Cenozoic evolution of the Yakutat–North American collision zone, southeast Alaska

Dissertation
der Mathematisch-Naturwissenschaftlichen Fakultät
der Eberhard Karls Universität Tübingen
zur Erlangung des Grades eines
Doktors der Naturwissenschaften
(Dr. rer. nat.)

vorgelegt von
Sarah Falkowski
aus Celle

Tübingen
2015

Gedruckt mit Genehmigung der Mathematisch-Naturwissenschaftlichen Fakultät der Eberhard Karls Universität Tübingen.

Tag der mündlichen Qualifikation:	15.01.2016
Dekan:	Prof. Dr. Wolfgang Rosenstiel
1. Berichterstatter:	Prof. Dr. Eva Enkelmann
2. Berichterstatter:	Prof. Dr. Todd A. Ehlers

Cenozoic evolution of the Yakutat–North American collision zone, southeast Alaska

Dissertation

der Mathematisch-Naturwissenschaftlichen Fakultät
der Eberhard Karls Universität Tübingen
zur Erlangung des Grades eines
Doktors der Naturwissenschaften
(Dr. rer. nat.)

vorgelegt von
Sarah Falkowski
aus Celle

Tübingen
2015

Acknowledgments

First and foremost, I would like to thank my advisors Eva Enkelmann and Todd Ehlers. They gave me a scientific home and the resources, support, and time I needed to successfully finish this project. They also encouraged me to attend national and international conferences and present our work. These opportunities are highly valued by me. Eva taught me everything I needed to know about thorough lab work to produce the high-quality data presented here.

This project was made possible through funding from the Deutsche Forschungsgemeinschaft. Furthermore, a scholarship from the Fulbright Commission gave me the chance to work personally with Eva after she accepted a professorship at the University of Cincinnati and left Tübingen. In 2014, I spent six months at the Geology Department in Cincinnati, where I felt welcome. A scholarship from the Alaska Geological Society helped me to attend a conference in the USA and meet others working in the remote St. Elias Mountains.

I learned a lot from collaborations with Kerstin Drost, Jörg Pfänder, and Blanka Sperner during U-Pb and ^{40}Ar/^{39}Ar measurements. Under the supervision of Jörg and Blanka at TU Freiberg, I was able to conduct almost all ^{40}Ar/^{39}Ar measurements. Kerstin conducted the U-Pb measurements, Hartmut Schulz helped with the cathodoluminescence images. Konstanze Stübner was available for any scientific questions and did an admirable job running and fixing the thermochronology labs in Tübingen, as Eva did before. Konstanze conducted the AHe measurements for this study.

Dorothea Muehlbayer-Renner, Dagmar Kost, and Anja Obst supported the preparation of samples in the Tübingen and Freiberg labs.

The time I could spend in the diverse ESD group in Tübingen was inspiring and fun because of the great people and excellent scientists that Todd brought together. It was particularly great to have been able to discuss the geology of Alaska with David Grabowski, who collected the Alaskan samples together with Eva and Ann-Kathrin Schatz. Philipp Widmann assisted Eva and me in the collection of the Canadian samples.

Many thanks go to Daniel Falkowski and Matthias Nettesheim for their proofreading of some of the chapters.

I am especially grateful to Elena Grin for going through the PhD experience with me and to everyone who shared the office with me over the past years.

Contributions of others

About 75 % of the laboratory work (data collection), 90 % of the data analysis, and 90 % of the interpretation in writing and figures were done by me. Others contributed to this study in different ways, listed in the following.

1. Project idea

The idea for the project is from Prof. Eva Enkelmann (then University of Tübingen, now University of Cincinnati). Funding to her and Prof. Todd Ehlers (University of Tübingen) (PIs) was given by the Deutsche Forschungsgemeinschaft. I was involved in decisions in the course of the project in the years 2011–2015 and in one of the sampling campaigns in 2012 in the northern St. Elias Mountains, Yukon.

2. Sampling

Sampling in the southern St. Elias Mountains, Alaska, was conducted by Prof. Enkelmann and students Ann-Kathrin Schatz and David Grabowski in 2011. Philipp Widmann, MSc. student, assisted Prof. Enkelmann and me in the field in 2012. Three bedrock samples from the Fairweather Range, presented in Chapter 4, were collected by Dr. Peter J. Haeussler (USGS, Anchorage, Alaska, USA); one bedrock sample was collected by Prof. Terry L. Pavlis (University of Texas, El Paso, USA).

2. Analyses

Dr. Kerstin Drost (then University of Tübingen) conducted the zircon U-Pb analyses at the Department of Isotope Geochemistry of the University of Tübingen with my assistance. I prepared the samples under supervision of Dr. Drost and made cathodoluminescence images of the individual zircons under supervision of Dr. Hartmut Schulz from the Biogeology and Applied Paleontology Department of the University of Tübingen. Dr. Drost also supported me in the interpretation of the U-Pb data (Chapter 4).

Dr. Jörg Pfänder, the head of the argon laboratory at TU Freiberg, and Dr. Blanka Sperner (TU Freiberg) supported me during $^{40}Ar/^{39}Ar$ measurements of cobbles in the Freiberg laboratory. Under Dr. Pfänder's supervision, I prepared the samples and conducted most of the measurements presented in Chapter 4. He also helped me with the analysis of the $^{40}Ar/^{39}Ar$ data (Chapter 4). Bedrock $^{40}Ar/^{39}Ar$ measurements were conducted at Lehigh University by Bruce Idleman in the laboratory of Prof. Peter Zeitler.

Dr. Konstanze Stübner (University of Tübingen) conducted the apatite (U-Th)/He measurements at the University of Tübingen. The new University of Tübingen facilities to measure uranium, thorium, and samarium were set up by Dr. Stübner with help of Prof. Ronny Schönberg, Dr. Drost, and Elmar Reitter.

The zircon (U-Th)/He measurements were conducted at the University of Arizona in the laboratory of Prof. Peter Reiners. Samples for apatite and zircon (U-Th)/He analyses were prepared by me.

Prof. Enkelmann provided the apatite fission-track data presented in Chapter 5. I conducted zircon fission-track analyses (Chapters 3 and 5) under the supervision of Prof. Enkelmann.

3. Text, figures, and tables

Dr. Drost and Dr. Pfänder are responsible for the text about the analytical details of the U-Pb and $^{40}Ar/^{39}Ar$ measurements (Chapters 2.4.3 and 2.4.4), respectively. The remaining text of this thesis was written by me and edited by my supervisors Prof. Enkelmann and Prof. Ehlers. Parts of Chapters 2.6, 2.7, and 3 have been published in a similar form in *Falkowski, S., E. Enkelmann, and T. A. Ehlers [2014], Constraining the area of rapid and deep-seated exhumation at the St. Elias syntaxis, southeast Alaska, with detrital zircon fission-track analysis, Tectonics, 33, 597–616, doi: 10.1002/2013TC003408* and therefore went through a peer-review process.

I prepared all figures and tables. Dr. Drost provided the information in Table 2-1.

4. Scientific ideas

I developed interpretations in continuous discussion with my supervisors Prof. Enkelmann and Prof. Ehlers. Discussions with other members of our work group as well as other scientists working in the St. Elias Mountains, including Prof. Terry L. Pavlis (University of Texas, El Paso, USA), Prof. John I. Garver (Union College, New York, USA), and Prof. Kenneth D. Ridgway (Purdue University, Indiana, USA) inspired and helped me to interpret some of the data.

Table of Contents

List of Figures

List of Tables

Abstract

A better understanding of orogenic syntaxes is necessary in order to improve our knowledge of continental deformation, which impacts human life immensely. Orogenic syntaxes are kinematic transition zones and potentially concentrate large amounts of stress and strain, which can lead to frequent and high-magnitude earthquakes and mass wasting processes.

The St. Elias syntaxis in the St. Elias Mountains of southeast Alaska and adjacent western Canada recently gained attention for its high exhumation and erosion rates, and by comparison to the "tectonic aneurysm" model that was developed for the eastern and western Himalayan syntaxes. The St. Elias syntaxis is the area where transform motion along the Fairweather Fault segment of the Yakutat-North American plate boundary transitions into flat-slab subduction of the thick, oceanic Yakutat crust. Detailed studies of exhumation processes at the St. Elias syntaxis are hampered by its extensive glaciation. The approach in this study therefore comprises the use of detrital material from large and small glacio-fluvial catchments and the application of multiple thermo- and geochronometric dating techniques in order to reveal the long-term exhumation history of the syntaxial region and its relation to other parts of the orogen. Cooling age populations were extracted from sand-sized samples and complete cooling histories (500–65 °C) and provenance information (U-Pb dates, lithology) were obtained from glacially transported cobbles and interpreted in combination with previously published and new bedrock thermo- and geochronologic ages.

A total of 4905 new single-grain zircon fission-track (ZFT) ages (~430–0.2 Ma) of modern, sand-sized detrital samples from 47 different catchments covering an area of almost 45,000 km^2, 1350 new single-grain apatite fission-track (AFT) ages (~433–1 Ma) of modern, sand-sized detrital samples from 15 of the 47 catchments, five ZFT bedrock ages (~154–9.4 Ma), three bedrock biotite $^{40}Ar/^{39}Ar$ ages (~42–5 Ma), as well as data of 27 cobble-sized detrital samples with 21 zircon U-Pb ages (~277–31 Ma), eight amphibole $^{40}Ar/^{39}Ar$ ages (~276–16 Ma), seven biotite $^{40}Ar/^{39}Ar$ ages (~50–42 Ma), four zircon (U-Th)/He ages (~35–4.8 Ma), four AFT ages (~17–1.6 Ma), and six apatite (U-Th)/He ages (~4.2–0.6 Ma) are presented.

Two large-scale terrane subduction and accretion phases influenced the upper crustal cooling of the study area; the Jurassic–Cretaceous accretion of the Wrangellia Composite Terrane to the former North American margin and the ongoing flat-slab subduction and collision of the Yakutat microplate. The Fairweather plate boundary segment has been transpressional in nature since at least 30 Ma and collision of the Yakutat microplate with the North American Plate began ~15–12 Ma. Rapid exhumation in the St. Elias syntaxis area began ~10 Ma and was confined by an unmapped, ice covered, discrete structure northeast of the northern Fairweather Fault and possibly the Fairweather Fault itself, most likely forming a one-sided, positive flower structure. The locus of rapid exhumation shifted southwest into the central syntaxis area at

~5 Ma and exhumation rate and depth were increased, causing ~10 km of exhumation ~5–2 Ma. This occurred probably due to a combination of i) an increase in the compressional component of Yakutat-North American convergence, ii) the subduction of increasingly thicker oceanic crust of the wedge-shaped Yakutat microplate, and iii) a change in erosional patterns and rates due to 6–5 Ma onset of glaciation. Pliocene exhumation might have been accommodated by a two-sided, positive flower structure centered at the northern Fairweather Fault, but with deep exhumation focused on the North American Plate. After ~2 Ma, the focus of most rapid exhumation migrated farther south to the lower plate of the syntaxial region (Yakutat microplate).

Overall, the results indicate that syntaxial regions should be treated as 4D-problems with spatio-temporally heterogeneously distributed deformation and exhumation. If process rates are high, as in the case of the St. Elias and Himalayan syntaxes, then, the dynamics of these regions are likely to respond very quickly (0.5–1.0 Myr) to changes in tectonic, rheologic, and climatic settings.

Zusammenfassung

Kontinentale Deformation beeinflusst die Gestalt der Erdoberfläche und hat dadurch einen großen Einfluss auf das Leben auf der Erde. Die Untersuchung von Gebirgssyntaxen, den Bereichen starker Krümmung in sonst geradlinig verlaufenden Gebirgszügen, ist ein wichtiger Schritt zu einem besseren Verständnis von Deformationsprozessen. Einige Syntaxen sind durch extreme Verformung gekennzeichnet, was zu starken Erdbeben und anderen Massenbewegungen, wie Hangrutschungen, führen kann.

Die St. Elias Syntaxis im gleichnamigen Gebirge in Südostalaska und angrenzenden Gebieten Westkanadas weist sehr hohe Erosions- und Gesteinsexhumierungsraten auf. Vergleichbar hohe Werte sind aus der östlichen und westlichen Syntaxis des Himalayas bekannt und wurden dort unter anderem mit dem Modell des „tectonic aneurysm" erklärt. Die St. Elias Syntaxis stellt einen kinematischen Übergangsbereich zwischen zwei Segmenten der Plattengrenze zwischen der Yakutat Mikroplatte und der Nordamerikanischen Platte dar. Dextrale Seitenverschiebung entlang der Fairweather-Störung geht innerhalb der St. Elias Syntaxis in flache Subduktion der ozeanischen Yakutat-Kruste über. Das gesamte St. Elias Gebirge ist vergletschert, was eine detaillierte Untersuchung von Exhumierungsprozessen erheblich erschwert. Diese Studie zeigt, dass dieses Problem durch Untersuchung von Detritus, der aktiven, fluvioglazialen Systemen entnommen wurde und daher hauptsächlich von Gletschern erodiertem Material entspricht, umgangen werden kann.

Mithilfe verschiedener thermo- und geochronologischer Datierungsmethoden kann die Exhumierungsgeschichte der Syntaxis über einen Temperaturbereich von 500–65 °C sowie die Provenanz (U-Pb Datierung, Lithologie) von Sand- und Geröllproben rekonstruiert und zusammen mit publizierten thermochronologischen Daten von Sandproben und Festgesteinen interpretiert werden.

Insgesamt werden in dieser Studie 4905 neue Zirkonspaltspur-Einzelkornalter (~430–0,2 Ma) von 47 Sandproben, die 47 verschiedenen Gletschereinzugsgebieten mit einer Gesamtfläche von fast 45000 km^2 entsprechen, und 1350 neue Apaptitspaltspur-Einzelkornalter (~433–1 Ma) von Sandproben aus 15 der 47 Einzugsgebiete präsentiert. Des Weiteren wurden 27 Geröllproben anhand von 21 Zirkon U-Pb Analysen (~277–31 Ma), acht Amphibol ^{40}Ar/^{39}Ar Analysen (~276–16 Ma), sieben Biotit ^{40}Ar/^{39}Ar Analysen (~50–42 Ma), vier Zirkon (U-Th)/He Analysen (~35–4,8 Ma), vier Apatitspaltspur-Analysen (~17–1.6 Ma), sowie sechs Apatit (U-Th)/He Analysen (~4.2–0,6 Ma) datiert. An neun Festgesteinsproben wurden fünf Zirkonspaltspurdatierungen (~154–9,4 Ma) und vier Biotit ^{40}Ar/^{39}Ar Datierungen (~42–5 Ma) vorgenommen.

Die Daten zeigen zwei Phasen von Subduktion und Akkretion von Terranen, die für das Abkühlen der oberen Kruste im Arbeitsgebiet verantwortlich waren; die jurassisch–kretazische Akkretion des Wrangellia Composite Terrane an den damaligen

Rand der Nordamerikanischen Platte sowie die noch andauernde Subduktion und Kollision der Yakutat Mikroplatte. Das Fairweather-Segment der Plattengrenze ist seit etwa 30 Mio. Jahren von Transpression gekennzeichnet; die Kollision der Yakutat Mikroplatte mit der Nordamerikanischen Platte begann vor 15–12 Mio. Jahren.

Die schnelle Gesteinsexhumierung in der St. Elias Syntaxis setzte vor etwa 10 Mio. Jahren ein und war von einer nicht kartierten, heute mit Eis bedeckten Störung nordöstlich der Fairweather-Störung und möglicherweise der Fairweather-Störung selbst begrenzt, was sich strukturgeologisch wahrscheinlich durch eine einseitige, positive „flower structure“ geäußert hat. Der Fokus der schnellen Exhumierung hat sich vor etwa 5 Mio. Jahren nach Südwesten verschoben, begleitet von einer Erhöhung der Exhumierungsrate und –tiefe. So wurden zwischen 5 Ma und 2 Ma ungefähr 10 km an Gestein exhumiert. Ausgelöst wurde diese konzentrierte Deformation vermutlich durch eine Kombination von drei, interagierenden Faktoren: i) der Erhöhung der Kompressionskomponente der Plattenkonvergenz, ii) der Subduktion von zunehmend mächtigerer, ozeanischer Kruste der keilförmigen Yakutat Mikroplatte, sowie iii) veränderter Erosionsmuster und -raten durch die vor 6–5 Mio. Jahren einsetzende Vergletscherung des Gebirges. Die schnelle, pliozäne Exhumierung, die sich um die Fairweather-Störung konzentrierte, wurde strukturell von einer zweiseitigen „flower structure“ getragen, wobei die tiefe Exhumierung auf die Nordamerikanische Platte beschränkt war. Vor etwa 2 Mio. Jahren wanderte der Fokus der stärksten Deformation weiter nach Süden auf die subduzierende Yakutat Mikroplatte.

Zusammenfassend veranschaulichen die Ergebnisse, dass Syntaxen als vierdimensionales Problem behandelt werden müssen, da Deformation und Exhumierung zeitlich und räumlich variabel sind. In Syntaxen sind hohe Prozessraten, wie im Fall der St. Elias Syntaxis und der Syntaxen des Himalayas, möglich. Dadurch passen sich geodynamische Prozesse schnell (innerhalb von 0,5 bis 1 Mio. Jahren) an tektonische, rheologische und klimatische Änderungen an.

1 Introduction

1.1 Motivation and hypotheses

Deformation at convergent and transform plate boundaries poses potentially fatal hazards to human life through earthquakes and related mass movements. This deformation and its spatial and temporal distribution are influenced by and interact with climate via the redistribution of mass [e.g., *Beaumont et al.*, 1992, 1999; *Willett*, 1999; *Whipple*, 2009; *Enkelmann et al*., 2015a], but this system is not well understood. Furthermore, plate corner settings can play an important role in localizing stress and strain and may result in high process rates. Potential positive feedbacks can emerge between efficient erosion, advection of heat and mass in the upper crust towards the surface, consequent crustal weakening, increased topographic relief and elevation, and the amount of precipitation [e.g., *Zeitler et al.*, 2001; *Koons et al.*, 2002, 2013; *Bendick and Ehlers*, 2014]. The model of localized feedback mechanisms between tectonic, erosional, and climatic processes is known as "tectonic aneurysm" [*Zeitler et al.*, 2001]. However, the model that was first developed for the eastern and western Himalayan syntaxes was recently challenged and is under debate in terms of relative contributions of the different processes [e.g., *Zeitler et al.*, 2001, 2014; *Koons et al.*, 2002, 2010, 2013; *Enkelmann et al.*, 2009; *Bendick and Ehlers*, 2014; *Wang et al.*, 2015]. While *Zeitler et al.* [2001, 2014] and *Koons et al.* [2002, 2010, 2013] consider local erosion as the driving mechanism, *Bendick and Ehlers* [2014] highlight the importance of geometric stiffening of the subducting plate in syntaxial regions to initiate very localized rapid exhumation.

In order to improve the understanding of plate boundary and continental deformation, the need to study plate corner regions and their influence on far-field deformation, surface processes, and climatic systems arises. One of the key components is to compile observational datasets of deformation, exhumation, and erosional characteristics of plate corners to provide a more complete overview of different tectonic and climatic settings as well as differences and similarities in deformation modes at different plate corners. These data can eventually be fed into large-scale geodynamic models and help to evaluate contending models.

Prior to this study, comprehensive structural and geo- and thermochronologic datasets existed only for the Himalayan syntaxes, particularly the eastern syntaxis in the Namche Barwa-Gyala Peri massif, [e.g., *Burg et al.*, 1998; *Zeitler et al.*, 1989, 2001, 2014; *Finnegan et al.*, 2008; *Stewart et al*., 2008; *Booth et al.*, 2009; *Enkelmann et al.*, 2011]. This study contributes long-term exhumation characteristics for the wider St. Elias syntaxis area in southeast Alaska and southwest Yukon, which has recently gained attention through the discovery of very rapid exhumation rates (>3 mm/yr) on million-year time scale and its comparison to exhumation mechanisms at the Himalayan syntaxes [*Enkelmann et al.*, 2009, 2010; *Koons et al.*, 2010, 2013]. However, spatio-temporal constraints for the rapid exhumation at the St. Elias syntaxis are not well studied and their investigation is severely hampered by the extensive ice cover of the coastal St. Elias Mountains. At the same time however, the collocation of large glaciers that cause extremely efficient glacial erosion [e.g., *Hallet et al.*, 1996] and active mountain building offers a prime opportunity to study tectonic-climatic interactions [e.g., *Bruhn et al.*, 2004; *Spotila et al.*, 2004; *Berger and Spotila*, 2008; *Enkelmann et al.*, 2010; *Spotila and Berger*, 2010; *Headley et al.*, 2013].

The working hypotheses for this study are:

(1) Subduction of the Yakutat plate corner results in localized rapid and deep exhumation at the St. Elias syntaxis.

(2) Exhumation mechanisms at the St. Elias syntaxis can be described as nascent "tectonic aneurysm" similar to the more developed Himalayan syntaxes.

(3) Detrital sampling is the most suitable approach to reveal the cooling history beneath the thick and extensive ice cover of the St. Elias Mountains.

Related questions addressed in the following chapters include:

What is the spatial evolution of exhumation at the St. Elias syntaxis? What is the role of glaciers in the concentration of deformation? What is the role of the inferred Connector Fault, which supposedly transfers strain from the Yakutat-North American plate boundary inland? (Chapter 3)

What is the temporal evolution of exhumation at the St. Elias syntaxis? What is the depth of exhumation? Can sufficient provenance information be obtained from detrital material to trace detrital cooling and exhumation signals to its origin? (Chapter 4)

What structures accommodate exhumation in the St. Elias syntaxis area? What are the inboard effects of exhumation processes at the St. Elias syntaxis? (Chapter 5)

1.2 Definition of "syntaxis" and "plate corner"

In studies that deal with orogenic syntaxes or plate corners, definitions of the terms "syntaxis" and "plate corner" are often vague, if given at all. In order to avoid misunderstandings which setting or which characteristics are discussed, a clear definition is required. One concrete definition is given by *Bendick and Ehlers* [2014], who use the term "syntaxis" for "narrow, cuspate region[s] linking two adjacent subduction segments, including both downgoing and overriding material, rather than all orogenic bends generically". In this study of the St. Elias syntaxis, "syntaxis" is used in the broader sense of "a sharp bend in an orogenic belt" [*Suess*, 1904], as the St. Elias syntaxis forms the transition zone between the transform and subduction segments of the plate boundary between the Yakutat microplate and the North American Plate. Also, both upper (North American Plate) and lower (Yakutat microplate) plates are considered as syntaxial region. The lower plate part of this region is considered as Yakutat plate corner, which is translated northwestward into the bend in the southeast Alaskan margin (Figure 1-1).

1.3 Outline of this thesis

This thesis is subdivided into six chapters. The following Chapter 2 provides methodological background on thermo- and geochronology, the analytical procedures used during this study, and how thermochronology can be used to reconstruct the evolution of mountain belts. Furthermore, an overview of the geologic and tectonic history of the Chugach-St. Elias Mountains and previous thermochronometric ages is given. Knowledge of the geologic background is crucial in order to understand the thermal record of rocks that experienced various geologic histories depending on the terrane and the location along and across strike of the orogen they originate from. In later chapters, more specific geologic information for the different study areas will be given.

For the purpose of clarity, the results of this study are divided into three chapters that can be considered as substudies that either focus on different geographic locations (Figure 1-1) and/or use different analytical approaches to address the above stated hypotheses and questions.

Chapter 3 focuses on mapping of the areal extent of rapid and deep exhumation in the St. Elias syntaxis region using detrital zircon fission-track (ZFT) analysis on 26 glacio-fluvial sand samples from the eastern part of the St. Elias syntaxis and the Fairweather Range (Figure 1-1).

Chapter 4 focuses on the investigation of glacially transported cobble-sized detritus from the Seward-Malaspina and Hubbard-Valerie Glacier catchments, which together drain almost the entire St. Elias syntaxis area (Figure 1-1). Multiple geo- and thermochronometric methods were applied on individual samples, including apatite and zircon (U-Th)/He dating (AHe and ZHe, respectively), apatite FT (AFT) analysis, zircon U-Pb dating, and biotite and amphibole $^{40}Ar/^{39}Ar$ analysis. This analytical approach allows the reconstruction of the provenance of the samples and their cooling histories over temperatures of 500–65 °C. Chapter 4 also includes a comprehensive synthesis of cooling histories from the entire Chugach-St. Elias Mountains and Fairweather Range in order to put the cooling characteristics obtained from the cobbles of the syntaxis area into a regional perspective. Overall, Chapter 4 provides information on the temporal evolution of syntaxial exhumation as well as constraints on the amount of rock exhumation.

Chapter 5 comprises ZFT and AFT analyses of detrital, sand-sized samples from 21 glacio-fluvial catchments located in the northern part of the St. Elias Mountains and eastern Wrangell Mountains (Figure 1-1). Only two thermochronologic studies have been published before from the Canadian side of the mountain range, both analyzing bedrock from the high Icefield Ranges region [*Dodds and Campbell*, 1988; *Spotila and Berger*, 2010]. Thus, the new detrital analyses, together with five bedrock samples, constitute a major advancement for revealing the thermal history of this large region, stretching from the syntaxis north to the Denali Fault (Figure 1-1).

The final Chapter 6 provides a summary of the main outcomes of this study and addresses the hypotheses from Chapter 1.1.

Peer-reviewed publications of the results of this thesis can be found in *Falkowski et al. [2014], doi: 10.1002/2013TC003408*; *Falkowski et al. [2016], doi: 10.1002/2015 TC004086*; and *Falkowski and Enkelmann [2016], doi: 10.1130/L508.1*.

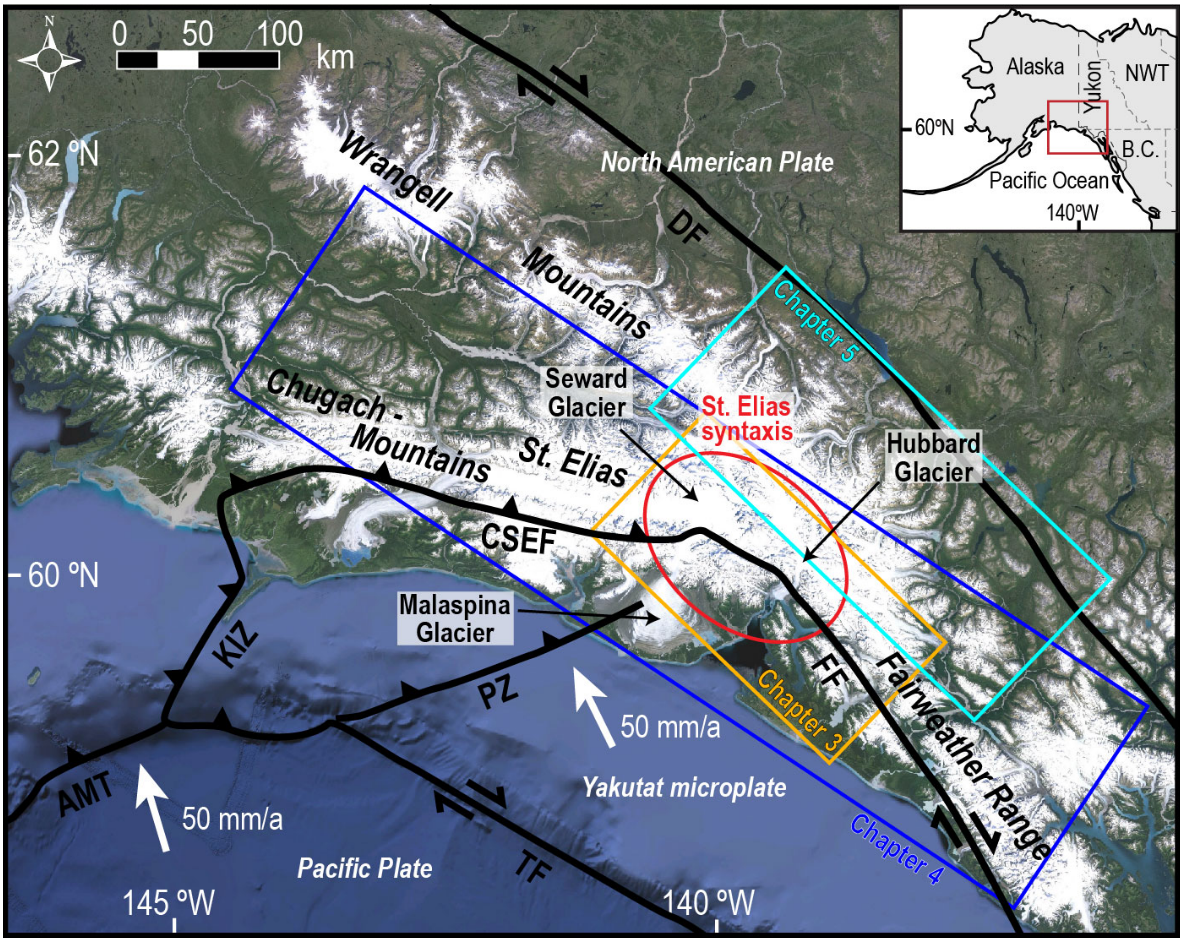

Figure 1-1. Satellite image of the Chugach-St. Elias and Wrangell Mountains in southeast Alaska and adjacent western Canada (Google Earth, August 2015). The red ellipsis indicates the St. Elias syntaxis area; the rectangles mark the study areas investigated in Chapters 3 (yellow), 4 (blue), and 5 (turquoise). NWT: Northwest Territories, B.C.: British Columbia, DF: Denali Fault, CSEF: Chugach-St. Elias Fault, FF: Fairweather Fault, KIZ: Kayak Island Zone, PZ: Pamplona Zone, TF: Transition Fault, AMT: Aleutian Megathrust. Plate motion vectors after *Plattner et al.* [2007] and *Elliott et al.* [2010].

2 Background

This chapter provides the theoretical background of the thermo- and geochronometric methods and concepts. An overview of commonly used methods with corresponding closure temperatures is shown in Figure 2-1. The aim of this chapter is not to give an exhaustive review of the methods but a brief overview of the principles and concepts of the techniques and analytical procedures used in this study. Furthermore, a description of the regional geologic and tectonic setting of the St. Elias Mountains, in particular the St. Elias syntaxis area, is given and results of previous exhumation studies conducted in the St. Elias Mountains are summarized.

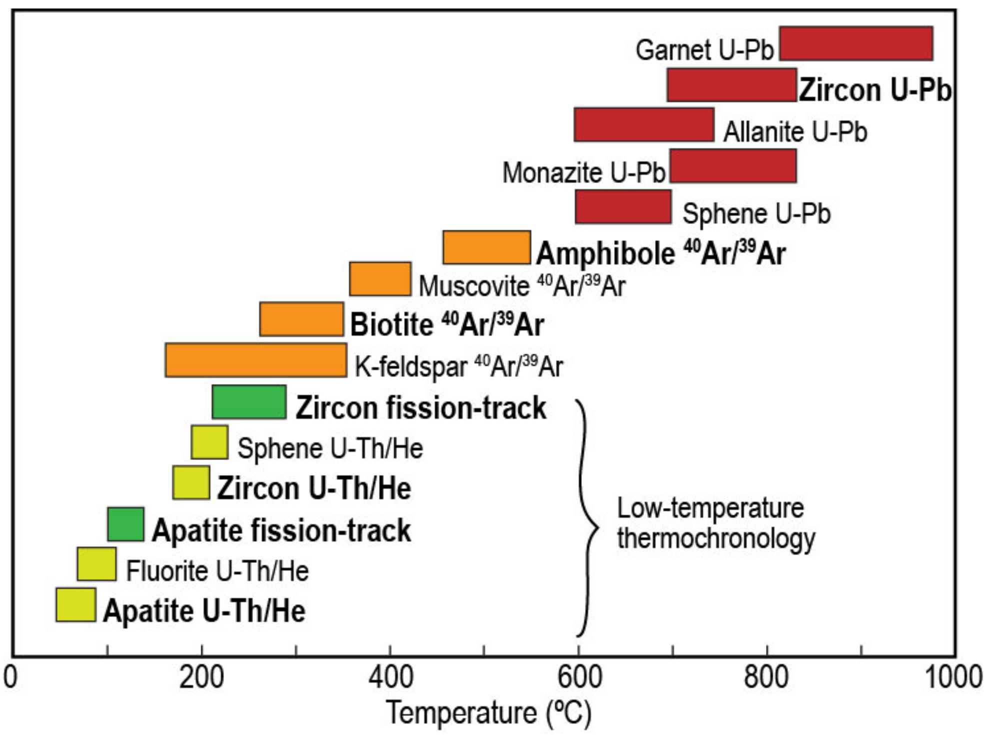

Figure 2-1. Closure temperatures of different thermo- and geochronometric systems. All systems from AHe to ZFT are commonly described as low-temperature thermochronology. The U-Pb systems can be grouped as geochronologic methods that characterize formation or recrystallization of crystals from melts. The systems with bold labels were used in this study. Temperature sensitivities after *Gleadow and Duddy* [1981], *Harrison* [1981], *Harrison et al.* [1985], *Copeland et al.* [1988], *Mezger et al.* [1989, 1993], *Parrish* [1990], *Foland* [1994], *Scott and St-Onge* [1995], *Brandon et al.* [1998], *Farley* [2000], *Reiners et al.* [2004], *Reiners and Brandon* [2006]; *Harrison et al.* [2009].

2.1 Noble gas thermochronometry

Geochronometry uses the radiometric decay of radioactive isotopes into stable isotopes in order to determine the time of formation of a certain mineral. Noble gas thermochronometry, in contrast, exploits the radiometric decay and temperature-dependent diffusion of the daughter products to study the thermal history of rocks since their formation [e.g., *Hurley*, 1954; *Dodson* 1973; *Berger and York*, 1981; *Zeitler et al.*, 1987]. After *Rutherford and Soddy*'s [1903] publication of the law of radioactive decay, *Ramsay and Soddy*'s [1903] finding that helium accumulates in material, which decays by α-emission, and *Rutherford*'s [1905] suggestion to use radioactivity to measure geologic time, the general age equation is given by **Equation 1**:

$$t = \frac{1}{\lambda} \ln\left(1 + \frac{D}{P}\right)$$

where t is the age, λ the decay constant, and D and P the concentration of daughter products and parent isotopes, respectively. Noble gas thermochronometry used in this study is based on the nuclear decay of ^{40}K ($^{40}Ar/^{39}Ar$ technique) or ^{238}U, ^{235}U, ^{232}Th, and ^{147}Sm ((U-Th)/He technique) that produces ^{40}Ar and ^{4}He, respectively, and the temperature-dependent accumulation (retention) of the decay products. Determining the concentration of parent isotopes and daughter products thus enables the calculation of the cooling age, the time that passed since the rock sample cooled through the closure temperature (T_c) [*Dodson*, 1973]. The concept of T_c is visualized in Figure 2-2.

2.1.1 $^{40}Ar/^{39}Ar$ thermochronometry

The $^{40}Ar/^{39}Ar$ method is based on the decay of ^{40}K to radiogenic ^{40}Ar. Therefore, all minerals that contain sufficient concentrations of potassium are suited for dating. Commonly, K-feldspar, micas, and amphibole, or whole-rock samples are used [e.g., *McDougall and Harrison*, 1988]. K-feldspar presents an exception to the equivalence of grain size and diffusion domain, which makes multidomain diffusion analysis necessary. This yields a more detailed view on the thermal history of the dated minerals [e.g., *Lovera et al.*, 1989, 1991].

The $^{40}Ar/^{39}Ar$ technique developed from the conventional K-Ar technique [*Aldrich and Nier*, 1948], where potassium and argon were measured separately at different aliquots of the same sample [e.g., *Dalrymple and Lanphere*, 1969]. In the $^{40}Ar/^{39}Ar$ method, ^{40}K is indirectly measured through ^{39}Ar, which is produced by the $^{39}K(n,p)^{39}Ar$ reaction during neutron irradiation in a nuclear reactor and the $^{40}K/^{39}K$ ratio is constant and known [*Merrihue and Turner*, 1966]. The advantages of using the $^{40}Ar/^{39}Ar$ ratio to calculate cooling ages are that measurements are single isotopic analyses of high precision on smaller sample sizes and that simultaneous measurements of all argon isotopes are possible. Furthermore, several cooling ages can be produced from a single sample through step-heating analyses, which yields insight into the distribution of radiogenic ^{40}Ar relative to ^{40}K (through ^{39}Ar; Figure 2-3) [e.g., *Merrihue and Turner*, 1966; *McDougall and Harrison*, 1988]. The knowledge of the distribution enables to evaluate the obtained cooling age in terms of the thermal history of the sample; for example thermal disturbances and argon loss can be detected and potentially corrected for [e.g., *Turner*, 1968; *Lanphere and Dalrymple*, 1976, 1978; *Heizler and Harrison*, 1988; *Kelley*, 2002]. For an illustration of the concept of step-heating analyses and age spectra, relatively simple cooling scenarios of idealized minerals and the resulting radiogenic ^{40}Ar concentration profiles and $^{40}Ar/^{39}Ar$ age spectra are depicted in Figure 2-3. For a thorough review the reader is referred to *McDougall and Harrison* [1988] and *Harrison and Zeitler* [2005].

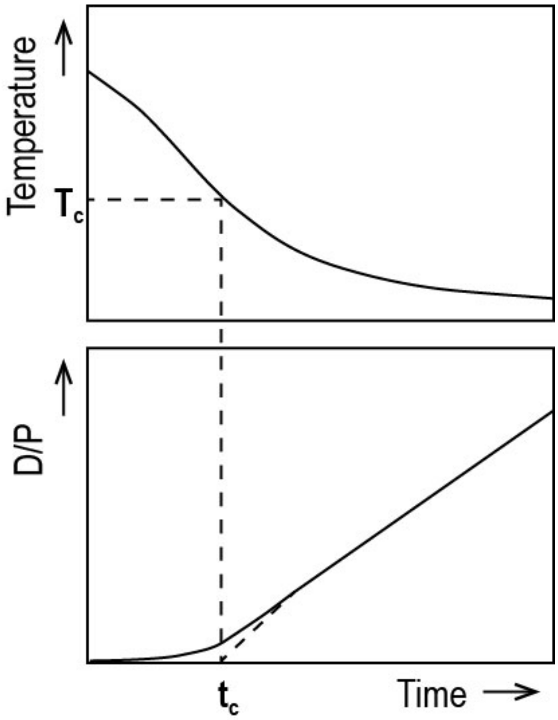

Figure 2-2. Definition of closure temperature, where time t_c corresponds to the apparent age of the mineral. The lower diagram shows the developing daughter/parent ratio (D/P) over time with decreasing temperature (as shown in the upper diagram). At higher temperatures the system remains open (D/P=0) and all daughter products are lost by diffusion. With decreasing temperature daughter products are partially retained, marked by the curved portion of the lower curve. When the temperature drops further (to the closure temperature T_c and below), diffusive loss becomes negligible (at time t_c) and the D/P ratio increases constantly marked by the linear portion of the lower curve. Modified after *Dodson* [1973].

Each heating step of the sample releases an increasing fraction of argon within an ultrahigh vacuum system and yields a $^{40}Ar/^{39}Ar$ ratio (for analytical procedures see Chapter 2.4.3 and *Pfänder et al.* [2014]) and thereby an age that can be plotted against the fraction of ^{39}Ar released to report the age spectrum (Figure 2-3). Important corrections of the measured isotope ratios include corrections for argon isotopes produced by interfering neutron reactions with other elements (mainly calcium and chlorine) during irradiation, and for trapped argon that contains non-radiogenic ^{40}Ar [*McDougall and Harrison*, 1988]. The latter correction bears an important assumption, namely that such argon is atmospheric in composition with $^{40}Ar/^{36}Ar=298.6 \pm 0.3$ [*Lee et al.*, 2006]. This assumption is not always true, for example, if the infinite sink assumption is not fulfilled due to fluid flow, varying temperatures, or fluid or melt inclusions [e.g., *Lanphere and Dalrymple*, 1976; *Heizler and Harrison*, 1988; *McDougall and Harrison*, 1988; *Kelley*, 2002]. The presence of excess Ar ($^{40}Ar/^{36}Ar \gg 298.6$) is not necessarily obvious from age spectra, which could still exhibit plateaus. This problem of apparently undisturbed, because flat, age spectra can become an issue for biotite $^{40}Ar/^{39}Ar$ dating, as biotite tends to break down during step heating, i.e., diffusion during the higher temperature steps can level the ^{40}Ar and ^{39}Ar concentrations and lead to apparent age plateaus toward the end of the age spectrum [e.g., *McDougall and Harrison*, 1988; *Roberts et al.*, 2001; *Kuiper*, 2002; *Harrison and Zeitler*, 2005]. One way to evaluate the potential presence and the nature of excess argon is the use of isochron [*Merrihue and Turner*, 1966] and inverse isochron diagrams [*Turner*, 1971; *Roddick et al.*, 1980], for which a detailed summary is given by *McDougall and Harrison* [1988] or *Kuiper* [2002], who stressed the importance of utilizing all available methods of age spectra and (inverse) isochron diagrams for data evaluation.

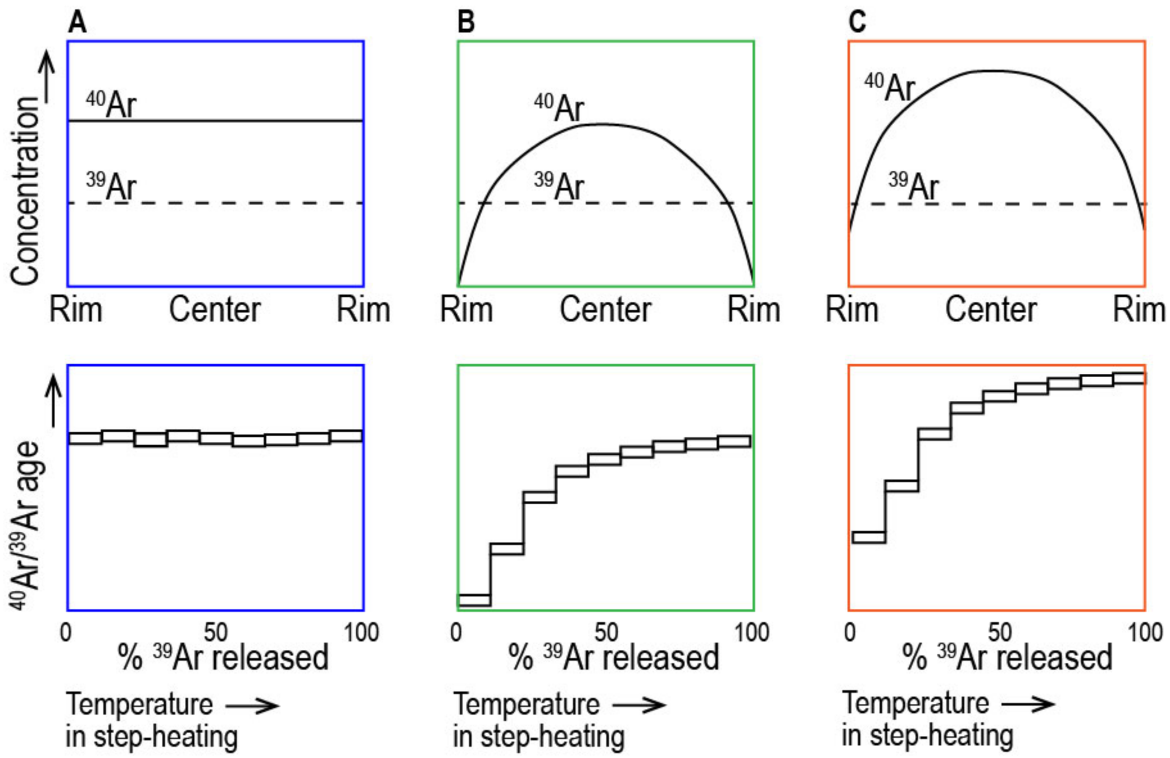

Figure 2-3A–C. Sketch of the resulting age spectra (lower three panels) of ^{40}Ar and ^{39}Ar concentrations (upper three panels) of idealized minerals. Modified after *McDougall and Harrison* [1988] and *Harrison and Zeitler* [2005]. (A) Rapid, monotonous, undisturbed cooling below the T_c results in a flat age spectrum (i.e., a plateau). The concentrations of ^{40}Ar and ^{39}Ar yield a constant ratio as both isotopes are derived from potassium and occur at similar positions within the crystal lattice, and exhibit a similar transport behavior. (B) This age spectrum is the result of recent diffusive argon loss, i.e., a decreased ^{40}Ar concentration at the rims of the crystal, which is seen in the lower temperature steps of step-heating analysis first. ^{39}Ar remains unaffected as it is induced by neutron irradiation of ^{39}K. (C) This age spectrum represents diffusive argon loss like in B, but then the mineral continued to uniformly accumulate ^{40}Ar. In age spectra that show these kinds of steps with low ages at the beginning increasing toward the end of the spectrum ('staircase'), the oldest age(s) reflect the minimum crystallization age of the mineral and the youngest age(s) reflect the time of the thermal event that affected the system last.

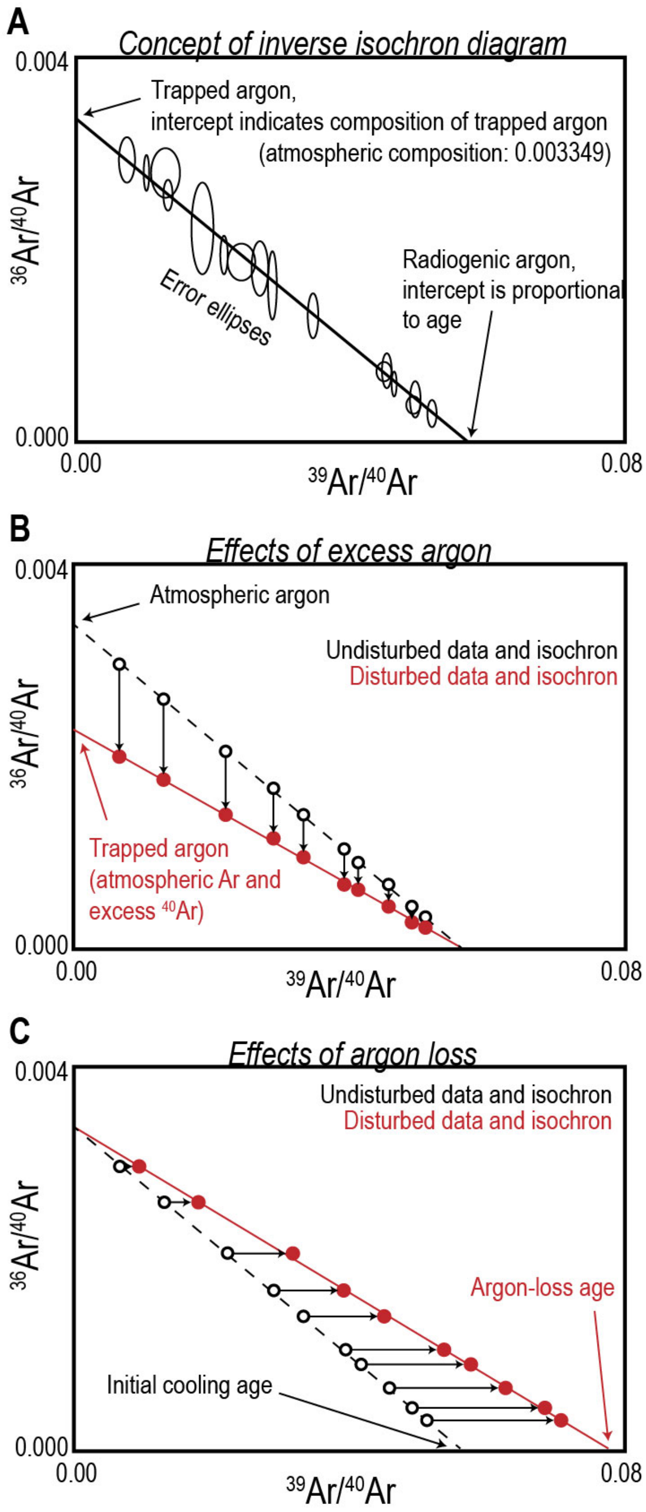

Figure 2-4A–C. Concept of the inverse isochron diagram (A) and effects of excess argon (B) and argon loss (C) on the isochron. The intercept of the isochron with the $^{36}Ar/^{40}Ar$ axis gives the composition of the trapped argon; the intercept with the $^{39}Ar/^{40}Ar$ axis is proportional to the inverse isochron age. The incorporation of excess argon does not change the inverse isochron age if the trapped argon/radiogenic argon remains the same for all data points (A). If argon is lost, the $^{36}Ar/^{40}Ar$ ratio does not change because argon isotope remain unfractionated during escape from a mineral, but the $^{39}Ar/^{40}Ar$ ratio changes because ^{40}Ar is lost while ^{39}Ar (representing ^{39}K) remains in the mineral (C). If all ^{40}Ar is lost, the inverse isochron age gives the end of the time over which argon loss occurred (C). If argon loss is not complete, the age is meaningless. Illustration modified from *Kuiper* [2002].

Isochron or inverse isochron diagrams are a method to determine the cooling age but also the initial argon composition. The usefulness of the isochron diagram has some limitations, namely the highly correlated errors on both axes due to the use of the least precisely measurable argon isotope, ^{36}Ar, to which both the total amount of ^{40}Ar and ^{39}Ar are normalized [e.g., *McDougall and Harrison*, 1988]. Therefore, the inverse isochron diagram is the preferred method used together with age spectra in this study (Chapter 4). The inverse isochron method plots $^{36}Ar/^{40}Ar$ against $^{39}Ar/^{40}Ar$ (Figure 2-4). If the argon composition in the sample is a mixture of trapped and radiogenic argon, the data points obtained from the step-heating analyses will exhibit a linear relationship and the $^{36}Ar/^{40}Ar$-axis intercept ($^{39}Ar/^{40}Ar=0$, no radiogenic ^{40}Ar) will give the ratio of the trapped argon component (atmospheric and/or excess argon), and the $^{39}Ar/^{40}Ar$-axis intercept ($^{36}Ar/^{40}Ar=0$, all argon is radiogenic as ^{36}Ar is not produced by radioactive decay) will give the $^{40}Ar/^{39}Ar$ age (Figure 2-4A) [*Turner*, 1971; *Roddick et al.*, 1980; *Heizler and Harrison*, 1988]. If an excess ^{40}Ar component is present and is homogeneously distributed, the $^{36}Ar/^{40}Ar$-axis intercept of the inverse isochron will be lowered (reflecting $^{40}Ar/^{36}Ar \gg 298.6$), but the $^{39}Ar/^{40}Ar$-axis intercept, the inverse isochron age, remains unchanged (Figure 2-4B) [*Heizler and Harrison*, 1988; *Kuiper*, 2002]. If the age spectrum of the same sample is then corrected with the actual $^{40}Ar/^{36}Ar$ ratio obtained from the inverse isochron diagram, it should yield the same age as the inverse isochron. Even if no correction is possible, for example, in the case of argon loss (Figure 2-4C) or a combination of argon loss and excess argon, or if excess argon is not evenly distributed within the minerals dated (i.e., the argon concentration is not a simple two-component mix of radiogenic and trapped argon), a verified data evaluation is ensured and potential inconsistencies can be revealed when using both age spectra and (inverse) isochron diagrams [*Kuiper*, 2002].

2.1.2 (U-Th)/He thermochronometry

After it had been one of the first radiometric dating techniques tested at the beginning of the 20th century [*Rutherford*, 1905], the AHe system was discarded as being unsuited for geochronometric dating due to its apparent helium leakage. Only in the late 1980s the method was rediscovered as potential thermochronometer with its ages being a measure of cooling below low temperatures and not the formation of the rock [*Zeitler et al.*, 1987]. Since then, efforts in experimental work and modeling studies on quantification of diffusion kinetics [e.g., *Wolf et al.*, 1998; *Farley*, 2000], non-diffusional factors on helium loss or retention [e.g., *Farley et al.*, 1996; *Green and Duddy*, 2006; *Shuster et al.*, 2006; *Flowers et al.*, 2009; *Gautheron et al.*, 2009], and influences of topography and advection on the heat flow of the shallow crust [e.g., *Mancktelow and Grasemann*, 1997; *House et al.*, 1998; *Braun*, 2002; *Ehlers and Farley*, 2003] paved the way for an appropriate interpretation of (U-Th)/He ages. Different mineral phases can be used but the best-studied and commonly used phases are apatite and zircon (see Figure 2-1 for T_c) [e.g., *Farley*, 2000, 2002; *Reiners et al.*, 2004].

Ages are calculated based on the equation for helium ingrowth (**Equation 2**):

$$^{4}He = 8\times{}^{238}U\left(e^{\lambda_{238}t}-1\right) + 7\times{}^{235}U\left(e^{\lambda_{235}t}-1\right) + 6\times{}^{232}Th\left(e^{\lambda_{232}t}-1\right) + {}^{147}Sm\left(e^{\lambda_{147}t}-1\right)$$

where λ_{238}, λ_{235}, λ_{232}, and λ_{147}, are the decay constants of the radioactive isotopes ^{238}U, ^{235}U, ^{232}Th, and ^{147}Sm, respectively, that emit 8, 7, 6 and 1 α-particles, respectively, during their decay chain to a stable isotope. This equation can be solved iteratively [*Vermeesch*, 2008] or non-iteratively [*Meesters and Dunai*, 2005] for t, the time since helium is effectively accumulated. The contribution of samarium to the helium production is only relevant in apatites, where samarium-derived helium constitutes typically 0.1–10 % [e.g., *Fitzgerald et al.*, 2006].

The (U-Th)/He age calculation requires a correction for non-diffusional loss of helium due to ejection of α-particles outside the crystal boundaries. When α-particles are emitted they travel on average ~5–22 μm (the so-called stopping distance, which is mineral-specific) in arbitrary directions from the decay center [*Farley et al.*, 1996; *Ketcham et al.*, 2011]. If the decay occurs within the range of the stopping distance to the crystal rim, helium can be ejected. This process needs to be accounted for by the α- or F_T-correction that introduces a factor for the total fraction of α-particles that would be retained in an idealized crystal with homogeneous U-Th (-Sm) distribution [*Farley et al.*, 1996]. The fractional loss of helium depends on the size and geometry of the analyzed crystal and hence, larger and euhedral grains require a smaller correction factor and are therefore favorable for analysis. The reader is referred to *Zeitler et al.* [1987], *Farley* [2000, 2002], *Ehlers and Farley* [2003], and *Harrison and Zeitler* [2005] for a more comprehensive view on the (U-Th)/He method.

2.2 Fission-track thermochronometry

Fission-track thermochronometry differs from other radiometric methods insofar as the measured daughter product is not an isotope, but a trail of physical damage called fission-track that forms due to the highly energetic, spontaneous fission of the ^{238}U nucleus in non-conductive minerals and glasses [*Price and Walker*, 1963; *Fleischer et al.*, 1975]. In a general view, the annealing of fission-tracks can be described by thermal diffusion through which the damage trails are progressively shortened and eventually vanish. On geologic time scales, this happens instantaneously at high temperatures above T_c (Figure 2-2) and the so-called Partial Annealing Zone (PAZ) in fission-track thermochronometry [*Gleadow and Duddy*, 1981; *Gleadow and Fitzgerald*, 1987]. At temperatures within the PAZ tracks are accumulated but partially shortened (annealed), while below the PAZ tracks are more or less completely preserved and accumulated [*Donelick et al.*, 1990]. Track annealing rates depend on several factors, such as cooling rate, composition (in apatites), track orientation with respect to crystallographic axes, or the amount of radiation damage accumulated in the crystal lattice. The kinetics of track annealing can be examined in laboratory experiments, or natural settings such as boreholes or exposed crustal sections [reviews in *Gallagher et al.*, 1998; *Tagami and O'Sullivan*, 2005].

Fission-tracks have initial lengths of ~11 μm in zircon and ~16 μm in apatite [e.g., *Fleischer et al.*, 1975] with nearly circular cross sections of ~8 nm in zircon [*Bursill and Braunshausen*, 1990] and ~6–10 nm in apatite [*Paul*, 1993], the minerals commonly used for fission-track thermochronometry. Chemical etching can widen the tracks to several μm to make them visible under an optical microscope [e.g., *Price and Walker*, 1962]. For the FT dating technique, the etched tracks are then counted under the microscope [e.g., *Hurford*, 1990]. The current practice of fission-track dating that is used in this study is the external detector method (EDM) [*Hurford*, 1990]. The analytical procedures are described in more detail in Chapter 2.4.2, but in general, they involve the determination of the amount of parent isotopes and daughter products in the same grain by counting induced and spontaneous fission-tracks, respectively. The number of spontaneous fission-tracks is a direct measure of ^{238}U fission events per volume unit, and the number of irradiation-induced tracks in an external muscovite detector is a measure of the amount of ^{238}U via ^{235}U, with the $^{238}U/^{235}U$ ratio being constant and known [e.g., *Hurford*, 1990].

The resulting age is then calibrated via the zeta-age technique [*Hurford and Green*, 1982, 1983; *Hurford*, 1990], which uses **Equation 3**:

$$t = \frac{1}{\lambda_D} \ln\left\{1 + \lambda_D \zeta \rho_D G \left(\frac{\rho_s}{\rho_i}\right)\right\}$$

where t is the thermochronometric age, λ_D the decay constant of α-emission of ^{238}U, ζ the zeta calibration factor, ρ_D the induced track density in a muscovite detector irradiated with a dosimeter of known uranium concentration with the samples as a measure of the neutron fluence, G the integrated geometry factor of the etched surface, and ρ_s and ρ_i the surface densities of etched spontaneous and induced tracks, respectively. The zeta factor is first determined by counting tracks of reference samples of known age, which makes it an individual factor specific to every fission-track counter and analytical setup, and it evolves over time with analyses of additional age standards. The age of unknown samples can then be determined with reference to the age standards included in the zeta factor. For details about the fission-track method, specifics to ZFT and AFT, and applications, the reader is referred to *Fleischer et al.* [1975], *Hurford* [1990], *Wagner and Van den haute* [1992], *Gallagher et al.* [1998], and *Reiners and Ehlers* [2005].

2.3 Zircon U-Pb geochronometry

After *Rutherford* [1905] first suggested using the decay of radioactive isotopes to measure geologic time, *Boltwood* [1907] showed that lead is the stable end product of the ^{238}U decay series and found constant Pb/U ratios in minerals from rocks of the same age and higher ratios in rocks that were supposedly older. He determined the first radiometric ages of minerals. *Holmes* [1911] then recognized the potential of zircon as an effective geochronometer and used it to commence defining the Phanerozoic time scale [*Holmes and Lawson*, 1927]. Much later ^{232}Th and ^{235}U were identified to also contribute radiogenic lead [*Rutherford*, 1929; *Dempster*, 1935].

With the decay series of ^{238}U to $^{206}Pb+8\alpha+6\beta^-$, ^{235}U to $^{207}Pb+7\alpha+4\beta^-$, and ^{232}Th to $^{208}Pb+6\alpha+4\beta^-$, three 'clocks' should reflect the same time of uranium and thorium ingrowth into the zircon crystal at igneous crystallization when measuring parent/daughter ratios of $^{238}U/^{206}Pb$, $^{235}U/^{207}Pb$, and $^{232}Th/^{208}Pb$. However, the uranium series generally appear more reliable, possibly due to different behavior of uranium and thorium, and partly because of the more precise determination of the ^{238}U and ^{235}U decay constants [*Jaffey et al.*, 1971]. The $^{206}Pb/^{238}U$ and $^{207}Pb/^{235}U$ ratios are plotted in the commonly used concordia diagram that shows the curve of compositions for which the uranium decay systems yield the same age [*Wetherill*, 1956]. Data points that lie on the curve are concordant, data points above or more often below the concordia are discordant and indicate lead loss.

The precision of measurements of the isotopic abundances has drastically improved with the development of the quantitative mass spectrometry [*Nier*, 1938; 1939a,b] and further improved with analytical developments that allowed for higher precision measurements of increasingly smaller sample sizes down to single grains and parts of single grains [e.g., *Lancelot et al.*, 1976; *Schärer and Allègre*, 1982a,b]. Reviews of analytical methodology can, for example, be found from *Ireland and Williams* [2003], *Parrish and Noble* [2003], *Košler and Sylvester* [2003], and, concerning the historical development, from *Davis et al.* [2003]. The analysis of single grains and parts of grains significantly improved the theoretical understanding especially related to apparent lead loss manifested in discordant U-Pb ages, which was a long-standing problem in the methodology [e.g., *Mezger and Krogstad*, 1997; *Davis et al.*, 2003]. Sensitive high-resolution ion microprobe (SHRIMP) measurements, for example, could show that zircons commonly consist of a mixture of concordant and discordant phases rather than that many zircons were affected by continuous or episodic lead loss as long thought [*Grünenfelder et al.*, 1964; *Steiger and Wasserburg*, 1966, 1969; *Gebauer et al.*, 1989]. It was also shown that zircon U-Pb ages could be preserved in high-grade thermal events, even melting, and that older zircon parts may serve as crystal nucleus in melts, or that older zircons can experience metamorphic overgrowth [e.g., *Poldervaart and Eckelmann*, 1955; *Grünenfelder et al.*, 1964; *Gebauer et al.*, 1989]. The issue of lead loss, however, could not be entirely resolved [e.g., *Mezger and Krogstadt*, 1997; *Davis et al.*, 2003], even though analytical techniques allow identifying likely concordant phases and avoiding discordant phases [review in *Davis et al.*, 2003]. Further understanding of internal zircon structure and the possibility to avoid discordant parts arose from back-scatter electron (BSE) or cathodoluminescence (CL) imaging prior to single-zircon analysis [e.g., *Vavra*, 1990], as done in this study with CL imaging (Figure 2-5).

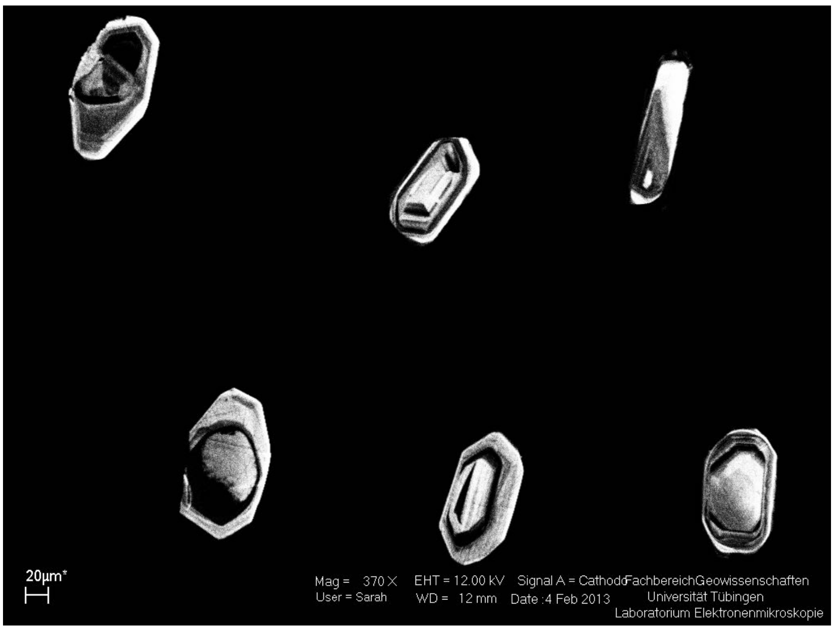

Figure 2-5. Example of cathodoluminescence imagery of six of the zircons analyzed (Chapter 4).

2.4 Analytical procedures

2.4.1 Apatite and zircon (U-Th)/He analysis

The mineral separation of all samples followed standard procedures. From mineral separates, clear apatites and zircons of sufficient size (width >80 µm) and without visible inclusions, impurities, and fractures were picked using cross-polarized binocular microscopes. Three single aliquots per apatite separate and two single aliquots per zircon separate were packed in niobium tubes after measuring their dimensions for alpha-ejection correction after *Farley et al.* [1996]. Helium, uranium, and thorium (and samarium on apatites) were measured at Patterson helium-extraction lines with 960 nm diode lasers and ICP-MS at the University of Tübingen (apatites) and the University of Arizona, USA (zircons). Apatite grains were heated for 5 min at 11 A and zircon grains for 10 min at 20 A. Each grain was re-heated and re-analyzed to make sure that the grain was degassed entirely in the first step. Concentrations of uranium, thorium, and samarium were determined by isotope dilution using the Thermo Scientific iCAP Qc ICP-MS equipped with an all-PFA sample introduction system at the Isotope Geochemistry Department of the University of Tübingen. Apatite samples together with the niobium-tubes were spiked with a calibrated mixed spike of ^{233}U+ ^{230}Th+^{149}Sm and dissolved over night in 2 ml 5 % HNO_3 + 0.1 % HF at 65 °C. The grain mass of each sample was estimated from measured ^{43}Ca concentrations assuming 39.4 wt-% calcium in apatite. For the zircons, the uranium and thorium concentrations were measured by ICP-MS at the Arizona Radiogenic Helium Dating Laboratory at the University of Arizona. The analytical errors of the mass spectrometer measurements are generally very low (<2 %) in contrast to the reproducibility of the sample age. Therefore, mean AHe and ZHe ages and standard deviations are commonly reported.

2.4.2 Apatite and zircon fission-track analysis

Zircon and apatite separates were obtained by using standard mineral separation procedures at the University of Tübingen. Zircons were mounted in Teflon, ground and polished to obtain even internal crystal surfaces, and etched for 12–32 h (detrital samples) and 10–27 h (bedrock samples) at 228 °C in a KOH:NaOH eutectic melt to reveal spontaneous fission tracks. Etching times depend on the radiation damage of individual zircons, which is a function of the cooling age and uranium content [*Garver and Kamp*, 2002; *Garver*, 2003]. As detrital samples contain zircons with various cooling ages and uranium contents, three mounts per sample were etched for different times. One mount per bedrock sample, three mounts per detrital sample, and Fish Canyon Tuff standard mounts were covered with uranium-free muscovite detectors and irradiated at the FRM-II nuclear reactor (Garching, Germany) or at the radiation center of Oregon State University (USA) to induce ^{235}U fission. Irradiation packages also held two to three IRMM541 uranium dosimeter glasses, also covered with muscovite detectors, to monitor neutron flux during irradiation. In each irradiation package, four to three standards were included.

Apatites were mounted in epoxy resin, ground, polished, and etched in 5.5 M nitric acid for 20 s to widen the spontaneous fission-tracks. As for zircon samples, the external detector method is applied and mounts were covered with a muscovite detector and prepared for irradiation at Oregon State University. IRMM540 dosimeter glasses as well as Durango standards were included in the irradiation package. After irradiation of zircon and apatite samples, the detectors were etched in 48 % hydrofluoric acid for 25 min to reveal induced fission-tracks.

Fission-tracks were counted using a Zeiss AxioImager microscope equipped with an AutoScan stage system at 1000x magnification. For the detrital ZFT samples, 1–3 mounts were used to analyze a representative grain population with regard to different degrees of radiation damage. Per sample, ~100 single-grain ages were analyzed using the ζ-calibration method [*Hurford*, 1990]. For extraction of detrital age components the software BINOMFIT [*Brandon*, 1992, 1996] was used. This method decomposes the measured age distribution into component age populations that are characterized by the peak age that gives the average ZFT age of each population, the age range of the population, and the relative size of the population with respect to the entire age distribution in percentage.

2.4.3 Biotite and amphibole $^{40}Ar/^{39}Ar$ analysis

The $^{40}Ar/^{39}Ar$ analysis of cobbles was carried out at Argonlabor Freiberg, TU Freiberg, Germany. Samples with no or very little alteration of amphibole and biotite, as observed in thin sections, were selected. Handpicked separates of 100–300 µm grain size were repeatedly washed in deionized water using an ultrasonic bath. About 5–10 mg of biotite and up to 300 mg of amphibole were wrapped in aluminum foil and placed along with fluence monitors in holes on aluminum discs for irradiation, which was done at the LVR-15 research reactor of the Nuclear Research Institute in Řež, Czech Republic. Irradiation duration was 4 h at a reactor power of 5 MW and a thermal neutron fluence of ca. 2.4x1013 n/cm^{2}s at a thermal-to-fast neutron ratio of ca. 2.2.

Irradiated samples were unwrapped and amphiboles were loaded into small molybdenum-crucibles for stepwise heating, which was performed using a CreaTec high-temperature furnace system [*Pfänder et al.*, 2014]. Heating time was 15 min per temperature step. Micas were loaded into holes with 3x1 mm (diameter x depth) on copper holders, and degassing was done using a floating energy controlled New Wave CO_2 laser system with a defocussed beam (3 mm diameter), operated in continuous mode at a wavelength of 10.6 µm. Heating time was 5 min per temperature step. The released gas was purified for 10 min by two GP50 getter pumps, one at room temperature and one at ~400 °C. Argon isotope abundances were measured in static mode on a GV Instruments ARGUS noble gas-mass spectrometer equipped with five faraday cups and 10^{12} Ω resistors on mass positions 36 to 39 and a 10^{11} Ω resistor on mass position 40. Each measurement comprises 45 scans at 10 s integration time each. A detailed description of the system as well as typical blank levels and airshot ratios is given in *Pfänder et al.* [2014].

Mass bias was corrected by assuming linear mass-dependent isotope fractionation and by using an atmospheric $^{40}Ar/^{36}Ar$ ratio of 298.6 ± 0.3 [*Lee et al.*, 2006]. Raw-data reduction and time-zero intercept calculations were done using an in-house developed MATLAB software package. Isochron, inverse isochron and plateau ages have been calculated with the Excel Add-In ISOPLOT 3.7 [*Ludwig*, 2012]. Fish Canyon Tuff sanidine was used as flux monitor (28.305 ± 0.036 Ma [*Renne et al.*, 2010]) and the decay constants of *Renne et al.* [2010] served as base for all calculations. Age uncertainties are reported on the 1σ-confidence level following the recommendation of *Renne et al.* [2009]. J-values and interference correction factors along with temperature steps, raw data and intensity intercepts are given in Appendix B (Dataset B-2).

2.4.4 Zircon U-Th-Pb analysis

After heavy mineral separation, up to 80 zircon crystals per sample were hand-picked under a binocular microscope and set in epoxy mounts. Mounts were polished to approximately half the zircon thickness and imaged in cathodoluminescence (CL) mode under the scanning electron microscope of the Biogeology and Applied Paleontology Department of the University of Tübingen (LEO 1450 VP Scanning electron microscope/Oxford Instruments). The latter is done to reveal internal textures of the zircon crystals such as growth zoning, metamorphic overgrowth, or inherited cores, to assist choosing the optimal location for laser spot analysis. When, in few cases, metamorphic overgrowth or older cores were suspected from CL-images, two to three ablation spots were chosen accordingly.

Uranium-thorium-lead isotopic analyses were acquired using a Thermo Scientific iCAP Qc quadrupole ICP-MS (inductively coupled plasma-mass spectrometer) and a Resonetics RESOlution M-50 excimer laser at the Isotope Geochemistry Department of the University of Tübingen. Operating conditions are listed in Table 2-1. After 30 s of gas blank measurement, laser ablation data were collected for another 30 s. The data were processed offline in a spreadsheet-based program. Data reduction included correction for gas blank as well as for time-dependent, instrumental and laser-induced fractionation. Fractionation correction was done by bracketing the unknowns with GJ1 zircon standard (608 Ma, ~430 ppm uranium; *Jackson et al.* [2004]) and applying the intercept method for the $^{206}Pb/^{238}U$ ratio. Reference zircon Plešovice (337 Ma, ~800 ppm uranium; *Sláma et al.* [2008]) was treated as unknown and provided a quality control.

Table 2-1. Instrument settings and operating conditions for U-Th-Pb analyses

Instrument	Thermo Scientific iCAP Qc
Forward Power	1550 W
Coolant gas flow	14.0 l/min
Sample gas flow	0.87 l/min
Sampling depth	5.0 mm
Data acquisition protocol	Time-resolved analysis
Isotopes determined	^{202}Hg, ^{204}(Hg + Pb), ^{206}Pb, ^{207}Pb, ^{208}Pb, ^{232}Th, ^{235}U, ^{238}U
Acquisition mode	Peak jumping, one point per peak
Dwell time	10 ms
Cones	Ni, skimmer with sensitivity insert
Laser-ablation system	Resonetics RESOlution M-50
Laser type/ wavelength	Excimer 193 nm
Pulse duration	20 ns
Energy density	2.6 J/cm^2
ThO^+/Th^+	< 1.0%
Nominal spot diameter	33 μm
Sampling strategy	Spot
Laser repetition rate	5 Hz
He gas flow	600 ml/min
N_2 gas flow	5 ml/min

2.5 Reconstruction of orogenic evolution from thermochronology

Thermochronometric ages indicate the time of cooling of a mineral below a certain temperature. This cooling can be due to thermal relaxation after magmatic or metamorphic events, instant cooling and crystallization during a volcanic eruption, or due to exhumational cooling. The latter is the aspect most scientist, who want to study the evolution and state of different tectonic settings, are interested in. Some assumptions concerning the thermochronometric system used or the study area always apply and thermal histories can become very complex, for example due to spatial and temporal variations in the thermal field of the crust. Nevertheless, thermochronometry is a very powerful tool to examine orogenic and landscape evolution and to quantify exhumation on geologic time scales [e.g., *Reiners and Brandon*, 2006].

In this context it is important to follow the terminology used to describe uplift, erosion, and exhumation in mountain belts to avoid misunderstandings [*England and Molnar*, 1990]. The term “uplift” can refer to “surface uplift” or “rock uplift”. “Surface uplift” means the displacement of the Earth's surface with respect to the geoid and is very difficult to measure. It can generally not be measured by thermochronology. “Rock uplift” describes the displacement of rocks with respect to the geoid, while “exhumation” refers to movement of rocks towards the Earth's surface. Exhumation occurs either by tectonic processes or by erosion, which both can remove significant volumes of overburden. Under the assumption that exhumation occurs solely by erosion and that a uniform thermal field exists in the study area, exhumation rates are often interpreted in terms of erosion rates.

There are several approaches to determine different aspects of the exhumation and erosion history of orogens. Bedrock samples yield the amount of exhumation at one point and can be used to examine temporal variation in exhumation. This can be done by either measuring multiple thermochronometric systems on the same sample or by exploiting the relationship between thermochronometric age and crustal depth in a vertical profile taken as a quasi-crustal section [*Wagner and Reimer*, 1972]. The latter approach avoids the assumption of a paleo-geothermal gradient, which is often not known and dependent on erosion rates [e.g., *Reiners and Brandon*, 2006].

Sampling over a wider area, possibly in horizontal, equal-elevation profiles, yields the spatial exhumation pattern, which helps studying the long-term kinematics of orogens, paleo-topography and its evolution through time, as well as structural features or climatically induced gradients in erosion [e.g., *House et al.*, 1998; *Braun*, 2002; *Reiners et al.*, 2003; *Reiners and Brandon*, 2006]. The potential concentration of erosion, exhumation, and deformation, like in the St. Elias or Himalayan syntaxes, can only be detected and mapped through a wide spatial coverage of samples. In this case, detrital samples are useful as they generally yield catchment-wide exhumation signals [e.g., *Garver et al.*, 1999; *Bernet and Garver*, 2005]. It is possible to sample modern detritus or in the past deposited sediments. The interpretation of thermochronometer ages from sedimentary samples is complicated by the fact that the ages can be younger or older than, or equal to, the depositional age of the sediment. When sediments are deposited they can be reheated by burial above T_c of the thermochronometric system(s) used, which means they are thermally reset and record in the following the thermal history of the sedimentary basin (Figure 2-6). In contrast, unreset sediments record the thermal history of their source area (Figure 2-6). Partially reset samples were not sufficiently reheated to fully reset the thermochronometric "clock" and contain mixed ages that have no geologic meaning (Figure 2-6). The depositional age of sediments studied for thermochronology must therefore be known. Then, detrital thermochronometer ages can be interpreted in the context of geologic and tectonic events that caused cooling [e.g., *Garver et al.*, 1999; *Bernet and Garver*, 2005].

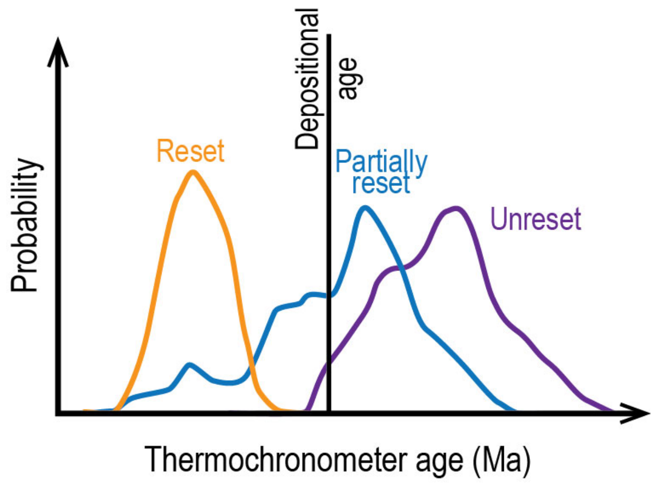

Figure 2-6. Schematic illustration of detrital thermochronometric age distributions of sedimentary samples that are reset (orange), partially reset (blue), and unreset (purple). After *Bernet and Garver* [2005].

2.6 Tectonic and geologic overview of the St. Elias Mountains

The St. Elias Mountains are the result of the ongoing oblique subduction and collision of the 15–30 km thick oceanic plateau of the Yakutat microplate the North American margin in southeast Alaska (Figure 2-7) [e.g., *Plafker et al.*, 1994; *O'Sullivan and Currie*, 1996; *Eberhart-Phillips et al.*, 2006; *Christeson et al.*, 2010; *Worthington et al.*, 2012]. This process can be regarded as continued formation of the western North American continent, where terrane amalgamation and subduction-related processes have occurred since the Mesozoic [e.g., *Armstrong*, 1988].

Three mountain ranges formed related to the north-northwestward translation of the Yakutat microplate. At the transform segment of the Yakutat-North American plate boundary formed the Fairweather Range in a transpressional setting (Figure 1-1). At the more convergent plate boundary formed the Chugach-St. Elias Mountains and above the eastern Yakutat slab edge formed the volcanic Wrangell Mountains (Figure 1-1) [e.g., *Plafker et al.*, 1989; *Richter et al.*, 1990; *Pavlis et al.*, 2004]. The three mountain ranges join together in the St. Elias syntaxis region, which is characterized by a bend in geologic structures, extreme local relief (up to 5000 m), abundant large-magnitude (M≥7) seismicity (Figure 2-8A), and extensive glaciation. Transpressional motion along the plate boundary (dextral Fairweather Fault) transitions across the St. Elias syntaxis into flat-slab subduction and accretion of the Cenozoic sedimentary cover of the western Yakutat microplate [e.g., *Plafker et al.*, 1994; *Bruhn et al.*, 2004, 2012; *Chapman et al.*, 2012]. The accumulation of strain in the syntaxis area, particularly north of the Hubbard Glacier terminus (Figure 1-1), can be observed in the magnitude of vertical velocities in thermo-kinematic models [*Koons et al.*, 2010] and in GPS data [*Elliott et al.*, 2010; *Marechal et al.*, 2015].

The oblique convergence between the Yakutat microplate and the North American Plate is today distributed between northeast striking folds and thrusts west of the current deformational front (Pamplona Zone, Malaspina Fault) (Figures 2-7 and 2-8), and southeast striking thrusts in the Yakutat foothills as observed in seismicity and GPS velocity models (Figure 2-8) [*Doser and Lomas*, 2000; *Elliott et al.*, 2010, 2013; *Doser*, 2014]. The far-field effect of the Yakutat convergence is expressed in large strike-slip faults, such as the Denali Fault (Figure 2-7), that facilitate counterclockwise rotation of the entire southern Alaska block [e.g., *Bruhn et al.*, 2004; *Pavlis et al.*, 2004; *Elliott et al.*, 2013]. The northern Fairweather Fault has been ascribed a significant compressional component [e.g., *Bruhn et al.*, 2004; *McAleer et al.*, 2009], even though geodetic studies do not record significant modern transpression at the northern end of the strike-slip fault itself [e.g., *Fletcher and Freymueller*, 2003; *Elliott et al.*, 2010]. Furthermore, convergent deformation is transferred inland into the Northern Cordillera [*Mazzotti and Hyndman*, 2002; *Elliott et al.*, 2010; *Finzel et al.*, 2011a], and to the Denali Fault [e.g., *Koons et al.*, 2010; *Benowitz et al.*, 2011, 2012]. A direct transfer of strain from the Fairweather Fault to the Denali Fault has been suggested to occur via the active Totschunda Fault and a suggested transfer fault called the Connector Fault (Figure 2-8) [e.g., *St. Amand*, 1957; *Richter and Matson*, 1971; *Lahr and Plafker*, 1980; *Spotila and*

Berger, 2010]. Evidence that the Connector Fault exists and is active come from GPS models and earthquake relocation studies [*Elliott et al.*, 2013; *Doser*, 2014].

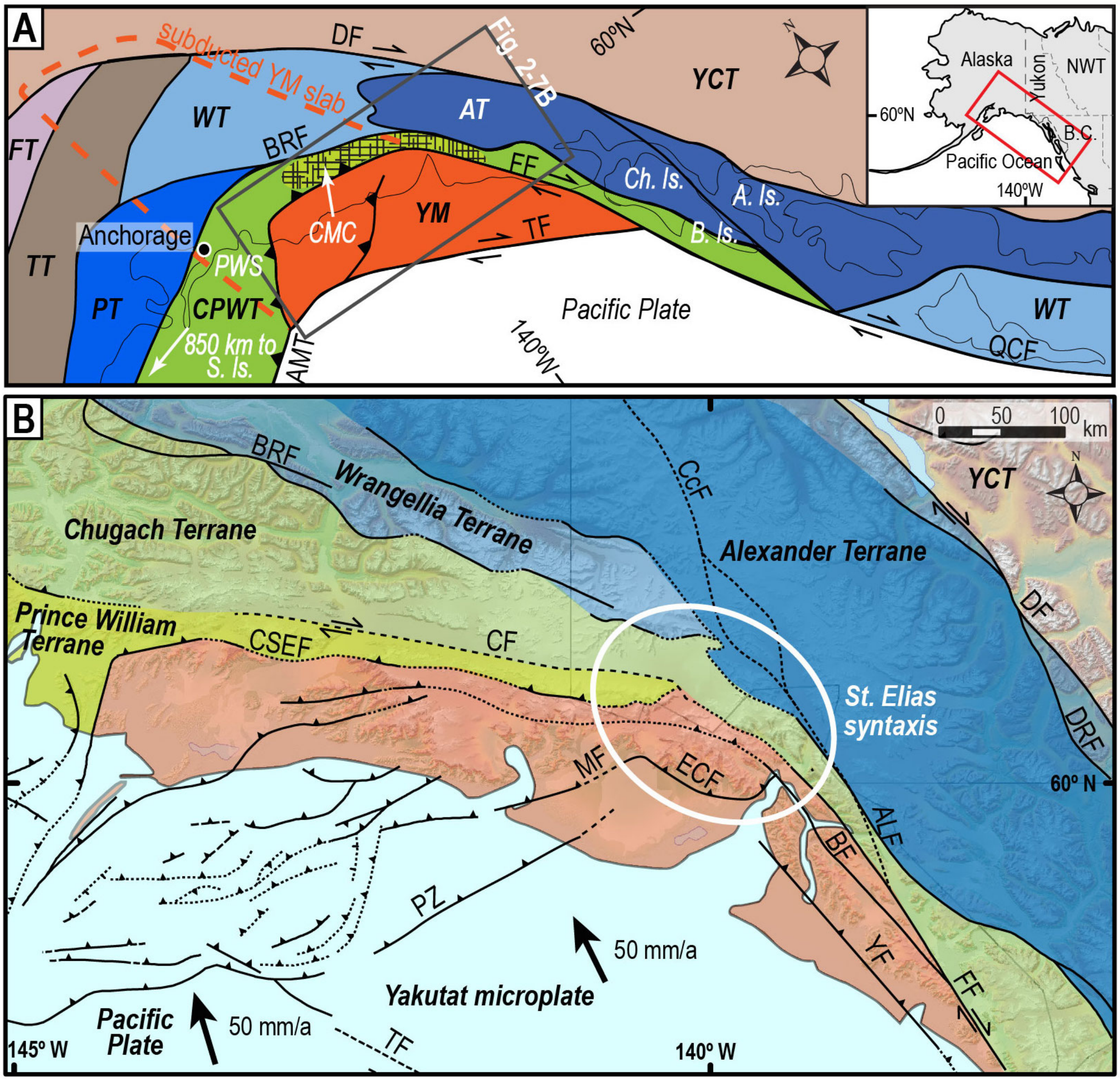

Figure 2-7A,B. Simplified overview of the terranes accreted to the western North American margin (A) and with detail of southeast Alaska (B). The dark grey box in (A) marks the extent of the map in (B). The Yakutat microplate is actively colliding with the North American Plate in southeast Alaska and subducts beneath Alaska. The dashed orange outline marks the subducted portion of the Yakutat microplate (after *Eberhart-Phillips et al.* [2006]). Inset map (A): NWT: Northwest Territories, B.C.: British Columbia. (A, B) CMC: Chugach Metamorphic Complex, DF: Denali Fault, DRF: Duke River Fault, BRF: Border Ranges Fault, FF: Fairweather Fault, TF: Transition Fault, QCF: Queen Charlotte Fault, AMT: Aleutian Megathrust, CcF: Connector Fault, CSEF: Chugach-St. Elias Fault, MF: Malaspina Fault, ECF: Esker Creek Fault, BF: Boundary Fault, YF: Yakutat Fault, PZ: Pamplona Zone, CF: Contact Fault, FT: Farewell Terrane, TT: Togiak Terrane, PT: Peninsular Terrane, WT: Wrangellia Terrane, AT: Alexander Terrane, CPWT: Chugach-Prince William Terrane, YCT: Yukon Composite Terrane, YM: Yakutat microplate, Ch. Is.: Chichagof Island, B. Is.: Baranof Island, A. Is.: Admiralty Island, S. Is.: Sanak Island, PWS: Prince William Sound. Plate motion vectors after *Plattner et al.* [2007] and *Elliott et al.* [2010]; terranes and faults after *Plafker et al.* [1994] and *Colpron and Nelson* [2011].

The study area comprises previously accreted terranes (Wrangellia Composite Terrane, Chugach-Prince William Terrane) and the currently subducting and accreting Yakutat microplate (Figure 2-7). The type of rocks as well as depositional or emplacement ages are important factors in exhumation and provenance studies, especially when considering detrital samples, to reconstruct the time-temperature history of the sediment source. Therefore, a review of the geology of the accreting rocks is given here. In general, knowledge of the geology in the extensively ice-covered St. Elias Mountains is inferred from the geology and tectono-stratigraphic relationships of the ice-free ridges in the mountain range [e.g., *Hudson et al.*, 1977a,b; *Plafker et al.*, 1989, 1994; *Israel*, 2004; *Pavlis et al.*, 2004; *Richter et al.*, 2006; *Chapman et al.*, 2012].

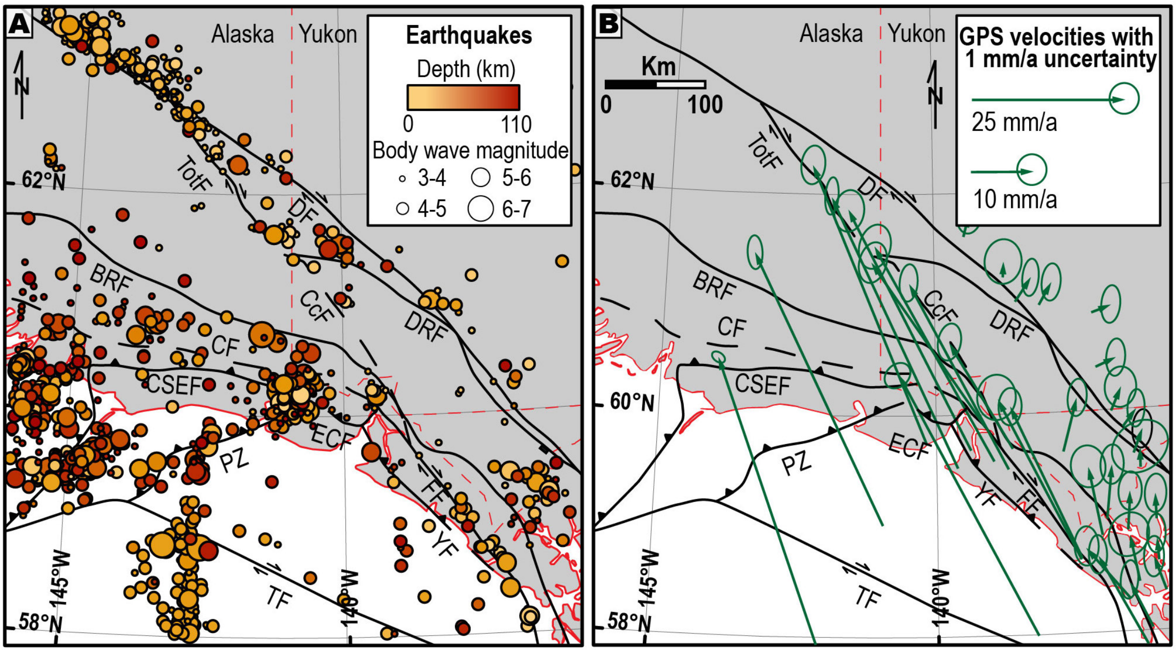

Figure 2-8A,B. Modern deformational field of southeast Alaska and adjacent southwest Yukon and northwest British Columbia. (A) Earthquake data from IRIS SeismicQuery database, body wave magnitude ≥ 3, 1964–2012. (B) GPS velocities from *Elliott et al.* [2010, 2013]. (A and B) DF: Denali Fault, TotF: Totschunda Fault, DRF: Duke River Fault, CcF: Connector Fault, BRF: Border Ranges Fault, CF: Contact Fault, CSEF: Chugach-St. Elias Fault, PZ: Pamplona Zone, ECF: Esker Creek Fault, FF: Fairweather Fault, YF: Yakutat Fault, TF: Transition Fault.

Wrangellia Composite Terrane

The Wrangellia Composite Terrane is bounded by the Denali Fault to the north and the Border Ranges Fault to the south and stretches along the entire western margin of the North American continent (Figure 2-7) [*Jones et al.*, 1977; *Nokleberg et al.*, 1994]. In the study area, the Wrangellia Composite Terrane encompasses the Wrangellia Terrane and the Alexander Terrane, which probably have been linked tectonically since the Late Devonian and became juxtaposed in the Late Pennsylvanian [*Gardner et al.*, 1988; *Beranek et al.*, 2014; *Israel et al.*, 2014]. In the early Mesozoic, the Peninsular

Terrane collided with the Wrangellia-Alexander Terrane to form the Wrangellia Composite Terrane, which accreted to the North American margin during Middle Jurassic–mid-Cretaceous time resulting in regional deformation and metamorphism [e.g., *Gardner et al.*, 1988; *Plafker et al.*, 1989; *Nokleberg et al.*, 1994; *Trop et al.*, 2002].

The Wrangellia Composite Terrane is composed of Cambrian–Late Triassic backarc basin strata, volcanic island arcs and Upper Triassic greenstone and limestone [e.g., *Hillhouse et al.*, 1977; *Nokleberg et al.*, 1994]. Overlying strata include Upper Jurassic–Lower Cretaceous flysch (e.g., Gravina Nutzotin belt) and Paleogene alluvial strata in the Denali Fault area, as well as Oligocene–Recent Wrangell lava [e.g., *Berg et al.*, 1972; *Jones et al*., 1977; *Richter et al.*, 1990; *Plafker et al.*, 1994]. The Wrangellia Composite Terrane is associated with various phases of arc magmatism and abundantly intruded by Upper Jurassic–Cretaceous plutons and is pervasively metamorphosed [e.g., *Dodds and Campbell*, 1988; *Nokleberg et al.*, 1994]. Late Cretaceous–Cenozoic strike-slip movement along the Denali Fault transported the Wrangellia Composite Terrane northward and resulted in its disintegration [e.g., *Plafker et al*., 1994].

Chugach and Prince William terranes

The Chugach and Prince William terranes represent a Cretaceous–Eocene accretionary complex of compositionally uniform deep-water turbidites derived from a Late Cretaceous–Paleocene volcanic arc with Jurassic meta-plutonic basement, most likely the Coast Plutonic Complex [*Dumoulin*, 1988; *Farmer et al.*, 1993; *Garver and Davidson*, 2015]. In the study area, the Chugach Terrane is composed of the Maastrichtian Valdez Group and the Prince William Terrane comprises the Paleocene–lower Eocene Orca Group (Figure 2-7B) [e.g., *Plafker et al.*, 1994]. In the St. Elias Mountains, the Chugach and Prince William terranes are mainly characterized by the ~55–50 Ma, greenschist–amphibolite facies Chugach Metamorphic Complex (Figure 2-7A), which formed during a spreading-ridge subduction event that is associated with the near-trench Sanak-Baranof plutonic belt [e.g., *Sisson and Hollister*, 1988; *Gasser et al.*, 2011]. The Sanak-Baranof granitoids intruded the accretionary sediments diachronously from ~62–47 Ma, younging eastward from Sanak Island to Baranof Island (Figure 2-7A) [*Hudson et al.*, 1977a, 1979].

Yakutat microplate

The Yakutat microplate is a ~15–30 km thick, northwestward tapering oceanic plateau that is overlain in the east by Campanian–lower Paleocene Yakutat Group flysch and mélange sequences, which represent a remnant accretionary complex metamorphosed to zeolite-prehnite-pumpellyite facies [*Plafker*, 1987; *Hudson et al.*, 1977b; *Dusel-Bacon et al.*, 1993]. In the west, the Yakutat microplate is overlain by ≤10 km thick, eastward thinning Cenozoic strata of the Poul Creek, Kulthieth, and Yakataga formations [*Ferris et al.*, 2003; *Eberhart-Phillips et al.*, 2006; *Gulick et al.*, 2007; *Christeson et al.*, 2010, *Worthington et al.*, 2010, 2012]. These strata were sourced from the Coast Plutonic Complex (lower Paleocene–Miocene Poul Creek and Kulthieth formations) and the Chugach and Prince William terranes (latest Miocene–Holocene Yakataga Formation) [*Perry et al.*, 2009].

2.7 Previous thermochronometric ages of the southern St. Elias Mountains

A large thermo- and geochronologic dataset has been produced for southeast Alaska. The focus of the studies lay on the convergent part of the Chugach-St. Elias Mountains [e.g., *Spotila et al.*, 2004; *Berger et al.*, 2008; *Berger and Spotila*, 2008; *Enkelmann et al.*, 2008, 2009, 2010; *Meigs et al.*, 2008; *Perry et al.*, 2009] and, to a smaller extent, on the Fairweather Range [*O'Sullivan et al.*, 1997; *McAleer et al.*, 2009] (Figure 2-9). Little is known about the syntaxis area itself [*O'Sullivan and Currie*, 1996; *Enkelmann et al.,* 2009, 2010*; Spotila and Berger*, 2010].

The dataset is dominated by bedrock AHe analyses, which has a closure temperature of ~65 °C [*Farley*, 2000] and therefore reflects rock exhumation from upper crustal (~2–3 km) depths, assuming a normal geothermal gradient. Those studies revealed rapid, shallow exhumation in southeast Alaska, particularly in the fold-and-thrust belt west of the Pamplona Zone (Figure 2-7B) [e.g., *Berger and Spotila*, 2008; *Meigs et al.*, 2008; *Enkelmann et al.*, 2010]. Deeper and longer-lived exhumation is suggested to occur along a corridor enveloping the Fairweather Fault [*McAleer et al.*, 2009]. *McAleer et al.* [2009] found rapid, rather uniform exhumation along the Fair-weather Fault that accelerated 5–3 Ma closest to the fault (Figure 2-9). The glacial cover of the St. Elias Mountains is a challenge to sampling for exhumation studies and resulted in sampling of mostly bedrock from higher, ice-free elevations. To overcome this shortcoming and obtain samples from beneath the ice, material of glacial outwash and rivers was collected along the strike of the Chugach-St. Elias Range for ZFT analyses [*Enkelmann et al.,* 2008, 2009, 2010]. The relatively high closure temperature of the ZFT system (250±40 °C; e.g., *Brandon et al.* [1998]) and the resistance of zircons to weathering during erosion and sediment transport make detrital ZFT analysis particularly suitable to quantify long-term exhumation [e.g. *Rahl et al.*, 2007]. This strategy revealed rapid, deep-seated exhumation at the St. Elias syntaxis underneath the Seward Glacier (Malaspina Glacier samples) and north of it (Chitina River sample) (arrows in Figure 2-9) [*Enkelmann et al.,* 2009, 2010]. Based on these observations, *Enkelmann et al.* [2010] speculated that rapid exhumation also occurs within the Hubbard Glacier catchment, what motivates this study to extend the detrital sampling to the regions farther north (northern St. Elias Mountains) and east (northern Fairweather Range).

The generally high exhumation rates in the convergent setting are assisted by high glacial erosion rates that are estimated to be among the highest in the world with up to 10 mm/yr on time scales of 10^4 yr based on sedimentation rates offshore [*Hallet et al.*, 1996; *Jaeger et al.*, 1998; *Sheaf et al.*, 2003] and ≥2 mm/yr over 10^6 yr time scales based on thermochronology [e.g., *Enkelmann et al.*, 2009; *McAleer et al.*, 2009; *Spotila and Berger*, 2010]. Glaciation of the Chugach-St. Elias Mountains began ~5.6 Ma and intensified at the Plio-Pleistocene transition [*Lagoe et al.*, 1993].

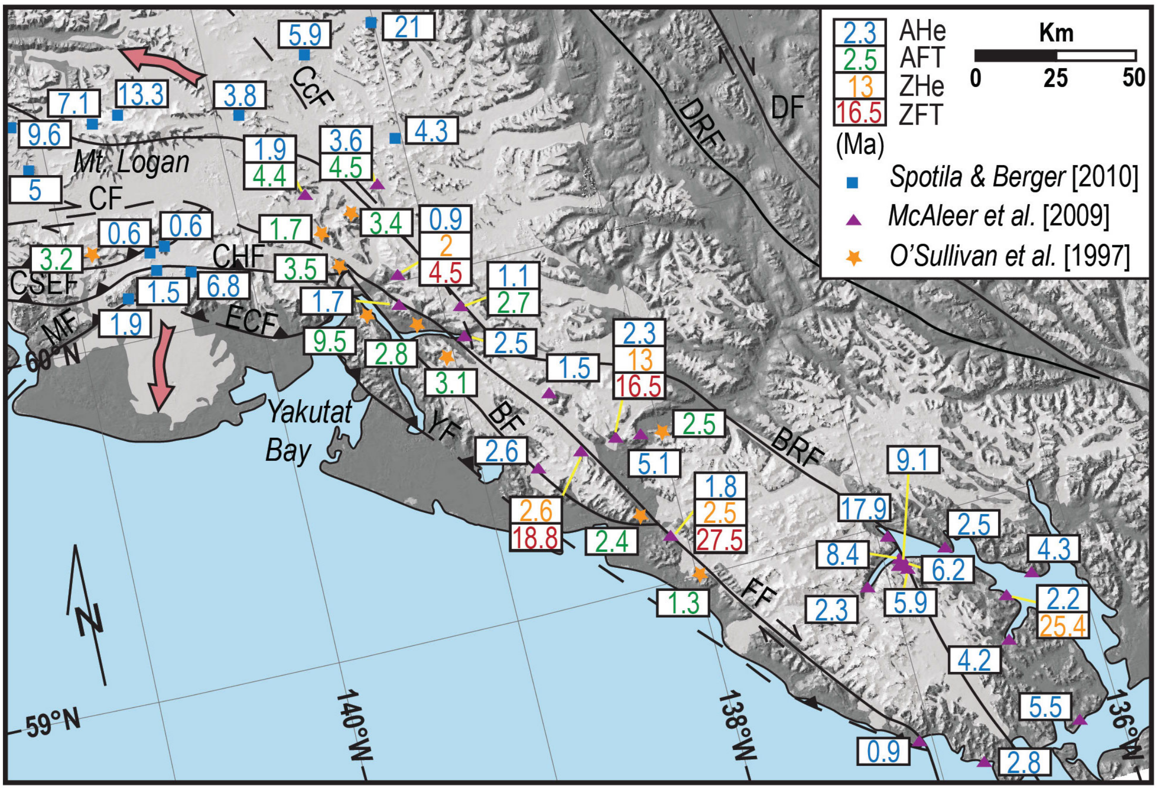

Figure 2-9. Bedrock thermochronometric ages from the Fairweather Fault and St. Elias syntaxis areas. Detrital ZFT samples from the Malaspina Glacier and Chitina River (reddish arrows indicate their transport directions) yield major young age populations of 3–2 Ma [*Enkelmann et al.*, 2009, 2010]. DF: Denali Fault, DRF: Duke River Fault, CcF: Connector Fault, BRF: Border Ranges Fault, CF: Contact Fault, CSEF: Chugach-St. Elias Fault, CHF: Chaix Hills Fault, FF: Fairweather Fault, BF: Boundary Fault, MF: Malaspina Fault, ECF: Esker Creek Fault, YF: Yakutat Fault.

3 Spatial extent of rapid and deep-seated exhumation at the St. Elias syntaxis

3.1 Significance

The distribution of deformation at convergent plate boundaries and zones of rapid exhumation in particular have long attracted the interest of Earth scientists, who aim to understand the interactions between climate, surface processes, and tectonics [e.g., *Koons*, 1987, 1990; *Beaumont et al.*, 1992; *Willett et al.*, 1993, 2003; *Zeitler et al.*, 2001; *Whipple*, 2009]. Deformation at orogenic syntaxes is less well studied and understood than orogenic wedges that are commonly described with critical taper models [*Chapple*, 1978; *Dahlen et al.*, 1984] and for which analog and numerical models of tectonic and erosional processes exist [e.g., *Willett et al.*, 1993, 2003; *Storti and McClay*, 1995; *Whipple*, 2009]. Orogenic syntaxes, however, play an important role in the deformation of convergent plate boundaries because those areas are complex structural transition zones and characterized by concentration of stresses resulting in high strain rates, surface uplift, and a potential for a coupling with surface processes and climate. Based on petrographic and thermochronometric observation, as well as numerical models, the Himalayan syntaxes are one of the key areas where such a strong coupling is suspected [e.g., *Zeitler et al.*, 2001; *Koons et al.*, 2013]. This mechanism results in a localized weakening of the crust due to efficient fluvial incision that removes the strong frictional upper crust and leads to surface uplift and the formation of extreme local relief. Together, these mechanisms are hypothesized to promote erosion and rapid exhumation of rocks and thereby promoting additional crustal deformation and localized weakening [*Zeitler et al.*, 2001]. Detrital ZFT analysis of sediments from the Malaspina-Seward glacial catchment revealed that very rapid and deep-seated rock exhumation occurs in the St. Elias syntaxis region of the Chugach-St. Elias Mountains in southeast Alaska (Figure 2-9) [*Enkelmann et al.*, 2009]. Because of this, the overall syntaxis tectonic setting, the coincidence of rapid exhumation and beginning glaciation of the orogen (~5.6 Ma; *Lagoe et al.* [1993]), as well as results of geodynamic numerical models, the St. Elias syntaxis has been proposed to represent an early stage of the same processes observable at the Himalayan syntaxes [*Enkelmann et al.*, 2009, 2010; *Koons et al.*, 2010, 2013]. However, documentation of the complete extent of rapid exhumation is needed prior to interpretation of the underlying mechanisms and timing of events in the St. Elias syntaxis region.

This study improves the observational record of syntaxes deformation by investigating the spatial extent of rapid, deep-seated exhumation at the St. Elias syntaxis (Figure 2-7B). In order to extract the long-term exhumation history, detrital ZFT ages of 26 glacio-fluvial sand-sized samples were analyzed. Samples were collected from catchments along the northernmost part of the plate-bounding Fairweather transform fault, just where motion begins to transition into flat-slab subduction of the Yakutat microplate (Figure 2-7B). In this study, it can be demonstrated that the area of rapid and deep-seated exhumation extends farther north and southeast from the St. Elias syntaxis than previously suggested [*Enkelmann et al.*, 2009, 2010] and that significant deformation and exhumation occur in both colliding plates in the wider syntaxis region, but that deep exhumation is focused on the North American Plate. The exhumation history obtained from detrital ZFT thermochronometric ages differs from that obtained from bedrock analysis [e.g., *O'Sullivan et al.*, 1997; *McAleer et al.*, 2009] and therefore proves to be invaluable for ice-covered areas and an essential complement to bedrock data.

3.2 Sampling

In total, 26 glacio-fluvial catchments from the northwestern part of the Fairweather Range and the St. Elias syntaxis region were sampled that have individual areas of ~3–5673 km^2 and span elevations of 0–5792 m a.s.l. (Table 3-1 and Figure 3-1). The total area covered amounts to ~11,000 km^2. Sampling spots were chosen to maximize the area covered and to obtain cooling age distributions from catchments with varying distances to the Fairweather Fault. Additionally, material was sampled from the Hubbard Glacier, which is the main glacial system that drains the high ice field of the St. Elias syntaxis region to the east (Figure 3-1). The 26 catchments correspond to 25 samples of modern glacial river sands (2–3 kg, medium- to coarse-sized) and one artificial sand sample (HUB1) generated by crushing and mixing hundreds of pebbles collected at the beach at the eastern shore of southern Yakutat Bay (Figure 3-1). This location has been considered the 970–1290 A.D. termination of the Hubbard Glacier [*Richter et al.*, 2006], but more recent seismic studies suggest that most areas of Yakutat Bay were dominated by morainal banks and advances of the Malaspina Glacier rather than the Hubbard Glacier [*Elmore et al.*, 2013]. However, the Hubbard Glacier probably advanced in a relatively narrow trough in eastern Yakutat Bay [*Elmore et al.*, 2013] and might still be the glacial system that deposited the pebbles collected at HUB1 site. This implies that with sample HUB1 most probably the majority of the study area and all the three terranes were sampled. For all other samples, catchment areas and elevation ranges were calculated using a 30 m resolution digital elevation model (ASTER GDEM, Advanced Spaceborne Thermal Emission and Reflection Radiometer Global Digital Elevation Model). In the following, samples are named YAKD+sample number, while corresponding catchments are marked for distinction as Y+sample number (e.g., Y1 describes the catchment belonging to sample YAKD1).

Table 3-1. Detrital samples and corresponding catchments in the southern St. Elias Mountains

Sample	Latitude (°N)/ Longitude (°W)	Name	Catchment area [km^2]	Elevation range [m]	Terrane
YAKD1	59.7767/ 139.5752	Aquadulce Creek	45	1–1385	YM
YAKD2	59.9051/ 139.5897	no name	18	6–1300	YM
YAKD3	59.9220/ 139.5176	Henry Glacier and others	40	19–1323	YM
YAKD29	59.9294/ 139.3952	Alexander Glacier	7	7–1159	YM
YAKD31	59.8617/ 139.2253	no name	6	3–547	YM
YAKD32	59.8116/ 139.3578	Hendrickson Glacier	26	10–1382	YM
YAKD33	59.7660/ 139.1653	Hidden Glacier	124	38–1713	YM
YAKD34	59.7006/ 139.2797	no name	19	2–1661	YM
YAKD35	59.5997/ 139.2275	Fourth Glacier	83	6–1612	YM
YAKD37	60.0627/ 139.5306	no name	2	70–1619	YM
YAKD39	60.0547/ 139.5491	Miller Glacier	23	11–1969	YM
YAKD40	60.0334/ 139.5568	Haenke Glacier	56	11–2401	YM
YAKD41	59.9967/ 139.6121	Turner Glacier	214	12–4191	YM
YAKD42	59.9396/ 139.6690	Black Glacier	6	25–1755	YM
YAKD43	59.9260/ 139.7279	Galiano Glacier	14	21–1980	YM
YAKD44	59.9244/ 139.7931	Atrevida Glacier	34	79–2000	YM
YAKD45	59.8799/ 139.9355	Lucia and Hayden Glaciers	73	37–3614	YM
YAKD46	59.4144/ 139.0081	Harlequin Lake	817	26–1768	YM, CT
YAKD55	59.8001/ 138.9639	West Nunatak Glac-ier	172	0–1676	YM, CT
YAKD30	59.8700/ 139.1104	Butler Glacier and others	81	49–2532	YM, CT
YAKD4	59.9958/ 139.3500	Variegated Glacier	59	106–2560	WCT, CT
YAKD5	59.9886/ 139.3935	Hubbard Glacier	3646	18–5792	WCT, CT
YAKD38	60.0404/ 139.5425	Valerie and Hubbard Glaciers	4050	16–4751	WCT, CT
YAKD57	59.8144/ 138.9237	Art Lewis and East Nunatak Glaciers	457	0–2771	WCT, CT
YAKD60	59.8537/ 139.0886	no name	40	0–1700	WCT, CT
HUB1	59.5417/ 139.8634	Previous Hubbard Glacier terminus (?)	>5000 (?)	0–5792 (?)	Probably WCT, CT, YM

Note: YM: Yakutat microplate, WCT: Wrangellia Composite Terrane, CT: Chugach Terrane.

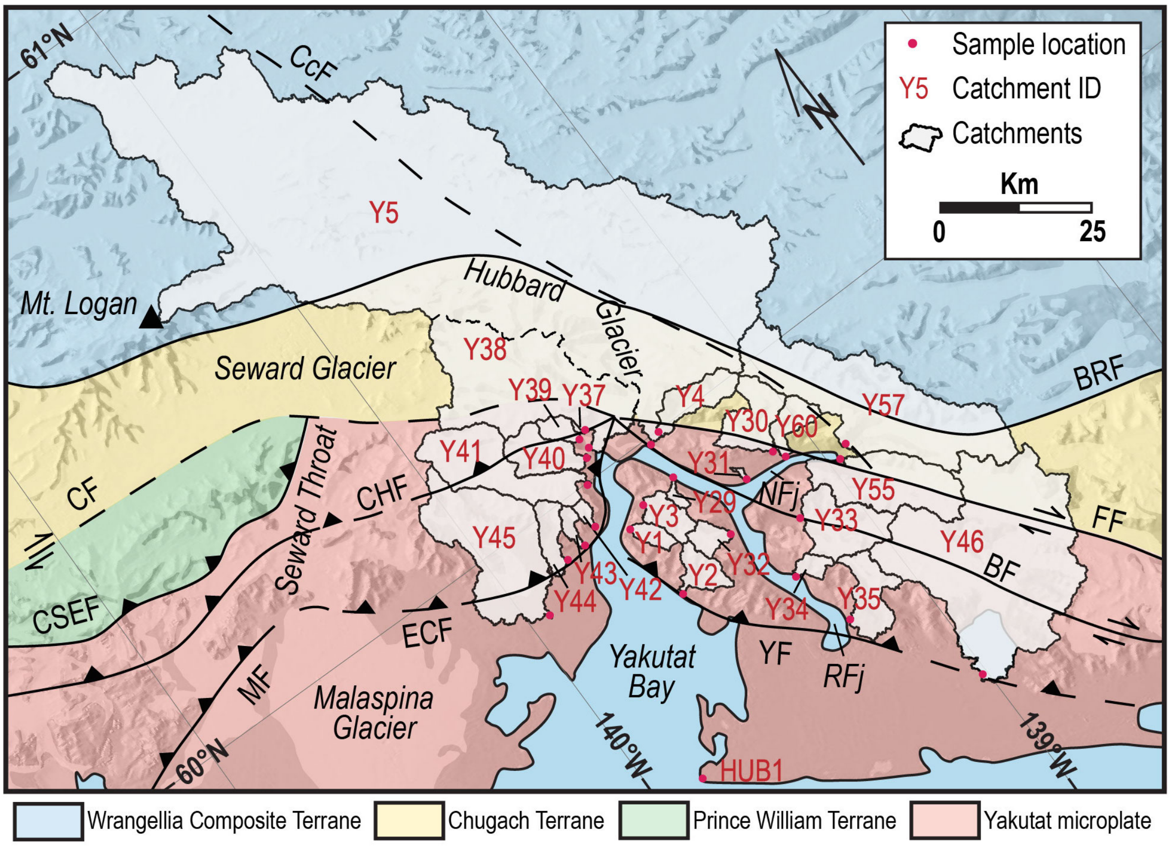

Figure 3-1. Detrital sample locations and corresponding catchments of the Yakutat foothills and Hubbard Glacier. CcF: Connector Fault, BRF: Border Ranges Fault, CF: Contact Fault, CSEF: Chugach-St. Elias Fault, CHF: Chaix Hills Fault, FF: Fairweather Fault, BF: Boundary Fault, YF: Yakutat Fault, ECF: Esker Creek Fault, MF: Malaspina Fault, NFj: Nunatak Fjord, RFj: Russell Fjord.

3.3 Results

In total, 2718 single grains yielded ZFT ages ranging from 293 Ma to 0.2 Ma (Table 3-2). All single-grain results are presented in Appendix B (Dataset B-1). Each of the 26 samples encompasses 2–5 age populations with peaks between 267 ± 64 Ma and 1.2 ± 0.7 Ma (here and in the following the reported errors are 1 σ) (Table 3-2 and Figure 3-2). The probability density plots in Figure 3-2 are arranged according to the location of the catchments on the different terranes. This classification illustrates the differences in age distributions of the Yakutat microplate and terranes of the North American Plate (Wrangellia Composite and Chugach terranes).

3.3.1 Yakutat microplate

The major age populations of the Yakutat microplate are all older than 30 Ma, the exception being YAKD31 that is located close to the Fairweather Fault and shows a major age population with 87 % of all grains with a peak at 4.8 ± 0.4 Ma (Table 3-2 and Figure 3-2). Few other samples of the Yakutat microplate exhibit young (≤5 Ma) age populations in small proportions. These samples are YAKD34 and YAKD35, which are located next to each other on eastern Russell Fjord (Figure 3-1) (both with a young age population of 4.6 ± 0.6 Ma, 7 % and 8 %, respectively; Table 3-2 and Figure 3-2), YAKD1 and YAKD2, located next to each other on the eastern Yakutat Bay shoreline (Figure 3-1) (youngest age populations of 2.4 ± 0.3 Ma (6 %) and 2.1 ± 0.6 Ma (2 %), respectively; Table 3-2 and Figure 3-2), as well as YAKD40 on western Disenchantment Bay (4.3±0.5 Ma, 10 %; Table 3-2 and Figure 3-1).

3.3.2 Wrangellia Composite and Chugach terranes

The age populations of the North American Plate are dominated by young (≤5 Ma) age peaks; in particular, ~3 Ma is a recurring age peak, e.g., the two samples collected from the Hubbard Glacier YAKD5: 3.1 ± 0.3 Ma (46 %) and YAKD38: 3.1 ± 0.2 Ma (59 %); the Variegated Glacier located just east of Hubbard Glacier YAKD4: 3.6 ± 0.3 Ma (68 %) or YAKD60: 3 ± 0.3 Ma (49 %) located north of Nunatak Fjord (Table 3-2 and Figure 3-1). Single-grain ages range from 184.2 Ma to 0.2 Ma and age peaks from 80.7 ± 6.4 Ma (27 %) to 1.2 ± 0.7 Ma (6 %) (Table 3-2). While on the Yakutat microplate a clear trend in the age distribution cannot be observed, a trend of increasing ages along strike of the Fairweather Fault toward the eastern end of the study area (YAKD55, YAKD57, and YAKD46) becomes apparent for the catchments north of the Fairweather Fault (Table 3-2 and Figure 3-2).

3.3.3 Chugach Terrane and Yakutat microplate

Catchments that largely overlap the Fairweather fault zone comprise grains originating from both plates (Y55 and Y46; Figure 3-1) and yield a large age population of around 30 Ma (YAKD55: 29 ± 2 Ma, 74 %; YAKD46: 33.1 ± 2.3 Ma, 60 %). Also, Y30, which has its larger area on the Chugach Terrane, shows a significant (11 %) age population at 29.1 ± 2.6 Ma (Table 3-2 and Figure 3-2).

3.3.4 Yakutat microplate and North American Plate composite samples

To obtain a robust picture of the cooling signals of the two tectonic regions, the ZFT ages of catchments of the North American Plate (Wrangellia Composite and Chugach terranes: Y38, Y5, Y4, Y30, Y60, and Y57; cf. Figure 3-1) and catchments of the Yakutat microplate (Y45, Y44, Y43, Y42, Y1, Y2, Y3, Y32, and Y35; cf. Figure 3-1) were combined, respectively (Figure 3-3). Catchments comprising both plates were not included in the composite samples. In general, the North American Plate cooling signal is characterized by a very large (73 %) young (≤5 Ma) cooling age fraction that comprises two major age populations with peaks at 5.1 ± 0.4 Ma (36 %) and 2.7 ± 0.2 Ma (37 %). Ages from Yakutat microplate catchments are mostly older, and 73 % of all ages constitute two age populations that peak at 67 ± 4.8 Ma (39 %) and 45 ± 4.1 Ma (34 %) (Figure 3-3). The oldest age populations of the composite North American Plate and the Yakutat microplate peak at 75 ± 5.3 Ma (8 %) and 115 ± 8.5 Ma (10 %), respectively. The two composite samples have two peaks in common, one around 30 Ma and another at 15–12 Ma (Figure 3-3). The HUB1 sample differs from the others insofar as it is an artificial sand sample and its catchment presumably includes all the three terranes. It contains by far the largest (52 %) comparatively old (113.9 ± 7.1 Ma) age peak (Table 3-2). The third age population of 33.9 ± 2.2 Ma (25 %) compares well with the ~30 Ma populations that both plates have in common (Figure 3-3). This age peak appears strikingly similar to the 115 ± 8.5 Ma (10 %) of the Yakutat microplate composite plot. The 6 ± 0.4 Ma (23 %) HUB1 age population is similar to age populations of catchments on the North American Plate (Table 3-2).

3.4 Discussion

3.4.1 Comparison with bedrock thermochronometric ages

With the current dataset there is no way of identifying from which elevations the dated grains originated, but it is generally expected that rocks yielding the youngest cooling ages are from low elevations and that cooling ages increase with increasing elevation. It is assumed that the largest portion is eroded at valley bottoms by subglacial processes, even though mountain flanks and tops certainly contribute material through mass wasting processes [e.g., *Arsenault and Meigs*, 2005].

The assumption of intense subglacial erosion can be supported when comparing detrital to bedrock thermochronometric ages of the same drainage basin. Only few bedrock ZFT ages exist, usually from higher elevations above the ice, but they do not detect the very young ages detrital studies reveal (Figure 2-9) [*Enkelmann et al.*, 2009, 2010; this study]. Neither do lower-temperature thermochronometers, like AFT or AHe, yield ages at high elevations young enough to correspond to the very young detrital ZFT age signals from low elevations (Figure 2-9) [*O'Sullivan and Currie*, 1996; *O'Sullivan et al.*, 1997; *Berger et al.*, 2008; *McAleer et al.*, 2009; *Spotila and Berger*, 2010]. Even though, for example, a bedrock sample from the Y4 catchment from an elevation of 1600 m a.s.l. yielded a ZFT age of 4.5 ± 0.3 Ma, a ZHe age of 1.96 ± 0.1 Ma, and an AHe age of 0.89 ± 0.1 Ma [*McAleer et al.*, 2009] (Figure 2-9), the majority (74 %) of YAKD4 grains are 3.6 ± 0.3 Ma and younger (Table 3-2).

3.4.2 Interpretation of detrital thermochronometric ages

ZFT age populations derived from catchments comprising sedimentary rocks can be younger or older than, or equal to the sediment deposition age (Figure 2-6). ZFT age populations that are younger than deposition characterize thermally reset sediments, whereby an unreset sediment sample is characterized by cooling ages predating deposition [e.g., *Brandon et al.*, 1998]. A partially reset or mixed detrital sample contains cooling ages both older and younger than deposition. Therefore, it is crucial to know the deposition age of the sediments and in the best case more about the geo logic history, like metamorphic phases. The Wrangellia Composite Terrane contains various

Table 3-2. Detrital ZFT results from the St. Elias syntaxis and Yakutat foothills

Sample	N	Age range [Ma]	Peak 1 [Ma]	Peak 2 [Ma]	Peak 3 [Ma]	Peak 4 [Ma]	Peak 5 [Ma]
Yakutat microplate							
YAKD1	104	1.1–181.5	2.4 ± 0.3 (6%)	31.5 ± 2.5 (29%)	49.4 ± 3.8 (39%)	91.4 ± 7.7 (26%)	
YAKD2	104	2.1–165.3	2.1 ± 0.6 (2%)	25.7 ± 2.8 (5%)	45.9 ± 3.6 (35%)	65.2 ± 6.3 (32%)	91.2 ± 8.3 (26%)
YAKD3	104	23.4–167.0	26.3 ± 9.7 (1%)	51.1 ± 6.3 (27%)	67.6 ± 5.9 (65%)	119.8 ± 14.4 (7%)	
YAKD29	102	22.9–126.7	33.6 ± 8.5 (7%)	43.9 ± 4 (46%)	68.8 ± 5.1 (47%)		
YAKD31	105	1.8–137.1	4.8 ± 0.4 (87%)	42.4 ± 12.5 (13%)			
YAKD32	104	17.5–207.7	27.7 ± 2.7 (12%)	55.3 ± 4 (59%)	103.4 ± 9.1 (29%)		
YAKD33	104	11.4–109.6	14.9 ± 2.6 (4%)	24.1 ± 2.2 (32%)	33.3 ± 2.6 (48%)	62.6 ± 5 (16%)	
YAKD34	105	2.6–178.4	4.6 ± 0.6 (7%)	23.5 ± 2.9 (4%)	47.9 ± 3.6 (46%)	85.6 ± 6.5 (43%)	
YAKD35	106	1.7–254.3	4.6 ± 0.6 (8%)	33.6 ± 2.7 (33%)	63.1 ± 4.7 (51%)	139.4 ± 17.1 (8%)	
YAKD37	105	21.7–293.3	38 ± 3.6 (21%)	84 ± 6.6 (64%)	196.7 ± 26.6 (15%)		
YAKD39	104	13.6–276.8	22.9 ± 2.3 (13%)	47.5 ± 3.8 (35%)	91.6 ± 6.8 (50%)	266.8 ± 63.5 (2%)	
YAKD40	105	2.1–256.8	4.3 ± 0.5 (10%)	22.6 ± 2.7 (12%)	47.6 ± 3.8 (39%)	84 ± 6.7 (39%)	
YAKD41	103	32.8–158.5	48.4 ± 3.9 (30%)	74.9 ± 5.4 (65%)	139.6 ± 20.7 (5%)		
YAKD42	105	6–100.2	8.2 ± 1.1 (5%)	19.9 ± 1.6 (39%)	41.4 ± 3.6 (44%)	71.2 ± 10 (12%)	
YAKD43	105	14.0–117.0	21.6 ± 2.4 (9%)	35.9 ± 2.9 (30%)	58.7 ± 4.2 (61%)		
YAKD44	105	16.6–146.2	26.8 ± 6.3 (7%)	41.7 ± 4.8 (45%)	60.1 ± 6.1 (36%)	101.2 ± 15 (12%)	
YAKD45	104	18.9–168.4	25 ± 9 (3%)	37.5 ± 3.7 (23%)	65 ± 5 (56%)	112.3 ± 11.5 (18%)	
Yakutat microplate and Chugach Terrane							
YAKD30	106	0.7–38.3	3.3 ± 0.2 (89%)	29.1 ± 2.6 (11%)			
YAKD46	105	2.4–140.7	5.6 ± 2 (4%)	15.6 ± 1.6 (13%)	33.1 ± 2.3 (60%)	88.9 ± 8.0 (23%)	
YAKD55	105	11.5–73.7	17.4 ± 1.8 (7%)	29 ± 2 (74%)	44.5 ± 4.4 (19%)	44.9 ± 4 (7%)	
Chugach and Wrangellia Composite Terrane							
YAKD4	103	0.6–18.7	1.2 ± 0.7 (6%)	3.6 ± 0.3 (68%)	7.5 ± 1 (18%)		
YAKD5	105	0.2–64.8	3.1 ± 0.3 (46%)	6.1 ± 0.5 (39%)	12.6 ± 1.4 (8%)		
YAKD38	105	1.1–184.2	3.1 ± 0.2 (59%)	27.4 ± 2.4 (14%)	80.7 ± 6.4 (27%)		
YAKD57	105	2.7–155.2	6.7 ± 0.6 (37%)	19.2 ± 1.6 (36%)	57.9 ± 4.6 (27%)		
YAKD60	105	1.5–11.6	3 ± 0.3 (49%)	5.1 ± 0.4 (47%)	9 ± 1.6 (4%)		
Probably all three terranes							
HUB1	105	2.5–275.2	6 ± 0.4 (23%)	33.9 ± 2.2 (25%)	113.9 ±7.1(52%)		

Note: Binomially fitted peak ages of age populations using BINOMFIT [*Brandon*, 1992, 1996]. N: number of dated grains per sample, 1 σ errors for the peak age. The size of the age population with respect to the total number of grains analyzed per sample is given in percentage. Dosimeter glass: IRMM541; ζ factor: 117.7±7.1 cm^2a.

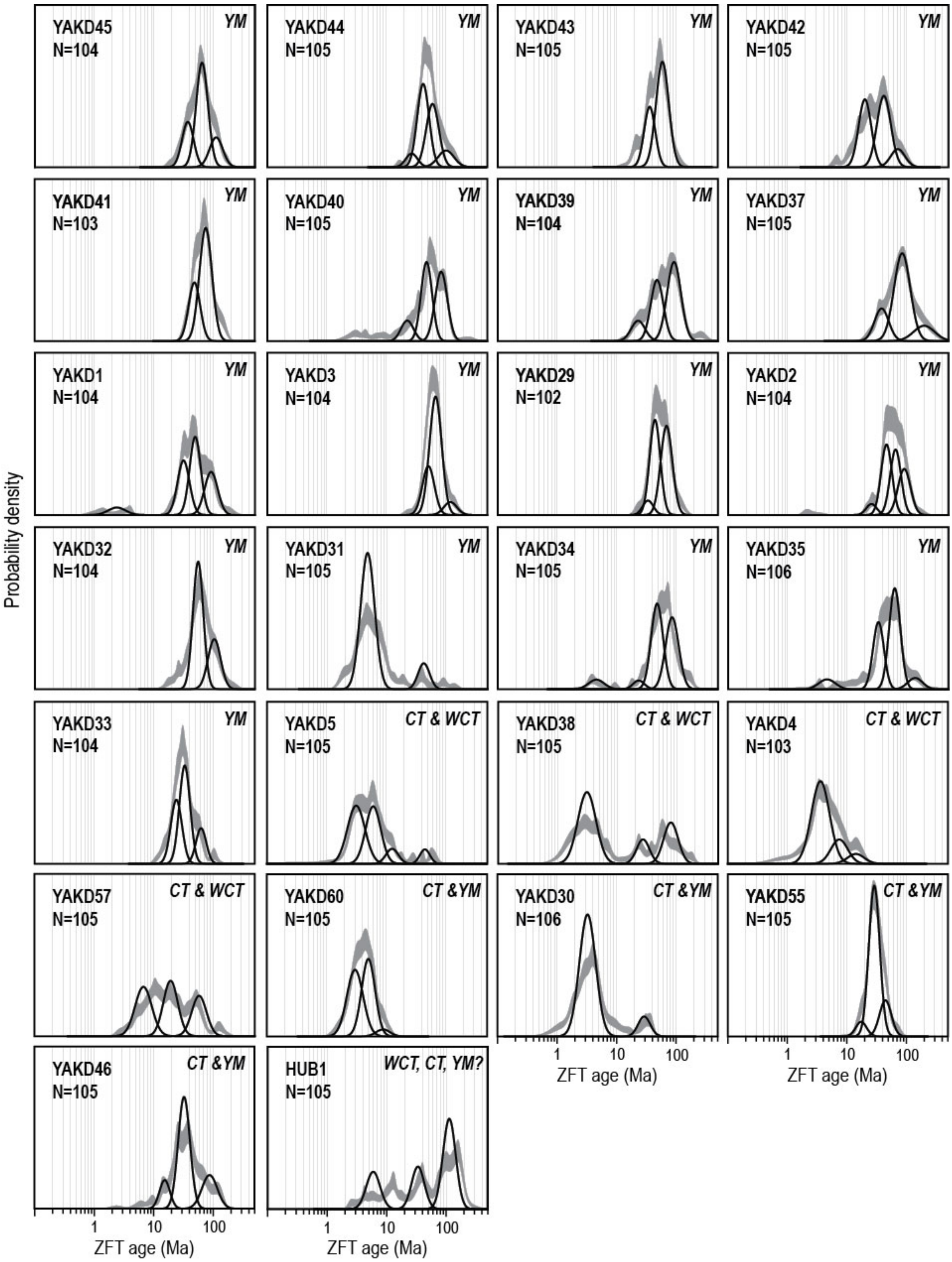

Figure 3-2. Results of binomial peak fitting using BINOMFIT [*Brandon*, 1992, 1996]. Age distributions are decomposed into component age populations. Black curves: fitted peaks; grey curves: measured age distributions (with 1σ uncertainty). Plots are sorted by sample locations on Yakutat microplate (YM), Chugach and Wrangellia Composite terranes (CT & WCT), Chugach Terrane and Yakutat microplate (CT &YM), and possibly all three terranes for HUB1 (WCT, CT, YM?). Single-grain ages can be found in Appendix B (Dataset B-1).

rocks, which have a wide age range generally older than Early Cretaceous, predating all the ZFT age populations found in the study area (≤115 ± 8.5 Ma, Figure 3-3). Chugach Terrane sediments (in the study area of the Valdez Group) were continuously accreted to the margin from the Late Cretaceous to the Eocene [e.g., *Plafker*, 1987; *Dumoulin*, 1988] until spreading-ridge subduction occurred ~55–50 Ma, when the rocks became intruded and metamorphosed to greenschist and amphibolite facies to build the Chugach Metamorphic Complex and reset most of the thermochronometric ages [e.g., *Sisson and Pavlis*, 1993; *Gasser et al.*, 2011]. The Yakutat Group sequences have a similar origin as accretionary sediments of Campanian–earliest Paleocene age [*Plafker*, 1987; *Landis*, 2007] and experienced various predepositional, syndepositional, and postdepositional heating and cooling histories.

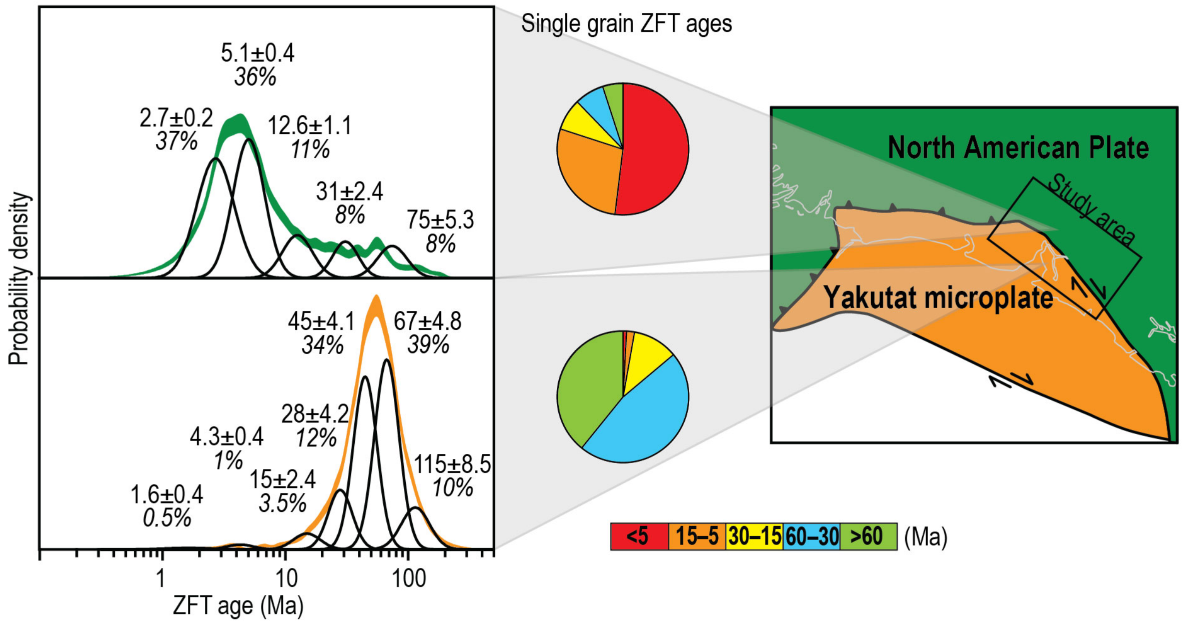

Figure 3-3. Composite ZFT age probability density plots for the North American Plate (YAKD38, YAKD5, YAKD4, YAKD30, YAKD60, and YAKD57) and Yakutat microplate (YAKD45, YAKD44, YAKD43, YAKD42, YAKD1, YAKD2, YAKD3, YAKD32, and YAKD35). Peak ages (in Ma) as well as the percentage of the grains composing that age population are given. Additionally, composite pie charts of single-grain ages are shown.

The fact that several age populations were obtained for each sample ranging from 267 ± 64 Ma to 1.2 ± 0.7 Ma (Table 3-2 and Figure 3-2) indicates that the exposed rocks in the study area experienced maximum temperatures well above, below, and around the ZFT closure temperature. As a consequence, some ages are reset, some are unreset, and some are partially reset, respectively (cf. Figure 2-6).

Unreset cooling ages can be associated with the thermal history of the source terrain of the sediments and might be used as provenance tool. It is important to note that the ZFT dataset alone cannot discriminate between specific causes for cooling, i.e., magmatic or metamorphic resetting, a regional relaxation or local variations of the geothermal gradient, or exhumational cooling due to tectonics or erosion. For a better interpretation of exhumational versus post-magmatic/metamorphic cooling, and provenance, higher-temperature dating techniques would be necessary. However, interpretations in the context of the known geologic history are possible. For instance, due to the lack of recent magmatic activity in the study area [e.g., *Hudson et al.*, 1977a] and the ZFT and U-Pb double dating on detrital material from the Seward-Malaspina Glacier and regions west of it [*Enkelmann et al.*, 2008, 2009], the largest part of ZFT ages from the North American Plate are interpreted to reflect reset ages and thus the time of cooling due to rock exhumation from depths below the ZFT closure temperature.

In the following, the age populations of the two composite samples (Figure 3-3) will be discussed as they provide a robust ZFT age signal for the Yakutat and North American plates. Figure 3-4 provides an overview of the spatial distribution of single-grain cooling ages of this and previous detrital ZFT studies from the wider area [*Enkelmann et al.*, 2008, 2009, 2010]. Ages in the pie charts are binned roughly according to previously recognized tectonic phases at the southeastern Alaskan margin. Those are i) the Mesozoic history of what is now the southern Alaskan margin with subduction, arc magmatism, and sediment accretion (>60 Ma) [e.g., *Plafker et al.*, 1994], ii) processes related to spreading-ridge subduction, which are metamorphism, magmatism, and reorganization of plate motions and boundaries (the transition from subduction to transform motion) (60–30 Ma) [e.g., *Haeussler et al.*, 2003], iii) Yakutat subduction-related cooling of the regional North American Plate, in particular of the Chugach Terrane (30–15 Ma) [*Perry et al.*, 2009], iv) the approximate onset of Yakutat collision (15–5 Ma) [e.g., *Plafker et al.*, 1994; *Pavlis et al.*, 2004]; and v) the time when rapid and deep exhumation occurs at the St. Elias syntaxis and glaciation of the orogen began (<5 Ma) [e.g., *Lagoe et al.*, 1993; *Enkelmann et al.*, 2010].

3.4.3 Late Cretaceous–Eocene cooling

The only composite age population peak that is clearly related to source area cooling (unreset sediment) is the 115 ± 8.5 Ma peak from the Yakutat microplate (10 % of all grains; Figure 3-3). Most studies suggest an origin of the Yakutat microplate between today's Baranof Island and Vancouver Island with a source terrain in the Wrangellia Composite Terrane and possibly in the Coast Plutonic Complex of British Columbia [e.g., *Plafker*, 1987; *Haeussler et al.*, 2003; *Perry et al.*, 2009; *Worthington et al.*, 2012]. The North American margin experienced a long and more or less continuous history of arc magmatism [e.g., *Hollister*, 1982; *Armstrong*, 1988], which involved pulses of uplift and deep exhumation [e.g., *Hollister*, 1979, 1982; *Plafker et al.*, 1994; *Gehrels et al.*, 2009]. Solely from the ~115 Ma ZFT age population it is not feasible to determine the provenance, but it would match the history of the Coast Plutonic Complex.

The 75 ± 5.3 Ma (8 %, North American Plate) and 67 ± 4.8 Ma (39 %, Yakutat microplate) age peaks fall into the time interval of deposition of Valdez Group and Yakutat Group, respectively. The ~67 Ma age peak is particularly large and also appears as 70–60 Ma age populations in individual catchments (Figures 3-3 and 3-4). These could either reflect post-magmatic/metamorphic or exhumational cooling in the sediment source area or reheating during sediment deposition. Processes of sediment burial, tectonic reworking, and low-grade metamorphism are obvious in the exposed Yakutat Group flysch and mélange sequences [e.g., *Hudson et al.*, 1977b; *Plafker et al.*, 1994] and resulted in reset or partially reset ZFT ages.

The second major age population (34 %) of the composite Yakutat microplate peaks at 45 ± 4.1 Ma (Figure 3-3) and appears in individual catchments as well (Table 3-2). This cooling signal postdates the time of Yakutat Group deposition and coincides with plate reorganization and slab window development following the ~55–50 Ma spreading-ridge subduction [e.g., *Hudson and Plafker*, 1982; *Stock and Molnar*, 1988; *Sisson and Pavlis*, 1993; *Bradley et al.*, 2003]. Effects have been most pronounced in the Chugach and Prince William Terranes (Chugach Metamorphic Complex and Sanak-Baranof intrusives), but the Yakutat microplate was affected as well, albeit to a smaller degree [e.g., *Hudson et al.*, 1977a; *Plafker*, 1987].

3.4.4 Oligocene cooling

The ZFT age populations discussed in the following are younger than deposition (reset sediment) and related to processes associated with subduction (and later collision) of the Yakutat microplate (<30 Ma single-grain ages, Figure 3-4). A widespread, on both plates appearing age population peaks at ~30 Ma (Table 3-2 and Figure 3-3). It occurs in especially large portions in catchments close to the Fairweather fault zone, e.g., Y55 (29 ± 2 Ma, 74 %; Table 3-2). That the age signal is observed on both plates is interesting because the Yakutat microplate was not adjacent to the Chugach/ Wrangellia part of the study area 30 Ma but hundreds of kilometers south. Thus, the age peak could reflect the same thermal event affecting the entire northern Cordillera or is merely a coincidence and reflect different geological events that happened to occur at approximately the same time. A ~30 Ma cooling and resetting of thermochronometric systems occurred in other sites as well. *Perry et al.* [2009] and *Enkelmann et al.* [2010] report ZFT age population peaks of ~33–25 Ma in the Chugach Mountains west of the syntaxis area and even in the Prince William Sound area farther west (Figure 2-7A) similar ZFT cooling ages were found and generally attributed to Yakutat subduction [*Izykowski et al.*, 2011; *Carlson*, 2012]. The rocks of the North American Plate in the study area are not located above the downgoing Yakutat slab, and the Yakutat microplate part was located farther south, but strain accumulation and deformation could still have translated along the transform plate boundary and caused transpression reflected in the ~30 Ma cooling phase. Recent structural data [*Chapman et al.*, 2012] suggest a Miocene transition from basement-involved transpression to fold- and thrust-style deformation in the syntaxis area around the Malaspina Glacier supporting the existence of a transpressional plate boundary at ~30 Ma.

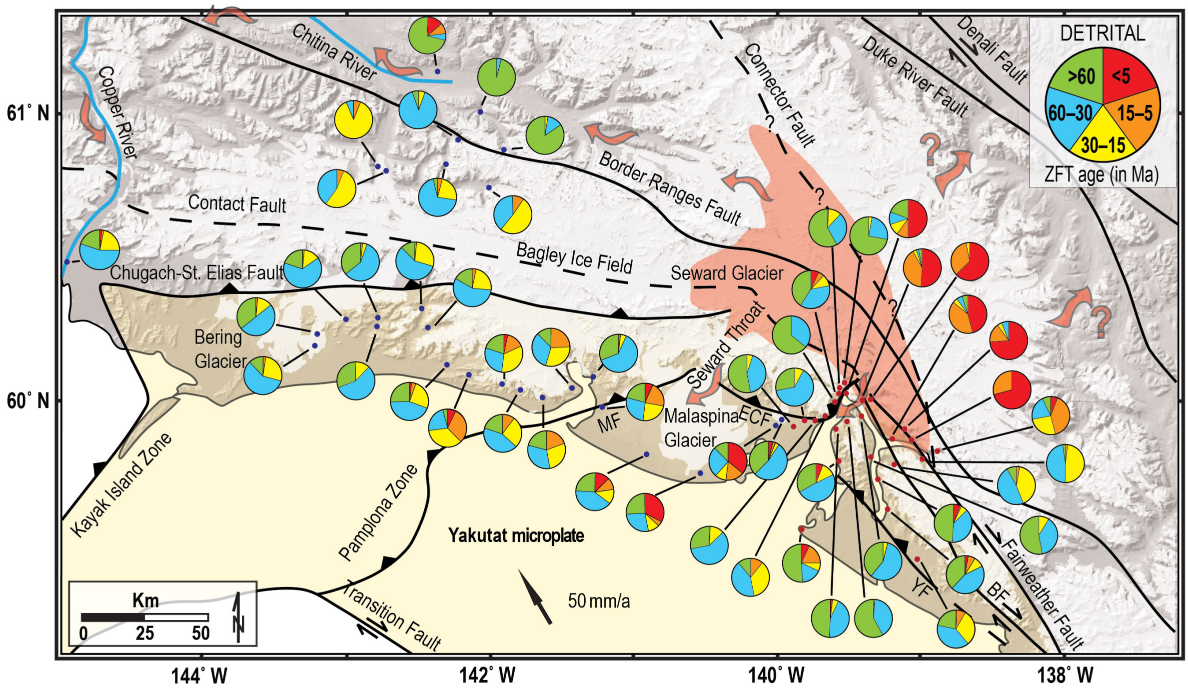

Figure 3-4. Pie charts of detrital single-grain ZFT ages of this study (red dots) and studies by *Enkelmann et al.* [2008, 2009, 2010] (blue dots). The reddish area outlines the area of rapid, deep exhumation on catchment scale. Arrows mark the transport direction of rapidly exhumed material. Single-grain ages of this study can be found in Appendix B (Dataset B-1).

3.4.5 Miocene cooling

The character of the Yakutat basement as a wedge-shaped oceanic plateau delivers a good explanation for the onset of exhumation in Southeast Alaska due to subduction of a buoyant slab, which may have initiated in the late Eocene [*Finzel et al.*, 2011b]. With continued translation along the Fairweather Fault and underthrusting beneath the North American Plate, the oceanic crust entering the deformational front became thicker and thicker (~15–30 km), resulting in increased upper and lower plates coupling [*Gulick et al.*, 2007; *Worthington et al.*, 2012]. The thermochronologic record might be able to capture the increasing resistance to subduction of the Yakutat microplate and the beginning of collision. If this is the case, the 12.6 ± 1.1 Ma (11 %) and possibly the 15 ± 2.4 Ma (3.5 %) composite age populations of the North American Plate and the Yakutat microplate, respectively (Figure 3-3), are candidates for recording deformation and exhumation of both plates due to the onset of collision. The Fairweather Fault may have developed a stronger compressional component in response to increasing and localizing strain around the fault bend of the syntaxis.

This exhumational event is in agreement with episodic exhumation at Mt. Logan with one phase occurring at ~14 Ma (AFT data) [*O'Sullivan and Currie*, 1996] or the ZHe study of cobbles from the Seward-Malaspina Glacier catchment showing an ~12 Ma cooling age population in Yakutat microplate and North American Plate lithologies [*Grabowski et al.*, 2013]. Many other studies in the Chugach-St. Elias Mountains using different thermochronometric methods (AHe, AFT, and ZFT) yielded 14–13 Ma cooling ages, too [*Enkelmann et al.*, 2008; *Meigs et al.*, 2008]. If all of these ages of detrital and bedrock samples are associated with beginning Yakutat collision in the mid-Miocene, then exhumation must have occurred rapidly in order to produce approximately the same cooling ages in different thermochronometric systems with different closure temperatures.

Figure 3-5 offers a synthesis of the tectonic history of the two parts of the study area in combination with the composite cooling signals presented in Figure 3-3. It illustrates how the histories of the two plates became common with time and continuing subduction of the Yakutat lithosphere.

3.4.6 Pliocene–Pleistocene cooling

3.4.6.1 Yakutat microplate

Even though collision of the Yakutat microplate with the North American Plate appears to cause very rapid uplift and exhumation of Yakutat Group rocks, as indicated by thermochronometric, sedimentary, geodetic, seismic, and paleoseismologic data [e.g., *O'Sullivan et al.*, 1997; *Doser and Lomas*, 2000; *Plafker and Thatcher*, 2008; *McAleer et al.*, 2009; *Elliott et al.*, 2010; *Spotila and Berger*, 2010], it does not cause exhumation deep enough to dominate the ZFT record of the Yakutat microplate (Table 3-2 and Figures 3-2 to 3-5). The few catchments that display ≤5 Ma cooling ages are located on the hanging walls of thrust faults that could explain recent, deeper exhumation due to thrusting and erosion (Table 3-2 and Figures 3-1 and 3-4). Y1 and Y2 (age peaks at ~2.5–2 Ma; Table 3-2), as well as Y34 and Y35, (age peaks at ~4.6 Ma; Table 3-2) are located on the hanging wall of the Yakutat Fault (Figure 3-1), so is Y46 (Figure 3-1), but the catchment is large and the small (4 %) peak at 5.6 ± 2 Ma may or may not be derived from exhumation on the Yakutat Fault. However, when comparing the Y46 age distribution with those of adjacent catchments, it seems likely that the ~5.6 Ma, reset ages are associated with the Yakutat Fault.

If this is true, then there exists a northwestward trend of younger reset age populations from Y46 to Y34/Y35 to Y1/Y2 (Figure 3-1). This would point to differential exhumation on the fault with stronger exhumation on the northwestern part. The Yakutat Fault has been identified in structural, geodetic, and seismic studies to be one of today's active faults in the Yakutat foothills to accommodate deformation [e.g., *Bruhn et al.*, 2004; *Elliott et al.*, 2010; *Plafker and Thatcher*, 2008]. For example, this fault was one of the structures that was activated during the 1899 Mw=8.1 and Mw=8.2 Yakutat Bay earthquakes in addition to the Boundary Fault and the Bancas Point Fault (parallel to the western Disenchantment Bay shoreline, Figure 3-1) [*Plafker and Thatcher*, 2008]. The Y40 catchment that also contains a young, reset ZFT age population (4.3 ± 0.5 Ma, 10 %; Table 3-2) is located on the western shore of Disenchantment Bay (Figure 3-1), where the largest coseismic uplift (14 m) during the 1899 earthquakes has been observed [*Tarr and Martin*, 1912; *Plafker and Thatcher*, 2008]. The new data from this study suggest uplift and exhumation of hanging wall blocks near the active structures in Disenchantment Bay and the Yakutat foothills.

3.4.6.2 Wrangellia Composite and Chugach Terranes

The most striking finding of this study is that the area of recent, deep-seated rock exhumation is more extensive than previously suggested and focused on the North American Plate (Figure 3-4). The area is confined to the southeast by the catchments Y55 and Y57 that do not show the very young ages of catchments farther west (Figures 3-1 and 3-4).

In this area, rapid and deep exhumation seems to be spatially limited by the intersection of the inferred Connector Fault with the Fairweather Fault (Figure 3-4). The southern limit is given by the Fairweather fault zone and its prolongation to the Contact Fault and the western limit by the western boundary of the Seward Glacier catchment (Figure 3-4) [*Enkelmann et al.*, 2009, 2010]. The northern boundaries cannot be constrained with the current dataset, and studies on the Canadian side of the St. Elias Mountains are needed. So far, the area appears to be ~4800 km^2 large (average of ~130×37 km) based on the outlines of investigated catchments in this and *Enkelmann et al.*'s [2008, 2009, 2010] studies and the inferred position of the Connector Fault as boundary (Figure 3-4).

3.5 Geodynamic Implications

3.5.1 Transpressional structures at the St. Elias syntaxis

Collisional deformation within the Yakutat microplate is accommodated in form of southeast- and northeast-striking thrust faults in the Yakutat foothills and west of Yakutat Bay, respectively [e.g., *Bruhn et al.*, 2004, 2012; *Pavlis et al.*, 2004; *Elliott et al.*, 2010; *Chapman et al.*, 2012]. Based on geomorphologic observations, structural reconstructions, and bedrock thermochronometry, it has been discussed that compressional structures exist on the northern side of the Fairweather Fault as well [*Bruhn et al.*, 2004, 2012; *McAleer et al.*, 2009; *Spotila and Berger*, 2010]. Due to the ice cover and the sparse seismograph network coverage, this has always been highly speculative.

The inferred Connector Fault has long been suggested to transfer strain from the Fairweather Fault directly to the Denali Fault via the Totschunda Fault, an active southern splay of the Denali Fault (Figure 2-8) [e.g., *St. Amand*, 1957; *Richter and Matson*, 1971; *Lahr and Plafker*, 1980; *Doig*, 1998; *Koons et al.*, 2010]. Furthermore, the Connector Fault, but also the Duke River Fault, have been taken as candidates to be responsible for a lack of pronounced seismic activity along the eastern Denali Fault by bypassing this fault segment via the Totschunda Fault and a fault connected with it (Figure 2-8) [e.g., *Richter and Matson*, 1971; *Doig*, 1998; *Eberhart-Phillips et al.*, 2003; *Kalbas et al.*, 2008]. Only recently, *Doser* [2014] demonstrated through an earthquake

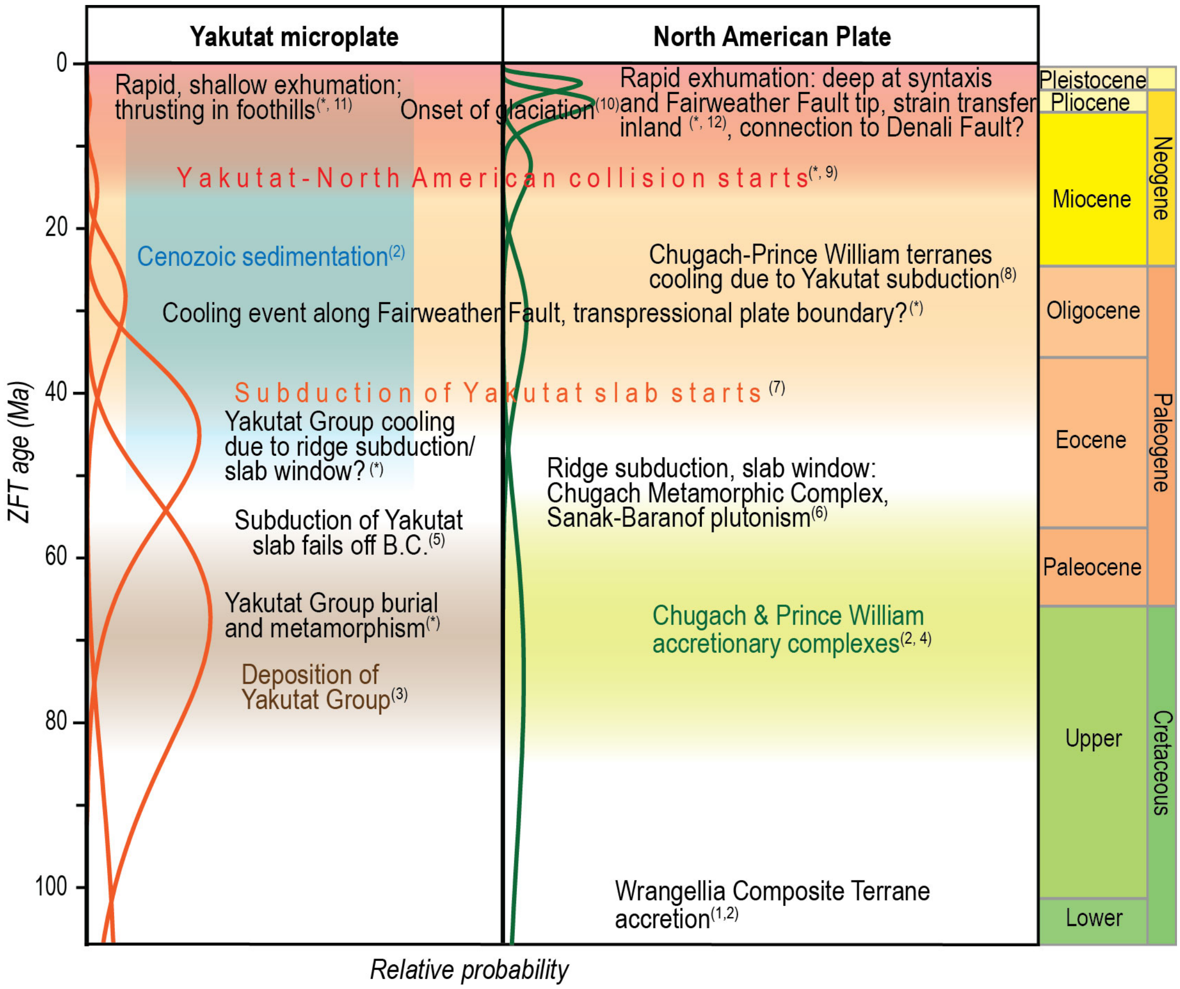

Figure 3-5. Summary of tectonic events and composite fitted peaks (as in Figure 3-4) for the study area. (1) *Jones et al.* [1977]; (2) e.g., *Plafker* [1987], *Plafker et al.* [1994]; (3) *Plafker* [1987], *Landis* [2007]; (4) *Dumoulin* [1988]; (5) *Worthington et al.* [2012]; (6) e.g., *Hudson et al.* [1979], *Hudson and Plafker* [1982], *Pavlis and Sisson* [1995]; (7) *Finzel et al.* [2011b]; (8) *Perry et al.* [2009], *Enkelmann et al.* [2010], *Benowitz et al.* [2011], *Carlson* [2012], *Grabowski et al.* [2013]; (9) *O'Sullivan and Currie* [1996], *Grabowski et al.* [2013]; (10) *Lagoe et al.* [1993]; (11) e.g., *Doser and Lomas* [2000], *Bruhn et al.* [2004], *Plafker and Thatcher* [2008], *Elliott et al.* [2010]; (12) *Enkelmann et al.* [2009, 2010], *Grabowski et al.* [2013]; and (*) this study.

relocation study that the Connector Fault is an active seismogenic structure to connect the Fairweather Fault with the Denali Fault. Like *Doser* [2014], *Kalbas et al.* [2008] discussed that the Totschunda Fault and the Connector Fault could have established only recently, but they also stated that if the Art Lewis Fault beneath Art Lewis Glacier (north of Nunatak Fjord, Figure 3-1) was the southern segment of the Connector Fault, it may have been active for up to 2.7 Myr based on its high dextral displacement of ~16 km (written communication between G. Plafker and Kalbas et al. in *Kalbas et al.* [2008]). This location of the southern Connector Fault agrees with the location suggested by others [*Spotila and Berger*, 2010; *Bruhn et al.*, 2012] and the southeastern constraint of the area of rapid and deep exhumation found here (Figure 3-4). If this indeed represents a segment of the Connector Fault, it must be even older than 2.7 Myr and have a significant compressional component over geologic time to accommodate deep exhumation and expose Pliocene and younger ZFT ages.

However, many aspects remain uncertain. The seismic data are still difficult to interpret because they are diffuse and sparse and suggest a different site of intersecting Fairweather and Connector Faults, which is closer to the Hubbard Glacier termination north of Disenchantment Bay (Figure 2-8) rather than at the end of Nunatak Fjord (Figures 3-1 and 3-4) [*Doser*, 2014]. The data basis is too poor to truly evaluate discrepancies between modern deformation and long-term deformation, but so far, it seems that the activity of structures on the northern side of the Fairweather Fault is longer-lived than suggested by the geophysical data. Further thermochronometric studies on the northern side of the mountain range will constrain the northern limit of rapid and deep exhumation as well as the role and location of possible structures to accommodate exhumation, and may also shed light on questions pertaining the bypassing of the eastern Denali Fault through structures like the Connector Fault or the Duke River Fault.

3.5.2 Possible drivers of rapid and deep exhumation in the St. Elias syntaxis region

The detrital ZFT thermochronometric record of the North American Plate in the St. Elias syntaxis region is dominated by two cooling phases at ~5.1 Ma and ~2.7 Ma (Figure 3-5). These signals are intriguing because they correlate well with changes in the depositional character of the Yakataga Formation, the youngest (6–5 Ma to Recent) of the Cenozoic sediment sequences in the Gulf of Alaska and onshore mainly west of Yakutat Bay. *Lagoe et al.* [1993] interpreted from the sedimentary record that the onset of tidewater glaciation occurred at 6.5–5.0 Ma, followed by a relative warm mid-Pliocene interval between 4.2 Ma and 3.5–3.0 Ma and a subsequent intensification and expansion of glaciation at 3.5–3.0 Ma consistent with Northern Hemisphere climate change and glacial expansion. *Lagoe et al.* [1993] found that the growth of glaciers at the beginning of the Pliocene was due to regional cooling and surface uplift that in turn affected local climate change. Some trends in sediment accumulation changes could be explained well by paleoclimatic indicators, while other changes could only be explained as effect of tectonics, e.g., the structural deformation of sediments offshore since the Pleistocene [*Lagoe and Zellers*, 1996].

The ~5.1 Ma ZFT cooling signal falls into the time of onset of glaciation and the ~2.7 Ma acceleration in exhumation rate occurs shortly after glacial intensification after the relatively warmer mid-Pliocene interval. It cannot be said whether there exists a link between the onset of glaciation and a tectonic response or a tectonically induced exhumation and surface uplift phase, which caused topography high enough to support alpine glaciers. There are two possible tectonic drivers for rapid exhumation in the St. Elias syntaxis region that may have coincided with each other and with climate change: i) continuously increasing resistance to subduction of the buoyant, eastward thickening Yakutat crust [*Gulick et al.*, 2007; *Worthington et al.*, 2012] and ii) a change in Pacific-North American relative plate motions resulting in increased compression of the Yakutat-North American convergence [*Engebretson et al.*, 1985]. However, the influence of this plate motion change (10°–15°) and the timing (estimates range from ~8–5 Ma) remain uncertain, as discussed by *Haeussler et al.* [2008].

Based on the exhumation pattern, a likely scenario is that oblique crustal convergence at the bend of the margin and significantly increasing crustal thickness since 15–12 Ma resulted in strain localization in the syntaxis region (Figure 3-5). With even thicker oceanic crust entering the deformational front and a possible increase in transpression at the plate boundary, strain accumulation at the bend resulted in the initiation of new structures to transfer strain northward into the continent at the Miocene-Pliocene boundary. Interestingly, a ~6–5 Ma exhumation phase has been discovered at the central and western Denali Fault [*Fitzgerald et al.*, 1995; *Haeussler et al.*, 2008] and correlates within error with the ~5.1 Ma exhumation signal from the syntaxis region. This signal was not found in thermochronometric studies of the Seward-Malaspina Glacier outwash, where, however, the 3–2 Ma signal was found [*Enkelmann et al.*, 2009; *Grabowski et al.*, 2013]. This observation could imply that the areal extent of rapid and deep exhumation increased slightly westward when glacial processes evolved and intensified. It is important to note that the rates of deep exhumation did not increase throughout the entire orogen at that time but remain focused on the North American Plate around the syntaxis and, to a somewhat lesser degree, close to the active structure of the Fairweather Fault running south [*McAleer et al.*, 2009].

3.5.3 Glacial erosion

Several important implications for glacial erosion of the St. Elias orogen can be drawn from investigating exhumation pattern. High rates of rock uplift and exhumation can only be maintained when erosion rates can keep up with surface uplift. Pliocene–Recent erosion rates are high based on inferences from sedimentation rates in the stratigraphic record of the glaciomarine-marine Yakataga Formation offshore and onshore [e.g., *Hallet et al.*, 1996; *Lagoe and Zellers*, 1996; *Sheaf et al.*, 2003; *Meigs et al.*, 2006]. Hence, glaciers have been efficient as erosional agents at the active convergent margin, though modern (10^1–10^2 yr) effective erosion rates of >10 mm/yr exceed by far longer-term rates (maximum estimate of ≥6 mm/yr for the Pliocene) [*Hallet et al.*, 1996; *Lagoe and Zellers*, 1996; *Meigs et al.*, 2006]. This high modern rate may be an artifact of episodic evacuation of material weathered over a longer time period (10^2–10^4 yr), but it still leaves erosion rates of several mm/yr over millennia. For example, *Sheaf et al.* [2003] estimated an average of 5.1 mm/yr over the Holocene.

Exhumation rates determined with thermochronometry can, under some assumptions, be taken as erosion rates. Quaternary exhumation rates in the St. Elias orogen have been interpreted as glacial erosion rates [e.g., *Berger and Spotila*, 2008; *Enkelmann et al.*, 2009; *McAleer et al.*, 2009] and can therefore be compared to erosion rate estimates from the stratigraphic record. *McAleer et al.* [2009] determined exhumation rates of ~2 mm/yr (maximum 2.8 mm/yr) close to the Fairweather Fault (<10 km) and averaged >0.5 mm/yr for the entire plate margin (including the Fairweather fault zone along a distance of ~250 km to the south of the study area, Figure 2-9) since ~5 Ma. *Enkelmann et al.* [2009] and *Grabowski et al.* [2013] gave Quaternary exhumation rates for the Seward-Malaspina glacial catchment of 2–2.7 mm/yr. These values are similar to exhumation rates implied by the youngest ZFT age peak of this study at ~2.7 Ma. Assuming a one-dimensional steady state rock exhumation, a rate of ~2.3 mm/yr and a closure depth of 6 km are suggested [*Reiners and Brandon*, 2006].

In summary, long-term erosion rates are roughly consistent between different methodological approaches, indicating an increase with the beginning of glaciation ~6–5 Ma (~0.013 mm/yr to 0.2 mm/yr) [*Lagoe and Zellers*, 1996], a further increase to up to ≥6 mm/yr over the Pliocene, followed by rates of ≤2 mm/yr [*Lagoe and Zellers*, 1996] or ~2 mm/yr as in the thermochronologic record [*Enkelmann et al.*, 2009; *McAleer et al.*, 2009; *Grabowski et al.*, 2013; this study].

The observed exhumation pattern also suggest that glacial erosion might be particularly efficient where it coincides with active structures and pervasively fractured rocks as it is probably the case in the syntaxis region and along the Fairweather Fault [*Headley et al.*, 2013]. The comparison between the detrital data and the bedrock thermochronology data further suggests that glacial erosion dominates in valleys similar to *Enkelmann et al.*'s [2009] results. This difference suggests vertically differential erosion, which agrees with observations of old preserved mountain peaks like at Mt. Logan [*O'Sullivan and Currie*, 1996; *Spotila and Berger*, 2010].

3.5.4 Comparison to the Himalayan syntaxes

The St. Elias syntaxis has been proposed to represent an early stage of a geodynamic feedback mechanism not yet fully evolved into something like the Himalayan syntaxes [*Enkelmann et al.*, 2009; *Koons et al.*, 2010, 2013]. In the eastern and western Himalayan syntaxes, the Tsangpo and Indus Rivers, respectively, deeply incise the high mountain massifs and remove and transport material with exceptionally high rates, creating ~7000 m of local relief [e.g., *Zeitler et al.*, 2001; *Koons et al.*, 2002; *Finnegan et al.*, 2008; *Stewart et al.*, 2008]. The general tectonic setting of an indenting plate corner is similar for the Indian and Alaskan syntaxes, and efficient erosion agents remove material from the systems. The areal extent, as known at the moment, is of similar order, where deep exhumation affects an area of ~4800 km^2 at the St. Elias syntaxis and ~5000 km^2 at the eastern Himalayan syntaxis [*Enkelmann et al.*, 2011]. In contrast to the Himalayas, where rivers incise bedrock in steep gorges, a wide network of glaciers accomplishes erosion in the St. Elias orogen. The glaciers that cover the syntaxis region and active structures appear to be particularly efficient and may interact with rock exhumation. However, with the current knowledge of the St. Elias syntaxis, it is difficult to compare it to the Himalayan syntaxes or other convergent settings at that matter. Further thermochronometric studies of the northern side of the mountain range will help to constrain the northern limit of rapid and deep exhumation and locate possible structures to accommodate this, and the use of higher-temperature thermochronometric systems will allow examining the degree of thermal disturbance of the crust.

3.6 Summary

This chapter emphasizes the complexity of orogenic syntaxis regions and that those settings must be treated as 4D-problems with spatially and temporally variable distribution of deformation. Furthermore, the results presented here are a further step in understanding the complex characteristics of the St. Elias syntaxis and contribute to the discussion about mechanisms, timing of events, glacial erosion, and the distribution of strain in the zone of transition from transpression to subduction. The finding of a more extensive area of rapid and deep exhumation will have to be taken into account for structural reconstructions, geodynamic models, and future sampling strategies. The main points of this chapter are as follows.

1) ZFT cooling age pattern of Yakutat microplate and North American Plate reveal two different tectonic regimes. While cooling of North American Plate rocks is dominantly related to Pliocene–Recent collision, Yakutat Group rocks mainly reflect their depositional and post-depositional heating in the latest Cretaceous and Eocene, respectively. The recent exhumation of Yakutat Group rocks is rapid, too, but mainly along shallow paths.

2) Composite samples reveal several cooling phases related to subduction and collision of the Yakutat microplate at the North American Plate margin. Those may be due to transpression-related cooling on both plates (~30 Ma), onset of collision (15–12 Ma), and localized strain in the St. Elias syntaxis region and efficient glacial erosion on the North American Plate (~5.1 Ma, ~2.7 Ma).

3) The area of recent deep exhumation is larger than previously known. It extends from the St. Elias syntaxis to the north and southeast. The southern limit is the Fairweather Fault and its prolongation to the Contact Fault; the western limit is the western boundary of the Seward Glacier catchment, and the Connector Fault could be the eastern limit.

4) The localization of strain and deep exhumation in the St. Elias syntaxis region appears to be the result of coevolving tectonic and climatic systems since the Pliocene. Tectonic processes were presumably the major driver in localizing strain and exhumation but only through efficient glacial erosion and evacuation of material could the high rates of exhumation be maintained.

5) Glacial erosion is focused in valleys and produces in combination with high rates of tectonic uplift the great relief of the St. Elias syntaxis region.

4 Cooling histories of the St. Elias syntaxis from cobbles

4.1 Significance

Two different sampling strategies for thermochronology, bedrock and detrital sampling, have previously been used to quantify the exhumation history of the St. Elias Mountains [e.g., *O'Sullivan et al.*, 1997; *Enkelmann et al.*, 2008, 2009; *Berger et al.*, 2008; *McAleer et al.*, 2009; *Grabowski et al.*, 2013; Chapter 3]. Bedrock data suffer from a biased signal because those samples can only be taken in the foothills or at high-elevation, ice-free ridges, while the youngest rocks that record the most rapid exhumation are expected to occur at low elevations in the glaciated valleys [e.g., *Fitzgerald and Gleadow*, 1990]. Sand-sized detritus from rivers draining the glaciated valleys yields the cooling record from the entire catchment, including those parts above and below the ice, and revealed the presence of very rapidly exhumed rocks in the syntaxis area through ≤5 Ma zircon fission-track (ZFT) ages [*Enkelmann et al.*, 2009, 2010; Chapter 3]. However, the inherent problem of sand is the decrease in spatial resolution of provenance and with that the cooling signal. Furthermore, it is difficult to extract fresh (unweathered) minerals from detritus for reliable higher-temperature thermochronometric analyses like $^{40}Ar/^{39}Ar$ dating, which are necessary to examine timing and depth of rapid exhumation.

To overcome these problems, cobble-sized detritus from the Seward-Malaspina and Hubbard-Valerie glaciers, which lie within the main catchments of the St. Elias syntaxis area, are used. Cobbles have the advantage that information about individual lithologies in the source region are preserved and that fresh minerals, undamaged from transport, are available for multiple dating techniques. In this study, zircon U-Pb dating and lithologic information from thin sections are used to explore the provenance of 27 cobbles from the two glacial catchments. In order to quantify the cooling history of the rocks through a large temperature range (500–60 °C), amphibole and biotite $^{40}Ar/^{39}Ar$ dating, AFT dating, as well as AHe and ZHe dating is used.

Additionally, four bedrock samples from the Fairweather Range east of the syntaxial region have been analyzed for biotite $^{40}Ar/^{39}Ar$ cooling ages for comparison of higher-temperature cooling outside the St. Elias syntaxis. To better understand the cooling history of the syntaxis area and show the applicability of using cobbles, the new data are put into regional geologic context of the Cenozoic orogenic evolution by extracting typical cooling histories from published geo- and thermochronologic bedrock data from along orogenic strike.

4.2 Seward-Malaspina and Hubbard-Valerie glacial catchments

The Seward-Malaspina (~3,900 km^2) and Hubbard-Valerie (~4,050 km^2) glacial systems cover the syntaxial region and are surrounded by the highest peaks of the orogen (up to 5959 m at Mt. Logan) (Figure 4-1). The Seward Ice Field, with ice thicknesses of >600–800 m [*Rignot et al.*, 2013], drains south through the narrow 4–6 km wide Seward Throat into the ~80 km wide Malaspina piedmont glacier (Figure 4-1), which is up to 600 m thick and extends to 400 m b.s.l. [*Rignot et al.*, 2013]. The current deformational front of the Cenozoic fold-and-thrust belt runs underneath the western part of the Malaspina lobe, with shallow northwest-dipping thrusts characterized by frequent, shallow seismic activity [e.g., *Doser and Lomas*, 2000; *Bruhn et al.*, 2004; *Cotton et al.*, 2014]. Northeast-dipping thrust and reverse faults within the Yakutat basement bound the Malaspina lobe to the northeast (Figure 4-1). A partly exposed mountain ridge east of Mt. Logan separates the Seward Ice Field in the south from the Hubbard Glacier to the north (Figure 4-1). The 500–950 m thick ice of the Hubbard Glacier flows for >100 km southeast before it turns south and drains into Disenchantment Bay (Figure 4-1), making it the largest tidewater glacier in Alaska [*Molnia*, 2008; *Rignot et al*., 2013]. Close to its terminus, the Hubbard Glacier is joined by the ~40 km long Valerie Glacier from the west. The Fairweather Fault runs beneath the Hubbard Glacier snout and along the Valerie Glacier valley (Figure 4-1).

4.3 Methods

4.3.1 Samples

This study builds on the analyses of *Grabowski et al.* [2013], who investigated 59 cobbles (10–30 cm in size) using petrographic thin sections and ZHe dating to identify the lithologies that were exhumed most rapidly under the Seward-Malaspina Glacier. Samples were collected on top of the debris-covered outer lobe of the Malaspina Glacier as outwash is directly shed into the ocean (Figure 4-1). Sample selection of a variety of representative lithologies was mainly based on the potential presence of datable mineral phases [*Grabowski et al.*, 2013]. The sample set is therefore neither representative of the abundance of rock types (cf. point counting by *Grabowski et al.* [2013]) nor of a quantitative analysis of catchment erosion. In this study, a subset of 22 cobbles that yielded enough datable mineral phases were analyzed. These cobbles are denoted "MAL" (for Malaspina). Additionally, five cobbles from the sediment fan built up at the western Hubbard Glacier terminus (Figure 4-1), which are denoted "HUB" (for Hubbard), were analyzed. The sediment fan constitutes a mix of sediment from the Hubbard and Valerie glaciers and therefore both catchments are considered as the source.

4.3.2 Provenance and cooling histories

The provenance of 21 Seward-Malaspina cobbles was examined using petrographic analyses of thin sections and zircon U-Pb dating. For one Seward-Malaspina cobble and the five Hubbard cobbles, no crystallization ages are available and the provenance is based on petrographic information and $^{40}Ar/^{39}Ar$ ages.

The cooling histories of individual cobbles were reconstructed using multiple thermochronometer analyses with different closure temperatures: amphibole and biotite $^{40}Ar/^{39}Ar$ dating with closure temperatures of 500 ± 50 °C [*Harrison*, 1981] and 300 ± 50 °C [*Harrison et al.*, 1985], respectively, ZHe analyses reflecting a 180 ± 20 °C [*Reiners et al.*, 2004] closure temperature, as well as AFT with 110 ± 10 °C [*Gleadow and Duddy*, 1981] and AHe dating with 60 ± 15 °C [*Farley*, 2000] closure temperatures (Figure 3).

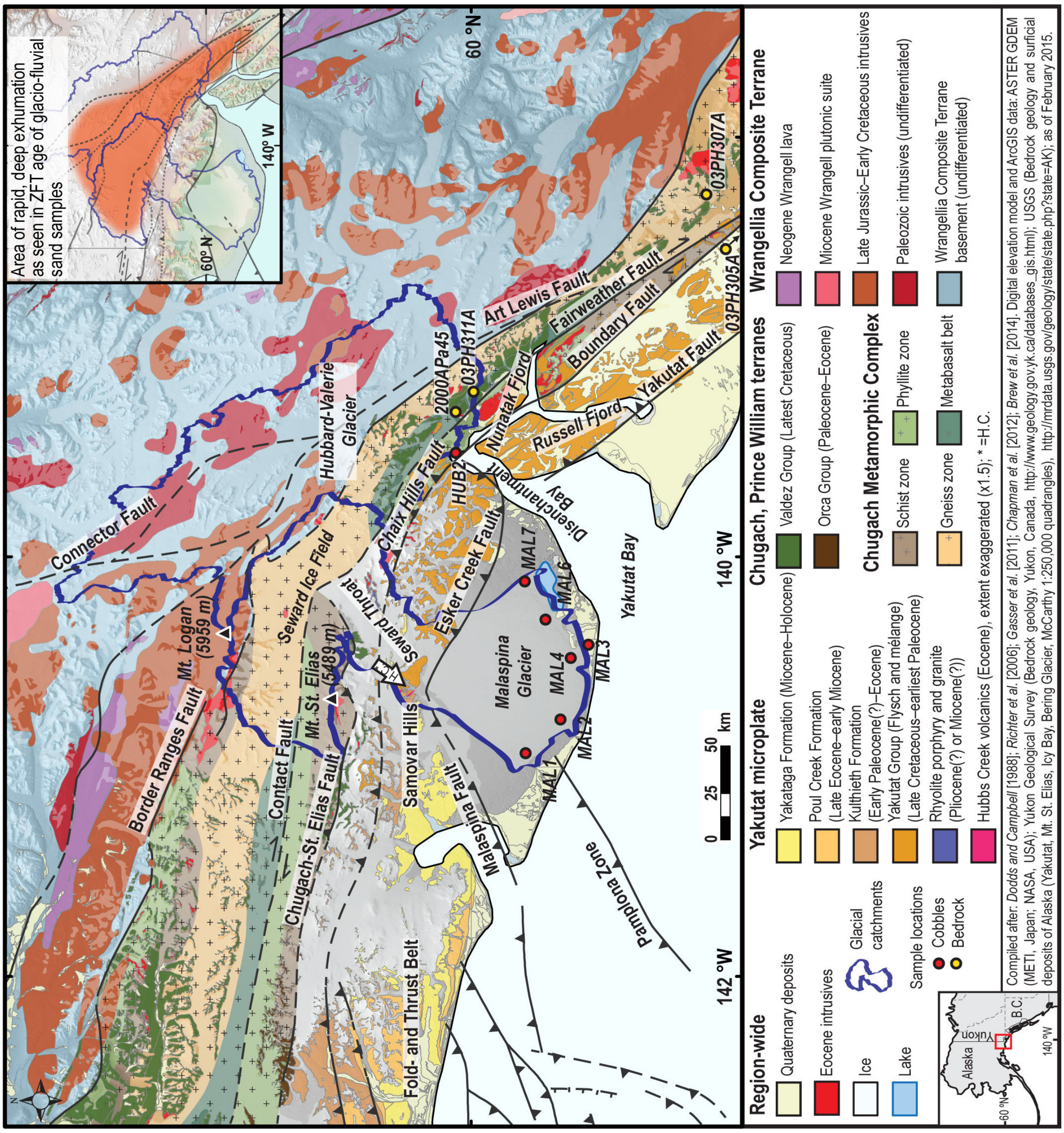

Figure 4-1. Geologic overview of the Chugach-St. Elias Mountains and Fairweather Range including cobble and bedrock sample locations. For exact sample location of 03PH305A see Figure 4-5. The inset map displays the area of most rapid and deep exhumation in the St. Elias syntaxis and northern Fairweather Fault areas based on ≤5 Ma ZFT cooling ages from sand-sized detritus [*Enkelmann et al.*, 2009, 2010; Chapter 3].

4.4 Results

4.4.1 Zircon U-Pb analysis

The interpretation of zircon U-Pb ages depends on the sample type analyzed. Generally, zircon U-Pb ages of magmatic rocks refer to the magmatic event and zircon crystallization from the melt, while zircons with metamorphic overgrowth in higher-grade metamorphic rocks yield the age of metamorphism. Furthermore, both magmatic and metamorphic zircons can contain old zircon cores that survived incorporation in melt and metamorphism. In sedimentary rocks, the zircon U-Pb age distribution of the source terrain(s) is reflected in the rock sample. This can also be the case for metasediments, as zircon U-Pb ages do not become completely reset during metamorphism [e.g., *Mezger and Krogstad*, 1997].

A summary of the ages for each sample is presented in Table 4-1 and concordia diagrams are shown in Figure 4-2. The details of the single-grain analyses of individual samples can be found in Appendix B (Table B-1). Of the 21 MAL cobbles, eight magmatic cobbles with a range of magmatic ages between 277.1 ± 6.7 Ma and 30.8 ± 0.8 Ma (Table 4-1) were dated. These cobbles show no zircons with inherited older cores (Table B-1). Two pyroclastic cobbles yielded ages around 50 Ma, which represent the time of the volcanic eruption(s) (Table 4-1). As the single-grain ages show a slight spread in both samples (Figure 4-2 and Table B-1), the cobbles may represent reworked volcanic material from more than one eruption.

The eleven metamorphic cobbles include six metasedimentary and five meta-igneous rocks (Table 4-1). The metasedimentary cobbles show Carboniferous–Eocene age distributions ranging between ~493 Ma and ~48 Ma (concordant ages only) with the vast majority being <200 Ma (Table B-1). Age distributions of single-grain ages of metasedimentary cobbles reflect the age distribution of their source area, which is discussed later in the text. One of these cobbles (MAL4-16) includes a zircon with a metamorphic rim that may reflect ~48 Ma metamorphism causing overgrowth on a ~57 Ma zircon (Table B-1). The meta-igneous cobbles yield Early Jurassic–Eocene protolith ages between 181.6 ± 0.8 Ma and 52.3 ± 7.3 Ma (Table 4-1). Zircons of meta-igneous cobbles do not show prominent metamorphic rims, which means their crystallization age was determined but not the time of the metamorphic event.

It is notable that half of the protolith crystallization ages and crystallization ages are around 50 Ma (Table 4-1).

4.4.2 $^{40}Ar/^{39}Ar$ analysis

Of eight amphibole samples measured, five yielded meaningful $^{40}Ar/^{39}Ar$ cooling ages that range between 181.0 ± 0.6 Ma and 15.8 ± 0.4 Ma (1 σ) (Table 4-2). The remaining three show i) one argon profile that is too disturbed for an age estimate (amphibolite MAL1-14), ii) one argon loss profile suggesting a minimum crystallization age of ~276 Ma and a maximum age of ~139 Ma thermal resetting (HUB2-3, meta-

Table 4-1. Cobble sample list and summary of zircon U-Pb ages

Sample	Latitude (°N) Longitude (°W)	Lithology	Zircon U-Pb age [Ma] (2σ)	N	Remarks
MAL1-8	59.8592 140.89585	Migmatitic gneiss	-	-	No zircons
MAL1-14		Amphibolite	30.8 ± 0.8	4	Crystallization age
MAL1-19		Aplite	46.4 ± 1.0	6	Crystallization age
MAL2-4	59.77705 140.78952	Granitoid	50.8 ± 1.0	17	Crystallization age
MAL2-10		Paragneiss	335–81/ 83.8 ± 1.3	19/ 11	Detrital age range/max. depositional age of sedimentary protolith
MAL2-16		Micaschist	72–49	17	Detrital age range
MAL3-2	59.70058 140.40393	Pyroclastic	50–46	8	Detrital age range
MAL3-8		Orthogneiss	52.3 ± 7.3	2	Lower intercept, proto-lith age
MAL3-19		Granitoid	277.1 ± 6.7	4	Crystallization age
MAL4-5	59.74943 140.48363	Paragneiss	60–48/ 49.4 ± 0.5	18/ 6	Detrital age range/max. depositional age of sedimentary protolith
MAL4-6		Igneous mylonite	53.3 ± 0.3	19	Igneous protolith age
MAL4-9		Orthogneiss	150.0 ± 1.0	29	Protolith age
MAL4-16		Paragneiss	279–56/ 56.3 ± 0.6/ 48.7 ± 0.9	16/ 7/ 2	Detrital age range/max. depositional age of sedimentary proto-lith/metamorphic age
MAL4-21		Metasedimentary mylonite	493–58	21	Detrital age range of sedimentary protolith
MAL6-5	59.81708 140.30245	Orthogneiss	151.0 ± 0.7	39	Protolith age
MAL6-23		Orthogneiss	52.4 ± 0.4	28	Protolith age
MAL6-24		Paragneiss	76–50/ 52.8 ± 0.5	20/ 13	Detrital age range/youngest population
MAL7-2	59.8669 140.10847	Gabbro	49.4 ± 0.4	10	Crystallization age
MAL7-3		Meta-quartzdiorite	181.6 ± 0.8	29	Protolith age
MAL7-6		Pyroclastic	50.3 ± 0.3	31	Crystallization age
MAL7-14		Granitoid	50.9 ± 1.4	13	Crystallization age
MAL7-20		Granitoid	48.5 ± 0.6	23	Crystallization age
HUB2-2	60.040383 139.54253	Granitoid	-	-	No analysis
HUB2-3		Meta-quartzdiorite	-	-	No analysis
HUB2-5		Granodiorite	-	-	No analysis
HUB2-7		Hornblende-gabbro	-	-	No analysis
HUB2-8		Mylonite	-	-	No analysis

Note: Unless otherwise noted the reported zircon U-Pb ages represent concordia ages for (meta-)igneous rocks and age ranges for (meta-)sedimentary rocks, whereas the number of single-grain analyses used to obtain the value(s) is given in the neighboring column (N). In addition, the maximum depositional age for sedimentary rocks or proto-liths and the age of metamorphism are given when conclusive (notes in the Remarks column). Single-grain analyses can be found in Appendix B (Table B-1).

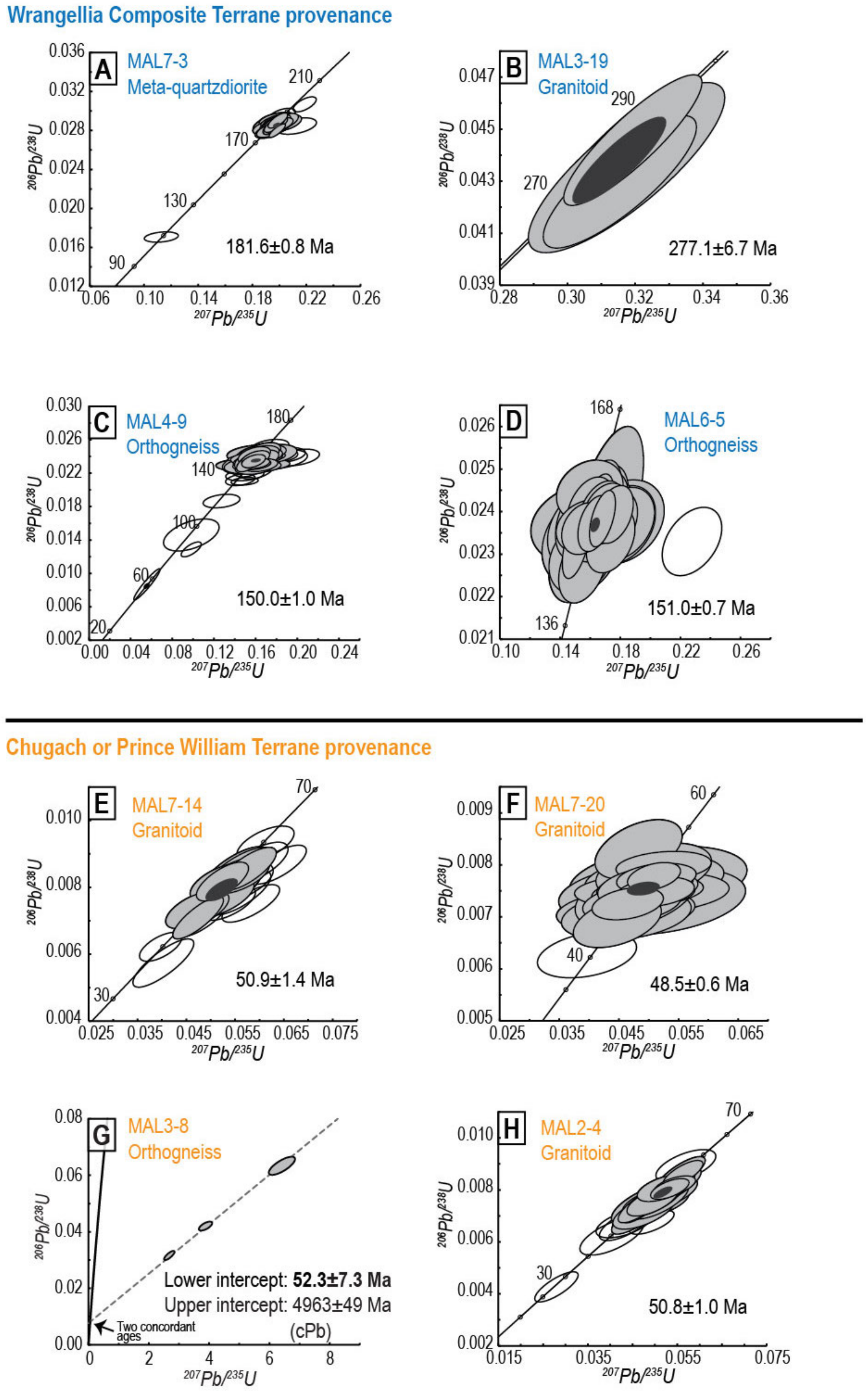

Figure 4-2, continued on next page

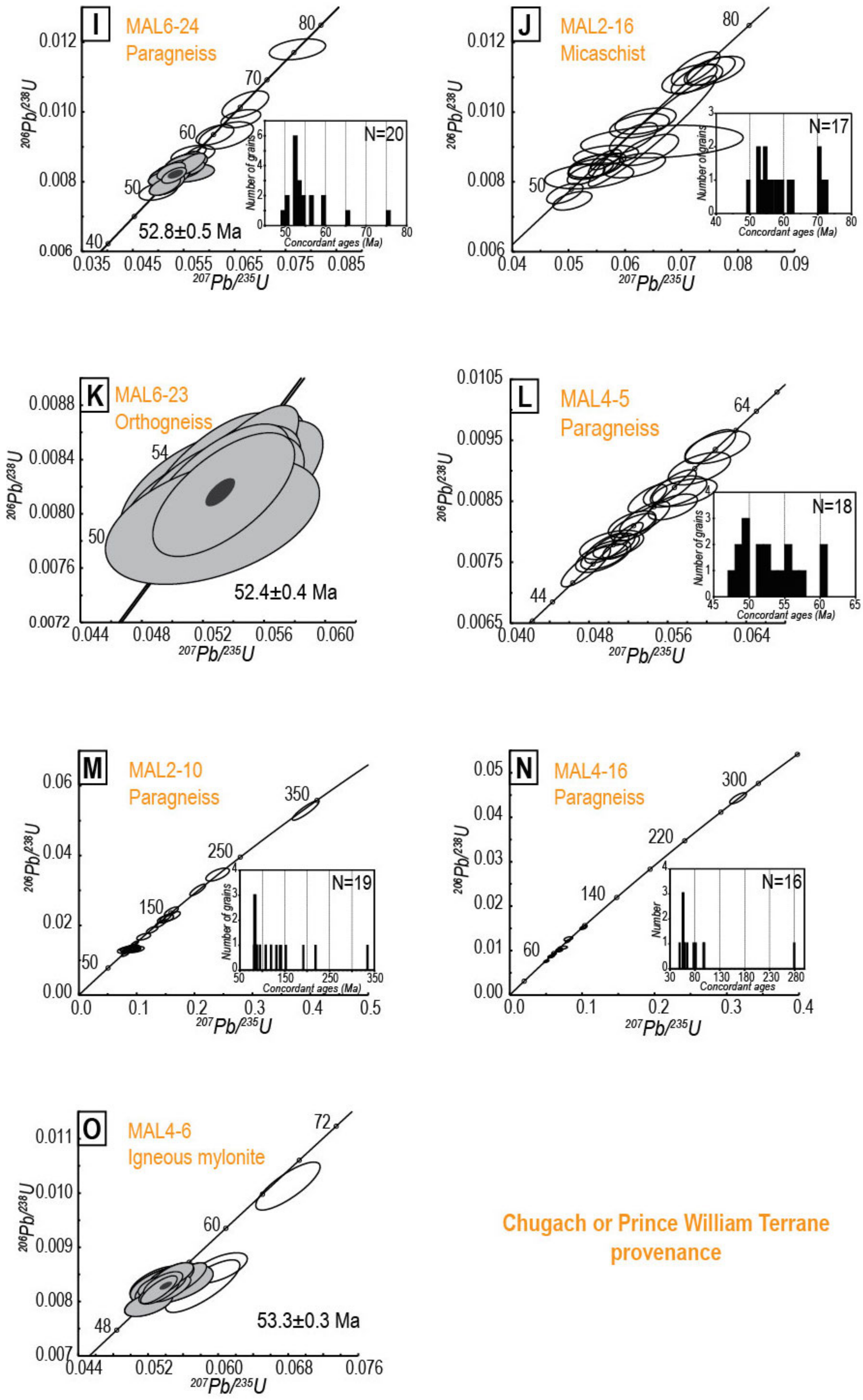

Figure 4-2, continued on next page

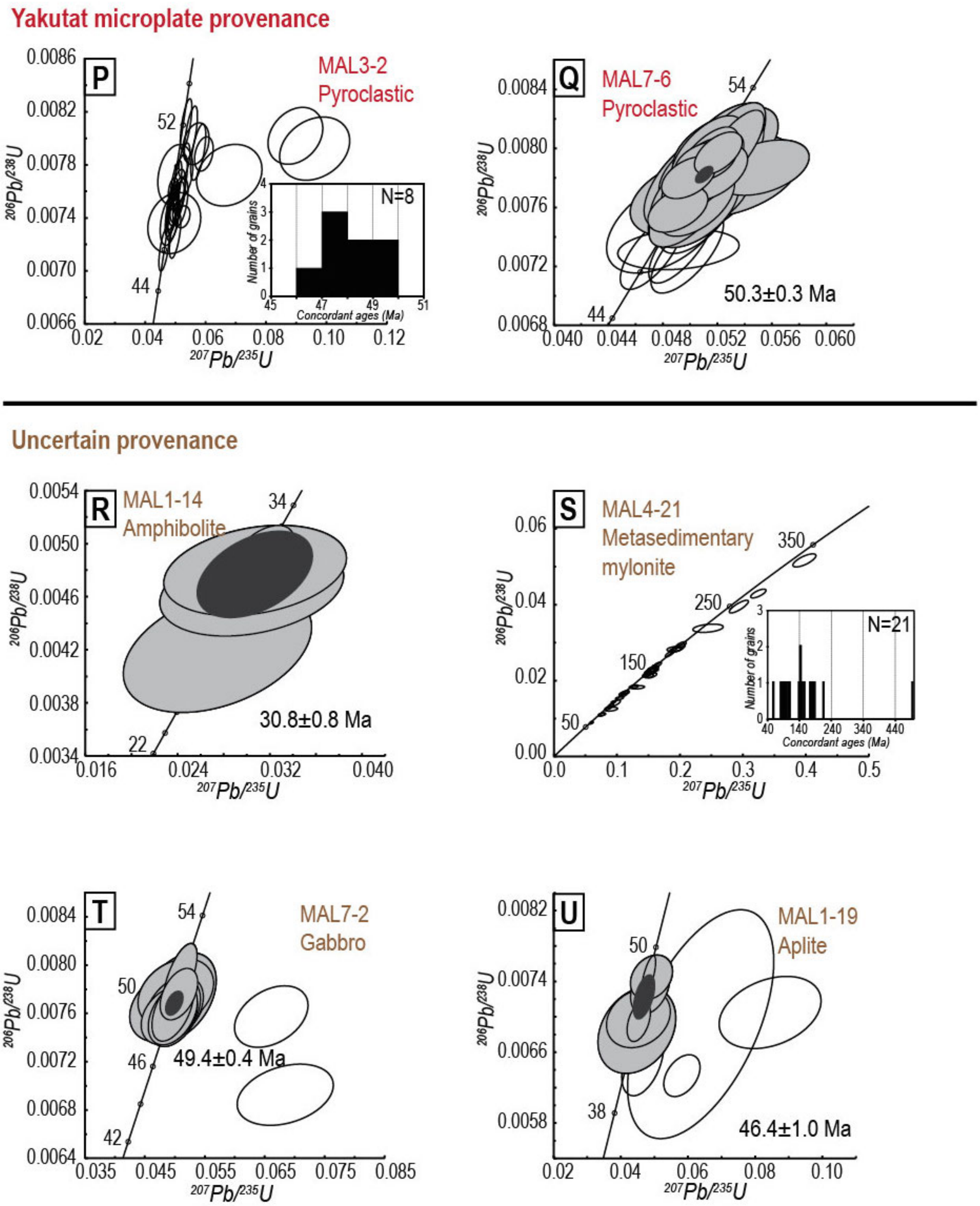

Figure 4-2A–U. Concordia diagrams of all MAL samples analyzed for U-Th-Pb, sorted by sample provenance. Additional histograms with concordant ages are given for (meta-)sedimentary samples. Ages used for concordia age calculation are presented by grey ellipses; hollow ellipses have been excluded for concordia age calculations. Concordia ages are marked with filled black ellipses. Error ellipses and age errors are 2 σ. Data were plotted using ISOPLOT add-in for Microsoft Excel. Single-grain analyses can be found in Appendix B (Table B-1).

quartzdiorite), and iii) one profile characterized by a combination of argon loss and excess argon (gabbro MAL7-2) (Table 4-2, Figure 4-3L,H, and N). However, for MAL7-2, the inverse isochron data in combination with its crystallization age of ~49 Ma (Table 4-1) justifies the use of an age of 42.0±2.7 Ma (Table 4-2). The seven biotite $^{40}Ar/^{39}Ar$ cooling ages of the cobbles range between 50.4±0.2 Ma and 41.8±0.3 Ma, which are all plateau ages comprising at least 75% of the ^{39}Ar (Table 4-2).

Three of the four bedrock biotite $^{40}Ar/^{39}Ar$ analyses yielded interpretable cooling ages that are presented in Table 4-3 and Figure 4-3P–S as well as in Appendix B (Dataset B-2). The ages range between 42.4 ± 1.1 Ma and ~5–3.5. Ma (Table 4-3). Biotite from tonalite 03PH305A experienced argon loss and does not provide a reliable age. Argon analysis of biotite from the mylonitic tonalite 2000APa45 does not yield a robust cooling age, but suggests cooling through ~300 °C between 5 Ma and ~3.5 Ma (Table 4-3). This sample is from a tonalite intrusion of Eocene age located just north of the Fairweather Fault at its northern tip at the Hubbard Glacier terminus (Figure 4-1). The only other Pliocene $^{40}Ar/^{39}Ar$ cooling age from the St. Elias Mountains is known from an amphibolite-facies schist ~110 km farther southeast just south of the Fairweather Fault [*Hudson et al.*, 1977b]. The meaning of the age, i.e., whether it represents (localized) contact metamorphism due to an unexposed pluton or exhumational cooling, is not known [*Hudson et al.*, 1977b].

4.4.3 Zircon and apatite (U-Th)/He analysis

The new ZHe ages from the HUB cobbles are presented in Table 4-4. Three of the HUB cobbles yield reproducible ages of 34.84 ± 3.0 Ma (HUB2-2), 5.79 ± 1.33 Ma (HUB2-5), and 4.82 ± 0.02 Ma (HUB2-8). For HUB2-3 single-grain ages are 10.34 Ma and 24.18 Ma (Table 4-4). Because the younger of the single-grain ages is younger than the AFT age of that sample (17.2 ± 1.4 Ma; Table 4-5), the true ZHe age is suggested to be closer to the older of the two zircon aliquots, i.e., 24 Ma.

ZHe ages of the Seward-Malaspina cobbles were published by *Grabowski et al.* [2013]. They measured 59 Seward-Malaspina cobbles and obtained five distinct ZHe age populations: ~2.7 Ma, ~12 Ma, ~27 Ma, ~36 Ma and ~53 Ma. The youngest four of the age populations are represented in the subset of cobbles (Table 4-6). Those have been interpreted as being associated with subduction and collision processes of the Yakutat microplate with the North American Plate since the late Eocene [*Grabowski et al.*, 2013]. The new HUB cobble ZHe ages fall into the same age range (Table 4-6).

AHe ages of six MAL cobbles range between 6.52 ± 0.87 Ma and 0.64 ± 0.03 Ma (Table 4-4). This result is consistent with other published AHe ages from the wider St. Elias syntaxis area and has been interpreted in terms of high precipitation and glacial erosion rates as well as Quaternary fault activity [e.g., *Spotila and Berger*, 2010; *Enkelmann et al.*, 2015b].

Table 4-2. Summary of cobble $^{40}Ar/^{39}Ar$ ages

Sample	Lithology	Min.	Total gas age [Ma] (1σ)	WMPA [Ma] (1σ) MSWD, % of ^{39}Ar	IIA [Ma] (1σ) MSWD, $^{40}Ar/^{36}Ar$ Steps used/total # steps
HUB2-2	Granitoid	Bt	49.8±0.3	**50.0±0.3** 0.1, 88.8	50.1±1.0 0.1, 275±110 4–17/17
HUB2-8	Mylonite	Bt	49.7±0.5	**49.8±0.3** 0.01, 89.8	50.0±2.5 0.01, 267±220 4–21/21
MAL2-10	Paragneiss	Bt	50.2±0.2	**50.4±0.2** 0.2, 96.8	50.7±0.6 0.1, 261±58 3–20/20
MAL2-16	Micaschist	Bt	47.9±0.2	**48.0±0.2** 0.2, 96.0	48.0±1.4 0.2, 301±86 4–16/16
MAL3-8	Orthogneiss	Bt	41.4±0.2	**41.8±0.3** 0.1, 74.9	41.5±1.7 0.1, 372±570 7–19/19
MAL6-23	Orthogneiss	Bt	48.4±0.1	**48.7±0.2** 0.2, 93.4	49.5±0.6 0.1, 276±26 4–21/21
MAL6-24	Gneiss	Bt	48.5±0.2	**48.8±0.2** 0.2, 85.2	49.3±0.8 0.2, 274±38 6–20/20
HUB2-3	Meta-quartz-diorite	Am	248.3±0.2	na	276.0±1.8* 0.1, 308±14 25–28/28
HUB2-5	Granodiorite	Am	148.7±0.2	151.5±0.6 0.5, 26.6	**151.2±1.1** 0.1, 311±15 20–25/25
HUB2-7	Hornblende-Gabbro	Am	24.3±0.5	**25.5±0.4** 0.2, 99.8	26.1±0.6 2.8, 296±2 1–19/19
MAL1-8	Migmatitic gneiss	Am	16.3±0.5	**15.8±0.4** 0.5, 100	15.8±0.8 0.5, 306±8 1–21/21
MAL1-14	Amphibolite	Am	602.0±1.4	na	na**
MAL6-23	Orthogneiss	Am	50.9±0.1	**51.2±0.2** 0.3, 97.7	51.4±0.5 0.3, 290±12 7–25/25
MAL7-2	Gabbro	Am	62.4±0.2	na	42.0±2.7 1.4, 409±10 13–19/20
MAL7-3	Meta-quartz-diorite	Am	175.2±0.2	**181.0±0.6** 1.0, 90.2	180.6±1.4 1.8, 311±21 10–23/24

Note: Min.: Mineral; WMPA: weighted mean plateau age; MSWD: mean square weighted deviation; IIA: inverse isochron age; Bt: biotite; Am: amphibole. *Argon loss-profile with ~276 Ma as minimum crystallization age and ~139 Ma as maximum age of thermal resetting; **Very disturbed profile, no age estimate possible. Ages in bold font are used in the interpretation. Details can be found in Appendix B (Dataset B-2).

Table 4-3. Bedrock cooling ages from the Fairweather Range

Sample	T_c [°C]	60±15	180±20	250±40	300±50	Lithology, Terrane
	Lat (°N)/ Long (°W) Elevation	Apatite (U-Th)/He [Ma] (1σ)	Zircon (U-Th)/He [Ma] (1σ)	Zircon fission-track [Ma] (1σ)	Biotite $^{40}Ar/^{39}Ar$ [Ma] (1σ)	
2000APa45	60.03214/ 139.328241 309 m	-	-	-	~5–3.5	Mylonitic tonalite, CT
03PH305A	59.1281/ 138.089 88 m	1.82 ± 0.5* N=31	2.45 ± 0.17* N=2	27.5 ± 1.5* N=15	-	Tonalite, YM
03PH307A	59.4378/ 138.2429 243 m	2.34 ± 0.33* N=16	13 ± 0.8* N=2	16.5 ± 0.8* N=15	42.4 ± 1.1	Granodiorite, CT
03PH311A	60.0225/ 139.2058 1610 m	0.89 ± 0.11* N=22	1.96 ± 0.09* N=2	4.5 ± 0.3* N=15	35.3 ± 0.5	Granite, CT

Note: T_c: closure temperature of the different thermochronometric systems after *Harrison et al.* [1985], *Brandon et al.* [1998], *Farley* [2000], and *Reiners et al.* [2004]. *Ages from *McAleer et al.* [2009], who used multiple multi-aliquot AHe analysis; N: Number of grains analyzed, CT: Chugach Terrane, YM: Yakutat microplate. No reliable age could be determined for 03PH305A, possibly due to argon loss. For details of the analyses see Figure 4-3 and Dataset B-2 in Appendix B.

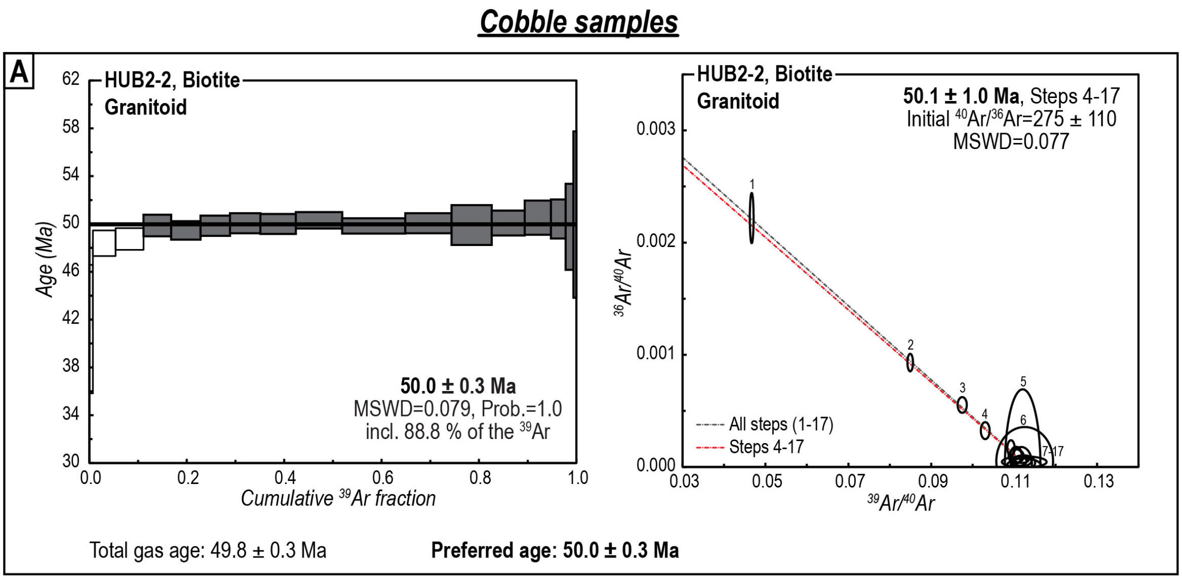

Figure 4-3, continued on next page

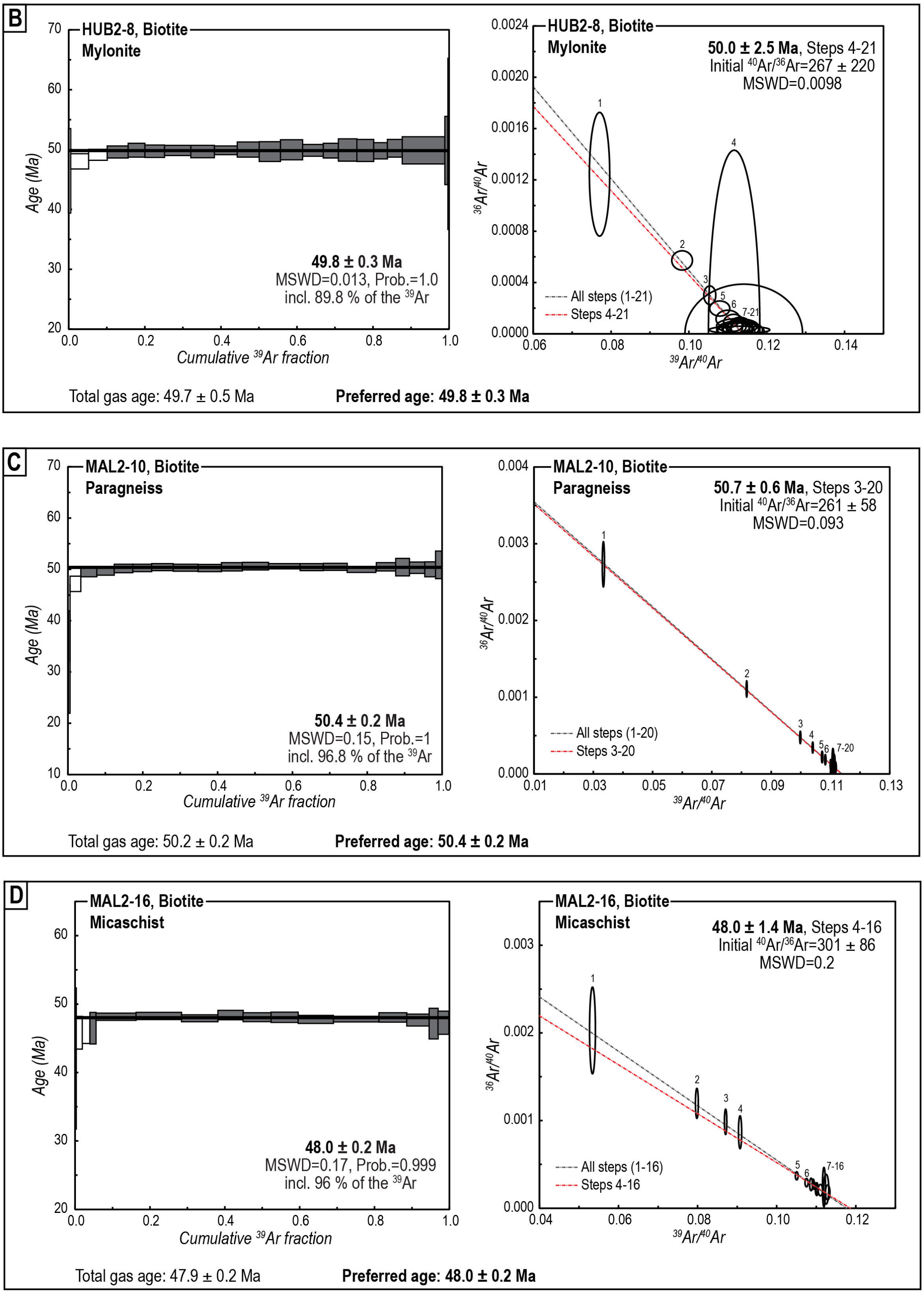

Figure 4-3, continued on next page

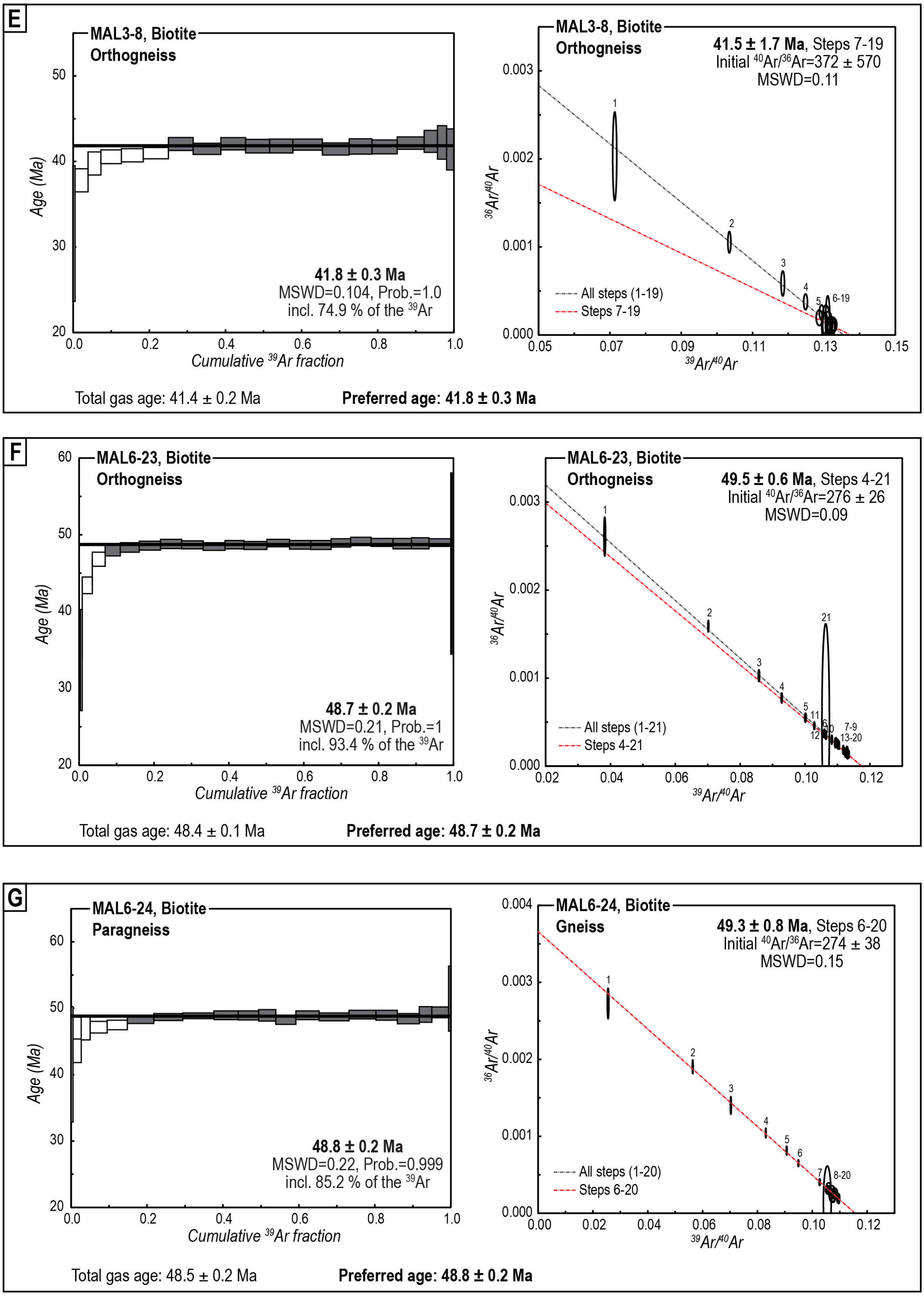

Figure 4-3, continued on next page

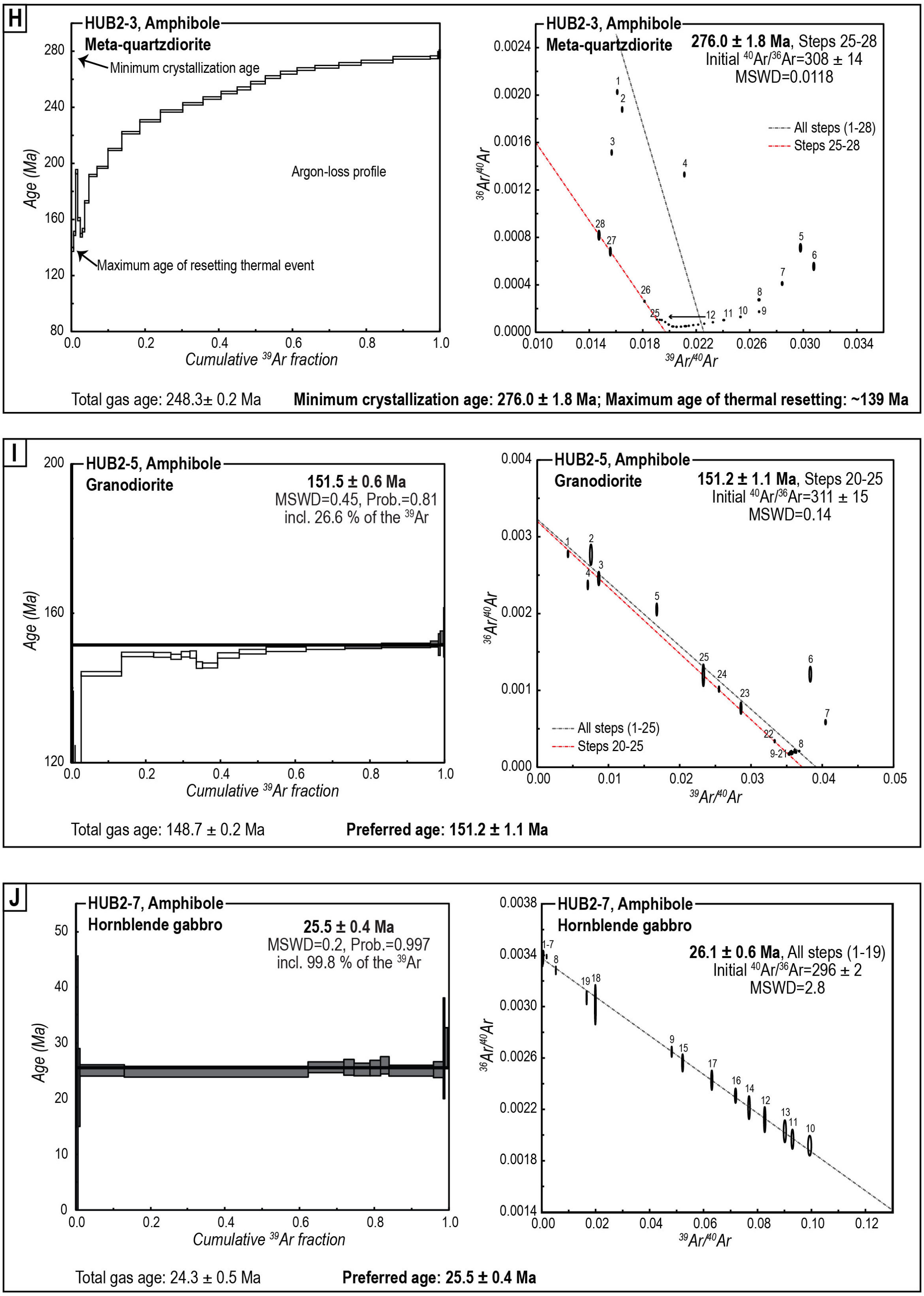

Figure 4-3, continued on next page

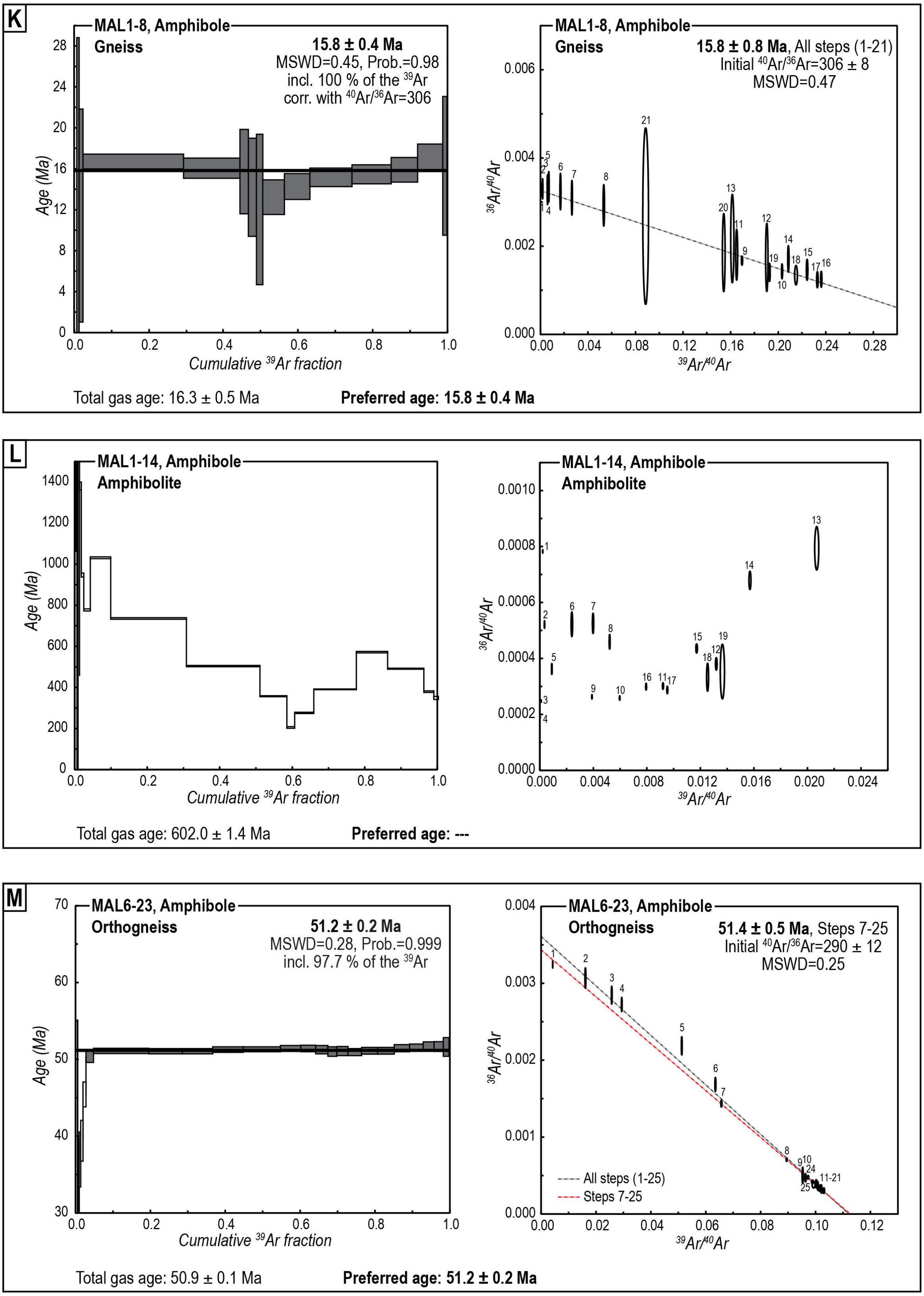

Figure 4-3, continued on next page

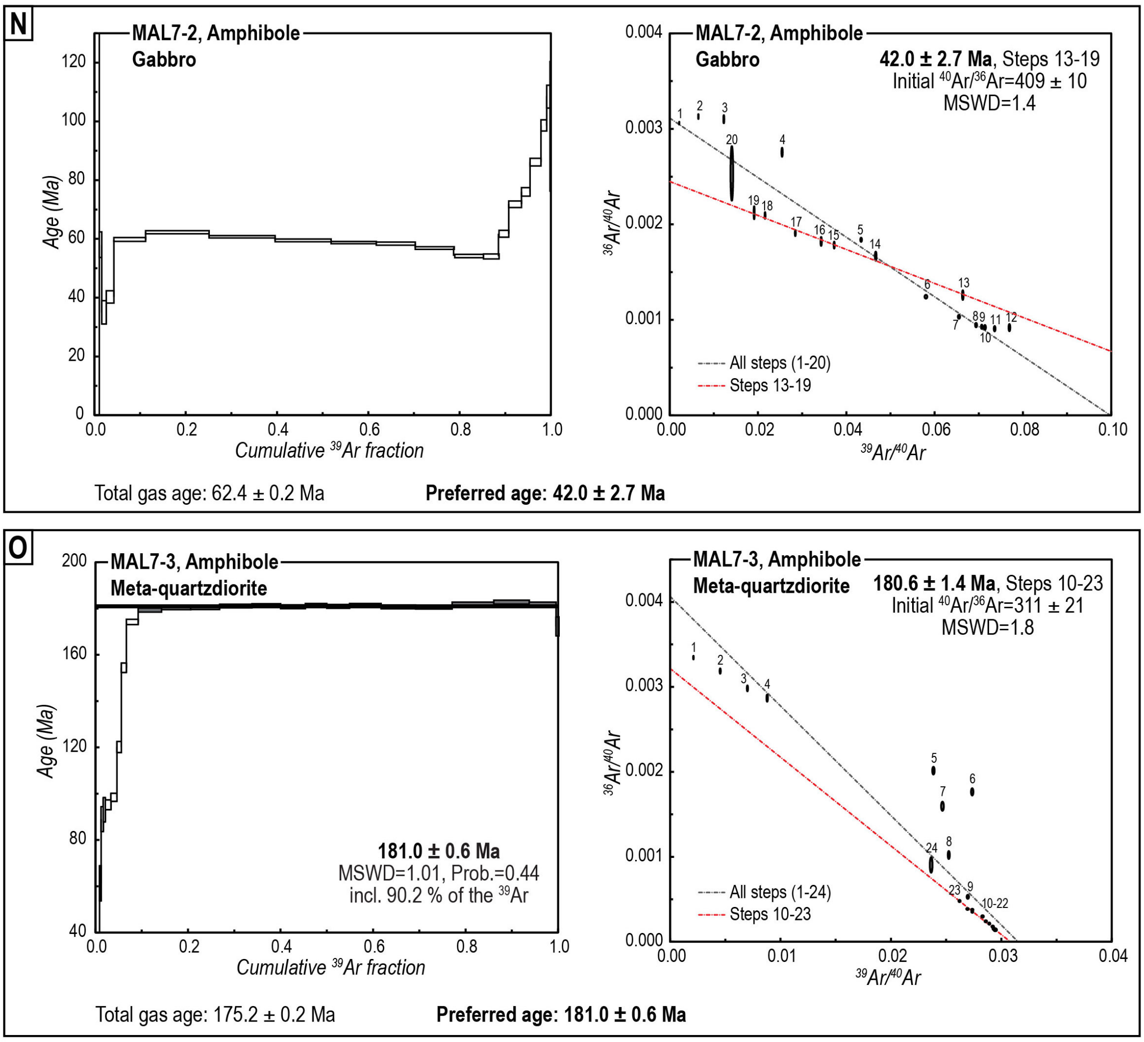

Bedrock samples

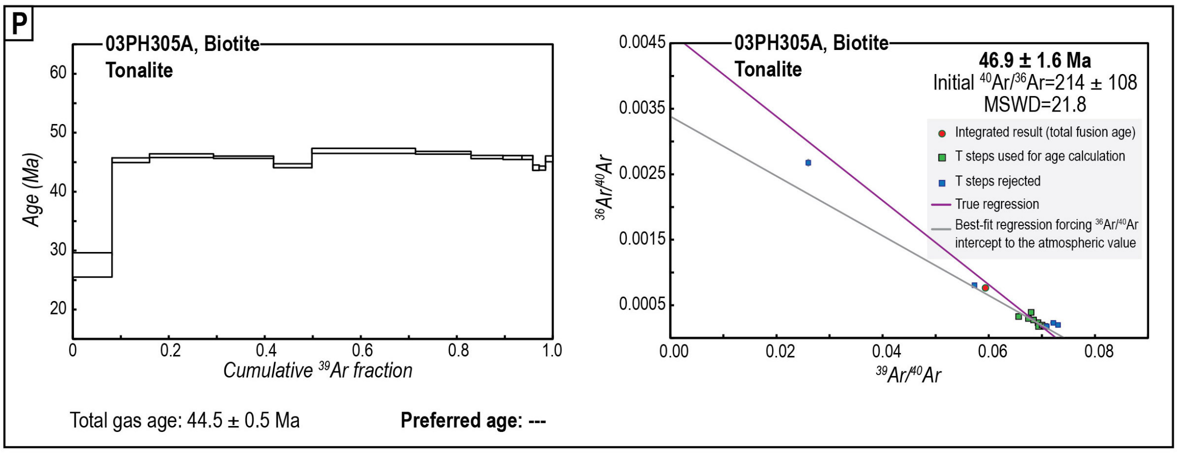

Figure 4-3, continued on next page

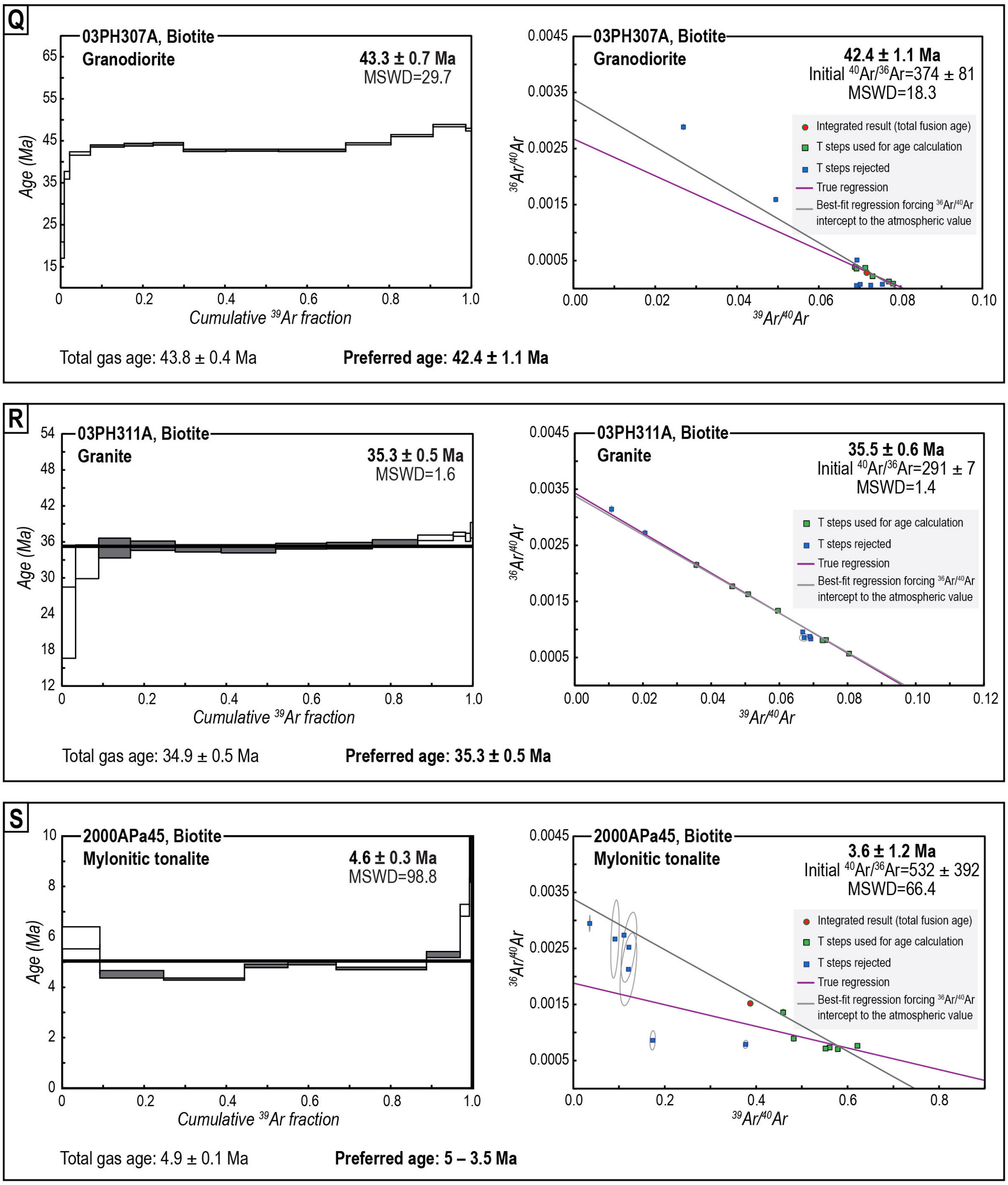

Figure 4-3A–S. Ar-Ar age spectra and inverse isochron diagrams for biotite and amphibole samples of cobbles (A–O) and bedrock (P–S). Temperature steps marked in white/grey in the age spectra are rejected from/used for the age calculation. Boxes in age spectra and ellipses in the inverse isochron diagrams represent 1 σ errors. The error ellipses in the inverse isochron diagrams of bedrock samples are often smaller than the data points (quadrangles). All ages are given with 1 σ errors. Argon analyses on biotite and amphibole separates of cobble samples were conducted at the Argonlab of the Technical University of Freiberg and data evaluation was undertaken using an in-house developed, MATLAB-based script and the Microsoft Excel Add-in ISOPLOT 3.7 [*Ludwig*, 2012]. For the atmospheric $^{40}Ar/^{36}Ar$ composition, the value of *Lee et al.* [2006] was used (298.6 ± 0.3). Problematic cobble samples are MAL7-2 and HUB2-5. Gabbro sample MAL7-2 does not yield a meaningful plateau age, likely due to a combination of argon loss and the presence of excess argon. However, the inverse isochron diagram reveals a

good correlation of steps 13–19 with an age of 42.0 ± 2.7 Ma and an initial $^{40}Ar/^{36}Ar$ of 409 ± 10. Even though the steps show a low proportion of radiogenic argon in combination with low potassium/calcium ratios, the correlation of steps 13–19 and the fact that an $^{40}Ar/^{39}Ar$ age of ~42 Ma is consistent with the U-Pb age of that sample (49.4 ± 0.4 Ma; Table 4-1) justifies using an age of 42 ± 3 Ma for MAL7-2. The amphiboles from granodiorite HUB2-5 experienced argon loss. However, taking only consistent steps 20–25 in the inverse isochron diagram yields a robust age estimate (151.2 ± 1.1 Ma) with only little excess argon and steps 20–25 also yield a plateau age of ~151.5 Ma. Therefore, the inverse isochron age is used as a best age estimate.
Analyses of biotite bedrock samples were conducted at the Noble Gas Geochronology Laboratory at Lehigh University, USA, where for the atmospheric $^{40}Ar/^{36}Ar$ composition the value of *Nier* [1950] was used (295.5). There, data were evaluated using ArArCALC [*Koppers*, 2002]. Biotite from tonalite 03PH305A experienced argon loss and does not provide a reliable age (P). Biotite from granite 03PH311A may also have experienced some argon loss, indicated by slightly lower than atmospheric initial $^{40}Ar/^{36}Ar$ values (R). Nonetheless, the plateau age of 35.3 ± 0.5 Ma is taken as best estimate, noted that it might be slightly too low. Biotite from granodiorite 03PH307A exhibits both argon loss and excess argon. Rejecting data points with too low ages, i.e., those that represent gas fractions from domains that underwent argon loss, the inverse isochron age can be used as a best age estimate (Q; Table 4-2).
For details of the analyses see Dataset B-2 in Appendix B.

Table 4-4. Zircon and apatite (U-Th)/He data of HUB and MAL cobbles

Sample ID_ Aliquot#	Mineral	4-He [mol]	238-U [mol]	235-U [mol]	232-Th [mol]	147-Sm [mol]	α-uncorrected age [Ma]	Ft	α-corrected age [Ma]	Mean age [Ma] (1σ)
HUB2-2_1	Zircon	2.01E-14	5.34E-13	3.92E-15	1.66E-13	na	27.17	0.73	36.96	
HUB2-2_2	Zircon	2.91E-14	8.52E-13	6.26E-15	2.11E-13	na	24.99	0.76	32.72	34.84 ± 3.0
HUB2-3_1	Zircon	4.37E-14	3.86E-12	2.84E-14	1.71E-12	na	7.94	0.77	10.34	
HUB2-3_2	Zircon	4.37E-14	5.80E-12	4.26E-14	4.29E-12	na	18.52	0.77	24.18	17.26 ± 9.78
HUB2-5_1	Zircon	1.04E-13	1.83E-11	1.35E-13	5.05E-12	na	4.14	0.85	4.85	
HUB2-5_2	Zircon	8.69E-14	1.07E-11	7.83E-14	4.72E-12	na	5.72	0.85	6.73	5.79 ± 1.33
HUB2-8_1	Zircon	1.85E-14	3.49E-12	2.56E-14	1.40E-12	na	3.76	0.78	4.81	
HUB2-8_2	Zircon	2.09E-14	4.08E-12	3.00E-14	1.23E-12	na	3.71	0.77	4.83	4.82 ± 0.02
MAL1-8_1	Apatite	-	-	-	-	-	-	-	-	
MAL1-8_2	Apatite	2.28E-17	1.09E-14	8.03E-17	0.00E+00	3.29E-15	1.61	0.76	2.13	
MAL1-8_3	Apatite	6.28E-18	4.48E-15	3.29E-17	0.00E+00	3.71E-15	1.08	0.70	1.54	1.84 ± 0.41
MAL2-10_1	Apatite	6.85E-15	1.15E-12	8.47E-15	0.00E+00	9.64E-13	4.58	0.78	5.90	
MAL2-10_2	Apatite	1.19E-14	1.71E-12	1.26E-14	3.21E-14	1.11E-12	5.35	0.75	7.13	6.52 ± 0.87
MAL2-10_3	Apatite	9.60E-15	5.39E-14	3.96E-16	0.00E+00	3.30E-14	135.78	0.75	~~181.02~~	
MAL2-16_1	Apatite	1.19E-15	2.94E-13	2.16E-15	2.34E-14	4.01E-13	3.06	0.77	3.99	
MAL2-16_2	Apatite	7.59E-16	1.95E-13	1.43E-15	1.84E-14	3.65E-13	2.92	0.71	4.09	
MAL2-16_3	Apatite	2.82E-15	6.31E-13	4.63E-15	3.78E-14	6.94E-13	3.39	0.75	4.54	4.20 ± 0.29
MAL3-8_1	Apatite	7.78E-17	1.42E-13	1.04E-15	1.18E-14	1.23E-13	0.41	0.63	0.66	
MAL3-8_2	Apatite	1.16E-16	1.32E-13	9.68E-16	1.48E-14	1.19E-13	0.66	0.63	1.05	
MAL3-8_3	Apatite	4.94E-17	7.26E-14	5.33E-16	3.80E-14	7.70E-14	0.47	0.59	0.79	0.83 ± 0.20
MAL6-23_1	Apatite	1.23E-14	2.79E-12	2.05E-14	1.34E-12	5.96E-13	3.07	0.77	4.00	
MAL6-23_2	Apatite	1.13E-14	2.73E-12	2.01E-14	1.55E-12	5.49E-13	2.83	0.79	3.58	
MAL6-23_3	Apatite	1.33E-14	3.83E-12	2.81E-14	1.51E-12	7.16E-13	2.47	0.75	3.29	3.62 ± 0.35
MAL7-3_1	Apatite	3.74E-16	5.17E-13	3.80E-15	6.17E-13	6.23E-14	0.44	0.67	0.66	
MAL7-3_2	Apatite	4.80E-16	2.80E-13	2.06E-15	3.29E-13	8.38E-14	1.04	0.68	~~1.54~~	
MAL7-3_3	Apatite	3.47E-16	4.89E-13	3.59E-15	5.17E-13	7.75E-14	0.44	0.71	0.62	0.64 ± 0.03

Note: Ft: α-ejection correction factor [*Farley et al.*, 1996]. MAL2-10_3 and MAL7-3_2 were rejected as outliers.

4.4.4 Apatite fission-track analysis

Three AFT ages are reported as pooled ages because they passed the χ^2-test (i.e., χ^2>5 %); they are 17.2 ± 1.4 Ma, 3.8 ± 2 Ma and 1.6 ± 1.0 Ma (1 σ; Table 4-5). HUB2-5 is reported as a mean age (4.8 ± 1.3 Ma, 1 σ; Table 4-5) as it failed the χ^2-test (i.e., χ^2<5 %), which indicates a larger scatter between single-grain ages. Reset sedimentary bedrock samples or igneous bedrock samples, as in this case, should generally pass the test, demonstrating that individual grains belong to the same cooling age population [*Galbraith*, 1981]. However, if track counts are small, as in the case of HUB2-5, where eight of 27 grains yielded zero spontaneous track counts and the remaining grains do not exceed seven spontaneous track counts, the χ^2-probablility is not a reliable statistic [e.g., *Galbraith*, 2005].

Previous studies in the syntaxis area report indistinguishable Plio-Pleistocene AHe, ZHe, and AFT ages, indicating rapid cooling of the rocks through 180 °C or 110 °C to at least 60 °C [e.g., *O'Sullivan et al.*, 1997; *Enkelmann et al.*, 2009; *McAleer et al.*, 2009; *Grabowski et al.*, 2013; Chapter 3]. Similarly, samples HUB2-3, HUB2-5, and MAL1-8 yielded indistinguishable AFT and/or He ages (Table 4-6). In contrast, HUB2-2 preserves a ZHe age (35 Ma) that may represent exhumation associated with flat-slab subduction of the Yakutat microplate, whereas the AFT age (4 Ma) reflects Pliocene tectonics and surface processes in the St. Elias syntaxis area [e.g., *Enkelmann et al.*, 2009, 2010; Chapter 3].

Table 4-5. Summary of apatite fission-track data of HUB cobbles

Sample ID	N	N_s	N_i	ρ_s [cm^{-2}]	ρ_i [cm^{-2}]	ρ_d [cm^{-2}]	χ^2 (%)	Age [Ma] (1σ)
HUB2-2	10	4	63	8.83E+03	1.06E+05	5.12E+05	14.75	3.8 ± 2.0
HUB2-3	25	206	715	1.55E+05	5.05E+05	5.07E+05	5.97	17.2 ± 1.4
HUB2-5	27	40	608	2.97E+04	3.98E+05	5.02E+05	0.006	4.8 ± 1.3
HUB2-7	8	3	108	6.67E+03	1.89E+05	4.96E+05	43.14	1.6 ± 1.0

Note: AFT ages calculated using the external detector method and a ζ-factor of 237 ± 5 cm^{2}a (E.E.) for dosimeter glass IRMM540; for χ^2>5 % the pooled age is reported, for χ^2<5 % the mean age is reported; N: number of grains dated, Ns, Ni: number of spontaneous and induced tracks, respectively; ρs, ρi: spontaneous and induced track densities, respectively, ρd: induced track density in external detector over dosimeter glass.

4.5 Discussion

Here, a discussion of the cobble provenance is followed by a discussion of their cooling histories with respect to their sources. Table 4-6 summarizes the interpretation of cobble provenance. Then, in order to put the cooling histories from the syntaxis area into a broader context and compare cobble to bedrock cooling histories, a review of available thermochronometric data and a discussion of integrated cooling histories for the orogen and their tectonic implications are provided.

4.5.1 Cobble provenance

4.5.1.1 Wrangellia Composite, Chugach Terrane, and Prince William Terrane

Early Cretaceous and older U-Pb and $^{40}Ar/^{39}Ar$ cooling ages are typical for rocks of the Wrangellia Composite Terrane [e.g., *Dodds and Campbell*, 1988; *Plafker et al.*, 1994; *O'Sullivan and Currie*, 1996; *Enkelmann et al.*, 2010]. For example, widespread Upper Jurassic plutonic rocks have been mapped at the southern margin of the Wrangellia Composite Terrane including the northern part of the Seward-Malaspina catchment and most of the Hubbard catchment [e.g., *Armstrong*, 1988; *Dodds and Campbell*, 1988; *Israel*, 2004]. The Wrangellia Composite Terrane provenance of Early Cretaceous and older cobbles becomes even more evident considering that the crystallization ages of the remaining cobbles are around 50 Ma (Table 4-6). Those ~50 Ma ages are characteristic of the early Eocene metamorphism and magmatism in the Chugach and Prince William terranes (Chugach Metamorphic Complex, Figure 4-1). The $^{40}Ar/^{39}Ar$ cooling ages of both biotite and amphibole from those cobbles yielding ~50 Ma U-Pb crystallization ages are just a few million years younger and thus indicate rapid initial cooling, which is consistent with the current understanding of the cooling history of the Chugach Metamorphic Complex [e.g., *Sisson et al.*, 2003; *Gasser et al.*, 2011].

Six metasedimentary cobbles yield detrital U-Pb age distributions (Tables 4-1 and 4-6) but the number of zircon analyses per sample (N=16–21; Table 4-1) is not high enough to quantitatively compare them to previously published detrital zircon age distributions of the studied terranes [e.g., *Gehrels et al.*, 2009; *Amato and Pavlis*, 2010; *Kochelek et al.*, 2011; *Rick et al.*, 2014]. Qualitatively, the range of the youngest zircons (55–49 Ma; Table B-1) of micaschist MAL2-16, and paragneisses MAL4-16 and MAL4-5, is typical of the Orca Group of the Prince William Terrane [e.g., *Davidson et al.*, 2011]. The occurrence of micaschist is also typical for the Prince William Terrane (Figure 4-1). The age range and distribution of paragneiss MAL2-10 (335–81 Ma) resembles that of the Valdez Group of the Chugach Terrane [e.g., *Rick et al.*, 2014]. The provenance of the metasedimentary mylonite MAL4-21 (Table 4-6) is not easily assignable and discussed in Chapter 4.5.1.3.

4.5.1.2 Yakutat microplate

The pyroclastic cobbles assigned to the Yakutat microplate (MAL3-2, MAL7-6; Table 4-6) yield crystallization ages indistinguishable from the ~50 Ma ages that were argued here to represent the Chugach Metamorphic Complex. However, their lithology is distinctly different. The cobbles are reworked pyroclastic material from early Eocene volcanic eruptions. The sediments must have been reheated, probably by burial, to have their ZHe ages reset at temperatures ≥180 °C, followed by exhumation ~8–6 Ma (Table 4-6). In the study area, such a scenario is only known for the Yakutat microplate. The only lower Eocene volcanics are the Hubbs Creek Volcanics of the Samovar Hills (arrow in Figure 4-1) (written communication with T. L. Pavlis, 2015). *Plafker* [1987]

Table 4-6. Summary of cooling ages and zircon U-Pb ages of MAL and HUB cobbles

	Cooling ages				Provenance tools	
T_c [°C]	60±15 <u>110±10</u>	180±20	300±50	500±50		
Sample	**Apatite -(U-Th)/He -<u>Fission-track</u> [Ma] (1σ)**	**Zircon (U-Th)/He [Ma] (1σ)**	**Biotite $^{40}Ar/^{39}Ar$ [Ma] (1σ)**	**Amphibole $^{40}Ar/^{39}Ar$ [Ma] (1σ)**	**Zircon U-Pb [Ma] (2σ)**	**Cobble lithology**
				Wrangellia Composite Terrane provenance		
MAL7-3	0.64 ± 0.03	3.0 ± 0.2	-	181.0 ± 0.6	181.6 ± 0.8	**Meta-quartzdiorite**; Qtz, Fsp, Hbl; Qtz and Fsp strongly altered, Hbl with cracks and inclusions
HUB2-3	<u>17.2 ± 1.4</u>	*~24 –17*	-	276.0 ± 1.8 (Min. crystall.)	-	**Meta-quartzdiorite**; strongly altered, Ser in Fsp; Chl, Bt in Am; greenschist facies, retrograde alteration
HUB2-5	<u>4.8 ± 1.3</u>	5.79 ± 1.3	-	151.2 ± 1.1	-	**Granodiorite**; Qtz, Fsp, Am
MAL3-19	-	11 ± 1.9	-	-	277.1 ± 6.7	**Granitoid;** Bt, Pl, Hbl, Opx, Cpx, Op
MAL4-9	-	32.3 ± 10.1	-	-	150.0 ± 1.0	**Orthogneiss**; Kfs, Grt, Bt, Qtz
MAL6-5	-	36.9 ± 9.9	-	-	151.0 ± 0.7	**Orthogneiss**; Qtz, Bt, Chl, Ms, Fsp
				Chugach and Prince William Terrane provenance		
MAL7-14	-	2.4 ± 0.2	-	-	50.9 ± 1.4	**Granitoid**; Fsp, Bt, Qtz, Ms, Chl
MAL7-20	-	2.5 ± 0.3	-	-	48.5 ± 0.6	**Granitoid**; Pl, Hbl, Opx, Cpx, Ap
MAL3-8	0.83 ± 0.2	2.6 ± 0.3	41.8 ± 0.3	-	52.3 ± 7.3	**Orthogneiss**; Qtz, Bt, Fsp, Px, some Ms, Ep
MAL2-4	-	13.3 ± 1.6	-	-	50.8 ± 1.0	**Granitoid** (Qtz-diorite?); Qtz, Fsp to Ser, Px
MAL6-24	-	14.5 ± 0.8	48.8 ± 0.2	-	76–50	**Paragneiss**; Bt, Fsp, Qtz, Ep
MAL2-16	4.2 ± 0.29	15.5 ± 0.7	48.0 ± 0.2	-	72–49	**Micaschist**; Bt, Chl, Fsp with Ep and Ser, Grt, Qtz
MAL6-23	3.6 ± 0.35	15.5 ± 1.5	48.7 ± 0.2	51.2 ± 0.2	52.4 ± 0.4	**Orthogneiss**; Bt, Qtz, Fsp, Cpx, some Ms
MAL4-5	-	16.4 ± 1.3	-	-	60–48	**Paragneiss**; Pl, Qtz, Bt, small Ms, small Grt
MAL2-10	6.5 ± 0.87	16.7 ± 5.6	50.4 ± 0.2	-	335–81	**Paragneiss**; Bt, Qtz, Pl, Ms, Grt

Continued on next page

		Cooling ages				Provenance tools
T_c [°C]	60±15 110±10	180±20	300±50	500±50		
Sample	**Apatite -(U-Th)/He -Fission-track [Ma] (1σ)**	**Zircon (U-Th)/He [Ma] (1σ)**	**Biotite $^{40}Ar/^{39}Ar$ [Ma] (1σ)**	**Amphibole $^{40}Ar/^{39}Ar$ [Ma] (1σ)**	**Zircon U-Pb [Ma] (2σ)**	**Cobble lithology**
MAL4-16	-	16.8 ± 2.6	-	-	279–56	**Paragneiss**; Qtz, Fsp, Bt, Chl
MAL4-6	-	29.2 ± 1.4	-	-	53.3 ± 0.3	**Igneous mylonite**; Fsp, Qtz, Bt
HUB2-2	3.8 ± 2.0	34.8 ± 3	50.0 ± 0.3	-	-	**Granitoid**; FSp, Qtz, Bt, Chl, Op (Py?)
HUB2-8	-	4.8 ± 0.02	49.8 ± 0.3	-	-	**Mylonite**; Qtz, Fsp, Bt, Am; few Am altered
			Yakutat microplate provenance			
MAL3-2	-	6.2 ± 1	-		50–46	**Pyroclastic**
MAL7-6	-	8.4 ± 1.9	-		50.3 ± 0.3	**Pyroclastic**
			Uncertain provenance			
MAL1-14	-	2.2 ± 0.3	-	-	30.8 ± 0.8	**Amphibolite**; Act, Pl
MAL1-19	-	2.3 ± 0.4	-	-	46.4 ± 1.0	**Aplite**; Fsp, Qtz, Grt; magmatic formation
MAL1-8	1.84 ± 0.41	2.4 ± 0.5	-	15.8 ± 0.4	-	Fine-grained, strongly deformed migmatitic **gneiss**; Am, Fsp, Ep; Ep developing in foliation, Am a little altered
MAL7-2	-	3.2 ± 1.03	-	42.0 ± 2.7	49.4 ± 0.4	**Gabbro**; 80% Pl, light green Am, Cpx in Am strongly altered, no/low metamorphic grade
MAL4-21	-	20.5 ± 1.3	-		493–58	**Metasedimentary mylonite**; Bt, Grt, Ep, Ms, Qtz, Kfs
HUB2-7	1.6 ± 1.0	-	-	25.5 ± 0.4	-	**Hornblende-gabbro**; Hbl, Pl, Qtz; medium-grained

Note: Cobbles are sorted by their provenance. T_c is the closure temperature of the thermochronometric systems after *Farley* [2000], *Gleadow and Duddy* [1981], *Reiners et al.* [2004], *Harrison et al.* [1985], *Harrison* [1981]. ZHe data of MAL cobbles from *Grabowski et al.* [2013]. Mineral abbreviations following *Kretz* [1983]. Min. crystall.: minimum crystallization age.

described the sequence as hundreds of meters of basalt, agglomerate, and tuff that overlie, possibly conformably, rocks of the Yakutat Group. Whole-rock K-Ar minimum crystallization ages and biostratigraphy of the overlying unit support an age of about 50 ± 3.9 Ma [*Plafker*, 1987]. Thus, the age of the Hubbs Creek Volcanics corresponds to the zircon U-Pb ages of the two pyroclastic cobbles. Resetting of the ZHe system through reheating may have occurred with burial by Eocene–Holocene sediments. Mid-Eocene to upper Miocene–lower Pliocene strata are missing due to an erosional event some time between the early Miocene and the latest Miocene–earliest Pliocene [*Chapman et al.*, 2012]. If those sediments were thick enough (at least 6–7 km with an assumed paleo-geothermal gradient of 25–30 °C/km) the scenario fits the crystallization age and latest Miocene exhumation of the two cobbles (Table 4-6).

4.5.1.3 Cobbles of uncertain provenance

The provenance of six cobbles is unclear, because their crystallization and cooling ages are either not known from the study area (MAL1-8, MAL1-14, MAL1-19, MAL7-2, HUB2-7; Table 4-6), or not distinct (MAL4-21; Table 4-6). The metasedimentary mylonite MAL4-21 yields a U-Pb single-grain age distribution of 493–58 Ma, with most ages 190–80 Ma (Tables 4-1 and B-1). The range and distribution does neither resemble Valdez nor Orca Group, and no $^{40}Ar/^{39}Ar$ cooling ages are available (Table 4-6). The overall age distribution and the range of youngest zircons in sample MAL4-21 is similar to the mélange of the McHugh Complex, the northernmost and oldest belt of the Chugach accretionary complex that has been mapped in Prince William Sound and a potential equivalent on Baranof Island (Figure 2-7A) [*Haeussler et al.*, 2005; *Amato and Pavlis*, 2010], but is not known from the study area. The U-Pb single-grain age distribution is also similar to the distribution of the Yakutat Group exposed in the Seward-Malaspina catchment [*Enkelmann et al.*, 2009]. Thus, this cobble could be either from the Border Ranges suture zone in the oldest, northernmost belt of the Chugach Terrane, if it occurs continuously along the entire terrane, or from the Yakutat Group close to the Yakutat-Chugach suture zone (Fairweather-Contact Fault connection; Figure 4-1). Both faults have been active at different times during the Cenozoic to cause the mylonitic fabric [e.g., *Roeske et al.*, 2003; *Bruhn et al.*, 2004].

Three cobbles of uncertain provenance have younger than Eocene zircon U-Pb crystallization or amphibole $^{40}Ar/^{39}Ar$ cooling ages. The amphibolite MAL1-14 yields a U-Pb age of 30.8 ± 0.8 Ma, and the migmatitic gneiss MAL1-8 and the gabbro HUB2-7 have amphibole $^{40}Ar/^{39}Ar$ cooling ages of 15.8 ± 0.4 Ma and 25.5 ± 0.4 Ma, respectively (Table 4-6). Only a few ages have been reported that are that young: conventional K-Ar ages and $^{40}Ar/^{39}Ar$ ages ranging between ~23 Ma and ~15 Ma from the Fairweather Range, particularly from the Chugach Terrane in the Nunatak Fjord and Hubbard terminus areas (Figure 4-1) [e.g., *Hudson et al.*, 1977a,b; *Loney and Himmelberg*, 1983; *Smart et al.*, 1996; *Sisson et al.*, 2003; *Gasser et al.*, 2011]. *Gasser et al.* [2011] interpreted the $^{40}Ar/^{39}Ar$ cooling ages of the Nunatak area as a slower cooling of the Chugach Metamorphic Complex than in its western and central parts west of the syntaxis due to differences in convergent components at the plate margin. *Sisson et al.* [2003] associated an early Miocene amphibole $^{40}Ar/^{39}Ar$ cooling age with an eastward tilting of the area east of the Fairweather Fault and then a later, Neogene cooling due to uplift and exhumation in response to deformation in the Fairweather fault zone.

An alternative to explaining the $^{40}Ar/^{39}Ar$ cooling age of gabbro HUB2-7 with exhumational cooling at the plate boundary is thermal relaxation after Oligocene intrusion, which might also be reflected by the 30.8 ± 0.8 Ma U-Pb age of amphibolite MAL1-14 (Table 4-6). Mafic intrusions are not mapped within the study area, but are known from a narrow mafic-ultramafic belt farther southeast in the Fairweather Range, and as far south as Chichagof and Baranof islands (Figure 2-7A). These intrusions have been interpreted as being associated with transpression at the Fairweather Fault [e.g., *Rossman*, 1963; *Plafker and MacKevett*, 1969; *Loney et al.*, 1975; *Loney and Himmelberg*, 1983]. As the St. Elias syntaxis area is extensively ice-covered, hitherto undetected Oligocene mafic intrusions may occur in the Hubbard and Seward Glacier region as well, either due to in place intrusion or displacement along the Fairweather Fault. The only known occurrence of a possibly Oligocene gabbro is at Mt. Newton, just east of Mt. St. Elias (Figure 4-1) [*Hudson et al.*, 1977b; *Dodds and Campbell*, 1988].

In summary, a Chugach Terrane origin of the uncertain cobbles is most likely, a Yakutat microplate origin is possible, and a Wrangellia Composite Terrane origin is unlikely.

4.5.2 New cooling histories from the St. Elias syntaxis

The time-temperature plot of Figure 4-4 shows the new cooling ages from the Seward-Malaspina and Hubbard-Valerie cobbles and the three bedrock samples from the Fairweather Range. By combining similar cooling paths of different samples, five dominant paths (1–5 in Figure 4-4B, C) can be distinguish Cooling path 1 comprises the majority of cobbles with Chugach and Prince William provenance and is characterized by rapid early Eocene cooling to ~300 °C after early Eocene crystallization and metamorphism in the Chugach Metamorphic Complex, followed by a period of slowed cooling reflected by ~37–2.5 Ma ZHe ages (Figure 4-4B).

Cooling path 2 combines Chugach and Prince William Terrane cobbles exhibiting renewed acceleration of cooling to ZHe closure in the Miocene. Further cooling to AHe closure and surface temperature occurred in the late Miocene–Pleistocene (Figure 4-4C), which are interpreted as exhumational cooling in the absence of heat sources in the study region at that time [e.g., *Plafker et al.*, 1994]. Other cobbles and a bedrock sample (03PH311A) of the Chugach and Prince William Terrane did not cool to ZHe closure in the Miocene, like those of path 2, but during a rapid cooling phase in the Plio-Pleistocene (path 3 in Figure 4-4B, C). Not only rocks of the Chugach and Prince William but also of the Wrangellia Composite Terrane and possibly of the Yakutat microplate (uncertain provenance cobbles) cooled rapidly through ZFT to AHe closure temperatures in the St. Elias syntaxis area (Figure 4-4C). This cooling path 3 may describe the same path as detrital sand samples from the syntaxis that led to the confine-

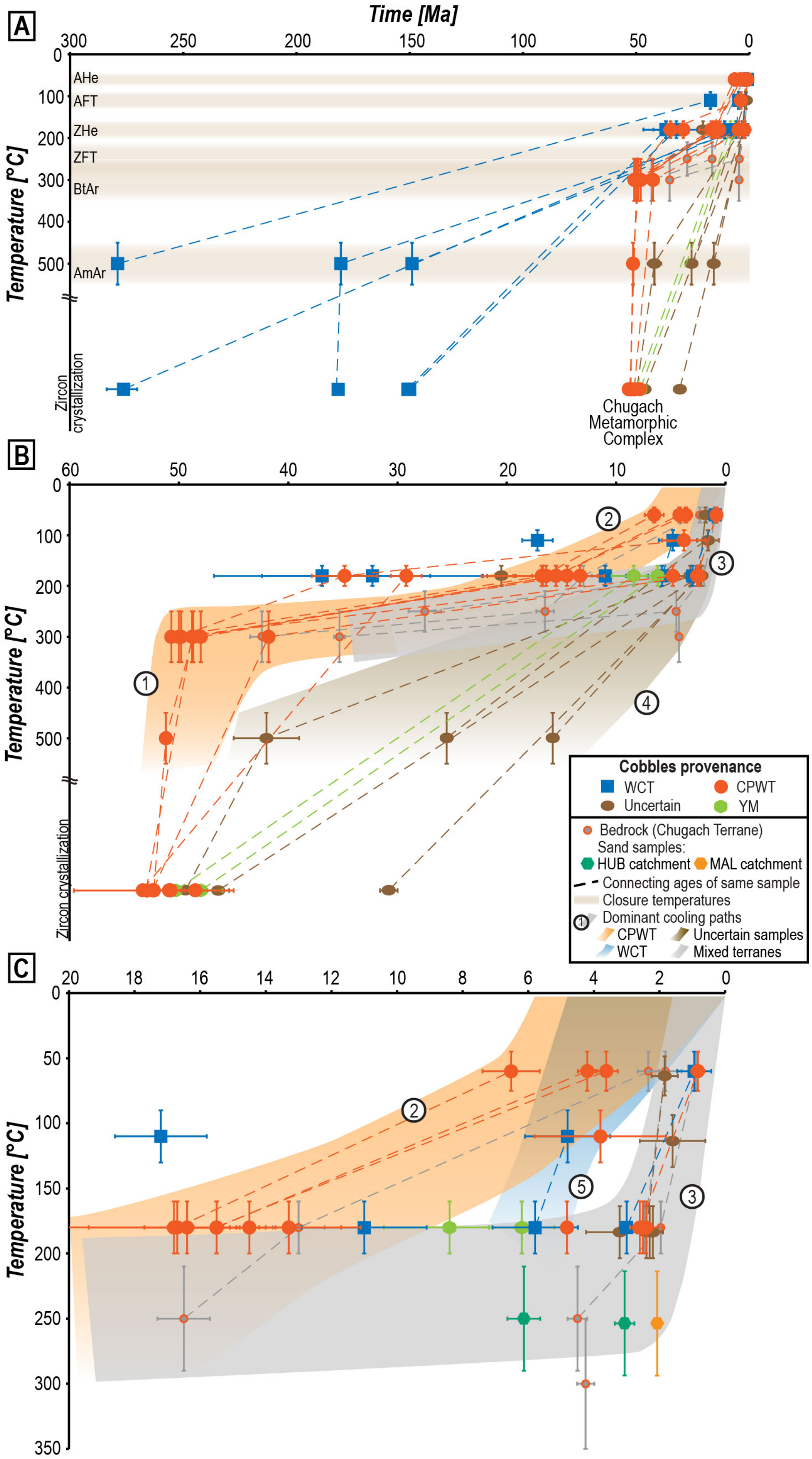

Figure 4-4A–C. Time-temperature plots of all cooling ages from this chapter and previous thermochronometric ages of the three bedrock samples with new $^{40}Ar/^{39}Ar$ ages (A), zoomed into 60–0 Ma (B) and 20–0 Ma (C). Dominant cooling paths are marked in colored bands and numbered in (B) and (C). The colors of the paths relate to the provenance of the samples describing the path. In (C), the youngest ZFT cooling age populations of sand samples from the MAL and HUB catchments are given for comparison (see text for details).

ment of the area of rapid, deep exhumation (inset map in Figure 4-1) [*Enkelmann et al.*, 2009; Chapter 3]. The youngest ZFT age population from three Seward-Malaspina sand samples is 2.1 ± 0.1 Ma with 30 % of the grains dated (N=312; yellow polygon symbol in Figure 4-4C) and the youngest two ZFT age populations from a Hubbard-Valerie sand sample are 6.1 ± 0.5 Ma and 3.1 ± 0.3 Ma with 46 % and 39 % of the grains dated (N=105; dark green polygon symbols in Figure 4-4C). The fact that cobbles from different terranes exhibit this cooling pattern supports the conclusions by *Grabowski et al.* [2013], who suggested based on the lithology of the cobbles with young ZHe ages a large areal extent of rapid exhumation in the Seward-Malaspina catchment and beyond.

Cooling path 4 combines the cobbles of uncertain provenance that yielded younger than early Eocene crystallization or amphibole $^{40}Ar/^{39}Ar$ cooling ages (Figure 4-4). Eocene to Miocene cooling is poorly confined and different for all cobbles in this group but for the lower-temperature cooling, this path follows the Plio-Pleistocene part of path 3 with the exception of MAL4-21, which has a ZHe age of ~21 Ma (Figure 4-4B).

Cooling path 5 highlights the rapid cooling from ZHe to AFT closure of a Wrangellia Composite Terrane cobble at ~5 Ma, similar to cooling observed at Mt. Logan [*O'Sullivan and Currie*, 1996].

4.5.3 Regional cooling histories

A discussion of the St. Elias syntaxis cooling history in a regional context requires division of the Chugach-St. Elias Mountains into four areas (Area 1–4) along orogenic strike (Figure 4-5). For each area, time-temperature plots were created and the dominant cooling paths were identified (Figures 4-6 to 4-9). Note that in the plots, bedrock and cobble cooling ages are plotted together and, with the exception of the Mt. Logan profile (Area 2; Figures 4-5 and 4-7), elevation differences are not marked.

4.5.3.1 Area 1

Area 1 is located west of the syntaxial region in the Chugach Mountains and contains only rocks from the Chugach and Prince William terranes to avoid data from the coastal, thermochronologically unreset fold-and-thrust belt [e.g., *Meigs et al.*, 2008; *Enkelmann et al.*, 2010], and the Oligocene–Recent Wrangell Volcanic Field to the north (Figure 4-5) [*Richter et al.*, 1990]. Cooling of this area is characterized by early Eocene–Oligocene post-magmatic and post-metamorphic cooling of the Chugach Metamorphic Complex (path 1) and post-Oligocene exhumational cooling of path 2 (Figure 4-6). Additionally, Oligocene–Miocene cooling of rocks from ZFT to AHe closure occurred (path 6; Figure 4-6), probably in response to flat-slab subduction of the Yakutat microplate. The younger AHe ages of this area that also describe cooling path 2 (Figure 4-6) are located at elevations >2000 m in the eastern part of the area, close to the syntaxis, where the new data also form cooling path 2 (Figure 4-4). The wide age range in the AHe ages in this area displays the high sensitivity of these thermochrono-

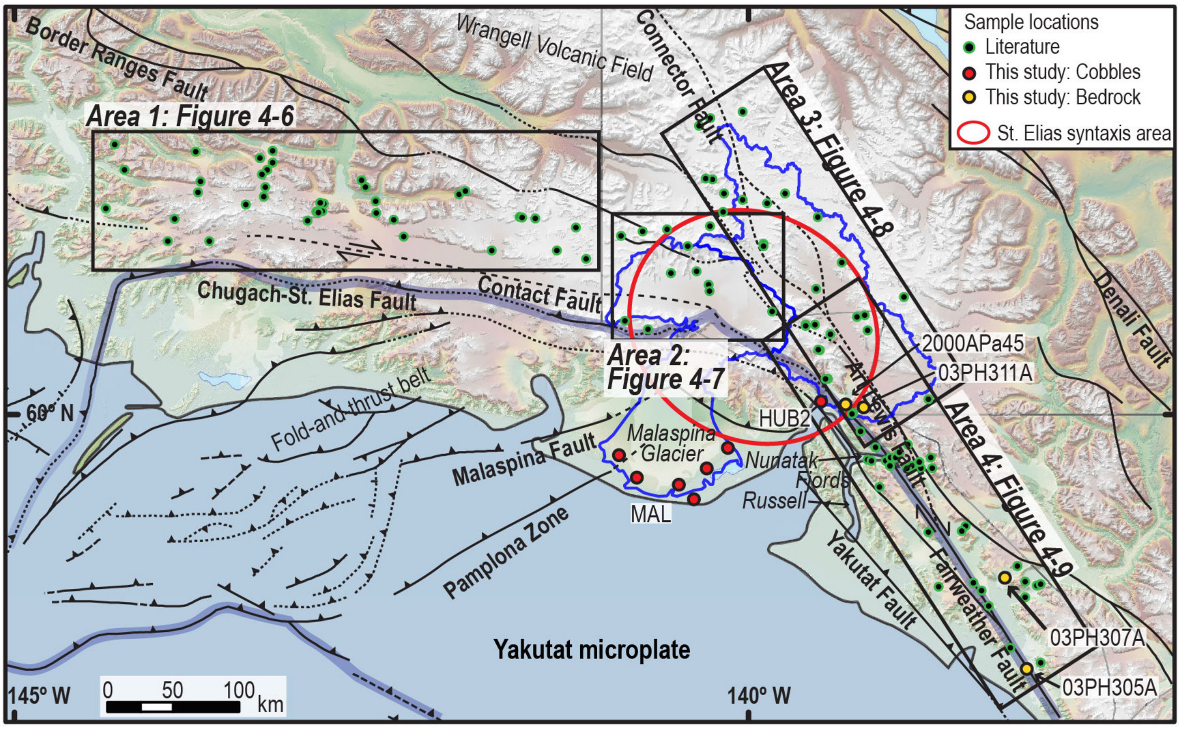

Figure 4-5. Digital elevation model of the Chugach-St. Elias Mountains and Fairweather Range showing Areas 1–4, for which time-temperature plots and cooling histories from previously published bedrock and new cobble and bedrock data were reconstructed. Details of sample locations and IDs can be found in Appendix A and B (Figures A-1 to A-4, Dataset B-3).

metric systems to changes in erosion and topography [e.g., *Ehlers and Farley*, 2003].

4.5.3.2 Area 2

Area 2 comprises the Seward Ice Field region (Figure 4-5) and includes the MAL cobbles (Figure 4-7). The main cooling paths 1–4 of the new data are supported by the few bedrock samples from this area, but additional information on the cooling history come from the ~4000 m elevation profile at Mt. Logan [O'Sullivan and Curries, 1996; Enkelmann et al., 2010; Spotila and Berger, 2010]. Paths L1, L2, and L3 represent the upper, middle, and lower part of the exposed Mt. Logan profile, respectively (Figure 4-7). As expected, samples from the lower part of the profile reveal younger cooling ages than samples collected at higher elevations. The two Wrangellia Composite Terrane cobbles that lie within uncertainty in path L1 or L2 (MAL4-9, MAL6-5; Figure 4-7) and the Chugach/Prince William cobble MAL4-6 with a ~29 Ma ZHe cooling age (Figure 4-4B) are thus very likely derived from Mt. Logan from >3000 m. The Wrangellia Composite Terran cobbles are sourced from the Jurassic Mt. Logan Batholith and the Chugach Terrane cobble from the Eocene King Peak Pluton of Mt. Logan. Mt. Logan cooling paths L1 and L2 are distinct from other post-early Eocene cooling paths (Figure 22) as these rocks were collected at higher elevations than other bedrock samples. Cobble samples complement the profile for lower, ice-covered elevations (<1780 m) and show path 3 cooling with rapid Plio-Pleistocene exhumational cooling (Figure 4-7).

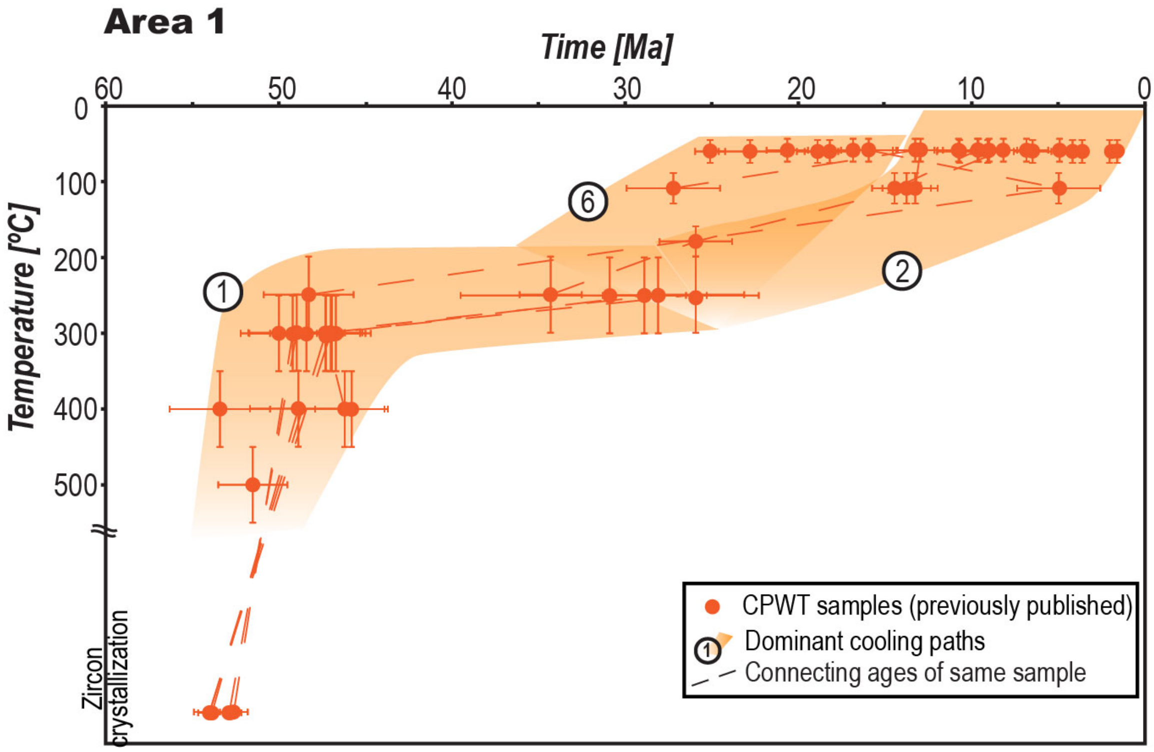

Figure 4-6. Time-temperature plot of Area 1 (cf. Figure 4-5). CPWT: Chugach and Prince Williams terranes. Data from *Hudson et al.* [1979], *Spotila et al.* [2004], *Spotila and Berger* [2008], *Berger et al.* [2008], *Meigs et al.* [2008], *Spotila and Berger* [2010], and *Gasser et al.* [2011]. Sample details in Appendix B (Dataset B-3).

4.5.3.3 Area 3

The Hubbard-Valerie catchment and immediate surroundings constitute Area 3, which includes the HUB cobbles and is mainly composed of Wrangellia Composite Terrane rocks (Figures 4-5 and 4-8). Therefore, many Paleozoic–Mesozoic ages of the higher-temperature systems are present and the Chugach Metamorphic Complex cooling of path 1 is only roughly defined by a few samples from the southern part of Area 3 (Figure 4-8). Cooling path 2 is not discernible here, but paths 3 and 4 are. Path 3 is only seen in Chugach Terrane samples in this area, but a few relatively young, Neogene Wrangellia Composite Terrane bedrock AHe cooling ages from elevations >2000 m are available from the northern syntaxis area that fit into cooling path 5 (Figures 4-4 and 4-8).

4.5.3.4 Area 4

Area 4 overlaps with the southern part of Area 3 and is the northern part of the Fairweather fault zone. Area 4 is underlain by rocks of Wrangellia Composite and Chugach terranes and Yakutat microplate (Figures 4-5 and 4-9), which explains the additional complexity of cooling histories compared to western areas. Paths 1, 3, and 4 occur here as well, but additional paths 7 and 8 are defined by Chugach Terrane and Yakutat microplate samples, respectively (Figure 4-9). Even though cooling path 1 of the Chugach Metamorphic Complex occurs here like in the areas to the west, path 7 shows a deviation from that. Samples that define path 7 are derived from the Chugach Metamorphic Complex that cooled later than path 1, around 35 Ma, to temperatures of 300 °C, but equally rapid. Other samples of the Chugach Terrane/Chugach Metamorphic Complex cooled at a slower rate and are contained in path 4, including the only sample for which a crystallization age is available in this area [*Gasser et al.*, 2011].

All of these samples are close to the Fairweather Fault and mostly from the Nunatak Fjord area (Figures 4-5 and A-4). This makes it likely that the HUB cobble of uncertain provenance (HUB2-7; Table 4-6, Figure 4-9) is derived from the Chugach Terrane west or east of the Hubbard Glacier terminus. This pattern is here interpreted as reflecting transpressional deformation at the plate boundary, especially within the zone of strain accumulation at the northern tip of the Fairweather Fault, where it begins to bend (Figure 4-5). The mylonitic tonalite 2000APa45 (Table 4-3) and schist 68Apr57F [*Hudson et al.*, 1977b] of Pliocene biotite $^{40}Ar/^{39}Ar$ ages are both located within the Fairweather fault zone (Figures 4-5, 4-9, and A-4) and indicate significant shear deformation at the Fairweather Fault in the Pliocene, when rapid exhumation began in the syntaxis and northern Fairweather Fault areas.

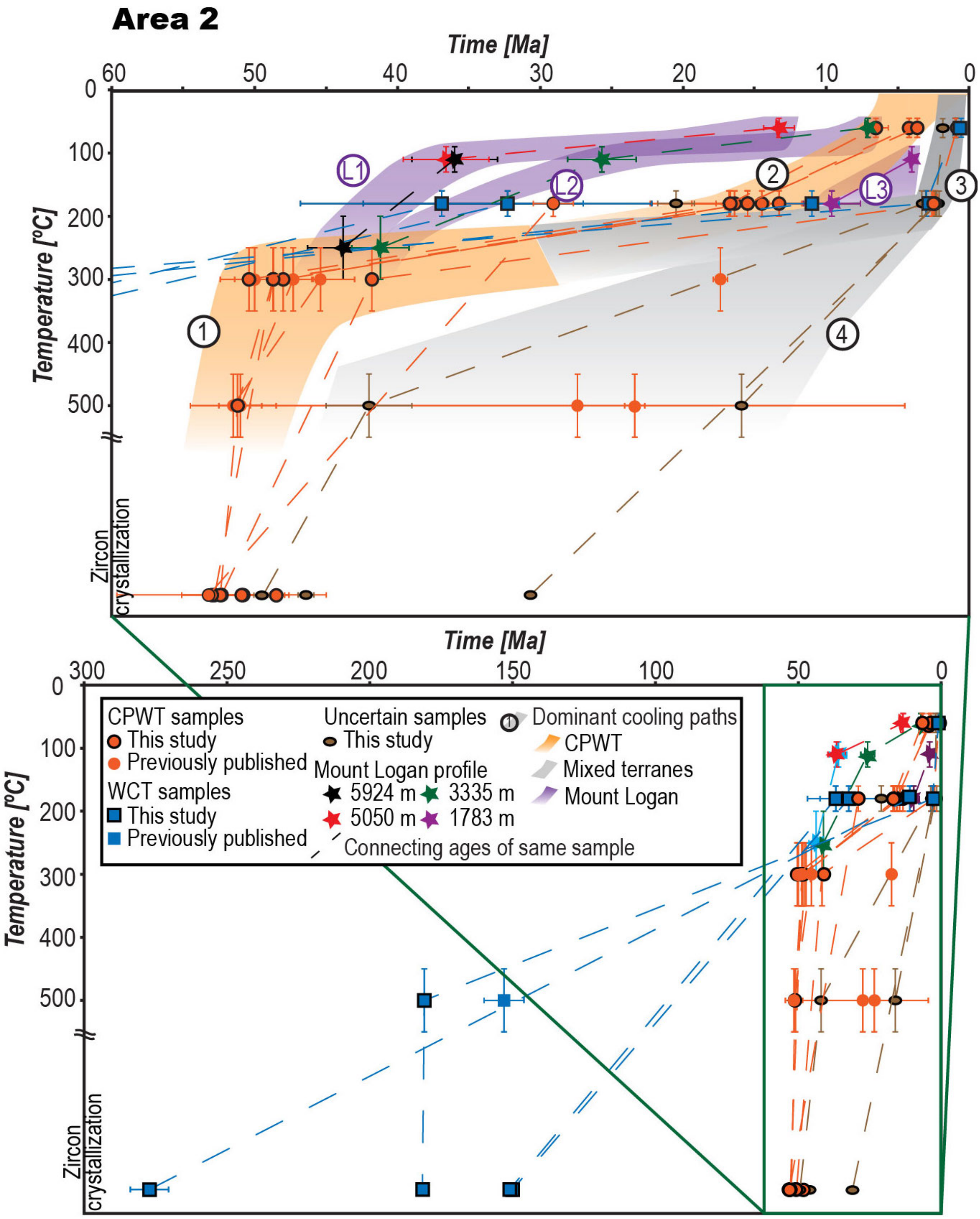

Figure 4-7. Time-temperature plot of Area 2 (cf. Figure 4-5). CPWT: Chugach and Prince Williams terranes, WCT: Wrangellia Composite Terrane. Data from *Hudson et al.* [1977a], *Dodds and Campbell* [1988], *O'Sullivan and Currie* [1996], *Enkelmann et al.* [2010], *Spotila and Berger* [2010], and this chapter. Sample details in Appendix B (Dataset B-3).

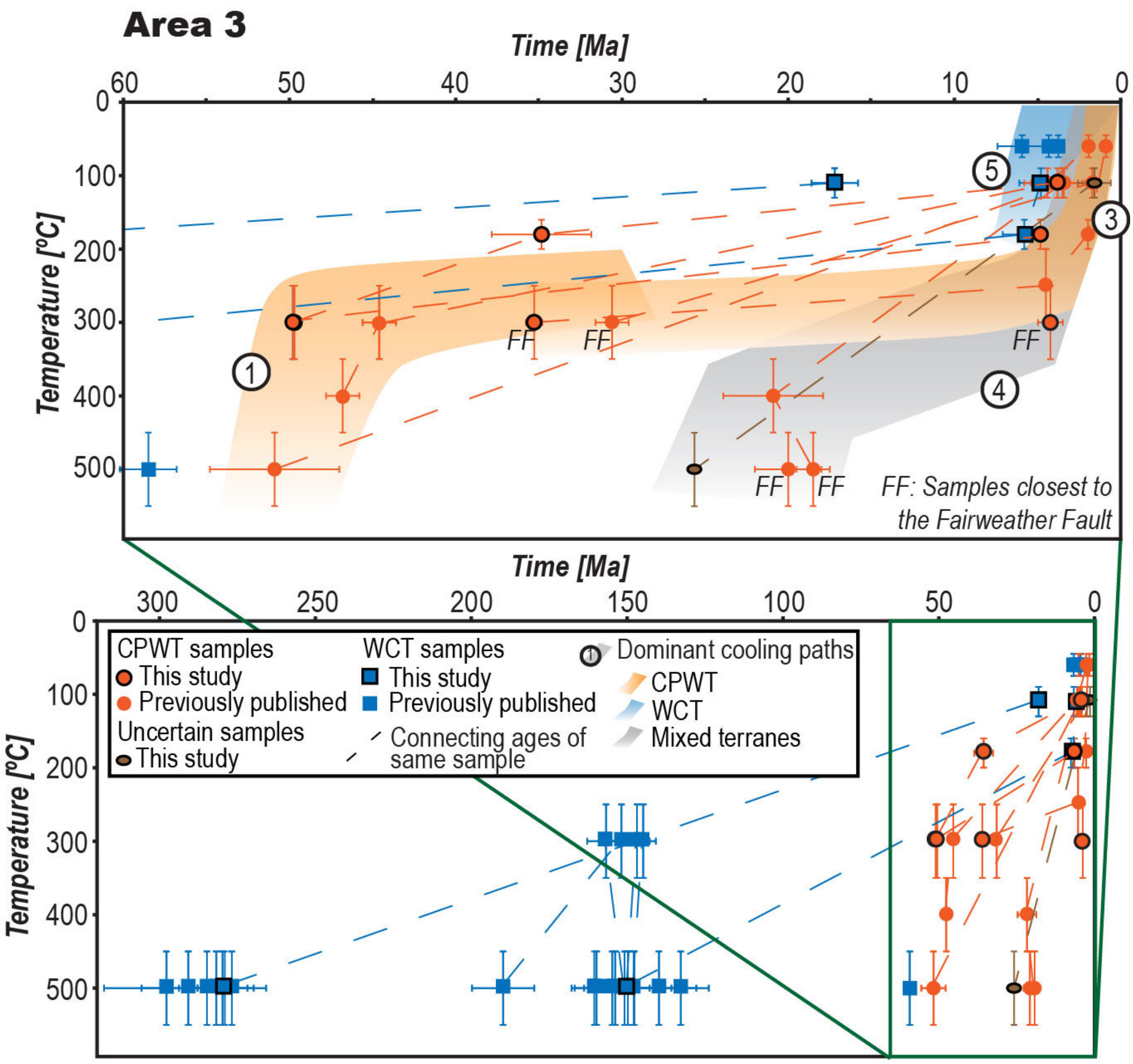

Figure 4-8. Time-temperature plot of Area 3 (cf. Figure 4-5). CPWT: Chugach and Prince Williams terranes, WCT: Wrangellia Composite Terrane. Data from *Hudson et al.* [1977a,b], *Dodds and Campbell* [1988], *O'Sullivan et al.* [1997], *McAleer et al.* [2009], *Spotila and Berger* [2010], and this chapter. Sample details in Appendix B (Dataset B-3).

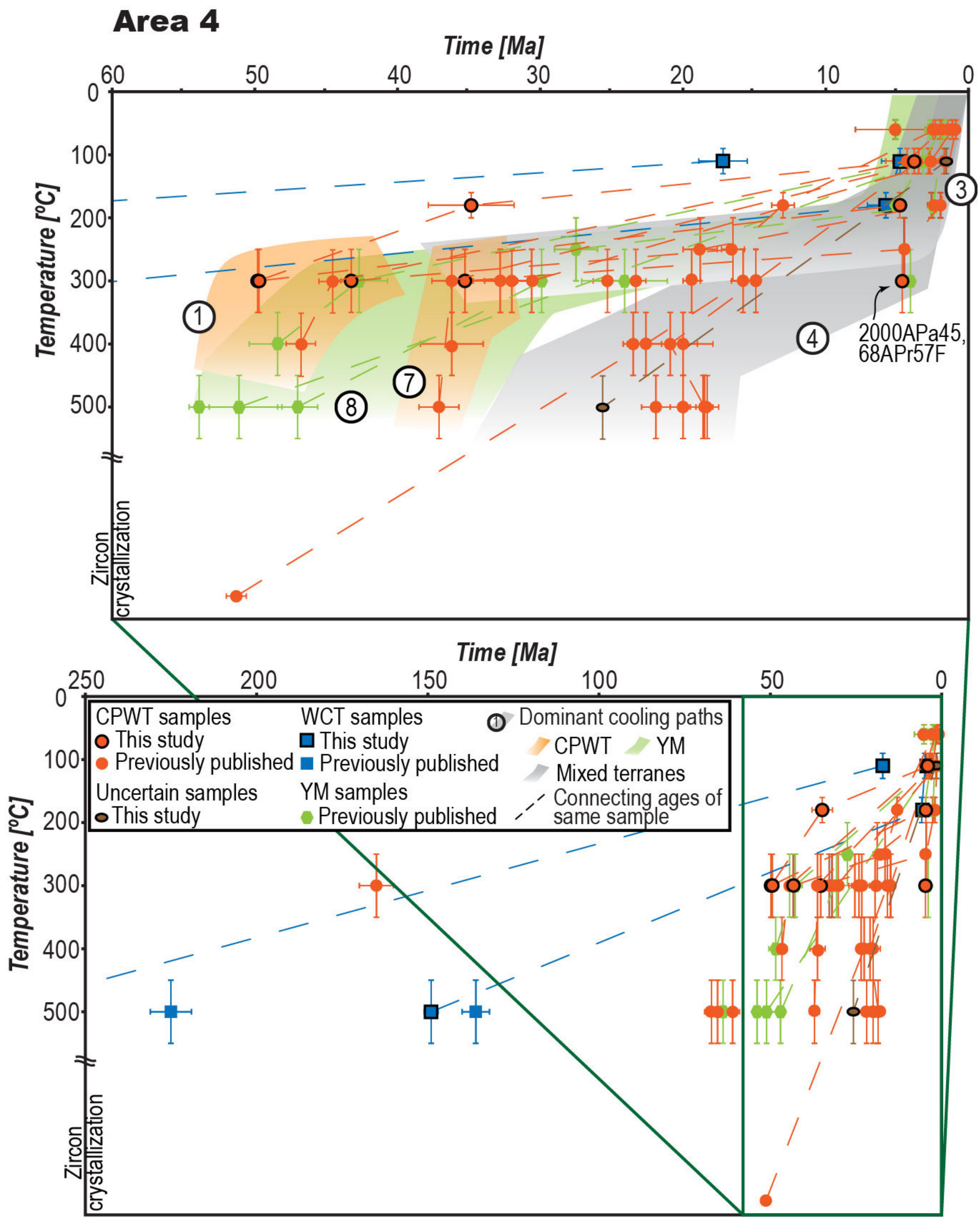

Figure 4-9. Time-temperature plot of Area 4 (cf. Figure 4-5). CPWT: Chugach and Prince Williams terranes, WCT: Wrangellia Composite Terrane, YM: Yakutat microplate. Sample IDs that are specifically named in the text are given. Data from *Hudson et al.* [1977a,b], *Dodds and Campbell* [1988], *O'Sullivan et al.* [1997], *Sisson et al.* [2003], *McAleer et al.* [2009], *Enkelmann et al.* [2015b], and this chapter. Sample details in Appendix B (Dataset B-3).

4.5.4 Summary of cooling histories of the Chugach-St. Elias Mountains

Figure 4-10 summarizes the spatio-temporally non-uniform cooling histories along the developing Cenozoic Alaskan margin. A brief interpretation of the cooling paths 1–8, as extracted from Figures 4-4 and 4-6 to 4-9, in relation to the tectonic setting and geologic events is given in Figure 4-10 as well. Additionally, Figure 4-11 displays a time scale with the main tectonic and geologic events of the study area in relation to the time-temperature plot of the main cooling paths as explained in Figure 4-10.

The compilation of thermochronometric data revealed magmatic, metamorphic, and exhumational cooling of the Chugach-St. Elias Mountains due to Mesozoic–Cenozoic accretion, subduction, and collision at the North American margin. Paleozoic–Mesozoic cooling is mostly recorded in the Wrangellia Composite Terrane north of the Border Ranges Fault, which acted as backstop to Cenozoic accretion and collision of the Yakutat microplate [e.g., *Roeske et al.*, 2003; *Enkelmann et al.*, 2008, 2010]. The Wrangellia Composite Terrane exhibits younger, Neogene and Quaternary exhumational cooling only in the syntaxis area (path 5; Figures 4-10 and 4-11) [*O'Sullivan and Currie*, 1996; *Enkelmann et al.*, 2010; *Spotila and Berger*, 2010; *Grabowski et al.*, 2013; Chapter 3].

The Eocene cooling history of the entire margin, mainly south of the Border Ranges Fault with exception of the syntaxis area, is characterized by spreading-ridge subduction, near-trench plutonism, and the formation and rapid initial cooling of the Chugach Metamorphic Complex (path 1; Figures 4-10 and 4-11) at rates of ~30–180 °C/Myr in an overall compressional tectonic setting [*Gasser et al.*, 2011, 2012]. The influence of the subsequently formed transpressional plate boundary in the eastern area becomes evident through the more variable post-Eocene cooling (paths 1, 4, 7, and 8; Figures 4-10 and 4-11). Significant transpressional deformation at the plate boundary since the Oligocene is indicated by exhumational cooling (paths 7, 8, and partly 4; Figures 4-10 and 4-11) [e.g., *Sisson et al.*, 2003; *Gasser et al.*, 2011; *McAleer et al.*, 2009; Chapter 3] and by transpression-related mafic intrusions with subsequent magmatic cooling (path 4; Figures 4-10 and 4-11) [e.g., *Rossman*, 1963; *Plafker and MacKevett*, 1969; *Loney and Himmelberg*, 1983]. Path 4 in the Fairweather Range and St. Elias syntaxis is relatively poorly confined in its >200 °C path due to highly variable cooling over short horizontal distances. Thermal overprinting and partial thermal overprinting of country rocks by Eocene–Miocene mafic intrusions (Figure 4-11) may have contributed to the variable cooling history of the eastern part of the orogen.

The effects of flat-slab subduction of Yakutat microplate since the late Eocene/Oligocene include exhumation of the upper plate as reflected in paths 2 and 6 in the syntaxis and western area (Figures 4-10 and 4-11) [e.g., *Enkelmann et al.*, 2008; *Perry et al.*, 2009]. Path 2 might also represent the mid-Miocene onset of collision between the Yakutat and North American plates (Figure 4-11), similar to signals observed in thermochronology of detrital sand samples and bedrock samples from Mt. Logan (Figures 4-4 and 4-7).

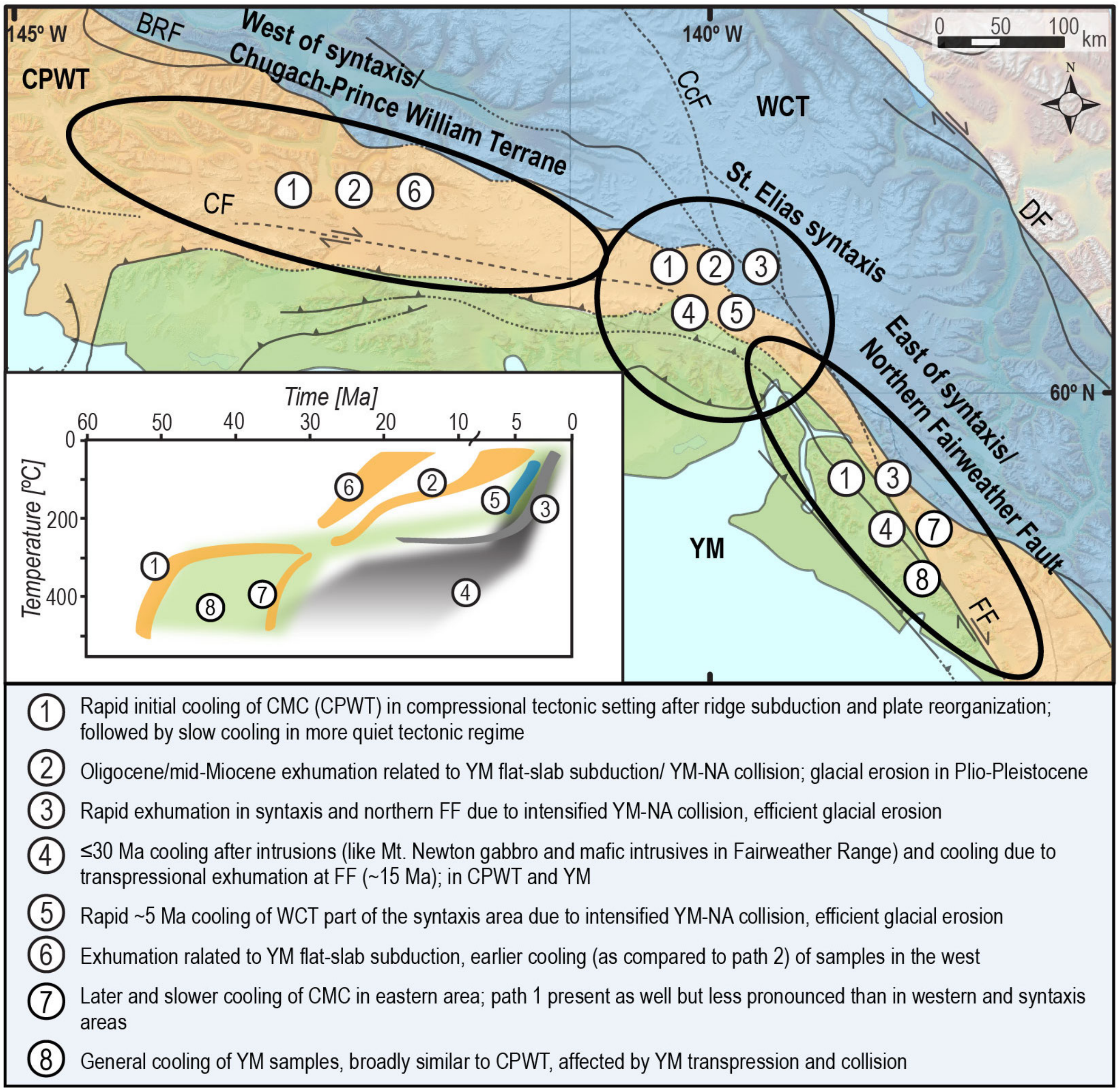

Figure 4-10. Summary of dominant cooling paths of Areas 1–4, reduced to three areas at the St. Elias syntaxis (Areas 2 and 3; Figure 4-5), and areas west (Area 1; Figure 4-5) and east (Area 2; Figure 4-5) of the syntaxis. The colors and numbers of cooling paths in the time-temperature plot correspond to cooling path numbers and colors in Figures 4-6 to 4-9 and in the map of this figure. A brief explanation of cooling paths is given at the bottom. BRF: Border Ranges Fault, CcF: Connector Fault, DF: Denali Fault, CF: Contact Fault, FF: Fairweather Fault, WCT: Wrangellia Composite Terrane, CPWT: Chugach-Prince William Terrane, YM: Yakutat microplate, CMC: Chugach Metamorphic Complex, NA: North American Plate.

Paths 3 and 5 reflect the localized, rapid Pliocene exhumation of the St. Elias syntaxis and northern Fairweather Fault areas due to the ongoing indentation of the Yakutat plate corner (Figures 4-10 and 4-11). Cooling path 3 has been revealed by detrital sand samples and is here shown mainly by cobble samples and supported by some bedrock samples of different terranes (Figures 4-6 to 4-9). Path 5 occurs in the Wrangellia part of the syntaxis and indicates an earlier onset of rapid exhumation (Figure 4-10). Processes that may have influenced deformation at the end of the Miocene include i) lateral thickening of the Yakutat microplate crust (>25 km) that enters the deformational front [*Christeson et al.*, 2010; *Worthington et al.*, 2012], ii) and increase in the convergent component of plate collision [*Engebretson et al.*, 1985], and iii) the beginning of glaciation [e.g., *Lagoe et al.*, 1993] (Figure 4-11). The localization of strain in the syntaxis area and the glaciation that intensified ~2.6 Ma due to Northern Hemisphere cooling may have led to efficient glacial erosion focused on highly stressed, easily erodible rocks in valleys [*Lagoe et al.*, 1993; *White et al.*, 1997; *Grabowski et al.*, 2013; *Headley et al.*, 2013].

4.5.5 Implications for the evolution of syntaxis exhumation

The provenance information and cooling histories obtained from cobbles help to decipher the development of exhumation in the St. Elias syntaxis, where relatively few samples have been dated so far. The most important data from the syntaxis are the Mt. Logan bedrock profile and detrital sand samples from the Malaspina Glacier [*O'Sullivan and Currie*, 1996; *Enkelmann et al.*, 2009]. It could be shown that cobbles complement bedrock and sand samples well, because they combine the advantages of both methods. Like sand-sized detritus, cobbles are derived from ice-covered and ice-free elevations, and, like on bedrock samples, multiple thermochronometric dating techniques can be applied on the cobbles. Furthermore, multi-grain analyses can be conducted on cobbles, like on bedrock, to obtain high-precision dates for, for example, the AHe system. This is not possible on sand samples, where single-grain analyses are necessary.

Cooling paths from cobbles from different elevations were obtained, which show that the onset of rapid exhumation was at ~5 Ma. Moreover, complete cooling histories could be derived for the first time from the syntaxis area and could be compared to the cooling and exhumation record from other parts of the orogen. This comparison showed similarities but also distinct differences that emphasize the transitional position of the St. Elias syntaxis between the transpressive setting of the Fairweather plate boundary in the east and the compressional and subduction setting to the west in the fold-and-thrust belt and Chugach Mountains (Figure 4-10).

The St. Elias syntaxis and the northern Fairweather fault zone, especially in the Nunatak Fjord area, have previously been established as rapidly exhuming by thermochronometric, structural, petrographic, and geophysical data, which is supported here [e.g., *Hudson et al.*, 1977b; *O'Sullivan et al.*, 1997; *Sisson et al.*, 2003; *Enkelmann et al.*, 2009; *McAleer et al.*, 2009; *Gasser et al.*, 2011; *Grabowski et al.*, 2013; *Marechal et al.*, 2015; Chapter 3]. For the first time, the higher-temperature cooling history of rocks sourced from the most rapidly and deeply exhuming area under the ice of the Seward-Malaspina and Hubbard-Valerie glaciers is provided here. This sets important brackets on the maximum amount and the duration of rapid rock exhumation, which allows comparing the St. Elias syntaxis with other regions. The St. Elias syntaxis has been compared to the eastern and western Himalayan syntaxes, where rocks of lower plate affinity and intrusions from lower crustal depth are exhumed and where <1 Ma biotite $^{40}Ar/^{39}Ar$ and ZFT ages are observed [*Zeitler et al.*, 1989, 2001, 2014; *Enkelmann et al.*,

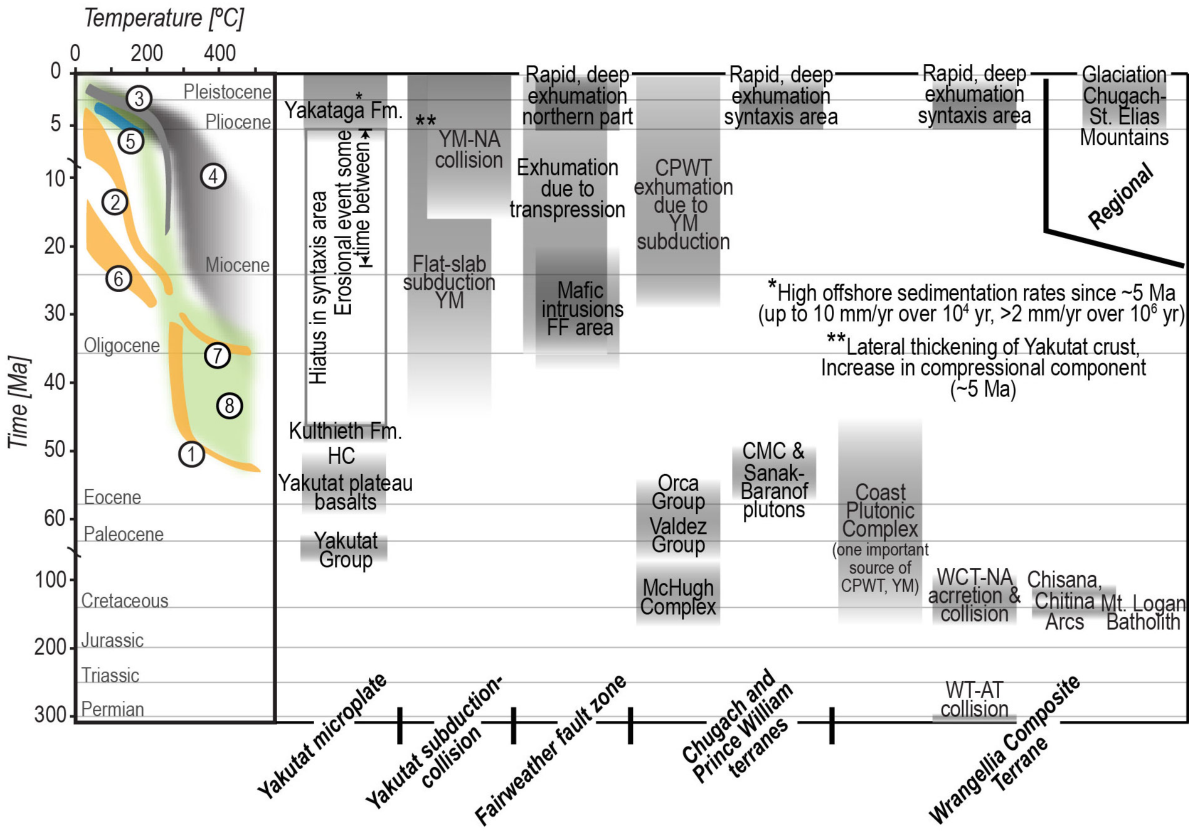

Figure 4-11. Overview of cooling histories of the Chugach-St. Elias Mountains and Fairweather Range (time-temperature plots as in Figure 4-10) and tectonic and geologic events ordered by area. Note the breaks in the time axis after 100 Ma and 10 Ma. Fm: Formation, HC: Hubbs Creek Volcanics, YM: Yakutat microplate, NA: North American Plate, FF: Fairweather Fault, CPWT: Chugach-Prince William Terrane, CMC: Chugach Metamorphic Complex, WCT: Wrangellia Composite Terrane, WT: Wrangellia Terrane, AT: Alexander Terrane. Data compiled after *Hudson et al.* [1977a,b], *Loney and Himmelberg* [1983], *Engebretson et al.* [1985], *Davis and Plafker* [1986], *Plafker* [1987], *Dodds and Campbell* [1988], *Dumoulin* [1988], *Farmer et al.* [1993], *Lagoe et al.* [1993], *Plafker et al.* [1994], *Pavlis and Sisson* [1995], *Hallet et al.* [1996], *Lagoe and Zellers* [1996], *O'Sullivan and Currie* [1996], *Sheaf et al.* [2003], *Enkelmann et al.* [2008, 2009, 2010, 2015b], *Gehrels et al.* [2009], *McAleer et al.* [2009], *Perry et al.* [2009], *Amato and Pavlis* [2010], *Finzel et al.* [2011b], *Gasser et al.* [2011], *Chapman et al.* [2012], *Worthington et al.* [2012], *Grabowski et al.* [2013], and this study.

2011]. The higher-temperature $^{40}Ar/^{39}Ar$ systems of the cobbles in the St. Elias Mountains are generally much older (Table 4-6), and rocks at the high mountain peaks reveal Eocene AFT and ZFT cooling ages [*O'Sullivan and Currie*, 1996], indicating a relatively short duration of rapid exhumation in the syntaxis area. Exhumation rates of 3 mm/yr or higher could not have been sustained for more than a few million years without producing young $^{40}Ar/^{39}Ar$ ages and removing the entire uppermost crustal layer with the older cooling record.

The amount of rapidly exhumed rocks since 5 Ma is confined between the closure temperature isotherms of the young ZFT system (>250–300 °C) and the biotite $^{40}Ar/^{39}Ar$ system (300 ± 50 °C) of the cobbles, at ~300 °C. Using a geothermal gradient of 20–30 °C/km thus suggests a maximum amount of exhumation of 10–15 km and most likely less if heat advection is taken into account [*Reiners and Brandon*, 2006]. This maximum estimate is up to 25–30 km less than the observed exhumation in the Himalayan syntaxes [*Booth et al.*, 2009].

Based on a recent synthesis of thermochronometric, geophysical, and geologic data, *Enkelmann et al.* [2015a] suggested that the high exhumation rates that developed beginning ~5 Ma in the syntaxis and north of the northernmost Fairweather Fault have decreased since ~2 Ma and that the focus of most rapid exhumation shifted southward to its current location on the deforming Yakutat microplate in the Malaspina Glacier and Disenchantment Bay area (Figure 4-1). Such a short duration of 2–3 Myr of rapid exhumation is in agreement with the observed limited amount of exhumation indicated by the higher-temperature $^{40}Ar/^{39}Ar$ data.

The only relatively young biotite $^{40}Ar/^{39}Ar$ cooling age (~5–3.5 Ma; Table 4-6) from the syntaxis area is mylonitic tonalite 2000APa45, which is not representative of the rapidly exhuming area, but directly of the Fairweather Fault. It supports a change in conditions (tectonic, climatic, erosional, or a combination of two or all mechanisms) around 5 Ma that resulted in intensified Yakutat-North American collision in the syntaxial region and significant shear on the Fairweather transform fault that resulted in the mylonitization and biotite growth or thermal resetting.

4.6 Summary

This chapter demonstrates the applicability of cobble-sized detrital thermochronology in partly inaccessible catchments without losing provenance information. Cobbles combine the advantages of bedrock and sand-sized samples. The spatial coverage of sampling in ice-covered catchments is large and multiple thermochronometric dating of unweathered mineral phases is possible, as well as multi-grain analyses.

For the St. Elias Mountains, detrital material is invaluable for obtaining an exhumation signal from the lower elevations of ice-filled valleys. By using cobbles, the exhumation record from multiple thermochronometers can be linked to provenance. The synthesis of geo- and thermochronologic data obtained from the different sampling approaches yields a comprehensive perspective on the cooling and exhumation history of the St. Elias orogen and particularly the ongoing indentation of the Yakutat plate corner in the North American margin. An onset of rapid exhumation at the syntaxis and northern side of the northern Fairweather Fault at ~5 Ma is supported by the cooling histories of cobbles from the Seward-Malaspina and Hubbard-Valerie catchments. The higher-temperature systems reveal that the amount of exhumation since ~5 Ma must have been limited to ~10 km or depths of ~300 °C, which further supports the interpretation of a shift in the location of focused, rapid exhumation from the North American Plate part of the syntaxial region to the southern syntaxial region on the Yakutat microplate. Thus, the geo- and thermochronometric data presented here provide a baseline set of data that can be used in future geodynamic models.

5 Upper crustal cooling of the northern St. Elias Mountains

5.1 Significance

The Wrangellia Composite Terrane is the classic example of an accreted and displaced terrane within the terrane mosaic of the western North American margin [*Jones et al.*, 1972; *Coney et al.*, 1980]. The composite terrane has been studied to understand continental growth by terrane subduction and accretion processes, and its spatial and temporal transitions between convergent, transpressional, and extensional tectonics [e.g., *Coney et al.*, 1980; *Rusmore and Woodsworth*, 1991; *Andronicos et al.*, 1999, 2003; *Gehrels et al.*, 2009; *Israel et al.*, 2013].

This chapter investigates the Wrangellia Composite Terrane of the northern St. Elias Mountains in southwest Yukon and adjacent Alaska and British Columbia (Figure 5-1). This area has been influenced by two accretionary and collisional events; the Late Jurassic–mid Cretaceous Wrangellia Composite Terrane accretion to the North American margin, and the late Eocene–Present flat-slab subduction, accretion, and collision of the Yakutat microplate [e.g., *Nokleberg et al.*, 1994; *Plafker et al.*, 1994]. The Wrangellia Composite Terrane has generally been ascribed the role of the backstop to Cenozoic accretion at its southern margin [e.g., *Pavlis and Roeske* 2007; *Enkelmann et al.*, 2010]. However, geophysical data and large-scale geodynamic models suggest that deformation from the current plate boundary is partly transferred inland to the northern margin of the Wrangellia Composite Terrane and to the eastern deformational front of the North American Cordillera (e.g., Mackenzie Mountains in the Northwest Territories) [e.g., *Lahr and Plafker*, 1980; *Mazzotti and Hyndman*, 2002; *Koons et al.*, 2010; *Doser*, 2014]. Effects of the Yakutat flat-slab subduction within the Wrangellia Composite Terrane are evident from areas above the downgoing slab in south-central Alaska and at its edge north of the Alaska Range [e.g., *Enkelmann et al.*, 2008; *Finzel et al.*, 2011b; *Brennan and Ridgway*, 2015]. The study area is located east of the downgoing slab and north and northeast of the indenting Yakutat plate corner, the St. Elias syntaxis area (Figure 5-1). Only few studies investigating the Wrangellia Composite Terrane exhumation in the northern syntaxial region exist, all suggesting a limited amount of Cenozoic exhumation [*O'Sullivan and Currie*, 1996; *Enkelmann et al.*, 2008, 2010; *Spotila and Berger*, 2010].

To obtain the long-term exhumation history of this remote, rugged, and extensively glaciated area, detrital ZFT and AFT analyses were used. The detrital approach proved to be very powerful to investigate the exhumation of rocks above and below the ice fields and glaciers of the southern St. Elias Mountains [*Enkelmann et al.*, 2008, 2009, 2015a; Chapter 3]. Modern glacio-fluvial samples allow analyzing sand-sized material that represents the entire catchment, including the lower-elevation portions below the ice, which are expected to record the most recent exhumational cooling. Here, the first comprehensive dataset (3537 single-grain ages) recording the late Mesozoic–Cenozoic cooling and exhumation in the northern St. Elias Mountains is presented. Furthermore,

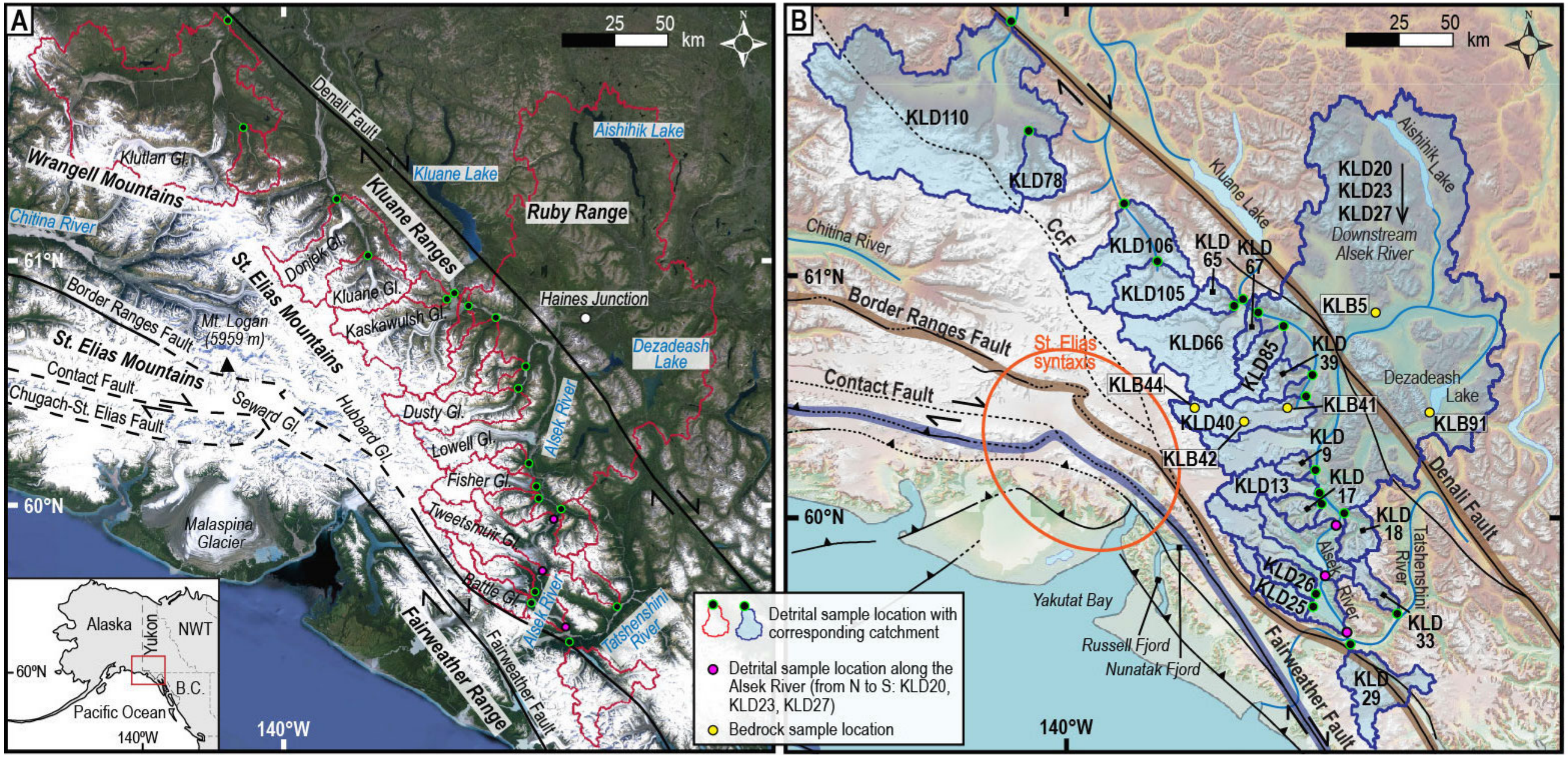

Figure 5-1A,B. Satellite image (A; GoogleEarth) and DEM (B; ASTER GDEM, 30 m; NASA and METI) of the St. Elias and western Wrangell mountain ranges, as well as Fairweather, Kluane, and Ruby ranges. The names of the main glaciers draining the northern St. Elias Mountains are given; Gl.: Glacier (A). Sampled catchments are outlined (A and B) and sample/catchment names are placed either within the catchment or indicated by a line (B). Note that the large Alsek catchment (KLD20, KLD23, KLD27) comprises most of the glacial catchments of the eastern study area. CcF: Connector Fault, B.C.: British Columbia, NWT: Northwest Territories.

the temporal and spatial far-field effects of the Yakutat subduction and collision to the north and northeast of the syntaxial area and the downgoing Yakutat slab are quantified.

5.2 Geology of the northern St. Elias Mountains and Ruby Range

5.2.1 Yukon-Tanana Terrane

The geology north of the Denali Fault comprises from south to north the Kluane metamorphic assemblage, the Coast Plutonic Complex to which the Ruby Range Batholith and Dezadeash Batholith belong, as well as rocks of the Aishihik metamorphic layered assemblages and Aishihik Plutonic Complex (Figure 5-2A) [*Erdmer and Mortensen*, 1993; *Johnston and Erdmer*, 1995; *Johnston and Canil*, 2007].

The Aishihik metamorphic assemblages are late Proterozoic–Mississippian in age and comprise >6 km thick continental margin and mixed volcano-sedimentary sequences [*Johnston et al.*, 1996; *Johnston and Canil*, 2007]. The ~186 Ma intrusion of the Aishihik Plutonic Complex is associated with Early Jurassic regional metamorphism and folding [*Johnston et al.*, 1996]. The Kluane metamorphic assemblage is described as a 12 km thick, homogeneous sequence of schist and gneiss, which includes amphibolite layers and minor ultramafic rocks [*Mezger*, 2000]. Detrital zircons suggest a maximum depositional age of 95 Ma and metamorphic overprint at 84 Ma due to southwestward thrusting of Yukon-Tanana rocks over the Kluane metamorphic assemblage, which in turn were thrust over sediments of the Dezadeash Group [e.g., *Eisbacher*, 1976; *Israel et al.*, 2011]. This deformation was associated with a regional event of folding, faulting, and metamorphism along the inboard margin of the Wrangellia Composite Terrane interpreted as its final collision with the former North American margin in the mid-Cretaceous [e.g., *Trop and Ridgway*, 2007].

Stitching and deformation of Yukon-Tanana and Wrangellia Composite terranes occurred during the Late Cretaceous–Eocene with the intrusion of plutons of the Kluane Arc [*Plafker et al.*, 1989]. These plutons are part of the widespread 85–45 Ma Coast Plutonic Complex that stretches southward along southeast Alaska and the coast of British Columbia, where it was dated to 175–45 Ma [e.g., *Armstrong*, 1988; *Erdmer and Mortensen*, 1993; *Gehrels et al.*, 2009]. In the study area, the Ruby Range Batholith has been dated by zircon U-Pb analysis to 57–50 Ma and associated with renewed metamorphism of the country rocks [*Erdmer and Mortensen*, 1993; *Mezger et al.*, 2001].

5.2.2 Wrangellia Composite Terrane

The Wrangellia Composite Terrane comprises the Alexander, Wrangellia, and Peninsular terranes, of which the Alexander and Wrangellia terranes occur in the study area. Alexander and Wrangellia terranes have a common tectonic history since at least the Late Devonian and were stitched together by Upper Pennsylvanian plutons

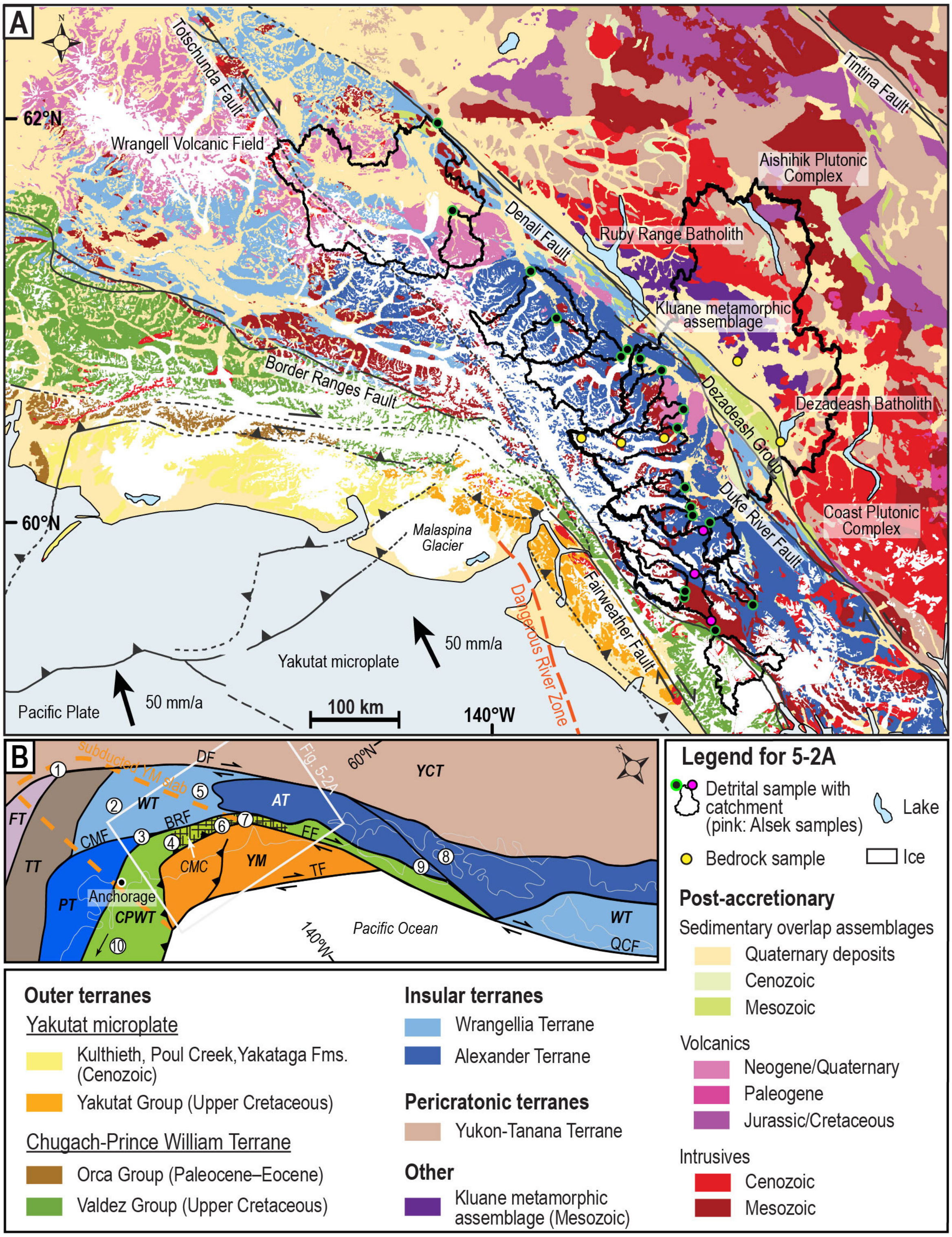

Figure 5-2A,B. Geologic (A) and terrane (B) map of the study area. (B) DF: Denali Fault, CMF: Castle Mountain Fault, BRF: Border Ranges Fault, FF: Fairweather Fault, TF: Transition Fault, QCF: Queen Charlotte Fault, YCT: Yukon Composite Terrane, FT: Farewell Terrane, TT: Togiak Terrane, WT: Wrangellia Terrane, PT: Peninsular Terrane, AT: Alexander Terrane, CPWT: Chugach-Prince William Terrane, YM: Yakutat microplate, CMC: Chugach Metamorphic Complex. Numbers indicate locations of 1: central Alaska Range, 2: Talkeetna Mountains, 3: Matanuska Valley, 4: Chugach Mountains, 5: Wrangell Mountains, 6: St. Elias Mountains, 7: St. Elias syntaxis, 8: Admiralty Island, 9: Baranof Island, 10: 850 km to Sanak Island. Terranes after *Colpron and Nelson* [2011], plate motion vectors after *Plattner et al.* [2007] and *Elliott et al.* [2010], geologic maps from i) Alaska: USGS, Alaska geologic map data, http://mrdata.usgs.gov/geology/state/state.php?state=AK, as of February 2015, ii) Yukon: Bedrock Geology 250K, http://data.geology.gov.yk.ca/Compilation/3, as of February 2015, and iii) British Columbia: Ministry of Energy, Mines, and Petroleum Resources, British Columbia, BC_digital_geology_II83, http://www.empr.gov.bc.ca/mining/geoscience/bedrockmapping/ages/bcgeomap.aspx, as of March 2015.

with Early Permian K-Ar cooling ages [*Gardner et al.*, 1988; *Israel et al.*, 2014], The Duke River Fault represents the suture between them (Figure 5-2). In the study area, the oldest strata of the Alexander Terrane are Cambrian–Upper Triassic siliciclastic, carbonate, and volcanic strata that formed as part of an arc-backarc system [e.g., *Dodds and Campbell*, 1992; *Beranek et al.*, 2012]. The Wrangellia Terrane is composed of the Sicker and Skolai island arc system and Carboniferous–lower Permian backarc basin strata of the Station Creek and Hasen Creek formations. The Icefield Ranges plutonic suite (290–270 Ma) is the last record of the Skolai/Sicker Arc in basement rocks of the study area [*Dodds and Campbell*, 1988; *Israel*, 2004; *Beranek et al.*, 2014; *Israel et al.*, 2014]. The Wrangellia Composite Terrane further comprises the Upper Triassic (230 Ma) Nikolai Greenstone, which is the result of a short-lived, voluminous volcanic episode and which is overlain by supratidal and sabkha facies Chitistone Limestone [e.g., *Hillhouse*, 1977; *Armstrong and MacKevett*, 1982; *Nokleberg et al.*, 1994]. In the study area, Nikolai Greenstone is exposed along the southern side of the Denali Fault [*Israel*, 2004]. In the same area and to smaller parts within the Upper Jurassic–Lower Cretaceous Dezadeash Group (Figure 5-2), intrusives of the Kluane Ranges plutonic suite occur, which represent remnants of the Lower Cretaceous (120–105 Ma; Figure 5-3A) Chisana Arc that formed during the subduction of the Wrangellia Composite Terrane at the former North American margin [e.g., *Csejtey et al.*, 1982; *Plafker et al.*, 1989, 1994; *McClelland and Gehrels*, 1990]. The Chisana Arc formed ~30–50 km north of the Upper Jurassic–Lower Cretaceous (160–130 Ma; Figure 5-3A) Chitina Arc, which is represented by the St. Elias plutonic suite (dark red colors within the catchments in Figure 5-2) [*Dodds and Campbell*, 1988]. This northward migration of the magmatic arc could indicate a shallowing of the subduction angle and/or removal of the forearc crust due to tectonic erosion [*Dodds and Campbell*, 1988; *Plafker et al.*, 1989; *Clift et al.*, 2005; *Trop and Ridgway*, 2007].

In the Late Jurassic, the Wrangellia Composite Terrane has already been close to the former North American margin and backarc sedimentation occurred along the inboard margin of the Wrangellia Composite Terrane [e.g., *Trop and Ridgway*, 2007]. In the study area, this is represented by the Upper Jurassic–Lower Cretaceous (160–137 Ma) Dezadeash Group (Figure 5-2), which is described as >3 km thick deep-sea fan turbidites sourced from the adjacent Chitina Arc [e.g., *Berg et al.*, 1972; *Eisbacher*, 1976; *Lowey*, 1992]. Starting in the Late Cretaceous, strike-slip motion along the Denali Fault displaced the sediments into their current position (Figure 5-2) [e.g., *Eisbacher*, 1976; *Israel*, 2004].

Post-accretionary sediments are exposed in the Denali fault zone in form of the Paleocene–Oligocene alluvial-fluvial Amphitheater Formation, which reflects one of the small pull-apart basins along the transpressional Denali Fault [e.g., *Plafker et al.*, 1994; *Israel et al.*, 2006]. Dextral transpression in the Wrangellia Composite Terrane has been associated with rapid (~120–210 mm/yr) north to northeast subduction of the Kula Plate (or Resurrection Plate according to *Bradley et al.* [2003] and *Haeussler et al.* [2003]) beneath Alaska since the Late Cretaceous [*Engebretson et al.*, 1985; *Plafker et al.*, 1994]. Prior to ~85 Ma, slower, east to northeast subduction (~70–120 mm/yr) had caused more orthogonal convergence or sinistral transpression [*Engebretson et al.*, 1985; *Plafker et al.*, 1994].

Local transtension in the Duke River Fault area led to the leakage of Miocene Wrangell lavas that overlie much of the Amphitheater sediments (Figure 5-2) [*Skulski et al.*, 1991, 1992; *Israel et al.*, 2006]. In contrast to this lava occurrence in Yukon, the main 26–0.2 Ma Wrangell Volcanic Field in the Wrangell Mountains in Alaska (Figure 5-2) comprises typical intraplate calc-alkaline volcanics from the progressive oblique subduction of the Yakutat lithosphere [*Richter et al.*, 1990]. Besides Quaternary glacial, fluvial, and lacustrine unconsolidated deposits, the Wrangell lavas are the youngest terrane-overlapping deposits [e.g., *Richter et al.*, 1990; *Israel*, 2004].

5.2.3 Previous thermochronometric ages of the northern St. Elias Mountains

The general exhumation and erosion history of the study area can only be derived from the geology of the ice-free ridges, K-Ar dates of intrusives and the better-studied areas to the west and southeast. During Late Jurassic–Cretaceous time, the Wrangellia Composite Terrane can be described as high-standing and affected by multiple phases of magmatic activity, regional metamorphism, exhumation, erosion, and sediment deposition in fore- and backarc basins at its in- and outboard margins [e.g., *Trop and Ridgway*, 2007]. The magmatic phases in the study area are documented by *Dodds and Campbell* [1988, 1992], who mapped the area and provided a large number of hornblende and biotite K-Ar cooling ages for southwest Yukon and adjacent areas in Alaska and British Columbia (Figure 5-3B). These K-Ar ages are mainly from igneous rocks and have generally been interpreted as emplacement ages. The rocks have been assigned to the Icefield Ranges suite (290–270 Ma), which is a part of the terrane definition, as well as the most abundant St. Elias suite (160–130 Ma) and the Kluane Ranges suite (120–105 Ma). Ages of Wrangell lavas and Kluane metamorphic assemblage were also obtained (Figure 5-3B) [*Dodds and Campbell*, 1988; *Richter et al.*, 1990; *Erdmer and Mortensen*, 1993]. No quantitative post-collisional exhumation record exists from thermochronometric dates for the northern St. Elias Mountains. Only few low-temperature thermochronometric ages (AHe) have been reported from the study area, of which four yield Late Miocene and younger ages (Figure 5-3B) that have been interpreted to record erosional exhumation [*Spotila and Berger*, 2010].

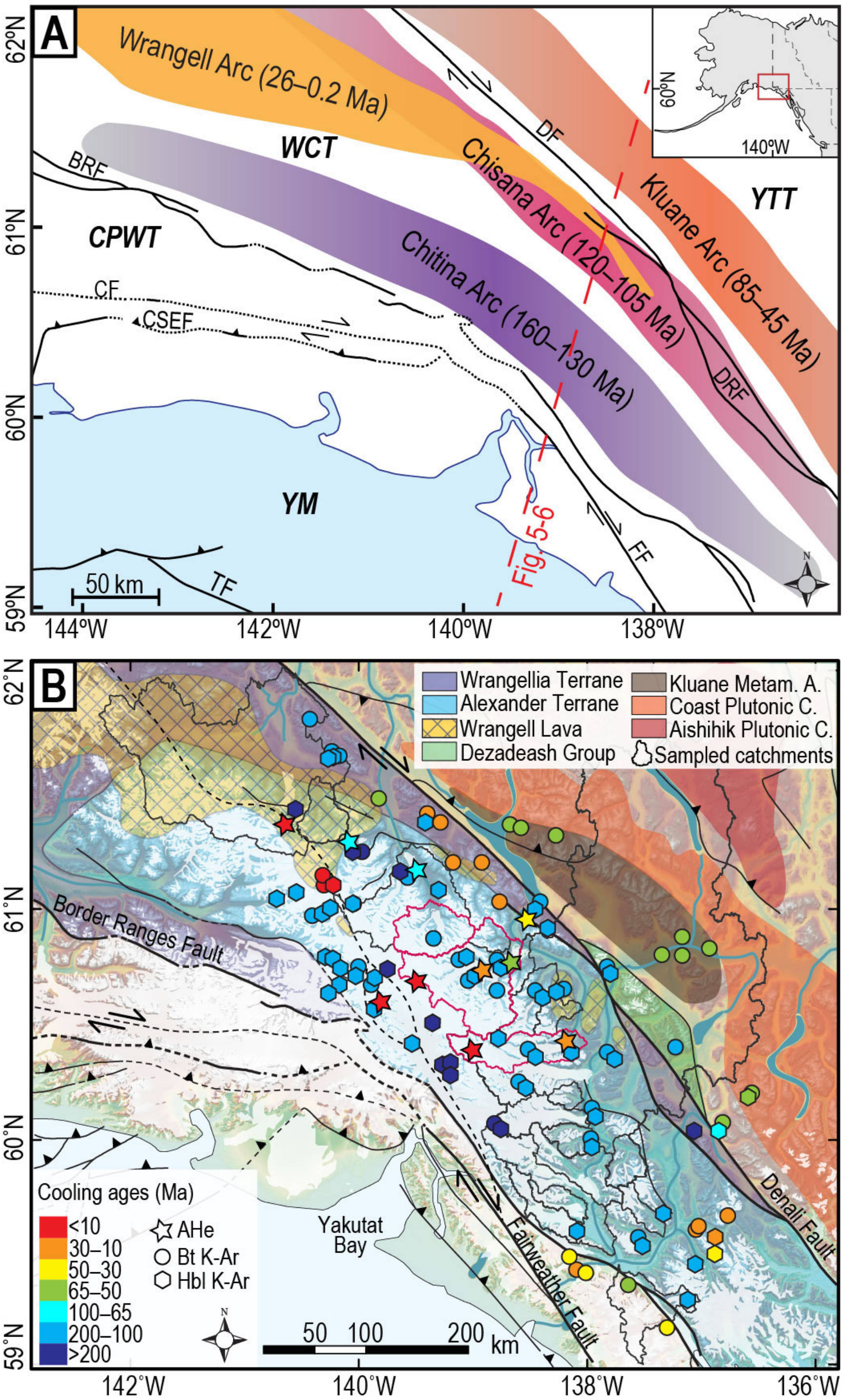

Figure 5-3A,B. (A) Magmatic arcs of the Wrangellia Composite and southern Yukon-Tanana terranes in the study area after *Dodds and Campbell* [1988], *Plafker et al.* [1994], and *Trop and Ridgway* [2007]. The red dashed line marks the profile of Figure 5-6. YTT: Yukon-Tanana Terrane, WCT: Wrangellia Composite Terrane, CPWT: Chugach-Prince William Terrane, YM: Yakutat microplate, DF: Denali Fault, DRF: Duke River Fault, BRF: Border Ranges Fault, CF: Contact Fault, CSEF: Chugach-St. Elias Fault, FF: Fairweather Fault. (B) Existing thermochronometer ages of southwest Yukon. K-Ar ages from *Dodds and Campbell* [1988] with the exception of biotite K-Ar ages from the Kluane metamorphic assemblage [*Farrar et al.*, 1988; *Erdmer and Mortensen*, 1993]. AHe ages from *Spotila and Berger* [2010]. Sampled catchments are marked; pink-outlined catchments have also been analyzed by *Enkelmann et al.* [2015a]. A.: Assemblage, C.: Complex.

5.3 Sampling

In total, 21 glacial and glacio-fluvial catchments in the northern St. Elias Mountains (19 catchments) and eastern Wrangell Mountains (two catchments) were sampled (Figures 5-1 and 5-2, Table 5-1). Sampling locations were chosen to include all large glaciers that drain the high Icefield region, which comprises the Hubbard Glacier catchment and the core of the syntaxial region (Figure 5-1A). Smaller catchments located farther inland in the Kluane Ranges were also sampled in order to be able to better confine exhumation signals obtained from regions closer to the St. Elias syntaxis (Figure 5-1A). Three samples are from different locations along the Alsek River, which crosses the entire St. Elias Mountains transporting material from Aishihik Lake north of the Denali Fault into the Gulf of Alaska (from north to south KLD20, KLD23, KLD27; Figure 5-1). Note that the Alsek River catchment encompasses most of the catchments in the eastern study area (KLD23, KLD20, KLD25, KLD26, KLD18, KLD17, KLD13, KLD9, KLD40, KLD39, KLD85, KLD67; Figure 5-1B). Catchment KLD110 comprises catchment KLD78, catchment KLD105 is contained within KLD106, and catchment KLD66 lies within the reaches of catchment KLD65 (Figure 5-1B).

At each sample location, 3–5 kg of medium- to coarse-grained sand was collected. Additionally, five bedrock samples (1–3 kg each) have been collected that allow comparing their ZFT ages to the detrital cooling age record (Figure 5-1B, Table 5-2).

5.4 Results

5.4.1 Bedrock zircon fission-track analysis

Five bedrock ZFT ages from samples located within the analyzed catchments are presented in Table 5-2. Two bedrock samples from the upper Alsek River catchment yield ZFT ages of ~43 Ma (KLB5) and ~110 Ma (KLB91). Sample KLB5 was taken from a granitoid belonging to the Coast Plutonic Complex that intruded the Kluane metamorphic assemblage (Figures 5-2 and 5-3B). U-Pb and K-Ar ages from the Kluane metamorphic assemblage and the Ruby Range Batholith suggest that KLB5 has early Eocene crystallization and K-Ar cooling ages. Graywacke KLB91 is taken from the Upper Jurassic–Lower Cretaceous Dezadeash Group and exhibits a mid-Cretaceous cooling age that is probably related to regional deformation during Wrangellia Composite Terrane collision, either due to exhumation or metamorphic resetting.

Three granitoid samples from the east-west elongated Dusty catchment (KLD40, Figure 5-1) exhibit increasingly younger ZFT ages of ~154 Ma, ~101 Ma, and ~9.4 Ma from east to west and with increasing elevations (1383–2637 m a.s.l.; Table 5-2). According to the geological map of southwest Yukon [*Israel*, 2004] the westernmost sample KLB44 was collected from the early Permian (290–270 Ma) Icefield Ranges plutonic suite, and KLB41 and KLB42 represent intrusions of the Upper Jurassic–Lower Cretaceous St. Elias plutonic suite. This indicates that sample KLB41 cooled below ZFT closure temperature shortly following its emplacement, while KLB42 either cooled much slower or experienced a heating event and was reset during mid-

Table 5-1. Detrital samples and corresponding catchments in the northern St. Elias Mountains

Sample	Latitude (°N)/ Longitude (°W)	Glacier/stream name	Catchment area (km²)	Terrane
KLD9	60.1755/ 138.0282	Between Dusty and Lowell Glaciers	142	AT
KLD13	60.0746/ 137.9578	Fisher Glacier	540	AT
KLD17	60.0355/ 137.9487	Plug, Tough, and Super Cub Creeks (S of Fisher Glacier)	262	AT
KLD18	59.9917/ 137.7755	E side Alsek River, E of Tweetsmuir Glacier	341	AT
KLD20	59.9427/ 137.8286	Alsek River, downstream of Fisher Glacier	16,997	AT, YTT, WT
KLD23	59.7288/ 137.9442	Alsek River, downstream of Tweedsmuir Glacier	17,687	AT, YTT, WT
KLD25	59.6033/ 138.0264	Battle Glacier	410	AT
KLD26	59.6302/ 138.0249	Vern Ritchie Glacier	270	AT
KLD27	59.4961/ 137.7543	Alsek River, downstream of Battle Glacier	19,255	AT, YTT, WT
KLD29	59.4498/ 137.7180	Konamoxt, Staircase, Melbern, Tikke, Grand Pacific, Moxt, Jarl, and Hay Glaciers	888	CT, AT
KLD33	59.5738/ 137.3309	Henshi Creek (?)	236	AT
KLD39	60.5689/ 138.0397	Felsite Glacier, Felsite Creek	236	AT
KLD40	60.4803/ 138.1062	Dusty Glacier	843	AT
KLD65	60.8760/ 138.6269	Kaskawulsh, Stairway, and Atrypa Glaciers, Canada Creek	1,752	AT
KLD66	60.8469/ 138.6771	Canada Creek	193	AT
KLD67	60.8254/ 138.4923	Maxwell Glacier	164	AT
KLD78	61.5497/ 140.4056	St. Clare and Bull Creeks (E of Klutlan Glacier)	460	AT (WVF)
KLD85	60.7683/ 138.2723	Disappointment Glacier	480	AT
KLD105	61.0251/ 139.3327	Kluane Glacier	707	AT
KLD106	61.2564/ 139.6159	Donjek and Kluane Glaciers	1,944	AT
KLD110	61.9872/ 140.5581	White River (Klutlan, Nesham, Brabazon, Mount Wood, Russell, Giffin, Guerin, Natazhat, Brooke, Lime, and Middle Fork Glaciers, St. Clare and Bull Creeks)	6,067	WT, AT (WVF)

Note: Catchment statistics were calculated using ArcGIS and a 30 m DEM (ASTER GDEM, NASA and METI). AT: Alexander Terrane, WT: Wrangellia Terrane, CT: Chugach Terrane, YTT: Yukon-Tanana terrane, WVF: Wrangell Volcanic Field.

Table 5-2. Bedrock ZFT ages from the Alexander and Yukon-Tanana terranes

Sample	Latitude (°N) Longitude (°W)	Elevation (m)	Location	Lithology	ZFT age (Ma) ±1σ
KLB5	60.8142 137.4896	681	Catchment of KLD20, 23, 27 (W side Pine Lake)	Granitoid (CPC)	43.2±3.5 N=7
KLB91	60.4086 137.0494	725	Catchment of KLD20, 23, 27 (SW side Dezadeash Lake)	Graywacke (Dezadeash Group)	109.9±8.9 N=10
KLB41	60.4277 138.2428	1383	Catchment of KLD40 (Dusty Glacier terminus, east)	Granite (St. Elias p.s.)	154.2±10.7 N=13
KLB42	60.4027 138.6824	1750	Catchment of KLD40 (central)	Granite (St. Elias p.s.)	101.4±6.1 N=18
KLB44	60.4282 139.0935	2637	Catchment of KLD40 (west)	Granodiorite (Ice. R. p.s.)	9.4±0.6 N=37

Note: N: number of individual zircons analyzed per sample. CPC: Coast Plutonic Complex, p.s.: plutonic suite, Ice. R.: Icefield Ranges. The ZFT ages represent pooled ages, as all samples demonstrated age homogeneity by passing the χ^2-test [e.g., *Galbraith*, 2005]. ζ=119.6±5.4 cm^2a; dosimeter glass: IRMM541.

Cretaceous collision, which left KLB41 unaffected even though the samples were taken only ~20 km apart from another (Figure 5-1B).

The youngest cooling age of ~9.4 Ma of KLB44 reflects exhumational cooling and occurs in roughly the same area as a young AHe age of ~4.3 Ma reported by *Spotila and Berger* [2010] (red star in Dusty catchment in Figure 5-3B), indicating ~40 °C/Myr cooling in the upper part of the Dusty catchment between ZFT and AHe closure depths.

5.4.2 Detrital fission-track analysis

In the following, the results of 21 detrital, glacio-fluvial samples, all of which were dated by ZFT analysis (2187 new ZFT single-grain ages) and 15 of them also by AFT analysis (1350 new AFT single-grain ages), are reported. Results of ZFT and AFT analyses are summarized in Table 5-3, which divides the ZFT and AFT age populations into time intervals that follow roughly different regional tectonic settings. Figures 5-1 and 5-5 illustrate the spatial distribution of ZFT and AFT age populations, respectively, for different time interval. All ages are reported with 1σ-errors in tables, figures, and text. Single-grain ages and peak-fitting results are provided in Appendix A and B (Figures A-5 and A-6, Datasets B-4 and B-5).

5.4.2.1 Detrital zircon fission-track analysis

Three detrital ZFT samples exist from the study area and have been published by *Enkelmann et al.* [2015a]. These are samples K12, K5, and K11, which coincide with samples KLD40, KLD65, and KLD105, respectively (Figure 5-3B). For a more robust cooling age distribution (larger number of grains per sample), the matching samples were accordingly combined in the analysis (Table 5-3). Individual results for samples KLD40, KLD65, and KLD105 can be found in Appendix A and B (Figure A-5, Dataset B-4).

Each sample yielded 2–4 different age populations with age peaks that range between 253.8 ± 28.9 Ma (14 %, KLD110) and 2.0 ± 0.6 Ma (2.3 %, KLD65+K5) (Table 5-3). The percentages in brackets indicate the fraction of single grains that is contained within the age population and is thus a measure of the size of the age-population with respect to the entire sample. The age population is characterized by its peak age (average age). The width of the age peaks (Figures A-5 and A-6) reflects the relative standard deviation as fraction of the peak age.

Most age peaks fall into the Cretaceous time (Figure 5-4A,B); some cluster around ~130 Ma and ~120–115 Ma, while Late Cretaceous age peaks show a wide range (Table 5-3). Early Cenozoic detrital ZFT age populations show some common age peaks in the range 55–40 Ma, that can be seen in eight of the samples throughout the study area (Table 5-3, Figure 5-4C). In contrast, three age populations with ~25–22 Ma age peaks (KLD17, KLD25, KLD27; Table 5-3) occur in the southern study area close to or, in the case of catchment KLD29, in the Chugach Terrane in the vicinity of the Yakutat-North American plate boundary (Table 5-3, Figures 5-2 and 5-4D).

The largest young age populations are derived from the two catchments located in the Wrangell Volcanic Field (KLD78, KLD110; Table 5-3, Figures 5-2 and5-4D) and are therefore considered to be of volcanic origin and reflect instantaneous cooling at the time of eruption. The very small ~2 Ma ZFT age population (2.3 %) in catchment KLD65/K5 (Table 5-3) is also interpreted as volcanic signal, either from Wrangell lava or ash.

The youngest (<10 Ma) non-volcanic ZFT cooling age peaks occur in catchments KLD13 (6.5 ± 0.8 Ma, 11 %), KLD27 (9.7 ± 1.2 Ma, 3.8 %), and KLD40/K12 (6.7 ± 0.3 Ma, 69.1 %) (Table 5-3). Catchments KLD13 and KLD40/K12 lie within the ~19,200 km^2-large Alsek River catchment of sample KLD27 (Figure 5-1). Considering the fact that the other two samples collected from the Alsek River upstream of KLD27 do not contain such young ZFT ages, the young ages of KLD27 are derived from the southern part of the Alsek catchment.

The ZFT age distributions also contain few, yet significant (mostly >10 %), Jurassic and older age peaks (>145 Ma; Table 5-3), mainly ~165–150 Ma. It is possible that no older cooling record is preserved, but it should also be noted that with increasing cooling age or uranium content it becomes increasingly difficult to date zircons by the fission-track method due to overlapping track densities. In many samples, a few grains (<7) could not be dated due to track densities that were too high.

Table 5-3. Detrital zircon and apatite fission-track results of KLD samples

Sample	Min	N	Age range [Ma]	Peak ages of distribution components ± 1σ [Ma] [Grain fraction in %]						
				≤5 Ma	15–5 Ma	35–15 Ma	60–35 Ma	100–60 Ma	145–100 Ma	≥145 Ma
KLD9	Zr	102	214–45					67.1±5.1 [12.3]	119.7±6.4 [87.7]	
	Ap	72	375–36					86.3±6.2 [70.8]		153.2±20.1 [29.2]
KLD13	Zr	106	220–4		6.5±0.8 [10.8]				115.5±6.1 [89.2]	
	Ap	104	433–22				49.1±12.0 [25.0]	83.5±6.1 [72.5]		331.0±70.1 [2.5]
KLD17	Zr	106	360–22			24.5±7.5 [1.8]		71.1±10.4 [10.7]	122.9±13.1 [66.5]	191.6±44.0 [21.1]
KLD18	Zr	104	256–105						129.9±20.9 [14.7]	155.7±9.6 [85.3]
	Ap	33	316–9			34.7±3.5 [63.4]			129.5±14.1 [36.6]	
KLD20	Zr	103	238–58					90.7±8.5 [22.2]	133.8±7.7 [77.8]	
	Ap	95	245–7		17.9±2.5 [15.1]			66.6±5.7 [48.5]	105.5±10.7 [36.4]	
KLD23	Zr	105	236–36				49.1±11.8 [2.8]	88.6±7.5 [32.4]	125.2±7.7 [64.8]	
	Ap	105	132–3		10.6±0.8 [60.6]	33.4±3.0 [33.7]		81.0±12.0 [5.7]		
KLD25	Zr	105	218–13			21.7±2.7 [4.0]	45.6±2.9 [50.7]		102.8±6.8 [45.2]	
KLD26	Zr	105	263–6		15.8±3.0 [5.0]		40.0±4.3 [9.4]	84.7±6.9 [52.6]	121.8±12.1 [33.0]	
	Ap	73	108–3		9.4±1.0 [70.0]		47.2±5.6 [30.0]			
KLD27	Zr	105	430–8		9.7±1.2 [3.8]			99.7±9.7 [21.0]		158.0±9.0 [75.2]
	Ap	107	132–3		11.3±1.1 [37.3]	29.5±2.7 [40.7]		74.9±6.7 [22.0]		
KLD29	Zr	105	161–11		14.3±1.5 [9.0]	23.9±1.3 [52.7]	44.8±3.2 [19.8]	91.1±6.6 [18.5]		
	Ap	103	80–2		13.1±1.3 [54.3]	21.1±4.1 [34.1] 31.5±8.4 [11.6]				
KLD33	Zr	104	279–76						107.4±12.3 [14.4] 134.1±7.7 [85.6]	
	Ap	95	173–3		8.7±2.4 [34.2]	18.6±3.7 [45.8] 32.3±4.7 [20.0]				
KLD39	Zr	102	197–47				60.4±8.5 [7.7]	78.5±7.7 [11.5]	104.0±7.4 [11.6]	150.7±16.2 [6.1]
	Ap	106	266–8			18.7±1.9 [15.3]		62.5±14.3 [20.8] 91.3±6.7 [63.8]		

Continued on next page

Sample	Min	N	Age range [Ma]	Peak ages of distribution components ± 1σ [Ma] [Grain fraction in %]						
				≤5 Ma	15–5 Ma	35–15 Ma	60–35 Ma	100–60 Ma	145–100 Ma	>≥145 Ma
KLD40+ K12*	Zr	205	237–2		6.7±0.3 [69.1]			88.0±3.4 [30.9]		
KLD40	Ap	105	224–1		8.8±0.9 [54.5]			85.0±5.1 [45.5]		
KLD65+ K5*	Zr	214	262–0.7	2.0±0.6 [2.3]			55.1±3.3 [12.6]	84.1±4.1 [40.7]	112.5±6.0 [32.2]	171.9±11.9 [12.1]
KLD65	Ap	52	335–38				58.5±5.7 [40.9]		102.8±9.5 [59.1]	
KLD66	Zr	103	294–49					77.3±5.6 [34.8]	116.5±9.9 [58.3]	166.1±83.2 [6.9]
KLD67	Zr	103	195–43				59.1±5.0 [13.9	87.5±5.9 [46.8]	119.8±8.1 [39.3]	
	Ap	97	332–21				50.4±7.2 [33.5]	74.2±9.1 [56.0]		164.2±35.4 [10.5]
KLD78	Zr	104	69–1	2.5±1.5 [3.0]	9.3±0.8 [48.7] 12.8±1.1 [41.3]		46.1±4.1 [7.1]			
KLD85	Zr	105	206–34				44.4±5.2 [8.7]	68.8±12.7 [24.6] 87.2±7.5 [51.5]	130.5±12.2 [15.2]	
	Ap	105	300–1		12.2±0.9 [63.6]			100.3±6.1 [36.4]		
KLD105+ K11*	Zr	200	231–30				48.3±3.5 [12.2]	88.3±9.3 [50.6]	111.4±13.4 [30.0]	148.8±86.1 [7.2]
KLD105	Ap	98	281–21			31.4±13.2 [4.4]		88.4±4.9 [95.6]		
KLD106	Zr	103	251–52					71.3±6.8 [29.2] 100.1±9.3 [47.9]	143.5±14.1 [22.9]	
KLD110	Zr	104	547–3		6.2±0.7 [16.1] 10.9±0.6 [58.0]		51.5±4.3 [11.5]			253.8±28.9 [14.4]

Note: Min: Mineral phase dated; N: number of grains dated per sample. Binomial peak fitting using BINOMFIT [*Brandon*, 1992; 1996]. ZFT: ζ=119.6±5.4 cm^2a (SF), dosimeter glass: IRMM541; AFT: ζ=237.0±5.0 cm^2a (EE), dosimeter glass: IRMM540-R. *Samples K5, K11, and K12 from *Enkelmann et al.* [2015a] from the same catchments as KLD65, KLD105, and KLD40, respectively. Individual results for KLD65, KLD105, and KLD40 can be found in Appendix A and B (Figure A-5, Dataset B-4). ZFT for K5, K11, K12: ζ=403.9±11.6 cm^2a (EE), dosimeter glass: CN5.

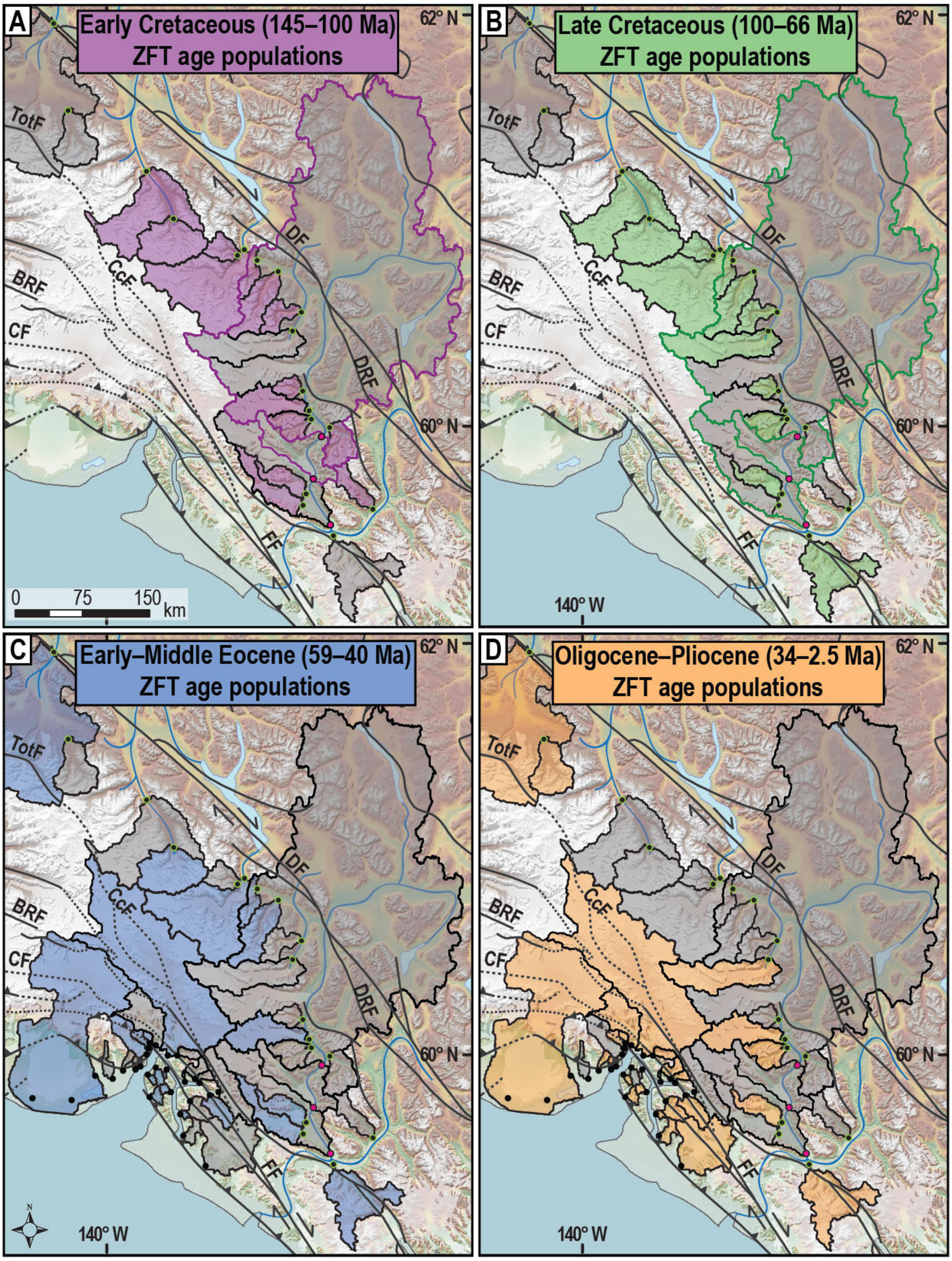

Figure 5-4A–D. Spatial distribution of ZFT cooling age populations through time. For C and D, results of detrital ZFT analyses by *Enkelmann et al.* [2009] and Chapter 3 were included. As those samples cover the Chugach-Prince William and Yakutat microplate, which are Late Cretaceous–early Eocene in age, these catchments are not included in A and B. Only age populations comprising >5 % of the grains of the sample are considered here.

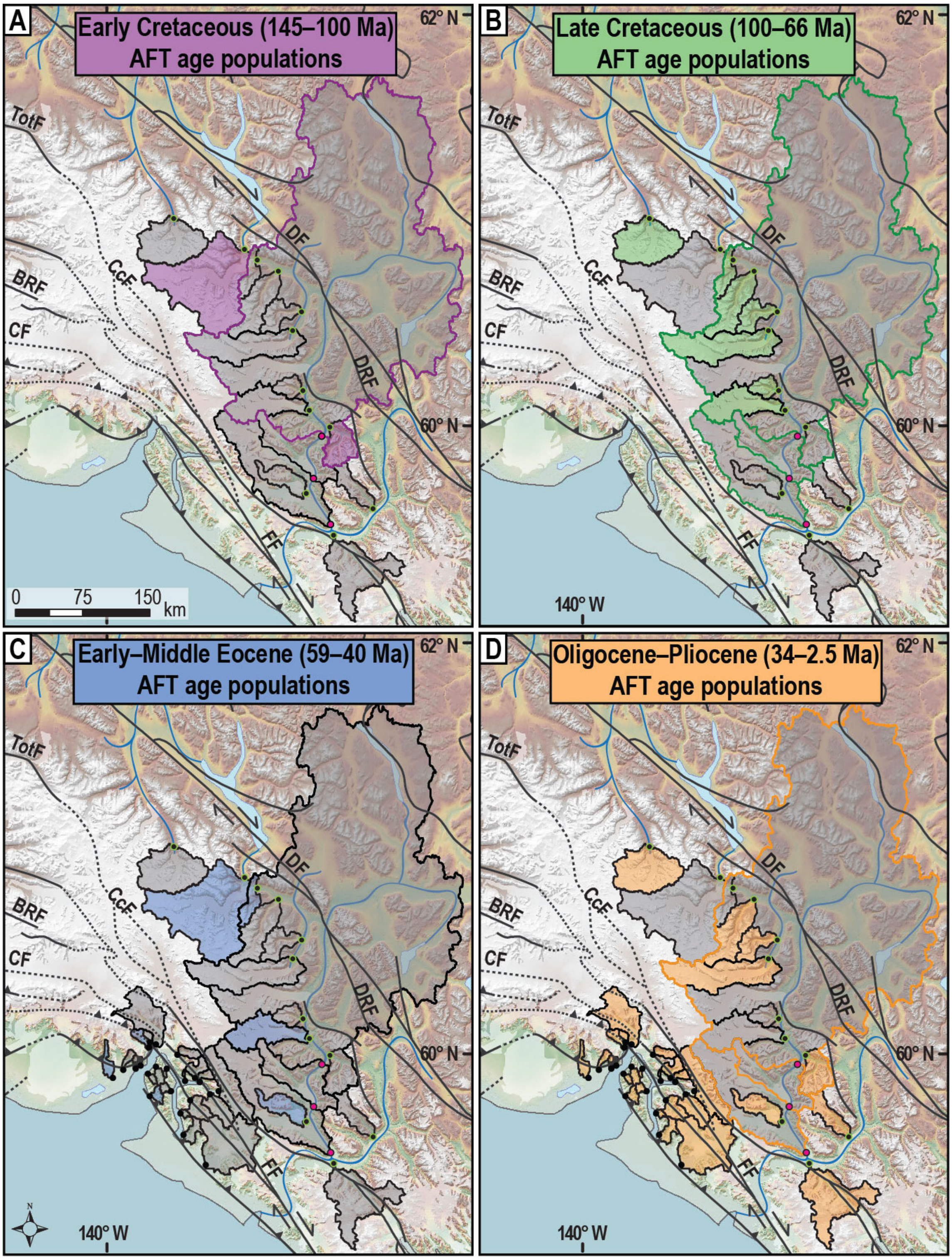

Figure 5-5A–D. Spatial distribution of AFT cooling age populations through time. For C and D, results of detrital AFT analyses by *Enkelmann et al.* [2015a] were included. As their samples cover the Chugach-Prince William and Yakutat microplate, which are Late Cretaceous–early Eocene in age, these catchments are not included in A and B. Only age populations comprising >5 % of the grains of the sample are considered here.

5.4.2.2 Detrital apatite fission-track analysis

The 15 AFT samples each yielded 2–3 age populations that range between 331.0 ± 70.1 Ma (2.5 %, KLD13) and 8.7 ± 2.4 Ma (34 %, KLD33), but are mostly Late Cretaceous–Miocene (Table 5-3). More or less distinct age clusters can be observed at ~90–80 Ma and around 30 Ma (Table 5-3). With the exception of KLD105+K11, samples with an ~30 Ma age population (11.6–63.4 %; Table 5-3) occur in the southern part of the study area. Furthermore, some samples contain late Miocene ~13–8 Ma AFT age populations (KLD23, KLD26, KLD27, KLD29, KLD33, KLD40, KLD85; Table 5-3) which are mostly located in the southern part as well, but also farther north in catchments KLD40 and KLD85.

5.4.2.3 Comparison of zircon and apatite fission-track data

From the samples that were analyzed for both ZFT and AFT, an overall trend of younger AFT than ZFT ages is observed (Table 5-3), which is expected due to the higher T_c of ZFT (~250 °C) than AFT (~110 °C). The direct comparison of certain ZFT and AFT age peaks is not straightforward. *Garver et al.* [1999] pointed out that such a comparison requires caution especially because of the difference in precision of ZFT and AFT age. The precision of ZFT ages is commonly higher due to the typically higher uranium content in zircon (>100 ppm) compared to apatite (<100 ppm), resulting in a better track counting statistic for zircons, particularly when applied to detrital material that require single-grain analysis. *Garver et al.* [1999] came to the conclusion that a proper comparison can be done when apatite counting statistics are good (≥100 grains) and when there are only few ZFT and AFT component age populations (1–2) that are well separated in time (>20–30 % of their peak age). Most of the samples yielded ≥3 ZFT age populations and 2–3 AFT age populations due to the heterogeneous geology and varying catchment sizes. Nevertheless, in most cases it is possible to compare ZFT and AFT age peaks (Table 5-3). For example, in KLD20 ZFT age peaks of ~134 Ma (78 %) and ~91 Ma (22 %) match with AFT age peaks of ~106 Ma (36 %) and ~67 Ma (49 %), respectively, which indicates roughly uniform cooling of ~5 °C/Myr between ~134–67 Ma. An additional AFT age peak of ~18 Ma (15 %) that has no equivalent in the ZFT age distribution suggests a younger cooling phase that does not exhume rocks from depths of zircon closure, but shallower from below the AFT closure depth. In many samples, ZFT and AFT age peaks can be matched, but it becomes indeed difficult when several age peaks are close together in time, for example in KLD26 (Table 5-3). There are other ZFT and AFT age peaks that are indistinguishable within error but more certainly equivalent (e.g., KLD18, KLD27, KLD29; Table 5-3). These indicate very rapid cooling through both ZFT and AFT closure temperatures at the time of the age peak. Conversely, age peaks that are separated by long time intervals reflect slow cooling (e.g., ~2 °C/Myr for sample KLD33 between ~107 Ma (ZFT) and ~32 Ma (AFT); Table 5-3).

It is important to note that the comparison of ZFT and AFT data from detrital samples is based on the assumption that zircon and apatite are equally abundant in rocks composing the catchments. However, zircons and apatites do not necessarily have to be sourced from the same lithology and elevation within the catchment. This is for example reflected in the fact that not all samples that yielded zircons also yielded sufficient apatites for dating. Variations in the abundance of apatite and zircon within the sediment source region can result in discrepancies between the ZFT and AFT age components. For example, for sample KLD13, a ZFT age population with a peak age of ~7 Ma (11 %) was obtained, whereas the youngest AFT age peak is ~49 Ma (25 %) (Table 5-3). Similar problems are found in samples KLD9 and KLD67 that yielded older AFT than ZFT age populations (Table 5-3). Thus, the potential discrepancy between zircon and apatite occurrence needs to be kept in mind when interpreting ZFT and AFT age distributions in relation to each other.

5.5 Discussion

5.5.1 Mesozoic cooling

Knowledge of the general geologic and tectonic history of the area is crucial for the interpretation of the ZFT and AFT age populations in terms of causes of rock cooling. For a better illustration of the tectonic setting during different time intervals schematic cross sections through the study area are shown (Figure 5-6).

Carboniferous–Early Cretaceous ZFT and AFT age populations are dominated by magmatic phases and associated metamorphism that reset almost the entire previous thermal record of the Cambrian–Upper Triassic basement rocks of the Wrangellia Composite Terrane. The Late Jurassic cooling age populations (around 155 Ma) of the Alexander Terrane are assignable to subduction-related magmatic activity and subsequent cooling of the Chitina Arc (Figures 5-3A and 5-6A), and therefore to the widespread St. Elias plutonic suite [e.g., *Dodds and Campbell*, 1988; *Plafker et al.*, 1989, 1994]. After cessation of Chitina Arc activity (~130 Ma), rocks cooled probably due to thermal relaxation after the magmatic intrusion, as recorded by the large group of ≤130 Ma ZFT and AFT age peaks (Table 5-3). Erosional exhumation must have played a role in cooling of the rocks as well, as collision of the Wrangellia Composite Terrane with the North American margin intensified during the Early Cretaceous [e.g., *Trop and Ridgway*, 2007].

Renewed magmatic activity and heating of the study area began ~120 Ma with the construction of the Chisana Arc (Figure 5-6A) [*Dodds and Campbell*, 1988; *Plafker et al.*, 1989, 1994]. A record of the Chisana Arc (Kluane Ranges plutonic suite or volcaniclastic flysch of the Dezadeash Group) could only occur within the Alsek River samples. However, no age signal is detected (Table 5-3). The larger part of the study area has been in a forearc position during the late Early Cretaceous and no sedimentary basin strata have been mapped in the area. Therefore, cooling age populations of this time might reflect an uplifted area experiencing erosion.

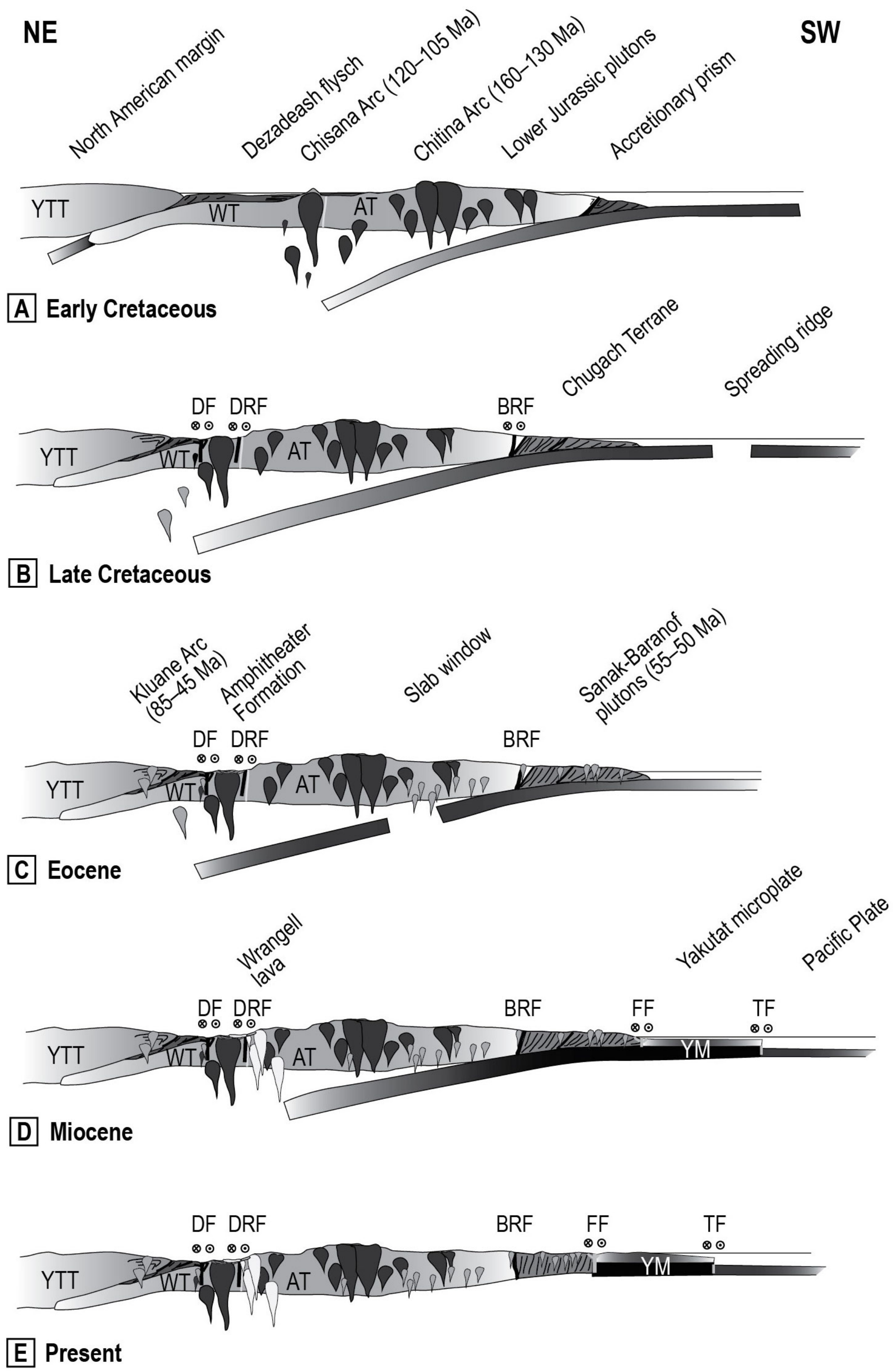

Figure 5-6A–E. Schematic cross sections of the Cretaceous through Recent tectonic evolution of the northwestern North American margin in the area of modern southeastern Alaska and western Yukon. The location of the cross section is marked in Figure 5-3A. The cross sections are constructed after cross sections from *Trop and Ridgway* [2007] who presented the tectonic evolution of south-central Alaska. YTT: Yukon-Tanana Terrane, WT: Wrangellia Terrane, AT: Alexander Terrane, YM: Yakutat microplate, DF: Denali Fault, DRF: Duke River Fault, BRF: Border Ranges Fault, FF: Fairweather Fault, TF: Transition Fault.

The detrital age populations further contain mid-Cretaceous ZFT and AFT age peaks (Table 5-3) that are most likely indicative of metamorphism and deformation due to the final accretion of the Wrangellia Composite Terrane to the North American margin [e.g., *McClelland and Gehrels*, 1990; *Dodds and Campbell*, 1992; *Ridgway et al.*, 2002]. Late Cretaceous accretion processes as well as subduction along the southern margin of the Wrangellia Composite Terrane caused deformation, erosion, and exhumation, which probably contributed to cooling [e.g., *Plafker et al.*, 1989]. The Coast Plutonic Complex in British Columbia also records high exhumation and erosion rates during the Cretaceous, which is well documented in the vast accretionary complex of the Chugach-Prince William Terrane [e.g., *Hollister* 1979, 1982; *Farmer et al.*, 1993; *Gehrels et al.*, 2009; *Garver and Davidson*, 2015].

During the same time interval, the Denali Fault developed in response to rapid oblique subduction (Figure 5-6B) [*Engebretson et al.*, 1985; *Plafker et al.*, 1994]. Up to 400 km of dextral strike-slip displacement have been accommodated along the Denali Fault since the Late Cretaceous [e.g., *Eisbacher*, 1976; *Lowey*, 1998]. The Duke River Fault, part of the southern Denali fault system, was also active at 100 Ma or even earlier [*Cobbett et al.*, 2010]. Furthermore, the Border Ranges Fault accommodated hundreds of kilometers of right-lateral displacement during latest Cretaceous–early Eocene time [*Little and Naeser*, 1989; *Smart et al.*, 1996; *Roeske et al.*, 2003; *Garver and Davidson*, 2015]. Consequently, the Wrangellia Composite Terrane was situated in a transpressional setting, bounded by two dextral strike-slip fault systems. This setting likely resulted in a high-stress regime causing uplift, erosion and exhumation. Deformation might have been more effective at the northern margin of the Wrangellia Composite Terrane close to the Denali Fault (Figure 5-4B), as the Border Ranges Fault has been described as backstop to southward accretion and one-sided (south) deformation [e.g., *Little and Naeser*, 1989; *Pavlis and Roeske*, 2007]. Late Cretaceous ZFT and AFT age populations are in fact more abundant in catchments in the central and northern Wrangellia Composite Terrane (Table 5-3, Figures 5-4 and 5-5).

Overall, the fact that a large fraction of the widespread Late Jurassic–Cretaceous cooling record is preserved, indicates generally slow cooling of the study area due to exhumation since then.

5.5.2 Cenozoic cooling of the Yukon-Tanana Terrane

The Yukon-Tanana Terrane experienced extensive Eocene magmatism and metamorphism (Figure 5-6C) that is recorded in the 43 Ma ZFT age of bedrock sample KLB5 (Table 5-2) [e.g., *Eisbacher*, 1976; *Erdmer and Mortensen*, 1993; *Mezger et al.*, 2001]. The upper Alsek catchment mostly comprises rocks of the Coast Plutonic Complex and Eocene metamorphic assemblages, and should therefore yield Eocene ZFT cooling ages or Early Cretaceous ages indicative of the Dezadeash Group (Table 5-2, Figure 5-3B). However, this is not the case, most likely because of the morphology of the large Alsek catchment and long transport distance (up to ~270 km). The catchment is characterized by low-relief topography north of the Denali Fault and sand-sized material is probably deposited in the wide valleys before the river enters the more rugged topography of the St. Elias Mountains, where the river forms steep valleys and canyons (Figure 5-1). The sand-sized material collected along the southern part of the Alsek River thus originates from the large glaciers that drain the high Icefield region. This means that the assumption of a detrital sample representing the catchment-wide cooling history is not valid for such a large catchment characterized by varying topographic characteristics and sediment storage.

5.5.3 Cenozoic cooling of the Wrangellia Composite Terrane

With the exception of the detrital ZFT record of the eastern Wrangell Mountains, Cenozoic age populations can mainly be interpreted in terms of cooling due to exhumation. Paleocene–mid Eocene ZFT and AFT age populations (~60–45 Ma, mainly ~50–45 Ma; Table 5-3) occur throughout the study area (Figures 5-4C and 5-5C). This time is well recognized in the geologic record of southern Alaska documenting Eocene spreading-ridge subduction (Figure 5-6C) [e.g., *Hudson et al.*, 1977a, 1979; *Pavlis and Sisson*, 1995]. The inboard (north of the Border Ranges Fault) effects of the spreading-ridge subduction are not well understood, but Eocene episodes of uplift, coarse-grained non-marine sedimentation, and magmatism farther west on the Wrangellia Composite Terrane (Matanuska Valley and Talkeetna Mountains; Figure 5-2B) suggest an influence of the migrating slab window beneath southern Alaska [*Trop et al.*, 2003; *Trop and Ridgway*, 2007]. The presence of distinct Paleocene–mid Eocene ZFT and AFT age populations in the study area probably indicates this influence in two ways. Firstly, prior to spreading-ridge subduction, the downgoing oceanic crust became increasingly younger and thicker, which resulted in a stronger coupling with the upper plate, and secondly, the slab window allows for an upwelling of hot mantle material, which together can result in the uplift and erosion of the upper plate as well as an increase in the geothermal gradient [e.g., *Thorkelson and Taylor*, 1989; *Cloos*, 1993; *Bradley et al.*, 2003].

Large early Oligocene age peaks are only obtained from apatites in the southern study area (the Oligocene age population of KLD105+K11 is neglected because of its small size and large error; Table 5-3). The fact that only apatites show these age populations indicates that only depths to AFT closure were affected by ~30 Ma exhumation (~3–4.5 km with a 25–35 °C/km estimated paleogeothermal gradient). Furthermore, late Oligocene–Miocene cooling age populations of mainly apatites, but also zircons, (~24–6 Ma; Table 5-3) occur in the southern part of the study area, even though some also occur father north in catchments KLD39, KLD40/K12, and KLD85 (Figures 5-4D and 5-5D). Oligocene–Miocene exhumation was probably caused by flat-slab subduction of the Yakutat microplate and transpression along the Fairweather Fault (Figure 5-6D) [e.g., *Enkelmann et al.*, 2008; *Finzel et al.*, 2011b; Chapter 3].

5.5.4 Inboard effects of the Yakutat subduction/collision

The subduction of the increasingly thicker Yakutat microplate has been affecting southern Alaska since the onset of flat-slab subduction in the late Eocene [*Finzel et al.*, 2011b] and intensified since the mid-Miocene [e.g. *O'Sullivan and Currie*, 1996; *Meigs et al.*, 2008; *Grabowski et al.*, 2013]. Figure 5-7 illustrates the detrital ZFT and AFT cooling signals of the study area in comparison to the northern Fairweather Fault area, the southern St. Elias Mountains and the Chugach Mountains in form of single-grain pie charts. It is important to note that single-grain ages have large uncertainties and are not used for the interpretation of cooling phases. Nonetheless, the visualization with pie charts gives a good overview of the spatial distribution of ZFT and AFT cooling ages. For example, the Oligocene–Miocene cooling ages are represented by the orange-colored bins that mainly occur in the AFT charts in the study area. However, those ages are far more widespread and make up larger fractions in both AFT and ZFT data in the catchments near the active plate boundary comprising the Chugach-Prince William Terrane and the Yakutat microplate in the south (Figure 5-7).

The latter two terranes comprise lower Eocene and older, mainly Upper Cretaceous sedimentary strata and the Oligocene–Miocene ages represent reset cooling signals due to exhumation related to Yakutat subduction and collision [*Enkelmann et al.*, 2008, 2009; Chapter 3]. Especially KLD29, which is located closest to the plate boundary, shows in ZFT and AFT age populations and single-grain age distribution similarities to the previously acquired cooling history to the west, i.e., typical age populations of ~30 Ma, ~20 Ma, and ~15 Ma (Table 5-3). Also similar to the area farther west, cooling ages increase abruptly north of the Border Ranges Fault, as seen in samples CH46, CH21, and WR23 from *Enkelmann et al.* [2008] (Figure 5-7).

Most evidence for the effects of Yakutat flat-slab subduction and collision are derived from sedimentologic and thermochronologic studies in the Chugach and Talkeetna mountain ranges, as well as the Alaska Range, all west of the study area and located above the subducted Yakutat slab [e.g., *Trop and Ridgway*, 2007; *Enkelmann et al.*, 2008; *Finzel et al.*, 2011b; *Arkle et al.*, 2013; *Benowitz et al.*, 2014; *Brennan and Ridgway*, 2015]. The study area has been influenced by the passage of the northeastern edge of the Yakutat slab (Figure 5-6D) [e.g., *Richter et al.*, 1990; *Skulski et al.*, 1991, 1992; *Trop et al.*, 2012]. Thus, the Yakutat flat-slab subduction affected the study area located north of the Border Ranges Fault and increased plate coupling resulting in uplift, erosion, and exhumation, similarly to areas farther west. However, the amount of exhumation is significantly smaller in the study area, compared to the regions above the slab (Chugach Mountains), as the Oligocene–Miocene cooling signal is not as large and widespread and mostly observed in apatites. Reasons for the limited exhumation are probably the shorter duration that the Yakutat slab has been present beneath the study area and the igneous and highly metamorphosed, and therefore strong, rocks of the Wrangellia Composite Terrane.

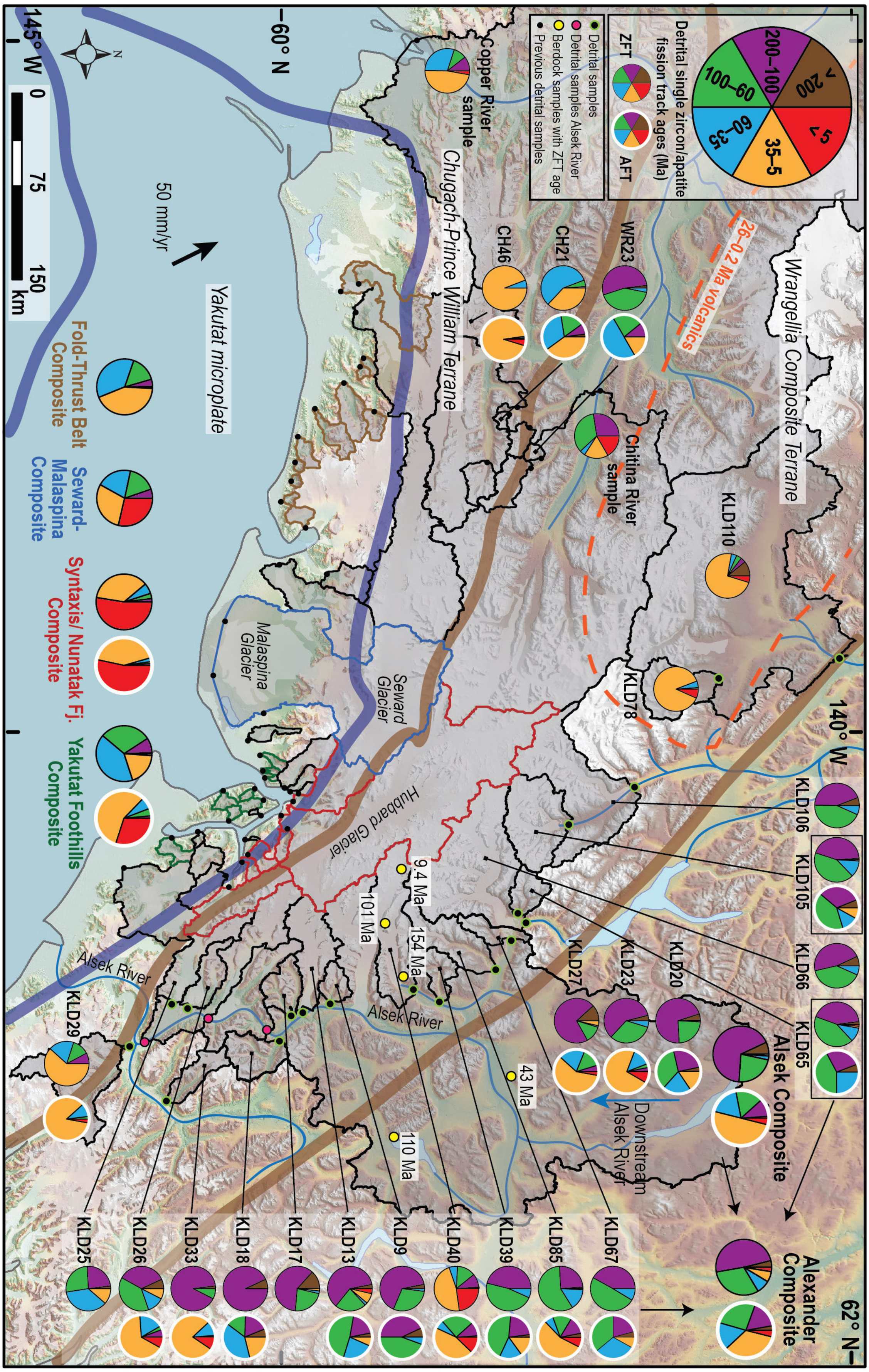

Figure 5-7 caption on next page

Figure 5-7. Detrital ZFT and AFT ages from *Enkelmann et al.* [2008, 2009, 2010] and Chapters 3 and 5. Single-grain ages are presented as pie charts binned with regard to tectonic events. Each of the smaller pie charts represents one detrital sample, whereas each of the larger pie charts represents a composite sample where several catchments with similar age distribution were combined to reflect the age distribution of an area with a more robust signal (higher number of single-grain ages). The five new bedrock ZFT ages are marked on the map as well. Thick blue lines outline the Yakutat microplate, thick brown lines outline the Wrangellia Composite Terrane with the Denali Fault in the north and the Border Ranges Fault in the south. Single-grain ages can be found in Appendix B (Datasets B-1, B-4, and B-5).

5.5.5 Concentration of stress and strain in the St. Elias syntaxial region

Since ~5 Ma, stresses created by the oblique Yakutat subduction-collision concentrate in the St. Elias syntaxis, where dextral transform motion transitions into oblique convergence and subduction [*Enkelmann et al.*, 2010; Chapter 3]. Possible drivers for this concentration of stress and strain are i) a change in Pacific Plate motion at ~5 Ma resulting in a larger compressional component at the Yakutat-North American plate boundary, ii) the increasingly thicker oceanic crust of the wedge-shaped Yakutat lithosphere entering the deformational front (Pamplona Zone, Figure 5-8C) in the syntaxial area, and iii) the beginning of glaciation of the area ~5.6 Ma [*Engebretson et al.*, 1985; *Lagoe et al.*, 1993; *White et al*., 1997; *Worthington et al.*, 2012]. The focusing of stress in the St. Elias syntaxis resulted in a complex structural setting, abundant and frequent large-magnitude (Mw=7–8) seismic activity, and very rapid exhumation of ~10 km of rocks beginning at ~5 Ma, as seen in very large detrital ZFT age populations (up to 90 %) of ≤5 Ma in catchments in the syntaxial region (Seward-Malaspina and Syntaxis/ Nunatak Fjord composite charts in Figure 5-7) [*Plafker and Thatcher*, 2008; *Enkelmann et al.*, 2009; *Bruhn et al.*, 2012; *Doser*, 2014; Chapter 3]. Support for the high rates of exhumation came from detrital AFT data of those samples with virtually the same age population peaks, indicating rapid cooling of the rocks through ZFT and AFT closure [*Enkelmann et al.*, 2015a]. Such high rates of exhumation (>3 mm/yr) cannot have been sustained for more than a few million years, as they would have removed the entire crustal layer recording older exhumation at high elevations, which is not the case [e.g., *O'Sullivan and Currie*, 1996]. *Enkelmann et al.* [2015a] indeed showed that the focus of deformation and the area of most rapid exhumation shifted southward after ~2 Ma using thermochronology data integrated with geophysical and structural data and surface processes models (Figure 5-8C).

The area of rapid Pliocene exhumation has been defined based on detrital ZFT age distributions from the southern St. Elias Mountains and the southern part of the inferred Connector Fault (Art Lewis Fault) has been interpreted as its eastern boundary (Figures 5-7 and 5-8A, C) [Chapter 3]. The new data from the northern St. Elias Mountains are all from east of the inferred fault trace of the Connector Fault (after *Spotila and Berger* [2010]). No ≤5 Ma ZFT age populations occur in the study area (Table 5-3,

Figure 5-7), which supports the existence of a southwest-dipping reverse or thrust fault resulting in differential exhumation on either side (Figure 5-8B). Geological and geophysical studies suggest that strain transfer inland along a discrete fault with lateral displacement can only be a young feature (≤1 Myr) [*Lahr and Plafker*, 1980; *Doser*, 2014; *Marechal et al.*, 2015]. The Art Lewis Fault, in contrast, may have been active for several million years [written communication between Plafker, G. and *Kalbas et al.*, 2008]. The Connector Fault/Art Lewis Fault has been interpreted as strike-slip fault, but additional vertical displacement, at least in the past, is in the overall transpressional tectonic setting likely.

The youngest (7–6 Ma; Table 5-3) ZFT age populations of the study area in KLD13 and KLD40 occur adjacent to the area of rapid Pliocene exhumation (Figure 5-8A). The ~7 Ma ZFT age population (69 %; Table 5-3) in KLD40 could moreover be confined to the western part of the Dusty catchment based on a comparison to the bedrock ZFT ages from the catchment (Table 5-2, Figure 5-7). Young (10–5 Ma) ZFT and AFT age populations from the Alsek catchment as well as 10–5 Ma AFT populations from smaller catchments could also be shown to occur in the southern study area to the east of the syntaxial region. The characteristic of similar ZFT and AFT age peaks as in the syntaxis [*Enkelmann et al.*, 2015a] is also valid for KLD40 (Table 5-3, Figure 5-7). This indicates that the area of rapid exhumation extended northeastward, or was located farther northeast of the syntaxis before 5 Ma and shifted subsequently to the south (Figure 5-8C). The rate of exhumation was not as high as in the area of Pliocene rapid exhumation as the signal is not as widespread and, with the exception of KLD40 and KLD13, mostly only seen in AFT results.

The area of ~10–5 Ma rapid exhumation can be outlined as in Figure 5-8C, even though it should be noted that its southern and western extent is uncertain (dashed outline in Figure 5-8C), as in those areas ≤5 Ma exhumation signals prevail and conceal a possible ~10–5 Ma signal. It is also uncertain to which extent the large Hubbard Glacier catchment was affected by the ~10–5 Ma exhumation phase. But that part of it exhumed rapidly during this time interval is clearly evident in the detrital ZFT age components of the Hubbard catchment [Chapter 3]. Beside a ~3 Ma detrital ZFT age population (46 %), the Hubbard detrital sample also yielded a ~6 Ma ZFT age peak (39 %), similar to the age populations in KLD40 and KLD13 (Table 5-3).

5.5.6 Structural implications for the syntaxial region

How was the late Miocene (~10–5 Ma) deformation distributed; diffuse or along discrete structures? The distribution of bedrock ages in catchment KLD40 (decreasing with increasing elevation) and the stark contrast in age over a short distance indicate at least one unmapped, ice-covered fault east of KLB44 (Table 5-2, Figures 5-7 and 5-8B). At ~5 Ma the rate of exhumation increased and the area of rapid exhumation was reduced in size or moved and its northeastern limit shifted southwestward. During this time exhumation was rapid and deep-seated [*Enkelmann et al.*, 2009; Chapter 3]. After ~2 Ma the focus of deformation shifted farther southward (Figure 5-8C) as a result of the interactions between rheologic and tectonic modification of the Yakutat microplate and global climate shifts resulting in intensification of glaciation. The high sedimentation rates on the Yakutat microplate resulted in the development of a décollement allowing a shift of deformation towards the south and emergence of the southern St. Elias Mountains that intercepts with the atmosphere resulting in the modern precipitation pattern that focuses erosion in the southern apex of the syntaxis region [*Enkelmann et al.*, 2015a]. In the southern locus, exhumation is rapid, but shallower along the northeast and northwest dipping thrust and revers faults [e.g., *Enkelmann et al.*, 2015b].

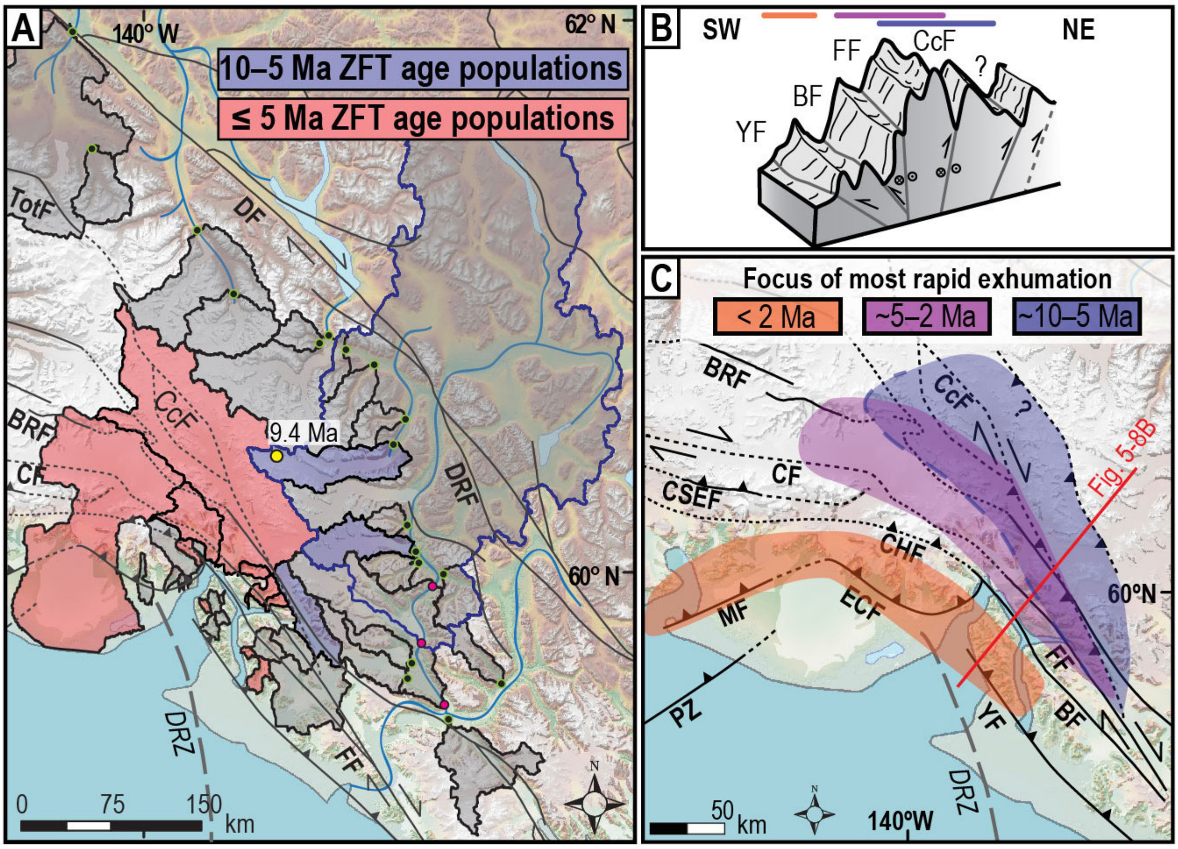

Figure 5-8A–C. (A) Locations of catchments with >5 % of 10–5 Ma (purple) and ≤5 Ma (red) detrital ZFT age populations from *Enkelmann et al.* [2009], and Chapters 3 and 5. Age populations representing young volcanics are excluded. (B) Schematic block model of the structures in the St. Elias syntaxis area. The colored bars at the top indicate the migrating focus of most rapid exhumation through time. (C) Map view of the migrating focus of most rapid exhumation ~10–5 Ma, ~5–2 Ma, and <2 Ma based on detrital ZFT and AFT age populations and bedrock thermochronometric ages. Note that the outline of the ~10–5 Ma area of rapid exhumation is uncertain especially in the south and west (dashed line), where <5 Ma exhumation signals overprinted possible earlier signals. (A–C) TotF: Totschunda Fault, DF: Denali Fault, DRF: Duke River Fault, CcF: Connector Fault, BRF: Border Ranges Fault, CF: Contact Fault, FF: Fairweather Fault, CSEF: Chugach-St. Elias Fault, CHF: Chaix Hills Fault, ECF: Esker Creek Fault, MF: Malaspina Fault, BF: Boundary Fault, YF: Yakutat Fault, PZ: Pamplona Zone, DRZ: Dangerous River Zone.

Field observations in the St. Elias Mountains are hindered by glaciation. Therefore, most of the knowledge about the structural geology is based on studies of the ice-free southern ridges of the St. Elias Mountains [e.g., *Pavlis et al.*, 2004, 2012; *Chapman et al.*, 2012], seismic and paleoseismic studies [e.g., *Plafker and Thatcher*, 2008; *Doser*, 2014], and GPS models [e.g., *Elliott et al.*, 2010, 2013; *Marechal et al.*, 2015]. *Bruhn et al.* [2012] combined geomorphic analysis of high-resolution images of bedrock and ice-flow pattern with the seismic record of large earthquakes in the syntaxis region. This comprehensive study suggested that deformation is partly accommodated by several one-sided, positive flower structures in the Yakutat foothills, on the northern side of the northern Fairweather Fault, and at Mt. Logan.

The new data, which record a longer-term deformation history, suggest a larger-scale, two-sided, positive flower structure with a migrating focus of deformation through time (Figure 5-8C). This structure is located on both sides of the northern Fairweather Fault and the areas of Hubbard and Seward glaciers, including an unmapped, south-dipping fault system on the northern side of the Fairweather Fault (Figure 5-8C) as is also predicted by geodynamic modeling [*Koons et al.*, 2010]. Whether the flower structure developed as one- or two-sided cannot be said, as the older, >5 Ma, record from the southern (Yakutat microplate) side is displaced westward along the Fairweather Fault and thus becomes bent and deformed as it passes the syntaxis and is possibly eroded. In any case, the northern side of the flower structure developed ~10 Ma, until deformation and exhumation shifted southwestward and caused rapid and deep-seated exhumation in the center of the flower structure located in the area covered by the Hubbard and Seward glaciers [Chapter 3]. At this time, the flower structure was two-sided with contemporaneous thrusting on the southern side of the Fairweather Fault as recorded by some ~6–4 Ma detrital ZFT age populations in the hanging wall of the Yakutat Fault [Chapter 3]. However, rapid and deep exhumation was confined to the north side of the Fairweather Fault on the North American Plate. As discussed above, deformation appears to have shifted south after ~2 Ma [*Enkelmann et al.*, 2015a], which implies that the northern side of the flower structure was abandoned, or at least that deformation and exhumation decreased significantly in that area. This is consistent with the analysis of *Bruhn et al.* [2012] and geophysical observations that do not indicate a current concentration of deformation in the Connector Fault area [*Enkelmann et al.*, 2015a; *Marechal et al.*, 2015]. However, it should be noted that particularly in the northern St. Elias Mountains only few seismic and GPS stations exist, which might affect models of the current stress field.

5.6 Summary

The new detrital ZFT and AFT age distributions from the northern St. Elias Mountains reveal the long-term cooling history of the Wrangellia Composite Terrane that records two major collisional events. The Late Jurassic–mid-Cretaceous accretion of the Wrangellia Composite Terrane to the former North American margin almost fully reset the thermal record of the study area. Erosional exhumation has since been overall slow as the Jurassic–Cretaceous record is well preserved. However, despite the inboard position of the study area to the northeast of the northwestward moving Yakutat microplate, the effects of Yakutat flat-slab subduction and oblique collision are clearly evident.

Furthermore, the data support the southern part of the Connector Fault (Art Lewis Fault) as being the limit of rapid and deep-seated Pliocene exhumation in the St. Elias syntaxis area [Chapter 3]. This area of rapidly exhuming rocks extended farther northeastward in the late Miocene (~10–5 Ma), reaching into the southeastern part of the study area of Chapter 5.

The data suggest the existence of an unmapped, ice-covered, southwest-dipping fault located northeast of the Connector Fault and indicate a large-scale, positive flower structure with a migrating focus of deformation through time. In the late Miocene, deformation and rock exhumation was accommodated along the Fairweather Fault and southwest-dipping faults north of the Border Ranges Fault. With a change in plate motions, glaciation of the area, and lateral changes in subducting slab thickness, the focus of deformation shifted southward at ~5 Ma and caused rapid and deep-seated exhumation in the center of the two-sided flower structure between Connector Fault and thrust faults in the Yakutat foothills, but with rapid and deep exhumation only along and north of the Fairweather Fault. The southward shift continued and since ~2 Ma deformation and the most rapid exhumation is concentrated along northeast dipping thrust faults that parallel the northern Fairweather Fault and along the northwest-dipping, shallow thrust of the fold-and-thrust belt.

6 Conclusion

The St. Elias Mountains situated in southeast Alaska and adjacent areas of western Canada are the highest coastal mountains on Earth. Their remote, rugged, and extensively glaciated location makes access a logistic and financial challenge. No roads extend into the mountains and most areas can only be sampled via helicopter. Despite those difficulties, the St. Elias Mountains became one of the best-dated orogens in the world over the last few years. The detrital thermochronologic dataset obtained in this study contributes significantly to the understanding of exhumation in the wider St. Elias syntaxis area and its relation to other parts of the orogen, including the inboard region.

Detrital thermochronology yielded integrated long-term cooling and exhumation signals from a large area and thus gave insight into the regional tectonic history.

1) Two large-scale terrane subduction and accretion phases are recorded in cooling signals of the study area; the Jurassic–Cretaceous accretion of the Wrangellia Composite Terrane to the former North American margin and the ongoing flat-slab subduction and collision of the Yakutat microplate.
2) The transform plate boundary between the Yakutat microplate and the North American Plate has been characterized by transpression since at least ~30 Ma and exhibits highly variable cooling due to Oligocene–Recent transpression-related exhumation and Oligocene–earliest Miocene magmatism.
3) Flat-slab subduction of the Yakutat microplate and upper/lower plate-coupling has been affecting the St. Elias syntaxis area, the western St. Elias and Chugach mountains as well as wide areas of south-central Alaska in terms of uplift, exhumation, and erosion since the Oligocene.
4) The onset of collision of the Yakutat microplate with the North American Plate can be constrained to the mid-Miocene (~15–12 Ma).
5) The St. Elias syntaxis is emphasized as transitional zone between transpression to the east and oblique subduction to the west. The syntaxis area shows aspects of cooling histories found to the east and west as well as distinct cooling phases unique to the syntaxis area.
6) Tectonic and climatic systems changed at the beginning of the Pliocene and coevolved since. Extremely efficient glacial erosion in mountain valleys played an important role in redistributing large amounts of material and creating the high relief of the St. Elias Mountains.

The main findings concerning the spatio-temporal evolution of exhumation and structural implications for the St. Elias syntaxis are:

1) There exists an area of rapid exhumation at the St. Elias syntaxis, but it is not a stable feature. Extent, location, and depth of rapid exhumation changed through time.
2) Rapid exhumation began ~10 Ma in the northern St. Elias Mountains northeast of the Fairweather Fault and shifted southwestward at ~5 Ma accompanied by an increase in rate and depth of exhumation. The amount of Pliocene exhumation has been ~10 km, or reaching depths of ~300 °C, north of the Fairweather Fault in an area ~4,800 km^2 large. After ~2 Ma, the focus of deformation shifted farther southward to the thrust and reverse faults south of the Fairweather Fault in the Malaspina and Yakutat foothills area on the Yakutat microplate.
3) The extent of rapid exhumation appears to be confined by discrete structures including at least one unmapped fault in the northern St. Elias Mountains, the southern Connector Fault (Art Lewis Fault), the Fairweather Fault, and thrust faults of the Yakutat foothills and Malaspina area, including the Boundary, Yakutat, Esker Creek, and Chaix Hills faults. At least in the Pliocene, these structures have formed a large-scale, two-sided flower structure.
4) Reasons for the concentration of stress and strain in the St. Elias syntaxis area are likely a combination of i) the collisional tectonics that intensified with the increasing thickness of the wedge-shaped Yakutat crust, ii) a change in Pacific Plate motion at ~5 Ma resulting in a larger compressional component of the Yakutat-North American convergence, and iii) the coevolving climatic system that resulted in efficient glacial erosion in a dynamic mountainous landscape since the Pliocene. Vast amounts of material have been transported out of the St. Elias Mountains and deposited offshore.
5) The migrating focus of deformation and the involvement of different structures over time need to be included in geodynamic models of the Yakutat subduction and collision. For example, models of inland strain transfer or exhumation mechanisms require adaption for the larger amount of strain accommodated by the wider St. Elias syntaxis area than previously known.

These findings address **hypothesis (1)** from Chapter 1.1:

Subduction of the Yakutat plate corner results in localized rapid and deep exhumation at the St. Elias syntaxis.

The data indicate that the subduction of the Yakutat plate corner resulted in localized rapid and, at times, deep exhumation, which was induced by tectonic processes. However, tectonic-climatic interactions and efficient glacial erosion play an important role in the modification of exhumation processes.

Moreover, this study bears implications for syntaxial regions in general.

1) Syntaxes must be treated as four-dimensional settings with a spatio-temporally heterogeneous distribution of deformation. These regions cannot be considered

as locally stable over long time intervals and are likely to adapt quickly to changing tectonic, rheologic, and climatic systems, which in turn are influenced by evolving topography and surface processes. The development of feedback mechanisms between tectonic, climatic, and surface processes is probable.

2) The St. Elias syntaxis has been compared with the eastern and western Himalayan syntaxes and the same exhumation mechanisms, even though in different stages, have been inferred. This study, however, suggests a different evolution and possibly different mechanisms for exhumation at the St. Elias syntaxis.
3) A large observational dataset of the development of exhumation at the Yakutat plate corner is provided here, which is important for future geodynamic models. This study also highlights the lack of an encompassing understanding of syntaxes at this point and that more data from syntaxes in different locations are required to evaluate contending exhumation models and contributing processes (tectonic, climatic, erosional).
4) It is crucial for future studies to give definitions of the terms “plate corner” and “syntaxis”, which have previously been vague. A clear definition is essential to avoid misunderstandings and generalizations of settings that might actually not be related.

These findings address **hypothesis (2)** from Chapter 1.1 only partly.

Exhumation mechanisms at the St. Elias syntaxis can be described as nascent “tectonic aneurysm” similar to the more developed Himalayan syntaxes.

The results highlight the differences between the eastern and western Himalayan syntaxes and the St. Elias syntaxis. However, different exhumation models cannot be evaluated with the data. Results rule out that processes similar to the Himalayan syntaxes are at play but cannot rule out that the same processes started to develop but then evolved into different mechanisms.

Hypothesis (3) from Chapter 1.1 can be confirmed.

Detrital sampling is the most suitable approach to reveal the cooling history beneath the thick and extensive ice cover of the St. Elias Mountains.

Detrital thermochronology proved to be very powerful in revealing the exhumation history from below the ice cover of the St. Elias Mountains. The innovative approach of detrital sampling can be summarized as follows.

1) The use of sand-sized detritus facilitated a large sampling coverage, including elevations above and below the ice of 47 catchments with a total area of almost 45,000 km^2. Previous bedrock samples resulted in a biased dataset, as thermochronometric ages were mainly taken from high elevations, while the most recent exhumation signals are sourced from the ice-filled valleys from low elevations.

2) The problem of lost provenance information that accompanies the use of sand-sized samples was overcome by using cobble-sized detritus. Cobbles combine the advantages of detrital sand (large spatial coverage, material from below the glaciers) and bedrock samples (unweathered mineral phases for multiple thermochronometric dating). Hence, complete cooling histories can be obtained and linked to lithology and provenance.

References

Aldrich, L. T., and A. O. Nier (1948), Argon 40 in potassium minerals, *Phys. Rev., 74*, 876–877, doi: 10.1103/PhysRev.74.876.

Amato, J. M., and T. L. Pavlis (2010), Detrital zircon ages from the Chugach Terrane, southern Alaska, reveal multiple episodes of accretion and erosion in a subduction complex, *Geology, 38*, 459–462, doi: 10.1130/G30719.1.

Andronicos, C. L., L. S. Hollister, C. M. Davidson, and D. H. Chardon (1999), Kinematic and tectonic significance of transpressive structures within the Coast Plutonic Complex, British Columbia, *J. Struct. Geol., 21*, 229–243, doi: 10.1016/S0191-8141(98)00117-5.

Andronicos, C. L., D. H. Chardon, L. S. Hollister, G. E. Gehrels, and G. J. Woodsworth (2003), Strain partitioning in an obliquely convergent orogen, plutonism, and synorogenic collapse: Coast Mountains Batholith, British Columbia, Canada, *Tectonics, 22*, doi: 10.1029/2001TC001312.

Arkle, J. C., P. A. Armstrong, P. J. Haeussler, M. G. Prior, S. Hartman, K. L. Sendziak, and J. A. Brush (2013), Focused exhumation in the syntaxis of the western Chugach Mountains and Prince William Sound, Alaska, *Geol. Soc. Am. Bull., 125*, 776–793, doi: 10.1130/B30738.1.

Armstrong, A. K., and E. M. MacKevett (1982), Stratigraphy and diagenetic history of the lower part of the Triassic Chitistone Limestone, Alaska, *U.S. Geol. Surv. Prof. Paper 1212-A*, A1-A26.

Armstrong, R. L. (1988), Mesozoic and Early Cenozoic magmatic evolution of the Canadian Cordillera, *GSA Special Papers*, *218*, 55–92, doi: 10.1130/SPE218-p55.

Arsenault, A. M., and A. J. Meigs (2005), Contribution of deep-seated bedrock landslides to erosion of a glaciated basin in southern Alaska, *Earth Surf. Process. Landforms, 30*, 1111–1125, doi: 10.1002/esp.1265.

Beaumont, C., P. Fullsack, and J. Hamilton (1992), Erosional control of active compressional orogens, in *Thrust Tectonics*, edited by K. R. McClay, 1–18, Chapman and Hall.

Beaumont, C., H. Kooi, and S. D. Willett (1999), Coupled tectonic-surface process models with applications to rifted margins and collisional orogens, in *Geomorphology and Global Tectonics*, edited by M.A. Summerfield, 29–55, John Wiley and Sons Ltd.

Bendick, R., and T. A. Ehlers (2014), Extreme localized exhumation at syntaxes initiated by subduction geometry, *Geophys. Res. Lett., 41*, 5861–5867, doi: 10.1002/2014GL061026.

Benowitz, J. A., P. W. Layer, P. Armstrong, S. E. Perry, P. J. Haeussler, P. G. Fitzgerald, and S. VanLaningham (2011), Spatial variations in focused exhumation along a continent-scale strike-slip fault: The Denali Fault of the eastern Alaska Range, *Geosphere, 7*, 455–467, doi: 10.1130/GES00589.1.

Benowitz, J. A., P. J. Haeussler, P. W. Layer, P. B. O'Sullivan, W. K. Wallace, and R. J. Gillis (2012), Cenozoic tectono-thermal history of the Tordrillo Mountains, Alaska: Paleocene-Eocene ridge subduction, decreasing relief, and Late Neogene faulting, *Geochem. Geophys. Geosyst., 13*, Q04009, doi: 10.1029/2011GC003951.

Benowitz, J. A., P. W. Layer, and S. Vanlaningham (2014), Persistent long-term (c. 24 Ma) exhumation in the Eastern Alaska Range constrained by stacked thermochronology, *Geol. Soc. London Special Puplications, 378*, 225–243, doi: 10.1144/SP378.12.

Beranek, L. P., C. R. van Staal, S. M. Gordee, W. C. McClelland, S. Israel., and M. Mihalynuk (2012), Tectonic significance of Upper Cambrian–Middle Ordovician mafic volcanic rocks on the Alexander Terrane, Saint Elias Mountains, northwestern Canada, *J. Geol., 120*, 293–314, doi: 10.1086/664788.

Beranek, L. P., C. R. van Staal, W. C. McClelland, N. Joyce, and S. Israel (2014), Late Paleozoic assembly of the Alexander-Wrangellia-Peninsular composite terrane, Canadian and Alaskan Cordillera, *Geol. Soc. Am. Bull., 126*, 1531–1550, doi:10.1130/B31066.1.

Berg, H. C., D. L. Jones, and D. H. Richter (1972), Gravina-Nutzotin Belt: Tectonic significance of an upper Mesozoic sedimentary and volcanic sequence in southern and southeastern Alaska, *U.S. Geol. Surv. Prof. Paper 800D*, D1–D24.

Berger, A. L., and J. A. Spotila (2008), Denudation and deformation in a glaciated orogenic wedge: The St. Elias orogen, Alaska, *Geology, 36*, 523–526, doi: 10.1130/G24883A.1.

Berger, A. L., J. A. Spotila, J. B. Chapman, T. L. Pavlis, E. Enkelmann, N. A. Ruppert, and J. T. Buscher (2008), Architecture, kinematics, and exhumation of a convergent orogenic wedge: A thermochronological investigation of tectonic-climatic interactions within the central St. Elias orogen, Alaska, *Earth Planet. Sci. Lett., 270*, 13–24, doi: 10.1016/j.epsl.2008.02.034.

Berger, G. W., and D. York (1981), Geothermometry from $^{40}Ar/^{39}Ar$ dating experiments, *Geochim. Cosmochim. Acta, 45*, 795–811, doi: 10.1016/0016-7037(81)90109-5.

Bernet, M., and J. I. Garver (2005), Fission-track analysis of detrital zircon, *Rev. Mineral. Geochem., 58*, 205–237, doi: 10.2138/rmg.2005.58.8.

Boltwood, B. B. (1907), On the ultimate disintegration products of the radioactive elements. Part II. The disintegration products of uranium, *Am. J. Sci., 23*, 77–88, doi: 10.2475/ajs.s4-23.134.78.

Booth, A. L., C. P. Chamberlain, W. S. Kidd, and P. K. Zeitler (2009), Constraints on the metamorphic evolution of the eastern Himalayan syntaxis from geochronologic and petrologic studies of Namche Barwa, *Geol. Soc. Am. Bull., 121*, 385–407, doi: 10.1130/B26041.1.

Bradley, D. C., T. M. Kusky, P. J. Haeussler, R. J. Goldfarb, M. L. Miller, J. A. Dumoulin, S. W. Nelson, and S. M. Karl (2003), Geologic signature of Early Tertiary ridge subduction in Alaska, in *Geology of a transpressional orogen developed during ridge-trench interaction along the North Pacific margin, Geol. Soc. Am. Special Paper, 371*, edited by V. B. Sisson et al., 19–49, Geological Society of America, Boulder, CO.

Brandon, M. T. (1992), Decomposition of fission-track grain-age distributions, *Am. J. Sci., 292*, 535–564, doi: 10.2475/ajs.292.8.535.

Brandon, M. T. (1996), Probability density plot for fission-track grain-age samples, *Radiat. Meas., 26*, 663–676, doi: 10.1016/S1350-4487(97)82880-6.

Brandon, M. T., M. K. Roden-Tice, and J. I. Garver (1998), Late Cenozoic exhumation of the Cascadia accretionary wedge in the Olympic Mountains, northwest Washington State, *Geol. Soc. Am. Bull., 110*, 985–1009, doi: 10.1130/0016-7606(1998)110<0985:LCEOTC>2.3.CO;2.

Braun. J (2002), Quantifying the effect of recent relief change on age-elevation relationships, *Earth Planet. Sci. Lett., 200*, 331–343, doi: 10.1016/S0012-821X(02)00638-6.

Brennan, P.R., and K. D. Ridgway (2015), Detrital zircon record of Neogene exhumation of the central Alaska Range: A far-field upper plate response to flat-slab subduction, *Geol. Soc. Am. Bull.*, doi: 10.1130/B31164.1.

Bruhn, R. L., T. L. Pavlis, G. Plafker, and L. Serpa (2004), Deformation during terrane accretion in the Saint Elias orogen, Alaska, *Geol. Soc. Am. Bull., 116*, 771–787, doi: 10.1130/B25182.1.

Bruhn, R. L., J. Sauber, M. M. Cotton, T. L. Pavlis, E. Burgess, N. A. Ruppert, and R. R. Forster (2012), Plate margin deformation and active tectonics along the northern edge of the Yakutat Terrane in the Saint Elias orogen, Alaska, and Yukon, Canada, *Geosphere, 8*, 1384–1407, doi: 10.1130/GES00807.1.

Burg, J.-P., P. Nievergelt, F. Oberli, D. Seward, P. Davy, J.-C. Maurin, Z. Diao, and M. Meier (1998), The Namche Barwa syntaxis: evidence for exhumation related to compressional crustal folding, *J. Asian Earth Sci., 16*, 239–252, doi: 10.1016/S0743-9547(98)00002-6.

Bursill, L. A., and G. Braunshausen (1990), Heavy-ion irradiation tracks in zircon, *Philos. Mag. A, 62*, 395–420, doi: 10.1080/01418619008244787.

Carlson, B. M. (2012), Cooling and provenance revealed through detrital zircon fission track dating of the Upper Cretaceous Valdez Group and Paleogene Orca Group in Western Prince William Sound, Alaska, *Proceedings from the 25th Keck Geology Consortium Undergraduate Research Symposium*, Amherst MA, 8–16.

Csejtey, B. Jr., D. P. Cox, R. C. Evarts, G. D. Stricker, and H. L. Foster (1982), The Cenozoic Denali Fault System and the Cretaceous accretionary development of southern Alaska, *J. Geophys. Res. Solid Earth, 87*, 3741–3754, doi: 10.1029/JB087iB05p03741.

Chapman, J. B., T. L. Pavlis, R. L. Bruhn, L. L. Worthington, S. P. Gulick, and A. L. Berger (2012), Structural relationships in the eastern syntaxis of the St. Elias orogen, Alaska, *Geosphere, 8*, 105–126, doi: 10.1130/GES00677.

Chapple, W. M. (1978), Mechanics of thin-skinned fold-and-thrust belts, *Geol. Soc. Am. Bull., 89*, 1189–1198, doi: 10.1130/0016–7606(1978)89<1189:MOTFB>2.0.CO;2.

Christeson, G. L., S. P. Gulick, H. J. Van Avendonk, L. L. Worthington, R. S. Reece, and T. L. Pavlis (2010), The Yakutat Terrane: Dramatic change in crustal thickness across the Transition Fault, Alaska, *Geology, 38*, 895–898, doi: 10.1130/G31170.1.

Clift, P. D., T. L Pavlis, S. M. DeBari, A. E. Draut, M. Rioux, and P. B. Kelemen (2005), Subduction erosion of the Jurassic Talkeetna-Bonanza arc and the Mesozoic accretionary tectonics of western North America, *Geology, 33*, 881–884, doi: 10.1130/G21822.1.

Cloos, M. (1993), Lithospheric buoyancy and collisional orogenesis: Subduction of oceanic plateaus, continental margins, island arcs, spreading ridges, and seamounts, *Geol. Soc. Am. Bull., 105*, 715–737, doi: 10.1130/0016-7606(1993)105<0715:LBACOS>2.3.CO;2.

Cobbett, R., S. Israel., and J. Mortensen (2010), The Duke River Fault, southwest Yukon: Preliminary examination of the relationship between Wrangellia and the Alexander terrane, in *Yukon Exploration and Geology 2009*, edited by K. E. MacFarlane et al., 143–158, Yukon Geological Survey.

Colpron, M., and J. L. Nelson (2011), A Paleozoic NW Passage and the Timanian, Caledonian and Uralian connections of some exotic terranes in the North American Cordillera, in *Arctic Petroleum Geology*, edited by A. M. Spencer et al., Geol. Soc. London, Memoirs, 35, 463–484, doi: 10.1144/M35.31.

Coney, P. J., D. J. Jones, and J. W. Monger (1980), Cordilleran suspect terranes, *Nature, 288*, 329–333, doi: 10.1038/288329a0.

Copeland, P., R. R. Parrish, and T. M. Harrison (1988), Identification of inherited radiogenic Pb in monazite and its implications for U-Pb systematics, *Nature, 333*, 760–763, doi: 10.1038/333760a0.

Cotton, M. M., R. L. Bruhn, J. Sauber, E. Burgess, and R. R. Forster (2014), Ice surface morphology and flow on Malaspina Glacier, Alaska: Implications for regional tectonics in the St. Elias orogen, *Tectonics, 33*, 581–595, doi: 10.1002/2013TC003381.

Dalrymple, G. B., and M. A. Lanphere (1969), *Potassium-argon dating: principles, techniques and applications to geochronology*, Freeman, San Francisco, CA, 258 p.

Dahlen, F. A., J. Suppe, and D. Davis (1984), Mechanics of fold-and-thrust belts and accretionary wedges: Cohesive Coulomb Theory, *J. Geophys. Res., 89*, 10087–10101, doi: 10.1029/JB089iB12p10087.

Davidson, C., J. I. Garver, H. L. Hilbert-Wolf, and B. Carlson (2011), Maximum depositional age of the Paleocene to Eocene Orca flysch, Prince William Sound, Alaska, paper presented at GSA Annual Meeting Minneapolis.

Davis, A. S., and G. Plafker (1986), Eocene basalts from the Yakutat terrane: Evidence for the origin of an accretionary terrane in southern Alaska, *Geology, 14*, 963–966, doi: 10.1130/0091-7613(1986)14<963:EBFTYT>2.0.CO;2.

Davis, D. W., T. E. Krogh, and I. S. Williams (2003), Historical development of zircon geochronology, *Rev. Mineral. Geochem., 53*, 145–181, doi: 10.2113/0530145.

Dempster, A. J. (1935), Isotopic constitution of uranium, *Nature, 136*, 180–180, doi: 10.1038/136180a0.

Dodds, C. J., and P. B. Campbell (1988), Potassium-argon ages of mainly intrusive rocks in the Saint Elias Mountains, Yukon and British Columbia, *Geological Survey of Canada paper 87-16*.

Dodds, C. J., and R. B. Campbell (1992), Overview, legend, and mineral deposit tabulations for geology of SW Kluane Lake (115G & F[E1/2]), Mount Saint Elias (115B & C[E1/2]), SW Dezadeash (115A), NE Yakutat (114O), and Tatshenshini (114P) map areas, Yukon Territory and British Columbia, *Geol. Surv. Can. Open Files 2188–2191*, 85 p.

Dodson, M. H. (1973), Closure temperature in cooling geochronological and petrological systems, *Contr. Mineral. Petrol., 40*, 259–274, doi: 10.1007/BF00373790.

Doig, R. (1998), Paleoseismological evidence from lake sediments for recent movement on the Denali and other faults, Yukon Territory, Canada, *Tectonophysics, 296*, 363–370, doi: 10.1016/S0040-1951(98)00152-8.

Donelick, R. A., Roden, M. K., Mooers, J. D., B. S. Carpenter, and D. S. Miller (1990), etchable length reduction of induced fission tracks in apatite at room temperature (≈23°C): crystallographic orientation effects and "initial" mean lengths, *Int. J. Radiat. Appl. Instrum. Part D, 17*, 261–265, doi: 10.1016/1359-0189(90)90044-X.

Doser, D. I., and R. Lomas (2000), The transition from strike-slip to oblique subduction in southeastern Alaska from seismological studies, *Tectonophysics, 316*, 45–65, doi: 10.1016/S0040-1951(99)00254-1.

Doser, D. I. (2014), Seismicity of Southwestern Yukon, Canada, and its relation to slip transfer between the Fairweather and Denali fault systems, *Tectonophysics, 611*, 121–129, doi: 10.1016/j.tecto.2013.11.018.

Dumoulin, J. A. (1988), Sandstone petrographic evidence and the Chugach-Prince William terrane boundary in southern Alaska, *Geology, 16*, 456–460, doi: 10.1130/0091-7613(1988)016<0456:SPEATC>2.3.CO;2.

Dusel-Bacon, C., B. Csejtey, H. L. Foster, E. O. Doyle, W.J. Nokleberg, and G. Plafker (1993), Distribution, facies, ages, and proposed tectonic associations of regionally metamorphosed rocks in east- and south-central Alaska, *U.S. Geol. Surv. Prof. Pap. 1497-C*.

Eberhart-Phillips, D., P. J. Haeussler, J. T. Freymueller, A. D. Frankel, C. M. Rubin, P. Craw, N. A. Ratchkovski, G. Anderson, G. A. Carver, A. J. Crone, T. E. Dawson, H. Fletcher, R. Hansen, E. L. Harp, R. A. Harris, D. P. Hill, S. Hreinsdóttir, R. W. Jibson, L. M. Jones, R. Kayen, D. K. Keefer, C. F. Larsen, S. C. Moran, S. F. Personius, G. Plafker, B. Sherrod, K. Sieh, N. Sitar, and W. K. Wallace (2003), The 2002 Denali Fault earthquake, Alaska: A large magnitude, slip-partitioned event, *Science, 300*, 1113–1118 doi: 10.1126/science.1082703.

Eberhart-Phillips, D., D. H. Christensen, T. M. Brocher, R. Hansen, N. A. Ruppert, P. J. Haeussler, and G. A. Abers (2006), Imaging the transition from Aleutian subduction to Yakutat collision in central Alaska, with local earthquakes and active source data, *J. Geophys. Res., 111*, B11303, doi: 10.1029/2005JB004240.

Ehlers, T. A., and K. A. Farley (2003), Apatite (U-Th)/He thermochronometry: methods and applications to problems in tectonic and surface processes, *Earth Planet. Sci. Lett., 206*, 1–14, doi: 10.1016/S0012-821X(02)01069-5.

Eisbacher, G.H. (1976), Sedimentology of the Dezadeash flysch and its implications for strike-slip faulting along the Denali Fault, Yukon Territory and Alaska, *Can. J. Earth Sci., 13*, 1495–1513, doi: 10.1139/e76-157.

Elliott, J. L., C. F. Larsen, J. T. Freymueller, and R. J. Motyka (2010), Tectonic block motion and glacial isostatic adjustment in southeast Alaska and adjacent Canada constrained by GPS measurements, *J. Geophys. Res., 115*, B09407, doi: 10.1029/2009JB007139.

Elliott, J. L., J. T. Freymueller, and C. F. Larsen (2013), Active tectonics of the St. Elias orogen, Alaska, observed with GPS measurements, *J. Geophys. Res. Solid Earth, 118*, 5625–5642, doi: 10.1002/jgrb.50341.

Elmore, C. R., S. P. Gulick, B. Willems, and R. Powell (2013), Seismic stratigraphic evidence for glacial expanse during glacial maxima in the Yakutat Bay Region, Gulf of Alaska, *Geochem. Geophys. Geosyst, 14*, 1294–1311, doi: 10.1002/ggge.20097.

Engebretson, D. C., A. Cox, and R. G. Gordon (1985), Relative motions between oceanic and continental plates in the Pacific basin, *Spec. Pap. Geol. Soc. Am., 206*, 1–60, doi: 10.1130/SPE206-p1.

England, P., and P. Molnar (1990), Surface uplift, uplift of rocks, and exhumation of rocks, *Geology, 18*, 1173–1177, doi: 10.1130/0091-7613(1990)018<1173:SUUORA>2.3.CO;2.

Enkelmann, E., J. I. Garver, and T. L. Pavlis (2008), Rapid exhumation of ice-covered rocks of the Chugach-St. Elias orogen, SE-Alaska. *Geology, 36*, 915–918, doi: 10.1130/G2252A.1.

Enkelmann, E., P. K. Zeitler, T. L. Pavlis, J. I. Garver, and K. D. Ridgway (2009), Intense localized rock uplift and erosion in the St. Elias orogen of Alaska, *Nat. Geosci., 2*, 360–363, doi: 10.1038/NGEO502.

Enkelmann, E., P. K. Zeitler, J. I. Garver, T. L. Pavlis, and B. P. Hooks (2010), The thermochronological record of tectonic and surface process interaction at the Yakutat–North American collision zone in southeast Alaska. *Am. J. Sci., 310*, 231–260, doi: 10.2475/04.2010.01.

Enkelmann, E., T. A. Ehlers, P. K. Zeitler, and B. Hallet (2011), Denudation of the Namche Barwa antiform, eastern Himalaya, *Earth Planet. Sci. Lett., 307*, 323–333, doi: 10.1016/j.epsl.2011.05.004.

Enkelmann, E., P. O. Koons, T. L. Pavlis, B. Hallet, A. Barker, J. L. Elliott, J. I. Garver, S. P. Gulick, R. M. Headley, G. L. Pavlis, K. D. Ridgway, N. A. Ruppert, and H. J. Van Avendonk (2015a), Cooperation among tectonic and surface processes in the St. Elias Range, Earth's highest coastal mountains, *Geophys. Res. Lett.*, 5838–5846, doi: 10.1002/2015GL064727.

Enkelmann, E., P. G. Valla, and J.-D. Champagnac (2015b), Low-temperature thermochronology of the Yakutat plate corner, St. Elias Range (Alaska): bridging short-term and long-term deformation, *Quat. Sci. Rev., 113*, 23–38, doi: 10.1016/j.quascirev.2014.10.019.

Erdmer, P., and J. K. Mortensen (1993), A 1200-km-long Eocene metamorphic-plutonic belt in the northwestern Cordillera–Evidence from southwest Yukon, *Geology, 21*, 1039–1042, doi: 10.1130/0091-7613(1993)021<1039:AKLEMP>2.3.CO;2.

Falkowski, S., E. Enkelmann, and T. A. Ehlers (2014), Constraining the area of rapid and deep-seated exhumation at the St. Elias syntaxis, southeast Alaska, with detrital zircon fission-track analysis, *Tectonics, 33*, 597–616, doi: 10.1002/2013TC003408.
Farley, K. A. (2000), Helium diffusion from apatite: general behavior as illustrated by Durango fluorapatite. *J. Geophys. Res., 105*, 2903–2914, doi: 10.1029/1999JB900348.
Farley, K. A. (2002), (U-Th)/He dating: Techniques, calibrations, and applications, *Rev. Mineral. Geochem., 47*, 819–844, doi: 10.2138/rmg.2002.47.18.
Farley, K. A., R. A. Wolf, and L. T. Silver (1996), The effects of long alpha-stopping distances on U-Th/He dates, *Geochim. Cosmochim. Acta, 60*, 4223–4230, doi: 10.1016/S0016-7037(96)00193-7.
Farmer, G. L., R. Ayuso, and G. Plafker (1993), A Coast Mountains provenance for the Valdez and Orca groups, southern Alaska, based on Nd, Sr, and Pb isotopic evidence, *Earth Planet. Sci. Lett., 116*, 9–21, doi: 10.1016/0012-821X(93)90042-8.
Farrar, E., A. H. Clark, D. A. Archibald, and D. C. Way (1988), Potassium-argon age of granitoid pluton rocks, southwest Yukon Territory, Canada, Isochron/West, 51, 19–23.
Ferris, A., G. A. Abers, D. H. Christensen, and E. Veenstra (2003), High resolution image of the subducted Pacific (?) Plate beneath central Alaska, 50–150 km depth, *Earth Planet. Sci. Lett., 214*, 575–588, doi: 10.1016/S0012-821X(03)00403-5.
Finnegan, N. J., B. Hallet, D. R. Montgomery, P. K. Zeitler, J. O. Stone, A. M. Anders, and L. Yuping (2008), Coupling of rock uplift and river incision in the Namche Barwa-Gyala Peri massif, Tibet, *Geol. Soc. Am. Bull., 120*, 142–155, doi: 10.1130/B26224.1.
Finzel, E. S., L. M. Flesch, and K. D. Ridgway (2011a), Kinematics of a diffuse North America-Pacific-Bering plate boundary in Alaska and western Canada, *Geology, 39*, 835–838, doi: 10.1130/G32271.1.
Finzel, E. S., J. M. Trop, K. D. Ridgway, and E. Enkelmann (2011b), Upper plate proxies for flat-slab subduction processes in southern Alaska, *Earth Planet. Sci. Lett.*, *303*, 348–360, doi: 10.1016/j.epsl.2011.01.014.
Fitzgerald, P. G., and J. W. Gleadow (1990), New approaches in fission track geochronology as a tectonic tool: Examples from the Transantarctic Mountains, *Int. J. Radiat. Appl. Instrum. Part D, 17*, 351–357, doi:10.1016/1359-0189(90)90057-5.
Fitzgerald, P. G., R. B. Sorkhabi, T. F. Redfield, E. Stump (1995), Uplift and denudation of the central Alaska Range: A case study in the use of apatite fission-track thermochronology to determine absolute uplift parameters, *J. Geophys. Res, 100*, 20175–20191, doi: 10.1029/95JB02150.
Fitzgerald, P. G., S. L. Baldwin, L. E. Webb, and P. B. O' Sullivan (2006), Interpretation of (U-Th)/He single grain ages from slowly cooled crustal terranes: A case study from the Transantarctic Mountains of southern Victoria Land, *Chem. Geol., 225*, 91–120, doi: 10.1016/j.chemgeo.2005.09.001.
Fleischer, R. L., P. B. Price, and R. M. Walker (1975), *Nuclear tracks in solids: principles and applications*, University of California Press, Berkeley, CA, USA.
Fletcher, H. J., and J. T. Freymueller (2003), New constraints on the motion of the Fairweather Fault, Alaska, from GPS observations, *Geophys. Res. Lett., 30*, 1139, 10.1029/2002GL016476.
Flowers, R. M., R. A. Ketcham, D. L. Shuster, K. A. Farley (2009), Apatite (U-Th)/He thermochronometry using a radiation damage accumulation and annealing model, *Geochim. Cosmochim. Acta, 73*, 2347–2365, doi: 10.1016/j.gca.2009.01.015.
Foland, K. A. (1994), Argon diffusion in feldspars, in *Feldspars and their reactions*, edited by I. Parsons, 415–447, Kluwer, Amsterdam.

Galbraith, R. F. (1981), On statistical models for fission track counts, *J. Int. Ass. Math. Geol., 13*, 471–478, doi: 10.1007/BF01034498.

Galbraith, R. F. (2005), *Interdisciplinary statistics, Statistics for fission track analysis*, Boca Raton, FL, USA, Chapman & Hall/CRC, Taylor & Francis Group, 219 p.

Gallagher, K., R. W. Brown, and C. Johnson (1998), Fission-track analysis and its applications to geological problems, *Annu. Rev. Earth Planet. Sci., 26*, 519–572, doi: 10.1146/annurev.earth.26.1.519.

Gardner, M. C., S. C. Bergman, G. W. Cushing, E. M. MacKevett, G. Plafker, R. B. Campbell, C. J. Dodds, W. C. McClelland, and P. A. Mueller (1988), Pennsylvanian pluton stitching of Wrangellia and the Alexander Terrane, Wrangell Mountains, Alaska, *Geology, 16*, 967–971, doi:10.1130/0091-7613(1988)016<0967:PPSOWA> 2.3.CO;2.

Garver, J. I. (2003), Etching zircon age standards for fission-track analysis, *Radiat. Meas., 37*, 47–53, doi: 10.1016/S1350-4487(02)00127-0.

Garver, J. I., and P. J. Kamp (2002), Integration of zircon color and zircon fission-track zonation patterns in orogenic belts: Application to the Southern Alps, New Zealand, *Tectonophysics, 349*, 203–219, doi: 10.1016/S0040-1951(02)00054-9. 10.1130/G2252A.1.

Garver, J. I., and C. M. Davidson (2015), Southwestern Laurentian zircons in Upper Cretaceous flysch of the Chugach-Prince William terrane in Alaska, *Am. J. Sci., 315*, 537–556, doi: 10.2475/06.2015.02.

Garver, J. I., M. T. Brandon, M. Roden-Tice, and P. J. Kamp (1999), Exhumation history of orogenic highlands determined by detrital fission-track thermochronology, *Geol. Soc. London Special Publications, 154*, 283–304, doi: 10.1144/GSL.SP.1999.154.01.13.

Gasser, D., E. Bruand, K. Stüwe, D. A. Foster, R. Schuster, B. Fügenschuh, and T. L. Pavlis (2011), Formation of a metamorphic complex along an obliquely convergent margin: Structural and thermochronological evolution of the Chugach Metamorphic Complex, southern Alaska, *Tectonics, 30*, TC2012, doi: 10.1029/2010TC002776.

Gasser, D., D. Rubatto, E. Bruand, and K. Stüwe (2012), Large-scale, short-lived metamorphism, deformation, and magmatism in the Chugach Metamorphic Complex, southern Alaska: A SHRIMP U-Pb study of zircon, *Geol. Soc. Am. Bull., 124*, 886–905, doi: 10.1130/B30507.1.

Gautheron, C., L. Tassan-Got, J. Barbarand, and M. Pagel (2009), Effect of alpha-damage annealing on apatite (U-Th)/He thermochronology, *Chem. Geol., 266*, 157–170, doi: 10.1016/j.chemgeo.2009.06.001.

Gebauer, D., I. S. Williams, W. Compston, M. Grünenfelder (1989), The development of the Central European continental crust since the Early Archaean based on conventional and ion-microprobe dating of up to 3.84 b.y. old detrital zircons, *Tectonophysics, 157*, 81–96, doi: 10.1016/0040-1951(89)90342-9.

Gehrels, G. E., M. E. Rusmore, G. J. Woodsworth, M. L. Crawford, C. L. Andronicos, L. S. Hollister, P. J. Patchett, M. N. Ducea, R. F. Butler, K. Klepeis, C. M. Davidson, R. M. Friedman, J. W. Haggart, J. B. Mahoney, W. A. Crawford, D. Pearson, and J. Girardi (2009), U-Th-Pb geochronology of the Coast Mountains batholith in north-coastal British Columbia: Constraints on age and tectonic evolution, *Geol. Soc. Am. Bull., 121*, 1341–1361, doi: 10.1130/B26404.1.

Gleadow, A. J., and I. R. Duddy (1981), A natural long-term track annealing experiment for apatite, *Nucl. Tracks, 5*, 169–174, doi: 10.1016/0191-278X(81)90039-1.

Gleadow, A. J., and P. G. Fitzgerald (1987), Uplift history and structure of the Transantarctic Mountains: new evidence from fission track dating of basement apatites in the Dry Valley area, southern Victoria Land, Earth Planet. *Sci. Lett, 82*, 1–14, doi: 10.1016/0012-821X(87)90102-6.

Grabowski, D. M., E. Enkelmann, and T. A. Ehlers (2013), Spatial extent of rapid denudation in the glaciated St. Elias syntaxis region, SE Alaska, *J. Geophys. Res. Earth Surf., 118*, 1921–1938, doi: 10.1002/jgrf.20136.

Green, P. F., and I. R. Duddy (2006), Interpretation of apatite (U-Th)/He ages and fission track ages from cratons, *Earth Planet. Sci. Lett., 244*, 541–547, doi: 10.1016/j.epsl.2006.02.024.

Grünenfelder, M., F. Hofmänner, and N. Grögler (1964), Heterogenität akzessorischer Zirkone und die petrographische Deutung ihrer Uran/Blei-Zerfallsalter: II, Präkambrische Zirkonbildung im Gotthardmassiv, *Schweiz. Mineral. Petrogr. Mitt., 44*, 543–558.

Gulick, S. P., L. A. Lowe, T. L. Pavlis, J. V. Gardner, and L. A. Mayer (2007), Geophysical insights into the Transition Fault debate: Propagating strike slip in response to stalling Yakutat block subduction in the Gulf of Alaska, *Geology, 35*, 763–766, doi: 10.1130/G2358A.1.

Haeussler, P. J., D. C. Bradley, R. E. Wells, and M. L. Miller (2003), Life and death of the Resurrection Plate: Evidence for its existence and subduction in the northeastern Pacific in Paleocene-Eocene time, *Geol. Soc. Am. Bull., 115*, 867–880, doi: 10.1130/0016-7606(2003)115<0867:LADOTR>2.0.CO;2.

Haeussler, P. J., G. E. Gehrels, and S. M. Karl (2005), Constraints on the age and provenance of the Chugach Accretionary Complex from detrital zircons in the Sitka Graywacke near Sitka, Alaska, in Studies by the U.S. Geol. Surv. in Alaska, 2004, *U.S. Geol. Surv. Prof. Pap. 1709-F*.

Haeussler, P. J., P. O'Sullivan, A. L. Berger, and J. A. Spotila (2008), Neogene exhumation of the Tordrillo Mountains, Alaska, and correlations with Denali (Mount McKinley), in *Active Tectonics and Seismic Potential of Alaska*, *Geophys. Monogr. Ser.*, vol. 179, edited by J. T. Freymueller et al., 269–285, American Geophysical Union, Washington, D. C., doi: 10.1029/179GM15.

Hallet, B., L. Hunter, and J. Bogen (1996), Rates of erosion and sediment evacuation by glaciers: A review of field data and their implications, *Global Planet. Change, 12*, 213–235, doi: 10.1016/0921-8181(95)00021-6.

Harrison, T. M. (1981), Diffusion of 40Ar in hornblende, *Contrib. Mineral. Petrol., 78*, 324 331, doi: 10.1007/BF00398927.

Harrison, T. M., and P. K. Zeitler (2005), Fundamentals of noble gas thermochronometry, *Rev. Mineral. Geochem.*, 58, 123–149, doi: 10.2138/rmg.2005.58.5.

Harrison, T. M., I. Duncan, and I. McDougall (1985), Diffusion of ^{40}Ar in biotite: Temperature, pressure and compositional effects, *Geochim. Cosmochim. Acta, 49*, 2461–2468, doi: 10.1016/0016-7037(85)90246-7.

Harrison, T. M., J. Célérier, A. B. Aikman, J. Hermann, M. T. Heizler (2009), Diffusion of ^{40}Ar in muscovite, *Geochim. Cosmochim. Acta, 73*, 1039–1051, doi: 10.1016/j.gca.2008.09.038.

Headley, R. M., E. Enkelmann, and B. Hallet (2013), Examination of the interplay between glacial processes and exhumation in the Saint Elias Mountains, Alaska, *Geosphere, 9*, 229–241, doi: 10.1130/GES00810.1.

Heizler, M. T., and T. M. Harrison (1988), Multiple trapped argon isotope components revealed by ^{40}Ar/^{39}Ar isochron analysis, *Geochim. Cosmochim. Acta, 52*, 1295–1303, doi: 10.1016/0016-7037(88)90283-9.

Hillhouse, J. W. (1977), Paleomagnetism of the Triassic Nikolai Greenstone, McCarthy Quadrangle, Alaska: *Can. J. Earth Sci., 14*, 2578–2592, doi: 10.1139/e77-223.

Holmes, A. (1911), The association of lead with uranium in rock-minerals, and its application to the measurement of geologic time, *Proc. R. Soc. London, Ser. A, 85*, 248–256.

Holmes, A., and R. W. Lawson (1927), Factors involved in the calculation of the ages of radioactive minerals, *Am. J. Sci., 13*, 327–344, doi: 10.2475-ajs.s5-13.76.327.

House, M. A., B. P. Wernicke, and K. A. Farley (1998), Dating topography of the Sierra Nevada, California, using apatite (U-Th)/He ages, *Nature, 396*, 66–69, doi: 10.1038/23926.

Hudson, T., G. Plafker, and D. L. Turner (1977a), Metamorphic rocks of the Yakutat-St. Elias area, south-central Alaska, *Journal of Research of the USGS, 5*, 173–184.

Hudson, T., G. Plafker, and M. A. Lanphere (1977b), Intrusive rocks of the Yakutat-St. Elias area, south-central Alaska, *Journal of Research of the USGS, 5*, 155–172.

Hudson, T., G. Plafker, and Z. E. Peterman (1979), Paleogene anatexis along the Gulf of Alaska margin, *Geology, 7*, 573–577, doi: 10.1130/0091-7613(1979)7<573:PAATGO>2.0.CO;2.

Hudson, T., and G. Plafker (1982), Paleogene metamorphism of an accretionary flysch terrane, eastern Gulf of Alaska, *Geol. Soc. Am. Bull., 93*, 1280–1290, doi: 10.1130/0016-7606(1982)93<1280:PMOAAF>2.0.CO;2.

Hurford, A. J. (1990), Standardization of fission-track dating calibration: Recommendation by the Fission Track Working Group of the I.U.G.S. Subcommission on Geochronology, *Chem Geol., 80*, 171–178, doi: 10.1016/0168-9622(90)90025-8.

Hurford, A. J., and P. F. Green (1982), A users' guide to fission track dating calibration, *Earth Planet. Sci. Lett., 59*, 343–354, doi: 10.1016/0012-821X(82)90136-4.

Hurford, A. J., and P. F. Green (1983), The zeta age calibration of fission-track dating, *Chem. Geol., 41*, 285–317, doi: 10.1016/S0009-2541(83)80026-6.

Hurley, P.M. (1954), The helium age method and the distribution and migration of helium in rocks, in *Nuclear Geology*, edited by H. Faul, Wiley & Sons, 301–329.

Hollister, L. S. (1979), Metamorphic and crustal displacements: New insights, *Episodes, 1979*, 3–8.

Hollister, L. S. (1982), Metamorphic evidence for rapid (2 mm/yr) uplift of a portion of the Central Gneiss Complex, Coast Mountains, B.C., *Can. Mineral., 20*, 319–332.

Ireland, T. R., and I. S. Williams (2003), Considerations in zircon geochronology by SIMS, *Rev. Mineral. Geochem., 53*, 215–241, doi: 10.2113/0530215.

Israel, S. A. (2004), Geology of southwestern Yukon, *YGS Open File 2004-16*, scale 1:250000, Yukon Geological Survey, Whitehorse, YT.

Israel, S. A., A. M. Tizzard, and J. Major (2006), Bedrock geology of the Duke River area, parts of NTS 115G/2, 3, 4, 6, and 7, southwestern Yukon, in *Yukon Exploration and Geology 2005*, edited by D. S. Emond et al., 139–154, Yukon Geological Survey.

Israel, S. A., D. Murphy, V. Bennett, J. Mortensen, and J. L. Crowley (2011), New insight into the geology and mineral potentail of the Coast Belt in southwestern Yukon, in *Yukon Exploration and Geology 2010*, edited by K. E. MacFarlane et al., 101–123, Yukon Geological Survey.

Israel, S. A., L. A. Kennedy, and R. M. Friedman (2013), Strain partitioning in accretionary orogens, and its effects on orogenic collapse: Insight from western North America, *Geol. Soc. Am. Bull., 125*, 1260–1281, doi: 10.1130/B30777.1.

Israel, S. A., L. Beranek, R. M. Friedman, and J. L. Crowley (2014), New ties between the Alexander terrane and Wrangellia and implications for North American Cordilleran evolution, *Lithosphere*, doi: 10.1130/L364.1.

Izykowski, T. M., E. R. Milde, and J. I. Garver (2011), Fission-track dating of reset detrital zircon from the Valdez Group (Thompson Pass) and Orca Group (Cordova): Implications for the thermal evolution of the Chugach-Prince William terrane, Alaska, *Geol. Soc. Am. Abstracts with Programs*, 43(4), 81.

Jackson, S. E., N. J. Pearson, W. L. Griffin, and E. A. Belousova (2004), The application of laser ablation-inductively coupled plasma-mass spectrometry to in situ U-Pb zircon geochronology, *Chem. Geol., 211*, 47–69, doi: 10.1016/j.chemgeo.2004.06.017.

Jaeger, J. M., C. A. Nittrouer, N. D. Scott, and J. D. Milliman (1998), Sediment accumulation along a glacially impacted mountainous coastline: north-east Gulf of Alaska, *Basin Res., 10*, 155–173, doi: 10.1046/j.1365-2117.1998.00059.x.

Jaffey, A. H., K. F. Flynn, L. E. Glendenin, W. C. Bentley, and A. M. Essling (1971), Precision measurement of half-lives and specific activities of ^{235}U and ^{238}U, *Phys. Rev. C, 4*, 1889–1906, doi: 10.1103/PhysRevC.4.1889.

Johnston, S. T., and P. Erdmer (1995), Hot-side-up aureole in southwest Yukon and limits on terrane assembly of the northern Canadian Cordillera, *Geology, 23*, 419–422, doi: 10.1130/0091-7613(1995)023<0419:HSUAIS>2.3.CO;2.

Johnston, S. T., and D. Canil (2007), Crustal architecture of SW Yukon, northern Cordillera, Implications for crustal growth in a convergent margin orogen, *Tectonics, 26*, TC1006, doi: 10.1029/2006TC001950.

Johnston, S. T., J. K. Mortensen, and P. Erdmer (1996), Igneous and metaigneous age constraints for the Aishihik metamorphic suite, southwest Yukon, *Can. J. Earth Sci., 33*, 1543–1555, doi: 10.1139/e96-117.

Jones, D. L., W. P. Irwin, and A. T. Ovenshine (1972), Southeastern Alaska–A displaced continental fragment?, *U.S. Geol. Surv. Prof Paper 800B*, B211–B217.

Jones, D. L., N. J. Silberling, and J. Hillhouse (1977), Wrangellia - A displaced terrane in northwestern North America, *Can. J, Earth Sci., 14*, 2565–2577, doi: 10.1139/e77-222.

Kalbas, J. L., A. M. Freed, and K. D. Ridgway (2008), Contemporary fault mechanics in southern Alaska, in *Active tectonics and seismic potential of Alaska, Geophys. Monogr. Ser.*, vol. 179, edited by J. T. Freymueller et al., 321–336, American Geophysical Union, Washington, D. C., doi: 10.1029/179GM18.

Kelley, S. (2002), Excess argon in K-Ar and Ar-Ar geochronology, *Chem. Geol., 188*, 1–22, doi: 10.1016/S0009-2541(02)00064-5.

Ketcham, R. A., C. Gautheron, L. Tassan-Got (2011), Accounting for long alpha-particle stopping distances in (U-Th-Sm)/He geochronology: refinement of the baseline case, *Geochim. Cosmochim. Acta, 75*, 7779–7791, doi: 10.1016/j.gca.2011.10.011.

Kochelek, E. J., J. M. Amato, T. L. Pavlis, and P. D. Clift (2011), Flysch deposition and preservation of coherent bedding in an accretionary complex: Detrital zircon ages from the Upper Cretaceous Valdez Group, Chugach Terrane, Alaska, *Lithosphere, 3*, 265–274, doi: 10.1130/L131.1.

Koons, P. O. (1987), Some thermal and mechanical consequences of rapid uplift: an example from the Southern Alps, New Zealand, *Earth Planet. Sci. Lett., 86*, 307–319, doi: 10.1016/0012-821X(87)90228-7.

Koons, P. O. (1990), Two-sided orogen: Collision and erosion from the sandbox to the Southern Alps, New Zealand, *Geology, 18*, 679–682, doi: 10.1130/0091-7613(1990)018<0679:TSOCAE>2.3.CO;2.

Koons, P. O., P. K. Zeitler, C. P. Chamberlain, D. Craw, and A. S. Meltzer (2002), Mechanical links between erosion and metamorphism in Nanga Parbat, Pakistan Himalaya, *Am. J. Sci, 302*, 749–773, doi: 10.2475/ajs.302.9.749.

Koons, P. O., B. P. Hooks, T. L. Pavlis, P. Upton, and A. D. Barker (2010), Three-dimensional mechanics of Yakutat convergence in the southern Alaskan plate corner, *Tectonics, 29*, TC4008, doi: 10.1029/2009TC002463.

Koons, P. O., P. K. Zeitler, and B. Hallet (2013), Tectonic aneurysms and mountain building, in *Treatise on Geomorphology, Tectonic Geomorphology*, vol. 5, edited by J. Shroder and L.A. Owen, 318–349, Academic Press, San Diego, CA.

Koppers, A. A. (2002), ArArCALC—software for 40Ar/39Ar age calculations, *Comput. Geosci., 28*, 605–619, doi: 10.1016/S0098-3004(01)00095-4.

Košler, J., and P. J. Sylvester (2003), Present trends and the future of zircon in geochronology: laser ablation ICPMS, *Rev. Mineral. Geochem., 53*, 243–275, doi: 10.2113/0530243.

Kretz, R. (1983), Symbols for rock-forming minerals, *Am. Mineral., 68*, 277–279.

Kuiper, Y. D. (2002), The interpretation of inverse isochron diagrams in ^{40}Ar/^{39}Ar geochronology, *Earth Planet. Sci. Lett., 203*, 499–506, doi: 10.1016/S0012-821(02)00833-6.

Landis, P. (2007), Stratigraphic framework and provenance of the Eocene-Oligocene Kulthieth Formation, Alaska: Implications for paleogeography and tectonics of the Early Cenozoic continental margin of northwestern North America, M.S. thesis, Purdue University, West Lafayette, IN.

Lagoe, M. B., C. H. Eyles, N. Eyles, and C. Hale (1993), Timing of Late Cenozoic tidewater glaciation in the far North Pacific, *Geol. Soc. Am. Bull., 105*, 1542–1560, doi: 10.1130/0016-7606(1993)105<1542:TOLCTG>2.3.CO;2.

Lagoe, M. B., and S. D. Zellers (1996), Depositional and microfaunal response to Pliocene climate change and tectonics in the eastern Gulf of Alaska, *Mar. Micropaleontol., 27*, 121–140, doi: 10.1016/0377-8398(95)00055-0.

Lahr, J. C., and G. Plafker (1980), Holocene Pacific-North American plate interaction in southern Alaska: Implications for the Yakataga seismic gap, *Geology, 8*, 483–486, doi: 10.1130/0091-7613(1980)8<483:HPAPII>2.0.CO;2.

Lancelot, J., A. Vitrac, and C. J. Allègre (1976), Uranium and lead isotopic dating with grain-by-grain zircon analysis: A study of complex geological history with a single rock, *Earth Planet. Sci. Lett., 29*, 357–366, doi: 10.1016/0012-821X(76)90140-0.

Lanphere, M. A., and G. B. Dalrymple (1976), Identification of excess ^{40}Ar by the ^{40}Ar/^{39}Ar age spectrum technique, *Earth Planet. Sci. Lett, 32*, 141–148, doi: 10.1016/0012-821X(76)90052-2.

Lanphere, M. A., and G. B. Dalrymple (1978), The use of ^{40}Ar/^{39}Ar data in evaluation of disturbed K-Ar systems, *U.S. Geol. Surv. Open-file Report 78-701*, 241–243.

Lee, J.-Y., K. Marti, J. P. Severinghaus, K. Kawamura, H.-S. Yoo, J. B. Lee, and J. S. Kim (2006), A redetermination of the isotopic abundances of atmospheric Ar, *Geochim. Cosmochim. Acta, 70*, 4507–4512, doi: 10.1016/j.gca.2006.06.1563.

Little, T. A., and C. W. Naeser (1989), Tertiary tectonics of the Border Ranges Fault Systems, Chugach Mountains, Alaska: Deformation and uplift in a forearc setting, *J. Geophys. Res. Solid Earth, 94*, 4333–4359, doi: 10.1029/JB094iB04p04333.

Loney, R. A., D. A. Brew, L. J. Muffler, and J. S. Pomeroy (1975), Reconnaissance geology of Chichagof, Baranof, and Kruzof Islands, Alaska, *U.S. Geol. Surv. Prof. Pap., 792*, 105 p.

Loney, R. A., and G. R. Himmelberg (1983), Structure and petrology of the La Perouse gabbro intrusion, Fairweather Range, southeastern Alaska, *J. Petrol., 24*, 377–423, doi: 10.1093/petrology/24.4.377.

Lovera, O. M., F. M. Richter, and T. M. Harrison (1989), The ^{40}Ar/^{39}Ar thermochronometry for slowly cooled samples having a distribution of diffusion domain sizes, *J. Geophys. Res, 94*, 17917–17935, doi: 10.1029/JB094iB12p17917.

Lovera, O. M., F. M. Richter, and T. M. Harrison (1991), Diffusion domains determined by 39Ar released during step heating, *J. Geophys. Res, 96*, 2057–2069, doi: 10.1029/90JB02217.
Lowey, G. W. (1992), Variation in bed thickness in a turbidite succession, Dezadeash Formation (Jurassic-Cretaceous), Yukon, Canada–Evidence of thinning-upward and thickening-upward cycles, *Sediment. Geol., 78*, 217–232, doi: 10.1016/0037-0738(92)90021-I.
Lowey, G. W. (1998), A new estimate of the amount of displacement on the Denali Fault system based on the occurrence of carbonate megaboulders in the Dezadeash Formation (Jura-Cretaceous), Yukon, and the Nutzotin Mountains sequence (Jura-Cretaceous), Alaska, *Bull. Can. Petrol. Geol., 46*, 379–386.
Ludwig, K. R. (2012), Isoplot 3.75 A geochronologic toolkit for Microsoft Excel, Berkeley Geochronology Center Special Publications No. 5, Berkeley Geochronology Center, CA, 75 p.
Mancktelow, N. S., and B. Grasemann (1997), Time-dependent effects of heat advection and topography on cooling histories during erosion, *Tectonophysics, 270*, 167–195, doi: 10.1016/S0040-1951(96)00279-X.
Marechal, A., S. Mazzotti, J. L. Elliott, J. T. Freymueller, and M. Schmidt (2015), Indentor-corner tectonics in the Yakutat-St. Elias collision constrained by GPS, *J. Geophys. Res. Solid Earth, 120*, 3897–3908, doi: 10.1002/2014JB011842.
Mazzotti, S., and R. D. Hyndman (2002), Yakutat collision and strain transfer across the northern Canadian Cordillera, *Geology, 30*, 495–498, doi: 10.1130/0091-7613(2002)030<0495:YCASTA>2.0.CO;2.
McClelland, W. C., and G. E. Gehrels (1990), Geology of the Duncan Canal shear zone: Evidence for Early to Middle Jurassic deformation of the Alexander Terrane, southeastern Alaska, *Geol. Soc. Am. Bull., 102*, 1378–1392, doi: 10.1130/0016-7606(1990)102<1378:GOTDCS>2.3.CO;2.
McDougall, I., and T. M. Harrison (1988), *Geochronology and thermochronology by the $^{40}Ar/^{39}Ar$ method*, Oxford Monographs on Geology and Geophysics No. 9, Oxford University Press, New York, 212 p.
McAleer, R. J., J. A. Spotila, E. Enkelmann, and A. L. Berger (2009), Exhumation along the Fairweather Fault, southeastern Alaska, based on low-temperature thermochronometry, *Tectonics, 28*, TC1007, doi: 10.1029/2007TC002240.
Meesters, A. G., and T. J. Dunai (2005), A noniterative solution of the (U-Th)/He age equation, *Geochem. Geophys. Geosys., 6*, doi: 10.1029/2004GC000834.
Meigs, A. J., W. C. Krugh, K. Davis, and G. Bank (2006), Ultra-rapid landscape response and sediment yield following glacier retreat, Icy Bay, southern Alaska, *Geomorphology, 78*, 207–221, doi: 10.1016/j.geomorph.2006.01.029.
Meigs, A. J., S. Johnston, J. I. Garver, and J. A. Spotila (2008), Crustal-scale structural architecture, shortening, and exhumation of an active, eroding orogenic wedge (Chugach/St. Elias Range, southern Alaska), *Tectonics, 27*, TC4003, doi: 10.1029/2007TC002168.
Merrihue, C., and G. Turner (1966), Potassium-argon dating by activation with fast neutrons, *J. Geophys. Res., 71*, 2852–2857, doi: 10.1029/JZ071i011p02852.
Mezger, J. E. (2000), 'Alpine-type' ultramafic rocks of the Kluane metamorphic assemblage, southwest Yukon: Oceanic crust fragments of a late Mesozoic back-arc basin along the northern Coast Belt, in *Yukon Exploration and Geology, 1999*, edited by D. S. Emond, and L. H. Weston, 127–138, Exploration and Geological Services Division, Yukon, Indian and Northern Affairs Canada.
Mezger, J. E., R. A. Creaser, P. Erdmer, and S. T. Johnston (2001), A Cretaceous back-arc basin in the Coast Belt of the northern Canadian Cordillera: Evidence from geochemical and neodymium

isotope characteristics of the Kluane metamorphic assemblage, southwest Yukon, *Can. J. Sci., 38*, 90–103, doi: 10.1139/e00-076.
Mezger, K., G. N. Hanson, S. R. Bohlen (1989), U-Pb systematics of garnet: dating the growth of garnet in the late Archean Pikwitonei granulite domain at Cauchon and Natawahunan Lakes, Manitoba, Canada, *Contrib. Mineral. Petrol., 101*, 136–148, doi: 10.1007/BF00375301.
Mezger, K., B. A. van der Pluijm, E. J. Essene, and A. N. Halliday (1993), U-Pb geochronology of the Grenville Orogen of Ontario and New York; constraints on ancient crustal tectonics, *Contrib. Mineral. Petrol., 114*, 13–26, doi: 10.1007/BF00307862.
Mezger, K., and E. J. Krogstad (1997), Interpretation of discordant U-Pb zircon ages: An evaluation, *J. Metamorph. Geol., 15*, 127–140, doi: 10.1111/j.1525-1314.1997.00008.x.
Molnia, B. F. (2008), Glaciers of North America: Glaciers of Alaska, in Satellite Image Atlas of Glaciers of the World, edited by R.S. Williams Jr., and J.G. Ferrigno, *U.S. Geol. Surv. Prof. Pap. 1386-K*, U.S. Geol. Surv., Washington, D.C., 521 p.
Nier, A.O. (1938), Variations in the relative abundances of the isotopes of common lead from various sources, *J. Am. Chem. Soc., 60*, 1571–1576, doi: 10.1021/ja01274a016.
Nier, A. O. (1939a), The isotopic constitution of uranium and the half-lives of the uranium isotopes, I, *Phys. Rev., 55*, 150–153, doi: 10.1103/PhysRev.55.150.
Nier, A. O. (1939b), The isotopic constitution of radiogenic leads and the measurement of geologic time, II, *Phys. Rev., 55*, 153–163, doi: 10.1103/PhysRev.55.153.
Nier, A. O. (1950), A redetermination of the relative abundances of the isotopes of carbon, nitrogen, oxygen, argon, and potassium, *Phys. Rev., 77*, 789–793, doi: 10.1103/PhysRev.77.789.
Nokleberg, W. J., G. Plafker, and F. H. Wilson (1994), Geology of south-central Alaska, in The geology of Alaska, *The geology of North America*, G-1, edited by G. Plafker, and H. C. Berg, pp. 311–366, GSA, Boulder, CO.
O'Sullivan, P. B., and L. D. Currie (1996), Thermotectonic history of Mt Logan, Yukon Territory, Canada: Implications of multiple episodes of Middle to Late Cenozoic denudation, *Earth Planet. Sci. Lett.*, *144*, 251–261, doi: 10.1016/0012-821X(96)00161-6.
O'Sullivan, P. B., G. Plafker, and J. M. Murphy (1997), Apatite fission-track thermotectonic history of crystalline rocks in the northern Saint Elias Mountains, Alaska, in *Geological Studies in Alaska by the USGS*, *USGS Prof. Pap., 1574,* edited by J. A. Dumoulin and J. E. Gray, 283–294.
Parrish, R. R. (1990), U-Pb dating of monazite and its application to geologic problems, *Can. J. Sci., 27*, 1431–1450, doi: 10.1139/e90-152.
Parrish, R. R., and S. R. Noble (2003), Zircon U-Th-Pb geochronology by isotope dilution–thermal ionization mass spectrometry (ID-TIMS), *Rev. Mineral. Geochem., 53*, 183–213, doi: 10.2113/0530183.
Paul, T. A. (1993), Transmission electron microscopy investigation of unetched fission tracks in fluorapatite–physical process of annealing, *Nucl. Tracks Radiat. Meas., 21*, 507–511, doi: 10.1016/1359-0189(93)90190-K.
Pavlis, T. L., and V. B. Sisson (1995), Structural history of the Chugach metamorphic complex in the Tana River region, eastern Alaska: A record of Eocene ridge subduction, *Geol. Soc. Am. Bull., 7*, 1333–1355, doi: 10.1130/0016-7606(1995)107<1333:SHOTCM>2.3.CO;2.
Pavlis, T. L., and S. M. Roeske (2007), The Border Ranges fault system, southern Alaska, *Geol. Soc. Am. Bull., 431*, 95–127, doi: 10.1130/2007.2431(05).
Pavlis, T. L., C. Picornell, and L. Serpa (2004), Tectonic processes during oblique collision: Insights from the St. Elias orogen, northern North American Cordillera, *Tectonics, 23*, TC3001, doi: 10.1029/2003TC001557.

Pavlis, T. L., J. B. Chapman, R. L. Bruhn, K. Ridgway, L. L. Worthington, S. P. Gulick, and J. Spotila (2012), Structure of the actively deforming fold-thrust belt of the St. Elias orogen with implications for glacial exhumation and three-dimensional tectonic processes, *Geosphere, 8*, 991–1019, doi: 10.1130/GES00753.1.

Perry, S. E., J. I. Garver, and K. D. Ridgway (2009), Transport of the Yakutat Terrane, southern Alaska: Evidence from sediment petrology and detrital zircon fission-track and U/Pb double dating, *J. Geol., 117*, 156–173, doi: 10.1086/596302.

Pfänder, J. A., B. Sperner, L. Ratschbacher, A. Fischer, M. Meyer, M. Leistner, and H. Schaeben (2014), High-resolution $^{40}Ar/^{39}Ar$ dating using a mechanical sample transfer system combined with a high-temperature cell for step heating experiments and a multicollector ARGUS noble gas mass spectrometer, *Geochem., Geophys., Geosyst., 15*, 1–14, doi: 10.1002/2014GC005289.

Plafker, G. (1987), Regional geology and petroleum potential of the northern Gulf of Alaska continental margin, in *Geology and resource potential of the continental margin of western North America and adjacent ocean basins*, Earth Science Series, vol. 6, edited by D. W. Scholl et al., 229–268, Circum-Pacific Council for Energy and Mineral Resources, Houston, TX.

Plafker, G., and E. M. MacKevett (1969), Mafic and ultramafic rocks from a layered pluton at Mount Fairweather, Alaska, in Geological Survey Research 1970, *U.S. Geol. Surv. Prof. Pap. 700-B*, B21–B26.

Plafker, G., and W. Thatcher (2008), Geological and geophysical evaluation of the mechanisms of the great 1899 Yakutat Bay earthquakes, in *Active tectonics and seismic potential of Alaska, Geophys. Monogr. Ser.*, vol. 179, edited by J. T. Freymueller et al., 215–236, American Geophysical Union, Washington, D. C., doi: 10.1029/179GM12.

Plafker, G., W. J. Nokleberg, and J. S. Lull (1989), Bedrock geology and tectonic evolution of the Wrangellia, Peninsular, and Chugach Terranes along the Trans-Alaskan Crustal Transect in the Chugach Mountains and southern Copper River Basin, Alaska, *J. Geophys. Res. Solid Earth, 94*, 4255–4295, doi: 10.1029/JB094iB04p04255.

Plafker, G., J. C. Moore, and G. R. Winkler (1994), Geology of the southern Alaska margin, in *The Geology of North America*, vol. G-1, *The Geology of Alaska*, edited by G. Plafker and H. C. Berg, 389–449, Geological Society of America, Boulder, CO.

Plattner, C., R. Malservisi, T. H. Dixon, P. LaFemina, G. F. Sella, J. Fletcher, and F. Suarez-Vidal (2007), New constraints on relative motion between the Pacific Plate and Baja California microplate (Mexico) from GPS measurements, *Geophys. J. Int., 170*, 1373–1380, doi: 10.1111/j.1365-246X.2007.03494.x.

Poldervaart, A., and F. D. Eckelmann (1955), Growth phenomena in zircon of autochthonous granites, *Geol. Soc. Am. Bull., 66*, 947–948, doi: 10.1130/0016-7606(1955)66[947:GPIZOA]2.0.CO;2.

Price, P. B., and R. M. Walker (1962), Chemical etching of charged-particle tracks in solids, *J. Appl. Phys., 33*, 3407–3412, doi: 10.1063/1.1702421.

Price, P. B., and R. M. Walker (1963), Fossil tracks of charged particles in mica and the age of minerals, *J. Geophys. Res., 68*, 4847–4862, doi: 10.1029/JZ068i016p04847.

Rahl, J. M., T. A. Ehlers, and B. A. van der Pluijm (2007), Quantifying transient erosion of orogens with detrital thermochronology from syntectonic basin deposits, *Earth Planet. Sci. Lett., 256*, 147–161, doi: 10.1016/j.espl.2007.01.020.

Ramsay, W., and F. Soddy (1903), Experiments in radioactivity and the production of helium from radium, *Proc. R. Soc. London, 72*, 204–207.

Reiners, P. W., T. A. Ehlers, S. G. Mitchell, and D. R. Montgomery (2003), Coupled spatial variations in precipitation and long-term erosion rates across the Washington Cascades, *Nature, 426*, 645–647, doi: 10.1038/nature02111.

Reiners, P. W., T. L. Spell, S. Nicolescu, K. A. Zanetti (2004), Zircon (U-Th)/He thermochronometry: He diffusion and comparison with ^{40}Ar/^{39}Ar dating, *Geochim Cosmochim. Acta, 68*, 1857–1887, doi: 10.1016/j.gca.2003.10.021.

Reiners, P. W., and M. T. Brandon (2006), Using thermochronology to understand orogenic erosion, *Annu. Rev. Earth Planet. Sci., 34*, 419–466, doi: 10.1146/annurev.earth.34.031405.125202.

Reiners, P. W., and T. A. Ehlers (2005), *Low-temperature thermochronology: techniques, interpretations, and applications*, Rev. Mineral. Geochem., 58, 622 p. Mineralogical Society of America, Geochemical Society, VA, USA.

Renne, P. R., A. L. Deino, W. E. Hames, M. T. Heizler, S. R. Hemming, K. V. Hodges, A. A. Koppers, D. F. Mark, L. E. Morgan, D. Phillips, B. S. Singer, B. D. Turrin, I. M. Villa, M. Villeneuve, and J. R. Wijbrans (2009), Data reporting norms for ^{40}Ar/^{39}Ar geochronology, *Quat. Geochronol., 4*, 346–352, doi: 10.1016/j.quageo.2009.06.005.

Renne, P. R., R. Mundil, G. Balco, K. Min, and K. R. Ludwig (2010), Joint determination of ^{40}K decay constants and ^{40}Ar*/40K for the Fish Canyon sanidine standard, and improved accuracy for ^{40}Ar/^{39}Ar geochronology, *Geochim. Cosmochim. Acta, 74*, 5349–5367, doi: 10.1016/j.gca.2010.06.017.

Richter, D. H., and N. A. Matson (1971), Quaternary faulting in the eastern Alaska Range, *Geol. Soc. Am. Bull.*, 82, 1529–1540, doi: 10.1130/0016-7606(1979)82[1529:QFITEA]2.0.CO;2.

Richter, D. H., J. G. Smith, M. A. Lanphere, G. B. Dalyrmple, B. L. Reed, and N. Shew (1990), Age and progression of volcanism, Wrangell volcanic field, Alaska, *Bull. Volcanol., 53,* 29–44, doi: 10.1007/BF00680318.

Richter, D. H., C. C. Preller, K. A. Labay, and N. B. Shew (2006), Geologic map of the Wrangell-St. Elias National Park and Preserve, Alaska, Scientific investigations map 2877, scale 1:350000, U.S. Geological Survey.

Rick, B. J., B. K. Frett, C. M. Davidson, and J. I. Garver (2014), U/Pb dating of detrital zircon from Seward to Baranof Island provides depositional links across the Chugach-Prince William Terrane in southeastern Alaska, Cordilleran Tectonics Workshop, UBC Okanagan, Abstracts, 35–36.

Rick, B. J. (2014), U/Pb dating of detrital zircons, Baranof Island, SE Alaska, in Short Contributions, 27th Annual Heck Symposium Volume.

Ridgway, K.D., J. M. Trop, W. J. Nokleberg, C. M. Davidson, and K. R. Eastham (2002), Mesozoic and Cenozoic tectonics of the eastern and central Alaska Range: Progressive basin development and deformation in a suture zone, *Geol. Soc. Am. Bull., 114*, 1480–1504, doi: 10.1130/0016-7606(2002)114<1480:MACTOT>2.0.CO;2.

Rignot, E., J. Mouginot, C. F. Larsen, Y. Gim, and D. Kirchner (2013), Low-frequency radar sounding of temperate ice masses in Southern Alaska, *Geophys. Res. Lett., 40*, 5399–5405, doi: 10.1002/2013GL057452.

Roberts, H. J., S. P. Kelley, and P. S. Dahl (2001), Obtaining geologically meaningful ^{40}Ar–^{39}Ar ages from altered biotite, *Chem. Geol., 172*, 277–290, doi: 10.1016/S0009-2541(00)00255-2.

Roddick, J. C., R. A. Cliff, and D. C. Rex (1980), The evolution of excess argon in Alpine biotites – A ^{40}Ar-^{39}Ar analysis, *Earth Planet. Sci. Lett., 48*, 185–208, doi: 10.1016/0012-821(80)90181-8.

Roeske, S. M., L. W. Snee, and T. L. Pavlis (2003), Dextral-slip reactivation of an arc-forearc boundary during Late Cretaceous–Early Eocene oblique convergence in the northern Cordillera, *GSA Special Paper, 371*, 141–169, doi: 10.1130/0-8137-2371-X.29.

Rossman, D. L. (1963), Geology and petrology of two stocks of layered gabbro in the Fairweather Range, Alaska, *U.S. Geol. Surv. Bull. 1121-F*, 50 p.

Rusmore, M. E., and G. J. Woodsworth (1991), Coast Plutonic Complex: A mid-Cretaceous contractional orogen, *Geology, 19*, 941–944, doi: 10.1130/0091-7613(1991)019<0941:CPCAMC>2.3.CO;2.

Rutherford, E. (1905), Present problems in radioactivity, *Pop. Sci. Monthly, 57*, 1–34.

Rutherford, E. (1929), Origin of actinium and the age of the Earth, *Nature, 123*, 313–314.

Rutherford, E., and F. Soddy (1903), Radioactive change, *Philos. Mag. Ser. 6, 5*, 576–591.

Schärer, U., and C. J. Allègre (1982a), Uranium-lead system in fragments of a single zircon grain, *Nature, 295*, 585–587, doi: 10.1038/295585a0.

Schärer, U., and C. J. Allègre (1982b), Investigation of the Archean crust by single-grain dating of detrital zircon: a greywacke of the Slave Province, Canada, *Can. J. Earth Sci., 19*, 1910–1918, doi: 10.1139/e82-169.

Scott, D. J., and M. R. St-Onge (1995), Constraints on Pb closure temperature in titanite based on rocks from the Ungava orogen, Canada: Implications for U-Pb geochronology and P-T-t path determinations, *Geology, 23*, 1123–1126, doi: 10.1130/0091-7613(1995)023<1123:COPCTI>2.3.CO;2.

Sheaf, M. A., L. Serpa, and T. L. Pavlis (2003), Exhumation rates in the St. Elias Mountains, Alaska, *Tectonophysics, 367*, 1–11, doi: 10.1016/S0040-1951(03)00124-0.

Shuster, D. L., R. M. Flowers, and K. A. Farley (2006), The influence of natural radiation damage on helium diffusion kinetics in apatite, *Earth Planet. Sci. Lett., 249*, 148–161, doi: 10.1016/j.epsl.2006.07.028.

Sisson, V. B., and L. S. Hollister (1988), Low-pressure facies series metamorphism in an accretionary sedimentary prism, southern Alaska, *Geology, 16*, 358–361, doi: 10.1130/0091-7613(1988)016<0358:LPFSMI>2.3.CO;2.

Sisson, V. B., and T. L. Pavlis (1993), Geologic consequences of plate reorganization: An example from the Eocene southern Alaska forearc, *Geology, 21*, 913–916, doi: 10.1130/0091-7613(1993)021<0913:GCOPRA>2.3.CO;2.

Sisson, V. B., A. R. Poole, N. R. Harris, H. C. Burner, T. L. Pavlis, P. Copeland, R. A. Donelick, and W. C. McClelland (2003), Geochemical and geochronologic constraints for genesis of a tonalite-trondhjemite suite and associated mafic intrusive rocks in the eastern Chugach Mountains, Alaska: A record of ridge-transform subduction, *GSA Special Paper, 371*, 293–326, doi: 10.1130/0-8137-2371-X.29.

Skulski, T., D. Francis, and J. Ludden (1991), Arc-transform magmatism in the Wrangell volcanic belt, *Geology, 19*, 11–14, doi: 10.1130/0091-7613(1991)019<0011:ATMITW>2.3.CO;2.

Skulski, T., D. Francis, and J. Ludden (1992), Volcanism in an arc-transform transition zone: The stratigraphy of the St. Clare Creek volcanic field, Wrangell volcanic belt, Yukon, *Can. J. Earth Sci., 29*, 446–461, doi: 10.1139/e92-039

Sláma, J., J. Košler, D. J. Condon, J. L. Crowley, A. Gerdes, J. M. Hanchar, M. S. Horstwood, G. A. Morris, L. Nasdala, N. Norberg, U. Schaltegger, B. Schoene, M. N. Tubrett, and M. J. Whitehouse (2008), Plešovice zircon - A new natural reference material for U-Pb and Hf isotopic microanalysis, *Chem. Geol., 249*, 1–35, doi: 10.1016/j.chemgeo.2007.11.005.

Smart, K. J., T. L. Pavlis, V. B. Sisson, S. M. Roeske, and L. W. Snee (1996), The Border Ranges fault system in Glacier Bay National Park, Alaska—evidence for major early Cenozoic dextral strike-slip motion, *Can. J. Earth Sci., 33*, 1268–1282, doi: 10.1139/e96-096.

Spotila, J. A., and A. L. Berger (2010), Exhumation at orogenic indentor corner under long-term glacial conditions: Example of the St. Elias orogen, southern Alaska, *Tectonophysics, 490*, 241–256, doi: 10.1016/j.tecto.2010.05.015.

Spotila, J. A., J. T. Buscher, A. J. Meigs, and P. W. Reiners (2004), Long-term glacial erosion of active mountain belts: Example of the Chugach-St. Elias Range, Alaska, *Geology, 32*, 501–504, doi: 10.1130/G20343.1.

St. Amand, P. (1957), Geological and geophysical synthesis of the tectonics of portions of British Columbia, the Yukon territory, and Alaska, *Geol. Soc. Am. Bull., 68*, 1343–1370, doi: 10.1130/0016-7606(1957)68[1343:GAGSOT]2.0.CO;2.

Steiger, R. H., and G. J. Wasserburg (1966), Systematics in the Pb^{208}-Th^{232}, Pb^{207}-U^{235}, and Pb^{206}-U^{238} systems, *J. Geophys. Res., 71*, 6065–6090, doi: 10.1029/JZ071i024p06065.

Steiger, R. H., and G. J. Wasserburg (1969), Comparative U-Th-Pb systematics in 2.7×10^9 yr plutons of different geologic histories, *Geochim. Cosmochim. Acta, 33*, 1213–1232, doi: 10.1016/0016-7037(69)90043-X.

Stewart, R. J., B. Hallet, P. K. Zeitler, M. A. Malloy, C. M. Allen, and D. Trippett (2008), Brahmaputra sediment flux dominated by highly localized rapid erosion from the easternmost Himalaya, *Geology*, 36, 711–714, doi: 10.1130/G24890A.1.

Stock, J., and P. Molnar (1988), Uncertainties and implications of the Late Cretaceous and Tertiary position of North America relative to the Farallon, Kula, and Pacific Plates, *Tectonics, 7*, 1339–1384, doi: 10.1029/TC007i006p01339.

Storti, F., and K. McClay (1995), Influence of syntectonic sedimentation on thrust wedges in analogue models, *Geology, 23*, 999–1002, doi: 10.1130/0091-7613(1995)<0999:IOSSOT>2.3CO;2.

Suess, E. (1904), *The face of the Earth (Das Antlitz der Erde), vol. 1*, Clarendon Press, Oxford, 604 p.

Tagami, T., and P. B. O'Sullivan (2005), Fundamentals of fission-track thermochronology, *Rev. Mineral. Geochem., 58*, 19–47, doi: 10.2138/rmg.2005.58.2.

Tarr, R.S., and L. Martin (1912), The earthquakes at Yakutat Bay, Alaska, in September, 1899; with a preface by G. K. Gilbert, *U.S. Geol. Surv. Prof. Pap., 69*, 135.

Thorkelson, D. J., and R. P. Taylor (1989), Cordilleran slab windows, *Geology, 17*, 833–836, doi: 10.1130/0091-7613(1989)017<0833:CSW>2.3.CO;2.

Trop, J. M., and K. D. Ridgway (2007), Mesozoic and Cenozoic tectonic growth of southern Alaska: A sedimentary basin perspective, in *Tectonic growth of a collisional continental margin: Crustal evolution of southern Alaska*, edited by K. D. Ridgway et al., 55–95, Geol. Soc. Am. Special Paper 431, doi: 10.1130/2007.2431(04).

Trop, J. M., K. D. Ridgway, J. D. Manuszak, and P. Layer (2002), Mesozoic sedimentary-basin development on the allochthonous Wrangellia Composite Terrane, Wrangell Mountains Basin, Alaska: A long-term record of terrane migration and arc construction, *Geol. Soc. Am. Bull., 114*, 693–717, doi: 10.1130/0016-7606(2002)114<0693: MSBDOT>2.0.CO;2.

Trop, J. M., K. D. Ridgway, and T. L. Spell (2003), Sedimentary record of transpressional tectonic and ridge subduction in the Tertiary Matanuska Valley–Talkeetna Mountains forearc basin, southern Alaska, in *Geology of a transpressional orogen developed during ridge-trench interaction along the North Pacific margin*, edited by V. B. Sisson et al., 89–118, Geol. Soc. Am. Special Paper 371, Boulder, CO, USA, doi: 10.1130/0-8137-2371-X.89.

Trop, J. M., W. K. Hart, D. Snyder, and B. Idleman (2012), Miocene basin development and volcanism along a strike-slip to flat-slab subduction transition: Stratigraphy, geochemistry, and geochronology of the central Wrangell volcanic belt, Yakutat-North America collision zone, *Geosphere, 8*, 805–834, doi: 10.1130/GES00762.1.

Turner, G. (1968), The distribution of potassium and argon in chondrites, in *Origin and distribution of the elements*, edited by L. H. Ahrens, 387–398, Pergamon London.

Turner, G. (1971), Argon 40-argon 39 dating: the optimization of irradiation parameters, *Earth Planet. Sci. Lett, 10*, 227–234, doi: 10.1016/0012-821X(71)90010-0.

Vavra, G. (1990), On the kinematics of zircon growth and its petrogenetic significance: a cathodoluminescence study, *Contrib. Mineral. Petrol., 106*, 90–99, doi: 10.1007/BF00306410.

Vermeesch, P. (2008), Three new ways to calculate average (U-Th)/He ages, *Chem. Geol., 249*, 339–347, doi: 10.1016/j.chemgeo.2008.01.027.

Wagner, G., and G. M. Reimer (1972) Fission track tectonics: the tectonic interpretation of fission track ages, *Earth Planet. Sci. Lett., 14*, 263–68, doi: 10.1016/0012-821X(72)90018-0.

Wagner, G., and P. Van den haute (1992), *Fission-track dating*, Kluwer Academic Publishers, 285 p.

Wang, P., D. Scherler, J. Liu-Zeng, J. Mey, J.-P. Avouac, Y. Zhang, and D. Shi (2015), Tectonic control of Yarlung Tsangpo Gorge revealed by a buried canyon in southern Tibet, *Science, 346*, 978–981, doi: 10.1126/science.1259041.

Wetherill, G. W. (1956), Discordant uranium-lead ages, I, *Trans., Am. Geophys. Union, 37*, 320–326, doi: 10.1029/TR037i003p00320.

White, J. M., T. A. Ager, D. P. Adam, E. B. Leopold, G. Liu, H. Jetté, and C. E. Schweger (1997), An 18 million year record of vegetation and climate change in northwestern Canada and Alaska: tectonic and global climatic correlates, *Palaeogeogr., Palaeoclimatol., Palaeoecol., 130*, 293–306, doi: 10.1016/S0031-0182(96)00146-0.

Whipple, K. X. (2009), The influence of climate on the tectonic evolution of mountain belts, *Nat. Geosci., 2*, 97–104, doi: 10.1038/ngeo413.

Willett, S. D., C. Beaumont, and P. Fullsack (1993), Mechanical model for the tectonics of doubly vergent compressional orogens, *Geology, 21*, 371–374, doi: 10.1130/0091-7613(1993)021<0371:MMFTTO>2.3.CO;2.

Willett, S. D. (1999), Orogeny and orography: The effects of erosion on the structure of mountain belt, *J. Geophys. Res. Solid Earth, 104*, 28957–28981, doi: 10.1029/1999JB900248.

Willett, S. D., D. Fisher, C. Fuller, Y. En-Chao, and L. Chia-Yu (2003), Erosion rates and orogenic-wedge kinematics in Taiwan inferred from fission-track thermochronometry, *Geology, 31*, 945–948, doi: 10.1130/G19702.1.

Wolf, R. A., K. A. Farley, and D. M. Kass (1998), Modeling on the temperature sensitivity of the apatite (U-Th)/He thermochronometer, *Chem. Geol., 148*, 105–114, doi: 10.1016/S0009-2541(98)00024-2.

Worthington, L. L., S. P. Gulick, and T. L. Pavlis (2010), Coupled stratigraphic and structural evolution of a glaciated orogenic wedge, *Tectonics, 29*, TC6013. doi: 10.1029/2010TC002723.

Worthington, L. L., H. J. Van Avendonk, S. P. Gulick, G. L. Christeson, and T. L. Pavlis (2012), Crustal structure of the Yakutat Terrane and the evolution of subduction and collision in southern Alaska, *J. Geophys, Res., 117*, B01102, doi: 10.1029/2011JB008493.

Zeitler, P. K., A. L. Herczeg, I. McDougall, and M. Honda (1987), U-Th-He dating of apatite: A potential thermochronometer, *Geochim. Cosmochim. Acta, 51*, 2865–2868, doi: 10.1016/0016-7037(87)90164-5.

Zeitler, P. K., J. F. Sutter, I. Williams, R. E. Zartman, and R. A. Tahirkheli (1989), Geochronology and temperature history of the Nanga Parbat–Haramosh Massif, Pakistan, *GSA Special Paper, 232*, 1–22, doi: 10.1130/SPE232–p1.

Zeitler, P. K., Meltzer, A. S., Koons, P. O., Craw, D., Hallet, B., Chamberlain, C. P., Kidd, W. S., Park, S. K., Seeber, L., Bishop, M., and Shroder, J. (2001), Erosion, Himalayan geodynamics, and the geomorphology of metamorphism, *GSA Today, 11*, 4–9, doi: 10.1130/1052-5173(2001)011<0004:EHGATG>2.0.CO;2.

Zeitler, P. K., A. S. Meltzer, L. Brown, W. S. Kidd, C. Lim, and E. Enkelmann (2014), Tectonics and topographic evolution of Namche Barwa and the easternmost Lhasa block, Tibet, *GSA Special Paper 507*, 23–58, doi:10.1130/2014.2507(02).

Appendix A

A1. Description

Appendix A contains Figures A-1 to A-4, which are detailed maps of the larger-scale map in Figure 4-5, as well as Figure A-5 and A-6, which are the results of binomial peak fitting of KLD samples (ZFT and AFT) from the northern St. Elias Mountains (Chapter 5).

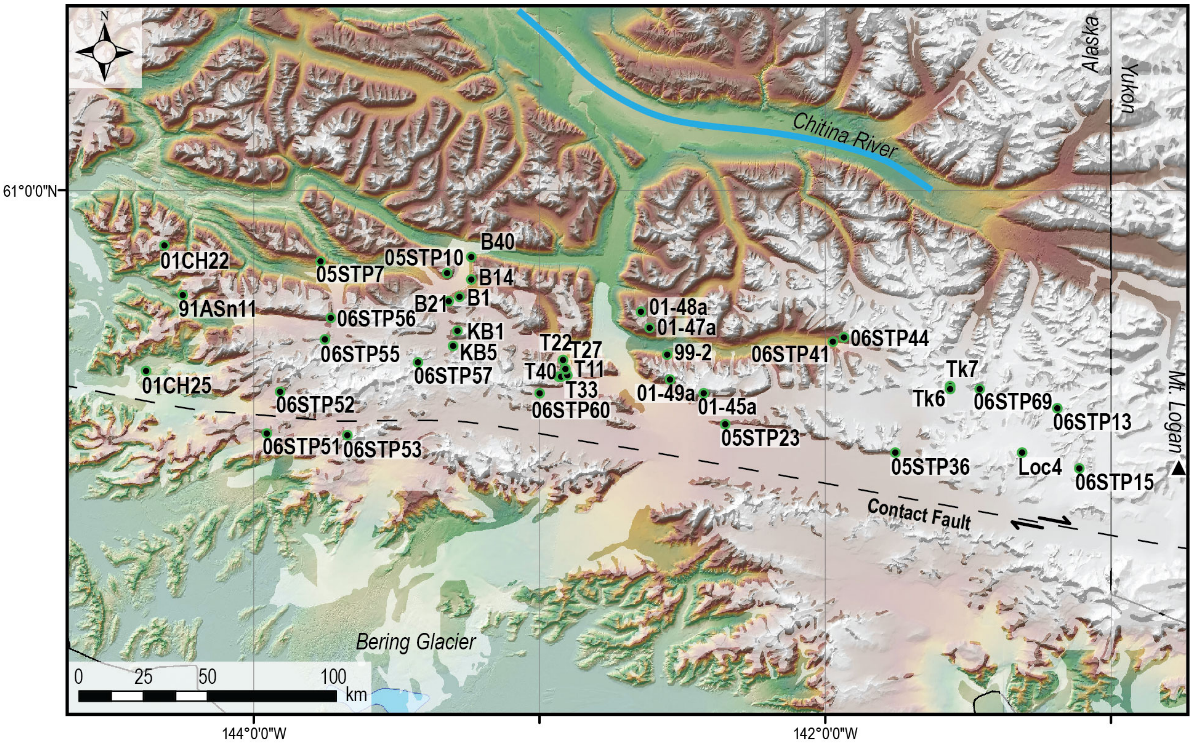

Figure A-1. DEM with locations and IDs of published samples used in Area 1 in Figures 4-5 and 4-6. For sample details see Dataset B-3.

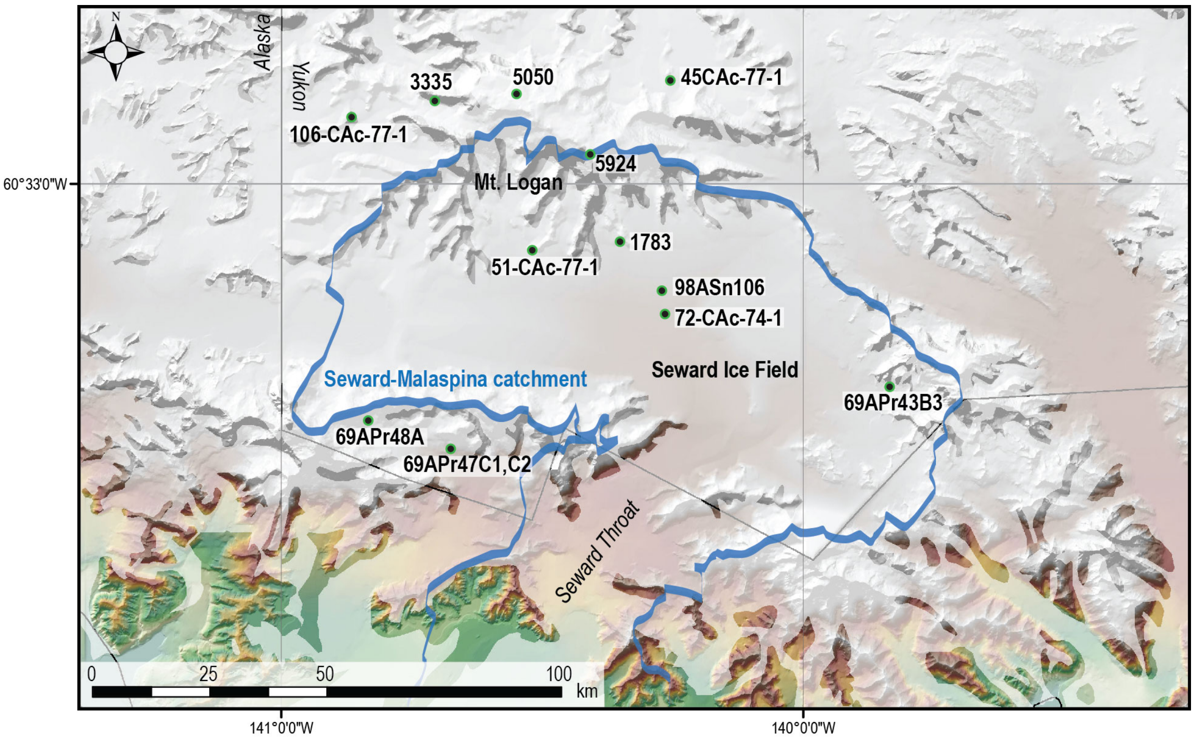

Figure A-2. DEM with locations and IDs of published samples used in Area 2 in Figures 4-5 and 4-7. For sample details see Dataset B-3.

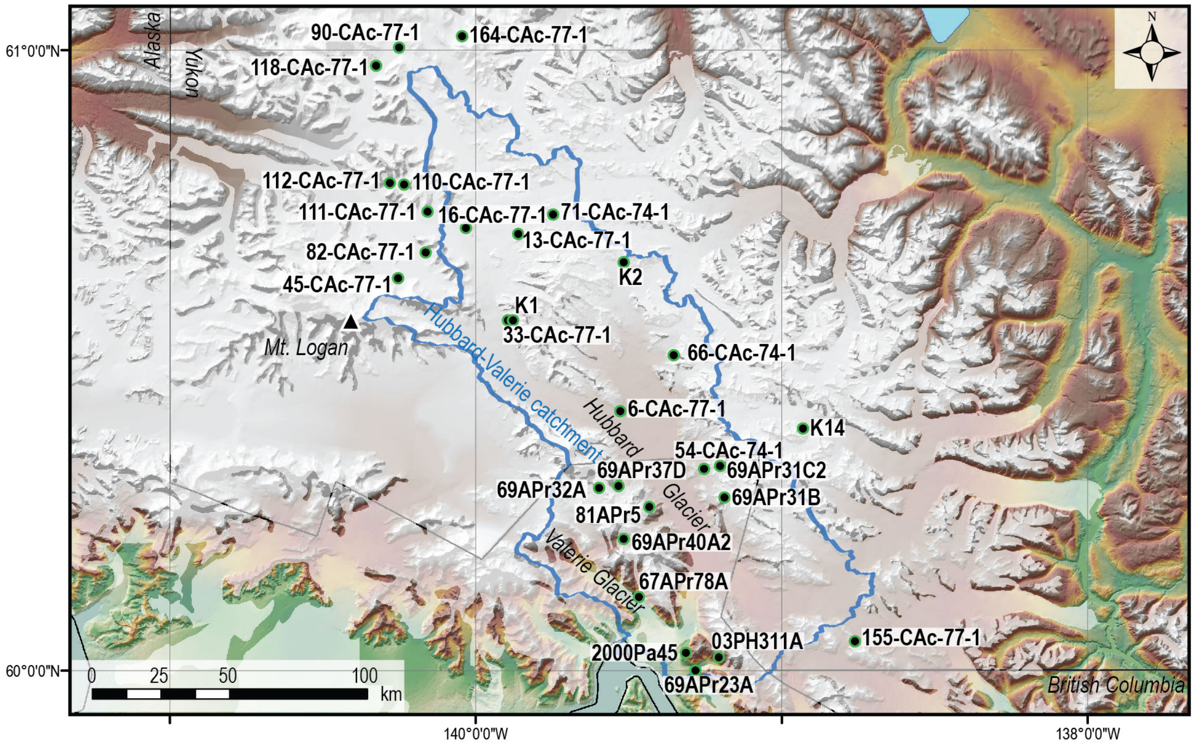

Figure A-3. DEM with locations and IDs of published samples used in Area 3 in Figures 4-5 and 4-8. For sample details see Dataset B-3.

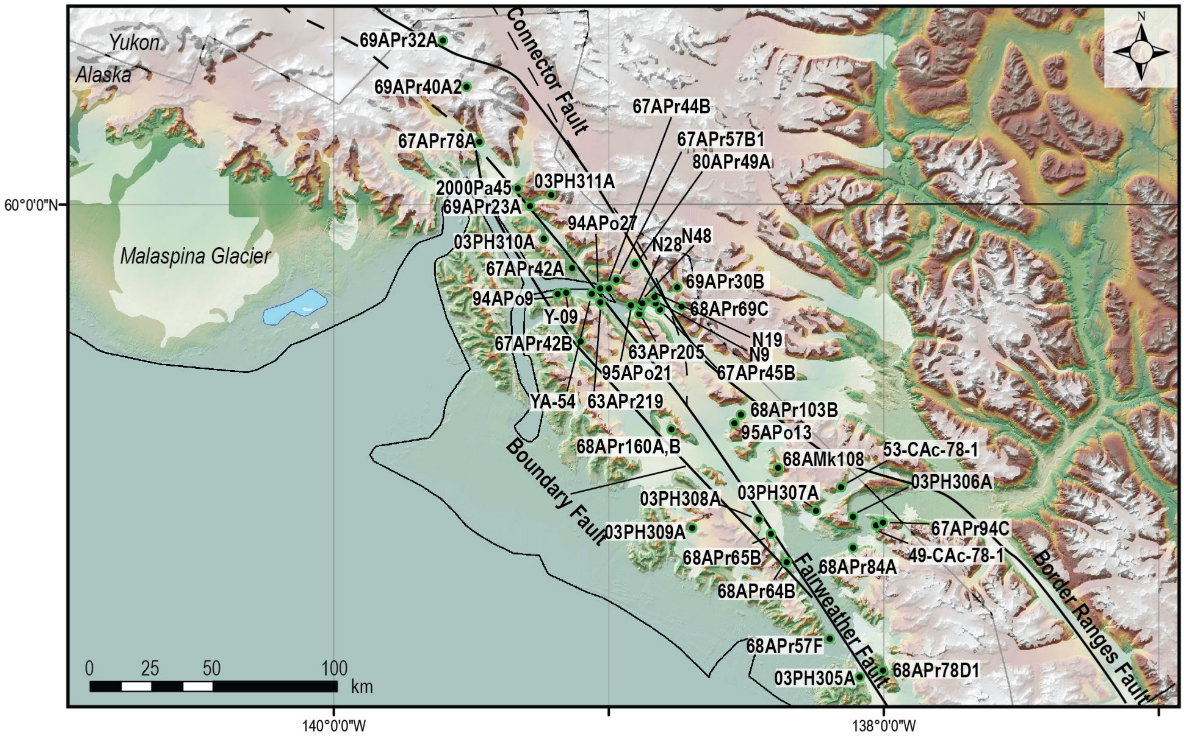

Figure A-4. DEM with locations and IDs of published samples used in Area 4 in Figures 4-5 and 4-9. For sample details see Dataset B-3.

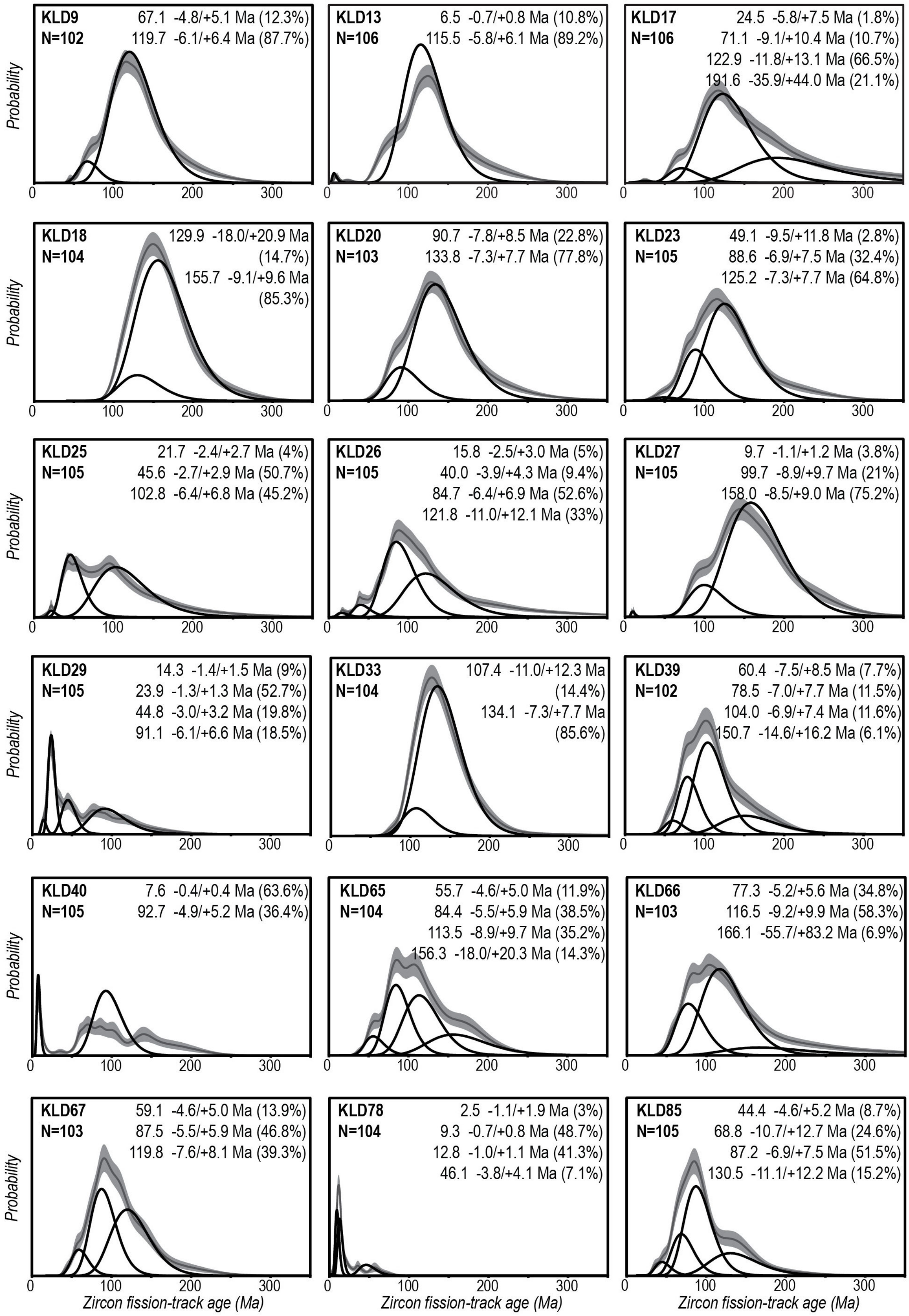

Figure A-5, continued on next page

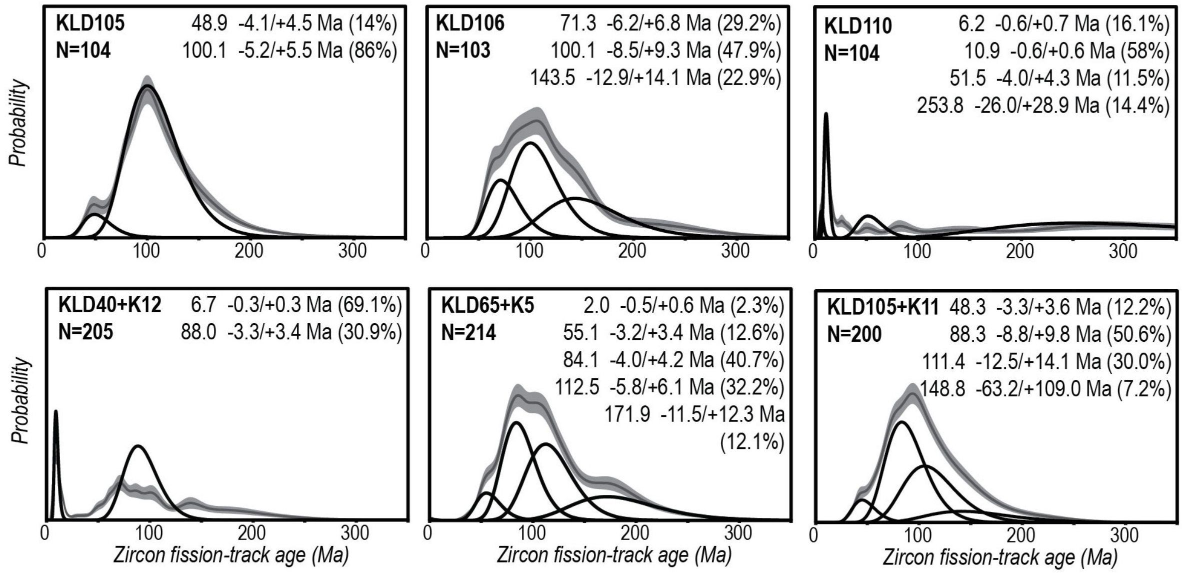

Figure A-5. Results of binomial peak fitting of ZFT ages of KLD samples using BINOMFIT [*Brandon*, 1992, 1996]. KLD40, KLD65, and KLD105 are combined with K12, K5, and K11, respectively, which are from the same catchments [*Enkelmann et al.*, 2015a]. Black curves: fitted peaks; grey curves: measured ZFT age distributions (1 σ). Given are the peak ages with asymmetric 1 σ error and the fraction of grains that make up the age population in that sample. N: number of dated grains per sample. This figure is in support of Table 5-3.

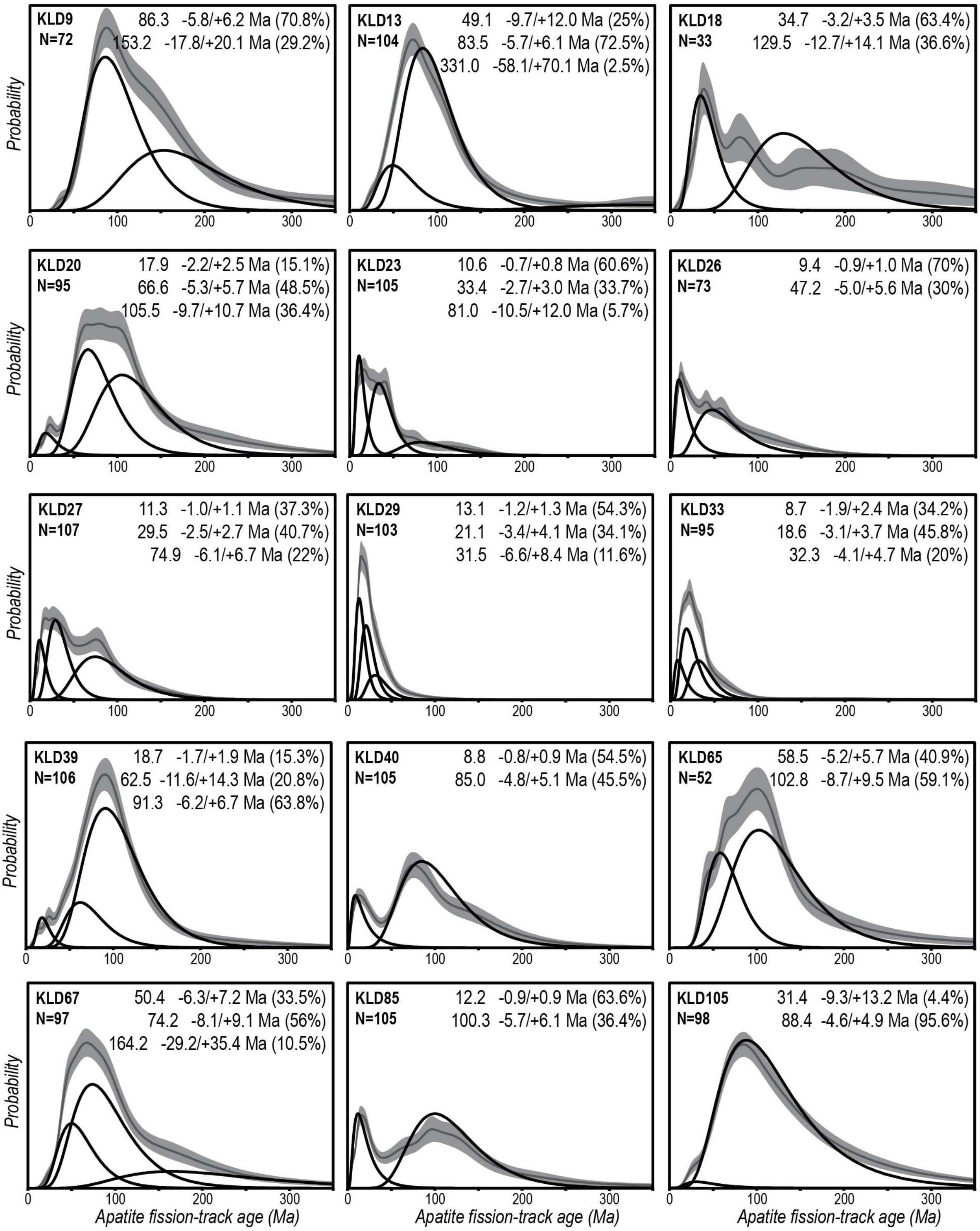

Figure A-6. Results of binomial peak fitting of AFT ages of KLD samples using BINOMFIT [*Brandon*, 1992, 1996]. Black curves: fitted peaks; grey curves: measured AFT age distributions (1 σ). Given are the peak ages with asymmetric 1 σ error and the fraction of grains that make up the age population in that sample. N: number of dated grains per sample. This figure is in support of Table 5-3.

Appendix B

B1. Description

A separate data disc contains Appendix B with Table B-1 and Datasets B-1 to B-5. Table B-1 contains zircon U-Th-Pb single-grain analyses presented in Chapter 4. Dataset B-1 contains the ZFT single-grains ages of YAKD and HUB1 samples presented in Chapter 3. Dataset B-2 contains $^{40}Ar/^{39}Ar$ analyses of cobbles and bedrock samples presented in Chapter 4. Dataset B-3 contains details of previously published samples compiled in Chapter 4. Datasets B-4 and B-5 contain ZFT and AFT single-grain ages, respectively, of KLD samples presented in Chapter 5.

Appendix B

B1. Description

This data disc contains Appendix B with Table B-1 and Datasets B-1 to B-5. Table B-1 contains zircon U-Th-Pb single-grain analyses presented in Chapter 4. Dataset B-1 contains the ZFT single-grains ages of YAKD and HUB1 samples presented in Chapter 3. Dataset B-2 contains $^{40}Ar/^{39}Ar$ analyses of cobbles and bedrock samples presented in Chapter 4. Dataset B-3 contains details of previously published samples compiled in Chapter 4 (References given in B2). Datasets B-4 and B-5 contain ZFT and AFT single-grain ages, respectively, of KLD samples presented in Chapter 5.

Table B-1. Laser ablation ICP-MS U-Pb data of single zircon grains from cobbles
Dataset B-1. Single grain zircon fission-track ages for YAKD samples
Dataset B-2. Analytical data of $^{40}Ar/^{39}Ar$ measurements of cobbles and bedrock samples
Dataset B-3. Data used in time-temperature plots of Areas 1–4 as presented in Figures 4-5 to 4-9 and Figures A-1 to A-4
- **B-3.1.** Data compilation of samples used in Area 1
- **B-3.2.** Data compilation of samples used in Area 2
- **B-3.3.** Data compilation of samples used in Area 3
- **B-3.4.** Data compilation of samples used in Area 4

Dataset B-4. Single-grain zircon fission-track ages of KLD samples
Dataset B-5. Single-grain apatite fission-track ages of KLD samples

B2. References

Berger, A. L., and J. A. Spotila (2008), Denudation and deformation in a glaciated orogenic wedge: The St. Elias orogen, Alaska, *Geology, 36*, 523–526, doi: 10.1130/G24883A.1.

Berger, A. L., J. A. Spotila, J. B. Chapman, T. L. Pavlis, E. Enkelmann, N. A. Ruppert, and J. T. Buscher (2008), Architecture, kinematics, and exhumation of a convergent orogenic wedge: A thermochronological investigation of tectonic-climatic interactions within the central St. Elias orogen, Alaska, *Earth Planet. Sci. Lett., 270*, 13–24, doi: 10.1016/j.epsl.2008.02.034.

Dodds, C. J., and P. B. Campbell (1988), Potassium-argon ages of mainly intrusive rocks in the Saint Elias Mountains, Yukon and British Columbia, *Geological Survey of Canada paper* 87-16.

Enkelmann, E., P. G. Valla, and J.-D. Champagnac (2015b), Low-temperature thermochronology of the Yakutat plate corner, St. Elias Range (Alaska): bridging short-term and long-term deformation, *Quat. Sci. Rev., 113*, 23–38, doi: 10.1016/j.quascirev.2014.10.019.

Enkelmann, E., P. K. Zeitler, J. I. Garver, T. L. Pavlis, and B. P. Hooks (2010), The thermochronological record of tectonic and surface process interaction at the

Yakutat–North American collision zone in southeast Alaska, *Am. J. Sci., 310*, 231–260, doi: 10.2475/04.2010.01.

Gasser, D., E. Bruand, K. Stüwe, D. A. Foster, R. Schuster, B. Fügenschuh, and T. L. Pavlis (2011), Formation of a metamorphic complex along an obliquely convergent margin: Structural and thermochronological evolution of the Chugach Metamorphic Complex, southern Alaska, *Tectonics, 30*, TC2012, doi: 10.1029/2010TC002776.

Grabowski, D. M., E. Enkelmann, and T. A. Ehlers (2013), Spatial extent of rapid denudation in the glaciated St. Elias syntaxis region, SE Alaska, *J. Geophys. Res. Earth Surf., 118*, 1921–1938, doi: 10.1002/jgrf.20136.

Hudson, T., G. Plafker, and M. A. Lanphere (1977a), Intrusive rocks of the Yakutat-St. Elias area, south-central Alaska, *Journal of Research of the U.S. Geol. Surv., 5*, 155–172.

Hudson, T., G. Plafker, and D. L. Turner (1977b), Metamorphic rocks of the Yakutat-St. Elias area, south-central Alaska, *Journal of Research of the U.S. Geol. Surv., 5*, 173–184.

Hudson, T., G. Plafker, and Z. E. Peterman (1979), Paleogene anatexis along the Gulf of Alaska margin, *Geology, 7*, 573–577, doi: 10.1130/0091-7613(1979)7<573:PAATGO>2.0.CO;2.

McAleer, R. J., J. A. Spotila, E. Enkelmann, and A. L. Berger (2009), Exhumation along the Fairweather Fault, southeastern Alaska, based on low-temperature thermochronometry, *Tectonics, 28*, TC1007, doi: 10.1029/2007TC002240.

Meigs, A. J., S. Johnston, J. I. Garver, and J. A. Spotila (2008), Crustal-scale structural architecture, shortening, and exhumation of an active, eroding orogenic wedge (Chugach/St. Elias Range, southern Alaska), *Tectonics, 27*, TC4003, doi: 10.1029/2007TC002168.

O'Sullivan, P. B., and L. D. Currie (1996), Thermotectonic history of Mt Logan, Yukon Territory, Canada: Implications of multiple episodes of Middle to Late Cenozoic denudation, *Earth Planet. Sci. Lett., 144*, 251–261, doi: 10.1016/0012-821X(96)00161-6.

O'Sullivan, P. B., G. Plafker, and J. M. Murphy (1997), Apatite fission-track thermotectonic history of crystalline rocks in the northern Saint Elias Mountains, Alaska, in *Geological Studies in Alaska by the U.S. Geol. Surv.*, edited by J. A. Dumoulin, and J. E. Gray, pp. 283–294, U.S. Geol. Surv. Prof. Pap., 1574.

Sisson, V. B., A. R. Poole, N. R. Harris, H. C. Burner, T. L. Pavlis, P. Copeland, R. A. Donelick, and W. C. McClelland (2003), Geochemical and geochronologic constraints for genesis of a tonalite-trondhjemite suite and associated mafic intrusive rocks in the eastern Chugach Mountains, Alaska: A record of ridge-transform subduction, *GSA Special Paper, 371*, 293–326, doi: 10.1130/0-8137-2371-X.29.

Spotila, J. A., J. T. Buscher, A. J. Meigs, and P. W. Reiners (2004), Long-term glacial erosion of active mountain belts, Example of the Chugach-St. Elias Range, Alaska, *Geology, 32*, 501–504, doi: 10.1130/G20343.1.

Spotila, J. A., and A. L. Berger (2010), Exhumation at orogenic indentor corner under long-term glacial conditions: Example of the St. Elias orogen, southern Alaska, *Tectonophysics, 490*, 241–256, doi: 10.1016/j.tecto.2010.05.015.

Table B-1. Laser ablation ICP-MS U-Pb data of single zircon grains from cobbles

Lead, U and Th concentrations were determined relative to GJ-1 zircon standard.
Isotopic ratios are corrected for gas blank, mass bias, laser-induced and time-dependant fractionation. A common Pb correction was not applied.
The $^{207}Pb/^{235}U$ ratio was calculated by $^{207}Pb/^{206}Pb \times ^{206}Pb/^{238}U \times 137.88$ using the corrected ratios.
Uncertainties were propagated by quadratic addition of the within-run standard error and the standard deviation of within-session reproducibility of GJ-1 zircon standard
A concordia age is given for analyses with a probability of concordance >0.15.

Analysis	Pb [ppm]	U [ppm]	Th [ppm]	Th/U	Isotopic ratios $^{206}Pb/^{204}Pb$	$^{208}Pb/^{232}Th$	±1s%	$^{207}Pb/^{206}Pb$	±1s%	$^{207}Pb/^{235}U$	±1s%	$^{206}Pb/^{238}U$	±1s%	Rho	Apparent ages (Ma) $^{208}Pb/^{232}Th$	±2s	$^{207}Pb/^{206}Pb$	±2s	$^{207}Pb/^{235}U$	±2s	$^{206}Pb/^{238}U$	±2s	Concordia age (Ma) age	±2s	MSWD	Probability	Remarks	Lithology
MAL4-6_1	10	1395	45	0.09	240	0.00182	9.02	0.04684	1.52	0.05405	2.21	0.00837	1.61	0.73	36.7	6.6	41.2	72.7	53.4	2.3	53.7	1.7	53.7	1.7	0.12	0.73	Outer part	Igneous mylonite
MAL4-6_1b	1	92	16	0.24	49	0.00516	5.88	0.04749	5.19	0.09285	5.35	0.01418	1.30	0.24	104.1	12.2	73.8	246.9	90.2	9.2	90.8	2.3	90.8	2.3	0.02	0.89	Inherited older core	
MAL4-6_2	4	464	40	0.18	214	0.00181	12.57	0.04925	2.86	0.04527	11.34	0.00667	10.98	0.97	36.5	9.2	159.8	134.0	45.0	10.0	42.8	9.4						
MAL4-6_3	22	3092	564	0.28	1265	0.00228	4.24	0.04685	1.70	0.05334	2.20	0.00826	1.39	0.63	46.0	3.9	41.5	81.5	52.8	2.3	53.0	1.5	53.0	1.5	0.08	0.78		
MAL4-6_5	42	1240	362	0.29	912	0.01370	4.47	0.05691	2.06	0.16137	3.76	0.02056	3.14	0.84	275.0	24.4	488.1	91.1	151.9	10.6	131.2	8.2						
MAL4-6_7	18	1949	503	0.36	806	0.00249	4.57	0.04734	1.78	0.05455	2.30	0.00836	1.45	0.63	50.3	4.6	66.2	84.6	53.9	2.4	53.7	1.6	53.7	1.6	0.09	0.77		
MAL4-6_8	30	3994	866	0.30	2446	0.00236	4.28	0.04704	1.27	0.05353	1.79	0.00825	1.26	0.71	47.6	4.1	51.1	60.6	52.9	1.8	53.0	1.3	53.0	1.3	0.00	0.95		
MAL4-6_9	35	5256	115	0.03	1911	0.00256	4.67	0.04678	1.29	0.05369	1.71	0.00832	1.12	0.65	51.7	4.8	37.9	61.8	53.1	1.8	53.4	1.2	53.4	1.2	0.25	0.61		
MAL4-6_10	7	893	64	0.15	453	0.00260	9.39	0.04755	1.33	0.05415	1.84	0.00826	1.28	0.69	52.6	9.9	77.0	63.1	53.5	1.9	53.0	1.3	53.0	1.4	0.57	0.45		
MAL4-6_11	15	2181	189	0.15	1428	0.00238	5.09	0.04712	1.31	0.05321	1.76	0.00819	1.17	0.67	48.0	4.9	55.1	62.7	52.6	1.8	52.6	1.2	52.6	1.2	0.01	0.94		
MAL4-6_12	13	1774	162	0.13	805	0.00266	4.50	0.04801	1.27	0.05453	1.74	0.00824	1.19	0.68	53.6	4.8	100.0	60.1	53.9	1.8	52.9	1.3						
MAL4-6_14	6	807	187	0.34	814	0.00258	4.48	0.04733	1.96	0.05517	2.26	0.00845	1.12	0.50	52.1	4.7	65.9	93.1	54.5	2.4	54.3	1.2	54.3	1.2	0.06	0.80		
MAL4-6_15	19	2589	672	0.37	635	0.00252	4.24	0.04687	1.31	0.05484	1.72	0.00849	1.11	0.65	50.8	4.3	42.7	62.6	54.2	1.8	54.5	1.2	54.5	1.2	0.14	0.71		
MAL4-6_17	12	1737	201	0.21	884	0.00240	4.71	0.04742	1.79	0.05205	2.16	0.00796	1.19	0.55	48.5	4.6	70.3	85.2	51.5	2.2	51.1	1.2	51.1	1.2	0.20	0.66		
MAL4-6_18	14	1503	115	0.12	1085	0.00255	5.18	0.05097	1.79	0.05822	2.98	0.00828	2.39	0.80	51.5	5.3	239.4	82.5	57.5	3.3	53.2	2.5						
MAL4-6_20	22	3073	330	0.14	2196	0.00281	4.30	0.04703	1.42	0.05351	1.99	0.00825	1.39	0.70	56.6	4.9	50.9	67.8	52.9	2.1	53.0	1.5	53.0	1.5	0.00	0.95		
MAL4-6_21	28	4020	619	0.22	816	0.00266	4.28	0.04711	1.42	0.05454	2.00	0.00840	1.41	0.70	53.6	4.6	54.6	67.8	53.9	2.1	53.9	1.5	53.9	1.5	0.00	0.98		
MAL4-6_22	16	2259	555	0.36	959	0.00235	4.38	0.04798	1.08	0.05471	1.58	0.00827	1.16	0.73	47.4	4.1	98.2	50.9	54.1	1.7	53.1	1.2						
MAL4-6_23	15	1845	359	0.35	699	0.00239	4.42	0.04683	1.80	0.05359	2.11	0.00830	1.09	0.52	48.2	4.3	40.5	86.0	53.0	2.2	53.3	1.2	53.3	1.2	0.09	0.77		
MAL4-6_24	33	4423	749	0.23	1963	0.00257	4.44	0.04719	1.32	0.05399	1.76	0.00830	1.17	0.66	52.0	4.6	58.7	62.8	53.4	1.8	53.3	1.2	53.3	1.2	0.03	0.86		
MAL4-6_25	28	3777	677	0.26	742	0.00256	4.36	0.04714	1.06	0.05459	1.68	0.00840	1.30	0.77	51.6	4.5	56.3	50.6	54.0	1.8	53.9	1.4	53.9	1.4	0.01	0.92		
MAL4-6_26	19	2503	242	0.18	842	0.00245	4.65	0.04829	1.26	0.05597	1.96	0.00841	1.50	0.77	49.5	4.6	113.5	59.3	55.3	2.1	54.0	1.6						
MAL4-6_27	8	977	125	0.22	366	0.00262	4.97	0.04766	3.03	0.05467	3.53	0.00832	1.81	0.51	52.8	5.2	82.3	143.7	54.0	3.7	53.4	1.9	53.4	1.9	0.16	0.69		
MAL4-6_28	20	2694	348	0.18	1176	0.00259	4.29	0.04694	0.98	0.05321	1.61	0.00822	1.27	0.79	52.4	4.5	46.1	46.7	52.6	1.6	52.8	1.3	52.8	1.3	0.08	0.78		
MAL4-6_29	7	887	86	0.16	831	0.00376	4.39	0.04788	2.13	0.07416	2.81	0.01123	1.84	0.65	75.9	6.7	93.3	100.6	72.6	3.9	72.0	2.6	72.0	2.6	0.18	0.68		
MAL4-6_30	20	2536	558	0.32	1073	0.00270	4.43	0.05063	1.69	0.06016	2.15	0.00862	1.33	0.62	54.6	4.8	224.0	78.1	59.3	2.5	55.3	1.5						
MAL4-6_31	12	1670	213	0.22	6288	0.00242	4.51	0.04603	1.84	0.05299	2.37	0.00835	1.49	0.63	48.9	4.4	-0.6	88.6	52.4	2.4	53.6	1.6	53.6	1.6	1.54	0.21		
MAL4-6_32	8	814	67	0.13	282	0.00506	4.56	0.04867	1.31	0.06797	2.21	0.01013	1.79	0.81	102.0	9.3	132.1	61.3	66.8	2.9	65.0	2.3						
MAL7-6_1	16	2136	733	0.49	528	0.00234	4.32	0.04665	1.59	0.04961	2.11	0.00771	1.38	0.66	47.3	4.1	31.6	76.0	49.2	2.0	49.5	1.4	49.5	1.4	0.22	0.64		Pyroclastic
MAL7-6_2	12	1605	552	0.49	967	0.00231	4.30	0.04870	1.34	0.04937	1.99	0.00735	1.48	0.74	46.7	4.0	133.6	62.9	48.9	1.9	47.2	1.4						
MAL7-6_3	13	1763	488	0.39	4083	0.00239	4.32	0.04778	1.10	0.05082	1.76	0.00771	1.37	0.78	48.3	4.2	88.4	52.2	50.3	1.7	49.5	1.4						
MAL7-6_4	10	1347	355	0.44	420	0.00246	4.40	0.05005	1.90	0.05412	2.45	0.00784	1.55	0.63	49.7	4.4	197.1	88.0	53.5	2.6	50.4	1.6						
MAL7-6_5	40	5064	3291	0.79	413	0.00277	4.36	0.05709	2.38	0.06211	2.75	0.00789	1.38	0.50	55.9	4.9	495.0	104.6	61.2	3.3	50.7	1.4						
MAL7-6_6	18	2380	914	0.46	977	0.00246	4.30	0.04690	1.40	0.04716	1.98	0.00729	1.40	0.71	49.6	4.3	43.9	66.8	46.8	1.8	46.8	1.3	46.8	1.3	0.01	0.93		
MAL7-6_7	8	1154	236	0.29	256	0.00238	4.41	0.04951	1.56	0.04978	2.19	0.00729	1.53	0.70	48.0	4.2	172.0	72.5	49.3	2.1	46.8	1.4						
MAL7-6_8	2	221	61	0.58	66	0.00248	4.93	0.04669	3.18	0.04818	3.65	0.00748	1.80	0.49	50.0	4.9	33.3	152.1	47.8	3.4	48.1	1.7	48.1	1.7	0.04	0.85		
MAL7-6_9	22	2596	1413	0.97	349	0.00196	4.78	0.04785	3.29	0.04993	3.54	0.00757	1.30	0.37	39.7	3.8	91.7	155.7	49.5	3.4	48.6	1.3	48.6	1.3	0.30	0.59		
MAL7-6_10	14	1941	579	0.37	816	0.00270	3.34	0.04738	1.80	0.05058	2.30	0.00774	1.43	0.62	54.6	3.6	68.6	85.6	50.1	2.3	49.7	1.4	49.7	1.4	0.19	0.66		
MAL7-6_11	17	2184	576	0.43	459	0.00261	3.68	0.04718	2.31	0.05105	2.66	0.00785	1.34	0.50	52.7	3.9	58.2	110.0	50.6	2.6	50.4	1.3	50.4	1.3	0.02	0.89		
MAL7-6_12	17	2365	832	0.44	412	0.00247	3.72	0.04750	1.72	0.04963	2.17	0.00758	1.32	0.61	49.8	3.7	74.6	81.7	49.2	2.1	48.7	1.3	48.7	1.3	0.40	0.53		
MAL7-6_13	17	2497	694	0.38	578	0.00272	3.26	0.04816	1.18	0.05303	1.84	0.00799	1.41	0.76	54.8	3.6	107.4	55.9	52.5	1.9	51.3	1.4						
MAL7-6_14	5	711	209	0.38	392	0.00279	3.56	0.04742	1.92	0.05242	2.42	0.00802	1.47	0.61	56.4	4.0	70.6	91.4	51.9	2.4	51.5	1.5	51.5	1.5	0.17	0.68		
MAL7-6_15	10	1516	396	0.42	609	0.00253	3.45	0.04765	1.37	0.05152	1.92	0.00784	1.34	0.70	51.1	3.5	81.7	65.1	51.0	1.9	50.4	1.3	50.4	1.3	0.91	0.34		
MAL7-6_16	17	2279	723	0.41	808	0.00259	3.46	0.04694	1.47	0.05110	1.96	0.00790	1.30	0.66	52.2	3.6	46.3	70.2	50.6	1.9	50.7	1.3	50.7	1.3	0.02	0.90		
MAL7-6_17	14	1978	478	0.37	937	0.00252	3.21	0.04665	1.68	0.05126	2.13	0.00797	1.30	0.61	50.9	3.3	31.4	80.6	50.8	2.1	51.2	1.3	51.2	1.3	0.24	0.62		
MAL7-6_18	10	1366	407	0.43	500	0.00251	3.37	0.04977	1.86	0.05372	2.33	0.00783	1.41	0.60	50.7	3.4	184.3	86.8	53.1	2.4	50.3	1.4						
MAL7-6_19	14	1974	551	0.47	372	0.00237	3.32	0.04913	1.82	0.05219	2.30	0.00770	1.40	0.61	47.8	3.2	154.3	85.4	51.7	2.3	49.5	1.4						
MAL7-6_20	9	1263	263	0.28	418	0.00244	3.43	0.04854	1.78	0.05053	2.28	0.00755	1.42	0.62	49.2	3.4	125.6	83.7	50.1	2.2	48.5	1.4						
MAL7-6_21	12	1749	409	0.33	2713	0.00249	3.39	0.04691	1.31	0.05059	1.89	0.00782	1.36	0.72	50.2	3.4	44.6	62.5	50.1	1.8	50.2	1.4	50.2	1.4	0.03	0.86		
MAL7-6_22	19	2437	693	0.39	1169	0.00258	3.35	0.04772	1.49	0.05293	2.01	0.00804	1.35	0.67	52.1	3.5	85.5	70.8	52.4	2.1	51.6	1.4	51.7	1.4	0.89	0.35		
MAL7-6_23	11	1552	407	0.37	734	0.00252	3.23	0.04811	2.17	0.05309	2.59	0.00800	1.41	0.55	50.8	3.3	104.6	102.5	52.5	2.7	51.4	1.4	51.4	1.4	1.04	0.31		
MAL7-6_26	15	2246	559	0.38	1347	0.00253	3.24	0.04734	1.77	0.05098	2.19	0.00781	1.28	0.59	51.1	3.3	66.2	84.5	50.5	2.2	50.2	1.3	50.2	1.3	0.14	0.71	No older inherited core suspected;	
MAL7-6_26b	18	2725	710	0.41	1532	0.00249	3.34	0.04760	1.44	0.05244	1.91	0.00799	1.25	0.65	50.2	3.3	79.6	68.5	51.9	1.9	51.3	1.3	51.3	1.3	0.67	0.41	two spots to check reproducibility	
MAL7-6_27	23	3332	1443	0.60	1077	0.00198	3.21	0.04668	1.44	0.05031	1.95	0.00782	1.32	0.67	40.0	2.6	32.9	69.1	49.8	1.9	50.2	1.3	50.2	1.3	0.25	0.62		
MAL7-6_28	13	1860	411	0.33	608	0.00240	3.24	0.04735	1.30	0.05139	1.79	0.00787	1.22	0.69	48.5	3.1	66.7	61.9	50.9	1.8	50.5	1.2	50.6	1.2	0.27	0.60		
MAL7-6_29	14	1872	786	0.53	882	0.00247	3.20	0.04797	1.89	0.05048	2.25	0.00763	1.22	0.54	49.8	3.2	97.7	89.5	50.0	2.2	49.0	1.2	49.0	1.2	1.15	0.28		
MAL7-6_30	8	1227	328	0.42	449	0.00249	3.92	0.04739	2.12	0.05116	2.48	0.00783	1.30	0.52	50.2	3.9	68.8	100.9	50.7	2.5	50.3	1.3	50.3	1.3	0.13	0.72		
MAL7-6_31	6	896	175	0.29	306	0.00245	3.46	0.04807	1.97	0.05065	2.50	0.00764	1.55	0.62	49.4	3.4	102.9	93.1	50.2	2.5	49.1	1.5	49.1	1.5	1.29	0.26		
MAL7-6_32	6	884	258	0.41	589	0.00251	3.30	0.04725	2.31	0.05207	2.61	0.00799	1.21	0.46	50.6	3.3	61.9	110.3	51.5	2.6	51.3	1.2	51.3	1.2	0.04	0.85		
MAL7-6_33	9	1204	306	0.36	451	0.00246	3.54	0.04701	1.85	0.05064	2.32	0.00781	1.39	0.60	49.7	3.5	49.7	88.4	50.2	2.3	50.2	1.4	50.2	1.4	0.00	0.99		
MAL7-6_34	11	1661	482	0.43	1370	0.00247	3.31	0.04820	2.14	0.05041	2.55	0.00759	1.38	0.54	49.8	3.3	108.9	101.3	49.9	2.5	48.7	1.3	48.7	1.3	1.36	0.24		
MAL7-6_35	3	468	150	0.49	175	0.00255	3.75	0.04724	3.27	0.04998	3.57	0.00767	1.42	0.40	51.4	3.9	61.3	155.9	49.5	3.4	49.3	1.4	49.3	1.4	0.02	0.88		
MAL7-6_36	18	2334	592	0.32	553	0.00243	3.11	0.04728	1.77	0.04989	1.83	0.00765	0.49	0.26	49.1	3.0	63.5	84.2	49.4	1.8	49.1	0.5	49.1	0.5	0.11	0.74		
MAL7-6_37	16	2134	609	0.57	306	0.00269	3.47	0.06659	3.31	0.07281	3.38	0.00793	0.69	0.20	54.2	3.8	824.9	138.2	71.4	4.7	50.9	0.7						
MAL7-6_38	14	1961	446	0.34	709	0.00241	3.20	0.04740	1.16	0.05208	1.38	0.00797	0.74	0.54	48.6	3.1	69.5	55.3	51.5	1.4	51.2	0.8	51.2	0.8	0.43	0.51		
MAL7-6_39	6	335	100	0.52	44	0.01638	24.58	0.24861	12.82	0.35733	15.70	0.01042	9.06	0.58	328.5	160.5	3175.9	406.2	310.2	85.7	66.9	12.1						
MAL7-6_40	2	223	55	0.36	113	0.00243	4.39	0.04898	3.80	0.05276	4.07	0.00781	1.47	0.36	49.0	4.3	146.8	178.0	52.2	4.1	50.2	1.5	50.2	1.5	1.11	0.29		
MAL7-6_41	22	2997	1103	0.51	871	0.00208	3.25	0.04669	1.48	0.04995	2.47	0.00776	1.97	0.80	42.0	2.7	33.5	70.9	49.5	2.4	49.8	2.0	49.8	2.0	0.21	0.64		
MAL7-6_42	5	491	103	0.87	68	0.00244	38.62	0.12086	10.70	0.12912	11.14	0.00775	3.10	0.28	49.3	38.1	1969.0	381.4	123.3	26.0	49.8	3.1						
MAL7-6_43	12	1773	496	0.44	495	0.00263	3.10	0.05096	2.33	0.05530	2.53	0.00787	0.97	0.39	53.1	3.3	239.0	107.6	54.7	2.7	50.5	1.0						
MAL7-6_44	6	777	251	0.48	361	0.00236	3.25	0.04780	1.78	0.05164	2.04	0.00783	0.99	0.49	47.6	3.1	89.5	84.6	51.1	2.0	50.3	1.0	50.3	1.0	0.84	0.36		
MAL7-6_45	5	682	170	0.36	286	0.00232	3.09	0.04872	3.62	0.04914	3.70	0.00732	0.77	0.21	46.7	2.9	134.5	170.4	48.7	3.5	47.0	0.7	47.0	0.7	1.00	0.32		
MAL7-6_46	17	2250	752	0.43	897	0.00267	3.12	0.04687	1.64	0.05113	1.79	0.00791	0.72	0.40	53.9	3.4	42.6	78.4	50.6	1.8	50.8	0.7	50.8	0.7	0.04	0.83		
MAL7-6_47	12	1622	434	0.40	991	0.00242	3.11	0.04874	1.15	0.05283	1.42	0.00786	0.83	0.59	48.9	3.0	135.6	53.8	52.3	1.4	50.5	0.8						
MAL7-6_48	13	1829	577	0.51	657	0.00199	3.41	0.04694	1.63	0.04910	1.83	0.00759	0.83	0.45	40.2	2.7	46.2	77.9	48.7	1.7	48.7	0.8	48.7	0.8	0.00	0.95		
MAL7-6_49	20	2856	1066	0.58	1342	0.00197	3.26	0.04637	1.44	0.04989	1.62	0.00780	0.74	0.46	39.7	2.6	17.0	69.1	49.4	1.6	50.1	0.7	50.1	0.7	0.93	0.33		
MAL7-6_50	2	283	76	0.43	142	0.00231	3.46	0.04645	2.04	0.04986	2.65	0.00779	1.69	0.64	46.6	3.2	20.9	98.0	49.4	2.6	50.0	1.7	50.0	1.7	0.36	0.55		
MAL4-9_1	1	75	10	0.10	54	0.00062	32.61	0.05026	3.77	0.14536	4.01	0.02120	1.34	0.33	12.5	8.1	182.0	175.9	137.8	10.4	135.3	3.6	135.3	3.6	0.27	0.60		Orthogneiss
MAL4-9_2	38	5656	78	0.02	1433	0.00264	3.17	0.04744	1.16	0.05532	1.57	0.00855	1.06	0.68	53.3	3.4	45.9	55.5	54.7	1.7	54.9	1.2	54.9	1.2	0.11	0.75		
MAL4-9_3	1	64	11	0.26	49	0.00646	3.72	0.05001	5.41	0.12725	5.69	0.01865	1.77	0.31	130.1	9.7	170.3	252.5	121.6	13.1	119.1	4.2	119.2	4.2	0.16	0.69		
MAL4-9_4	2	79	22	0.46	62	0.00805	3.68	0.06148	3.99	0.20015	4.34	0.02387	1.70	0.39	162.0	11.9	632.8	171.9	185.3	14.8	152.1	5.1						
MAL4-9_5	1	55	8	0.24	70	0.00786	5.31	0.04654	4.05	0.15522	4.29	0.02445	1.42	0.33	158.2	16.7	-0.4	195.2	146.5	11.7	155.7	4.4						
MAL4-9_6	2	81	15	0.25	83	0.00801	6.30	0.05011	3.51	0.15321	3.84	0.02242	1.56	0.41	161.2	20.2	174.7	163.9	144.7	10.4	142.9	4.4	142.9	4.4	0.15	0.70		
MAL4-9_7	1	49	8	0.24	60	0.00700	4.55	0.04942	5.32	0.16315	5.73	0.02421	2.14	0.37	140.9	12.8	142.1	249.8	153.5	16.4	154.2	6.5	154.2	6.5	0.01	0.92		
MAL4-9_9	1	43	6	0.25	34	0.00657	5.84	0.04869	5.87	0.15226	6.11	0.02293	1.71	0.28	132.4	15.4	107.2	277.4	143.9	16.5	146.1	4.9	146.1	4.9	0.08	0.78		
MAL4-9_10	1	94	3	0.08	109	0.00470	12.41	0.04935	9.75	0.09824	11.12	0.01460	5.36	0.48	94.8	23.5	138.6	457.7	95.2	20.3	93.4	10.0	93.4	10.0	0.04	0.85		
MAL4-9_11	1	63	11	0.27	66	0.00715	5.05	0.04962	4.94	0.16513	5.26	0.02441	1.81	0.34	143.9	14.5	151.4	231.4	155.2	15.2	155.4	5.6	155.4	5.6	0.00	0.97		
MAL4-9_12	2	211	7	0.05	92	0.00728	5.94	0.05593	2.86	0.09817	4.02	0.01287	2.83	0.70	146.6	17.4	424.9	127.7	95.1	7.3	82.5	4.6						
MAL4-9_13	4	165	44	0.36	204	0.00782	3.94	0.05129	2.12	0.16879	2.66	0.02414	1.60	0.60	157.5	12.4	228.0	98.2	158.4	7.8	153.8	4.9						
MAL4-9_14	1	39	7	0.28	41	0.00708	4.73	0.04819	6.84	0.15992	7.06	0.02434	1.73	0.24	142.5	13.4	81.7	324.9	150.6	19.9	155.0	5.3	155.0	5.3	0.21	0.64		
MAL4-9_15	1	52	7	0.20	90	0.00812	3.86	0.04890	3.58	0.16364	3.94	0.02455	1.65	0.42	163.5	12.6	116.5	168.7	153.9	11.3	156.3	5.1						
MAL4-9_16	1	46	8	0.32	56	0.00643	5.37	0.04914	6.32	0.15729	6.59	0.02348	1.84	0.28	129.5	13.9	127.9	297.6	148.3	18.3	149.6	5.5						
MAL4-9_17	4	74	7	0.07	35	0.20783	3.57	0.23858	3.85	0.80699	4.05	0.02481	1.26	0.31	3816.6	249.3	3092.3	122.8	600.8	37.1	158.0	3.9						

MAL4-9_18	1	49	5	0.25	64	0.00732	4.07	0.05610	4.89	0.18466	5.15	0.02415	1.61	0.31	147.4	12.0	430.9	218.0	172.1	16.4	153.8	4.9					
MAL4-9_19	1	47	7	0.32	48	0.00765	6.35	0.05723	5.22	0.18466	5.58	0.02367	1.96	0.35	154.1	19.5	475.1	230.8	172.1	17.7	150.8	5.9					
MAL4-9_20	1	46	7	0.23	33	0.00786	5.08	0.04927	6.93	0.15543	7.28	0.02314	2.23	0.31	158.3	16.0	133.8	325.9	146.7	20.0	147.5	6.5	147.5	6.5	0.01	0.93		
MAL4-9_21	1	57	10	0.26	47	0.00949	3.36	0.05063	4.65	0.16874	4.92	0.02445	1.60	0.33	191.0	12.8	197.4	216.0	158.3	14.5	155.7	4.9	155.7	4.9	0.15	0.70		
MAL4-9_22	1	49	8	0.25	38	0.00741	4.65	0.04926	3.07	0.15959	3.47	0.02377	1.61	0.46	149.2	13.8	133.1	144.5	150.3	9.7	151.4	4.8	151.4	4.8	0.06	0.80		
MAL4-9_23	1	62	9	0.24	64	0.00675	5.66	0.04972	4.00	0.16484	4.32	0.02433	1.64	0.38	135.9	15.4	154.8	187.3	154.9	12.5	154.9	5.0	154.9	5.0	0.00	1.00		
MAL4-9_24	1	58	15	0.36	61	0.00880	4.71	0.04982	3.95	0.16558	4.49	0.02438	2.14	0.48	177.2	16.6	159.8	185.0	155.6	13.0	155.3	6.6	155.3	6.6	0.00	0.96		
MAL4-9_25	2	88	11	0.30	129	0.00736	4.73	0.05019	3.06	0.16047	3.24	0.02319	1.08	0.33	148.2	14.0	203.9	141.8	151.1	9.1	147.8	3.2	147.8	3.2	0.60	0.44		
MAL4-9_26	3	97	20	0.89	73	0.00824	17.10	0.15353	6.98	0.43347	7.42	0.02048	2.50	0.34	166.0	56.6	2385.6	237.7	365.6	46.1	130.7	6.5						
MAL4-9_28	1	44	8	0.26	59	0.00731	6.18	0.04759	5.82	0.15580	5.88	0.02374	0.87	0.15	147.1	18.1	79.0	276.4	147.0	16.2	151.3	2.6	151.3	2.6	0.29	0.59		
MAL4-9_29	2	115	8	0.17	181	0.00733	6.74	0.04748	3.41	0.15462	4.01	0.02362	2.11	0.53	147.7	19.8	73.5	162.2	146.0	10.9	150.5	6.3	150.3	6.3	0.94	0.33		
MAL4-9_30	2	76	16	0.31	-2240	0.00749	4.30	0.05047	5.04	0.16712	5.16	0.02402	1.10	0.21	150.9	12.9	216.5	233.3	156.9	15.0	153.0	3.3	153.0	3.3	0.28	0.59		
MAL4-9_31	1	57	8	0.21	116	0.00707	7.28	0.05191	3.86	0.16440	4.09	0.02297	1.36	0.33	142.4	20.7	281.5	176.6	154.5	11.8	146.4	3.9						
MAL4-9_32	5	541	49	0.16	2385	0.00404	8.27	0.05560	2.98	0.05560	9.26	0.00869	8.77	0.95	81.6	13.5	19.8	143.1	54.9	9.9	55.8	9.7	55.5	9.7	0.26	0.61		
MAL4-9_33	2	83	22	0.39	385	0.00714	4.14	0.05068	4.49	0.15828	4.70	0.02265	1.40	0.30	143.7	11.9	226.3	207.6	149.2	13.1	144.4	4.0	144.4	4.0	0.59	0.44		
MAL4-9_34	8	429	83	0.28	200	0.00680	3.47	0.05090	2.04	0.15802	2.26	0.02252	0.98	0.43	137.1	9.5	236.1	94.0	149.0	6.3	143.6	2.8						
MAL4-9_35	2	112	31	0.41	106	0.00725	4.70	0.05158	3.47	0.14952	3.58	0.02102	0.89	0.25	145.9	13.7	267.0	159.0	141.5	9.5	134.1	2.4						
MAL4-9_36	2	105	6	0.08	159	0.00781	7.42	0.04771	2.55	0.15380	3.30	0.02338	2.10	0.64	157.2	23.2	85.1	120.8	145.3	8.9	149.0	6.2	148.7	6.2	1.16	0.28		
MAL4-9_37	3	218	30	0.17	331	0.00770	3.35	0.04977	3.08	0.10781	3.26	0.01571	1.06	0.33	155.1	10.4	184.4	143.6	104.0	6.5	100.5	2.1	100.5	2.1	1.30	0.25		
MAL4-9_39	2	104	24	0.55	71	0.00760	4.12	0.04915	4.57	0.15563	4.71	0.02296	1.15	0.24	153.0	12.6	155.2	213.8	146.9	12.9	146.4	3.3	146.4	3.3	0.01	0.93		
MAL4-9_41	6	246	46	0.24	294	0.00795	2.99	0.04888	2.62	0.15773	2.96	0.02346	1.38	0.47	160.0	9.5	136.3	123.2	148.7	8.2	149.5	4.1	149.5	4.1	0.05	0.83		
MAL4-9_42	1	42	6	0.23	80	0.00696	5.15	0.05339	4.34	0.17641	4.61	0.02403	1.57	0.34	140.3	14.4	339.5	196.5	165.0	14.1	153.1	4.7						
MAL4-9_43	1	60	10	0.47	59	0.00766	7.78	0.05273	5.65	0.16436	5.79	0.02267	1.28	0.22	154.2	23.9	311.1	257.2	154.5	16.7	144.5	3.7	144.5	3.7	1.52	0.22		
MAL4-9_44	1	49	7	0.19	88	0.00805	5.55	0.04885	4.71	0.15734	5.00	0.02342	1.68	0.34	162.0	17.9	134.2	221.5	148.4	13.9	149.3	5.0	149.3	5.0	0.02	0.89		
MAL4-9_46	2	81	13	0.24	157	0.00762	4.01	0.05029	4.06	0.17359	4.33	0.02511	1.51	0.35	153.4	12.3	201.4	188.3	162.5	13.0	159.9	4.8	159.9	4.8	0.19	0.66		
MAL4-9_47	1	39	5	0.19	53	0.00801	7.13	0.05071	3.68	0.16516	4.13	0.02370	1.88	0.45	161.3	22.9	220.4	170.4	155.2	11.9	151.0	5.6	151.0	5.6	0.64	0.43		
MAL4-9_48	1	43	5	0.18	48	0.00768	7.10	0.05351	5.32	0.17668	5.52	0.02403	1.50	0.27	154.6	21.9	342.9	240.6	165.2	16.9	153.1	4.6						
MAL4-9_49	1	72	7	0.15	159	0.00840	3.93	0.05039	4.39	0.16495	5.19	0.02382	2.77	0.53	169.2	13.2	205.2	203.5	155.0	15.0	151.8	8.3	151.8	8.3	0.27	0.61		
MAL4-9_50	1	41	5	0.19	92	0.00738	6.90	0.05062	4.15	0.16725	4.45	0.02405	1.59	0.36	148.6	20.4	215.2	192.3	157.0	13.0	153.2	4.8	153.2	4.8		0.53		
MAL4-9_52	3	131	18	0.19	274	0.00873	3.10	0.04987	4.03	0.15809	4.19	0.02308	1.16	0.28	175.7	10.8	180.1	187.9	149.0	11.7	147.1	3.4	147.1	3.4	0.12	0.73		
MAL4-9_53	1	61	8	0.19	159	0.00841	4.70	0.05267	3.56	0.16138	4.02	0.02231	1.89	0.47	169.2	15.8	306.0	162.0	151.9	11.4	142.2	5.3						
MAL4-9_54	1	61	9	0.19	101	0.01005	3.07	0.05001	4.84	0.14960	5.02	0.02178	1.31	0.26	202.1	12.4	186.3	225.5	141.6	13.3	138.9	3.6	138.9	3.6	0.17	0.68		
MAL4-9_55	44	6207	99	0.02	3568	0.00285	2.68	0.04758	1.01	0.05517	1.47	0.00844	1.07	0.73	57.6	3.1	68.7	48.1	54.5	1.6	54.2	1.2	54.2	1.2	0.36	0.55		
MAL4-9_56	1	70	11	0.18	1850	0.00966	4.57	0.05252	4.76	0.16440	4.92	0.02280	1.23	0.25	194.2	17.7	298.7	217.3	154.5	14.2	145.3	3.5	145.3	3.5	1.81	0.18		
MAL4-9_57	2	99	6	0.09	99	0.00879	4.66	0.04789	5.25	0.15626	5.40	0.02378	1.28	0.24	176.8	16.4	82.2	249.1	147.4	14.9	151.5	3.8	151.5	3.8	0.32	0.57		
MAL4-9_58	1	49	5	0.16	79	0.00832	4.38	0.05269	5.19	0.17560	5.53	0.02429	1.91	0.34	167.4	14.6	304.0	236.4	164.3	16.8	154.7	5.8	154.7	5.8	1.45	0.23		
MAL4-9_59	1	64	9	0.18	144	0.00919	5.56	0.04785	3.61	0.15836	4.03	0.02413	1.79	0.44	184.9	20.5	79.4	171.3	149.3	11.2	153.7	5.4	153.6	5.4	0.79	0.38		
MAL4-9_60	0.4	19	2	0.11	24	0.01157	6.79	0.04974	9.11	0.15713	9.22	0.02303	1.43	0.16	232.5	31.4	170.5	425.3	148.2	25.6	146.8	4.2	146.8	4.2	0.01	0.91		
MAL4-9_61	1	48	7	0.17	119	0.01047	2.92	0.05097	4.38	0.16670	4.60	0.02385	1.41	0.31	210.6	12.3	226.9	202.3	156.6	13.4	151.9	4.2	152.0	4.2	0.52	0.47		
MAL3-2_1	4	579	160	0.40	162	0.00242	2.11	0.04871	1.58	0.05154	1.92	0.00767	1.09	0.57	48.8	2.1	134.0	74.3	51.0	1.9	49.3	1.1						Pyroclastic
MAL3-2_2	19	2595	1020	0.70	317	0.00203	2.57	0.05468	2.01	0.05942	2.12	0.00788	0.67	0.32	41.0	2.1	399.0	90.2	58.6	2.4	50.6	0.7						
MAL3-2_3	35	4868	2059	0.51	1091	0.00241	1.33	0.04912	1.24	0.05114	1.41	0.00755	0.67	0.48	48.6	1.3	153.6	58.3	50.6	1.4	48.5	0.6						
MAL3-2_4	1	145	65	0.60	46	0.00269	2.92	0.04888	7.09	0.04961	7.20	0.00736	1.27	0.18	54.2	3.2	142.2	332.8	49.2	6.9	47.3	1.2	47.3	1.2	0.31	0.58		
MAL3-2_5	6	530	131	0.49	67	0.00855	6.06	0.16498	3.25	0.21827	3.38	0.00960	0.93	0.28	172.1	20.8	2507.3	109.2	200.5	12.3	61.6	1.1						
MAL3-2_6	13	1876	518	0.33	534	0.00283	1.53	0.04840	1.41	0.04964	1.51	0.00744	0.54	0.36	57.2	1.7	119.1	66.6	49.2	1.5	47.8	0.5						
MAL3-2_7	17	2390	670	0.35	1496	0.00267	1.73	0.04692	1.21	0.04924	1.31	0.00761	0.49	0.37	54.0	1.9	45.1	58.0	48.8	1.2	48.9	0.5	48.9	0.5	0.02	0.90		
MAL3-2_8	37	1831	649	0.40	44	0.02855	9.37	0.31260	7.47	0.57133	8.70	0.01326	4.47	0.51	568.9	105.3	3533.8	230.3	458.9	65.3	84.9	7.5						
MAL3-2_9	9	1309	374	0.48	236	0.00242	2.56	0.05335	2.16	0.05686	2.37	0.00773	0.96	0.41	48.9	2.5	343.6	98.0	56.2	2.6	49.6	1.0						
MAL3-2_10	81	336	116	0.49	20	0.65649	2.31	0.75768	1.55	17.52160	2.74	0.16772	2.27	0.83	10201.0	372.4	4844.2	44.3	2963.8	53.4	999.5	42.0						
MAL3-2_11	3	380	123	0.52	128	0.00239	1.91	0.05176	3.01	0.05680	3.12	0.00796	0.81	0.26	48.3	1.8	274.9	138.1	56.1	3.4	51.1	0.8						
MAL3-2_12	22	3028	1040	0.50	599	0.00207	2.20	0.04906	1.23	0.05298	1.41	0.00783	0.69	0.49	41.8	1.8	150.6	57.7	52.4	1.4	50.3	0.7						
MAL3-2_13	14	2016	467	0.32	583	0.00258	1.73	0.05132	1.80	0.05242	1.86	0.00741	0.46	0.25	52.0	1.8	255.1	82.9	51.9	1.9	47.6	0.4						
MAL3-2_14	2	228	83	0.39	51	0.00471	2.63	0.07599	5.07	0.08497	5.20	0.00811	1.17	0.22	94.9	5.0	1094.9	202.8	82.8	8.3	52.1	1.2						
MAL3-2_15	20	2704	1053	0.56	674	0.00208	2.09	0.04909	1.42	0.05129	1.58	0.00758	0.70	0.44	42.0	1.8	151.9	66.4	50.8	1.6	48.7	0.7						
MAL3-2_16	9	1274	304	0.33	553	0.00241	4.34	0.04865	1.80	0.05074	2.11	0.00757	1.09	0.52	48.7	4.2	130.8	84.9	50.3	2.1	48.6	1.1						
MAL3-2_17	14	1752	424	0.50	189	0.00301	5.92	0.08115	3.98	0.08972	4.13	0.00802	1.09	0.26	60.7	7.2	1225.1	156.4	87.2	6.9	51.5	1.1						
MAL3-2_18	4	624	231	0.47	133	0.00254	4.37	0.04717	2.34	0.04798	2.56	0.00738	1.03	0.40	51.2	4.5	57.8	111.6	47.6	2.4	47.4	1.0	47.4	1.0	0.03	0.85		
MAL3-2_19	5	577	128	0.41	64	0.00539	4.70	0.08798	4.77	0.09610	4.93	0.00792	1.23	0.25	108.7	10.2	1382.1	183.4	93.2	8.8	50.9	1.2						
MAL3-2_20	20	2894	1037	0.47	694	0.00230	4.62	0.04983	1.20	0.04991	1.54	0.00727	0.96	0.62	46.5	4.3	186.9	56.0	49.5	1.5	46.7	0.9						
MAL3-2_21	16	2336	685	0.39	492	0.00280	4.44	0.04973	1.23	0.05513	1.60	0.00804	1.03	0.64	56.5	5.0	182.2	57.2	54.5	1.7	51.6	1.1						
MAL3-2_22	20	2805	1048	0.58	1311	0.00186	4.34	0.04733	1.30	0.04862	1.66	0.00745	1.04	0.62	37.6	3.3	66.1	61.8	48.2	1.6	47.8	1.0	47.9	1.0	0.34	0.56		
MAL3-2_23	4	460	123	0.55	108	0.00380	6.09	0.09966	5.91	0.10750	6.03	0.00782	1.18	0.20	76.6	9.3	1617.8	220.2	103.7	11.9	50.2	1.2						
MAL3-2_24	8	1143	299	0.42	162	0.00247	4.50	0.05497	1.88	0.05914	2.09	0.00780	0.90	0.43	50.0	4.5	411.0	84.1	58.3	2.4	50.1	0.9						
MAL3-2_25	14	1908	502	0.38	485	0.00254	4.63	0.04790	1.09	0.05354	1.46	0.00811	0.97	0.67	51.3	4.7	94.4	51.5	53.0	1.5	52.0	1.0						
MAL3-2_26	25	3509	1590	0.56	843	0.00210	4.21	0.04683	1.18	0.04625	1.51	0.00716	0.94	0.62	42.4	3.6	40.6	56.5	45.9	1.4	46.0	0.9	46.0	0.9	0.04	0.85		
MAL3-2_27	7	1071	272	0.43	248	0.00373	4.38	0.06711	1.36	0.07557	1.76	0.00817	1.11	0.63	75.2	6.6	841.1	56.7	74.0	2.5	52.4	1.2						
MAL3-2_28	7	252	94	0.53	32	0.02602	5.16	0.29656	11.18	0.61256	11.32	0.01498	1.74	0.15	519.1	52.9	3452.4	347.0	485.2	89.3	95.9	3.3						
MAL3-2_29	4	244	99	2.08	34	0.00292	23.73	0.23152	7.66	0.25515	7.95	0.00799	2.09	0.26	59.0	28.0	3062.6	245.1	230.8	33.1	51.3	2.1						
MAL3-2_30	14	2029	774	0.62	1089	0.00201	4.25	0.04790	1.24	0.04935	1.61	0.00747	1.02	0.64	40.5	3.4	94.1	58.9	48.9	1.5	48.0	1.0						
MAL3-2_31	3	338	103	0.41	18	0.00523	5.91	0.10504	5.59	0.11502	5.79	0.00794	1.51	0.26	105.4	12.4	1715.1	205.6	110.6	12.2	51.0	1.5						
MAL3-2_32	4	262	92	0.72	45	0.00850	7.30	0.22745	5.27	0.31049	5.72	0.00990	2.21	0.39	171.1	24.9	3034.2	169.0	274.6	27.7	63.5	2.8						
MAL3-2_33	7	721	310	1.34	137	0.00181	5.32	0.08631	8.03	0.08583	8.35	0.00721	2.27	0.27	36.5	3.9	1345.2	310.3	83.6	13.4	46.3	2.1						
MAL3-2_34	3	353	119	0.80	77	0.00240	4.55	0.06371	6.40	0.06783	6.52	0.00772	1.23	0.19	48.5	4.4	732.0	271.2	66.6	8.4	49.6	1.2						
MAL3-2_35	16	2114	561	0.26	374	0.00605	4.55	0.08101	4.63	0.09045	4.73	0.00810	0.98	0.21	121.8	11.0	1221.6	181.8	87.9	8.0	52.0	1.0						
MAL3-2_36	9	785	237	0.35	68	0.01439	4.22	0.16861	4.78	0.24197	4.87	0.01041	0.97	0.20	288.8	24.2	2543.9	160.1	220.0	19.4	66.7	1.3						
MAL3-2_37	4	403	121	0.89	100	0.00262	4.40	0.05011	3.33	0.05061	3.61	0.00733	1.38	0.38	52.9	4.6	200.0	154.8	50.1	3.5	47.1	1.3						
MAL3-2_38	8	1046	240	0.33	266	0.00399	4.51	0.06005	2.36	0.06642	2.57	0.00802	1.01	0.39	80.4	7.2	605.3	102.2	65.3	3.3	51.5	1.0						
MAL3-2_39	19	2520	1161	0.54	516	0.00255	4.23	0.05287	1.39	0.05755	1.77	0.00790	1.10	0.62	51.4	4.3	323.1	62.9	56.8	2.0	50.7	1.1						
MAL3-2_40	14	1683	503	0.34	166	0.00593	4.27	0.08034	1.45	0.09482	1.72	0.00856	0.91	0.53	119.5	10.2	1205.4	57.3	92.0	3.0	54.9	1.0						
MAL3-2_41	12	1724	656	0.52	522	0.00237	4.23	0.04816	1.64	0.04915	1.89	0.00740	0.94	0.50	47.9	4.0	107.4	77.3	48.7	1.8	47.5	0.9						
MAL3-2_42	16	2303	707	0.39	427	0.00251	4.32	0.04741	1.32	0.04896	1.66	0.00749	1.00	0.60	50.7	4.4	70.0	62.7	48.5	1.6	48.1	1.0	48.1	1.0	0.48	0.49		
MAL3-2_43	1	181	64	0.58	64	0.00243	5.60	0.04692	4.58	0.04998	4.74	0.00773	1.20	0.25	49.0	5.5	45.3	219.0	49.5	4.6	49.6	1.2	49.6	1.2	0.00	0.97		
MAL3-2_44	6	644	191	0.67	85	0.00335	5.25	0.10705	3.22	0.11747	3.43	0.00796	1.19	0.35	67.6	7.1	1749.8	117.9	112.8	7.3	51.1	1.2						
MAL3-2_45	23	3243	1191	0.53	1201	0.00200	4.30	0.04759	1.21	0.05019	1.56	0.00765	0.98	0.63	40.3	3.5	78.8	57.5	49.7	1.5	49.1	1.0	49.1	1.0	1.04	0.31		
MAL3-2_46	6	456	120	0.24	63	0.02564	1.94	0.19113	7.63	0.32766	7.69	0.01243	1.00	0.13	511.8	19.6	2751.9	250.7	287.8	38.9	79.7	1.6						
MAL3-2_47	14	1991	614	0.35	787	0.00290	2.08	0.04985	1.72	0.05167	1.98	0.00752	0.98	0.50	58.5	2.4	188.2	80.0	51.2	2.0	48.3	0.9						
MAL4-5_1	11	1632	47	0.04	897	0.00279	3.76	0.04676	1.54	0.05238	1.89	0.00812	1.09	0.58	56.4	4.2	37.1	73.7	51.8	1.9	52.2	1.1	52.2	1.1	0.17	0.68		Paragneiss
MAL4-5_2	9	1201	38	0.04	383	0.00393	3.25	0.04844	2.08	0.05774	2.34	0.00864	1.07	0.46	79.3	5.1	121.1	98.1	57.0	2.6	55.5	1.2	55.5	1.2	1.71	0.19		
MAL4-5_3	13	1656	29	0.03	877	0.00255	4.92	0.04735	1.36	0.05367	1.95	0.00822	1.41	0.72	51.5	5.1	67.0	64.5	53.1	2.0	52.8	1.5	52.8	1.5	0.19	0.66	Outer part	
MAL4-5_3b	21	2797	60	0.06	1403	0.00253	7.40	0.04964	1.57	0.05927	1.89	0.00866	1.07	0.56	51.0	7.5	178.3	73.0	58.5	2.2	55.6	1.2					Inner part	
MAL4-5_4	16	1972	71	0.06	794	0.00286	2.50	0.04697	1.08	0.05659	1.70	0.00874	1.31	0.77	57.8	2.9	47.7	51.6	55.9	1.8	56.1	1.5	56.1	1.5	0.10	0.75		
MAL4-5_5	19	2838	54	0.03	2654	0.00284	2.32	0.04717	1.35	0.05055	1.72	0.00777	1.07	0.62	57.3	2.7	57.6	64.5	50.1	1.7	49.9	1.1	49.9	1.1	0.06	0.81		
MAL4-5_6	13	1901	67	0.06	427	0.00248	3.64	0.04878	1.50	0.05654	1.82	0.00841	1.03	0.56	50.0	3.6	137.2	70.4	55.8	2.0	54.0	1.1						
MAL4-5_7	13	1373	518	0.64	5656	0.00236	3.26	0.04754	1.99	0.05677	2.33	0.00866	1.21	0.52	47.6	3.1	76.5	94.6	56.1	2.5	55.6	1.3	55.6	1.3	0.19	0.66		
MAL4-5_8	15	1834	145	0.13	1315	0.00277	3.51	0.04657	1.27	0.06035	1.75	0.00940	1.20	0.69	56.0	3.9	27.4	60.9	59.5	2.0	60.3	1.4	60.3	1.4	1.18	0.28	Outer part	
MAL4-5_8b	10	1107	94	0.12	720	0.00344	2.31	0.04729	1.27	0.07081	1.78	0.01086	1.25	0.70	69.3	3.2	63.8	60.6	69.5	2.4	69.6	1.7	69.6	1.7	0.04	0.85	Inner part	
MAL4-5_9	6	260	37	0.23	348	0.00729	2.89	0.05385	2.15	0.18300	2.63	0.02465	1.52	0.58	146.8	8.4	364.7	97.0	170.6	8.3	157.0	4.7						
MAL4-5_10	7	1034	105	0.15	513	0.00285	3.50	0.04685	2.00	0.05530	2.39	0.00856	1.30	0.55	57.4	4.0	41.8	95.7	54.6	2.5	54.9	1.4	54.9	1.4	0.08	0.78		
MAL4-5_11	12	1101	155	0.50	310	0.00305	10.54	0.08778	5.31	0.10829	5.43	0.00895	1.14	0.21	61.5	12.9	1377.7	204.2	104.4	10.8	57.4	1.3						
MAL4-5_12	9	1113	265	0.31	481	0.00271	1.96	0.04674	1.29	0.04983	1.84	0.00773	1.31	0.71	54.6	2.1	35.7	61.9	49.4	1.8	49.7	1.3	49.6	1.3	0.20	0.65		
MAL4-5_13	47	6867	109	0.03	4564	0.00248	4.05	0.04732	0.74	0.05197	1.21	0.00797	0.96	0.79	50.0	4.0	65.5	35.4	51.4	1.2	51.1	1.0	51.2	1.0	0.65	0.42		
MAL4-5_14	9	1067	60	0.09	477	0.00324	3.37	0.04721	1.88	0.06109	2.22	0.00939	1.16	0.53	65.4	4.4	59.7	89.9	60.2	2.6	60.2	1.4	60.2	1.4	0.00	0.99		
MAL4-5_15	9	790	75	0.11	1712	0.00358	2.58	0.04721	1.85	0.04945	2.33	0.00760	1.42	0.61	72.3	3.7	59.7	88.0	49.0	2.2	48.8	1.4	48.8	1.4	0.06	0.80		
MAL4-5_16	8	1068	70	0.13	502	0.00237	2.70	0.04687	2.33	0.05031	2.65	0.00778	1.26	0.47	47.9	2.6	42.8	111.5	49.8	2.6	50.0	1.3	50.0	1.3	0.02	0.90		

MAL4-5_17	9	1296	50	0.05	2339	0.00291	2.90	0.04719	1.39	0.05253	1.80	0.00807	1.15	0.64	58.8	3.4	59.1	66.4	52.0	1.8	51.8	1.2	51.8	1.2	0.05	0.83	Outer part	
MAL4-5_17b	3	404	53	0.20	187	0.00247	2.65	0.04794	2.62	0.05559	2.87	0.00841	1.18	0.41	49.9	2.6	96.4	124.1	54.9	3.1	54.0	1.3	54.0	1.3	0.45	0.50	Inner part	
MAL4-5_18	9	1058	215	0.28	474	0.00277	1.94	0.04756	1.83	0.05925	2.19	0.00904	1.20	0.55	55.9	2.2	77.2	86.9	58.4	2.5	58.0	1.4	58.0	1.4	0.19	0.66		
MAL4-5_19	12	1361	168	0.32	496	0.00229	3.72	0.05486	1.59	0.07324	1.94	0.00968	1.10	0.57	46.3	3.4	406.6	71.3	71.8	2.7	62.1	1.4					Inner part	
MAL4-5_19b	18	2688	61	0.03	5997	0.00282	2.86	0.04798	1.07	0.05127	1.50	0.00775	1.04	0.70	56.9	3.3	98.4	50.8	50.8	1.5	49.8	1.0					Outer part	
MAL4-5_20	17	2303	207	0.12	1349	0.00281	2.11	0.04581	1.02	0.05396	1.50	0.00854	1.10	0.73	56.7	2.4	-12.6	49.4	53.4	1.6	54.8	1.2					Outer part	
MAL4-5_20b	6	650	90	0.31	267	0.00319	3.28	0.04627	1.59	0.06014	2.19	0.00943	1.51	0.69	64.5	4.2	11.9	76.4	59.3	2.5	60.5	1.8	60.4	1.8	1.65	0.20	Inner part	
MAL4-5_21	11	1371	112	0.11	576	0.00257	2.61	0.04657	1.18	0.04768	2.16	0.00743	1.81	0.84	51.9	2.7	27.1	56.7	47.3	2.0	47.7	1.7	47.7	1.7	0.53	0.47		
MAL4-5_22	11	1569	33	0.08	3206	0.00238	7.19	0.04730	1.60	0.04954	1.96	0.00759	1.14	0.58	48.1	6.9	64.6	76.3	49.1	1.9	48.8	1.1	48.8	1.1	0.17	0.68	Outer part	
MAL4-5_22b	13	1606	201	0.17	4019	0.00289	3.33	0.04610	1.79	0.05755	2.16	0.00905	1.20	0.56	58.3	3.9	2.8	86.5	56.8	2.4	58.1	1.4	58.1	1.4	1.69	0.19	Inner part	
MAL7-3_1	8	333	31	0.13	475	0.00952	2.93	0.05011	1.40	0.19612	1.81	0.02839	1.15	0.63	191.5	11.2	200.1	65.3	181.8	6.0	180.4	4.1	180.5	4.1	0.36	0.55		Meta-quartzdiorite
MAL7-3_2	8	324	35	0.16	363	0.00953	3.22	0.05007	1.77	0.19786	2.22	0.02866	1.34	0.60	191.7	12.3	198.2	82.5	183.3	7.5	182.2	4.8	182.2	4.8	0.15	0.70		
MAL7-3_3	4	173	15	0.12	322	0.00918	3.51	0.04986	1.64	0.19879	1.94	0.02892	1.03	0.53	184.8	12.9	188.3	76.4	184.1	6.5	183.8	3.7	183.8	3.7	0.01	0.91		
MAL7-3_4	4	144	11	0.10	174	0.01398	3.96	0.05421	2.58	0.21263	2.85	0.02845	1.21	0.42	280.6	22.1	379.7	116.3	195.8	10.2	180.8	4.3						
MAL7-3_5	4	175	16	0.13	322	0.00907	2.91	0.04949	2.78	0.19541	3.12	0.02864	1.41	0.45	182.5	10.6	171.0	130.2	181.2	10.4	182.0	5.1	182.0	5.1	0.03	0.87		
MAL7-3_6	15	582	41	0.11	1335	0.00958	2.99	0.04979	0.98	0.19557	1.58	0.02849	1.24	0.79	192.6	11.5	185.1	45.6	181.4	5.3	181.1	4.4	181.1	4.4	0.03	0.86		
MAL7-3_7	5	205	19	0.14	4910	0.00828	4.15	0.04957	1.74	0.20191	2.00	0.02954	1.00	0.50	166.7	13.8	174.9	81.2	186.7	6.9	187.7	3.7	187.6	3.7	0.10	0.75		
MAL7-3_8	8	310	26	0.12	936	0.00899	2.73	0.05026	2.02	0.19574	2.27	0.02825	1.03	0.45	180.9	9.8	207.1	94.1	181.5	7.6	179.6	3.6	179.6	3.6	0.34	0.56		
MAL7-3_9	4	163	21	0.17	216	0.00913	3.01	0.04971	2.23	0.19781	2.44	0.02886	1.01	0.41	183.7	11.0	181.7	104.1	183.3	8.2	183.4	3.6	183.4	3.6	0.00	0.97		
MAL7-3_10	5	204	24	0.16	384	0.00954	3.30	0.04918	2.24	0.19196	2.49	0.02831	1.09	0.44	191.8	12.6	156.5	105.1	178.3	8.2	180.0	3.9	179.9	3.9	0.20	0.65		
MAL7-3_11	5	191	18	0.13	-603	0.00900	3.06	0.04996	2.02	0.19599	2.25	0.02845	0.98	0.44	181.0	11.0	193.0	94.4	181.7	7.5	180.9	3.5	180.9	3.5	0.07	0.80		
MAL7-3_12	75	2950	360	0.17	3606	0.00892	2.71	0.05134	0.71	0.19817	1.24	0.02800	1.01	0.82	179.5	9.7	256.0	32.8	183.6	4.2	178.0	3.6						
MAL7-3_13	12	469	40	0.11	1024	0.00947	2.91	0.04973	1.46	0.19730	1.74	0.02877	0.95	0.54	190.6	11.0	182.5	68.4	182.8	5.8	182.9	3.4	182.9	3.4	0.00	0.99		
MAL7-3_14	8	323	31	0.13	543	0.00998	2.87	0.05012	1.99	0.19630	2.36	0.02841	1.26	0.54	200.7	11.5	200.5	92.7	182.0	7.9	180.6	4.5	180.6	4.5	0.18	0.67		
MAL7-3_15	10	410	34	0.12	618	0.00941	3.25	0.05103	1.70	0.20327	2.10	0.02889	1.22	0.58	189.3	12.2	242.0	78.7	187.9	7.2	183.6	4.4						
MAL7-3_16	6	250	20	0.11	354	0.00998	2.91	0.04975	1.65	0.19206	1.94	0.02800	1.03	0.53	200.7	11.6	183.2	77.0	178.4	6.4	178.0	3.6	178.0	3.6	0.02	0.89		
MAL7-3_17	6	253	25	0.14	555	0.00889	3.06	0.05056	1.99	0.19903	2.36	0.02855	1.27	0.54	179.0	10.9	221.0	92.6	184.3	8.0	181.5	4.5	181.5	4.5	0.71	0.40		
MAL7-3_18	11	426	31	0.11	5381	0.00903	2.60	0.04962	1.01	0.19858	1.49	0.02903	1.10	0.74	181.6	9.4	177.1	47.2	183.9	5.0	184.5	4.0	184.4	4.0	0.10	0.76		
MAL7-3_19	6	202	31	0.21	239	0.00907	2.63	0.04963	2.68	0.19881	2.90	0.02905	1.11	0.38	182.5	9.6	177.7	125.3	184.1	9.8	184.6	4.1	184.6	4.1	0.01	0.91		
MAL7-3_20	2	108	36	0.51	134	0.00476	3.54	0.04793	4.38	0.11276	4.56	0.01706	1.26	0.28	96.0	6.8	95.9	208.3	108.5	9.4	109.1	2.7	109.1	2.7	0.02	0.90		
MAL7-3_21	8	294	41	0.19	1374	0.00884	2.95	0.04983	1.71	0.19640	1.95	0.02858	0.93	0.48	178.0	10.4	187.2	80.0	182.1	6.5	181.7	3.3	181.7	3.4	0.02	0.89		
MAL7-3_22	8	313	26	0.12	7751	0.00931	3.14	0.05033	1.37	0.19667	1.90	0.02834	1.32	0.69	187.4	11.7	210.4	63.9	182.3	6.4	180.1	4.7	180.3	4.7	0.88	0.35		
MAL7-3_23	11	434	35	0.12	393	0.00873	2.86	0.04986	1.24	0.19806	1.79	0.02881	1.30	0.72	175.7	10.0	188.3	57.7	183.5	6.0	183.1	4.7	183.1	4.7	0.03	0.86		
MAL7-3_24	7	260	25	0.13	299	0.00919	3.08	0.04989	1.90	0.19217	2.17	0.02794	1.06	0.49	184.9	11.3	189.7	88.6	178.5	7.1	177.6	3.7	177.7	3.7	0.07	0.79		
MAL7-3_25	11	431	39	0.13	623	0.00867	2.97	0.04967	1.83	0.19795	2.18	0.02890	1.19	0.55	174.5	10.3	179.8	85.6	183.4	7.3	183.7	4.3	183.7	4.3	0.01	0.93		
MAL7-3_26	12	476	65	0.19	914	0.00916	2.86	0.05100	1.40	0.20028	1.72	0.02848	1.00	0.58	184.3	10.5	240.7	64.8	185.4	5.8	181.0	3.6						
MAL7-3_27	7	291	23	0.11	536	0.00897	3.11	0.05095	1.48	0.20131	1.75	0.02866	0.93	0.53	180.5	11.2	238.6	68.5	186.2	6.0	182.1	3.4						
MAL7-3_28	5	216	20	0.14	1016	0.00921	3.41	0.04971	1.60	0.19659	1.98	0.02868	1.16	0.59	185.4	12.6	181.2	74.7	182.2	6.6	182.3	4.2	182.3	4.2	0.00	0.98		
MAL7-3_29	10	378	35	0.13	555	0.00923	2.86	0.05171	1.22	0.21873	1.59	0.03068	1.02	0.64	185.7	10.6	272.6	56.2	200.9	5.8	194.8	3.9						
MAL7-3_30	6	240	31	0.19	328	0.00873	2.61	0.05009	1.87	0.19618	2.16	0.02841	1.07	0.50	175.7	9.1	199.2	87.2	181.9	7.2	180.6	3.8	180.6	3.8	0.18	0.67		
MAL7-3_31	5	172	21	0.19	425	0.00856	3.02	0.05162	1.91	0.20492	2.23	0.02879	1.14	0.51	172.4	10.4	268.7	88.0	189.3	7.7	183.0	4.1						
MAL7-3_32	6	259	21	0.11	407	0.00906	3.62	0.04971	1.10	0.19617	1.59	0.02862	1.15	0.72	182.2	13.1	181.6	51.5	181.9	5.3	181.9	4.1	181.9	4.1	0.00	0.99		
MAL7-3_33	5	198	19	0.16	317	0.00886	2.80	0.04952	2.20	0.19494	2.46	0.02855	1.10	0.45	178.3	9.9	172.3	103.1	180.8	8.2	181.5	3.9	181.5	3.9	0.03	0.86		
MAL6-5_1	2	70	16	0.29	57	0.00833	3.88	0.04853	5.31	0.15822	5.42	0.02365	1.11	0.20	167.8	13.0	125.3	249.7	149.1	15.1	150.7	3.3	150.6	3.3	0.04	0.84		Orthogneiss
MAL6-5_2	2	73	13	0.24	102	0.00802	3.28	0.04895	4.62	0.16113	5.08	0.02387	2.11	0.41	161.4	10.5	145.5	216.6	151.7	14.4	152.1	6.3	152.1	6.3	0.00	0.95		
MAL6-5_3	1	31	5	0.24	54	0.00866	10.46	0.04849	9.65	0.15855	9.80	0.02371	1.69	0.17	174.4	36.3	123.2	454.2	149.4	27.4	151.1	5.0	151.1	5.0	0.02	0.90		
MAL6-5_4	7	320	7	0.03	326	0.00847	7.99	0.04701	2.12	0.15079	2.58	0.02326	1.47	0.57	170.4	27.1	49.7	101.2	142.6	6.9	148.3	4.3						
MAL6-5_5	2	52	6	0.07	224	0.00829	8.44	0.05228	4.04	0.17107	4.39	0.02373	1.73	0.39	166.8	28.0	297.7	184.2	160.3	13.1	151.2	5.2						
MAL6-5_6	1	45	8	0.22	82	0.00872	4.80	0.04724	5.53	0.15953	5.66	0.02449	1.20	0.21	175.5	16.8	61.6	263.5	150.3	15.9	156.0	3.7	155.9	3.7	0.54	0.46		
MAL6-5_7	2	83	27	0.41	131	0.00883	4.56	0.05023	4.16	0.16366	4.42	0.02363	1.49	0.34	177.6	16.1	205.7	193.0	153.9	12.7	150.6	4.4	150.6	4.4	0.32	0.57		
MAL6-5_8	1	66	18	0.36	277	0.00855	4.18	0.05007	4.44	0.16617	4.71	0.02407	1.55	0.33	172.2	14.3	198.1	206.3	156.1	13.7	153.3	4.7	153.4	4.7	0.18	0.67		
MAL6-5_9	2	100	18	0.24	328	0.00822	3.95	0.05060	3.56	0.16691	3.81	0.02392	1.37	0.36	165.5	13.0	222.5	164.5	156.7	11.1	152.4	4.1	152.4	4.1	0.69	0.40	Outer part	
MAL6-5_9b	1	48	7	0.20	70	0.00869	6.21	0.05112	5.88	0.17019	6.03	0.02415	1.33	0.22	174.9	21.6	246.2	270.8	159.6	17.9	153.8	4.0	153.8	4.0	0.44	0.51	Inner part	
MAL6-5_10	3	141	25	0.26	186	0.00777	5.09	0.05316	2.80	0.17543	3.04	0.02394	1.16	0.38	156.4	15.9	335.5	127.0	164.1	9.2	152.5	3.5						
MAL6-5_11	2	72	13	0.25	106	0.00834	3.98	0.05032	3.77	0.16416	4.04	0.02366	1.45	0.36	167.8	13.3	209.8	174.6	154.3	11.6	150.7	4.3	150.8	4.3	0.44	0.51		
MAL6-5_12	1	61	9	0.22	106	0.00862	5.53	0.05159	4.66	0.17139	5.67	0.02410	3.24	0.57	173.5	19.1	267.2	213.9	160.6	16.9	153.5	9.8	153.5	9.8	1.05	0.30		
MAL6-5_13	2	78	10	0.19	166	0.00782	4.82	0.05514	5.00	0.18010	5.25	0.02369	1.60	0.30	157.5	15.1	417.8	223.5	168.1	16.3	150.9	4.8						
MAL6-5_14	1	38	7	0.27	99	0.00746	4.50	0.04809	5.59	0.15517	6.00	0.02340	2.20	0.37	150.3	13.5	103.8	264.1	146.5	16.4	149.1	6.5	149.1	6.5	0.12	0.73		
MAL6-5_15	2	84	15	0.23	178	0.00783	4.35	0.05286	4.07	0.17313	4.27	0.02376	1.31	0.31	157.7	13.7	322.7	184.9	162.1	12.8	151.3	3.9						
MAL6-5_16	1	48	8	0.20	74	0.00838	4.87	0.05010	4.60	0.16260	4.76	0.02354	1.24	0.26	168.7	16.4	199.7	213.8	153.0	13.6	150.0	3.7	150.0	3.7	0.21	0.65		
MAL6-5_17	1	45	7	0.22	40	0.00767	6.00	0.04970	5.82	0.16342	6.03	0.02385	1.57	0.26	154.5	18.5	180.8	271.7	153.7	17.3	151.9	4.7	151.9	4.7	0.04	0.83		
MAL6-5_18	3	120	40	0.40	156	0.00870	3.45	0.05109	1.76	0.16793	2.10	0.02384	1.14	0.54	175.1	12.0	245.0	81.2	157.6	6.1	151.9	3.4						
MAL6-5_19	4	159	67	0.54	173	0.00756	3.23	0.04979	2.58	0.16285	2.82	0.02372	1.13	0.40	152.3	9.8	185.2	120.5	153.2	8.0	151.1	3.4	151.2	3.4	0.31	0.58	Outer part	
MAL6-5_19b	0.5	18	2	0.11	22	0.03845	4.13	0.08987	8.13	0.32603	8.40	0.02631	2.13	0.25	762.7	61.9	1422.8	310.7	286.5	42.4	167.4	7.0					Inner part	
MAL6-5_20	1	47	5	0.21	46	0.00733	7.47	0.04744	6.40	0.15273	6.66	0.02335	1.83	0.27	147.6	22.0	71.4	305.0	144.3	18.0	148.8	5.4	148.8	5.4	0.27	0.60		
MAL6-5_21	10	88	8	2.27	26	0.01280	5.71	0.05093	5.44	0.16712	5.61	0.02380	1.40	0.25	257.1	29.2	237.6	251.1	156.9	16.4	151.6	4.2	151.6	4.2	0.45	0.50		
MAL6-5_22	2	89	19	0.30	72	0.00715	3.81	0.04680	4.16	0.15338	4.44	0.02377	1.56	0.35	144.0	10.9	38.8	199.3	144.9	12.0	151.5	4.7	151.3	4.7	1.37	0.24		
MAL6-5_23	1	51	7	0.18	73	0.00826	5.29	0.05017	3.86	0.16184	4.17	0.02340	1.59	0.38	166.2	17.5	202.8	179.4	152.3	11.8	149.1	4.7	149.1	4.7	0.35	0.56		
MAL6-5_24	1	59	11	0.24	109	0.00810	4.35	0.04952	4.21	0.16013	4.63	0.02345	1.91	0.41	163.1	14.1	172.4	197.0	150.8	13.0	149.5	5.7	149.5	5.7	0.05	0.82		
MAL6-5_25	1	49	7	0.17	301	0.01035	4.28	0.04699	5.46	0.15277	5.70	0.02358	1.61	0.28	208.1	17.7	48.5	261.5	144.4	15.4	150.3	4.8	150.2	4.8	0.65	0.42		
MAL6-5_26	2	91	20	0.29	91	0.00821	3.66	0.04946	3.95	0.15501	4.25	0.02273	1.58	0.37	165.2	12.1	169.6	184.7	146.3	11.6	144.9	4.5	144.9	4.5	0.07	0.79		
MAL6-5_27	2	75	13	0.21	72	0.00870	5.34	0.05022	4.39	0.16467	4.52	0.02378	1.07	0.24	175.1	18.6	205.2	204.1	154.8	13.0	151.5	3.2	151.5	3.2	0.27	0.60	Inner part	
MAL6-5_27b	2	96	16	0.24	251	0.00763	4.07	0.05388	3.57	0.17335	3.82	0.02333	1.35	0.35	153.7	12.5	366.2	161.4	162.3	11.5	148.7	4.0					Outer part	
MAL6-5_28	1	63	12	0.27	101	0.00768	6.33	0.04831	3.30	0.15941	3.74	0.02393	1.77	0.47	154.7	19.5	114.3	155.8	150.2	10.5	152.5	5.3	152.4	5.3	0.25	0.62		
MAL6-5_29	3	89	5	0.03	62	0.54459	15.53	0.18175	16.21	1.23453	20.32	0.04926	12.26	0.60	8787.5	2277.0	2668.9	537.0	816.4	241.9	310.0	74.4						
MAL6-5_30	2	70	8	0.16	82	0.00787	5.65	0.04906	3.71	0.15678	4.07	0.02318	1.67	0.41	158.5	17.8	150.9	174.0	147.9	11.2	147.7	4.9	147.7	4.9	0.00	0.97	Inner part	
MAL6-5_30b	1	49	8	0.22	46	0.00816	7.06	0.04867	5.51	0.15395	5.72	0.02294	1.55	0.27	164.3	23.1	132.0	259.0	145.4	15.6	146.2	4.5	146.2	4.5	0.01	0.91	Outer part	
MAL6-5_31	2	84	13	0.22	80	0.00827	5.25	0.04958	2.49	0.16378	2.95	0.02396	1.59	0.54	166.4	17.4	175.1	116.0	154.0	8.4	152.6	4.8	152.7	4.8	0.15	0.70		
MAL6-5_32	2	79	14	0.27	93	0.00759	5.43	0.04990	3.73	0.16288	4.04	0.02367	1.55	0.38	152.9	16.6	190.4	173.6	153.2	11.5	150.8	4.6	150.9	4.6	0.20	0.65		
MAL6-5_33	16	660	157	0.31	947	0.00820	4.62	0.04908	1.35	0.16792	1.74	0.02481	1.10	0.63	165.1	15.2	151.6	63.3	157.6	5.1	158.0	3.4	158.0	3.4	0.04	0.84		
MAL6-5_34	2	72	17	0.31	74	0.00846	5.82	0.05524	6.09	0.18096	6.32	0.02376	1.70	0.27	170.3	19.7	421.9	271.7	168.9	19.8	151.4	5.1						
MAL6-5_36	1	69	15	0.26	65	0.00966	5.01	0.05143	3.58	0.16984	3.79	0.02395	1.23	0.32	194.4	19.4	260.2	164.6	159.3	11.2	152.6	3.7	152.6	3.7	1.60	0.21		
MAL6-5_37	1	66	7	0.16	193	0.00741	6.75	0.04874	4.00	0.15904	4.25	0.02366	1.44	0.34	149.2	20.1	135.4	187.9	149.9	11.9	150.8	4.3	150.8	4.3	0.03	0.87		
MAL6-5_38	3	157	58	0.48	119	0.00799	4.74	0.05191	3.43	0.16919	3.74	0.02364	1.49	0.40	160.8	15.2	281.3	157.2	158.7	11.0	150.6	4.4						
MAL6-5_39	1	58	8	0.18	133	0.00821	7.09	0.04834	3.86	0.16009	4.09	0.02402	1.36	0.33	165.3	23.4	116.1	182.2	150.8	11.5	153.0	4.1	153.0	4.1	0.17	0.68		
MAL6-5_40	2	79	15	0.28	89	0.00744	5.67	0.04960	3.50	0.16471	4.00	0.02408	1.92	0.48	149.9	16.9	176.3	163.5	154.8	11.5	153.4	5.8	153.4	5.8	0.08	0.78		
MAL6-5_41	1	57	6	0.13	91	0.00751	8.69	0.05533	4.65	0.18094	4.88	0.02372	1.48	0.30	151.2	26.2	425.7	207.3	168.9	15.2	151.1	4.4						
MAL6-5_42	1	50	9	0.23	80	0.00886	5.90	0.04782	3.74	0.15564	3.89	0.02360	1.05	0.27	178.3	21.0	90.6	177.2	146.9	10.7	150.4	3.1	150.4	3.1	0.47	0.49		
MAL6-5_43	1	45	7	0.19	79	0.01025	5.08	0.04817	5.14	0.15313	5.56	0.02305	2.10	0.38	206.0	20.8	107.9	242.9	144.7	15.0	146.9	6.1	146.9	6.1	0.11	0.74		
MAL6-5_44	1	64	8	0.20	46	0.01568	5.28	0.07090	3.26	0.22774	3.55	0.02330	1.41	0.40	314.4	33.0	954.5	133.4	208.3	13.4	148.5	4.1						
MAL6-5_45	2	66	10	0.17	112	0.00944	4.79	0.05059	4.02	0.16696	4.49	0.02393	1.99	0.44	189.8	18.1	222.3	186.0	156.8	13.1	152.5	6.0	152.5	6.0	0.54	0.46		
MAL4-16_1	2	240	72	0.39	47	0.00329	4.63	0.04693	3.88	0.06433	4.14	0.00994	1.46	0.35	66.4	6.1	45.5	185.3	63.3	5.1	63.8	1.8	63.8	1.9	0.04	0.84		Paragneiss
MAL4-16_2	34	4434	1082	0.34	1788	0.00255	4.57	0.04745	1.30	0.05747	1.85	0.00878	1.32	0.71	51.4	4.7	72.1	61.8	56.7	2.0	56.4	1.5	56.4	1.5	0.26	0.61		
MAL4-16_3	121	2514	1822	0.85	8970	0.01306	4.53	0.05168	0.99	0.31558	1.51	0.04428	1.14	0.76	262.3	23.6	271.5	45.2	278.5	7.4	279.3	6.2	279.2	6.2	0.12	0.73		
MAL4-16_4	6	851	33	0.05	287	0.00287	5.26	0.04847	2.25	0.05106	2.56	0.00764	1.21	0.48	57.9	6.1	122.2	105.9	50.6	2.5	49.1	1.2	49.1	1.2	1.82	0.18		
MAL4-16_5	9	1357	30	0.02	320	0.00393	6.09	0.04507	1.89	0.04297	3.90	0.00691	3.41	0.87	79.3	9.6	-51.8	92.1	42.7	3.3	44.4	3.0					Inner part (U-rich)	
MAL4-16_5b	6	665	97	0.21	347	0.00372	4.99	0.04859	2.42	0.06843	2.70	0.01022	1.22	0.45	75.0	7.5	127.9	113.7	67.2	3.5	65.5	1.6	65.5	1.6	1.16	0.28	Inner part (U-poor)	
MAL4-16_6	49	3222	553	0.31	727	0.00506	4.58	0.04853	1.14	0.10264	1.58	0.01534	1.09	0.69	102.0	9.3	125.3	53.8	99.2	3.0	98.1	2.1	98.2	2.1	1.00	0.32		
MAL4-16_7	8	623	151	0.35	507	0.00502	4.62	0.04865	1.55	0.10186	1.94	0.01519	1.16	0.60	101.3	9.3	130.8	72.7	98.5	3.6	97.2	2.2	97.2	2.2	0.83	0.36		
MAL4-16_8	4	393	85	0.30	276	0.00413	4.81	0.04641	2.67	0.08099	3.06	0.01266	1.50	0.49	83.3	8.0	19.1	128.1	79.1	4.7	81.1	2.4	81.0	2.4	0.97	0.33		
MAL4-16_9	6	594	79	0.17	231	0.00367	4.70	0.04869	2.05	0.06799	2.42	0.01013	1.29	0.53	74.1	7.0	132.8	96.5	66.8	3.1	65.0	1.7	65.0	1.7	1.90	0.17		
MAL4-16_10	3	278	42	0.21	99	0.00365	4.31	0.04986	3.31	0.07319	3.55	0.01065	1.28	0.36	73.6	6.3	188.3	154.0	71.7	4.9	68.3	1.7						

MAL4-16_11	13	283	120	0.58	727	0.01418	3.93	0.05220	1.95	0.32537	2.33	0.04521	1.27	0.55	284.6	22.2	294.0	89.3	286.0	11.7	285.0	7.1	285.1	7.1	0.04	0.84		
MAL4-16_12	4	503	113	0.32	365	0.00286	4.04	0.04757	2.51	0.05679	2.88	0.00866	1.42	0.49	57.6	4.6	78.2	119.3	56.1	3.1	55.6	1.6	55.6	1.6	0.14	0.71		
MAL4-16_14	4	426	91	0.49	114	0.00290	4.81	0.04779	4.76	0.05718	5.02	0.00868	1.58	0.31	58.6	5.6	88.7	226.0	56.5	5.5	55.7	1.7	55.7	1.7	0.08	0.77		
MAL4-16_15	11	1291	168	0.19	589	0.00281	4.33	0.04814	1.54	0.06146	1.92	0.00926	1.14	0.59	56.7	4.9	106.4	73.0	60.6	2.3	59.4	1.3	59.4	1.3	1.61	0.20		
MAL4-16_16	6	711	122	0.22	322	0.00319	4.13	0.04749	1.97	0.05735	2.38	0.00876	1.33	0.56	64.5	5.3	73.8	93.7	56.6	2.6	56.2	1.5	56.2	1.5	0.14	0.71		
MAL4-16_17	11	1599	44	0.04	1527	0.00283	4.84	0.04776	1.85	0.04960	2.26	0.00753	1.29	0.57	57.1	5.5	87.2	88.0	49.2	2.2	48.4	1.2	48.4	1.2	0.76	0.38	Metamorphic rim	
MAL4-16_17b	3	405	108	0.36	434	0.00294	4.51	0.04722	4.80	0.05758	5.03	0.00884	1.51	0.30	59.4	5.4	60.6	229.0	56.8	5.6	56.8	1.7	56.8	1.7	0.00	0.97	Central part	
MAL4-16_18	6	643	74	0.15	317	0.00363	4.23	0.04971	2.29	0.06865	2.61	0.01002	1.25	0.48	73.2	6.2	181.4	106.8	67.4	3.4	64.2	1.6						
MAL4-16_19	18	1803	1398	0.89	623	0.00312	4.90	0.04765	1.67	0.06030	2.21	0.00918	1.46	0.66	63.0	6.2	81.9	79.2	59.5	2.6	58.9	1.7	58.9	1.7	0.33	0.56		
MAL4-16_20	9	852	158	0.25	2033	0.00405	4.01	0.04794	1.19	0.08012	1.69	0.01212	1.20	0.71	81.6	6.5	96.3	56.3	78.3	2.5	77.7	1.9	77.7	1.9	0.43	0.51		
MAL4-16_21	10	1181	217	0.27	340	0.00318	4.23	0.04779	2.62	0.05744	2.84	0.00872	1.11	0.39	64.1	5.4	88.9	124.3	56.7	3.1	55.9	1.2	56.0	1.2	0.28	0.60		
MAL4-16_22	23	2891	259	0.12	1773	0.00298	3.93	0.04821	1.04	0.05938	1.51	0.00893	1.09	0.73	60.1	4.7	109.6	49.0	58.6	1.7	57.3	1.2						
MAL4-21_1	12	425	151	0.46	435	0.00948	3.94	0.04925	0.93	0.18436	1.69	0.02715	1.41	0.83	190.8	15.0	159.9	43.8	171.8	5.3	172.7	4.8	172.5	4.8	0.34	0.56		Metasedimentary mylonite
MAL4-21_2	20	711	179	0.35	405	0.00925	4.01	0.05024	1.54	0.19827	2.09	0.02862	1.41	0.67	186.0	14.8	206.1	71.7	183.7	7.0	181.9	5.1	182.0	5.1	0.45	0.50		
MAL4-21_3	6	227	97	0.65	274	0.00812	4.41	0.05117	1.97	0.16815	2.48	0.02383	1.50	0.61	163.5	14.4	248.7	90.6	157.8	7.2	151.8	4.5						
MAL4-21_5	41	628	378	0.88	2046	0.02006	3.88	0.05733	1.12	0.50162	2.06	0.06346	1.73	0.84	401.5	30.9	504.4	49.3	412.8	14.0	396.6	13.3						
MAL4-21_6	20	1302	364	0.41	2271	0.00548	3.89	0.04977	1.16	0.11110	1.64	0.01619	1.17	0.71	110.5	8.6	184.1	54.0	107.0	3.3	103.5	2.4						
MAL4-21_7	28	1206	604	0.54	4430	0.00911	3.90	0.05002	1.15	0.15937	1.69	0.02311	1.25	0.74	183.3	14.2	195.8	53.3	150.2	4.7	147.3	3.6						
MAL4-21_8	7	511	184	0.52	444	0.00432	3.95	0.04894	1.97	0.08621	2.57	0.01278	1.64	0.64	87.2	6.9	145.2	92.8	84.0	4.1	81.8	2.7	81.8	2.7	1.80	0.18		
MAL4-21_9	3	217	44	0.26	150	0.00616	4.41	0.04886	2.06	0.11304	2.44	0.01678	1.31	0.54	124.1	10.9	141.0	96.7	108.7	5.0	107.3	2.8	107.3	2.8	0.48	0.49		
MAL4-21_10	27	1101	378	0.42	1948	0.00801	4.13	0.04928	1.09	0.16442	1.60	0.02420	1.17	0.73	161.2	13.3	161.0	51.3	154.6	4.6	154.1	3.6	154.2	3.6	0.07	0.79		
MAL4-21_11	9	415	150	0.47	853	0.00761	4.01	0.05301	1.45	0.15620	1.90	0.02137	1.23	0.65	153.2	12.3	329.1	65.9	147.4	5.2	136.3	3.3						
MAL4-21_12	2	130	35	0.40	183	0.00446	5.31	0.05278	4.34	0.09079	4.65	0.01248	1.68	0.36	89.9	9.5	319.2	197.6	88.2	7.9	79.9	2.7						
MAL4-21_13	9	524	96	0.32	288	0.00694	4.08	0.05087	1.75	0.15197	2.67	0.02167	2.02	0.76	139.8	11.4	235.1	81.0	143.6	7.2	138.2	5.5						
MAL4-21_14	7	394	106	0.53	227	0.00547	4.25	0.04907	1.91	0.11641	2.37	0.01721	1.40	0.59	110.3	9.4	151.2	89.8	111.8	5.0	110.0	3.1	110.0	3.1	0.82	0.36		
MAL4-21_15	8	296	42	0.21	611	0.00904	4.22	0.04976	1.24	0.20164	1.71	0.02939	1.17	0.69	181.9	15.3	183.7	58.0	186.5	5.8	186.7	4.3	186.7	4.3	0.01	0.92		
MAL4-21_16	13	1170	167	0.23	352	0.00480	3.85	0.04853	1.41	0.09064	1.97	0.01355	1.38	0.70	96.8	7.4	125.2	66.5	88.1	3.3	86.7	2.4	86.8	2.4	1.31	0.25		
MAL4-21_17	18	458	85	0.25	985	0.01666	3.91	0.05482	1.07	0.32459	1.54	0.04295	1.10	0.72	334.0	25.9	404.7	48.1	285.4	7.7	271.1	5.9						
MAL4-21_18	7	333	106	0.46	278	0.00666	3.87	0.05161	1.58	0.15107	1.86	0.02123	0.99	0.53	134.2	10.4	267.9	72.6	142.9	5.0	135.4	2.6						
MAL4-21_19	9	834	88	0.18	825	0.00493	4.05	0.04936	1.22	0.10091	1.73	0.01483	1.23	0.71	99.4	8.0	165.0	57.0	97.6	3.2	94.9	2.3					Inner part	
MAL4-21_19b	11	866	109	0.19	1062	0.00454	3.90	0.04765	1.35	0.09454	1.60	0.01439	0.86	0.54	91.5	7.1	81.9	64.2	91.7	2.8	92.1	1.6	92.1	1.6	0.10	0.75	Outer part	
MAL4-21_20	6	599	104	0.26	350	0.00452	4.12	0.04984	2.82	0.07640	3.05	0.01112	1.14	0.37	91.2	7.5	187.5	131.7	74.8	4.4	71.3	1.6						
MAL4-21_21	3	110	33	0.45	218	0.01053	4.24	0.05250	3.82	0.24470	4.05	0.03381	1.32	0.33	211.8	17.9	307.1	174.5	222.3	16.2	214.3	5.6	214.4	5.6	1.07	0.30		
MAL4-21_22	5	232	71	0.53	487	0.00714	3.83	0.05012	2.17	0.15685	2.37	0.02270	0.96	0.41	143.9	11.0	200.4	100.8	147.9	6.5	144.7	2.8	144.7	2.8	1.18	0.28		
MAL4-21_23	11	540	145	0.38	497	0.00708	3.97	0.04937	1.74	0.15262	2.10	0.02242	1.18	0.56	142.6	11.3	165.2	81.3	144.2	5.7	143.0	3.3	143.0	3.3	0.30	0.59		
MAL4-21_24	23	642	188	0.43	1562	0.01410	4.08	0.05392	1.23	0.29365	2.13	0.03950	1.74	0.82	283.0	23.0	367.6	55.5	261.4	9.8	249.7	8.5						
MAL4-21_25	17	2421	8	0.01	1028	0.01343	5.49	0.04742	0.98	0.05869	1.91	0.00898	1.64	0.86	269.6	29.4	70.5	46.5	57.9	2.2	57.6	1.9	57.6	1.9	0.30	0.58	Outer part	
MAL4-21_25b	12	182	77	0.68	1054	0.02313	3.95	0.05683	1.20	0.62303	1.40	0.07951	0.72	0.52	462.3	36.1	485.1	52.9	491.7	10.9	493.2	6.9	493.0	6.8	0.09	0.76	Inherited older core	
MAL4-21_26	16	587	221	0.50	609	0.00901	3.83	0.04981	1.69	0.19324	1.91	0.02814	0.89	0.47	181.3	13.8	186.0	79.0	179.4	6.3	178.9	3.1	178.9	3.1	0.03	0.86		
MAL4-21_27	5	297	64	0.25	443	0.00663	4.13	0.05038	2.34	0.09764	3.36	0.01406	2.41	0.72	133.6	11.0	212.5	108.8	94.6	6.1	90.0	4.3						
MAL4-21_28	12	1594	25	0.02	1236	0.00662	4.86	0.04897	1.46	0.05978	1.98	0.00885	1.34	0.68	133.4	12.9	146.5	68.5	59.0	2.3	56.8	1.5						
MAL4-21_29	34	695	139	0.25	2140	0.01774	3.78	0.05395	0.81	0.36477	1.36	0.04904	1.09	0.80	355.3	26.6	368.9	36.6	315.8	7.4	308.6	6.6						
MAL4-21_32	6	217	53	0.32	1100	0.00983	4.07	0.04908	2.48	0.19192	2.65	0.02836	0.94	0.36	197.7	16.0	151.4	116.4	178.3	8.7	180.3	3.4	180.3	3.4	0.25	0.62		
MAL4-21_33	3	222	44	0.29	215	0.00616	4.12	0.05303	3.10	0.13341	3.24	0.01825	0.95	0.29	124.2	10.2	330.0	141.0	127.2	7.8	116.6	2.2						
MAL4-21_34	22	392	184	0.54	11427	0.01592	4.50	0.05582	1.30	0.39774	1.89	0.05168	1.37	0.72	319.2	28.5	445.4	58.0	340.0	11.0	324.8	8.7						
MAL4-21_35	57	304	164	0.58	2388	0.06220	3.72	0.08353	0.88	1.53812	3.90	0.13355	3.80	0.97	1219.7	88.1	1281.7	34.5	945.8	48.6	808.1	57.8						
MAL4-21_36	41	2568	842	0.43	2144	0.00545	3.89	0.04941	0.79	0.11941	1.25	0.01753	0.98	0.78	109.8	8.5	167.1	36.8	114.5	2.7	112.0	2.2					Outer part	
MAL4-21_36b	33	2008	860	0.49	3758	0.00609	4.88	0.04853	1.25	0.11362	1.76	0.01698	1.23	0.70	122.8	11.9	125.4	58.9	109.3	3.6	108.5	2.7	108.6	2.7	0.32	0.57	Inner part	
MAL4-21_37	8	494	302	0.69	-3614	0.00594	4.11	0.04913	2.32	0.10417	2.51	0.01538	0.97	0.39	119.7	9.8	154.0	108.9	100.6	4.8	98.4	1.9	98.4	1.9	1.01	0.31		
MAL4-21_40	5	311	92	0.39	295	0.00620	3.99	0.04994	2.10	0.12675	2.35	0.01841	1.05	0.45	125.0	9.9	192.1	98.0	121.2	5.4	117.6	2.4						
MAL4-21_41	19	1006	309	0.51	1426	0.00700	3.81	0.04972	1.65	0.14830	2.13	0.02163	1.35	0.63	141.0	10.7	182.0	77.0	140.4	5.6	138.0	3.7	138.0	3.7	1.27	0.26		
MAL4-21_42	13	847	119	0.19	449	0.00564	2.89	0.04732	1.33	0.10818	1.81	0.01658	1.23	0.68	113.7	6.5	65.6	63.4	104.3	3.6	106.0	2.6	105.9	2.6	1.66	0.20		
MAL4-21_43	7	365	70	0.29	698	0.00683	3.01	0.04967	2.10	0.15329	2.62	0.02238	1.57	0.60	137.6	8.3	179.5	98.2	144.8	7.1	142.7	4.4	142.8	4.4	0.55	0.46		
MAL4-21_44	7	635	74	0.19	376	0.00635	3.79	0.05004	2.28	0.07630	2.83	0.01106	1.68	0.59	128.0	9.7	196.7	106.0	74.7	4.1	70.9	2.4						
MAL4-21_45	6	276	76	0.37	612	0.00916	2.81	0.04934	1.96	0.15715	2.30	0.02310	1.19	0.52	184.4	10.3	164.1	92.1	148.2	6.3	147.2	3.5	147.2	3.5	0.13	0.72		
MAL2-10_1	1	50	14	0.37	38	0.00434	5.80	0.04784	4.17	0.08468	4.99	0.01284	2.74	0.55	87.5	10.1	91.4	197.7	82.5	7.9	82.2	4.5	82.2	4.5	0.01	0.93		Paragneiss
MAL2-10_2	23	1162	496	0.67	1610	0.00665	3.40	0.04904	1.76	0.14970	2.76	0.02214	2.13	0.77	133.9	9.1	149.8	82.7	141.6	7.3	141.2	5.9	141.2	5.9	0.04	0.84		
MAL2-10_3	10	476	105	0.28	612	0.00734	3.46	0.04992	1.81	0.14129	2.85	0.02053	2.20	0.77	147.8	10.2	191.2	84.1	134.2	7.2	131.0	5.7	131.1	5.7	1.97	0.16		
MAL2-10_4	5	136	54	0.58	341	0.01060	3.57	0.05036	2.68	0.23987	3.47	0.03455	2.20	0.63	213.2	15.2	211.5	124.4	218.3	13.7	219.0	9.5	218.9	9.5	0.01	0.90		
MAL2-10_6	1	49	17	0.58	29	0.00424	4.37	0.05418	5.70	0.09787	6.30	0.01310	2.68	0.43	85.5	7.5	378.7	256.3	94.8	11.4	83.9	4.5						
MAL2-10_7	3	159	54	0.42	163	0.00552	3.71	0.04848	3.75	0.11209	4.39	0.01675	2.28	0.52	111.4	8.2	125.5	176.5	107.9	9.0	107.1	4.8	107.1	4.8	0.04	0.84		
MAL2-10_8	3	267	42	0.19	200	0.00507	3.97	0.04928	2.41	0.08007	3.29	0.01178	2.24	0.68	102.2	8.1	161.2	112.5	78.2	5.0	75.5	3.4						
MAL2-10_9	5	226	56	0.32	470	0.00804	3.46	0.05170	2.68	0.16124	3.60	0.02262	2.40	0.67	161.8	11.2	272.1	123.0	151.8	10.2	144.2	6.8						
MAL2-10_10	1	92	35	0.51	66	0.00410	4.18	0.04781	3.10	0.08364	3.76	0.01269	2.13	0.57	82.8	6.9	90.1	147.1	81.6	5.9	81.3	3.4	81.3	3.4	0.01	0.90		
MAL2-10_11	49	1041	183	0.24	5775	0.01797	3.35	0.05371	1.06	0.39205	2.43	0.05294	2.18	0.90	359.9	23.9	358.9	47.7	335.9	13.9	332.5	14.2	334.5	13.7	1.11	0.29		
MAL2-10_12	7	454	257	0.79	332	0.00473	3.38	0.04748	1.75	0.09658	2.77	0.01475	2.15	0.78	95.3	6.4	73.5	83.3	93.6	5.0	94.4	4.0	94.3	4.0	0.25	0.61		
MAL2-10_13	1	45	15	0.42	40	0.00446	5.10	0.04528	6.45	0.08060	7.06	0.01291	2.88	0.41	89.9	9.2	-40.7	313.3	78.7	10.7	82.7	4.7	82.6	4.7	0.67	0.41		
MAL2-10_14	1	68	19	0.50	51	0.00448	5.20	0.04971	5.53	0.09263	6.03	0.01352	2.41	0.40	90.4	9.4	181.3	257.7	90.0	10.4	86.5	4.1	86.5	4.1	0.51	0.47		
MAL2-10_15	1	68	17	0.34	129	0.00430	4.86	0.04872	4.71	0.08655	5.19	0.01288	2.19	0.42	86.7	8.4	134.4	221.4	84.3	8.4	82.5	3.6	82.5	3.6	0.21	0.64		
MAL2-10_16	1	76	14	0.38	95	0.00438	6.44	0.04887	7.67	0.08849	8.04	0.01313	2.41	0.30	88.4	11.4	141.6	360.0	86.1	13.3	84.1	4.0	84.1	4.0	0.10	0.75		
MAL2-10_17	1	98	24	0.33	117	0.00476	4.85	0.04886	4.16	0.09223	4.74	0.01369	2.29	0.48	96.0	9.3	141.3	195.1	89.6	8.1	87.6	4.0	87.7	4.0	0.29	0.59		
MAL2-10_18	7	362	131	0.54	581	0.00552	3.67	0.04909	2.39	0.12679	3.23	0.01873	2.17	0.67	111.3	8.1	152.2	112.2	121.2	7.4	119.6	5.1	119.7	5.1	0.33	0.57		
MAL2-10_19	2	142	39	0.28	80	0.00551	3.78	0.05308	4.48	0.09532	5.08	0.01302	2.39	0.47	111.0	8.4	332.4	203.2	92.4	9.0	83.4	4.0						
MAL2-10_20	4	188	50	0.23	409	0.00742	4.19	0.04732	1.58	0.08589	4.58	0.01316	4.30	0.94	149.4	12.5	65.5	75.1	83.7	7.4	84.3	7.2	84.1	7.2	0.25	0.62		
MAL2-10_21	1	48	17	0.47	37	0.00466	5.04	0.04783	6.34	0.08713	6.99	0.01321	2.95	0.42	94.0	9.5	90.6	300.5	84.8	11.4	84.6	5.0	84.6	5.0	0.00	0.97		
MAL2-10_22	10	340	102	0.44	516	0.00892	3.75	0.04941	1.57	0.20550	2.73	0.03017	2.23	0.82	179.4	13.4	167.3	73.2	189.8	9.5	191.6	8.4	191.2	8.4	0.44	0.51		
MAL2-10_23	5	211	93	0.59	389	0.00763	3.57	0.04839	2.18	0.15996	3.10	0.02397	2.20	0.71	153.5	10.9	118.6	102.8	150.7	8.7	152.7	6.6	152.5	6.6	0.45	0.50		
MAL2-10_24	4	217	45	0.31	551	0.00669	4.95	0.04972	3.14	0.14984	3.82	0.02186	2.17	0.57	134.8	13.3	182.0	146.4	141.8	10.1	139.4	6.0	139.4	6.0	0.33	0.57		
MAL2-10_25	45	1039	380	0.60	1752	0.01713	3.40	0.05507	1.16	0.36571	2.41	0.04817	2.11	0.88	343.3	23.2	414.9	51.9	316.5	13.1	303.3	12.5						
MAL6-23_1	7	901	160	0.24	383	0.00254	3.82	0.04738	2.22	0.05350	3.26	0.00819	2.39	0.73	51.3	3.9	68.4	105.5	52.9	3.4	52.6	2.5	52.6	2.5	0.09	0.76		Orthogneiss
MAL6-23_2	14	1973	216	0.15	704	0.00274	3.56	0.04659	1.55	0.05329	2.72	0.00830	2.23	0.82	55.4	3.9	28.4	74.2	52.7	2.8	53.3	2.4	53.2	2.4	0.45	0.50	Inner part	
MAL6-23_2b	3	370	59	0.21	268	0.00275	4.02	0.04673	2.96	0.05169	3.62	0.00802	2.09	0.58	55.6	4.5	35.3	141.7	51.2	3.6	51.5	2.1	51.5	2.1	0.05	0.82	Outer part	
MAL6-23_3	3	433	70	0.23	219	0.00262	4.07	0.04820	2.62	0.05275	3.45	0.00794	2.25	0.65	52.9	4.3	109.3	123.6	52.2	3.5	51.0	2.3	51.0	2.3	0.86	0.35		
MAL6-23_4	3	397	67	0.23	180	0.00271	4.50	0.04751	2.82	0.05356	3.64	0.00818	2.30	0.63	54.8	4.9	74.7	134.0	53.0	3.8	52.5	2.4	52.5	2.4	0.11	0.74		
MAL6-23_5	2	306	49	0.22	568	0.00263	4.68	0.04714	3.77	0.05303	4.41	0.00816	2.30	0.52	53.2	5.0	56.3	179.3	52.5	4.5	52.4	2.4	52.4	2.4	0.00	0.97		
MAL6-23_6	2	332	53	0.23	122	0.00267	5.01	0.04737	2.55	0.05356	3.41	0.00820	2.26	0.66	54.0	5.4	67.7	121.4	53.0	3.5	52.7	2.4	52.7	2.4	0.06	0.81		
MAL6-23_7	2	242	36	0.20	133	0.00286	4.99	0.04695	2.98	0.05346	3.81	0.00826	2.38	0.62	57.8	5.8	46.7	142.4	52.9	3.9	53.0	2.5	53.0	2.5	0.01	0.93		
MAL6-23_8	8	1028	137	0.19	1044	0.00265	5.00	0.04695	1.69	0.05344	2.70	0.00826	2.11	0.78	53.4	5.3	46.5	80.7	52.9	2.8	53.0	2.2	53.0	2.2	0.03	0.87	Middle part	
MAL6-23_8b	5	629	103	0.24	403	0.00250	4.74	0.04720	2.64	0.05399	3.52	0.00830	2.33	0.66	50.5	4.8	59.1	125.9	53.4	3.7	53.3	2.5	53.3	2.5	0.01	0.93	Inner part	
MAL6-23_8c	2	243	31	0.20	103	0.00253	5.17	0.04842	2.89	0.05484	3.73	0.00822	2.35	0.63	51.0	5.3	119.6	136.3	54.2	3.9	52.7	2.5	52.7	2.5	0.92	0.34	Outer part	
MAL6-23_9	2	283	40	0.19	307	0.00256	5.41	0.04624	3.62	0.05204	4.28	0.00816	2.29	0.53	51.6	5.6	10.0	173.9	51.5	4.3	52.4	2.4	52.4	2.4	0.24	0.62		
MAL6-23_10	4	555	97	0.21	339	0.00277	4.40	0.04617	2.55	0.05243	3.58	0.00824	2.51	0.70	55.8	4.9	6.4	122.7	51.9	3.6	52.9	2.6	52.8	2.6	0.59	0.44	Inner part	
MAL6-23_10b	3	391	68	0.24	399	0.00268	5.27	0.04765	2.48	0.05369	3.27	0.00817	2.14	0.65	54.0	5.7	81.9	117.5	53.1	3.4	52.5	2.2	52.5	2.2	0.25	0.62	Outer part	
MAL6-23_11	3	350	38	0.55	112	0.00269	7.52	0.04726	4.00	0.05256	4.65	0.00807	2.37	0.51	54.2	8.1	62.6	190.4	52.0	4.7	51.8	2.4	51.8	2.4	0.01	0.91		
MAL6-23_12	5	620	135	0.29	368	0.00270	4.77	0.04720	2.39	0.05384	3.27	0.00827	2.23	0.68	54.5	5.2	59.4	114.1	53.2	3.4	53.1	2.4	53.1	2.4	0.01	0.91		
MAL6-23_13	3	404	61	0.22	224	0.00288	4.53	0.04724	1.86	0.05456	2.77	0.00838	2.06	0.74	58.1	5.3	61.3	88.5	53.9	2.9	53.8	2.2	53.8	2.2	0.03	0.87		
MAL6-23_14	9	1198	185	0.22	677	0.00247	4.40	0.04767	1.63	0.05380	2.71	0.00818	2.17	0.80	49.8	4.4	83.0	77.3	53.2	2.8	52.5	2.3	52.6	2.3	0.61	0.44		
MAL6-23_15	3	373	65	0.23	199	0.00284	4.92	0.04730	3.03	0.05343	3.80	0.00819	2.29	0.60	57.3	5.6	64.3	144.3	52.9	3.9	52.6	2.4	52.6	2.4	0.03	0.87		
MAL6-23_16	35	4941	783	0.23	3626	0.00239	4.44	0.04735	0.98	0.05368	2.33	0.00822	2.11	0.91	48.3	4.3	66.8	46.6	53.1	2.4	52.8	2.2	52.8	2.2	0.36	0.55		
MAL6-23_17	8	1203	57	0.07	1159	0.00258	4.71	0.04734	2.44	0.05270	3.38	0.00807	2.34	0.69	52.1	4.9	66.4	116.3	52.1	3.4	51.8	2.4	51.8	2.4	0.06	0.80		
MAL6-23_18	2	262	39	0.22	-3074	0.00261	5.46	0.04724	3.48	0.05290	4.14	0.00812	2.23	0.54	52.7	5.8	61.6	166.1	52.3	4.2	52.1	2.3	52.1	2.3	0.01	0.91		
MAL6-23_19	3	362	65	0.25	121	0.00251	4.87	0.04716	2.38	0.05217	3.21	0.00802	2.16	0.67	50.7	4.9	57.2	113.3	51.6	3.2	51.5	2.2	51.5	2.2	0.01	0.92		

MAL6-23_20	3	387	65	0.24	169	0.00255	5.14	0.04700	3.85	0.05229	4.39	0.00807	2.12	0.48	51.4	5.3	49.4	183.8	51.8	4.4	51.8	2.2	51.8	2.2	0.00	0.98		
MAL6-23_21	2	280	42	0.20	128	0.00259	4.77	0.04707	2.22	0.05262	3.19	0.00811	2.28	0.72	52.4	5.0	52.7	106.1	52.1	3.2	52.1	2.4	52.1	2.4	0.00	0.99		
MAL6-23_22	3	405	63	0.21	363	0.00285	4.98	0.04727	3.61	0.05309	4.26	0.00815	2.25	0.53	57.6	5.7	62.7	172.2	52.5	4.4	52.3	2.3	52.3	2.3	0.01	0.90		
MAL6-23_23	2	292	44	0.22	197	0.00265	4.99	0.04694	2.76	0.05289	3.69	0.00817	2.45	0.66	53.6	5.3	46.3	132.1	52.3	3.8	52.5	2.6	52.5	2.6	0.01	0.93		
MAL6-23_24	2	202	25	0.16	292	0.00276	6.11	0.04804	4.88	0.05263	5.43	0.00795	2.39	0.44	55.7	6.8	101.4	230.8	52.1	5.5	51.0	2.4	51.0	2.4	0.18	0.67		
MAL6-23_25	4	472	94	0.27	351	0.00265	4.76	0.04754	2.71	0.05337	3.55	0.00814	2.29	0.64	53.5	5.1	76.4	129.1	52.8	3.7	52.3	2.4	52.3	2.4	0.14	0.71		
MAL3-19_1	37	638	708	1.18	763	0.01842	4.71	0.05173	1.16	0.31443	2.75	0.04409	2.50	0.91	369.0	34.4	273.3	53.2	277.6	13.4	278.1	13.6	277.8	13.2	0.03	0.86		Granitoid
MAL3-19_2	13	277	128	0.54	758	0.02127	4.26	0.05290	2.13	0.31743	3.73	0.04352	3.07	0.82	425.5	35.9	324.5	96.7	279.9	18.4	274.6	16.5	275.7	16.4	1.01	0.31		
MAL3-19_3	28	575	422	0.99	2184	0.01877	4.29	0.05324	1.65	0.31547	2.93	0.04298	2.42	0.83	375.9	32.0	339.0	75.0	278.4	14.3	271.2	12.9						
MAL3-19_4	33	628	309	0.60	1517	0.01992	4.22	0.05195	1.24	0.31929	2.61	0.04458	2.30	0.88	398.6	33.4	283.1	56.7	281.4	12.9	281.2	12.7	281.2	12.4	0.00	0.95		
MAL2-4_1	4	465	70	0.42	102	0.00379	5.94	0.04727	2.17	0.05621	3.27	0.00862	2.44	0.75	76.5	9.1	62.9	103.6	55.5	3.5	55.4	2.7	55.4	2.7	0.02	0.88		Granitoid (Quartzdiorite?)
MAL2-4_2	6	783	135	0.31	288	0.00381	4.44	0.04571	2.23	0.05076	3.50	0.00805	2.71	0.77	76.8	6.8	-17.5	107.8	50.3	3.4	51.7	2.8	51.6	2.8	1.72	0.19	Inner part	
MAL2-4_2b	2	218	16	0.13	125	0.00377	6.63	0.04659	3.82	0.05187	4.62	0.00807	2.61	0.56	76.0	10.1	28.3	183.4	51.3	4.6	51.8	2.7	51.8	2.7	0.07	0.80	Outer part	
MAL2-4_3	3	399	64	0.31	205	0.00376	4.49	0.04812	2.57	0.05325	4.38	0.00803	3.54	0.81	75.8	6.8	105.2	121.9	52.7	4.5	51.5	3.6	51.5	3.6	0.75	0.39		
MAL2-4_4	5	656	123	0.33	263	0.00365	1.69	0.04808	2.61	0.05329	3.31	0.00804	2.03	0.61	73.6	2.5	102.2	123.6	52.7	3.4	51.6	2.1	51.6	2.1	0.65	0.42		
MAL2-4_5	3	347	44	0.26	182	0.00323	3.27	0.04835	2.93	0.05439	3.51	0.00816	1.94	0.55	65.2	4.3	116.4	138.3	53.8	3.7	52.4	2.0	52.4	2.0	0.82	0.36		
MAL2-4_6	2	315	46	0.28	145	0.00312	2.06	0.04707	3.77	0.04900	4.40	0.00755	2.27	0.52	63.0	2.6	53.4	179.9	48.6	4.2	48.5	2.2	48.5	2.2	0.00	0.96	Inner part	
MAL2-4_6b	1	159	11	0.16	265	0.00460	3.56	0.04876	5.06	0.05015	6.08	0.00753	3.37	0.55	92.8	6.6	114.1	239.0	49.7	5.9	48.4	3.2	48.4	3.2	0.29	0.59	Outer part	
MAL2-4_7	4	496	84	0.31	296	0.00357	2.74	0.04742	2.29	0.04850	4.71	0.00749	4.11	0.87	72.0	3.9	47.8	109.3	48.1	4.4	48.1	3.9	48.1	3.9	0.00	1.00		
MAL2-4_8	2	238	26	0.23	230	0.00379	4.22	0.04710	4.94	0.04309	5.94	0.00670	3.29	0.55	76.5	6.4	31.8	236.7	42.8	5.0	43.0	2.8	43.0	2.8	0.01	0.92		
MAL2-4_9	3	402	57	0.27	642	0.00452	3.06	0.04818	3.41	0.04742	6.14	0.00721	5.11	0.83	91.1	5.6	85.7	162.0	47.0	5.7	46.3	4.7	46.3	4.7	0.23	0.63		
MAL2-4_10	3	400	62	0.32	167	0.00470	2.85	0.04668	3.87	0.05692	4.81	0.00893	2.86	0.59	94.7	5.4	10.6	186.2	56.2	5.3	57.3	3.3	57.3	3.3	0.26	0.61		
MAL2-4_11	2	274	29	0.20	232	0.00395	3.05	0.04852	4.59	0.04750	5.98	0.00717	3.84	0.64	79.7	4.8	102.6	217.0	47.1	5.5	46.0	3.5	46.0	3.5	0.26	0.61		
MAL2-4_12	2	308	51	0.32	120	0.00435	3.34	0.04757	5.46	0.04036	7.23	0.00621	4.75	0.66	87.8	5.9	56.0	260.3	40.2	5.7	39.9	3.8	39.9	3.8	0.02	0.90		
MAL2-4_13	3	411	43	0.20	360	0.00408	3.49	0.04861	3.01	0.05410	4.67	0.00815	3.57	0.76	82.3	5.7	107.2	142.4	53.5	4.9	52.3	3.7	52.3	3.7	0.57	0.45		
MAL2-4_14	3	385	38	0.20	327	0.00500	2.70	0.04650	2.89	0.04743	4.92	0.00747	3.97	0.81	100.9	5.4	1.6	139.4	47.1	4.5	48.0	3.8	47.9	3.8	0.45	0.50		
MAL2-4_15	4	480	68	0.29	211	0.00458	2.98	0.04881	4.31	0.05246	5.45	0.00787	3.33	0.61	92.3	5.5	117.2	203.2	51.9	5.5	50.5	3.4	50.5	3.4	0.41	0.52		
MAL2-4_16	2	307	37	0.23	276	0.00382	4.40	0.04756	3.93	0.04347	5.55	0.00669	3.92	0.71	77.0	6.8	55.6	187.7	43.2	4.7	43.0	3.4	43.0	3.4	0.02	0.89		
MAL2-4_17	4	529	73	0.28	647	0.00407	3.37	0.04785	3.59	0.05004	5.04	0.00766	3.54	0.70	82.2	5.5	70.1	171.0	49.6	4.9	49.2	3.5	49.2	3.5	0.06	0.81	Outer part	
MAL2-4_17b	5	626	102	0.32	256	0.00456	3.24	0.04747	1.76	0.05623	3.37	0.00867	2.87	0.85	92.0	6.0	51.3	84.2	55.5	3.6	55.6	3.2	55.6	3.2	0.01	0.92	Inner part	
MAL2-4_18	3	438	63	0.26	401	0.00445	3.17	0.04895	3.87	0.05074	5.42	0.00758	3.80	0.70	89.7	5.7	124.6	182.4	50.3	5.3	48.7	3.7	48.7	3.7	0.66	0.42		
MAL2-4_19	3	427	40	0.21	277	0.00489	3.55	0.04708	4.82	0.04786	6.48	0.00744	4.34	0.67	98.6	7.0	32.2	230.8	47.5	6.0	47.8	4.1	47.8	4.1	0.02	0.89		
MAL2-4_20	3	387	36	0.18	220	0.00383	3.86	0.05339	3.10	0.04929	4.16	0.00675	2.78	0.67	77.2	5.9	325.6	140.6	48.8	4.0	43.4	2.4						
MAL2-4_21	4	517	86	0.33	344	0.00428	2.90	0.04773	3.57	0.04941	4.73	0.00757	3.10	0.65	86.4	5.0	65.1	170.2	49.0	4.5	48.6	3.0	48.6	3.0	0.04	0.85		
MAL2-4_22	3	422	65	0.30	290	0.00418	3.76	0.04736	2.43	0.05580	3.97	0.00862	3.14	0.79	84.3	6.3	46.4	116.0	55.1	4.3	55.3	3.5	55.3	3.5	0.02	0.88		
MAL2-4_23	2	287	28	0.19	257	0.00466	3.05	0.04794	4.42	0.02798	7.10	0.00427	5.55	0.78	93.9	5.7	75.8	209.9	28.0	3.9	27.5	3.0	27.5	3.0	0.21	0.65		
MAL7-14_1	4	476	125	0.47	278	0.00413	2.59	0.04688	3.00	0.05239	4.17	0.00818	2.90	0.70	83.3	4.3	22.2	143.8	51.8	4.2	52.5	3.0	52.5	3.0	0.18	0.67		Granitoid
MAL7-14_2	3	365	72	0.37	652	0.00404	3.11	0.04675	3.43	0.03974	4.46	0.00622	2.84	0.64	81.5	5.1	15.6	165.1	39.6	3.5	40.0	2.3	40.0	2.3	0.09	0.77		
MAL7-14_3	3	420	93	0.47	424	0.00549	2.64	0.04995	3.19	0.05954	4.35	0.00872	2.95	0.68	110.6	5.8	172.6	148.9	58.7	5.0	56.0	3.3						
MAL7-14_4	3	441	111	0.48	249	0.00406	2.48	0.04721	4.37	0.05262	5.31	0.00815	3.01	0.57	81.9	4.0	39.5	209.1	52.1	5.4	52.3	3.1	52.3	3.1	0.02	0.90		
MAL7-14_5	4	521	140	0.51	263	0.00391	2.68	0.04887	2.57	0.04741	4.47	0.00710	3.66	0.82	78.9	4.2	121.7	120.9	47.0	4.1	45.6	3.3	45.5	3.3	1.51	0.22		
MAL7-14_7	3	385	70	0.38	467	0.00396	2.86	0.04762	3.65	0.05491	5.26	0.00843	3.78	0.72	79.9	4.6	60.2	174.0	54.3	5.6	54.1	4.1	54.1	4.1	0.00	0.94		
MAL7-14_8	3	434	89	0.40	173	0.00378	2.55	0.05004	3.14	0.05445	4.35	0.00796	3.01	0.69	76.2	3.9	177.0	146.6	53.8	4.6	51.1	3.1						
MAL7-14_9	3	419	95	0.44	360	0.00395	2.70	0.05054	3.78	0.05621	4.82	0.00813	3.00	0.62	79.7	4.3	200.7	175.4	55.5	5.2	52.2	3.1						
MAL7-14_10	3	383	83	0.45	219	0.00400	2.23	0.04982	2.76	0.04861	4.43	0.00714	3.47	0.78	80.6	3.6	167.0	128.8	48.2	4.2	45.8	3.2						
MAL7-14_11	4	534	134	0.50	209	0.00413	2.49	0.04862	3.89	0.05556	4.74	0.00836	2.70	0.57	83.3	4.1	110.6	183.9	54.9	5.1	53.6	2.9	53.6	2.9	0.37	0.54		
MAL7-14_12	3	386	92	0.45	160	0.00430	2.86	0.04827	3.59	0.05567	5.13	0.00843	3.66	0.71	86.8	4.9	93.5	169.9	55.0	5.5	54.1	3.9	54.1	3.9	0.21	0.65		
MAL7-14_13	3	460	95	0.38	251	0.00336	3.10	0.04636	3.94	0.04645	5.00	0.00733	3.07	0.62	67.7	4.2	-3.0	190.0	46.1	4.5	47.1	2.9	47.0	2.9	0.29	0.59		
MAL7-14_14	7	347	79	2.79	45	0.00417	3.39	0.04849	4.39	0.05290	6.07	0.00798	4.18	0.69	84.0	5.7	104.1	207.7	52.3	6.2	51.2	4.3	51.2	4.3	0.25	0.62		
MAL7-14_15	3	376	73	0.36	239	0.00402	2.85	0.04815	4.00	0.05473	5.44	0.00831	3.69	0.68	81.2	4.6	87.8	189.8	54.1	5.7	53.3	3.9	53.3	3.9	0.13	0.72		
MAL7-14_16	3	370	87	0.46	104	0.00371	3.58	0.05215	3.16	0.05592	4.70	0.00784	3.47	0.74	74.8	5.3	273.9	144.8	55.3	5.1	50.3	3.5						
MAL7-14_17	2	358	75	0.41	181	0.00405	2.89	0.04980	3.87	0.05249	4.96	0.00770	3.11	0.63	81.6	4.7	167.3	180.9	51.9	5.0	49.5	3.1	49.4	3.1	1.58	0.21		
MAL7-14_18	2	301	65	0.39	-1083	0.00331	3.84	0.05139	3.68	0.04031	6.33	0.00573	5.15	0.81	66.7	5.1	240.3	169.6	40.1	5.0	36.9	3.8						
MAL7-14_19	3	494	136	0.53	446	0.00339	2.49	0.05232	3.06	0.05380	4.10	0.00752	2.72	0.66	68.4	3.4	281.6	140.1	53.2	4.3	48.3	2.6						
MAL7-14_20	3	430	100	0.44	215	0.00363	2.58	0.05006	2.66	0.05411	3.88	0.00790	2.82	0.73	73.3	3.8	179.3	124.0	53.5	4.0	50.7	2.9						
MAL7-14_21	3	389	92	0.45	285	0.00350	3.15	0.05662	2.81	0.05824	4.15	0.00752	3.05	0.74	70.6	4.4	459.6	124.5	57.5	4.6	48.3	2.9						
MAL7-14_22	3	421	92	0.45	647	0.00408	2.74	0.05368	2.60	0.06373	3.78	0.00868	2.74	0.73	82.4	4.5	340.1	117.6	62.7	4.6	55.7	3.0						
MAL7-14_23	3	399	102	0.49	177	0.00393	2.73	0.04738	4.24	0.04756	5.28	0.00734	3.15	0.60	79.3	4.3	49.8	202.6	47.2	4.9	47.1	3.0	47.1	3.0	0.00	0.98		
MAL7-14_24	3	386	106	0.49	170	0.00346	2.55	0.04923	2.75	0.05760	4.13	0.00855	3.08	0.75	69.9	3.6	140.7	128.9	56.9	4.6	54.9	3.4	54.9	3.4	1.68	0.19		
MAL7-14_25	4	581	158	0.47	2375	0.00341	3.06	0.04812	3.15	0.06124	3.92	0.00930	2.33	0.60	68.8	4.2	86.9	149.2	60.4	4.6	59.7	2.8	59.7	2.8	0.13	0.72		
MAL7-20_1	0.2	30	6	0.31	17	0.00243	8.25	0.04885	11.29	0.05156	11.80	0.00771	3.42	0.29	49.0	8.1	122.7	531.8	51.0	11.8	49.5	3.4	49.5	3.4	0.07	0.79		Granitoid
MAL7-20_2	0.3	44	12	0.40	0	0.00269	7.11	0.05193	10.60	0.05198	11.18	0.00727	3.57	0.32	54.2	7.7	269.9	486.1	51.5	11.3	46.9	3.3	46.8	3.3	0.74	0.39		
MAL7-20_3	0.4	53	15	0.38	26	0.00256	5.63	0.04810	9.03	0.05089	9.39	0.00771	2.56	0.27	51.7	5.8	91.5	428.0	50.4	9.3	49.5	2.5	49.5	2.5	0.04	0.85		
MAL7-20_4	1	155	58	0.53	127	0.00256	3.91	0.04824	5.12	0.05125	5.33	0.00775	1.50	0.28	51.7	4.0	98.2	242.1	50.8	5.3	49.8	1.5	49.8	1.5	0.16	0.69		
MAL7-20_5	1	147	51	0.49	-104729	0.00253	5.34	0.04977	5.02	0.05106	5.27	0.00748	1.58	0.30	51.1	5.5	171.3	234.6	50.6	5.2	48.1	1.5	48.0	1.5	1.02	0.31		
MAL7-20_6	0.2	33	6	0.33	-91	0.00243	11.63	0.04699	7.90	0.04776	8.67	0.00741	3.56	0.41	49.0	11.4	35.3	378.3	47.4	8.0	47.6	3.4	47.6	3.4	0.00	0.95		
MAL7-20_7	1	109	36	0.46	85	0.00243	5.10	0.04802	6.75	0.04973	6.98	0.00755	1.79	0.26	49.1	5.0	86.8	320.1	49.3	6.7	48.5	1.7	48.5	1.7	0.06	0.81		
MAL7-20_8	1	115	21	0.27	647	0.00237	6.07	0.04772	5.94	0.04977	6.30	0.00761	2.10	0.33	47.9	5.8	71.8	282.6	49.3	6.1	48.9	2.0	48.9	2.0	0.03	0.87		
MAL7-20_9	1	201	87	0.69	67	0.00236	4.40	0.04796	6.06	0.05247	6.23	0.00798	1.44	0.23	47.6	4.2	83.5	287.7	51.9	6.3	51.2	1.5	51.2	1.5	0.05	0.82		
MAL7-20_10	1	82	27	0.94	28	0.00310	8.05	0.16019	7.43	0.17026	8.01	0.00775	3.00	0.37	62.6	10.1	2447.6	251.5	159.6	23.8	49.8	3.0						
MAL7-20_11	1	115	35	0.67	82	0.00258	6.96	0.04724	6.09	0.04470	6.75	0.00690	2.91	0.43	52.1	7.2	47.0	291.0	44.4	5.9	44.4	2.6	44.4	2.6	0.00	0.99		
MAL7-20_12	1	144	43	0.39	61	0.00263	4.98	0.04732	6.85	0.04715	7.16	0.00727	2.10	0.29	53.0	5.3	51.1	326.9	46.8	6.6	46.7	2.0	46.7	2.0	0.00	0.98		
MAL7-20_13	5	675	245	0.53	186	0.00261	4.04	0.04771	3.29	0.05086	3.58	0.00778	1.42	0.40	52.6	4.2	70.2	156.5	50.4	3.5	50.0	1.4	50.0	1.4	0.07	0.80		
MAL7-20_14	1	73	22	0.42	51	0.00268	5.66	0.04695	8.98	0.04833	9.14	0.00751	1.72	0.19	54.1	6.1	31.9	430.2	47.9	8.6	48.2	1.7	48.2	1.7	0.01	0.94		
MAL7-20_15	1	132	73	0.77	113	0.00238	4.98	0.04800	7.03	0.04907	7.22	0.00746	1.66	0.23	48.1	4.8	84.2	333.6	48.6	6.9	47.9	1.6	47.9	1.6	0.05	0.83		
MAL7-20_16	1	37	8	0.07	216	0.00212	11.20	0.04245	5.51	0.04828	6.18	0.00830	2.81	0.45	42.9	9.6	-215.9	276.8	47.9	5.8	53.3	3.0						
MAL7-20_17	0.2	23	4	0.24	50	0.00405	8.77	0.04832	6.68	0.04882	8.10	0.00738	4.58	0.57	81.8	14.3	99.7	315.9	48.4	7.7	47.4	4.3	47.4	4.3	0.11	0.74		
MAL7-20_18	0.3	47	11	0.42	19	0.00260	7.23	0.05044	9.16	0.05159	9.40	0.00747	2.10	0.22	52.6	7.6	199.4	425.4	51.1	9.4	48.0	2.0	48.0	2.0	0.46	0.50		
MAL7-20_19	0.3	41	13	0.39	28	0.00254	10.97	0.04724	10.86	0.04822	11.29	0.00745	3.09	0.27	51.3	11.2	44.9	519.0	47.8	10.6	47.9	2.9	47.9	2.9	0.00	0.99		
MAL7-20_20	0.4	55	14	0.38	706	0.00256	8.51	0.04795	9.20	0.04621	9.62	0.00704	2.79	0.29	51.6	8.8	80.1	437.0	45.9	8.6	45.2	2.5	45.2	2.5	0.02	0.87		
MAL7-20_21	0.2	32	7	0.32	21	0.00248	9.38	0.04733	9.99	0.04612	10.28	0.00712	2.40	0.23	50.1	9.4	48.9	477.4	45.8	9.2	45.7	2.2	45.7	2.2	0.00	0.99		
MAL7-20_22	1	201	78	0.53	137	0.00252	3.96	0.04622	5.22	0.04795	5.57	0.00758	1.96	0.35	50.8	4.0	-8.1	251.9	47.6	5.2	48.7	1.9	48.7	1.9	0.21	0.65		
MAL7-20_23	1	88	29	0.45	68	0.00256	4.88	0.04709	7.27	0.05081	7.79	0.00788	2.80	0.36	51.6	5.0	36.8	348.3	50.3	7.7	50.6	2.8	50.6	2.8	0.01	0.94		
MAL7-20_24	2	284	119	0.51	292	0.00268	3.86	0.04675	4.97	0.04644	5.26	0.00726	1.75	0.33	54.1	4.2	19.2	238.5	46.1	4.8	46.6	1.6	46.6	1.6	0.05	0.82		
MAL7-20_25	1	88	22	0.30	75	0.00260	4.58	0.04619	8.07	0.03964	8.57	0.00627	2.87	0.34	52.5	4.8	-10.2	389.7	39.5	6.6	40.3	2.3	40.3	2.3	0.07	0.79		
MAL1-19_1	2	243	16	0.11	365	0.00491	5.41	0.06711	3.47	0.05819	3.79	0.00633	1.53	0.40	99.0	10.7	825.9	144.8	57.4	4.2	40.7	1.2						Aplite
MAL1-19_2	1	184	11	0.14	97	0.00237	9.26	0.05234	4.91	0.04652	5.48	0.00649	2.44	0.44	47.7	8.8	283.2	224.8	46.2	5.0	41.7	2.0						
MAL1-19_3	0.5	64	4	0.09	19	0.01222	5.44	0.08754	6.95	0.08444	7.34	0.00705	2.36	0.32	245.5	26.5	1357.9	267.9	82.3	11.6	45.3	2.1						
MAL1-19_4	1	87	15	0.18	32	0.00354	4.62	0.04740	8.35	0.04530	8.57	0.00699	1.94	0.23	71.5	6.6	51.2	398.5	45.0	7.6	44.9	1.7	44.9	1.7	0.00	0.97		
MAL1-19_5	1	205	21	0.17	64	0.00250	6.12	0.04826	4.99	0.04918	5.18	0.00745	1.38	0.27	50.4	6.2	94.0	236.4	48.7	4.9	47.8	1.3	47.8	1.3	0.15	0.70		
MAL1-19_6	10	1842	127	0.10	1243	0.00275	3.50	0.04733	1.28	0.04832	1.80	0.00746	1.26	0.70	55.4	3.9	47.3	61.1	47.9	1.7	47.9	1.2	47.9	1.2	0.00	0.98		
MAL1-19_7	3	471	59	0.18	119	0.00242	5.74	0.04774	2.82	0.04540	3.12	0.00695	1.34	0.43	48.9	5.6	68.1	134.1	45.1	2.8	44.7	1.2	44.7	1.2	0.12	0.73		
MAL1-19_8	0.1	23	1	0.11	-62	0.00350	19.37	0.06741	11.66	0.06378	13.94	0.00692	7.64	0.55	70.6	27.3	834.0	486.0	62.8	17.0	44.4	6.8						
MAL1-19_9	1	52	3	0.39	17	0.01139	47.16	0.28351	7.46	0.27162	8.43	0.00701	3.93	0.47	229.0	215.3	3369.4	232.7	244.0	36.9	45.0	3.5						
MAL1-19_10	2	337	30	0.14	152	0.00225	7.56	0.04869	4.54	0.04873	4.81	0.00732	1.61	0.33	45.4	6.9	113.4	214.2	48.3	4.5	47.0	1.5	47.0	1.5	0.37	0.54		
MAL1-19_11	0.2	38	3	0.14	25	0.00298	13.70	0.04786	10.12	0.04483	10.53	0.00685	2.91	0.28	60.2	16.5	72.6	481.1	44.5	9.2	44.0	2.6	44.0	2.6	0.01	0.91		

MAL7-2_1	8	954	431	0.59	445	0.00260	3.59	0.04714	1.72	0.05092	2.24	0.00790	1.44	0.64	52.5	3.8	35.7	82.4	50.4	2.2	50.7	1.5	50.7	1.5	0.13	0.71		Gabbro
MAL7-2_2	2	285	68	0.32	184	0.00308	4.24	0.04815	3.13	0.05004	3.47	0.00760	1.49	0.43	62.2	5.3	86.1	148.5	49.6	3.4	48.8	1.4	48.8	1.4	0.25	0.62		
MAL7-2_3	1	206	91	0.64	75	0.00291	3.61	0.07227	4.55	0.06842	4.79	0.00693	1.49	0.31	58.8	4.2	975.8	185.5	67.2	6.2	44.5	1.3						
MAL7-2_4	2	223	90	0.60	112	0.00241	4.32	0.04659	5.01	0.04879	5.25	0.00766	1.57	0.30	48.6	4.2	7.2	241.2	48.4	5.0	49.2	1.5	49.2	1.5	0.12	0.72		
MAL7-2_5	2	322	127	0.54	277	0.00254	3.73	0.04783	3.68	0.04994	3.95	0.00764	1.44	0.36	51.4	3.8	70.0	175.0	49.5	3.8	49.1	1.4	49.1	1.4	0.06	0.81		
MAL7-2_6	2	250	97	0.92	100	0.00230	5.35	0.08655	5.62	0.08416	5.84	0.00712	1.59	0.27	46.4	5.0	1333.3	217.6	82.0	9.2	45.7	1.4						
MAL7-2_9	3	435	173	0.59	149	0.00239	3.95	0.04781	2.26	0.05071	2.52	0.00776	1.12	0.45	48.2	3.8	68.5	107.4	50.2	2.5	49.8	1.1	49.8	1.1	0.12	0.73		
MAL7-2_10	3	408	169	0.60	187	0.00259	4.00	0.04739	3.69	0.04912	3.91	0.00759	1.30	0.33	52.2	4.2	47.3	176.2	48.7	3.7	48.7	1.3	48.7	1.3	0.00	0.99		
MAL7-2_11	2	217	86	0.53	81	0.00253	3.86	0.04789	4.70	0.05060	5.08	0.00774	1.93	0.38	51.1	3.9	71.7	223.4	50.1	5.0	49.7	1.9	49.7	1.9	0.04	0.84		
MAL7-2_12	1	183	82	0.58	100	0.00249	4.12	0.04728	4.91	0.05018	5.13	0.00777	1.49	0.29	50.2	4.1	41.1	234.8	49.7	5.0	49.9	1.5	49.9	1.5	0.01	0.94		
MAL7-2_13	3	330	120	0.79	71	0.00207	5.54	0.06390	3.53	0.06609	3.79	0.00757	1.37	0.36	41.8	4.6	717.8	149.9	65.0	4.8	48.6	1.3						
MAL7-2_14	6	797	361	0.62	229	0.00245	3.67	0.04766	2.47	0.04968	2.85	0.00764	1.41	0.50	49.4	3.6	59.1	117.9	49.2	2.7	49.0	1.4	49.0	1.4	0.03	0.87		
MAL7-2_15	5	665	341	0.70	1497	0.00254	3.60	0.04792	3.07	0.04969	3.36	0.00760	1.37	0.41	51.4	3.7	71.8	146.2	49.2	3.2	48.8	1.3	48.8	1.3	0.10	0.75		
MAL6-24_1	7	857	106	0.15	3134	0.00364	2.84	0.04610	1.81	0.05250	2.18	0.00831	1.23	0.56	73.4	4.2	-10.6	87.2	52.0	2.2	53.3	1.3						Paragneiss
MAL6-24_2	19	2413	107	0.06	1076	0.00339	2.62	0.04749	1.18	0.05721	1.58	0.00879	1.06	0.67	68.3	3.6	60.5	56.1	56.5	1.7	56.4	1.2	56.4	1.2	0.02	0.88		
MAL6-24_4	4	605	45	0.11	11228	0.00275	3.27	0.04620	2.36	0.05132	2.60	0.00810	1.08	0.42	55.4	3.6	-6.2	114.1	50.8	2.6	52.0	1.1	52.0	1.1	1.08	0.30		
MAL6-24_5	7	704	135	0.34	452	0.00395	2.84	0.04796	2.32	0.06712	2.79	0.01021	1.56	0.56	79.8	4.5	83.2	109.9	66.0	3.6	65.5	2.0	65.5	2.0	0.10	0.75		
MAL6-24_6	3	345	67	0.25	521	0.00401	3.89	0.05265	3.70	0.06113	3.89	0.00847	1.18	0.30	80.8	6.3	299.7	168.9	60.2	4.6	54.4	1.3					Inner part	
MAL6-24_6b	3	402	45	0.14	203	0.00311	3.84	0.04740	2.20	0.05265	2.69	0.00811	1.56	0.58	62.7	4.8	54.7	104.8	52.1	2.7	52.0	1.6	52.0	1.6	0.00	0.96	Outer part	
MAL6-24_7	12	434	110	0.27	808	0.01467	2.31	0.05187	1.56	0.16261	2.20	0.02288	1.54	0.70	294.4	13.5	265.1	71.6	153.0	6.2	145.8	4.5						
MAL6-24_8	4	387	157	0.44	415	0.00339	2.62	0.04737	3.13	0.05392	3.36	0.00831	1.22	0.36	68.4	3.6	52.7	149.4	53.3	3.5	53.3	1.3	53.3	1.3	0.00	0.99		
MAL6-24_10	3	277	62	0.22	319	0.00405	3.58	0.04931	3.68	0.05570	3.90	0.00825	1.29	0.33	81.7	5.8	146.8	172.5	55.0	4.2	53.0	1.4	52.9	1.4	1.12	0.29		
MAL6-24_11	4	328	101	0.35	320	0.00399	2.23	0.04964	3.01	0.06335	3.46	0.00932	1.71	0.49	80.5	3.6	160.7	140.8	62.4	4.2	59.8	2.0	59.8	2.0	1.93	0.16		
MAL6-24_12	4	477	102	0.29	10093	0.00307	3.11	0.04783	2.14	0.06115	2.48	0.00934	1.26	0.51	62.0	3.9	73.1	101.8	60.3	2.9	59.9	1.5	59.9	1.5	0.07	0.80		
MAL6-24_13	2	290	27	0.12	-439	0.00460	3.63	0.04729	2.02	0.05439	3.02	0.00840	2.24	0.74	92.8	6.7	45.8	96.7	53.8	3.2	54.0	2.4	53.9	2.4	0.03	0.87		
MAL6-24_14	6	775	106	0.18	693	0.00328	3.33	0.04758	2.74	0.05546	3.07	0.00852	1.39	0.45	66.2	4.4	59.9	130.4	54.8	3.3	54.7	1.5	54.7	1.5	0.01	0.94		
MAL6-24_15	4	489	49	0.22	638	0.00298	4.36	0.04728	2.75	0.05002	3.09	0.00773	1.40	0.45	60.1	5.2	44.8	131.5	49.6	3.0	49.7	1.4	49.7	1.4	0.01	0.94		
MAL6-24_16	4	535	53	0.13	294	0.00358	2.74	0.04734	2.83	0.05683	3.09	0.00878	1.24	0.40	72.3	4.0	47.3	135.3	56.1	3.4	56.3	1.4	56.3	1.4	0.02	0.89		
MAL6-24_17	3	401	45	0.16	405	0.00269	4.62	0.04787	2.82	0.05496	3.09	0.00839	1.26	0.41	54.3	5.0	73.5	134.0	54.3	3.3	53.9	1.4	53.9	1.4	0.09	0.77		
MAL6-24_18	4	531	67	0.16	353	0.00291	2.87	0.04743	1.50	0.05308	1.87	0.00818	1.12	0.60	58.7	3.4	51.4	71.4	52.5	1.9	52.5	1.2	52.5	1.2	0.00	0.97	Two zircons grown together, Inner part of I	
MAL6-24_18b	10	1155	52	0.20	-8153	0.00147	16.69	0.05269	1.86	0.05343	2.21	0.00742	1.20	0.54	29.6	9.9	296.5	84.9	52.9	2.3	47.6	1.1					Two zircons grown together, Inner part of II	
MAL6-24_19	5	469	98	0.28	-3901	0.00387	2.45	0.04797	2.74	0.07735	2.93	0.01179	1.04	0.35	78.1	3.8	77.9	130.1	75.7	4.3	75.6	1.6	75.6	1.6	0.00	0.97		
MAL6-24_20	4	543	61	0.17	326	0.00275	4.43	0.05032	3.33	0.05544	3.56	0.00806	1.26	0.35	55.5	4.9	189.9	154.9	54.8	3.8	51.7	1.3					Outer part	
MAL6-24_20b	9	1048	81	0.14	1164	0.00337	4.85	0.04814	1.83	0.05211	2.38	0.00792	1.51	0.64	68.1	6.6	85.5	87.0	51.6	2.4	50.8	1.5	50.9	1.5	0.62	0.43	Inner part	
MAL6-24_22	10	1416	267	0.26	24011	0.00284	2.89	0.04760	1.98	0.05129	2.42	0.00788	1.40	0.58	57.2	3.3	58.4	94.3	50.8	2.4	50.6	1.4	50.6	1.4	0.03	0.87		
MAL6-24_23	10	1131	239	0.27	884	0.00347	2.47	0.04943	2.16	0.06623	2.42	0.00981	1.08	0.45	70.0	3.5	147.0	101.5	65.1	3.1	62.9	1.4						
MAL6-24_24	4	540	64	0.14	596	0.00325	2.82	0.04675	2.84	0.05231	3.12	0.00819	1.28	0.41	65.6	3.7	14.3	136.7	51.8	3.2	52.6	1.3	52.6	1.3	0.32	0.57		
MAL6-24_25	14	1735	77	0.07	1255	0.00250	5.13	0.04814	1.56	0.05626	2.15	0.00851	1.49	0.69	50.4	5.2	98.1	73.6	55.6	2.3	54.6	1.6	54.6	1.6	1.36	0.24		
MAL1-14_1	0.4	93	22	0.33	19	0.00191	5.42	0.04756	10.23	0.03044	10.69	0.00466	3.09	0.29	38.5	4.2	69.5	486.8	30.4	6.4	29.9	1.8	29.9	1.8	0.03	0.87		Amphibolite
MAL1-14_2	0.4	116	31	0.44	62	0.00135	5.75	0.04738	7.69	0.02690	8.13	0.00413	2.65	0.33	27.4	3.1	60.3	366.3	27.0	4.3	26.6	1.4	26.6	1.4	0.03	0.86		
MAL1-14_3	2	322	122	0.45	107	0.00173	4.11	0.04861	3.96	0.03123	4.30	0.00468	1.68	0.39	34.9	2.9	120.9	186.7	31.2	2.6	30.1	1.0	30.1	1.0	0.89	0.34		
MAL1-14_4	0.4	81	26	0.44	32	0.00164	7.06	0.04661	10.11	0.03073	10.51	0.00480	2.89	0.28	33.1	4.7	21.0	485.3	30.7	6.4	30.9	1.8	30.9	1.8	0.00	0.97		
MAL1-14_5	0.2	42	6	0.30	12	0.00118	12.88	0.04763	11.24	0.02746	12.12	0.00420	4.54	0.37	23.8	6.1	72.9	534.4	27.5	6.6	27.0	2.4	27.0	2.4	0.03	0.87		
MAL1-14_6	1	272	114	0.48	112	0.00196	3.29	0.04653	2.94	0.03150	3.36	0.00493	1.62	0.48	39.5	2.6	17.1	141.4	31.5	2.1	31.7	1.0	31.7	1.0	0.04	0.84		
MAL3-8_4	3	29	2	0.09	17	0.78044	3.43	0.67225	1.75	3.88230	2.33	0.04203	1.54	0.66	11659.6	612.4	4667.6	50.5	1610.0	38.0	265.4	8.0						Orthogneiss
MAL3-8_5	4	42	4	0.08	20	0.63212	2.98	0.61654	1.58	2.67897	2.63	0.03162	2.11	0.80	9901.5	468.7	4542.5	45.7	1322.7	39.3	200.7	8.3						
MAL3-8_6	3	16	3	0.27	16	0.43448	3.17	0.73706	1.84	6.41719	2.77	0.06336	2.07	0.75	7292.6	390.0	4799.9	52.8	2034.6	49.3	396.0	15.9						
MAL3-8_7	4	492	126	0.37	181	0.00269	3.37	0.04899	3.00	0.05478	3.33	0.00814	1.45	0.44	54.3	3.7	139.6	140.8	54.2	3.5	52.2	1.5	52.2	1.5	1.46	0.23		
MAL3-8_8	4	493	179	0.61	-7880	0.00246	3.20	0.04723	2.03	0.04989	2.46	0.00769	1.38	0.56	49.6	3.2	52.8	97.1	49.4	2.4	49.4	1.4	49.4	1.4	0.01	0.94		
MAL2-16_1	1	149	20	0.20	108	0.00281	6.86	0.04780	5.71	0.05366	6.00	0.00817	1.84	0.31	56.6	7.8	81.2	271.3	53.1	6.2	52.5	1.9	52.5	1.9	0.04	0.83		Micaschist
MAL2-16_2	4	584	148	0.35	595	0.00286	3.32	0.04683	2.72	0.05390	3.06	0.00838	1.41	0.46	57.7	3.8	32.4	130.5	53.3	3.2	53.8	1.5	53.8	1.5	0.11	0.74		
MAL2-16_3	3	339	100	0.39	119	0.00339	3.39	0.04736	3.13	0.06255	3.46	0.00961	1.49	0.43	68.4	4.6	59.1	149.0	61.6	4.1	61.7	1.8	61.7	1.8	0.00	0.97		
MAL2-16_4	4	488	92	0.25	192	0.00293	3.18	0.04704	2.91	0.05453	3.40	0.00844	1.76	0.52	59.2	3.8	43.2	139.2	53.9	3.6	54.1	1.9	54.1	1.9	0.02	0.88		
MAL2-16_5	4	500	101	0.26	639	0.00273	4.29	0.04945	2.39	0.05068	2.79	0.00746	1.45	0.52	55.0	4.7	161.5	111.6	50.2	2.7	47.9	1.4						
MAL2-16_6	5	597	181	0.39	393	0.00294	3.13	0.04718	3.23	0.05482	3.56	0.00846	1.60	0.44	59.3	3.7	50.3	154.4	54.2	3.8	54.3	1.7	54.3	1.7	0.00	0.96		
MAL2-16_7	10	418	170	0.44	-2053	0.00805	2.99	0.05053	1.68	0.12970	2.56	0.01868	1.93	0.75	162.0	9.7	211.6	78.0	123.8	6.0	119.3	4.6						
MAL2-16_8	8	642	63	0.21	1265	0.00322	8.93	0.04989	1.98	0.06484	7.14	0.00946	6.86	0.96	65.0	11.6	181.8	92.1	63.8	8.9	60.7	8.3						
MAL2-16_9	4	507	125	0.45	449	0.00269	4.15	0.04785	4.60	0.05889	5.00	0.00896	1.95	0.39	54.2	4.5	83.7	218.5	58.1	5.7	57.5	2.2	57.5	2.2	0.06	0.81	Inner part	
MAL2-16_9b	7	952	90	0.12	1395	0.00295	3.62	0.04684	2.19	0.04934	2.68	0.00767	1.54	0.58	59.6	4.3	33.0	104.8	48.9	2.6	49.2	1.5	49.2	1.5	0.10	0.76	Outer part	
MAL2-16_10	1	165	38	0.33	80	0.00336	4.16	0.05248	2.57	0.06433	3.28	0.00892	2.04	0.62	67.9	5.6	298.8	117.1	63.3	4.0	57.2	2.3						
MAL2-16_11	7	214	43	3.17	44	0.00271	7.45	0.05288	8.59	0.06654	8.84	0.00916	2.09	0.24	54.7	8.1	316.1	390.8	65.4	11.2	58.8	2.4	58.7	2.4	1.48	0.22		
MAL2-16_12	5	454	136	0.45	985	0.00327	3.16	0.04774	2.63	0.07192	3.06	0.01096	1.56	0.51	66.1	4.2	78.3	125.0	70.5	4.2	70.3	2.2	70.3	2.2	0.02	0.90		
MAL2-16_13	6	542	199	0.43	876	0.00433	3.11	0.04946	2.29	0.07604	2.74	0.01119	1.51	0.55	87.3	5.4	161.7	106.9	74.4	3.9	71.7	2.1						
MAL2-16_14	18	1796	20	0.02	1321	0.00321	6.88	0.04808	1.68	0.07225	2.31	0.01094	1.59	0.69	64.8	8.9	95.1	79.4	70.8	3.2	70.1	2.2	70.1	2.2	0.39	0.53		
MAL2-16_15	5	639	139	0.29	311	0.00284	3.41	0.04873	1.78	0.05682	2.38	0.00848	1.58	0.66	57.3	3.9	127.0	84.0	56.1	2.6	54.5	1.7						
MAL2-16_17	7	1124	93	0.13	-5732	0.00283	3.26	0.04704	2.13	0.05311	2.58	0.00822	1.46	0.56	57.1	3.7	43.2	101.8	52.5	2.6	52.7	1.5	52.7	1.5	0.04	0.85		
MAL2-16_19	8	884	214	0.38	824	0.00388	3.18	0.04883	1.95	0.07500	2.46	0.01118	1.49	0.61	78.3	5.0	131.6	91.7	73.4	3.5	71.7	2.1	71.7	2.1	1.64	0.20		
MAL2-16_20	5	534	57	0.17	1791	0.00322	3.97	0.04834	2.07	0.06150	2.83	0.00926	1.93	0.68	65.0	5.2	108.2	97.9	60.6	3.3	59.4	2.3	59.4	2.3	0.96	0.33		
MAL2-16_21	2	248	59	0.35	220	0.00258	4.46	0.04700	3.96	0.05661	4.17	0.00876	1.32	0.32	52.1	4.6	41.3	189.3	55.9	4.5	56.3	1.5	56.3	1.5	0.03	0.87		
MAL2-16_22	3	299	75	0.32	247	0.00341	3.49	0.04752	3.11	0.06362	3.49	0.00974	1.57	0.45	68.7	4.8	67.3	148.3	62.6	4.2	62.5	2.0	62.5	2.0	0.00	0.95		
MAL2-16_23	8	751	82	0.14	439	0.00397	3.34	0.04690	1.67	0.07252	2.42	0.01125	1.76	0.73	80.2	5.3	35.9	79.7	71.1	3.3	72.1	2.5	72.1	2.5	0.84	0.36		
MAL2-16_24	5	654	133	0.37	346	0.00290	3.74	0.05297	3.23	0.06166	3.65	0.00847	1.71	0.47	58.6	4.4	319.7	146.6	60.8	4.3	54.4	1.8						
MAL2-16_25	7	921	72	0.14	-17954	0.00234	4.03	0.04768	1.40	0.05660	1.96	0.00864	1.37	0.70	47.2	3.8	75.5	66.7	55.9	2.1	55.4	1.5	55.5	1.5	0.35	0.55		

Dataset B-1. Single grain zircon fission-track ages for YAKD samples

===================ZetaAge Program v. 4.8 (Brandon 8/13/02)===================

All samples dated by Sarah Falkowski (2012)

HUB1 (Alaska), modern 'artificial' sand

EFFECTIVE TRACK DENSITY FOR FLUENCE MONITOR (tracks/cm^2): 5.890E+05

RELATIVE ERROR (%): 1.58

EFFECTIVE URANIUM CONTENT OF MONITOR (ppm): 50.00

ZETA FACTOR AND STANDARD ERROR (yr cm^2): 117.70 7.10

SIZE OF COUNTER SQUARE (cm^2): 1.000E-06

Grain no.	**RhoS (cm^-2)**	**(Ns)**	**RhoI (cm^-2)**	**(Ni)**	**Squares**	**U+/-2s**		**Grain Age**	**Age (Ma) --95% CI--**	
1	3.94E+06	(71)	1.56E+06	(28)	18	132	50	87.0	55.7	140.1
2	1.04E+07	(83)	3.50E+06	(28)	8	297	112	101.6	65.8	162.0
3	6.25E+06	(100)	1.60E+07	(256)	16	1358	175	13.6	10.5	17.6
4	9.75E+06	(78)	4.25E+06	(34)	8	361	123	78.8	52.2	121.7
5	9.00E+06	(45)	1.74E+07	(87)	5	1477	319	17.9	12.2	26.0
6	5.83E+06	(35)	1.00E+06	(6)	6	85	67	194.8	83.6	563.2
7	1.00E+06	(28)	1.40E+07	(391)	28	1185	126	2.5	1.6	3.6
8	8.78E+06	(79)	1.89E+06	(17)	9	160	77	157.9	93.7	284.2
9	8.00E+06	(96)	2.83E+06	(34)	12	241	82	96.8	65.1	147.8
10	4.33E+06	(26)	2.17E+06	(13)	6	184	100	68.5	34.2	145.4
11	3.31E+06	(53)	2.13E+06	(34)	16	180	62	53.7	34.3	85.3
12	8.67E+05	(13)	1.00E+07	(150)	15	849	141	3.0	1.6	5.3
13	9.44E+05	(17)	2.56E+06	(46)	18	217	64	12.9	6.9	22.8
14	6.43E+05	(9)	1.50E+06	(21)	14	127	55	15.0	6.0	33.8
15	1.67E+06	(10)	3.50E+06	(21)	6	297	128	16.6	6.9	36.6
16	2.02E+06	(109)	1.65E+07	(892)	54	1402	104	4.3	3.4	5.4
17	8.69E+06	(139)	2.19E+06	(35)	16	186	63	135.8	93.6	202.6
18	5.77E+06	(173)	1.83E+06	(55)	30	156	42	107.9	79.4	149.0
19	7.78E+05	(14)	5.06E+06	(91)	18	429	91	5.4	2.8	9.4
20	8.60E+06	(86)	1.50E+06	(15)	10	127	65	194.0	112.9	360.5
21	8.67E+06	(78)	1.78E+06	(16)	9	151	74	165.5	97.0	303.2
22	1.75E+06	(7)	4.75E+06	(19)	4	403	183	12.9	4.5	31.7
23	4.17E+06	(25)	5.50E+06	(33)	6	467	162	26.3	14.9	45.4
24	1.00E+06	(16)	2.94E+06	(47)	16	249	73	11.9	6.2	21.2
25	1.00E+07	(50)	8.80E+06	(44)	5	747	225	39.3	25.7	60.3
26	3.67E+06	(33)	2.89E+06	(26)	9	245	96	43.8	25.4	76.2
27	7.56E+06	(68)	1.67E+06	(15)	9	141	72	154.0	88.2	289.7
28	7.38E+06	(118)	1.56E+06	(25)	16	133	53	160.8	104.6	258.1
29	9.44E+06	(85)	2.89E+06	(26)	9	245	96	111.9	71.8	180.9
30	1.25E+06	(15)	1.08E+06	(13)	12	92	50	39.8	17.7	90.8
31	6.45E+06	(129)	2.60E+06	(52)	20	221	61	85.3	61.5	120.1
32	9.00E+06	(36)	3.25E+06	(13)	4	276	150	94.5	49.5	194.5
33	3.33E+06	(20)	4.33E+06	(26)	6	368	143	26.7	14.1	49.5
34	1.44E+06	(13)	2.89E+06	(26)	9	245	96	17.4	8.2	34.9
35	8.75E+06	(35)	1.25E+06	(5)	4	106	91	231.9	93.9	748.7
36	9.50E+06	(171)	4.44E+06	(80)	18	377	85	73.4	54.9	98.1
37	7.05E+06	(141)	1.75E+06	(35)	20	149	50	137.7	95.0	205.4
38	1.67E+06	(10)	1.67E+06	(10)	6	141	87	34.6	12.9	92.2
39	2.15E+06	(28)	1.69E+06	(22)	13	144	61	43.9	24.3	80.5
40	1.83E+06	(11)	7.17E+06	(43)	6	608	185	9.0	4.1	17.5
41	6.81E+06	(143)	1.62E+06	(34)	21	137	47	143.7	98.8	215.3

42	4.20E+06 (63)	3.07E+06 (46)	15	260	77	47.3	31.8	70.7
43	1.65E+07 (99)	3.00E+06 (18)	6	255	119	186.5	113.5	326.8
44	6.00E+06 (240)	5.10E+06 (204)	40	433	62	40.6	32.5	50.7
45	1.15E+07 (69)	2.17E+06 (13)	6	184	100	179.6	100.0	353.3
46	6.25E+06 (200)	1.69E+06 (54)	32	143	39	126.9	93.8	174.7
47	7.70E+06 (462)	1.65E+06 (99)	60	140	28	159.1	124.4	203.4
48	3.75E+05 (3)	1.00E+06 (8)	8	85	58	13.4	2.2	54.0
49	3.25E+06 (52)	2.56E+06 (41)	16	218	68	43.8	28.5	67.6
50	8.28E+05 (24)	2.76E+06 (80)	29	234	53	10.4	6.3	16.6
51	3.44E+06 (31)	8.89E+05 (8)	9	75	52	131.0	60.1	329.9
52	8.30E+06 (83)	1.50E+06 (15)	10	127	65	187.4	108.8	348.8
53	8.12E+06 (211)	1.46E+06 (38)	26	124	40	189.0	134.1	274.1
54	8.00E+06 (80)	2.90E+06 (29)	10	246	91	94.6	61.5	150.2
55	8.17E+06 (49)	1.50E+06 (9)	6	127	83	183.4	91.0	423.1
56	5.67E+06 (68)	1.50E+06 (18)	12	127	59	128.8	76.5	230.1
57	1.20E+06 (12)	2.20E+06 (22)	10	187	79	19.0	8.5	39.8
58	1.04E+07 (83)	3.75E+06 (30)	8	318	116	94.9	62.1	149.3
59	1.75E+06 (7)	9.00E+06 (36)	4	764	254	6.9	2.5	15.4
60	6.91E+06 (76)	4.36E+06 (48)	11	370	107	54.6	37.6	80.1
61	1.52E+06 (41)	4.07E+06 (110)	27	346	67	12.9	8.8	18.7
62	9.58E+06 (115)	1.92E+06 (23)	12	163	67	170.1	109.0	278.5
63	7.17E+06 (43)	7.00E+06 (42)	6	594	183	35.4	22.6	55.5
64	7.17E+06 (86)	2.50E+06 (30)	12	212	77	98.3	64.5	154.4
65	5.33E+06 (32)	1.67E+06 (10)	6	141	87	108.8	52.9	248.3
66	8.33E+05 (5)	3.00E+06 (18)	6	255	119	9.8	2.8	26.9
67	1.25E+06 (20)	8.00E+06 (128)	16	679	122	5.5	3.2	8.7
68	6.30E+06 (126)	2.15E+06 (43)	20	183	56	100.5	70.8	145.7
69	7.31E+06 (117)	2.00E+06 (32)	16	170	60	125.1	84.4	191.1
70	6.27E+06 (94)	1.60E+06 (24)	15	136	55	133.7	85.3	218.8
71	1.44E+06 (52)	1.53E+06 (55)	36	130	35	32.7	21.9	48.7
72	8.88E+06 (71)	2.88E+06 (23)	8	244	101	105.6	65.6	177.2
73	6.00E+06 (36)	6.67E+05 (4)	6	57	53	294.5	110.8	1106.6
74	5.71E+05 (8)	2.86E+06 (40)	14	243	77	7.0	2.8	15.0
75	1.03E+07 (62)	3.67E+06 (22)	6	311	132	96.5	58.9	165.0
76	1.00E+06 (32)	9.06E+05 (29)	32	77	28	38.1	22.4	65.3
77	2.19E+06 (46)	2.33E+06 (49)	21	198	57	32.5	21.2	49.6
78	2.29E+06 (80)	6.23E+06 (218)	35	529	73	12.8	9.6	16.9
79	1.05E+06 (22)	9.57E+06 (201)	21	813	117	3.8	2.3	5.9
80	4.50E+05 (9)	5.25E+06 (105)	20	446	88	3.0	1.3	5.9
81	5.89E+06 (53)	2.56E+06 (23)	9	217	90	79.1	47.9	135.3
82	1.60E+06 (8)	1.40E+06 (7)	5	119	87	39.4	12.5	127.2
83	5.75E+06 (46)	1.13E+06 (9)	8	96	62	172.3	85.1	399.4
84	2.53E+06 (38)	1.20E+06 (18)	15	102	47	72.4	40.6	134.9
85	7.78E+06 (140)	1.67E+06 (30)	18	141	51	159.1	107.4	244.3
86	1.64E+06 (23)	5.71E+05 (8)	14	49	33	97.6	42.9	252.9
87	1.07E+06 (16)	6.40E+06 (96)	15	543	112	5.8	3.2	9.9
88	7.13E+06 (107)	1.47E+06 (22)	15	125	53	165.5	104.8	274.6
89	3.13E+05 (10)	1.59E+06 (51)	32	135	38	6.9	3.1	13.5
90	4.88E+06 (78)	1.06E+06 (17)	16	90	43	156.0	92.5	280.9
91	4.80E+06 (96)	2.40E+06 (48)	20	204	59	68.8	48.3	99.6
92	2.33E+06 (14)	7.67E+06 (46)	6	651	192	10.6	5.4	19.5
93	1.33E+06 (32)	1.33E+06 (32)	24	113	40	34.6	20.5	58.2
94	1.56E+06 (28)	5.33E+06 (96)	18	453	93	10.1	6.4	15.5
95	2.44E+06 (22)	6.67E+05 (6)	9	57	44	123.5	49.8	372.4
96	2.70E+06 (27)	2.30E+06 (23)	10	195	81	40.5	22.4	73.9
97	5.11E+05 (23)	3.96E+06 (178)	45	336	51	4.5	2.8	6.9

98	5.72E+06	(103)	1.11E+06	(20)	18	94	42	175.0	108.8	297.7
99	6.09E+06	(213)	1.20E+06	(42)	35	102	31	172.9	124.4	246.6
100	5.83E+06	(70)	1.50E+06	(18)	12	127	59	132.5	78.8	236.4
101	6.67E+05	(4)	4.83E+06	(29)	6	410	152	4.9	1.2	13.6
102	1.03E+07	(62)	3.17E+06	(19)	6	269	122	111.5	66.3	197.5
103	2.78E+06	(50)	3.89E+06	(70)	18	330	79	24.7	16.8	36.1
104	6.50E+06	(39)	3.17E+06	(19)	6	269	122	70.5	40.0	129.2
105	1.69E+06	(61)	1.58E+06	(57)	36	134	36	37.0	25.3	54.1

YAKD1 (Alaska), modern sand

EFFECTIVE TRACK DENSITY FOR FLUENCE MONITOR (tracks/cm^2): 5.940E+05
RELATIVE ERROR (%): 1.58
EFFECTIVE URANIUM CONTENT OF MONITOR (ppm): 50.00
ZETA FACTOR AND STANDARD ERROR (yr cm^2): 117.70 7.10
SIZE OF COUNTER SQUARE (cm^2): 1.000E-06

Grain no.	**RhoS (cm^-2)**	**(Ns)**	**RhoI (cm^-2)**	**(Ni)**	**Squares**	**U+/-2s**		**Grain Age**	**Age (Ma) --95% CI--**	
1	5.40E+06	(54)	2.10E+06	(21)	10	177	76	88.9	53.1	155.0
2	5.50E+06	(44)	4.38E+06	(35)	8	368	124	43.8	27.5	70.3
3	6.33E+06	(38)	5.17E+06	(31)	6	435	156	42.7	25.9	70.9
4	3.47E+06	(111)	1.22E+06	(39)	32	103	33	98.5	68.1	145.8
5	7.08E+06	(85)	5.33E+06	(64)	12	449	113	46.2	33.0	65.0
6	1.28E+07	(51)	5.75E+06	(23)	4	484	200	76.8	46.3	131.7
7	2.50E+06	(10)	7.50E+05	(3)	4	63	68	111.5	29.9	627.6
8	1.18E+07	(71)	8.83E+06	(53)	6	744	205	46.6	32.2	67.9
9	5.57E+06	(39)	2.86E+06	(20)	7	241	107	67.5	38.7	122.3
10	3.86E+06	(27)	3.43E+06	(24)	7	289	117	39.2	21.8	70.9
11	2.67E+06	(32)	2.00E+06	(24)	12	168	68	46.4	26.5	82.3
12	8.67E+06	(52)	1.67E+06	(10)	6	140	87	177.0	90.7	389.5
13	3.33E+06	(20)	6.67E+05	(4)	6	56	53	167.2	58.3	667.8
14	3.19E+06	(51)	1.50E+06	(24)	16	126	51	73.6	44.7	125.1
15	2.00E+06	(8)	7.50E+05	(3)	4	63	68	89.7	22.3	523.9
16	1.10E+07	(55)	8.40E+06	(42)	5	707	218	45.6	30.0	69.8
17	6.33E+06	(38)	7.17E+06	(43)	6	603	184	30.8	19.4	48.8
18	1.25E+07	(100)	5.00E+06	(40)	8	421	133	86.6	59.6	128.4
19	9.56E+06	(86)	1.03E+07	(93)	9	870	182	32.3	23.7	43.8
20	5.67E+06	(34)	6.33E+06	(38)	6	533	173	31.2	19.1	50.9
21	4.54E+06	(218)	3.13E+06	(150)	48	263	44	50.6	39.8	64.3
22	4.67E+06	(28)	5.67E+06	(34)	6	477	163	28.8	16.8	48.8
23	2.16E+06	(97)	7.56E+05	(34)	45	64	22	98.7	66.4	150.5
24	3.35E+06	(67)	1.25E+06	(25)	20	105	42	92.6	58.1	153.2
25	5.60E+06	(84)	1.80E+06	(27)	15	152	58	107.4	69.3	172.5
26	5.38E+06	(43)	3.75E+06	(30)	8	316	115	49.8	30.6	82.3
27	1.57E+07	(94)	1.28E+07	(77)	6	1080	248	42.5	31.1	58.3
28	1.26E+07	(63)	4.80E+06	(24)	5	404	164	90.7	56.2	152.0
29	7.67E+06	(69)	6.33E+06	(57)	9	533	142	42.2	29.3	61.0
30	9.53E+06	(286)	6.43E+06	(193)	30	542	80	51.6	41.4	64.1
31	9.35E+06	(159)	3.18E+06	(54)	17	267	73	101.9	74.6	141.6
32	1.21E+07	(109)	7.11E+06	(64)	9	599	150	59.2	43.1	82.0
33	2.25E+06	(90)	1.43E+06	(57)	40	120	32	54.9	39.0	78.0
34	4.92E+06	(59)	4.92E+06	(59)	12	414	108	34.9	23.9	50.9
35	1.04E+07	(94)	4.22E+06	(38)	9	355	115	85.7	58.4	128.5
36	5.67E+06	(34)	4.83E+06	(29)	6	407	150	40.8	24.2	69.4
37	2.40E+06	(36)	2.47E+06	(37)	15	208	68	33.9	20.8	55.2
38	2.50E+06	(40)	1.81E+06	(29)	16	153	56	48.0	29.1	80.2
39	8.75E+06	(140)	7.19E+06	(115)	16	605	114	42.4	32.2	55.7

40	5.50E+06	(	22)	9.50E+06	(	38)	4	800	259	20.3	11.4	35.0
41	2.47E+06	(	37)	2.47E+06	(	37)	15	208	68	34.9	21.5	56.5
42	4.00E+06	(	32)	2.13E+06	(	17)	8	179	86	65.2	35.3	125.2
43	1.89E+06	(	17)	2.00E+06	(	18)	9	168	78	33.0	16.0	67.6
44	1.01E+07	(	71)	6.43E+06	(	45)	7	541	161	54.9	37.3	81.6
45	6.13E+06	(	49)	8.25E+06	(	66)	8	694	172	25.9	17.5	38.1
46	1.13E+07	(	45)	1.53E+07	(	61)	4	1284	330	25.8	17.1	38.5
47	2.48E+06	(	67)	2.00E+06	(	54)	27	168	46	43.2	29.7	63.1
48	5.50E+06	(	44)	5.63E+06	(	45)	8	473	141	34.1	22.0	52.8
49	4.88E+06	(	39)	8.75E+05	(	7)	8	74	54	188.4	85.5	496.7
50	5.67E+06	(	119)	4.14E+06	(	87)	21	349	75	47.6	35.8	63.6
51	4.38E+06	(	57)	2.38E+06	(	31)	13	201	72	63.8	40.6	102.3
52	5.67E+06	(	119)	1.95E+06	(	41)	21	164	51	100.4	70.1	147.0
53	6.75E+06	(	108)	5.19E+06	(	83)	16	437	97	45.3	33.7	61.1
54	7.63E+06	(	122)	7.50E+06	(	120)	16	631	117	35.4	26.8	46.8
55	1.05E+07	(	42)	1.23E+07	(	49)	4	1031	295	29.9	19.3	46.1
56	3.07E+06	(	43)	1.50E+06	(	21)	14	126	55	70.9	41.4	125.9
57	6.33E+06	(	57)	6.56E+06	(	59)	9	552	144	33.7	23.0	49.3
58	2.67E+06	(	16)	1.67E+06	(	10)	6	140	87	55.4	23.8	136.5
59	3.33E+05	(	5)	5.20E+06	(	78)	15	438	100	2.3	0.7	5.5
60	1.25E+07	(	50)	4.25E+06	(	17)	4	358	171	101.4	58.0	187.6
61	4.33E+06	(	39)	2.11E+06	(	19)	9	178	81	71.1	40.3	130.3
62	6.92E+06	(	83)	5.83E+06	(	70)	12	491	118	41.3	29.7	57.7
63	1.33E+05	(	2)	4.93E+06	(	74)	15	415	97	1.0	0.1	3.5
64	2.50E+06	(	20)	3.00E+06	(	24)	8	253	102	29.1	15.2	54.9
65	6.28E+06	(	113)	3.17E+06	(	57)	18	267	71	68.8	49.7	96.5
66	2.89E+06	(	26)	1.56E+06	(	14)	9	131	69	64.3	32.6	133.2
67	5.78E+06	(	52)	4.22E+06	(	38)	9	355	115	47.6	30.8	74.4
68	9.17E+06	(	55)	6.50E+06	(	39)	6	547	175	49.1	32.0	76.0
69	9.75E+06	(	78)	7.88E+06	(	63)	8	663	168	43.1	30.5	61.1
70	1.21E+07	(	97)	5.25E+06	(	42)	8	442	136	80.1	55.4	118.0
71	5.96E+06	(	149)	3.12E+06	(	78)	25	263	60	66.4	50.2	88.5
72	1.80E+07	(	90)	2.04E+07	(	102)	5	1717	344	30.8	22.9	41.3
73	1.56E+06	(	14)	1.67E+06	(	15)	9	140	71	32.6	14.6	72.2
74	3.25E+06	(	26)	1.63E+06	(	13)	8	137	75	69.1	34.5	146.6
75	4.44E+05	(	4)	1.63E+07	(	147)	9	1375	231	1.0	0.3	2.5
76	8.58E+06	(	103)	5.17E+06	(	62)	12	435	111	57.8	41.8	80.6
77	4.80E+06	(	24)	8.00E+06	(	40)	5	673	213	21.0	12.1	35.6
78	1.06E+06	(	38)	9.39E+06	(	338)	36	790	89	3.9	2.7	5.5
79	6.89E+06	(	62)	3.44E+06	(	31)	9	290	104	69.4	44.5	110.5
80	1.00E+06	(	16)	1.14E+07	(	182)	16	957	145	3.1	1.7	5.1
81	1.00E+06	(	9)	1.78E+06	(	16)	9	150	74	19.8	7.7	47.1
82	5.73E+06	(	172)	2.67E+06	(	80)	30	224	51	74.5	55.7	99.5
83	5.67E+06	(	85)	6.20E+06	(	93)	15	522	109	31.9	23.4	43.3
84	3.08E+06	(	74)	3.42E+06	(	82)	24	288	64	31.5	22.7	43.7
85	1.13E+06	(	9)	1.75E+06	(	14)	8	147	78	22.6	8.6	55.6
86	1.87E+06	(	28)	2.20E+06	(	33)	15	185	64	29.6	17.2	50.5
87	7.44E+06	(	67)	8.78E+06	(	79)	9	739	167	29.6	21.0	41.5
88	3.08E+05	(	12)	7.95E+06	(	310)	39	669	79	1.4	0.7	2.4
89	3.38E+06	(	27)	2.63E+06	(	21)	8	221	96	44.7	24.4	83.2
90	4.40E+06	(	66)	3.07E+06	(	46)	15	258	76	49.9	33.8	74.4
91	1.02E+07	(	183)	2.67E+06	(	48)	18	224	65	131.6	95.7	184.8
92	4.00E+06	(	24)	3.17E+06	(	19)	6	267	121	43.9	23.1	84.8
93	2.75E+06	(	22)	1.13E+06	(	9)	8	95	62	84.0	37.7	207.6
94	5.08E+06	(	61)	4.42E+06	(	53)	12	372	102	40.1	27.3	59.1
95	6.88E+06	(	110)	4.31E+06	(	69)	16	363	88	55.4	40.7	76.1

96	5.00E+06	(40)	5.75E+06	(46)	8	484	143	30.3	19.3	47.4
97	5.90E+06	(59)	3.80E+06	(38)	10	320	104	54.0	35.4	83.4
98	6.22E+06	(56)	6.56E+06	(59)	9	552	144	33.1	22.5	48.6
99	2.80E+06	(56)	8.50E+05	(17)	20	72	34	113.4	65.5	208.2
100	4.06E+06	(65)	1.63E+06	(26)	16	137	53	86.5	54.4	142.1
101	5.20E+06	(26)	4.20E+06	(21)	5	354	153	43.1	23.4	80.5
102	4.57E+06	(96)	6.00E+06	(126)	21	505	91	26.6	19.9	35.6
103	1.80E+06	(27)	3.13E+06	(47)	15	264	77	20.1	12.0	32.9
104	1.00E+06	(6)	6.67E+05	(4)	6	56	53	51.6	12.4	247.9

YAKD2 (Alaska), modern sand55555

EFFECTIVE TRACK DENSITY FOR FLUENCE MONITOR (tracks/cm^2): 5.940E+05

RELATIVE ERROR (%): 1.58

EFFECTIVE URANIUM CONTENT OF MONITOR (ppm): 50.00

ZETA FACTOR AND STANDARD ERROR (yr cm^2): 117.70 7.10

SIZE OF COUNTER SQUARE (cm^2): 1.000E-06

Grain no.	**RhoS (cm^-2)**	**(Ns)**	**RhoI (cm^-2)**	**(Ni)**	**Squares**	**U+/-2s**		**Grain Age**	**Age (Ma) --95% CI--**	
1	6.07E+06	(91)	3.47E+06	(52)	15	292	81	60.8	42.8	87.3
2	7.43E+06	(208)	3.14E+06	(88)	28	265	57	81.8	62.1	107.7
3	1.56E+06	(14)	7.78E+05	(7)	9	65	48	68.8	26.3	201.6
4	4.56E+06	(41)	3.00E+06	(27)	9	253	97	52.8	31.8	89.2
5	5.81E+06	(93)	3.13E+06	(50)	16	263	74	64.6	45.4	93.1
6	1.08E+07	(43)	2.25E+06	(9)	4	189	123	162.6	79.8	378.6
7	1.11E+07	(122)	4.27E+06	(47)	11	360	105	89.9	63.9	128.8
8	8.75E+06	(35)	6.25E+06	(25)	4	526	209	48.7	28.4	84.8
9	1.15E+07	(46)	1.78E+07	(71)	4	1494	357	22.6	15.2	33.2
10	7.60E+06	(38)	4.20E+06	(21)	5	354	153	62.7	36.1	112.6
11	1.43E+07	(57)	5.00E+06	(20)	4	421	186	98.4	58.6	172.9
12	1.31E+07	(92)	7.86E+06	(55)	7	661	179	58.1	41.2	82.8
13	8.50E+06	(119)	2.36E+06	(33)	14	198	69	124.4	84.4	188.9
14	5.50E+06	(44)	3.38E+06	(27)	8	284	109	56.6	34.4	95.1
15	1.11E+07	(78)	1.14E+07	(80)	7	962	217	34.0	24.5	47.1
16	6.00E+06	(24)	4.75E+06	(19)	4	400	182	43.9	23.1	84.8
17	2.26E+06	(61)	1.67E+06	(45)	27	140	42	47.2	31.6	71.0
18	4.54E+06	(159)	2.51E+06	(88)	35	212	45	62.7	47.1	83.4
19	2.78E+06	(89)	1.59E+06	(51)	32	134	38	60.6	42.6	87.4
20	6.67E+06	(60)	3.00E+06	(27)	9	253	97	77.0	48.3	126.2
21	7.56E+06	(68)	5.56E+06	(50)	9	468	132	47.3	32.4	69.7
22	1.00E+07	(50)	3.20E+06	(16)	5	269	133	107.6	60.8	202.5
23	5.10E+06	(245)	2.48E+06	(119)	48	209	39	71.4	55.7	91.6
24	9.53E+06	(143)	3.27E+06	(49)	15	275	79	101.0	72.8	142.8
25	8.33E+06	(175)	4.38E+06	(92)	21	369	78	66.0	49.9	87.2
26	6.78E+06	(122)	5.44E+06	(98)	18	458	93	43.3	32.4	58.0
27	3.50E+06	(28)	1.13E+06	(9)	8	95	62	106.6	49.7	257.0
28	7.33E+06	(88)	4.33E+06	(52)	12	365	101	58.8	41.3	84.6
29	2.10E+06	(42)	3.55E+06	(71)	20	299	71	20.7	13.7	30.7
30	2.15E+06	(43)	1.70E+06	(34)	20	143	49	44.0	27.5	71.2
31	7.67E+06	(92)	5.08E+06	(61)	12	428	110	52.5	37.6	73.8
32	4.83E+06	(169)	2.31E+06	(81)	35	195	44	72.3	54.1	96.5
33	7.67E+06	(92)	5.83E+06	(70)	12	491	118	45.8	33.2	63.4
34	9.75E+06	(117)	3.67E+06	(44)	12	309	93	92.1	64.8	133.5
35	3.09E+06	(34)	2.82E+06	(31)	11	237	85	38.2	22.8	64.3
36	1.10E+07	(165)	8.20E+06	(123)	15	690	126	46.7	35.9	60.7
37	5.38E+06	(43)	3.25E+06	(26)	8	274	107	57.4	34.6	97.4
38	1.12E+07	(67)	3.83E+06	(23)	6	323	134	100.6	62.2	169.3

39	1.30E+07	(104)	8.88E+06	(71)	8	747	178	51.0	37.3	70.0
40	4.50E+06	(81)	3.11E+06	(56)	18	262	70	50.3	35.4	72.1
41	5.00E+05	(15)	8.60E+06	(258)	30	724	93	2.1	1.1	3.4
42	6.25E+06	(75)	2.17E+06	(26)	12	182	71	99.7	63.4	162.3
43	2.42E+06	(29)	1.25E+06	(15)	12	105	54	66.9	34.9	134.4
44	7.69E+06	(123)	4.69E+06	(75)	16	395	92	57.0	42.5	77.1
45	9.25E+06	(37)	4.25E+06	(17)	4	358	171	75.3	41.6	142.6
46	1.20E+07	(72)	8.00E+06	(48)	6	673	195	52.2	35.7	76.9
47	6.38E+06	(51)	4.75E+06	(38)	8	400	129	46.7	30.1	73.1
48	9.00E+06	(54)	6.00E+06	(36)	6	505	168	52.2	33.6	81.9
49	6.30E+06	(126)	4.65E+06	(93)	20	391	82	47.1	35.2	63.1
50	7.57E+06	(53)	1.00E+07	(70)	7	842	202	26.4	18.1	38.3
51	4.47E+06	(67)	3.80E+06	(57)	15	320	85	40.9	28.3	59.4
52	1.00E+07	(90)	8.33E+06	(75)	9	701	163	41.8	30.4	57.6
53	9.67E+06	(58)	5.00E+06	(30)	6	421	153	67.1	42.6	108.0
54	4.48E+06	(121)	1.89E+06	(51)	27	159	45	82.3	59.0	116.6
55	3.67E+06	(44)	1.75E+06	(21)	12	147	64	72.5	42.5	128.5
56	4.81E+06	(101)	4.33E+06	(91)	21	365	77	38.7	28.8	52.0
57	7.10E+06	(284)	3.70E+06	(148)	40	311	52	66.6	52.8	84.0
58	1.18E+07	(47)	9.75E+06	(39)	4	821	262	42.0	26.9	65.9
59	7.61E+06	(137)	3.17E+06	(57)	18	267	71	83.3	60.9	115.7
60	5.58E+06	(67)	3.58E+06	(43)	12	302	92	54.2	36.4	81.5
61	5.56E+06	(89)	7.38E+06	(118)	16	621	116	26.3	19.7	35.0
62	4.86E+06	(243)	3.92E+06	(196)	50	330	48	43.2	34.5	54.0
63	9.80E+06	(49)	7.60E+06	(38)	5	640	207	44.9	28.8	70.5
64	6.82E+06	(116)	6.18E+06	(105)	17	520	103	38.5	28.8	51.4
65	5.60E+06	(56)	2.20E+06	(22)	10	185	78	88.0	53.2	151.4
66	9.50E+06	(57)	6.33E+06	(38)	6	533	173	52.2	34.1	80.9
67	7.67E+06	(69)	5.00E+06	(45)	9	421	125	53.3	36.1	79.5
68	2.88E+06	(23)	1.75E+06	(14)	8	147	78	56.9	28.2	119.7
69	7.67E+06	(46)	7.50E+06	(45)	6	631	188	35.6	23.1	55.0
70	1.10E+07	(66)	4.33E+06	(26)	6	365	142	87.8	55.3	144.1
71	6.13E+06	(98)	2.00E+06	(32)	16	168	59	105.8	70.7	163.1
72	7.63E+06	(122)	3.06E+06	(49)	16	258	74	86.3	61.6	122.9
73	1.30E+07	(78)	3.67E+06	(22)	6	309	130	122.1	75.9	205.9
74	7.17E+06	(43)	6.33E+06	(38)	6	533	173	39.4	24.9	62.7
75	5.67E+06	(34)	2.83E+06	(17)	6	238	114	69.2	37.8	132.2
76	6.25E+06	(25)	4.50E+06	(18)	4	379	177	48.3	25.4	93.9
77	5.20E+06	(52)	2.30E+06	(23)	10	194	80	78.3	47.3	134.1
78	3.95E+06	(79)	1.85E+06	(37)	20	156	51	74.0	49.7	112.6
79	7.00E+06	(126)	2.67E+06	(48)	18	224	65	90.9	64.9	129.7
80	3.90E+06	(82)	2.43E+06	(51)	21	204	57	55.9	39.0	81.0
81	5.71E+05	(4)	7.29E+06	(51)	7	613	172	2.8	0.7	7.5
82	1.12E+07	(67)	4.33E+06	(26)	6	365	142	89.1	56.2	146.2
83	5.39E+06	(97)	3.33E+06	(60)	18	281	73	56.2	40.4	79.0
84	7.69E+06	(123)	2.31E+06	(37)	16	195	64	114.8	79.3	170.7
85	6.56E+06	(118)	3.00E+06	(54)	18	253	69	75.8	54.6	106.8
86	4.42E+06	(53)	2.08E+06	(25)	12	175	70	73.4	45.0	123.4
87	7.50E+06	(30)	4.75E+06	(19)	4	400	182	54.8	30.0	103.1
88	1.10E+07	(55)	3.60E+06	(18)	5	303	141	105.3	61.4	190.6
89	2.63E+06	(21)	2.25E+06	(18)	8	189	88	40.6	20.6	80.8
90	6.67E+06	(60)	3.22E+06	(29)	9	271	100	71.7	45.5	116.0
91	1.00E+07	(80)	4.38E+06	(35)	8	368	124	79.2	52.8	121.5
92	1.50E+06	(12)	1.38E+06	(11)	8	116	68	38.0	15.4	94.8
93	4.29E+06	(60)	5.36E+06	(75)	14	451	105	27.9	19.5	39.7
94	1.23E+07	(49)	5.75E+06	(23)	4	484	200	73.8	44.3	127.0

95	6.56E+06	(59)	2.33E+06	(21)	9	196	85	97.0	58.5	168.2
96	7.50E+06	(45)	1.50E+06	(9)	6	126	82	170.0	83.8	394.7
97	6.60E+06	(33)	5.20E+06	(26)	5	438	171	44.2	25.7	76.9
98	2.33E+06	(56)	1.13E+06	(27)	24	95	36	71.9	44.8	118.4
99	7.00E+05	(7)	3.00E+05	(3)	10	25	27	78.8	18.6	471.4
100	5.70E+06	(171)	3.23E+06	(97)	30	272	56	61.2	46.4	80.6
101	5.42E+06	(65)	4.58E+06	(55)	12	386	104	41.2	28.3	60.1
102	7.50E+06	(30)	3.25E+06	(13)	4	274	149	79.6	40.7	166.5
103	6.40E+06	(32)	6.00E+06	(30)	5	505	184	37.2	21.9	63.3
104	8.17E+06	(49)	6.00E+06	(36)	6	505	168	47.4	30.2	75.0

YAKD3 (Alaska), modern sand

EFFECTIVE TRACK DENSITY FOR FLUENCE MONITOR (tracks/cm^2): 5.940E+05
RELATIVE ERROR (%): 1.58
EFFECTIVE URANIUM CONTENT OF MONITOR (ppm): 50.00
ZETA FACTOR AND STANDARD ERROR (yr cm^2): 117.70 7.10
SIZE OF COUNTER SQUARE (cm^2): 1.000E-06

Grain no.	**RhoS (cm^-2)**	**(Ns)**	**RhoI (cm^-2)**	**(Ni)**	**Squares**	**U+/-2s**		**Grain Age (Ma) Age**	**--95% CI--**	
1	2.87E+06	(43)	2.13E+06	(32)	15	180	63	46.7	28.9	76.3
2	3.94E+06	(63)	2.56E+06	(41)	16	216	67	53.4	35.5	81.3
3	5.00E+06	(60)	1.00E+06	(12)	12	84	48	170.6	92.3	347.7
4	5.75E+06	(23)	4.75E+06	(19)	4	400	182	42.1	22.0	81.7
5	3.75E+06	(30)	1.75E+06	(14)	8	147	78	74.0	38.4	151.2
6	5.14E+06	(72)	3.43E+06	(48)	14	289	83	52.2	35.7	76.9
7	5.50E+06	(33)	2.67E+06	(16)	6	224	111	71.3	38.4	138.9
8	6.30E+06	(63)	3.80E+06	(38)	10	320	104	57.6	38.0	88.6
9	4.21E+06	(101)	2.54E+06	(61)	24	214	55	57.6	41.5	80.5
10	4.67E+06	(56)	3.00E+06	(36)	12	253	84	54.1	35.0	84.7
11	5.25E+06	(21)	4.25E+06	(17)	4	358	171	43.0	21.6	86.7
12	6.38E+06	(153)	4.71E+06	(113)	24	396	75	47.1	35.9	61.7
13	4.33E+06	(91)	2.14E+06	(45)	21	180	54	70.2	48.7	102.8
14	6.30E+06	(63)	2.70E+06	(27)	10	227	87	80.8	50.9	132.0
15	4.30E+06	(43)	3.10E+06	(31)	10	261	93	48.2	29.8	79.2
16	6.00E+06	(36)	5.00E+06	(30)	6	421	153	41.8	25.0	70.2
17	3.40E+06	(68)	2.50E+06	(50)	20	210	60	47.3	32.4	69.7
18	5.67E+06	(102)	2.94E+06	(53)	18	248	68	66.8	47.6	95.1
19	1.96E+06	(47)	1.08E+06	(26)	24	91	36	62.7	38.2	105.6
20	7.29E+06	(175)	1.79E+06	(43)	24	151	46	140.3	100.5	200.7
21	3.33E+06	(90)	1.74E+06	(47)	27	147	43	66.5	46.3	96.8
22	4.00E+06	(24)	6.00E+06	(36)	6	505	168	23.3	13.3	40.1
23	7.92E+06	(95)	2.08E+06	(25)	12	175	70	130.9	84.1	212.2
24	4.81E+06	(77)	2.25E+06	(36)	16	189	63	74.2	49.5	113.5
25	4.56E+06	(73)	3.00E+06	(48)	16	253	73	52.9	36.3	77.8
26	2.95E+06	(59)	1.70E+06	(34)	20	143	49	60.3	39.0	94.8
27	7.82E+06	(86)	2.55E+06	(28)	11	214	81	106.1	68.9	168.9
28	3.33E+06	(133)	1.95E+06	(78)	40	164	37	59.3	44.5	79.5
29	6.78E+06	(61)	2.78E+06	(25)	9	234	93	84.4	52.5	140.4
30	4.83E+06	(58)	1.75E+06	(21)	12	147	64	95.4	57.4	165.5
31	7.00E+06	(49)	3.29E+06	(23)	7	277	114	73.8	44.3	127.0
32	7.63E+06	(61)	4.63E+06	(37)	8	389	128	57.3	37.5	88.7
33	3.72E+06	(186)	2.06E+06	(103)	50	173	35	62.7	47.9	82.0
34	5.17E+06	(62)	3.42E+06	(41)	12	288	90	52.6	34.9	80.1
35	4.70E+06	(47)	2.40E+06	(24)	10	202	82	67.9	40.9	116.1
36	3.80E+06	(152)	2.48E+06	(99)	40	208	42	53.4	40.3	70.5
37	5.25E+06	(42)	2.25E+06	(18)	8	189	88	80.6	45.7	149.0

38	3.83E+06	(134)	2.37E+06	(83)	35	200	44	56.2	42.4	74.8
39	4.13E+06	(33)	2.25E+06	(18)	8	189	88	63.5	34.9	119.9
40	1.81E+06	(58)	1.06E+06	(34)	32	89	31	59.2	38.2	93.4
41	4.67E+06	(56)	3.08E+06	(37)	12	260	85	52.6	34.2	82.0
42	5.00E+06	(20)	2.75E+06	(11)	4	231	137	62.8	28.9	145.3
43	4.94E+06	(79)	3.88E+06	(62)	16	326	83	44.4	31.4	63.0
44	5.20E+06	(52)	3.00E+06	(30)	10	253	92	60.2	37.8	97.8
45	6.50E+06	(26)	4.50E+06	(18)	4	379	177	50.2	26.6	97.1
46	2.68E+06	(161)	8.67E+05	(52)	60	73	20	107.1	78.1	149.5
47	5.22E+06	(94)	2.33E+06	(42)	18	196	61	77.6	53.5	114.6
48	3.46E+06	(83)	2.04E+06	(49)	24	172	49	58.9	40.9	85.7
49	6.00E+06	(24)	3.25E+06	(13)	4	274	149	63.9	31.5	136.7
50	4.00E+06	(28)	1.86E+06	(13)	7	156	85	74.4	37.6	156.6
51	4.11E+06	(74)	9.44E+05	(17)	18	79	38	149.3	88.2	269.6
52	2.90E+06	(58)	1.95E+06	(39)	20	164	52	51.7	33.9	79.7
53	5.65E+06	(113)	4.65E+06	(93)	20	391	82	42.3	31.9	56.4
54	7.00E+06	(42)	3.67E+06	(22)	6	309	130	66.2	38.8	116.5
55	4.94E+06	(178)	2.28E+06	(82)	36	192	43	75.2	56.5	100.1
56	3.27E+06	(49)	2.53E+06	(38)	15	213	69	44.9	28.8	70.5
57	4.22E+06	(38)	3.67E+06	(33)	9	309	107	40.1	24.5	66.0
58	3.50E+06	(42)	2.75E+06	(33)	12	231	80	44.3	27.4	72.1
59	5.22E+06	(47)	4.00E+06	(36)	9	337	112	45.4	28.8	72.2
60	5.75E+06	(69)	3.08E+06	(37)	12	260	85	64.7	42.9	99.4
61	4.83E+06	(29)	2.50E+06	(15)	6	210	107	66.9	34.9	134.4
62	3.70E+06	(37)	1.60E+06	(16)	10	135	66	79.9	43.7	153.9
63	9.25E+06	(37)	6.50E+06	(26)	4	547	213	49.5	29.2	85.1
64	7.47E+06	(127)	3.29E+06	(56)	17	277	74	78.7	57.1	109.8
65	6.40E+06	(128)	3.00E+06	(60)	20	253	65	74.0	54.2	102.5
66	3.87E+06	(58)	1.27E+06	(19)	15	107	48	105.2	62.3	187.2
67	6.11E+06	(110)	3.11E+06	(56)	18	262	70	68.2	49.1	95.9
68	5.82E+06	(64)	2.27E+06	(25)	11	191	76	88.5	55.3	146.8
69	5.81E+06	(93)	2.81E+06	(45)	16	237	71	71.7	49.8	104.9
70	7.50E+06	(30)	3.50E+06	(14)	4	295	155	74.0	38.4	151.2
71	1.00E+07	(40)	1.10E+07	(44)	4	926	279	31.7	20.1	49.8
72	3.50E+06	(21)	2.50E+06	(15)	6	210	107	48.6	24.0	101.3
73	2.25E+06	(9)	2.00E+06	(8)	4	168	116	39.1	13.4	116.2
74	4.60E+06	(92)	2.70E+06	(54)	20	227	62	59.2	41.9	84.5
75	7.40E+06	(37)	4.00E+06	(20)	5	337	149	64.1	36.4	116.7
76	4.63E+06	(111)	2.25E+06	(54)	24	189	52	71.4	51.2	100.8
77	6.88E+06	(55)	4.50E+06	(36)	8	379	126	53.1	34.3	83.3
78	6.78E+06	(122)	3.22E+06	(58)	18	271	71	73.0	53.1	101.7
79	5.22E+06	(261)	2.18E+06	(109)	50	184	36	82.9	64.4	106.8
80	1.89E+06	(17)	6.67E+05	(6)	9	56	44	96.6	37.1	299.9
81	2.90E+06	(29)	1.40E+06	(14)	10	118	62	71.6	36.9	146.7
82	7.17E+06	(43)	6.67E+06	(40)	6	561	177	37.5	23.8	59.1
83	3.33E+06	(50)	1.60E+06	(24)	15	135	55	72.2	43.7	122.9
84	4.60E+06	(184)	2.25E+06	(90)	40	189	40	70.9	53.7	93.6
85	6.75E+06	(27)	3.50E+06	(14)	4	295	155	66.7	34.0	137.7
86	4.33E+06	(104)	2.17E+06	(52)	24	182	51	69.4	49.4	98.9
87	9.50E+06	(76)	3.38E+06	(27)	8	284	109	97.3	62.3	157.1
88	6.50E+06	(91)	2.21E+06	(31)	14	186	67	101.5	67.2	157.9
89	6.67E+06	(80)	3.00E+06	(36)	12	253	84	77.0	51.5	117.6
90	4.85E+06	(97)	2.10E+06	(42)	20	177	55	80.1	55.4	118.0
91	3.29E+06	(46)	1.00E+06	(14)	14	84	44	112.9	61.7	222.6
92	7.00E+06	(42)	5.50E+06	(33)	6	463	161	44.3	27.4	72.1
93	8.75E+06	(35)	3.75E+06	(15)	4	316	161	80.6	43.2	158.9

94	7.00E+06	(42)	4.33E+06	(26)	6	365	142	56.1	33.7	95.3
95	8.40E+06	(42)	4.00E+06	(20)	5	337	149	72.7	42.0	130.8
96	7.75E+06	(62)	2.63E+06	(21)	8	221	96	101.9	61.7	176.0
97	2.27E+06	(34)	1.47E+06	(22)	15	123	52	53.7	30.6	96.3
98	7.44E+06	(67)	4.33E+06	(39)	9	365	117	59.7	39.7	91.0
99	6.40E+06	(96)	3.60E+06	(54)	15	303	83	61.8	43.9	88.0
100	8.20E+06	(82)	5.30E+06	(53)	10	446	123	53.8	37.7	77.6
101	4.67E+06	(126)	1.96E+06	(53)	27	165	45	82.4	59.5	116.0
102	6.80E+06	(68)	4.30E+06	(43)	10	362	110	55.0	37.0	82.6
103	5.70E+06	(57)	3.10E+06	(31)	10	261	93	63.8	40.6	102.3
104	7.75E+06	(31)	5.00E+06	(20)	4	421	186	53.8	29.8	99.6

YAKD4 (Alaska), modern sand

EFFECTIVE TRACK DENSITY FOR FLUENCE MONITOR (tracks/cm^2): 5.930E+05
RELATIVE ERROR (%): 1.58
EFFECTIVE URANIUM CONTENT OF MONITOR (ppm): 50.00
ZETA FACTOR AND STANDARD ERROR (yr cm^2): 117.70 7.10
SIZE OF COUNTER SQUARE (cm^2): 1.000E-06

Grain no.	**RhoS (cm^-2)**	**(Ns)**	**RhoI (cm^-2)**	**(Ni)**	**Squares**	**U+/-2s**		**Grain Age**	**Age (Ma) --95%**	**CI--**
1	2.00E+06	(20)	4.90E+06	(49)	10	413	118	14.3	8.0	24.4
2	5.56E+05	(5)	8.00E+06	(72)	9	675	160	2.5	0.8	5.9
3	1.20E+06	(12)	8.30E+06	(83)	10	700	155	5.1	2.5	9.3
4	1.50E+06	(18)	4.00E+06	(48)	12	337	97	13.2	7.2	22.9
5	1.27E+06	(19)	3.07E+06	(46)	15	259	76	14.5	8.0	25.1
6	1.56E+06	(14)	1.13E+07	(102)	9	956	191	4.8	2.5	8.4
7	1.92E+06	(23)	1.47E+07	(177)	12	1244	191	4.6	2.8	7.0
8	1.60E+06	(8)	8.60E+06	(43)	5	725	221	6.6	2.6	14.0
9	3.17E+06	(19)	1.35E+07	(81)	6	1138	255	8.2	4.7	13.6
10	6.67E+05	(4)	2.17E+06	(13)	6	183	100	11.0	2.5	34.7
11	0.00E+00	(0)	4.67E+06	(28)	6	393	148	0.9	0.0	4.9
12	3.75E+05	(3)	4.00E+06	(32)	8	337	119	3.4	0.6	10.5
13	2.50E+05	(3)	5.08E+06	(61)	12	429	110	1.8	0.3	5.3
14	3.00E+05	(12)	3.98E+06	(159)	40	335	54	2.7	1.3	4.7
15	1.00E+06	(12)	2.67E+06	(32)	12	225	79	13.2	6.1	26.1
16	1.17E+06	(7)	9.83E+06	(59)	6	829	217	4.2	1.6	9.1
17	7.27E+05	(8)	4.09E+06	(45)	11	345	103	6.3	2.5	13.3
18	7.33E+05	(11)	4.73E+06	(71)	15	399	95	5.5	2.6	10.3
19	1.58E+06	(19)	3.67E+06	(44)	12	309	93	15.1	8.3	26.3
20	1.00E+06	(6)	2.00E+06	(12)	6	169	96	17.7	5.4	50.1
21	5.00E+05	(8)	5.19E+06	(83)	16	437	97	3.4	1.4	6.9
22	9.26E+05	(25)	6.93E+06	(187)	27	584	87	4.7	2.9	7.1
23	8.89E+05	(16)	7.28E+06	(131)	18	614	109	4.3	2.4	7.2
24	2.11E+06	(19)	8.78E+06	(79)	9	740	168	8.4	4.8	14.0
25	1.25E+05	(2)	6.00E+06	(96)	16	506	104	0.8	0.1	2.7
26	6.92E+05	(9)	9.54E+06	(124)	13	804	146	2.6	1.1	5.0
27	1.25E+06	(15)	7.58E+06	(91)	12	639	135	5.8	3.1	10.0
28	1.25E+06	(20)	1.51E+07	(242)	16	1275	169	2.9	1.7	4.6
29	3.33E+06	(20)	8.33E+06	(50)	6	703	199	14.0	7.9	23.9
30	3.13E+05	(5)	7.38E+06	(118)	16	622	116	1.5	0.5	3.6
31	1.00E+06	(12)	8.33E+06	(100)	12	703	142	4.2	2.1	7.6
32	7.50E+05	(9)	1.02E+07	(122)	12	857	157	2.6	1.1	5.1
33	5.00E+05	(4)	3.13E+06	(25)	8	263	105	5.8	1.4	16.2
34	1.00E+06	(12)	5.42E+06	(65)	12	457	114	6.5	3.2	12.0
35	0.00E+00	(0)	1.11E+06	(10)	9	94	58	2.5	0.1	15.6
36	0.00E+00	(0)	4.17E+05	(10)	24	35	22	2.5	0.1	15.6

37	6.25E+05	(	5)	8.25E+06	(	66)	8	696	172	2.7	0.8	6.5
38	1.57E+06	(	22)	1.16E+07	(	163)	14	982	157	4.7	2.9	7.4
39	5.56E+05	(	5)	5.11E+06	(	46)	9	431	127	3.9	1.2	9.5
40	6.67E+05	(	4)	4.67E+06	(	28)	6	393	148	5.2	1.3	14.2
41	3.33E+05	(	16)	4.52E+06	(	217)	48	381	53	2.6	1.4	4.3
42	1.83E+06	(	22)	8.58E+06	(	103)	12	724	144	7.5	4.5	11.9
43	1.00E+06	(	8)	9.75E+06	(	78)	8	822	187	3.6	1.5	7.4
44	1.29E+06	(	18)	1.19E+07	(	167)	14	1006	159	3.8	2.2	6.1
45	8.75E+05	(	14)	5.50E+06	(	88)	16	464	100	5.6	2.9	9.8
46	1.50E+06	(	12)	8.88E+06	(	71)	8	748	179	6.0	2.9	11.0
47	7.78E+05	(	7)	2.11E+06	(	19)	9	178	81	13.0	4.6	31.9
48	5.63E+05	(	9)	7.50E+06	(	120)	16	632	117	2.7	1.2	5.1
49	5.00E+05	(	5)	7.90E+06	(	79)	10	666	151	2.3	0.7	5.4
50	6.25E+04	(	1)	4.81E+06	(	77)	16	406	93	0.5	0.0	2.6
51	3.33E+05	(	4)	3.08E+06	(	37)	12	260	85	3.9	1.0	10.5
52	2.33E+06	(	35)	1.32E+07	(	198)	15	1113	162	6.2	4.2	8.9
53	2.95E+06	(	56)	2.32E+07	(	441)	19	1957	196	4.4	3.3	5.9
54	1.88E+05	(	3)	1.00E+06	(	16)	16	84	42	6.8	1.2	22.8
55	4.17E+05	(	10)	2.00E+06	(	48)	24	169	49	7.4	3.3	14.6
56	6.25E+05	(	10)	8.38E+06	(	134)	16	706	124	2.6	1.2	4.9
57	1.00E+06	(	8)	6.25E+06	(	50)	8	527	149	5.7	2.3	11.9
58	8.75E+05	(	7)	5.13E+06	(	41)	8	432	135	6.1	2.3	13.4
59	4.38E+05	(	7)	8.81E+06	(	141)	16	743	127	1.8	0.7	3.7
60	8.33E+05	(	10)	8.67E+06	(	104)	12	731	145	3.4	1.6	6.4
61	1.38E+06	(	33)	1.50E+07	(	360)	24	1265	139	3.2	2.2	4.6
62	2.13E+06	(	32)	4.00E+06	(	60)	15	337	87	18.6	11.7	29.0
63	1.70E+06	(	34)	1.70E+07	(	339)	20	1429	162	3.5	2.4	5.0
64	1.50E+06	(	12)	7.63E+06	(	61)	8	643	165	6.9	3.4	12.9
65	1.71E+06	(	24)	5.86E+06	(	82)	14	494	110	10.3	6.2	16.3
66	1.25E+06	(	10)	1.44E+07	(	115)	8	1212	229	3.1	1.4	5.8
67	5.83E+05	(	7)	6.58E+06	(	79)	12	555	126	3.2	1.2	6.7
68	1.72E+06	(	31)	1.78E+07	(	320)	18	1499	174	3.4	2.3	4.9
69	5.63E+05	(	9)	7.25E+06	(	116)	16	611	115	2.8	1.2	5.3
70	1.88E+06	(	15)	8.25E+06	(	66)	8	696	172	8.0	4.2	14.0
71	1.33E+06	(	8)	1.03E+07	(	62)	6	871	222	4.6	1.9	9.4
72	1.50E+06	(	12)	1.45E+07	(	116)	8	1223	230	3.7	1.8	6.6
73	2.50E+05	(	3)	2.33E+06	(	28)	12	197	74	3.9	0.7	12.1
74	1.25E+06	(	15)	1.15E+07	(	138)	12	970	168	3.8	2.1	6.5
75	2.50E+05	(	5)	2.70E+06	(	54)	20	228	62	3.3	1.0	8.0
76	1.43E+05	(	1)	8.29E+06	(	58)	7	699	184	0.7	0.0	3.5
77	3.75E+05	(	3)	1.00E+06	(	8)	8	84	58	13.5	2.2	54.3
78	0.00E+00	(	0)	8.33E+05	(	5)	6	70	60	5.2	0.2	38.0
79	1.24E+06	(	26)	8.86E+06	(	186)	21	747	112	4.9	3.1	7.4
80	2.60E+06	(	39)	2.83E+07	(	425)	15	2389	244	3.2	2.2	4.5
81	1.10E+06	(	23)	8.81E+06	(	185)	21	743	112	4.4	2.7	6.7
82	9.09E+05	(	10)	4.00E+06	(	44)	11	337	102	8.0	3.6	16.0
83	0.00E+00	(	0)	1.06E+06	(	19)	18	89	40	1.3	0.0	7.5
84	5.00E+05	(	3)	9.67E+06	(	58)	6	815	215	1.9	0.4	5.5
85	3.43E+06	(	48)	1.27E+07	(	178)	14	1072	164	9.4	6.7	13.0
86	7.11E+05	(	32)	7.53E+06	(	339)	45	635	72	3.3	2.2	4.7
87	5.00E+05	(	4)	4.13E+06	(	33)	8	348	121	4.4	1.1	11.9
88	8.06E+05	(	29)	8.44E+06	(	304)	36	712	85	3.3	2.2	4.9
89	8.00E+04	(	2)	3.32E+06	(	83)	25	280	62	0.9	0.1	3.1
90	6.67E+05	(	4)	6.17E+06	(	37)	6	520	171	3.9	1.0	10.5
91	4.67E+05	(	14)	4.50E+06	(	135)	30	379	66	3.7	1.9	6.3
92	4.38E+05	(	7)	2.19E+06	(	35)	16	184	62	7.1	2.6	15.9

93	7.14E+05	(5)	5.71E+06	(40)	7	482	152	4.5	1.3	11.1
94	1.20E+06	(18)	6.67E+06	(100)	15	562	114	6.3	3.6	10.4
95	3.13E+05	(5)	2.50E+06	(40)	16	211	67	4.5	1.3	11.1
96	7.00E+05	(7)	7.70E+06	(77)	10	649	149	3.2	1.2	6.9
97	6.52E+05	(15)	6.83E+06	(157)	23	576	94	3.4	1.8	5.7
98	4.17E+05	(5)	9.42E+06	(113)	12	794	151	1.6	0.5	3.7
99	4.17E+05	(5)	7.33E+06	(88)	12	618	133	2.0	0.6	4.8
100	1.00E+06	(14)	7.07E+06	(99)	14	596	121	5.0	2.6	8.7
101	5.00E+05	(4)	9.38E+06	(75)	8	790	184	1.9	0.5	5.0
102	3.33E+05	(2)	5.00E+06	(30)	6	422	153	2.5	0.3	9.2
103	5.67E+05	(17)	2.73E+06	(82)	30	230	51	7.3	4.0	12.3

YAKD5 (Alaska), modern sand

EFFECTIVE TRACK DENSITY FOR FLUENCE MONITOR (tracks/cm^2): 5.930E+05
RELATIVE ERROR (%): 1.58
EFFECTIVE URANIUM CONTENT OF MONITOR (ppm): 50.00
ZETA FACTOR AND STANDARD ERROR (yr cm^2): 117.70 7.10
SIZE OF COUNTER SQUARE (cm^2): 1.000E-06

Grain no.	**RhoS (cm^-2)**	**(Ns)**	**RhoI (cm^-2)**	**(Ni)**	**Squares**	**U+/-2s**		**Grain Age**	**Age (Ma) --95%**	**CI--**
1	2.50E+05	(4)	6.88E+05	(11)	16	58	34	13.0	2.9	42.7
2	2.00E+05	(4)	1.45E+06	(29)	20	122	45	5.0	1.2	13.7
3	1.05E+06	(21)	1.06E+07	(212)	20	894	126	3.5	2.1	5.4
4	8.40E+06	(42)	2.74E+07	(137)	5	2310	401	10.7	7.4	15.2
5	7.00E+05	(21)	6.90E+06	(207)	30	582	83	3.6	2.1	5.6
6	2.20E+06	(22)	2.20E+07	(220)	10	1855	257	3.5	2.1	5.4
7	7.33E+05	(11)	4.40E+06	(66)	15	371	92	5.9	2.8	11.1
8	7.50E+05	(3)	4.25E+06	(17)	4	358	172	6.4	1.2	21.3
9	1.88E+05	(3)	1.13E+06	(18)	16	95	44	6.1	1.1	19.9
10	9.26E+05	(25)	1.31E+07	(353)	27	1102	122	2.5	1.6	3.7
11	6.25E+05	(15)	9.58E+06	(230)	24	808	109	2.3	1.3	3.8
12	7.86E+05	(22)	7.00E+06	(196)	28	590	86	3.9	2.4	6.1
13	6.67E+05	(4)	9.00E+06	(54)	6	759	207	2.7	0.7	7.0
14	1.75E+06	(14)	8.63E+06	(69)	8	727	176	7.1	3.7	12.7
15	1.56E+06	(25)	1.05E+07	(168)	16	885	139	5.2	3.3	7.9
16	2.80E+06	(42)	1.62E+07	(243)	15	1366	180	6.1	4.2	8.4
17	3.33E+05	(5)	6.13E+06	(92)	15	517	109	2.0	0.6	4.6
18	8.67E+05	(13)	7.07E+06	(106)	15	596	117	4.3	2.2	7.6
19	2.00E+06	(10)	9.60E+06	(48)	5	809	234	7.4	3.3	14.6
20	3.50E+06	(35)	1.14E+07	(114)	10	961	182	10.7	7.1	15.8
21	1.00E+06	(9)	5.56E+05	(5)	9	47	40	61.7	18.9	234.4
22	5.00E+05	(3)	1.67E+06	(10)	6	141	87	10.8	1.9	40.6
23	2.50E+05	(4)	1.81E+06	(29)	16	153	56	5.0	1.2	13.7
24	3.60E+05	(9)	4.92E+06	(123)	25	415	76	2.6	1.1	5.0
25	2.14E+05	(3)	1.29E+06	(18)	14	108	51	6.1	1.1	19.9
26	1.33E+06	(12)	1.23E+07	(111)	9	1040	200	3.8	1.9	6.9
27	1.16E+06	(22)	9.37E+06	(178)	19	790	121	4.3	2.6	6.7
28	1.22E+06	(11)	3.56E+06	(32)	9	300	106	12.1	5.5	24.4
29	8.75E+05	(21)	1.09E+07	(261)	24	917	117	2.8	1.7	4.4
30	7.50E+05	(9)	1.05E+07	(126)	12	885	160	2.5	1.1	4.9
31	3.00E+05	(3)	1.50E+06	(15)	10	126	64	7.3	1.3	24.6
32	5.00E+06	(35)	2.17E+07	(152)	7	1831	302	8.1	5.4	11.7
33	3.75E+05	(18)	4.46E+06	(214)	48	376	53	3.0	1.7	4.8
34	1.38E+06	(11)	8.13E+06	(65)	8	685	171	6.0	2.8	11.3
35	4.00E+05	(6)	2.87E+06	(43)	15	242	74	5.0	1.7	11.5
36	1.13E+06	(17)	7.07E+06	(106)	15	596	117	5.6	3.1	9.4

37	5.50E+05	(11)	8.30E+06	(166)	20	700	111	2.3	1.1	4.3
38	7.69E+04	(1)	3.46E+06	(45)	13	292	87	0.9	0.0	4.5
39	1.68E+06	(42)	2.09E+07	(523)	25	1764	164	2.8	2.0	3.8
40	2.76E+06	(47)	1.53E+06	(26)	17	129	50	62.6	38.1	105.4
41	4.67E+05	(7)	5.27E+06	(79)	15	444	101	3.2	1.2	6.7
42	6.33E+05	(19)	4.47E+06	(134)	30	377	66	5.0	2.9	8.0
43	2.30E+06	(23)	3.00E+06	(30)	10	253	92	26.7	14.8	47.5
44	5.45E+05	(18)	1.42E+06	(47)	33	120	35	13.4	7.3	23.4
45	2.22E+06	(20)	2.16E+07	(194)	9	1818	267	3.6	2.1	5.7
46	7.50E+05	(30)	4.60E+06	(184)	40	388	58	5.7	3.7	8.4
47	6.67E+05	(6)	1.06E+07	(95)	9	890	184	2.3	0.8	5.0
48	9.33E+05	(28)	3.70E+06	(111)	30	312	60	8.8	5.6	13.4
49	3.53E+06	(53)	2.17E+07	(325)	15	1827	211	5.7	4.2	7.6
50	1.53E+06	(23)	5.93E+06	(89)	15	500	107	9.1	5.4	14.4
51	8.57E+05	(6)	4.00E+06	(28)	7	337	127	7.6	2.5	18.4
52	1.73E+06	(19)	8.18E+06	(90)	11	690	147	7.4	4.2	12.2
53	8.00E+06	(64)	1.54E+07	(123)	8	1296	237	18.2	13.2	24.8
54	3.25E+06	(26)	2.73E+07	(218)	8	2298	319	4.2	2.7	6.3
55	1.00E+06	(15)	7.67E+06	(115)	15	646	122	4.6	2.5	7.8
56	1.13E+06	(34)	4.83E+06	(145)	30	408	69	8.2	5.5	12.0
57	1.67E+06	(10)	5.50E+06	(33)	6	464	161	10.7	4.6	22.0
58	1.67E+05	(1)	1.50E+06	(9)	6	126	82	4.4	0.1	27.9
59	1.60E+07	(64)	1.95E+07	(78)	4	1644	375	28.6	20.2	40.3
60	3.33E+05	(2)	1.83E+06	(11)	6	155	91	6.7	0.7	29.0
61	2.28E+06	(57)	6.20E+06	(155)	25	523	85	12.8	9.3	17.5
62	1.38E+06	(22)	9.31E+06	(149)	16	785	131	5.2	3.1	8.1
63	7.56E+06	(136)	4.67E+06	(84)	18	393	87	56.2	42.5	74.8
64	4.17E+05	(5)	3.42E+06	(41)	12	288	90	4.4	1.3	10.8
65	0.00E+00	(0)	2.20E+06	(44)	20	185	56	0.6	0.0	3.1
66	2.73E+06	(30)	1.50E+07	(165)	11	1265	201	6.4	4.1	9.4
67	4.00E+05	(12)	1.90E+06	(57)	30	160	43	7.4	3.6	13.9
68	6.67E+04	(2)	7.00E+05	(21)	30	59	26	3.6	0.4	13.6
69	2.00E+06	(8)	6.75E+06	(27)	4	569	218	10.5	4.1	23.4
70	5.33E+05	(8)	4.60E+06	(69)	15	388	94	4.1	1.7	8.4
71	1.65E+06	(43)	8.81E+06	(229)	26	743	101	6.6	4.6	9.1
72	1.24E+06	(26)	9.29E+06	(195)	21	783	115	4.7	3.0	7.0
73	2.89E+06	(26)	1.60E+07	(144)	9	1349	228	6.3	4.0	9.6
74	1.14E+06	(32)	1.41E+07	(395)	28	1189	125	2.8	1.9	4.1
75	4.00E+05	(14)	1.77E+06	(62)	35	149	38	7.9	4.1	14.2
76	3.00E+06	(12)	1.68E+07	(67)	4	1412	347	6.3	3.1	11.7
77	2.13E+06	(51)	1.30E+07	(312)	24	1096	129	5.7	4.1	7.7
78	2.71E+06	(19)	1.33E+07	(93)	7	1120	234	7.2	4.1	11.8
79	8.92E+06	(214)	7.50E+06	(180)	24	632	96	41.3	32.8	52.1
80	0.00E+00	(0)	5.63E+05	(9)	16	47	31	2.8	0.1	17.7
81	3.64E+05	(4)	2.73E+06	(30)	11	230	84	4.8	1.2	13.2
82	4.81E+06	(77)	2.56E+06	(41)	16	216	67	65.1	44.1	97.6
83	8.10E+05	(17)	8.29E+06	(174)	21	699	108	3.4	1.9	5.6
84	4.81E+05	(13)	6.00E+06	(162)	27	506	81	2.8	1.5	4.9
85	5.57E+06	(39)	1.53E+07	(107)	7	1289	252	12.7	8.6	18.5
86	7.86E+05	(11)	1.07E+07	(150)	14	903	150	2.6	1.2	4.7
87	0.00E+00	(0)	7.67E+06	(92)	12	646	136	0.3	0.0	1.4
88	8.00E+05	(8)	1.18E+07	(118)	10	995	185	2.4	1.0	4.8
89	2.50E+05	(3)	1.58E+06	(19)	12	134	61	5.8	1.0	18.7
90	1.94E+06	(35)	2.12E+07	(382)	18	1789	192	3.2	2.2	4.5
91	3.13E+05	(5)	3.69E+06	(59)	16	311	81	3.0	0.9	7.3
92	1.20E+06	(12)	1.46E+07	(146)	10	1231	207	2.9	1.4	5.2

93	1.82E+05	(2)	5.73E+06	(63)	11	483	122	1.2	0.1	4.2
94	8.57E+05	(6)	7.00E+06	(49)	7	590	169	4.4	1.5	10.0
95	7.50E+05	(9)	6.67E+06	(80)	12	562	127	4.0	1.7	7.8
96	1.58E+06	(19)	8.75E+06	(105)	12	738	146	6.4	3.7	10.4
97	1.31E+06	(17)	8.15E+06	(106)	13	688	135	5.6	3.1	9.4
98	6.47E+05	(11)	6.59E+06	(112)	17	556	106	3.5	1.7	6.4
99	1.17E+05	(7)	1.38E+06	(83)	60	117	26	3.0	1.1	6.3
100	8.00E+05	(8)	5.70E+06	(57)	10	481	128	5.0	2.0	10.3
101	6.67E+05	(8)	7.67E+06	(92)	12	646	136	3.1	1.3	6.2
102	9.29E+05	(13)	8.57E+06	(120)	14	723	134	3.8	2.0	6.7
103	2.00E+06	(20)	2.25E+07	(225)	10	1897	260	3.1	1.9	4.9
104	1.80E+06	(36)	1.55E+07	(309)	20	1303	154	4.1	2.8	5.8
105	2.20E+06	(33)	1.21E+07	(181)	15	1017	154	6.4	4.2	9.3

YAKD29 (Alaska), modern sand
EFFECTIVE TRACK DENSITY FOR FLUENCE MONITOR (tracks/cm^2): 5.930E+05
RELATIVE ERROR (%): 1.58
EFFECTIVE URANIUM CONTENT OF MONITOR (ppm): 50.00
ZETA FACTOR AND STANDARD ERROR (yr cm^2): 117.70 7.10
SIZE OF COUNTER SQUARE (cm^2): 1.000E-06

Grain no.	**RhoS (cm^-2)**	**(Ns)**	**RhoI (cm^-2)**	**(Ni)**	**Squares**	**U+/-2s**		**Grain Age**	**Age (Ma) --95% CI--**	
1	9.00E+06	(54)	5.17E+06	(31)	6	436	156	60.4	38.2	97.2
2	4.93E+06	(74)	4.07E+06	(61)	15	343	88	42.2	29.6	60.2
3	9.75E+06	(117)	4.75E+06	(57)	12	401	106	71.1	51.5	99.5
4	8.64E+06	(121)	6.79E+06	(95)	14	572	118	44.3	33.5	58.6
5	7.38E+06	(59)	2.88E+06	(23)	8	242	100	88.5	54.2	150.3
6	8.08E+06	(97)	4.83E+06	(58)	12	408	107	58.0	41.5	81.9
7	8.13E+06	(122)	7.07E+06	(106)	15	596	117	40.0	30.1	53.3
8	4.07E+06	(110)	2.89E+06	(78)	27	244	56	49.0	36.3	66.4
9	5.20E+06	(52)	2.60E+06	(26)	10	219	85	69.2	42.6	115.5
10	1.10E+07	(44)	3.00E+06	(12)	4	253	143	125.5	66.0	261.0
11	3.73E+06	(56)	1.93E+06	(29)	15	163	60	66.9	42.1	108.7
12	8.17E+06	(49)	2.17E+06	(13)	6	183	100	129.0	69.8	259.3
13	1.00E+07	(60)	6.67E+06	(40)	6	562	178	52.1	34.4	79.8
14	1.18E+07	(71)	6.17E+06	(37)	6	520	171	66.5	44.2	101.9
15	3.50E+06	(21)	2.83E+06	(17)	6	239	114	42.9	21.6	86.5
16	8.44E+06	(135)	7.50E+06	(120)	16	632	117	39.1	29.8	51.4
17	7.57E+06	(53)	6.71E+06	(47)	7	566	165	39.2	26.0	59.4
18	9.25E+06	(37)	6.25E+06	(25)	4	527	209	51.3	30.2	89.0
19	6.53E+06	(111)	6.59E+06	(112)	17	556	106	34.5	25.9	46.0
20	8.00E+06	(40)	8.40E+06	(42)	5	708	218	33.2	21.0	52.4
21	3.08E+06	(37)	1.33E+06	(16)	12	112	55	79.8	43.6	153.7
22	1.01E+07	(161)	5.63E+06	(90)	16	474	101	62.0	46.7	82.3
23	5.13E+06	(41)	3.75E+06	(30)	8	316	115	47.5	29.0	78.7
24	5.11E+06	(46)	4.22E+06	(38)	9	356	115	42.1	26.8	66.5
25	5.43E+06	(38)	6.57E+06	(46)	7	554	163	28.8	18.2	45.2
26	8.67E+06	(52)	8.17E+06	(49)	6	689	197	36.9	24.5	55.7
27	5.00E+06	(60)	2.83E+06	(34)	12	239	82	61.2	39.6	96.2
28	4.44E+06	(80)	2.56E+06	(46)	18	215	64	60.3	41.5	88.7
29	6.39E+06	(115)	4.89E+06	(88)	18	412	89	45.4	34.1	60.7
30	7.60E+06	(38)	1.16E+07	(58)	5	978	258	22.9	14.7	35.0
31	4.91E+06	(172)	2.43E+06	(85)	35	205	45	70.0	52.6	93.1
32	9.64E+06	(135)	6.50E+06	(91)	14	548	116	51.5	38.5	68.8
33	7.33E+06	(88)	4.67E+06	(56)	12	393	105	54.6	38.6	77.8
34	8.33E+06	(100)	8.33E+06	(100)	12	703	142	34.8	26.1	46.4

35	8.00E+06	(48)	6.33E+06	(38)	6	534	173	43.9	28.1	69.1
36	8.00E+06	(48)	5.17E+06	(31)	6	436	156	53.7	33.6	87.3
37	3.60E+06	(18)	5.40E+06	(27)	5	455	174	23.3	12.1	43.7
38	4.94E+06	(79)	3.13E+06	(50)	16	263	75	54.8	38.0	79.9
39	1.37E+07	(82)	9.00E+06	(54)	6	759	207	52.7	37.0	75.8
40	9.00E+06	(54)	9.33E+06	(56)	6	787	211	33.6	22.7	49.7
41	6.33E+06	(76)	3.25E+06	(39)	12	274	88	67.5	45.4	102.1
42	1.36E+07	(68)	1.10E+07	(55)	5	927	251	43.0	29.7	62.5
43	7.00E+06	(63)	5.78E+06	(52)	9	487	135	42.1	28.7	62.1
44	5.13E+06	(41)	1.88E+06	(15)	8	158	80	94.1	51.4	183.1
45	1.11E+07	(111)	7.30E+06	(73)	10	616	145	52.8	39.0	72.0
46	9.00E+06	(54)	3.83E+06	(23)	6	323	134	81.1	49.2	138.5
47	6.00E+06	(36)	4.17E+06	(25)	6	351	140	50.0	29.3	86.8
48	6.50E+06	(52)	4.38E+06	(35)	8	369	124	51.6	33.0	81.6
49	8.38E+06	(134)	6.38E+06	(102)	16	538	108	45.6	34.4	60.6
50	9.33E+06	(56)	5.67E+06	(34)	6	478	163	57.1	36.7	90.3
51	6.50E+06	(52)	2.50E+06	(20)	8	211	93	89.7	53.0	158.7
52	7.17E+06	(43)	8.00E+06	(48)	6	675	195	31.2	20.2	48.1
53	2.65E+06	(90)	1.79E+06	(61)	34	151	39	51.2	36.6	72.2
54	1.11E+07	(100)	8.44E+06	(76)	9	712	164	45.7	33.6	62.5
55	5.11E+06	(46)	2.44E+06	(22)	9	206	87	72.3	42.8	126.3
56	9.83E+06	(59)	7.00E+06	(42)	6	590	182	48.8	32.3	74.3
57	4.50E+06	(54)	2.67E+06	(32)	12	225	79	58.5	37.2	93.7
58	9.50E+06	(57)	9.50E+06	(57)	6	801	213	34.8	23.7	51.2
59	5.00E+06	(45)	2.56E+06	(23)	9	215	89	67.7	40.3	117.3
60	6.50E+06	(52)	4.63E+06	(37)	8	390	128	48.8	31.5	76.6
61	4.88E+06	(78)	1.44E+06	(23)	16	121	50	116.7	73.0	194.8
62	2.67E+06	(16)	3.67E+06	(22)	6	309	131	25.4	12.4	50.4
63	7.14E+06	(150)	5.62E+06	(118)	21	474	88	44.2	33.7	57.8
64	9.00E+06	(36)	8.00E+06	(32)	4	675	238	39.1	23.6	65.0
65	5.20E+06	(104)	2.05E+06	(41)	20	173	54	87.7	60.7	129.3
66	1.15E+07	(46)	4.75E+06	(19)	4	401	182	83.5	48.3	151.1
67	7.50E+06	(30)	5.50E+06	(22)	4	464	196	47.3	26.5	86.1
68	1.43E+07	(86)	1.40E+07	(84)	6	1180	260	35.6	26.0	48.8
69	1.60E+07	(160)	6.80E+06	(68)	10	573	140	81.5	61.1	110.0
70	4.67E+06	(28)	2.83E+06	(17)	6	239	114	57.0	30.3	111.1
71	1.05E+07	(63)	4.67E+06	(28)	6	393	148	77.8	49.3	126.2
72	5.50E+06	(44)	2.38E+06	(19)	8	200	91	79.9	46.0	145.1
73	3.35E+06	(134)	2.90E+06	(116)	40	245	46	40.2	30.5	52.9
74	1.07E+07	(96)	5.56E+06	(50)	9	468	133	66.6	46.9	95.7
75	1.10E+07	(44)	7.25E+06	(29)	4	611	226	52.6	32.3	87.3
76	8.78E+06	(79)	7.56E+06	(68)	9	637	155	40.4	28.8	56.8
77	7.50E+06	(45)	5.33E+06	(32)	6	450	158	48.8	30.4	79.4
78	7.00E+06	(56)	5.13E+06	(41)	8	432	135	47.4	31.2	72.8
79	6.50E+06	(39)	2.83E+06	(17)	6	239	114	79.2	44.1	149.3
80	4.79E+06	(67)	2.43E+06	(34)	14	205	70	68.3	44.7	106.4
81	6.93E+06	(97)	7.93E+06	(111)	14	669	128	30.4	22.9	40.4
82	9.00E+06	(54)	5.67E+06	(34)	6	478	163	55.1	35.3	87.3
83	5.70E+06	(57)	2.40E+06	(24)	10	202	82	82.0	50.4	138.3
84	5.50E+06	(44)	1.75E+06	(14)	8	148	78	107.9	58.7	213.3
85	4.58E+06	(55)	4.17E+06	(50)	12	351	99	38.3	25.6	57.3
86	4.20E+06	(84)	3.05E+06	(61)	20	257	66	47.9	34.0	67.7
87	1.04E+07	(52)	6.60E+06	(33)	5	556	193	54.7	34.8	87.3
88	4.58E+06	(55)	1.75E+06	(21)	12	148	64	90.3	54.1	157.4
89	5.75E+06	(138)	2.75E+06	(66)	24	232	57	72.5	53.7	98.8
90	7.42E+06	(89)	6.50E+06	(78)	12	548	125	39.7	28.9	54.5

91	7.00E+06	(119)	3.53E+06	(60)	17	298	77	68.8	50.1	95.5
92	4.14E+06	(58)	3.64E+06	(51)	14	307	86	39.6	26.7	58.8
93	5.58E+06	(67)	3.00E+06	(36)	12	253	84	64.5	42.5	99.6
94	6.77E+06	(203)	3.83E+06	(115)	30	323	61	61.2	47.3	79.2
95	4.61E+06	(83)	2.39E+06	(43)	18	201	61	66.9	45.8	99.1
96	4.48E+06	(94)	1.95E+06	(41)	21	165	51	79.3	54.6	117.6
97	4.83E+06	(116)	2.33E+06	(56)	24	197	53	71.8	51.8	100.7
98	4.50E+06	(36)	3.00E+06	(24)	8	253	103	52.0	30.3	91.2
99	8.75E+06	(35)	2.75E+06	(11)	4	232	137	109.0	54.8	238.1
100	6.88E+06	(55)	5.75E+06	(46)	8	485	143	41.6	27.6	62.9
101	6.44E+06	(232)	3.39E+06	(122)	36	286	52	65.9	51.3	84.5
102	5.50E+06	(77)	4.29E+06	(60)	14	361	94	44.6	31.4	63.6

YAKD30 (Alaska), modern sand

EFFECTIVE TRACK DENSITY FOR FLUENCE MONITOR (tracks/cm^2): 5.930E+05
RELATIVE ERROR (%): 1.58
EFFECTIVE URANIUM CONTENT OF MONITOR (ppm): 50.00
ZETA FACTOR AND STANDARD ERROR (yr cm^2): 117.70 7.10
SIZE OF COUNTER SQUARE (cm^2): 1.000E-06

Grain no.	**RhoS (cm^-2)**	**(Ns)**	**RhoI (cm^-2)**	**(Ni)**	**Squares**	**U+/-2s**		**Grain Age**	**Age (Ma) --95%**	**CI--**
1	3.33E+04	(2)	1.02E+06	(61)	60	86	22	1.2	0.1	4.3
2	1.39E+06	(25)	1.59E+07	(286)	18	1340	164	3.1	1.9	4.6
3	1.46E+06	(35)	1.31E+07	(315)	24	1107	129	3.9	2.6	5.5
4	9.12E+05	(31)	6.15E+06	(209)	34	518	73	5.2	3.4	7.6
5	1.71E+06	(65)	1.26E+07	(479)	38	1063	103	4.8	3.6	6.3
6	2.03E+06	(71)	1.84E+07	(643)	35	1549	132	3.9	2.9	5.1
7	6.67E+04	(1)	4.87E+06	(73)	15	410	97	0.5	0.0	2.8
8	5.00E+05	(7)	3.71E+06	(52)	14	313	87	4.8	1.8	10.4
9	6.67E+04	(4)	6.33E+05	(38)	60	53	17	3.8	1.0	10.2
10	7.67E+05	(23)	4.37E+06	(131)	30	368	65	6.2	3.7	9.6
11	8.75E+05	(28)	7.41E+06	(237)	32	624	83	4.1	2.7	6.1
12	7.92E+05	(19)	5.08E+06	(122)	24	429	79	5.5	3.2	8.9
13	1.87E+06	(28)	3.87E+06	(58)	15	326	86	16.9	10.3	26.9
14	1.63E+05	(13)	1.21E+06	(97)	80	102	21	4.7	2.4	8.4
15	6.80E+05	(17)	9.16E+06	(229)	25	772	105	2.6	1.5	4.2
16	1.00E+06	(15)	4.80E+06	(72)	15	405	96	7.3	3.9	12.8
17	4.00E+05	(20)	3.22E+06	(161)	50	272	44	4.4	2.6	6.9
18	8.57E+05	(24)	5.86E+06	(164)	28	494	79	5.1	3.2	7.9
19	8.75E+05	(35)	7.18E+06	(287)	40	605	74	4.3	2.9	6.1
20	5.56E+05	(5)	5.00E+06	(45)	9	422	126	4.0	1.2	9.7
21	5.50E+05	(11)	7.70E+06	(154)	20	649	106	2.5	1.2	4.6
22	5.00E+05	(9)	5.44E+06	(98)	18	459	94	3.3	1.4	6.3
23	4.76E+04	(2)	8.33E+05	(35)	42	70	24	2.1	0.2	7.8
24	3.33E+05	(8)	1.96E+06	(47)	24	165	48	6.0	2.4	12.7
25	3.21E+05	(9)	2.36E+06	(66)	28	199	49	4.8	2.1	9.6
26	5.00E+05	(5)	3.80E+06	(38)	10	320	104	4.7	1.4	11.7
27	1.33E+05	(4)	3.33E+06	(100)	30	281	57	1.5	0.4	3.7
28	8.33E+05	(15)	2.11E+06	(38)	18	178	58	13.9	7.0	25.6
29	8.75E+05	(7)	3.63E+06	(29)	8	306	113	8.6	3.1	19.6
30	5.83E+05	(7)	4.08E+06	(49)	12	344	98	5.1	1.9	11.1
31	1.00E+06	(6)	9.33E+06	(56)	6	787	211	3.8	1.3	8.7
32	7.20E+05	(18)	8.92E+06	(223)	25	752	103	2.8	1.6	4.6
33	5.00E+05	(25)	5.80E+06	(290)	50	489	59	3.0	1.9	4.5
34	6.60E+06	(132)	7.55E+06	(151)	20	637	105	30.4	23.4	39.6
35	8.13E+05	(13)	7.56E+06	(121)	16	638	117	3.8	1.9	6.7

36	8.33E+05 (5)	1.15E+07 (69)	6	970	235	2.6	0.8	6.2
37	5.00E+05 (5)	7.20E+06 (72)	10	607	144	2.5	0.8	5.9
38	4.50E+06 (36)	4.13E+06 (33)	8	348	121	37.9	23.0	62.8
39	4.44E+05 (16)	4.08E+06 (147)	36	344	58	3.8	2.1	6.4
40	9.17E+05 (11)	1.12E+07 (134)	12	942	165	2.9	1.4	5.3
41	1.17E+06 (21)	1.01E+07 (182)	18	853	129	4.1	2.4	6.3
42	6.11E+05 (11)	2.44E+06 (44)	18	206	62	8.8	4.1	17.2
43	2.92E+05 (7)	7.29E+06 (175)	24	615	95	1.4	0.6	2.9
44	8.89E+05 (16)	7.33E+06 (132)	18	618	109	4.3	2.3	7.1
45	2.44E+06 (22)	3.22E+06 (29)	9	272	100	26.5	14.5	47.6
46	1.06E+06 (19)	1.31E+07 (236)	18	1105	148	2.8	1.7	4.5
47	2.29E+05 (16)	3.71E+06 (260)	70	313	40	2.2	1.2	3.6
48	8.67E+05 (13)	2.73E+06 (41)	15	230	72	11.2	5.4	21.1
49	1.75E+06 (28)	1.53E+07 (245)	16	1291	170	4.0	2.6	5.9
50	3.04E+05 (17)	3.96E+06 (222)	56	334	46	2.7	1.5	4.4
51	8.25E+05 (33)	8.78E+06 (351)	40	740	82	3.3	2.2	4.7
52	1.83E+06 (22)	2.50E+06 (30)	12	211	77	25.6	14.0	45.8
53	3.13E+05 (5)	1.44E+06 (23)	16	121	50	7.8	2.3	20.4
54	8.00E+05 (24)	1.64E+07 (493)	30	1386	132	1.7	1.1	2.6
55	2.50E+05 (10)	4.95E+06 (198)	40	417	61	1.8	0.8	3.3
56	6.79E+05 (19)	1.22E+07 (342)	28	1030	116	2.0	1.2	3.1
57	2.00E+05 (2)	3.60E+06 (36)	10	304	101	2.1	0.2	7.5
58	3.21E+05 (9)	5.50E+06 (154)	28	464	76	2.1	0.9	4.0
59	9.52E+05 (20)	4.29E+06 (90)	21	361	77	7.8	4.5	12.7
60	4.00E+05 (16)	4.10E+06 (164)	40	346	55	3.4	1.9	5.7
61	1.33E+06 (12)	2.28E+07 (205)	9	1921	275	2.1	1.0	3.7
62	1.13E+06 (17)	1.37E+07 (206)	15	1158	165	2.9	1.6	4.7
63	4.17E+05 (10)	7.75E+06 (186)	24	653	98	1.9	0.9	3.5
64	2.13E+06 (17)	1.68E+07 (134)	8	1412	248	4.5	2.5	7.4
65	7.00E+05 (7)	2.00E+06 (20)	10	169	75	12.4	4.4	30.0
66	5.00E+04 (2)	2.38E+06 (95)	40	200	41	0.8	0.1	2.7
67	1.33E+05 (2)	2.53E+06 (38)	15	214	69	2.0	0.2	7.1
68	1.56E+05 (5)	7.03E+06 (225)	32	593	81	0.8	0.2	1.8
69	6.67E+05 (10)	1.01E+07 (151)	15	849	141	2.3	1.1	4.4
70	2.00E+06 (50)	2.72E+06 (68)	25	229	56	25.6	17.4	37.5
71	6.67E+05 (20)	6.73E+06 (202)	30	568	82	3.5	2.1	5.5
72	8.75E+06 (35)	8.75E+06 (35)	4	738	249	34.8	21.2	57.2
73	4.00E+05 (4)	6.70E+06 (67)	10	565	139	2.2	0.6	5.6
74	2.67E+05 (4)	9.00E+06 (135)	15	759	133	1.1	0.3	2.7
75	2.33E+05 (7)	7.43E+06 (223)	30	627	86	1.1	0.4	2.3
76	2.86E+05 (6)	4.86E+06 (102)	21	410	82	2.1	0.7	4.6
77	5.71E+05 (8)	1.15E+07 (161)	14	970	156	1.8	0.7	3.5
78	5.50E+05 (11)	8.05E+06 (161)	20	679	109	2.4	1.2	4.4
79	1.13E+06 (27)	9.63E+06 (231)	24	812	110	4.1	2.6	6.1
80	6.25E+05 (15)	6.29E+06 (151)	24	530	88	3.5	1.9	5.9
81	4.40E+05 (11)	3.72E+06 (93)	25	314	66	4.2	2.0	7.7
82	4.11E+06 (74)	4.00E+06 (72)	18	337	80	35.8	25.5	50.2
83	8.33E+06 (75)	7.56E+06 (68)	9	637	155	38.4	27.3	54.1
84	2.50E+05 (5)	4.45E+06 (89)	20	375	80	2.0	0.6	4.8
85	1.14E+06 (24)	4.24E+06 (89)	21	357	76	9.5	5.7	14.9
86	1.10E+06 (22)	1.01E+07 (202)	20	852	123	3.8	2.3	5.9
87	3.57E+05 (20)	4.21E+06 (236)	56	355	48	3.0	1.8	4.7
88	2.11E+06 (19)	2.04E+07 (184)	9	1724	260	3.6	2.1	5.8
89	1.44E+06 (26)	1.83E+07 (329)	18	1541	177	2.8	1.8	4.1
90	1.20E+05 (6)	4.00E+06 (200)	50	337	49	1.1	0.4	2.3
91	1.67E+06 (20)	2.08E+07 (250)	12	1757	229	2.8	1.7	4.4

92	1.05E+06	(22)	9.43E+06	(198)	21	795	116	3.9	2.4	6.0
93	1.20E+06	(24)	1.64E+07	(327)	20	1379	158	2.6	1.6	3.9
94	1.08E+06	(13)	1.05E+07	(126)	12	885	160	3.6	1.9	6.4
95	5.33E+05	(8)	9.80E+06	(147)	15	826	139	1.9	0.8	3.8
96	1.25E+05	(2)	1.56E+06	(25)	16	132	52	3.0	0.3	11.2
97	1.17E+06	(14)	2.23E+07	(267)	12	1876	237	1.9	1.0	3.1
98	8.00E+05	(20)	5.72E+06	(143)	25	482	82	4.9	2.9	7.8
99	1.92E+06	(25)	1.41E+07	(183)	13	1187	179	4.8	3.0	7.3
100	3.22E+06	(29)	3.22E+06	(29)	9	272	100	34.8	20.1	60.3
101	1.38E+06	(11)	8.00E+06	(64)	8	675	169	6.1	2.9	11.5
102	1.07E+06	(16)	6.80E+06	(102)	15	573	115	5.5	3.0	9.3
103	1.88E+06	(15)	1.41E+07	(113)	8	1191	227	4.7	2.5	8.0
104	8.00E+05	(8)	8.20E+06	(82)	10	691	154	3.5	1.4	7.0
105	4.00E+05	(8)	6.15E+06	(123)	20	519	95	2.3	1.0	4.6
106	1.25E+06	(15)	1.39E+07	(167)	12	1173	185	3.2	1.7	5.3

YAKD31 (Alaska), modern sand

EFFECTIVE TRACK DENSITY FOR FLUENCE MONITOR (tracks/cm^2): 5.930E+05
RELATIVE ERROR (%): 1.58
EFFECTIVE URANIUM CONTENT OF MONITOR (ppm): 50.00
ZETA FACTOR AND STANDARD ERROR (yr cm^2): 117.70 7.10
SIZE OF COUNTER SQUARE (cm^2): 1.000E-06

Grain no.	**RhoS (cm^-2)**	**(Ns)**	**RhoI (cm^-2)**	**(Ni)**	**Squares**	**U+/-2s**		**Grain Age**	**Age (Ma) --95%**	**CI--**
1	1.70E+06	(63)	8.89E+06	(329)	37	750	86	6.7	5.0	8.8
2	1.48E+06	(31)	6.86E+06	(144)	21	578	98	7.5	4.9	11.1
3	1.13E+07	(102)	4.22E+06	(38)	9	356	115	92.8	63.6	138.5
4	1.96E+06	(53)	1.54E+07	(415)	27	1296	134	4.5	3.3	6.0
5	5.40E+06	(54)	1.91E+07	(191)	10	1610	238	9.9	7.1	13.4
6	1.00E+06	(6)	8.00E+06	(48)	6	675	195	4.5	1.5	10.2
7	2.33E+06	(56)	2.18E+07	(523)	24	1837	171	3.7	2.8	4.9
8	1.76E+06	(44)	1.40E+07	(349)	25	1177	131	4.4	3.1	6.0
9	4.00E+05	(6)	7.40E+06	(111)	15	624	120	1.9	0.7	4.2
10	6.67E+05	(10)	2.00E+05	(3)	15	17	18	111.3	29.9	626.6
11	7.69E+05	(10)	4.92E+06	(64)	13	415	104	5.5	2.5	10.7
12	2.00E+06	(24)	2.08E+07	(249)	12	1750	228	3.4	2.1	5.1
13	1.86E+06	(26)	8.79E+06	(123)	14	741	135	7.4	4.6	11.3
14	7.22E+05	(13)	5.44E+06	(98)	18	459	94	4.7	2.4	8.3
15	7.78E+05	(7)	6.00E+06	(54)	9	506	138	4.6	1.7	10.0
16	2.80E+06	(56)	1.02E+07	(203)	20	856	123	9.6	7.0	13.0
17	1.28E+06	(23)	8.94E+06	(161)	18	754	121	5.0	3.1	7.8
18	1.33E+06	(20)	8.13E+06	(122)	15	686	126	5.8	3.4	9.2
19	2.58E+06	(31)	1.11E+07	(133)	12	935	164	8.2	5.3	12.1
20	1.50E+06	(12)	6.25E+06	(50)	8	527	149	8.5	4.1	15.9
21	2.00E+05	(5)	5.20E+05	(13)	25	44	24	13.7	3.7	40.0
22	2.40E+06	(24)	1.86E+07	(186)	10	1568	235	4.5	2.8	6.9
23	5.25E+05	(21)	3.83E+06	(153)	40	323	53	4.8	2.9	7.6
24	1.08E+07	(65)	2.67E+06	(16)	6	225	111	139.2	80.5	257.6
25	1.36E+06	(38)	8.25E+06	(231)	28	696	94	5.8	4.0	8.1
26	2.33E+06	(21)	9.89E+06	(89)	9	834	178	8.3	4.9	13.4
27	2.08E+06	(25)	1.92E+07	(230)	12	1616	219	3.8	2.4	5.8
28	7.86E+05	(11)	4.57E+06	(64)	14	385	97	6.1	2.9	11.5
29	1.47E+06	(22)	4.87E+06	(73)	15	410	97	10.6	6.2	17.1
30	1.93E+06	(27)	8.57E+06	(120)	14	723	134	7.9	5.0	12.0
31	2.33E+06	(14)	2.83E+06	(17)	6	239	114	28.7	13.1	61.7
32	2.00E+06	(24)	1.57E+07	(189)	12	1328	197	4.5	2.8	6.8

33	2.58E+06 (31)	1.45E+07 (174)	12	1223	189	6.2	4.1	9.2
34	5.00E+06 (90)	4.22E+06 (76)	18	356	82	41.2	30.0	56.7
35	1.25E+06 (5)	5.50E+06 (22)	4	464	196	8.1	2.3	21.4
36	1.17E+06 (21)	1.18E+07 (213)	18	998	140	3.5	2.1	5.4
37	9.17E+05 (11)	1.58E+06 (19)	12	134	61	20.3	8.7	44.6
38	9.38E+05 (15)	1.74E+07 (278)	16	1465	182	1.9	1.0	3.2
39	2.67E+06 (56)	6.86E+06 (144)	21	578	98	13.6	9.8	18.6
40	4.58E+05 (11)	7.67E+06 (184)	24	646	97	2.1	1.0	3.8
41	8.75E+05 (7)	1.29E+07 (103)	8	1086	216	2.4	0.9	5.1
42	1.33E+06 (8)	6.33E+06 (38)	6	534	173	7.5	3.0	16.0
43	1.08E+06 (26)	1.06E+07 (254)	24	892	115	3.6	2.3	5.4
44	1.22E+06 (33)	1.09E+07 (295)	27	921	111	3.9	2.6	5.6
45	4.76E+05 (20)	6.40E+06 (269)	42	540	68	2.6	1.6	4.1
46	5.50E+05 (11)	1.11E+07 (222)	20	936	129	1.8	0.9	3.2
47	1.67E+06 (20)	5.17E+06 (62)	12	436	111	11.3	6.4	18.9
48	7.62E+05 (16)	5.38E+06 (113)	21	454	86	5.0	2.7	8.4
49	1.76E+06 (37)	6.95E+06 (146)	21	586	99	8.9	6.0	12.8
50	6.00E+06 (36)	1.12E+07 (67)	6	942	231	18.8	12.1	28.5
51	5.00E+05 (18)	3.67E+06 (132)	36	309	55	4.8	2.7	7.8
52	1.00E+06 (9)	4.56E+06 (41)	9	384	120	7.8	3.3	16.0
53	2.19E+05 (7)	1.69E+06 (54)	32	142	39	4.6	1.7	10.0
54	1.16E+07 (93)	1.20E+07 (96)	8	1012	208	33.7	25.1	45.4
55	4.72E+06 (118)	4.12E+06 (103)	25	347	69	39.8	29.8	53.2
56	3.33E+05 (4)	2.42E+06 (29)	12	204	75	5.0	1.2	13.7
57	1.57E+06 (33)	1.03E+07 (217)	21	871	121	5.3	3.6	7.7
58	2.15E+06 (43)	1.00E+07 (200)	20	843	122	7.5	5.3	10.5
59	5.00E+05 (6)	5.67E+06 (68)	12	478	116	3.2	1.1	7.1
60	1.10E+07 (55)	4.40E+06 (22)	5	371	157	86.3	52.1	148.7
61	3.33E+05 (5)	1.07E+06 (16)	15	90	44	11.1	3.1	31.1
62	7.08E+05 (17)	5.00E+06 (120)	24	422	78	5.0	2.8	8.3
63	1.50E+06 (18)	1.01E+07 (121)	12	850	157	5.2	3.0	8.6
64	1.25E+06 (10)	1.13E+07 (90)	8	949	202	3.9	1.8	7.5
65	1.17E+06 (7)	5.33E+06 (32)	6	450	158	7.8	2.8	17.6
66	3.75E+05 (9)	4.50E+06 (108)	24	379	74	3.0	1.3	5.7
67	9.00E+05 (18)	6.00E+06 (120)	20	506	94	5.3	3.0	8.6
68	1.25E+06 (5)	1.05E+07 (42)	4	885	273	4.3	1.3	10.5
69	2.15E+06 (58)	1.69E+07 (456)	27	1424	141	4.4	3.3	5.9
70	5.00E+06 (60)	2.16E+07 (259)	12	1820	233	8.1	6.0	10.8
71	3.54E+05 (17)	4.38E+06 (210)	48	369	52	2.9	1.6	4.6
72	4.50E+05 (18)	4.93E+06 (197)	40	415	61	3.2	1.8	5.2
73	4.17E+05 (10)	1.92E+06 (46)	24	162	48	7.7	3.4	15.2
74	1.67E+06 (20)	9.42E+06 (113)	12	794	151	6.2	3.6	10.0
75	1.70E+06 (17)	1.15E+07 (115)	10	970	183	5.2	2.9	8.6
76	7.33E+05 (11)	4.20E+06 (63)	15	354	90	6.2	2.9	11.7
77	1.83E+06 (11)	2.02E+07 (121)	6	1700	313	3.2	1.5	5.9
78	4.25E+06 (34)	1.91E+07 (153)	8	1613	265	7.8	5.2	11.3
79	5.00E+05 (16)	5.94E+06 (190)	32	501	74	3.0	1.6	4.9
80	3.75E+05 (3)	1.50E+06 (12)	8	126	72	9.1	1.6	32.3
81	2.79E+06 (67)	2.54E+06 (61)	24	214	55	38.2	26.6	55.0
82	6.00E+05 (9)	4.80E+06 (72)	15	405	96	4.4	1.9	8.8
83	5.80E+06 (87)	4.13E+06 (62)	15	349	89	48.8	34.8	68.7
84	1.83E+06 (33)	1.68E+07 (302)	18	1415	169	3.8	2.6	5.5
85	6.00E+05 (6)	9.20E+06 (92)	10	776	163	2.3	0.8	5.1
86	5.83E+05 (7)	9.50E+06 (114)	12	801	152	2.2	0.8	4.6
87	4.00E+05 (4)	3.50E+06 (35)	10	295	99	4.1	1.0	11.2
88	6.17E+06 (37)	1.15E+07 (69)	6	970	235	18.7	12.2	28.3

89	1.05E+06	(22)	5.81E+06	(122)	21	490	90	6.3	3.8	10.0
90	1.23E+06	(37)	6.13E+06	(184)	30	517	78	7.0	4.8	10.0
91	9.29E+06	(65)	5.14E+06	(36)	7	434	144	62.6	41.1	96.9
92	9.58E+05	(46)	1.09E+07	(522)	48	917	85	3.1	2.2	4.2
93	1.18E+06	(33)	8.82E+06	(247)	28	744	97	4.7	3.1	6.7
94	3.33E+05	(15)	6.16E+06	(277)	45	519	64	1.9	1.0	3.2
95	3.33E+05	(4)	3.25E+06	(39)	12	274	88	3.7	0.9	9.9
96	1.15E+06	(31)	1.20E+07	(324)	27	1012	117	3.4	2.2	4.8
97	5.00E+05	(9)	1.04E+07	(187)	18	876	131	1.7	0.8	3.3
98	4.00E+05	(8)	2.20E+06	(44)	20	185	56	6.4	2.6	13.6
99	4.00E+05	(4)	1.90E+06	(19)	10	160	73	7.6	1.8	22.1
100	0.00E+00	(0)	8.00E+04	(4)	50	7	6	6.6	0.2	52.7
101	5.00E+05	(7)	5.00E+06	(70)	14	422	101	3.6	1.4	7.6
102	8.75E+05	(21)	5.79E+06	(139)	24	488	84	5.3	3.2	8.4
103	2.00E+05	(5)	1.84E+06	(46)	25	155	46	3.9	1.2	9.5
104	1.70E+06	(17)	1.88E+07	(188)	10	1585	236	3.2	1.8	5.2
105	7.41E+05	(20)	4.52E+06	(122)	27	381	70	5.8	3.4	9.2

YAKD32 (Alaska), modern sand
EFFECTIVE TRACK DENSITY FOR FLUENCE MONITOR (tracks/cm^2): 5.920E+05
RELATIVE ERROR (%): 1.58
EFFECTIVE URANIUM CONTENT OF MONITOR (ppm): 50.00
ZETA FACTOR AND STANDARD ERROR (yr cm^2): 117.70 7.10
SIZE OF COUNTER SQUARE (cm^2): 1.000E-06

Grain no.	**RhoS (cm^-2)**	**(Ns)**	**RhoI (cm^-2)**	**(Ni)**	**Squares**	**U+/-2s**		**Grain Age**	**Age (Ma) --95% CI--**	
1	7.58E+06	(91)	4.17E+06	(50)	12	352	100	63.0	44.2	90.9
2	6.69E+06	(234)	2.09E+06	(73)	35	176	41	110.2	82.7	146.7
3	1.08E+07	(65)	1.13E+07	(68)	6	957	233	33.2	23.3	47.4
4	7.44E+06	(67)	7.44E+06	(67)	9	629	154	34.8	24.4	49.5
5	3.79E+06	(53)	1.29E+06	(18)	14	109	51	101.2	58.8	183.6
6	1.20E+07	(48)	8.00E+06	(32)	4	676	238	52.0	32.6	84.0
7	2.63E+06	(71)	2.56E+06	(69)	27	216	52	35.8	25.3	50.6
8	9.50E+06	(152)	5.19E+06	(83)	16	438	97	63.3	47.3	84.8
9	5.12E+06	(128)	2.48E+06	(62)	25	209	53	71.4	52.4	98.5
10	7.38E+06	(59)	3.00E+06	(24)	8	253	103	84.8	52.2	142.5
11	2.23E+06	(67)	9.00E+05	(27)	30	76	29	85.6	54.3	139.3
12	8.43E+06	(118)	6.64E+06	(93)	14	561	117	44.0	33.3	58.5
13	7.42E+06	(89)	4.58E+06	(55)	12	387	105	56.1	39.7	80.0
14	3.17E+06	(152)	2.35E+06	(113)	48	199	38	46.6	35.6	61.2
15	8.29E+06	(58)	1.86E+06	(13)	7	157	86	152.1	83.6	302.3
16	4.28E+06	(124)	1.97E+06	(57)	29	166	44	75.2	54.6	104.9
17	6.04E+06	(151)	4.92E+06	(123)	25	416	76	42.6	32.6	55.6
18	7.33E+06	(132)	4.06E+06	(73)	18	343	81	62.6	46.7	84.6
19	7.00E+06	(42)	5.67E+06	(34)	6	479	164	42.9	26.6	69.5
20	1.62E+07	(81)	3.60E+06	(18)	5	304	142	153.8	92.5	272.2
21	7.88E+06	(63)	3.38E+06	(27)	8	285	109	80.5	50.8	131.6
22	1.06E+07	(127)	7.92E+06	(95)	12	669	138	46.3	34.6	62.0
23	5.70E+06	(114)	3.45E+06	(69)	20	291	71	57.3	42.1	78.5
24	1.00E+07	(40)	4.25E+06	(17)	4	359	172	81.0	45.2	152.5
25	7.67E+06	(46)	3.83E+06	(23)	6	324	134	69.1	41.2	119.5
26	3.75E+06	(90)	1.79E+06	(43)	24	151	46	72.4	49.9	106.7
27	6.67E+05	(8)	1.25E+06	(15)	12	106	54	18.7	6.8	46.6
28	6.00E+06	(36)	7.33E+06	(44)	6	619	187	28.5	17.8	45.2
29	2.84E+06	(125)	9.77E+05	(43)	44	83	25	100.3	70.6	145.3
30	7.25E+06	(58)	3.25E+06	(26)	8	274	107	77.0	47.9	127.5

31	1.75E+06	(21)	1.25E+06	(15)	12	106	54	48.4	23.9	101.0
32	3.97E+06	(151)	2.39E+06	(91)	38	202	43	57.4	43.2	76.4
33	3.88E+06	(62)	6.25E+05	(10)	16	53	33	209.7	108.9	456.4
34	1.80E+06	(18)	7.00E+05	(7)	10	59	43	87.8	35.6	249.1
35	6.43E+06	(180)	4.04E+06	(113)	28	341	65	55.2	42.4	71.8
36	7.75E+06	(62)	3.88E+06	(31)	8	327	117	69.1	44.4	110.2
37	7.50E+06	(60)	4.13E+06	(33)	8	348	121	62.9	40.6	99.4
38	4.74E+06	(199)	3.45E+06	(145)	42	292	49	47.6	37.2	60.8
39	9.67E+06	(116)	3.42E+06	(41)	12	289	90	97.6	68.0	143.0
40	2.06E+06	(33)	1.50E+06	(24)	16	127	51	47.6	27.4	84.2
41	1.08E+07	(65)	9.33E+06	(56)	6	788	211	40.3	27.8	58.7
42	3.80E+06	(19)	5.00E+06	(25)	5	422	168	26.5	13.8	49.9
43	1.92E+06	(23)	1.75E+06	(21)	12	148	64	38.0	20.1	72.2
44	6.63E+06	(159)	5.13E+06	(123)	24	433	79	44.8	34.4	58.4
45	8.63E+06	(69)	6.63E+06	(53)	8	560	154	45.2	31.1	65.9
46	6.47E+06	(97)	3.67E+06	(55)	15	310	84	61.1	43.5	86.7
47	1.20E+07	(48)	1.50E+07	(60)	4	1267	328	27.8	18.6	41.4
48	6.44E+06	(58)	3.89E+06	(35)	9	328	111	57.4	37.2	90.0
49	1.21E+07	(97)	8.38E+06	(67)	8	707	174	50.2	36.4	69.7
50	4.92E+06	(59)	1.83E+06	(22)	12	155	65	92.3	56.1	158.4
51	9.22E+06	(83)	3.22E+06	(29)	9	272	101	98.6	64.2	156.2
52	7.17E+06	(43)	6.83E+06	(41)	6	577	180	36.4	23.2	57.3
53	1.05E+07	(147)	4.21E+06	(59)	14	356	93	86.1	63.3	118.6
54	1.20E+07	(84)	5.86E+06	(41)	7	495	154	70.9	48.3	105.7
55	8.83E+06	(53)	5.67E+06	(34)	6	479	164	54.0	34.5	85.7
56	4.21E+06	(118)	2.39E+06	(67)	28	202	50	61.0	44.9	83.7
57	5.92E+06	(142)	3.79E+06	(91)	24	320	68	54.0	40.5	72.1
58	3.80E+06	(57)	1.73E+06	(26)	15	146	57	75.7	47.0	125.5
59	4.39E+06	(79)	3.00E+06	(54)	18	253	69	50.7	35.5	73.1
60	1.75E+07	(70)	7.75E+06	(31)	4	655	234	78.0	50.6	123.2
61	3.74E+06	(187)	1.94E+06	(97)	50	164	34	66.7	50.8	87.5
62	3.37E+06	(101)	1.40E+06	(42)	30	118	36	83.1	57.6	122.1
63	9.00E+06	(45)	4.20E+06	(21)	5	355	153	73.9	43.4	130.7
64	3.17E+06	(92)	1.79E+06	(52)	29	151	42	61.3	43.2	87.9
65	4.11E+06	(74)	2.94E+06	(53)	18	249	68	48.4	33.6	70.3
66	3.79E+06	(106)	1.11E+06	(31)	28	94	33	117.6	78.6	181.6
67	6.55E+06	(72)	2.27E+06	(25)	11	192	76	99.2	62.5	163.2
68	5.33E+06	(64)	1.33E+06	(16)	12	113	56	136.8	79.1	253.5
69	3.78E+06	(34)	2.11E+06	(19)	9	178	81	61.8	34.4	114.8
70	7.83E+06	(47)	3.50E+06	(21)	6	296	128	77.2	45.5	136.0
71	1.48E+07	(89)	4.17E+06	(25)	6	352	140	122.3	78.3	198.9
72	3.46E+06	(90)	3.19E+06	(83)	26	270	60	37.7	27.6	51.4
73	6.50E+06	(26)	1.75E+06	(7)	4	148	108	126.0	54.4	344.0
74	9.30E+06	(186)	3.05E+06	(61)	20	258	66	105.2	78.5	143.0
75	8.33E+06	(50)	5.50E+06	(33)	6	465	161	52.5	33.2	84.1
76	5.75E+06	(23)	8.00E+06	(32)	4	676	238	25.0	14.0	44.1
77	9.33E+06	(56)	3.83E+06	(23)	6	324	134	83.9	51.1	143.0
78	4.50E+06	(135)	1.27E+06	(38)	30	107	35	122.2	85.1	180.1
79	6.90E+06	(138)	4.40E+06	(88)	20	372	80	54.3	40.5	72.7
80	5.86E+06	(41)	1.17E+07	(82)	7	989	220	17.4	11.6	25.6
81	4.35E+06	(174)	5.90E+06	(236)	40	498	67	25.7	20.4	32.3
82	4.62E+06	(134)	2.14E+06	(62)	29	181	46	74.8	55.0	102.8
83	2.30E+06	(23)	2.00E+06	(20)	10	169	75	39.9	21.0	76.5
84	5.10E+06	(51)	8.00E+05	(8)	10	68	46	214.8	103.7	520.7
85	6.30E+06	(63)	4.70E+06	(47)	10	397	116	46.5	31.4	69.4
86	4.33E+06	(78)	2.67E+06	(48)	18	225	65	56.3	38.9	82.5

87	2.00E+06	(40)	2.00E+06	(40)	20	169	53	34.8	21.8	55.2
88	1.43E+07	(57)	4.25E+06	(17)	4	359	172	115.0	66.6	210.9
89	1.20E+07	(60)	3.00E+06	(15)	5	253	129	136.8	77.6	259.2
90	6.83E+06	(41)	1.08E+07	(65)	6	915	228	22.0	14.5	33.0
91	6.22E+06	(56)	3.67E+06	(33)	9	310	107	58.7	37.6	93.3
92	7.71E+06	(54)	4.57E+06	(32)	7	386	136	58.4	37.1	93.5
93	7.00E+06	(35)	4.00E+06	(20)	5	338	150	60.5	34.1	110.6
94	7.59E+06	(205)	2.07E+06	(56)	27	175	47	126.0	93.6	172.6
95	4.55E+06	(173)	3.08E+06	(117)	38	260	49	51.2	39.4	66.7
96	7.00E+06	(98)	4.07E+06	(57)	14	344	91	59.6	42.6	84.1
97	8.50E+06	(68)	4.50E+06	(36)	8	380	126	65.3	43.1	100.8
98	9.22E+06	(166)	4.39E+06	(79)	18	371	84	72.6	54.2	97.2
99	3.15E+06	(41)	1.69E+06	(22)	13	143	60	64.4	37.6	113.6
100	1.00E+06	(6)	2.00E+06	(12)	6	169	96	17.6	5.4	50.0
101	8.50E+06	(68)	3.63E+06	(29)	8	306	113	80.9	51.9	129.7
102	6.10E+06	(61)	3.70E+06	(37)	10	313	103	57.1	37.4	88.4
103	9.30E+06	(93)	7.60E+06	(76)	10	642	148	42.5	31.0	58.4
104	3.94E+06	(63)	1.50E+06	(24)	16	127	51	90.4	56.0	151.5

YAKD33 (Alaska), modern sand
EFFECTIVE TRACK DENSITY FOR FLUENCE MONITOR (tracks/cm^2): 5.920E+05
RELATIVE ERROR (%): 1.58
EFFECTIVE URANIUM CONTENT OF MONITOR (ppm): 50.00
ZETA FACTOR AND STANDARD ERROR (yr cm^2): 117.70 7.10
SIZE OF COUNTER SQUARE (cm^2): 1.000E-06

Grain no.	**RhoS (cm^-2)**	**(Ns)**	**RhoI (cm^-2)**	**(Ni)**	**Squares**	**U+/-2s**		**Grain Age**	**Age (Ma) --95%**	**CI--**
1	2.57E+06	(36)	4.57E+06	(64)	14	386	97	19.6	12.6	29.9
2	1.09E+07	(131)	8.58E+06	(103)	12	725	144	44.1	33.2	58.6
3	2.23E+06	(58)	3.88E+06	(101)	26	328	66	20.0	14.2	27.9
4	6.17E+06	(74)	4.33E+06	(52)	12	366	102	49.4	34.2	71.8
5	4.75E+06	(38)	3.38E+06	(27)	8	285	109	48.8	29.1	83.1
6	3.83E+06	(23)	4.17E+06	(25)	6	352	140	32.0	17.3	58.6
7	8.50E+06	(51)	1.17E+07	(70)	6	985	237	25.4	17.3	36.9
8	5.33E+06	(48)	8.44E+06	(76)	9	713	165	22.0	15.0	32.0
9	1.52E+07	(91)	8.67E+06	(52)	6	732	203	60.6	42.7	87.0
10	2.77E+06	(97)	3.17E+06	(111)	35	268	51	30.4	22.9	40.3
11	3.56E+06	(32)	5.11E+06	(46)	9	432	127	24.2	14.9	38.8
12	9.22E+06	(83)	9.00E+06	(81)	9	760	170	35.6	25.9	49.0
13	8.69E+06	(252)	5.03E+06	(146)	29	425	72	59.8	47.2	75.7
14	7.05E+06	(148)	1.00E+07	(211)	21	849	120	24.4	19.2	31.1
15	5.06E+06	(81)	5.50E+06	(88)	16	465	100	32.0	23.3	43.8
16	2.67E+06	(32)	4.17E+06	(50)	12	352	100	22.3	13.8	35.4
17	2.28E+06	(41)	4.06E+06	(73)	18	343	81	19.6	13.0	29.1
18	5.57E+06	(156)	3.79E+06	(106)	28	320	63	51.0	38.8	67.0
19	2.60E+06	(26)	2.70E+06	(27)	10	228	87	33.5	18.8	59.5
20	1.67E+06	(20)	3.50E+06	(42)	12	296	91	16.6	9.2	28.9
21	1.44E+06	(39)	1.15E+06	(31)	27	97	35	43.6	26.6	72.3
22	1.18E+07	(71)	8.33E+06	(50)	6	704	199	49.2	33.8	72.2
23	2.50E+06	(45)	3.72E+06	(67)	18	314	77	23.4	15.6	34.6
24	4.40E+06	(44)	3.60E+06	(36)	10	304	101	42.4	26.7	67.8
25	2.72E+06	(49)	3.00E+06	(54)	18	253	69	31.6	21.0	47.3
26	5.67E+06	(51)	1.31E+07	(118)	9	1107	206	15.1	10.6	21.1
27	3.28E+06	(59)	4.33E+06	(78)	18	366	83	26.3	18.4	37.4
28	4.22E+06	(38)	3.89E+06	(35)	9	328	111	37.7	23.2	61.5
29	3.61E+06	(65)	4.11E+06	(74)	18	347	81	30.5	21.5	43.2

30	2.81E+06 (59)	3.38E+06 (71)	21	286	68	28.9	20.1	41.4
31	3.20E+06 (32)	4.10E+06 (41)	10	346	108	27.2	16.5	44.2
32	5.64E+06 (79)	3.43E+06 (48)	14	290	84	57.0	39.4	83.5
33	2.50E+06 (40)	3.63E+06 (58)	16	306	81	24.0	15.6	36.5
34	1.01E+07 (101)	6.30E+06 (63)	10	532	135	55.6	40.2	77.4
35	2.80E+06 (28)	2.50E+06 (25)	10	211	84	38.9	21.9	69.5
36	4.00E+06 (60)	6.67E+06 (100)	15	563	114	20.9	14.9	29.1
37	3.33E+06 (100)	3.97E+06 (119)	30	335	62	29.2	21.8	39.1
38	5.00E+06 (45)	2.67E+06 (24)	9	225	91	64.8	38.8	111.3
39	1.78E+06 (32)	3.17E+06 (57)	18	267	71	19.6	12.3	30.6
40	5.17E+06 (31)	4.67E+06 (28)	6	394	148	38.4	22.3	66.5
41	7.25E+06 (29)	8.75E+06 (35)	4	739	249	28.8	17.0	48.5
42	3.70E+06 (37)	3.60E+06 (36)	10	304	101	35.7	22.0	58.1
43	4.33E+06 (39)	3.78E+06 (34)	9	319	109	39.8	24.5	65.0
44	5.33E+06 (32)	4.83E+06 (29)	6	408	151	38.3	22.5	65.6
45	4.05E+06 (85)	4.62E+06 (97)	21	390	80	30.5	22.5	41.2
46	2.74E+06 (85)	3.77E+06 (117)	31	319	60	25.3	18.9	33.7
47	6.29E+06 (151)	7.04E+06 (169)	24	595	93	31.1	24.2	39.9
48	6.00E+06 (36)	1.02E+07 (61)	6	859	221	20.6	13.2	31.5
49	9.50E+06 (57)	9.33E+06 (56)	6	788	211	35.4	24.0	52.1
50	4.50E+06 (36)	6.13E+06 (49)	8	517	148	25.6	16.1	40.1
51	5.29E+06 (111)	7.38E+06 (155)	21	623	102	24.9	19.0	32.7
52	4.17E+06 (50)	5.58E+06 (67)	12	472	116	26.0	17.6	38.0
53	5.60E+06 (112)	1.85E+06 (37)	20	156	51	104.3	71.6	155.7
54	6.00E+06 (24)	7.00E+06 (28)	4	591	222	29.8	16.5	53.3
55	8.43E+06 (59)	1.04E+07 (73)	7	881	207	28.1	19.6	40.2
56	1.74E+06 (47)	1.81E+06 (49)	27	153	44	33.3	21.9	50.8
57	4.14E+06 (116)	6.50E+06 (182)	28	549	83	22.2	17.1	28.9
58	2.46E+06 (59)	2.25E+06 (54)	24	190	52	38.0	25.8	56.0
59	6.17E+06 (37)	8.50E+06 (51)	6	718	201	25.3	16.1	39.3
60	4.88E+06 (39)	4.88E+06 (39)	8	412	132	34.8	21.7	55.6
61	8.58E+06 (103)	9.42E+06 (113)	12	795	151	31.7	23.7	42.4
62	1.40E+07 (84)	8.50E+06 (51)	6	718	201	57.1	39.9	82.5
63	3.21E+06 (45)	4.14E+06 (58)	14	350	92	27.0	17.9	40.5
64	1.85E+06 (37)	1.75E+06 (35)	20	148	50	36.7	22.5	60.0
65	2.27E+06 (68)	2.80E+06 (84)	30	236	52	28.2	20.1	39.2
66	9.48E+06 (256)	8.78E+06 (237)	27	741	99	37.5	30.3	46.5
67	6.25E+05 (5)	1.38E+06 (11)	8	116	69	16.1	4.3	49.3
68	5.92E+06 (71)	4.00E+06 (48)	12	338	98	51.3	35.1	75.6
69	1.40E+06 (14)	3.30E+06 (33)	10	279	97	14.9	7.3	28.4
70	2.88E+06 (69)	3.38E+06 (81)	24	285	64	29.6	21.1	41.4
71	2.11E+06 (38)	3.06E+06 (55)	18	258	70	24.1	15.5	37.0
72	3.33E+06 (40)	3.33E+06 (40)	12	282	89	34.8	21.8	55.2
73	1.50E+06 (12)	3.13E+06 (25)	8	264	105	16.8	7.6	34.5
74	3.83E+06 (23)	1.18E+07 (71)	6	999	238	11.3	6.7	18.3
75	5.50E+06 (33)	4.50E+06 (27)	6	380	145	42.4	24.8	73.3
76	3.37E+06 (91)	3.44E+06 (93)	27	291	61	34.0	25.2	45.9
77	3.67E+06 (22)	2.67E+06 (16)	6	225	111	47.6	24.0	96.9
78	4.00E+06 (32)	7.38E+06 (59)	8	623	163	18.9	11.9	29.5
79	2.00E+06 (10)	4.40E+06 (22)	5	372	157	16.0	6.7	34.8
80	5.63E+06 (45)	3.00E+06 (24)	8	253	103	64.8	38.8	111.3
81	4.50E+06 (18)	2.75E+06 (11)	4	232	137	56.4	25.4	132.3
82	2.88E+06 (46)	3.75E+06 (60)	16	317	82	26.7	17.7	39.8
83	7.80E+06 (78)	8.10E+06 (81)	10	684	153	33.5	24.2	46.3
84	2.27E+06 (25)	5.09E+06 (56)	11	430	115	15.6	9.3	25.3
85	1.26E+07 (101)	1.25E+07 (100)	8	1056	213	35.1	26.3	46.8

86	3.75E+06	(60)	5.94E+06	(95)	16	501	104	22.0	15.6	30.7
87	5.26E+06	(163)	4.81E+06	(149)	31	406	68	38.0	29.5	48.9
88	2.13E+06	(17)	5.00E+06	(40)	8	422	133	14.9	7.9	26.7
89	9.87E+06	(148)	3.33E+06	(50)	15	282	80	102.1	73.8	143.7
90	4.50E+06	(36)	1.38E+06	(11)	8	116	69	111.9	56.5	243.9
91	6.58E+06	(158)	3.21E+06	(77)	24	271	62	71.0	53.8	94.6
92	7.39E+06	(133)	3.89E+06	(70)	18	328	79	65.8	48.9	89.3
93	3.50E+06	(56)	3.81E+06	(61)	16	322	83	31.9	21.8	46.6
94	4.88E+06	(117)	5.50E+06	(132)	24	465	82	30.8	23.4	40.6
95	7.00E+06	(28)	5.50E+06	(22)	4	465	196	44.1	24.4	80.9
96	5.25E+06	(21)	5.50E+06	(22)	4	465	196	33.2	17.4	63.2
97	2.60E+06	(26)	2.80E+06	(28)	10	236	89	32.3	18.2	57.1
98	4.90E+06	(49)	6.40E+06	(64)	10	541	136	26.6	18.0	39.3
99	2.70E+06	(27)	2.50E+06	(25)	10	211	84	37.5	21.0	67.3
100	2.44E+06	(44)	3.22E+06	(58)	18	272	72	26.4	17.4	39.7
101	3.44E+06	(31)	3.78E+06	(34)	9	319	109	31.7	18.8	53.1
102	2.06E+06	(33)	2.75E+06	(44)	16	232	70	26.1	16.1	41.9
103	3.42E+06	(41)	4.17E+06	(50)	12	352	100	28.5	18.4	44.0
104	4.00E+06	(64)	3.56E+06	(57)	16	301	80	39.0	26.9	56.8

YAKD34 (Alaska), modern sand

EFFECTIVE TRACK DENSITY FOR FLUENCE MONITOR (tracks/cm^2): 5.920E+05
RELATIVE ERROR (%): 1.58
EFFECTIVE URANIUM CONTENT OF MONITOR (ppm): 50.00
ZETA FACTOR AND STANDARD ERROR (yr cm^2): 117.70 7.10
SIZE OF COUNTER SQUARE (cm^2): 1.000E-06

Grain no.	**RhoS (cm^-2)**	**(Ns)**	**RhoI (cm^-2)**	**(Ni)**	**Squares**	**U+/-2s**		**Grain Age**	**Age (Ma) --95% CI--**	
1	9.40E+06	(47)	4.00E+06	(20)	5	338	150	81.0	47.4	144.4
2	9.88E+06	(79)	5.00E+06	(40)	8	422	133	68.3	46.2	102.7
3	6.33E+06	(76)	2.67E+06	(32)	12	225	79	82.0	53.8	128.2
4	2.80E+06	(28)	1.70E+06	(17)	10	144	69	56.9	30.2	110.9
5	6.00E+06	(24)	2.00E+06	(8)	4	169	116	102.3	45.2	263.8
6	7.71E+06	(108)	3.14E+06	(44)	14	265	80	84.8	59.3	123.4
7	1.07E+07	(64)	5.83E+06	(35)	6	493	166	63.3	41.4	98.5
8	1.55E+07	(93)	5.83E+06	(35)	6	493	166	91.7	61.8	139.4
9	1.03E+07	(62)	3.00E+06	(18)	6	253	118	118.2	69.6	212.3
10	7.60E+06	(38)	5.80E+06	(29)	5	490	181	45.4	27.3	76.4
11	1.25E+07	(50)	6.25E+06	(25)	4	528	210	69.1	42.1	116.6
12	5.63E+06	(169)	2.60E+06	(78)	30	220	50	75.0	57.0	99.5
13	9.05E+06	(172)	4.11E+06	(78)	19	347	79	76.1	56.8	101.9
14	5.00E+06	(50)	4.10E+06	(41)	10	346	108	42.3	27.5	65.6
15	6.20E+06	(31)	3.40E+06	(17)	5	287	138	63.0	34.0	121.3
16	7.42E+06	(178)	4.38E+06	(105)	24	370	73	58.7	44.8	76.8
17	3.75E+06	(90)	4.88E+06	(117)	24	412	77	26.8	20.1	35.6
18	5.00E+06	(25)	3.20E+06	(16)	5	270	133	54.0	27.9	108.3
19	6.07E+06	(255)	2.86E+06	(120)	42	241	45	73.5	57.3	94.0
20	4.53E+06	(136)	3.90E+06	(117)	30	329	62	40.3	30.7	53.1
21	4.38E+05	(7)	4.38E+05	(7)	16	37	27	34.8	10.4	115.4
22	3.87E+06	(93)	3.62E+06	(87)	24	306	66	37.1	27.4	50.4
23	1.21E+07	(241)	2.30E+06	(46)	20	194	57	179.5	131.1	251.4
24	4.20E+06	(42)	1.30E+06	(13)	10	110	60	110.6	59.0	224.8
25	7.11E+06	(64)	5.67E+06	(51)	9	479	134	43.6	29.7	64.2
26	5.31E+06	(85)	3.44E+06	(55)	16	290	78	53.6	37.7	76.7
27	6.47E+06	(110)	1.47E+06	(25)	17	124	49	150.8	97.7	242.8
28	9.00E+06	(45)	3.80E+06	(19)	5	321	146	81.6	47.1	147.8

29	7.50E+06	(	45)	4.83E+06	(	29)	6	408	151	53.7	33.0	88.9
30	8.83E+06	(	53)	5.17E+06	(	31)	6	436	156	59.2	37.4	95.4
31	7.17E+06	(	43)	1.67E+06	(	10)	6	141	87	146.3	73.6	326.2
32	6.05E+06	(	121)	4.25E+06	(	85)	20	359	78	49.4	37.1	66.0
33	4.39E+06	(	79)	3.89E+06	(	70)	18	328	79	39.2	28.0	54.9
34	3.75E+06	(	15)	1.25E+06	(	5)	4	106	90	101.6	36.0	357.7
35	1.10E+07	(	44)	4.00E+06	(	16)	4	338	167	94.5	52.7	179.6
36	4.60E+06	(	23)	6.40E+06	(	32)	5	541	190	25.0	14.0	44.1
37	7.83E+06	(	47)	2.50E+06	(	15)	6	211	107	107.5	59.6	207.0
38	9.71E+06	(	68)	6.29E+06	(	44)	7	531	160	53.6	36.2	80.2
39	7.50E+06	(	30)	6.00E+06	(	24)	4	507	205	43.4	24.5	77.5
40	9.17E+06	(	55)	5.67E+06	(	34)	6	479	164	56.0	36.0	88.7
41	5.67E+06	(	34)	5.67E+06	(	34)	6	479	164	34.8	21.0	57.6
42	8.44E+06	(	135)	3.94E+06	(	63)	16	333	84	74.1	54.6	101.7
43	1.44E+06	(	26)	1.44E+07	(	260)	18	1220	156	3.5	2.2	5.2
44	1.23E+07	(	49)	5.50E+06	(	22)	4	465	196	76.8	45.8	133.5
45	4.24E+06	(	89)	3.81E+06	(	80)	21	322	72	38.6	28.2	53.0
46	2.43E+06	(	34)	8.57E+05	(	12)	14	72	41	97.1	49.6	206.2
47	8.80E+06	(	88)	4.80E+06	(	48)	10	405	117	63.5	44.2	92.3
48	7.50E+06	(	45)	6.33E+06	(	38)	6	535	173	41.1	26.1	65.1
49	1.10E+07	(	66)	8.00E+06	(	48)	6	676	195	47.7	32.4	70.7
50	5.63E+06	(	45)	4.38E+06	(	35)	8	370	125	44.6	28.1	71.5
51	1.04E+07	(	73)	5.43E+06	(	38)	7	458	148	66.5	44.4	101.2
52	1.85E+07	(	74)	3.75E+06	(	15)	4	317	161	168.2	97.0	314.9
53	1.10E+07	(	55)	9.20E+06	(	46)	5	777	229	41.5	27.6	62.8
54	8.75E+05	(	7)	6.63E+06	(	53)	8	560	154	4.7	1.8	10.2
55	6.33E+06	(	38)	7.50E+06	(	45)	6	633	189	29.4	18.5	46.2
56	4.25E+06	(	17)	7.00E+06	(	28)	4	591	222	21.2	10.8	39.9
57	1.89E+06	(	17)	1.78E+06	(	16)	9	150	74	36.9	17.6	77.9
58	9.83E+06	(	59)	6.33E+06	(	38)	6	535	173	53.8	35.2	83.2
59	3.38E+06	(	27)	1.75E+06	(	14)	8	148	78	66.5	33.9	137.3
60	4.22E+06	(	38)	1.89E+06	(	17)	9	160	76	77.0	42.7	145.6
61	1.00E+07	(	80)	6.75E+06	(	54)	8	570	155	51.4	35.9	74.0
62	4.00E+05	(	2)	6.60E+06	(	33)	5	557	193	2.3	0.2	8.3
63	5.33E+06	(	80)	3.40E+06	(	51)	15	287	81	54.4	37.8	78.9
64	5.00E+05	(	7)	4.36E+06	(	61)	14	368	95	4.1	1.5	8.7
65	9.75E+06	(	39)	5.50E+06	(	22)	4	465	196	61.3	35.6	108.6
66	5.67E+06	(	102)	3.94E+06	(	71)	18	333	79	49.8	36.5	68.5
67	6.23E+06	(	81)	3.15E+06	(	41)	13	266	83	68.3	46.5	102.1
68	7.67E+06	(	46)	7.50E+06	(	45)	6	633	189	35.5	23.0	54.8
69	1.30E+07	(	52)	6.00E+06	(	24)	4	507	205	74.8	45.5	126.9
70	5.19E+06	(	83)	3.50E+06	(	56)	16	296	79	51.4	36.2	73.5
71	6.67E+06	(	40)	3.33E+06	(	20)	6	282	125	69.0	39.6	124.7
72	4.67E+06	(	56)	2.08E+06	(	25)	12	176	70	77.3	47.7	129.4
73	5.56E+05	(	10)	3.89E+06	(	70)	18	328	79	5.0	2.3	9.7
74	3.67E+06	(	22)	1.17E+06	(	7)	6	99	72	106.9	45.0	296.7
75	7.75E+06	(	31)	8.50E+06	(	34)	4	718	245	31.7	18.8	53.1
76	9.00E+06	(	45)	3.40E+06	(	17)	5	287	138	91.0	51.5	169.8
77	3.17E+06	(	38)	2.50E+06	(	30)	12	211	77	43.9	26.5	73.4
78	2.42E+06	(	29)	1.00E+06	(	12)	12	84	48	83.0	41.5	178.8
79	9.38E+06	(	75)	9.50E+06	(	76)	8	802	185	34.3	24.6	47.8
80	9.10E+06	(	91)	5.70E+06	(	57)	10	481	128	55.3	39.3	78.5
81	9.33E+06	(	56)	4.83E+06	(	29)	6	408	151	66.8	42.1	108.5
82	2.60E+06	(	39)	9.33E+05	(	14)	15	79	41	95.6	51.3	190.8
83	7.08E+06	(	85)	4.17E+06	(	50)	12	352	100	58.9	41.1	85.3
84	4.77E+06	(	62)	9.31E+06	(	121)	13	786	145	17.9	12.9	24.4

85	2.67E+06	(32)	1.42E+06	(17)	12	120	57	65.0	35.2	124.8
86	5.50E+06	(22)	1.00E+06	(4)	4	84	80	183.0	64.7	723.2
87	1.05E+07	(42)	3.75E+06	(15)	4	317	161	96.2	52.7	186.8
88	8.50E+06	(51)	2.00E+06	(12)	6	169	96	144.9	77.3	298.4
89	9.64E+06	(212)	3.32E+06	(73)	22	280	66	99.9	74.8	133.5
90	1.22E+06	(33)	4.59E+06	(124)	27	388	71	9.3	6.1	13.7
91	7.00E+05	(35)	6.28E+06	(314)	50	530	62	3.9	2.7	5.5
92	4.25E+06	(51)	2.42E+06	(29)	12	204	75	60.8	38.0	99.6
93	2.50E+06	(25)	3.10E+06	(31)	10	262	94	28.1	15.9	49.0
94	7.33E+06	(44)	4.50E+06	(27)	6	380	145	56.4	34.3	94.8
95	3.43E+06	(24)	1.86E+06	(13)	7	157	86	63.6	31.4	136.2
96	5.33E+06	(64)	4.33E+06	(52)	12	366	102	42.7	29.2	62.9
97	4.33E+06	(52)	1.75E+06	(21)	12	148	64	85.3	50.8	149.2
98	2.80E+06	(14)	1.60E+06	(8)	5	135	93	60.2	23.8	165.7
99	4.20E+06	(63)	2.07E+06	(31)	15	175	62	70.2	45.2	111.8
100	9.33E+06	(56)	3.83E+06	(23)	6	324	134	83.9	51.1	143.0
101	1.19E+07	(95)	5.88E+06	(47)	8	496	145	69.9	48.9	101.5
102	1.13E+07	(68)	5.50E+06	(33)	6	465	161	71.2	46.5	111.5
103	5.17E+06	(62)	3.83E+06	(46)	12	324	96	46.8	31.4	70.1
104	8.00E+06	(40)	6.20E+06	(31)	5	524	187	44.8	27.3	74.0
105	1.89E+06	(68)	1.61E+06	(58)	36	136	36	40.7	28.3	58.8

YAKD35 (Alaska), modern sand

EFFECTIVE TRACK DENSITY FOR FLUENCE MONITOR (tracks/cm^2): 5.920E+05
RELATIVE ERROR (%): 1.58
EFFECTIVE URANIUM CONTENT OF MONITOR (ppm): 50.00
ZETA FACTOR AND STANDARD ERROR (yr cm^2): 117.70 7.10
SIZE OF COUNTER SQUARE (cm^2): 1.000E-06

Grain no.	**RhoS (cm^-2)**	**(Ns)**	**RhoI (cm^-2)**	**(Ni)**	**Squares**	**U+/-2s**		**Grain Age**	**Age (Ma) --95% CI--**	
1	8.00E+05	(4)	1.40E+06	(7)	5	118	86	20.2	4.3	77.9
2	7.88E+06	(63)	9.13E+06	(73)	8	771	181	30.0	21.1	42.6
3	9.56E+06	(153)	4.94E+06	(79)	16	417	94	67.1	50.8	89.2
4	5.90E+06	(59)	3.30E+06	(33)	10	279	97	61.9	39.8	97.9
5	7.00E+06	(84)	6.17E+06	(74)	12	521	122	39.4	28.5	54.7
6	7.86E+06	(55)	4.43E+06	(31)	7	374	134	61.4	38.9	98.7
7	1.23E+07	(74)	5.50E+06	(33)	6	465	161	77.5	50.9	120.6
8	8.20E+06	(41)	2.00E+06	(10)	5	169	104	139.6	69.9	312.4
9	1.28E+07	(51)	7.00E+06	(28)	4	591	222	63.0	39.1	103.8
10	3.09E+06	(34)	2.55E+06	(28)	11	215	81	42.1	24.8	72.1
11	3.33E+06	(20)	2.83E+06	(17)	6	239	115	40.8	20.3	82.9
12	5.89E+06	(53)	5.22E+06	(47)	9	441	129	39.2	25.9	59.3
13	1.23E+06	(37)	2.47E+06	(74)	30	208	49	17.4	11.4	26.2
14	8.80E+06	(132)	4.20E+06	(63)	15	355	90	72.5	53.4	99.6
15	5.00E+06	(60)	2.92E+06	(35)	12	246	83	59.3	38.6	92.8
16	7.25E+06	(58)	2.63E+06	(21)	8	222	96	95.1	57.2	165.0
17	4.58E+05	(11)	5.50E+06	(132)	24	465	82	2.9	1.4	5.4
18	6.33E+05	(19)	3.47E+06	(104)	30	293	58	6.4	3.7	10.5
19	9.00E+06	(54)	4.83E+06	(29)	6	408	151	64.4	40.4	104.9
20	8.67E+06	(52)	5.00E+06	(30)	6	422	154	60.0	37.7	97.4
21	6.40E+06	(96)	4.67E+06	(70)	15	394	95	47.6	34.6	65.8
22	3.80E+06	(19)	1.80E+06	(9)	5	152	99	72.5	31.6	182.1
23	7.72E+06	(139)	3.39E+06	(61)	18	286	74	78.8	58.0	108.4
24	4.69E+06	(75)	3.38E+06	(54)	16	285	78	48.2	33.5	69.7
25	1.58E+07	(126)	3.38E+06	(27)	8	285	109	159.8	105.6	251.7
26	4.64E+06	(51)	4.18E+06	(46)	11	353	104	38.5	25.3	58.7

27	2.96E+06 (71)	1.50E+06 (36)	24	127	42	68.2	45.2	104.9
28	6.60E+06 (66)	3.60E+06 (36)	10	304	101	63.4	41.7	98.1
29	2.47E+06 (47)	1.53E+06 (29)	19	129	48	56.1	34.7	92.5
30	6.60E+06 (33)	1.00E+07 (50)	5	845	239	23.0	14.3	36.4
31	3.30E+06 (66)	4.00E+06 (80)	20	338	76	28.7	20.4	40.3
32	6.90E+06 (69)	4.90E+06 (49)	10	414	118	48.8	33.4	72.0
33	5.42E+06 (65)	4.25E+06 (51)	12	359	101	44.2	30.2	65.2
34	9.70E+06 (194)	6.10E+06 (122)	20	515	95	55.1	42.6	71.1
35	6.67E+06 (120)	1.72E+06 (31)	18	145	52	133.0	89.5	204.2
36	1.18E+07 (47)	6.50E+06 (26)	4	549	214	62.5	38.1	105.2
37	4.65E+06 (93)	6.55E+06 (131)	20	553	98	24.7	18.5	33.1
38	6.17E+06 (111)	5.44E+06 (98)	18	460	94	39.3	29.7	52.2
39	8.60E+06 (172)	4.05E+06 (81)	20	342	77	73.3	54.9	97.8
40	5.14E+06 (144)	2.54E+06 (71)	28	214	51	70.2	52.5	94.7
41	2.83E+06 (85)	1.17E+06 (35)	30	99	33	83.8	56.1	128.2
42	1.86E+06 (26)	1.29E+06 (18)	14	109	51	50.0	26.5	96.8
43	9.90E+06 (99)	2.30E+06 (23)	10	194	80	147.5	93.7	243.1
44	3.00E+06 (48)	3.69E+06 (59)	16	311	81	28.3	18.9	42.1
45	6.94E+06 (125)	3.39E+06 (61)	18	286	74	70.9	51.9	98.0
46	2.08E+06 (25)	5.25E+06 (63)	12	443	112	13.9	8.3	22.3
47	9.40E+06 (94)	1.90E+06 (19)	10	160	73	169.0	103.5	292.5
48	6.50E+06 (39)	4.83E+06 (29)	6	408	151	46.6	28.1	78.2
49	6.92E+06 (83)	2.08E+06 (25)	12	176	70	114.1	72.7	186.4
50	4.63E+06 (37)	1.88E+06 (15)	8	158	81	84.8	45.8	166.5
51	5.71E+06 (40)	3.29E+06 (23)	7	278	115	60.1	35.3	105.3
52	6.92E+06 (83)	6.58E+06 (79)	12	556	126	36.5	26.5	50.4
53	4.61E+06 (129)	2.11E+06 (59)	28	178	46	75.6	55.2	104.8
54	9.69E+06 (155)	7.13E+06 (114)	16	602	114	47.1	36.0	61.7
55	6.77E+06 (88)	6.46E+06 (84)	13	546	120	36.4	26.7	49.7
56	7.58E+06 (91)	4.58E+06 (55)	12	387	105	57.3	40.6	81.7
57	1.00E+06 (5)	4.00E+06 (20)	5	338	150	8.9	2.6	23.9
58	2.65E+06 (53)	2.55E+06 (51)	20	215	60	36.1	24.1	54.1
59	5.70E+06 (188)	5.85E+06 (193)	33	494	73	33.8	26.8	42.8
60	4.13E+06 (33)	5.00E+05 (4)	8	42	40	271.9	101.4	1030.5
61	9.75E+06 (39)	1.73E+07 (69)	4	1457	353	19.7	12.9	29.6
62	5.67E+06 (34)	4.33E+06 (26)	6	366	143	45.3	26.5	78.7
63	1.40E+07 (84)	9.33E+06 (56)	6	788	211	52.0	36.7	74.3
64	4.70E+06 (47)	3.30E+06 (33)	10	279	97	49.4	31.0	79.6
65	7.81E+06 (125)	6.25E+06 (100)	16	528	107	43.4	32.5	57.8
66	4.94E+06 (89)	1.83E+06 (33)	18	155	54	93.0	62.0	143.3
67	2.80E+06 (28)	1.70E+06 (17)	10	144	69	56.9	30.2	110.9
68	7.86E+06 (55)	7.14E+06 (50)	7	603	171	38.2	25.6	57.2
69	9.50E+06 (38)	8.00E+06 (32)	4	676	238	41.2	25.1	68.1
70	2.48E+06 (99)	1.28E+06 (51)	40	108	30	67.2	47.5	96.2
71	2.20E+06 (66)	2.10E+06 (63)	30	177	45	36.4	25.4	52.3
72	4.64E+06 (51)	4.64E+06 (51)	11	392	110	34.8	23.1	52.3
73	6.30E+06 (63)	6.70E+06 (67)	10	566	139	32.7	22.8	46.8
74	4.23E+06 (55)	3.23E+06 (42)	13	273	84	45.4	29.9	69.6
75	6.67E+05 (4)	1.00E+06 (6)	6	84	66	23.5	4.8	97.3
76	9.33E+06 (84)	7.44E+06 (67)	9	629	154	43.5	31.2	61.0
77	4.08E+06 (49)	1.25E+06 (15)	12	106	54	112.0	62.4	215.1
78	7.10E+06 (142)	2.90E+06 (58)	20	245	65	84.6	62.0	117.0
79	1.67E+05 (2)	4.17E+06 (50)	12	352	100	1.5	0.2	5.3
80	5.58E+06 (67)	3.92E+06 (47)	12	331	97	49.4	33.6	73.4
81	1.16E+07 (174)	5.27E+06 (79)	15	445	101	76.0	56.9	101.6
82	2.78E+05 (5)	1.56E+06 (28)	18	131	49	6.4	1.9	16.3

83	2.75E+06	(33)	2.33E+06	(28)	12	197	74	40.9	24.0	70.2
84	1.07E+07	(64)	5.67E+06	(34)	6	479	164	65.1	42.4	101.9
85	1.05E+07	(63)	1.10E+07	(66)	6	929	230	33.2	23.1	47.6
86	5.17E+06	(62)	3.42E+06	(41)	12	289	90	52.4	34.8	79.8
87	6.25E+06	(50)	2.00E+06	(16)	8	169	83	107.2	60.6	201.8
88	3.27E+06	(98)	1.70E+06	(51)	30	144	40	66.5	47.0	95.3
89	7.00E+06	(56)	4.00E+06	(32)	8	338	119	60.6	38.6	96.7
90	6.50E+06	(39)	1.23E+07	(74)	6	1042	244	18.4	12.1	27.4
91	7.06E+06	(113)	3.19E+06	(51)	16	269	76	76.6	54.7	108.9
92	5.56E+05	(10)	2.22E+06	(40)	18	188	59	8.8	3.9	17.7
93	1.44E+06	(23)	1.44E+06	(23)	16	121	50	34.8	18.6	64.7
94	5.71E+06	(40)	5.86E+06	(41)	7	495	154	33.9	21.4	53.7
95	4.00E+06	(48)	2.67E+06	(32)	12	225	79	52.0	32.6	84.0
96	1.34E+07	(67)	4.60E+06	(23)	5	389	161	100.2	62.0	168.8
97	3.67E+06	(88)	2.88E+06	(69)	24	243	59	44.3	31.9	61.6
98	4.08E+06	(98)	2.71E+06	(65)	24	229	57	52.3	37.8	72.7
99	4.37E+06	(131)	2.57E+06	(77)	30	217	50	59.0	44.2	79.3
100	2.50E+06	(20)	7.63E+06	(61)	8	644	165	11.5	6.5	19.2
101	6.92E+06	(83)	3.17E+06	(38)	12	267	87	75.5	51.0	114.0
102	7.50E+06	(30)	6.50E+06	(26)	4	549	214	40.0	22.9	70.5
103	2.50E+06	(40)	2.44E+06	(39)	16	206	66	35.6	22.3	56.9
104	8.71E+06	(61)	4.86E+06	(34)	7	410	140	62.1	40.3	97.5
105	2.44E+06	(39)	1.50E+06	(24)	16	127	51	56.2	33.1	97.8
106	1.67E+06	(45)	1.69E+07	(457)	27	1430	141	3.4	2.5	4.7

YAKD37 (Alaska), modern sand
EFFECTIVE TRACK DENSITY FOR FLUENCE MONITOR (tracks/cm^2): 5.930E+05
RELATIVE ERROR (%): 1.58
EFFECTIVE URANIUM CONTENT OF MONITOR (ppm): 50.00
ZETA FACTOR AND STANDARD ERROR (yr cm^2): 117.70 7.10
SIZE OF COUNTER SQUARE (cm^2): 1.000E-06

Grain no.	**RhoS (cm^-2)**	**(Ns)**	**RhoI (cm^-2)**	**(Ni)**	**Squares**	**U+/-2s**		**Grain Age**	**Age (Ma) --95% CI--**	
1	3.75E+06	(60)	1.56E+06	(25)	16	132	52	82.9	51.5	138.1
2	4.50E+06	(45)	2.20E+06	(22)	10	185	78	70.7	41.8	123.8
3	2.25E+06	(18)	5.00E+05	(4)	8	42	40	150.6	51.5	608.6
4	5.20E+06	(26)	4.00E+06	(20)	5	337	149	45.1	24.3	85.2
5	3.67E+06	(33)	4.22E+06	(38)	9	356	115	30.3	18.4	49.5
6	4.40E+06	(22)	2.60E+06	(13)	5	219	120	58.5	28.4	126.5
7	7.40E+06	(37)	2.80E+06	(14)	5	236	124	90.9	48.5	182.3
8	5.17E+06	(31)	1.17E+06	(7)	6	98	72	150.1	66.4	403.2
9	2.83E+06	(17)	1.50E+06	(9)	6	126	82	65.0	27.7	165.8
10	1.00E+06	(4)	2.50E+05	(1)	4	21	34	125.4	13.8	4679.9
11	6.50E+06	(65)	4.10E+06	(41)	10	346	108	55.0	36.7	83.5
12	2.17E+06	(26)	7.50E+05	(9)	12	63	41	98.9	45.6	240.2
13	5.25E+06	(42)	2.25E+06	(18)	8	190	88	80.5	45.7	148.7
14	3.90E+06	(39)	1.90E+06	(19)	10	160	73	70.9	40.2	130.1
15	3.83E+06	(23)	3.67E+06	(22)	6	309	131	36.4	19.4	68.4
16	6.20E+06	(62)	4.30E+06	(43)	10	363	111	50.1	33.4	75.7
17	5.50E+06	(22)	3.00E+06	(12)	4	253	143	63.3	30.2	140.4
18	9.38E+06	(75)	5.25E+06	(42)	8	443	137	61.9	42.0	92.7
19	4.25E+06	(68)	9.38E+05	(15)	16	79	40	155.0	88.8	291.6
20	6.88E+06	(55)	1.75E+06	(14)	8	148	78	134.5	74.7	261.8
21	5.25E+06	(21)	1.75E+06	(7)	4	148	108	102.3	42.7	285.3
22	6.78E+06	(61)	8.89E+05	(8)	9	75	51	256.3	125.5	614.2
23	1.78E+06	(16)	7.78E+05	(7)	9	66	48	78.3	31.0	225.4

24	1.89E+06	(17)	1.00E+06	(9)	9	84	55	65.0	27.7	165.8
25	7.67E+06	(46)	3.50E+06	(21)	6	295	128	75.7	44.5	133.6
26	5.50E+06	(33)	6.00E+06	(36)	6	506	168	31.9	19.3	52.6
27	4.00E+06	(24)	2.33E+06	(14)	6	197	104	59.3	29.6	124.0
28	1.78E+06	(16)	2.89E+06	(26)	9	244	95	21.5	10.7	41.5
29	5.50E+06	(22)	3.00E+06	(12)	4	253	143	63.3	30.2	140.4
30	7.06E+06	(113)	2.50E+06	(40)	16	211	67	97.6	67.7	143.8
31	1.00E+07	(40)	8.50E+06	(34)	4	717	245	40.9	25.3	66.6
32	1.75E+06	(14)	1.88E+06	(15)	8	158	80	32.5	14.5	72.0
33	3.64E+06	(51)	7.86E+05	(11)	14	66	39	158.0	82.7	335.7
34	7.26E+06	(138)	2.84E+06	(54)	19	240	65	88.4	64.2	123.6
35	4.60E+06	(46)	1.00E+06	(10)	10	84	52	156.6	79.4	347.5
36	9.00E+06	(36)	3.00E+06	(12)	4	253	143	102.9	53.0	217.5
37	9.25E+06	(37)	4.00E+06	(16)	4	337	166	79.8	43.6	153.7
38	5.88E+06	(47)	3.00E+06	(24)	8	253	103	67.8	40.8	115.9
39	5.00E+06	(30)	8.33E+05	(5)	6	70	60	200.8	79.9	657.0
40	2.50E+06	(15)	3.33E+06	(20)	6	281	124	26.2	12.4	53.6
41	4.71E+06	(99)	1.43E+06	(30)	21	120	44	113.7	75.3	177.3
42	3.33E+06	(50)	3.07E+06	(46)	15	259	76	37.8	24.8	57.7
43	8.50E+06	(34)	3.75E+06	(15)	4	316	161	78.2	41.8	154.6
44	8.13E+06	(65)	4.63E+06	(37)	8	390	128	60.9	40.2	93.9
45	6.20E+06	(62)	1.10E+06	(11)	10	93	55	191.5	101.8	401.8
46	5.63E+06	(45)	2.75E+06	(22)	8	232	98	70.7	41.8	123.8
47	9.50E+06	(76)	1.75E+06	(14)	8	148	78	185.0	105.3	353.3
48	5.50E+06	(22)	1.25E+06	(5)	4	105	90	148.1	56.5	499.5
49	7.38E+06	(59)	4.75E+06	(38)	8	401	130	53.9	35.3	83.3
50	6.00E+06	(30)	1.80E+06	(9)	5	152	99	113.9	53.6	272.9
51	4.63E+06	(37)	3.75E+06	(30)	8	316	115	42.9	25.8	71.8
52	5.39E+06	(97)	2.22E+06	(40)	18	187	59	83.9	57.7	124.5
53	5.75E+06	(46)	1.88E+06	(15)	8	158	80	105.4	58.4	203.3
54	7.75E+06	(93)	4.08E+06	(49)	12	344	98	65.8	46.1	95.1
55	1.07E+07	(64)	1.17E+06	(7)	6	98	72	305.3	144.5	777.2
56	4.75E+06	(57)	8.33E+05	(10)	12	70	43	193.4	99.8	423.1
57	4.56E+06	(114)	1.68E+06	(42)	25	142	44	93.8	65.5	137.1
58	3.50E+06	(21)	1.17E+06	(7)	6	98	72	102.3	42.7	285.3
59	4.60E+06	(46)	2.10E+06	(21)	10	177	77	75.7	44.5	133.6
60	5.67E+06	(51)	4.11E+06	(37)	9	347	114	47.9	30.8	75.2
61	9.00E+06	(54)	3.33E+06	(20)	6	281	124	93.1	55.2	164.3
62	9.33E+06	(56)	3.33E+06	(20)	6	281	124	96.5	57.4	169.8
63	5.50E+06	(22)	1.75E+06	(7)	4	148	108	107.1	45.1	297.2
64	4.06E+06	(65)	1.75E+06	(28)	16	148	55	80.3	51.0	129.9
65	2.90E+06	(29)	4.20E+06	(42)	10	354	109	24.1	14.4	39.5
66	7.17E+06	(43)	3.00E+06	(18)	6	253	118	82.4	46.9	151.9
67	7.50E+06	(30)	2.00E+06	(8)	4	169	116	127.7	58.3	322.4
68	6.33E+06	(38)	1.67E+06	(10)	6	141	87	129.7	64.5	292.0
69	4.83E+06	(58)	5.83E+05	(7)	12	49	36	277.3	130.3	710.8
70	1.07E+07	(64)	1.17E+06	(7)	6	98	72	305.3	144.5	777.2
71	5.00E+06	(40)	1.00E+06	(8)	8	84	58	169.5	80.0	418.1
72	5.90E+06	(118)	2.05E+06	(41)	20	173	54	99.4	69.4	145.6
73	6.88E+06	(55)	3.00E+06	(24)	8	253	103	79.2	48.5	133.9
74	6.60E+06	(66)	2.90E+06	(29)	10	245	90	78.7	50.3	126.4
75	5.78E+06	(52)	2.00E+06	(18)	9	169	79	99.5	57.7	180.8
76	5.60E+06	(28)	4.20E+06	(21)	5	354	153	46.3	25.4	85.7
77	7.80E+06	(117)	1.13E+06	(17)	15	96	46	233.9	142.0	413.2
78	6.00E+06	(24)	2.00E+06	(8)	4	169	116	102.5	45.3	264.3
79	3.50E+06	(14)	1.75E+06	(7)	4	148	108	68.6	26.3	201.3

80	7.67E+06	(46)	2.17E+06	(13)	6	183	100	121.2	65.2	244.7
81	5.63E+06	(45)	1.63E+06	(13)	8	137	75	118.6	63.7	239.8
82	2.67E+06	(16)	3.33E+05	(2)	6	28	36	256.5	65.3	2115.5
83	4.50E+06	(45)	1.50E+06	(15)	10	126	64	103.1	57.0	199.3
84	3.71E+06	(52)	3.71E+06	(52)	14	313	87	34.8	23.2	52.1
85	7.61E+06	(137)	7.83E+06	(141)	18	660	113	33.8	26.0	44.0
86	1.18E+07	(59)	4.60E+06	(23)	5	388	160	88.5	54.2	150.3
87	9.00E+06	(36)	2.00E+06	(8)	4	169	116	152.8	71.3	380.0
88	3.56E+06	(32)	2.33E+06	(21)	9	197	85	52.8	29.6	96.4
89	4.67E+06	(28)	3.17E+06	(19)	6	267	121	51.1	27.6	96.8
90	3.13E+06	(25)	1.88E+06	(15)	8	158	80	57.7	29.4	117.7
91	2.75E+06	(22)	1.38E+06	(11)	8	116	68	68.9	32.3	157.6
92	5.20E+06	(104)	1.70E+06	(34)	20	143	49	105.5	71.4	160.4
93	4.33E+06	(26)	3.17E+06	(19)	6	267	121	47.5	25.4	90.7
94	7.25E+06	(58)	2.13E+06	(17)	8	179	86	117.2	68.0	214.7
95	4.38E+06	(35)	2.13E+06	(17)	8	179	86	71.1	39.0	135.5
96	5.50E+06	(22)	1.50E+06	(6)	4	126	99	124.3	50.1	374.9
97	4.33E+06	(26)	4.67E+06	(28)	6	393	148	32.3	18.2	57.1
98	3.33E+06	(20)	2.00E+06	(12)	6	169	96	57.6	27.0	129.3
99	2.50E+06	(15)	2.17E+06	(13)	6	183	100	40.1	17.8	91.4
100	2.50E+06	(20)	1.75E+06	(14)	8	148	78	49.5	23.9	105.9
101	2.33E+06	(28)	9.17E+05	(11)	12	77	46	87.5	42.7	194.9
102	4.00E+06	(32)	1.63E+06	(13)	8	137	75	84.7	43.7	176.1
103	5.25E+06	(42)	4.88E+06	(39)	8	411	131	37.5	23.7	59.5
104	4.56E+06	(82)	2.17E+06	(39)	18	183	58	72.8	49.3	109.6
105	3.83E+06	(23)	1.83E+06	(11)	6	155	91	72.0	34.1	163.8

YAKD38 (Alaska), modern sand

EFFECTIVE TRACK DENSITY FOR FLUENCE MONITOR (tracks/cm^2): 5.930E+05
RELATIVE ERROR (%): 1.58
EFFECTIVE URANIUM CONTENT OF MONITOR (ppm): 50.00
ZETA FACTOR AND STANDARD ERROR (yr cm^2): 117.70 7.10
SIZE OF COUNTER SQUARE (cm^2): 1.000E-06

Grain no.	**RhoS (cm^-2)**	**(Ns)**	**RhoI (cm^-2)**	**(Ni)**	**Squares**	**U+/-2s**		**Grain Age**	**Age (Ma) --95% CI--**	
1	2.40E+06	(24)	3.40E+06	(34)	10	287	98	24.6	14.0	42.7
2	2.33E+06	(14)	6.67E+06	(40)	6	562	178	12.3	6.1	22.9
3	1.16E+06	(37)	1.52E+07	(485)	32	1278	123	2.7	1.8	3.7
4	7.60E+06	(76)	2.40E+06	(24)	10	202	82	109.1	68.6	180.6
5	3.20E+05	(8)	4.72E+06	(118)	25	398	74	2.4	1.0	4.8
6	7.25E+06	(87)	2.75E+06	(33)	12	232	80	91.1	60.6	140.5
7	1.05E+06	(21)	5.65E+06	(113)	20	476	91	6.5	3.9	10.4
8	9.44E+05	(17)	6.61E+06	(119)	18	557	103	5.0	2.8	8.3
9	3.75E+05	(9)	8.00E+06	(192)	24	675	100	1.7	0.7	3.2
10	4.50E+06	(18)	2.18E+07	(87)	4	1834	396	7.3	4.1	12.1
11	6.75E+06	(54)	3.88E+06	(31)	8	327	117	60.4	38.2	97.2
12	7.50E+05	(15)	5.60E+06	(112)	20	472	90	4.7	2.5	8.0
13	4.64E+06	(65)	2.71E+06	(38)	14	229	74	59.3	39.2	91.1
14	2.50E+05	(1)	8.25E+06	(33)	4	696	241	1.2	0.0	6.3
15	1.33E+06	(8)	1.02E+07	(61)	6	857	220	4.7	1.9	9.6
16	6.67E+05	(6)	9.11E+06	(82)	9	768	171	2.6	0.9	5.8
17	5.11E+06	(92)	3.22E+06	(58)	18	272	72	55.1	39.2	77.9
18	1.75E+06	(7)	1.50E+06	(6)	4	126	99	40.4	11.7	145.1
19	4.67E+05	(7)	1.09E+07	(163)	15	916	146	1.5	0.6	3.2
20	1.67E+05	(1)	5.17E+06	(31)	6	436	156	1.3	0.0	6.8
21	2.63E+06	(42)	1.34E+07	(214)	16	1128	158	6.9	4.8	9.6

22	3.63E+06 (29)	1.38E+06 (11)	8	116	68	90.5	44.4	201.1
23	1.90E+06 (19)	9.90E+06 (99)	10	835	169	6.7	3.9	11.0
24	6.75E+06 (81)	2.42E+06 (29)	12	204	75	96.4	62.7	152.9
25	7.43E+05 (26)	5.60E+06 (196)	35	472	69	4.7	2.9	7.0
26	6.67E+05 (4)	1.98E+07 (119)	6	1672	310	1.2	0.3	3.1
27	0.00E+00 (0)	1.33E+06 (12)	9	112	64	2.1	0.1	12.6
28	7.33E+06 (44)	4.33E+06 (26)	6	365	142	58.6	35.4	99.3
29	2.22E+06 (20)	1.78E+07 (160)	9	1499	241	4.4	2.6	7.0
30	1.08E+06 (13)	9.58E+06 (115)	12	808	153	4.0	2.0	7.0
31	5.33E+06 (32)	2.50E+06 (15)	6	211	107	73.6	39.0	146.4
32	4.29E+05 (6)	4.29E+06 (60)	14	361	94	3.6	1.2	8.1
33	3.13E+05 (5)	6.13E+06 (98)	16	516	105	1.8	0.6	4.3
34	7.78E+05 (14)	8.06E+06 (145)	18	679	115	3.4	1.8	5.8
35	4.78E+06 (86)	4.22E+06 (76)	18	356	82	39.4	28.6	54.4
36	3.75E+05 (3)	6.50E+06 (52)	8	548	152	2.1	0.4	6.2
37	4.20E+06 (63)	2.47E+06 (37)	15	208	68	59.0	38.8	91.2
38	6.67E+05 (24)	5.22E+06 (188)	36	440	66	4.5	2.8	6.8
39	5.33E+05 (16)	5.73E+06 (172)	30	483	75	3.3	1.8	5.4
40	9.52E+04 (2)	3.90E+06 (82)	21	329	73	0.9	0.1	3.2
41	3.13E+06 (25)	2.40E+07 (192)	8	2024	299	4.6	2.9	6.9
42	5.50E+06 (77)	3.57E+06 (50)	14	301	85	53.5	37.0	78.0
43	5.00E+05 (7)	7.29E+06 (102)	14	614	123	2.4	0.9	5.1
44	1.80E+06 (18)	1.18E+07 (118)	10	995	185	5.4	3.0	8.8
45	2.08E+06 (25)	2.50E+06 (30)	12	211	77	29.1	16.4	51.0
46	3.10E+05 (13)	7.90E+06 (332)	42	667	76	1.4	0.7	2.4
47	4.11E+06 (74)	2.17E+06 (39)	18	183	58	65.8	44.1	99.6
48	2.22E+05 (8)	3.03E+06 (109)	36	255	49	2.6	1.1	5.2
49	4.40E+06 (44)	7.20E+06 (72)	10	607	144	21.3	14.3	31.4
50	2.50E+05 (3)	5.17E+06 (62)	12	436	111	1.8	0.3	5.2
51	2.50E+05 (3)	5.83E+05 (7)	12	49	36	15.4	2.5	65.2
52	2.00E+06 (8)	1.50E+06 (6)	4	126	99	46.1	14.1	160.8
53	3.23E+05 (10)	6.90E+06 (214)	31	582	82	1.7	0.8	3.1
54	1.83E+06 (22)	2.50E+06 (30)	12	211	77	25.6	14.0	45.8
55	4.33E+06 (117)	6.48E+06 (175)	27	546	84	23.3	17.9	30.3
56	4.17E+05 (5)	8.67E+06 (104)	12	731	145	1.7	0.5	4.0
57	5.83E+05 (7)	6.75E+06 (81)	12	569	127	3.1	1.2	6.5
58	5.00E+05 (4)	1.55E+07 (124)	8	1307	238	1.2	0.3	3.0
59	9.00E+05 (36)	6.15E+06 (246)	40	519	68	5.1	3.5	7.3
60	6.13E+06 (49)	1.38E+06 (11)	8	116	68	151.9	79.2	323.6
61	5.00E+05 (5)	7.00E+06 (70)	10	590	142	2.6	0.8	6.1
62	1.06E+07 (211)	1.95E+06 (39)	20	164	53	185.5	132.1	267.8
63	1.00E+05 (1)	2.00E+06 (20)	10	169	75	2.0	0.0	10.9
64	2.50E+05 (6)	3.83E+06 (92)	24	323	68	2.3	0.8	5.1
65	3.33E+05 (4)	3.08E+06 (37)	12	260	85	3.9	1.0	10.5
66	1.15E+06 (15)	1.30E+07 (169)	13	1096	172	3.1	1.7	5.3
67	3.06E+06 (49)	1.38E+06 (22)	16	116	49	77.0	45.9	133.8
68	8.15E+05 (22)	1.41E+07 (380)	27	1187	127	2.0	1.2	3.1
69	3.75E+05 (6)	6.81E+06 (109)	16	574	111	2.0	0.7	4.3
70	6.67E+06 (40)	2.67E+06 (16)	6	225	111	86.1	47.6	164.9
71	6.22E+06 (56)	1.67E+06 (15)	9	141	72	128.0	72.2	243.6
72	4.00E+06 (48)	2.42E+06 (29)	12	204	75	57.4	35.6	94.4
73	1.67E+05 (2)	4.67E+06 (56)	12	393	105	1.3	0.1	4.7
74	2.75E+06 (44)	2.13E+06 (34)	16	179	61	45.0	28.1	72.5
75	2.67E+06 (32)	1.83E+06 (22)	12	155	65	50.5	28.5	91.1
76	2.00E+05 (6)	6.10E+06 (183)	30	514	78	1.2	0.4	2.5
77	7.31E+05 (19)	5.92E+06 (154)	26	499	82	4.3	2.5	7.0

78	4.07E+05	(11)	5.15E+06	(139)	27	434	75	2.8	1.3	5.1
79	6.00E+05	(12)	9.25E+06	(185)	20	780	117	2.3	1.1	4.1
80	1.30E+06	(26)	1.85E+06	(37)	20	156	51	24.5	14.2	41.5
81	1.63E+06	(13)	2.38E+06	(19)	8	200	91	23.9	10.8	50.8
82	7.00E+05	(21)	8.63E+06	(259)	30	728	93	2.9	1.7	4.4
83	2.63E+05	(15)	5.53E+06	(315)	57	466	54	1.7	0.9	2.8
84	5.63E+06	(45)	1.75E+06	(14)	8	148	78	110.3	60.1	217.8
85	8.00E+06	(48)	2.33E+06	(14)	6	197	104	117.6	64.5	231.0
86	2.83E+06	(17)	5.17E+06	(31)	6	436	156	19.2	9.9	35.6
87	1.11E+06	(10)	1.33E+06	(12)	9	112	64	29.1	11.2	73.1
88	3.88E+06	(31)	7.50E+05	(6)	8	63	50	174.1	73.6	508.4
89	1.13E+06	(18)	1.14E+07	(183)	16	964	146	3.5	2.0	5.6
90	2.00E+05	(6)	3.13E+06	(94)	30	264	55	2.3	0.8	5.0
91	2.89E+06	(130)	2.71E+06	(122)	45	229	42	37.1	28.2	48.8
92	5.56E+05	(25)	6.04E+06	(272)	45	510	64	3.2	2.0	4.8
93	1.00E+07	(40)	2.50E+06	(10)	4	211	130	136.5	68.2	305.9
94	3.75E+05	(6)	5.50E+06	(88)	16	464	100	2.4	0.8	5.4
95	3.33E+05	(6)	3.89E+06	(70)	18	328	79	3.1	1.1	6.8
96	5.00E+05	(14)	1.04E+06	(29)	28	87	32	16.9	8.2	32.9
97	2.50E+05	(7)	1.04E+06	(29)	28	87	32	8.6	3.1	19.6
98	3.75E+05	(12)	2.41E+06	(77)	32	203	47	5.5	2.7	10.1
99	3.40E+05	(17)	3.08E+06	(154)	50	260	43	3.9	2.2	6.4
100	8.25E+06	(66)	3.63E+06	(29)	8	306	113	78.7	50.3	126.4
101	7.80E+06	(39)	4.20E+06	(21)	5	354	153	64.3	37.1	115.1
102	6.67E+04	(2)	1.17E+06	(35)	30	98	33	2.1	0.2	7.8
103	2.60E+06	(39)	1.40E+06	(21)	15	118	51	64.3	37.1	115.1
104	1.92E+06	(23)	1.08E+06	(13)	12	91	50	61.1	29.9	131.5
105	5.42E+05	(13)	2.42E+06	(58)	24	204	54	7.9	3.9	14.4

YAKD39 (Alaska), modern sand

EFFECTIVE TRACK DENSITY FOR FLUENCE MONITOR (tracks/cm^2): 5.910E+05
RELATIVE ERROR (%): 1.58
EFFECTIVE URANIUM CONTENT OF MONITOR (ppm): 50.00
ZETA FACTOR AND STANDARD ERROR (yr cm^2): 117.70 7.10
SIZE OF COUNTER SQUARE (cm^2): 1.000E-06

Grain no.	**RhoS (cm^-2)**	**(Ns)**	**RhoI (cm^-2)**	**(Ni)**	**Squares**	**U+/-2s**		**Grain Age**	**Age (Ma) --95% CI--**	
1	9.33E+06	(56)	2.50E+06	(15)	6	212	108	127.6	72.0	242.8
2	9.50E+06	(38)	5.75E+06	(23)	4	486	201	57.1	33.3	100.4
3	3.00E+06	(15)	2.80E+06	(14)	5	237	125	37.1	16.7	82.9
4	6.75E+06	(54)	5.13E+06	(41)	8	434	135	45.6	29.9	70.2
5	3.17E+06	(38)	5.75E+06	(69)	12	486	118	19.2	12.5	28.8
6	6.09E+06	(67)	2.45E+06	(27)	11	208	79	85.4	54.2	139.0
7	9.17E+05	(11)	1.33E+06	(16)	12	113	56	24.0	10.0	54.7
8	7.25E+06	(87)	2.67E+06	(32)	12	226	79	93.6	62.0	145.1
9	7.75E+06	(31)	3.50E+06	(14)	4	296	156	76.1	39.6	154.9
10	6.88E+06	(55)	7.00E+06	(56)	8	592	159	34.1	23.0	50.4
11	4.11E+06	(37)	2.22E+06	(20)	9	188	83	63.8	36.3	116.1
12	1.00E+07	(60)	5.67E+06	(34)	6	479	164	61.0	39.5	95.8
13	4.38E+06	(70)	2.88E+06	(46)	16	243	72	52.7	35.8	78.2
14	4.92E+06	(64)	4.54E+06	(59)	13	384	100	37.6	26.0	54.5
15	4.43E+06	(31)	2.29E+06	(16)	7	193	95	66.7	35.6	130.7
16	8.00E+06	(48)	4.50E+06	(27)	6	381	146	61.4	37.7	102.4
17	9.83E+06	(118)	5.58E+06	(67)	12	472	116	60.9	44.8	83.6
18	2.33E+06	(21)	1.89E+06	(17)	9	160	77	42.8	21.5	86.2
19	6.50E+06	(78)	8.33E+05	(10)	12	71	44	262.1	138.3	563.0

20	1.00E+07	(40)	5.00E+06	(20)	4	423	187	68.9	39.6	124.5
21	1.04E+07	(52)	4.40E+06	(22)	5	372	157	81.4	48.8	140.8
22	4.00E+06	(32)	2.13E+06	(17)	8	180	86	64.9	35.2	124.6
23	6.13E+06	(49)	1.75E+06	(14)	8	148	78	119.6	65.7	234.7
24	1.64E+06	(23)	2.43E+06	(34)	14	205	70	23.5	13.2	41.0
25	1.05E+07	(126)	3.25E+06	(39)	12	275	88	111.1	77.3	163.5
26	9.29E+06	(130)	2.43E+06	(34)	14	205	70	131.2	89.8	197.4
27	3.42E+06	(41)	9.17E+05	(11)	12	78	46	127.0	65.1	274.0
28	7.20E+06	(36)	3.80E+06	(19)	5	321	146	65.3	36.7	120.6
29	4.57E+06	(32)	2.29E+06	(16)	7	193	95	68.8	36.9	134.5
30	4.33E+06	(52)	8.33E+06	(100)	12	705	142	18.1	12.7	25.5
31	1.17E+07	(70)	1.05E+07	(63)	6	888	225	38.5	27.0	55.1
32	3.80E+06	(76)	1.75E+06	(35)	20	148	50	74.9	49.7	115.3
33	1.63E+06	(13)	2.13E+06	(17)	8	180	86	26.6	11.9	57.9
34	5.50E+06	(22)	2.00E+06	(8)	4	169	116	93.8	40.9	244.0
35	9.00E+06	(72)	5.88E+06	(47)	8	497	145	53.0	36.2	78.3
36	3.25E+06	(39)	3.42E+06	(41)	12	289	90	33.0	20.7	52.4
37	6.17E+06	(37)	3.17E+06	(19)	6	268	122	67.1	37.8	123.6
38	3.33E+06	(20)	2.67E+06	(16)	6	226	111	43.2	21.4	89.2
39	2.94E+06	(47)	3.69E+06	(59)	16	312	81	27.7	18.4	41.3
40	6.17E+06	(37)	2.67E+06	(16)	6	226	111	79.5	43.5	153.2
41	1.03E+07	(103)	3.80E+06	(38)	10	321	104	93.3	64.0	139.3
42	8.17E+06	(49)	6.33E+06	(38)	6	536	174	44.7	28.7	70.1
43	1.42E+07	(85)	7.50E+06	(45)	6	635	189	65.3	45.0	95.9
44	9.80E+06	(49)	2.60E+06	(13)	5	220	120	128.6	69.6	258.4
45	8.00E+06	(32)	1.00E+06	(4)	4	85	80	263.4	97.9	1001.6
46	1.08E+07	(43)	7.50E+06	(30)	4	635	231	49.6	30.5	81.9
47	5.25E+06	(42)	5.88E+06	(47)	8	497	145	31.0	19.9	48.0
48	5.67E+06	(136)	2.58E+06	(62)	24	219	56	75.7	55.8	104.1
49	8.75E+06	(35)	3.25E+06	(13)	4	275	150	92.3	48.1	190.2
50	8.90E+06	(89)	3.90E+06	(39)	10	330	106	78.7	53.6	117.9
51	9.67E+06	(58)	3.17E+06	(19)	6	268	122	104.7	62.0	186.3
52	2.63E+06	(63)	1.79E+06	(43)	24	152	46	50.7	33.9	76.6
53	3.11E+06	(59)	1.11E+06	(21)	19	94	40	96.5	58.2	167.3
54	5.08E+06	(127)	1.68E+06	(42)	25	142	44	104.1	73.1	151.3
55	2.75E+06	(33)	1.42E+06	(17)	12	120	57	66.9	36.4	128.1
56	3.58E+06	(86)	1.38E+06	(33)	24	116	40	89.7	59.7	138.5
57	4.80E+06	(24)	3.20E+06	(16)	5	271	134	51.8	26.5	104.3
58	5.45E+06	(60)	4.82E+06	(53)	11	408	112	39.2	26.7	57.9
59	7.25E+06	(87)	2.00E+06	(24)	12	169	69	124.3	78.9	204.2
60	4.56E+06	(73)	1.13E+06	(18)	16	95	44	138.6	82.7	246.6
61	5.75E+06	(46)	1.63E+06	(13)	8	137	75	120.8	65.0	243.9
62	6.67E+06	(40)	2.83E+06	(17)	6	240	115	80.9	45.2	152.3
63	5.67E+06	(68)	4.08E+06	(49)	12	345	99	48.0	32.8	70.9
64	8.67E+06	(52)	3.67E+06	(22)	6	310	131	81.4	48.8	140.8
65	8.83E+06	(106)	3.08E+06	(37)	12	261	86	98.6	67.5	147.6
66	9.80E+06	(98)	3.90E+06	(39)	10	330	106	86.6	59.4	129.0
67	5.40E+06	(108)	2.05E+06	(41)	20	173	54	90.8	63.0	133.5
68	5.43E+06	(76)	2.29E+06	(32)	14	193	68	81.8	53.7	128.0
69	5.25E+06	(168)	2.41E+06	(77)	32	204	47	75.4	57.3	100.1
70	6.20E+06	(93)	5.33E+06	(80)	15	451	102	40.3	29.5	55.1
71	6.83E+06	(41)	2.50E+06	(15)	6	212	108	93.7	51.3	182.5
72	7.20E+06	(72)	2.30E+06	(23)	10	195	81	107.5	66.9	180.2
73	3.33E+06	(20)	5.83E+06	(35)	6	494	166	19.9	10.9	35.3
74	8.50E+06	(34)	2.00E+06	(8)	4	169	116	144.0	66.8	359.7
75	9.30E+06	(93)	1.10E+06	(11)	10	93	55	283.9	155.0	582.7

76	9.83E+06	(118)	5.75E+06	(69)	12	486	118	59.2	43.6	80.9
77	4.94E+06	(89)	4.39E+06	(79)	18	371	84	39.1	28.5	53.6
78	5.00E+06	(30)	3.17E+06	(19)	6	268	122	54.5	29.8	102.5
79	4.00E+06	(24)	1.83E+06	(11)	6	155	92	74.9	35.7	169.5
80	5.50E+06	(33)	2.00E+06	(12)	6	169	96	94.1	47.9	200.4
81	2.79E+06	(78)	1.25E+06	(35)	28	106	36	76.9	51.1	118.1
82	8.00E+06	(32)	1.03E+07	(41)	4	867	271	27.1	16.5	44.1
83	4.47E+06	(67)	2.93E+06	(44)	15	248	75	52.7	35.5	79.0
84	1.68E+07	(67)	5.00E+06	(20)	4	423	187	114.8	69.4	199.8
85	5.88E+06	(47)	4.88E+06	(39)	8	412	132	41.8	26.7	65.6
86	2.83E+06	(17)	4.00E+06	(24)	6	338	137	24.7	12.4	47.7
87	5.11E+06	(46)	4.56E+06	(41)	9	385	120	38.9	25.0	60.8
88	4.43E+06	(31)	7.14E+05	(5)	7	60	52	206.6	82.5	674.2
89	8.67E+06	(104)	2.92E+06	(35)	12	247	83	102.2	69.4	154.6
90	1.38E+07	(83)	5.50E+06	(33)	6	465	161	86.6	57.5	134.0
91	1.25E+06	(15)	1.17E+06	(14)	12	99	52	37.1	16.7	82.9
92	6.10E+06	(61)	3.90E+06	(39)	10	330	106	54.1	35.7	83.1
93	6.83E+06	(41)	6.33E+06	(38)	6	536	174	37.4	23.5	59.8
94	5.11E+06	(46)	7.78E+06	(70)	9	658	158	22.8	15.4	33.6
95	6.50E+06	(26)	4.75E+06	(19)	4	402	182	47.3	25.3	90.4
96	9.38E+05	(15)	2.44E+06	(39)	16	206	66	13.5	6.8	24.8
97	9.17E+06	(110)	3.17E+06	(38)	12	268	87	99.6	68.6	148.2
98	1.62E+06	(21)	2.62E+06	(34)	13	221	76	21.5	11.8	38.0
99	2.33E+06	(14)	2.17E+06	(13)	6	183	100	37.3	16.3	86.0
100	1.62E+06	(73)	5.33E+05	(24)	45	45	18	104.5	65.5	173.3
101	5.33E+06	(64)	1.50E+06	(18)	12	127	59	121.7	71.9	218.2
102	8.11E+06	(146)	5.00E+06	(90)	18	423	90	56.1	42.0	74.7
103	3.33E+06	(40)	1.42E+06	(17)	12	120	57	80.9	45.2	152.3
104	5.11E+06	(46)	7.11E+06	(64)	9	602	151	25.0	16.7	37.0

YAKD40 (Alaska), modern sand

EFFECTIVE TRACK DENSITY FOR FLUENCE MONITOR (tracks/cm^2): 5.910E+05
RELATIVE ERROR (%): 1.58
EFFECTIVE URANIUM CONTENT OF MONITOR (ppm): 50.00
ZETA FACTOR AND STANDARD ERROR (yr cm^2): 117.70 7.10
SIZE OF COUNTER SQUARE (cm^2): 1.000E-06

Grain no.	**RhoS (cm^-2)**	**(Ns)**	**RhoI (cm^-2)**	**(Ni)**	**Squares**	**U+/-2s**		**Grain Age**	**Age (Ma) --95% CI--**	
1	3.30E+06	(99)	2.43E+06	(73)	30	206	48	47.0	34.4	64.5
2	5.75E+06	(46)	4.38E+06	(35)	8	370	125	45.5	28.7	72.8
3	1.56E+05	(7)	2.07E+06	(93)	45	175	37	2.7	1.0	5.6
4	6.94E+06	(111)	2.81E+06	(45)	16	238	71	85.1	59.8	123.2
5	3.78E+06	(136)	1.39E+06	(50)	36	118	33	93.7	67.5	132.4
6	5.50E+06	(55)	3.30E+06	(33)	10	279	97	57.6	36.8	91.6
7	1.02E+07	(61)	5.67E+06	(34)	6	479	164	62.0	40.2	97.3
8	7.14E+06	(150)	2.48E+06	(52)	21	209	58	99.4	72.2	139.0
9	1.20E+06	(12)	9.00E+05	(9)	10	76	49	46.0	17.9	123.5
10	4.64E+06	(167)	3.00E+06	(108)	36	254	49	53.5	40.8	70.0
11	9.40E+06	(94)	3.10E+06	(31)	10	262	94	104.3	69.2	162.0
12	3.44E+06	(186)	1.11E+06	(60)	54	94	24	106.7	79.6	145.4
13	4.67E+06	(56)	5.83E+05	(7)	12	49	36	267.1	125.2	686.3
14	3.88E+06	(31)	3.75E+06	(30)	8	317	115	35.8	21.0	61.2
15	4.31E+06	(138)	1.91E+06	(61)	32	161	41	78.1	57.5	107.5
16	7.50E+06	(45)	4.33E+06	(26)	6	367	143	59.8	36.2	101.0
17	4.13E+06	(62)	3.87E+06	(58)	15	327	86	37.1	25.5	54.0
18	3.20E+06	(48)	6.27E+06	(94)	15	530	110	17.8	12.2	25.4

19	7.22E+05	(13)	3.72E+06	(67)	18	315	77	6.8	3.4	12.3
20	3.33E+06	(60)	1.06E+06	(19)	18	89	41	108.3	64.3	192.2
21	4.92E+06	(59)	4.75E+06	(57)	12	402	107	35.9	24.5	52.6
22	1.00E+06	(15)	1.53E+06	(23)	15	130	54	22.7	11.0	45.3
23	4.50E+06	(27)	2.00E+06	(12)	6	169	96	77.2	38.2	167.5
24	4.57E+06	(96)	3.38E+06	(71)	21	286	68	46.8	34.1	64.6
25	5.13E+06	(77)	3.07E+06	(46)	15	259	77	57.9	39.7	85.4
26	5.25E+06	(42)	3.25E+06	(26)	8	275	107	55.8	33.5	94.9
27	4.83E+06	(29)	8.33E+05	(5)	6	71	60	193.6	76.7	635.5
28	4.55E+05	(5)	2.55E+06	(28)	11	215	81	6.4	1.9	16.3
29	6.00E+06	(30)	7.20E+06	(36)	5	609	203	29.0	17.2	48.3
30	4.50E+06	(36)	1.63E+06	(13)	8	137	75	94.9	49.7	195.1
31	2.17E+06	(26)	1.25E+06	(15)	12	106	54	59.7	30.7	121.4
32	4.92E+06	(123)	5.12E+06	(128)	25	433	78	33.3	25.3	43.9
33	9.40E+06	(94)	6.70E+06	(67)	10	567	139	48.6	35.1	67.6
34	4.65E+06	(279)	3.05E+06	(183)	60	258	39	52.8	42.3	65.9
35	4.78E+06	(43)	5.00E+06	(45)	9	423	126	33.2	21.3	51.5
36	7.21E+06	(173)	7.21E+06	(173)	24	610	95	34.7	27.2	44.2
37	5.22E+06	(47)	4.22E+06	(38)	9	357	116	42.8	27.4	67.5
38	9.00E+06	(72)	3.50E+06	(28)	8	296	111	88.5	56.8	142.4
39	1.05E+06	(21)	3.90E+06	(78)	20	330	75	9.4	5.5	15.3
40	2.27E+06	(34)	1.60E+06	(24)	15	135	55	49.0	28.3	86.4
41	4.75E+06	(57)	2.50E+06	(30)	12	212	77	65.6	41.6	105.8
42	2.59E+06	(88)	9.12E+05	(31)	34	77	28	97.7	64.5	152.3
43	6.00E+06	(24)	3.75E+06	(15)	4	317	161	55.2	27.9	113.2
44	3.17E+06	(38)	3.92E+06	(47)	12	331	97	28.1	17.8	44.0
45	6.63E+06	(53)	2.25E+06	(18)	8	190	89	101.0	58.7	183.3
46	3.90E+06	(39)	1.90E+06	(19)	10	161	73	70.7	40.1	129.6
47	5.56E+05	(5)	2.22E+06	(20)	9	188	83	8.9	2.5	23.9
48	5.13E+06	(123)	1.58E+06	(38)	24	134	43	111.3	77.1	164.7
49	4.12E+06	(103)	2.72E+06	(68)	25	230	56	52.4	38.2	72.4
50	3.75E+06	(30)	2.00E+06	(16)	8	169	83	64.6	34.3	127.0
51	2.37E+06	(83)	1.34E+06	(47)	35	114	33	61.0	42.2	89.3
52	2.57E+05	(9)	5.71E+05	(20)	35	48	21	15.8	6.3	35.9
53	1.05E+07	(42)	9.25E+06	(37)	4	783	257	39.3	24.7	62.9
54	3.33E+06	(40)	1.17E+06	(14)	12	99	52	97.9	52.7	195.0
55	3.00E+06	(84)	1.79E+06	(50)	28	151	43	58.1	40.5	84.2
56	3.79E+06	(106)	3.07E+06	(86)	28	260	56	42.7	31.8	57.5
57	9.38E+06	(75)	3.50E+06	(28)	8	296	111	92.2	59.3	147.9
58	1.87E+06	(112)	1.37E+06	(82)	60	116	26	47.3	35.3	63.8
59	6.72E+06	(121)	2.50E+06	(45)	18	212	63	92.6	65.5	133.6
60	7.56E+06	(121)	3.25E+06	(52)	16	275	76	80.3	57.7	113.5
61	4.40E+06	(132)	1.77E+06	(53)	30	149	41	85.9	62.1	120.6
62	4.80E+06	(72)	2.20E+06	(33)	15	186	65	75.2	49.4	117.4
63	8.33E+06	(75)	4.44E+06	(40)	9	376	119	64.8	43.7	97.7
64	6.25E+06	(150)	3.08E+06	(74)	24	261	61	70.0	52.7	93.9
65	2.85E+06	(114)	1.80E+06	(72)	40	152	36	54.8	40.5	74.7
66	6.80E+06	(136)	3.75E+06	(75)	20	317	74	62.7	47.0	84.4
67	5.58E+06	(67)	4.08E+06	(49)	12	345	99	47.3	32.3	69.9
68	6.67E+05	(16)	7.50E+06	(180)	24	635	97	3.1	1.7	5.2
69	5.50E+06	(110)	8.55E+06	(171)	20	723	113	22.4	17.1	29.2
70	3.80E+06	(38)	1.30E+06	(13)	10	110	60	100.1	52.7	204.9
71	4.33E+06	(39)	4.11E+06	(37)	9	348	114	36.6	22.7	58.9
72	6.36E+06	(70)	8.27E+06	(91)	11	700	148	26.7	19.2	36.9
73	2.56E+06	(41)	1.69E+06	(27)	16	143	55	52.5	31.6	88.8
74	3.38E+06	(27)	5.00E+06	(40)	8	423	134	23.5	13.8	39.1

75	1.63E+06	(13)	3.50E+06	(28)	8	296	111	16.2	7.7	32.2
76	4.00E+06	(48)	3.67E+06	(44)	12	310	94	37.8	24.6	58.3
77	8.17E+06	(49)	3.33E+06	(20)	6	282	125	84.3	49.5	149.8
78	8.00E+04	(2)	8.40E+05	(21)	25	71	31	3.5	0.4	13.5
79	2.32E+06	(86)	1.27E+06	(47)	37	107	31	63.2	43.9	92.3
80	1.87E+06	(28)	1.07E+06	(16)	15	90	45	60.3	31.7	119.4
81	2.87E+06	(43)	1.73E+06	(26)	15	147	57	57.1	34.4	96.9
82	3.69E+06	(59)	2.06E+06	(33)	16	174	61	61.8	39.8	97.7
83	4.22E+06	(211)	2.16E+06	(108)	50	183	36	67.4	52.0	87.5
84	2.36E+06	(59)	1.48E+06	(37)	25	125	41	55.1	36.0	85.6
85	1.33E+06	(8)	1.17E+06	(7)	6	99	72	39.5	12.6	127.6
86	2.80E+06	(28)	1.70E+06	(17)	10	144	69	56.8	30.2	110.7
87	6.22E+06	(56)	2.00E+06	(18)	9	169	79	106.7	62.3	192.9
88	4.68E+06	(187)	1.58E+06	(63)	40	133	34	102.3	76.6	138.4
89	2.61E+06	(47)	1.06E+06	(19)	18	89	41	85.0	49.3	153.6
90	4.83E+06	(29)	5.50E+06	(33)	6	465	161	30.5	17.9	51.8
91	4.30E+06	(43)	1.90E+06	(19)	10	161	73	77.9	44.7	141.6
92	4.56E+06	(41)	5.78E+06	(52)	9	489	136	27.4	17.7	42.0
93	1.67E+05	(2)	3.42E+06	(41)	12	289	90	1.8	0.2	6.5
94	3.50E+06	(21)	5.17E+06	(31)	6	437	156	23.6	12.8	42.2
95	3.92E+06	(47)	2.25E+06	(27)	12	190	73	60.1	36.8	100.4
96	6.17E+06	(37)	2.83E+06	(17)	6	240	115	74.9	41.4	141.9
97	2.42E+06	(29)	6.00E+06	(72)	12	508	120	14.0	8.8	21.8
98	5.25E+06	(21)	1.75E+06	(7)	4	148	108	102.0	42.6	284.4
99	8.75E+05	(42)	6.90E+06	(331)	48	583	67	4.4	3.1	6.1
100	3.67E+06	(55)	2.27E+06	(34)	15	192	66	55.9	35.9	88.5
101	2.00E+05	(2)	2.50E+06	(25)	10	212	84	3.0	0.3	11.2
102	1.90E+05	(4)	3.00E+06	(63)	21	254	64	2.3	0.6	5.9
103	6.75E+06	(27)	4.00E+06	(16)	4	338	167	58.2	30.4	115.7
104	4.13E+06	(62)	2.60E+06	(39)	15	220	70	55.0	36.3	84.3
105	2.09E+06	(73)	8.57E+05	(30)	35	73	26	83.8	54.3	132.9

YAKD41 (Alaska), modern sand

EFFECTIVE TRACK DENSITY FOR FLUENCE MONITOR (tracks/cm^2): 5.910E+05
RELATIVE ERROR (%): 1.58
EFFECTIVE URANIUM CONTENT OF MONITOR (ppm): 50.00
ZETA FACTOR AND STANDARD ERROR (yr cm^2): 117.70 7.10
SIZE OF COUNTER SQUARE (cm^2): 1.000E-06

Grain no.	**RhoS (cm^-2)**	**(Ns)**	**RhoI (cm^-2)**	**(Ni)**	**Squares**	**U+/-2s**		**Grain Age**	**Age (Ma) --95% CI--**	
1	7.40E+06	(111)	3.53E+06	(53)	15	299	82	72.3	51.8	102.4
2	6.38E+06	(51)	3.63E+06	(29)	8	307	113	60.7	37.9	99.4
3	4.89E+06	(44)	3.56E+06	(32)	9	301	106	47.6	29.6	77.5
4	5.17E+06	(31)	3.83E+06	(23)	6	324	134	46.6	26.4	83.7
5	1.03E+07	(41)	7.25E+06	(29)	4	613	227	48.9	29.7	81.6
6	5.88E+06	(47)	3.88E+06	(31)	8	328	117	52.4	32.7	85.4
7	6.43E+06	(45)	4.86E+06	(34)	7	411	141	45.8	28.7	73.8
8	4.88E+06	(39)	2.75E+06	(22)	8	233	98	61.2	35.5	108.4
9	5.75E+06	(23)	3.25E+06	(13)	4	275	150	60.9	29.8	131.0
10	4.00E+06	(48)	2.17E+06	(26)	12	183	71	63.7	38.9	107.1
11	7.20E+06	(36)	5.60E+06	(28)	5	474	178	44.5	26.5	75.7
12	7.83E+06	(47)	3.00E+06	(18)	6	254	118	89.7	51.5	164.2
13	5.88E+06	(47)	3.00E+06	(24)	8	254	103	67.5	40.6	115.6
14	2.56E+06	(46)	1.33E+06	(24)	18	113	46	66.1	39.7	113.3
15	6.50E+06	(26)	5.25E+06	(21)	4	444	192	42.9	23.2	80.1
16	6.78E+06	(61)	5.67E+06	(51)	9	479	134	41.5	28.1	61.4

17	7.36E+06 (206)	2.86E+06 (80)	28	242	54	88.6	66.7	117.6
18	6.56E+06 (59)	2.56E+06 (23)	9	216	89	88.2	54.0	149.8
19	9.20E+06 (46)	4.60E+06 (23)	5	389	161	69.0	41.1	119.3
20	8.00E+06 (72)	3.78E+06 (34)	9	320	109	73.1	48.1	113.4
21	7.40E+06 (37)	3.60E+06 (18)	5	305	142	70.8	39.5	132.2
22	6.93E+06 (104)	2.87E+06 (43)	15	243	74	83.4	58.1	122.0
23	7.00E+06 (42)	1.83E+06 (11)	6	155	92	130.1	66.8	280.1
24	4.17E+06 (25)	1.50E+06 (9)	6	127	82	94.8	43.4	231.2
25	5.70E+06 (57)	2.70E+06 (27)	10	228	87	72.8	45.5	119.8
26	6.14E+06 (86)	5.79E+06 (81)	14	489	110	36.8	26.8	50.5
27	9.33E+06 (56)	4.00E+06 (24)	6	338	137	80.3	49.2	135.6
28	4.39E+06 (158)	1.83E+06 (66)	36	155	38	82.6	61.7	112.0
29	5.00E+06 (60)	2.50E+06 (30)	12	212	77	69.0	44.0	110.9
30	4.44E+06 (80)	2.94E+06 (53)	18	249	69	52.2	36.5	75.4
31	6.13E+06 (49)	4.63E+06 (37)	8	391	128	45.9	29.3	72.3
32	8.83E+06 (53)	2.83E+06 (17)	6	240	115	106.8	61.5	196.9
33	3.17E+06 (19)	2.17E+06 (13)	6	183	100	50.4	23.8	111.1
34	6.60E+06 (33)	3.40E+06 (17)	5	288	138	66.9	36.4	128.1
35	6.67E+06 (60)	4.11E+06 (37)	9	348	114	56.1	36.7	86.9
36	1.50E+06 (15)	1.00E+06 (10)	10	85	52	51.7	21.9	128.7
37	6.14E+06 (43)	2.43E+06 (17)	7	205	98	86.9	48.9	162.6
38	7.83E+06 (47)	4.67E+06 (28)	6	395	148	58.0	35.7	96.2
39	1.05E+07 (126)	5.00E+06 (60)	12	423	110	72.5	53.0	100.5
40	8.50E+06 (34)	2.00E+06 (8)	4	169	116	144.0	66.8	359.7
41	5.50E+06 (44)	2.25E+06 (18)	8	190	89	84.0	47.9	154.6
42	8.19E+06 (131)	1.75E+06 (28)	16	148	56	160.0	106.5	249.7
43	1.13E+07 (169)	8.80E+06 (132)	15	745	131	44.3	34.3	57.3
44	5.25E+06 (21)	1.50E+06 (6)	4	127	100	118.4	47.3	358.7
45	1.18E+07 (59)	5.40E+06 (27)	5	457	175	75.3	47.2	123.6
46	8.00E+06 (32)	2.25E+06 (9)	4	190	124	120.9	57.4	288.2
47	1.10E+07 (44)	1.15E+07 (46)	4	973	287	33.2	21.4	51.3
48	4.94E+06 (79)	3.19E+06 (51)	16	270	76	53.6	37.3	77.8
49	7.78E+06 (70)	2.44E+06 (22)	9	207	87	109.2	67.3	185.2
50	8.71E+06 (61)	3.86E+06 (27)	7	326	125	77.9	49.0	127.5
51	3.78E+06 (34)	4.00E+06 (36)	9	338	113	32.8	19.9	53.9
52	3.70E+06 (111)	1.83E+06 (55)	30	155	42	69.7	50.1	98.2
53	7.33E+06 (66)	3.67E+06 (33)	9	310	108	69.0	44.9	108.3
54	4.25E+06 (68)	2.81E+06 (45)	16	238	71	52.3	35.4	78.0
55	4.53E+06 (172)	2.89E+06 (110)	38	245	47	54.1	41.4	70.6
56	9.50E+06 (152)	4.69E+06 (75)	16	397	92	70.0	52.8	93.7
57	8.67E+06 (52)	6.17E+06 (37)	6	522	171	48.6	31.3	76.3
58	8.60E+06 (129)	4.60E+06 (69)	15	389	94	64.6	47.9	88.0
59	9.50E+06 (57)	7.00E+06 (42)	6	592	183	47.0	31.0	71.8
60	7.50E+06 (60)	2.88E+06 (23)	8	243	101	89.7	55.0	152.1
61	4.20E+06 (84)	1.90E+06 (38)	20	161	52	76.3	51.5	115.1
62	1.42E+07 (85)	7.33E+06 (44)	6	620	187	66.7	45.9	98.4
63	8.89E+06 (80)	4.33E+06 (39)	9	367	117	70.8	47.8	106.7
64	2.69E+06 (105)	1.10E+06 (43)	39	93	28	84.2	58.7	123.1
65	5.75E+06 (69)	2.25E+06 (27)	12	190	73	88.0	55.9	142.9
66	2.31E+06 (37)	8.13E+05 (13)	16	69	37	97.5	51.2	200.0
67	4.75E+06 (38)	2.25E+06 (18)	8	190	89	72.7	40.7	135.4
68	6.40E+06 (128)	1.50E+06 (30)	20	127	46	146.1	98.2	225.2
69	6.00E+06 (24)	3.50E+06 (14)	4	296	156	59.1	29.5	123.6
70	8.50E+06 (51)	2.17E+06 (13)	6	183	100	133.8	72.7	268.1
71	5.13E+06 (154)	2.20E+06 (66)	30	186	46	80.5	60.1	109.3
72	8.20E+06 (41)	4.80E+06 (24)	5	406	165	59.0	34.9	102.1

73	5.33E+06	(32)	4.50E+06	(27)	6	381	146	41.1	23.9	71.2
74	1.43E+07	(57)	4.50E+06	(18)	4	381	177	108.5	63.5	196.0
75	3.47E+06	(52)	2.40E+06	(36)	15	203	68	50.0	32.1	78.7
76	7.80E+06	(78)	7.30E+06	(73)	10	618	145	37.1	26.6	51.7
77	6.00E+06	(60)	3.50E+06	(35)	10	296	100	59.2	38.5	92.7
78	7.25E+06	(29)	2.75E+06	(11)	4	233	137	90.2	44.3	200.4
79	5.50E+06	(33)	2.50E+06	(15)	6	212	108	75.6	40.3	150.0
80	8.04E+06	(193)	3.04E+06	(73)	24	257	61	91.2	69.4	121.2
81	1.18E+07	(118)	5.40E+06	(54)	10	457	125	75.4	54.3	106.2
82	1.13E+07	(90)	5.63E+06	(45)	8	476	142	69.1	47.9	101.2
83	5.40E+06	(108)	3.85E+06	(77)	20	326	75	48.6	35.9	66.0
84	4.11E+06	(37)	4.22E+06	(38)	9	357	116	33.8	20.9	54.6
85	6.11E+06	(55)	1.89E+06	(17)	9	160	77	110.8	64.0	203.8
86	2.81E+06	(45)	8.13E+05	(13)	16	69	37	118.2	63.5	239.0
87	7.89E+06	(71)	3.56E+06	(32)	9	301	106	76.5	49.9	120.1
88	4.63E+06	(74)	1.13E+06	(18)	16	95	44	140.5	83.9	249.8
89	8.60E+06	(43)	5.20E+06	(26)	5	440	171	57.1	34.4	96.9
90	9.40E+06	(47)	5.20E+06	(26)	5	440	171	62.4	38.0	105.0
91	6.83E+06	(82)	4.08E+06	(49)	12	345	99	57.9	40.2	84.3
92	9.75E+06	(195)	4.85E+06	(97)	20	410	84	69.4	52.9	90.9
93	3.25E+06	(52)	1.63E+06	(26)	16	137	54	69.0	42.5	115.2
94	6.50E+06	(117)	4.00E+06	(72)	18	338	80	56.2	41.6	76.6
95	9.33E+06	(84)	6.67E+06	(60)	9	564	146	48.5	34.4	68.7
96	3.56E+06	(64)	1.44E+06	(26)	18	122	48	84.7	53.2	139.4
97	1.06E+07	(127)	7.67E+06	(92)	12	649	136	47.8	36.3	63.3
98	6.30E+06	(63)	4.20E+06	(42)	10	355	110	51.9	34.6	78.7
99	9.60E+06	(48)	2.80E+06	(14)	5	237	125	117.2	64.3	230.3
100	1.10E+07	(55)	4.20E+06	(21)	5	355	154	90.0	53.9	156.8
101	5.40E+06	(81)	2.73E+06	(41)	15	231	72	68.2	46.4	102.0
102	7.56E+06	(136)	4.00E+06	(72)	18	338	80	65.3	48.8	88.2
103	5.11E+06	(92)	2.22E+06	(40)	18	188	59	79.3	54.3	118.1

YAKD42 (Alaska), modern sand

EFFECTIVE TRACK DENSITY FOR FLUENCE MONITOR (tracks/cm^2): 5.900E+05

RELATIVE ERROR (%): 1.58

EFFECTIVE URANIUM CONTENT OF MONITOR (ppm): 50.00

ZETA FACTOR AND STANDARD ERROR (yr cm^2): 117.70 7.10

SIZE OF COUNTER SQUARE (cm^2): 1.000E-06

Grain no.	**RhoS (cm^-2)**	**(Ns)**	**RhoI (cm^-2)**	**(Ni)**	**Squares**	**U+/-2s**		**Grain Age**	**Age (Ma) --95% CI--**	
1	2.83E+06	(17)	3.67E+06	(22)	6	311	131	26.8	13.4	52.8
2	3.72E+06	(67)	5.06E+06	(91)	18	428	91	25.5	18.3	35.4
3	4.25E+06	(68)	2.44E+06	(39)	16	207	66	60.2	40.1	91.7
4	5.06E+06	(182)	4.14E+06	(149)	36	351	58	42.2	33.0	54.1
5	2.50E+06	(50)	1.29E+07	(257)	20	1089	140	6.8	4.9	9.2
6	2.44E+06	(44)	2.44E+06	(44)	18	207	62	34.6	22.3	53.8
7	5.50E+06	(33)	5.67E+06	(34)	6	480	164	33.6	20.2	55.9
8	1.63E+06	(13)	2.50E+06	(20)	8	212	94	22.6	10.3	47.5
9	3.42E+06	(41)	8.00E+06	(96)	12	678	140	14.8	10.0	21.6
10	1.28E+06	(32)	1.84E+06	(46)	25	156	46	24.2	14.9	38.7
11	7.17E+06	(43)	6.67E+06	(40)	6	565	178	37.2	23.6	58.7
12	2.29E+06	(48)	1.62E+06	(34)	21	137	47	48.8	30.8	78.1
13	5.71E+06	(40)	5.14E+06	(36)	7	436	145	38.5	23.9	62.1
14	2.70E+06	(73)	2.41E+06	(65)	27	204	51	38.9	27.4	55.2
15	5.13E+06	(41)	3.13E+06	(25)	8	265	105	56.6	33.7	97.1
16	6.25E+06	(25)	8.75E+06	(35)	4	742	250	24.8	14.2	42.5

17	1.92E+06	(23)	1.50E+06	(18)	12	127	59	44.1	22.9	86.7
18	1.67E+06	(20)	2.00E+06	(24)	12	169	69	28.9	15.1	54.5
19	1.40E+06	(14)	2.50E+06	(25)	10	212	84	19.5	9.3	38.8
20	5.75E+06	(23)	2.25E+06	(9)	4	191	124	87.2	39.4	214.4
21	1.07E+06	(16)	1.00E+06	(15)	15	85	43	36.9	17.1	80.0
22	4.50E+06	(45)	4.30E+06	(43)	10	364	111	36.2	23.3	56.4
23	2.75E+06	(33)	3.42E+06	(41)	12	290	90	27.9	17.1	45.2
24	1.83E+06	(11)	3.50E+06	(21)	6	297	128	18.3	7.9	39.4
25	1.31E+06	(21)	2.88E+06	(46)	16	244	72	15.9	9.0	27.1
26	5.43E+06	(38)	5.00E+06	(35)	7	424	143	37.6	23.1	61.2
27	4.63E+06	(37)	4.00E+06	(32)	8	339	119	40.0	24.3	66.3
28	1.42E+06	(17)	1.83E+06	(22)	12	155	66	26.8	13.4	52.8
29	2.67E+06	(16)	8.67E+06	(52)	6	734	204	10.8	5.7	19.0
30	2.08E+06	(25)	2.50E+06	(30)	12	212	77	28.9	16.3	50.8
31	2.10E+06	(21)	6.10E+06	(61)	10	517	133	12.0	6.9	19.9
32	2.00E+06	(36)	1.33E+06	(24)	18	113	46	51.8	30.1	90.7
33	4.67E+06	(28)	2.67E+06	(16)	6	226	111	60.2	31.7	119.2
34	5.17E+06	(62)	1.75E+06	(21)	12	148	64	101.2	61.3	174.9
35	8.50E+06	(51)	3.67E+06	(22)	6	311	131	79.7	47.7	138.0
36	1.74E+06	(47)	3.30E+06	(89)	27	279	60	18.3	12.6	26.4
37	3.67E+06	(33)	5.22E+06	(47)	9	443	129	24.4	15.1	38.8
38	1.94E+06	(31)	4.75E+06	(76)	16	403	93	14.2	9.0	21.8
39	1.19E+06	(43)	1.72E+06	(62)	36	146	37	24.1	15.9	36.1
40	2.28E+06	(41)	4.67E+06	(84)	18	395	87	17.0	11.3	24.9
41	4.60E+06	(23)	7.80E+06	(39)	5	661	211	20.5	11.7	35.1
42	8.13E+06	(65)	3.00E+06	(24)	8	254	103	93.0	57.8	155.4
43	1.28E+06	(23)	7.50E+06	(135)	18	636	111	5.9	3.6	9.3
44	6.17E+06	(74)	8.67E+06	(104)	12	734	146	24.7	18.0	33.6
45	7.00E+05	(28)	1.85E+06	(74)	40	157	37	13.2	8.2	20.5
46	2.04E+06	(51)	1.32E+06	(33)	25	112	39	53.4	33.8	85.4
47	3.00E+06	(30)	3.80E+06	(38)	10	322	104	27.4	16.4	45.3
48	1.00E+06	(6)	4.00E+06	(24)	6	339	137	8.9	2.9	21.8
49	1.27E+06	(19)	2.53E+06	(38)	15	215	70	17.4	9.4	30.8
50	2.25E+06	(18)	2.63E+06	(21)	8	222	96	29.7	14.9	58.5
51	3.25E+06	(65)	1.90E+06	(38)	20	161	52	59.0	39.0	90.6
52	5.25E+06	(21)	3.75E+06	(15)	4	318	162	48.3	23.8	100.7
53	3.38E+06	(27)	2.00E+06	(16)	8	169	84	58.1	30.4	115.5
54	3.00E+06	(27)	3.78E+06	(34)	9	320	109	27.6	16.0	47.0
55	3.33E+06	(30)	5.44E+06	(49)	9	461	132	21.3	13.0	34.1
56	2.55E+06	(28)	2.64E+06	(29)	11	223	83	33.5	19.2	58.2
57	1.60E+06	(8)	2.80E+06	(14)	5	237	125	20.0	7.2	50.5
58	3.92E+06	(94)	2.88E+06	(69)	24	244	59	47.1	34.2	65.3
59	1.71E+06	(24)	1.43E+06	(20)	14	121	54	41.5	22.0	79.1
60	3.22E+06	(29)	3.67E+06	(33)	9	311	108	30.5	17.8	51.7
61	2.00E+06	(80)	4.55E+06	(182)	40	386	58	15.3	11.5	20.4
62	1.80E+06	(18)	1.20E+06	(12)	10	102	58	51.6	23.7	117.6
63	3.27E+06	(49)	4.60E+06	(69)	15	390	94	24.6	16.7	36.0
64	4.20E+06	(42)	4.10E+06	(41)	10	347	108	35.5	22.5	55.9
65	3.92E+06	(47)	3.25E+06	(39)	12	275	88	41.7	26.7	65.5
66	4.17E+06	(25)	2.67E+06	(16)	6	226	111	53.8	27.8	107.9
67	2.20E+06	(33)	1.33E+06	(20)	15	113	50	56.9	31.8	104.6
68	2.90E+06	(29)	2.70E+06	(27)	10	229	88	37.2	21.3	65.2
69	3.40E+06	(102)	2.03E+06	(61)	30	172	44	57.7	41.7	80.7
70	3.33E+06	(80)	5.46E+06	(131)	24	463	82	21.2	15.8	28.2
71	3.00E+06	(48)	2.19E+06	(35)	16	185	63	47.4	30.1	75.5
72	5.17E+06	(31)	4.50E+06	(27)	6	381	146	39.7	23.0	69.1

73	8.00E+06	(72)	3.89E+06	(35)	9	330	111	70.9	46.8	109.5
74	2.69E+06	(43)	3.13E+06	(50)	16	265	75	29.8	19.3	45.7
75	3.80E+06	(57)	3.27E+06	(49)	15	277	79	40.3	27.0	60.2
76	1.35E+06	(27)	1.50E+06	(30)	20	127	46	31.2	17.8	54.2
77	3.67E+06	(22)	7.00E+06	(42)	6	593	183	18.2	10.3	31.1
78	4.25E+06	(51)	1.83E+06	(22)	12	155	66	79.7	47.7	138.0
79	1.83E+06	(11)	4.17E+06	(25)	6	353	140	15.4	6.8	32.1
80	1.54E+06	(37)	8.75E+05	(21)	24	74	32	60.7	34.8	109.2
81	2.42E+06	(29)	5.25E+06	(63)	12	445	113	16.0	9.9	25.2
82	2.00E+06	(10)	1.60E+06	(8)	5	136	93	43.1	15.4	125.4
83	2.80E+06	(56)	2.55E+06	(51)	20	216	61	38.0	25.5	56.7
84	4.50E+06	(36)	1.41E+07	(113)	8	1197	228	11.1	7.4	16.2
85	6.25E+06	(25)	1.30E+07	(52)	4	1102	306	16.7	9.9	27.4
86	3.58E+06	(43)	2.33E+06	(28)	12	198	74	53.0	32.3	88.6
87	1.00E+06	(6)	2.83E+06	(17)	6	240	115	12.5	4.0	32.5
88	3.69E+06	(48)	4.85E+06	(63)	13	411	104	26.4	17.7	39.1
89	5.72E+06	(103)	2.44E+06	(44)	18	207	62	80.6	56.3	117.6
90	4.25E+06	(34)	3.38E+06	(27)	8	286	109	43.5	25.5	75.0
91	4.17E+06	(50)	6.33E+06	(76)	12	537	124	22.8	15.6	33.0
92	2.60E+06	(13)	2.40E+06	(12)	5	203	115	37.5	15.8	89.6
93	1.80E+06	(27)	6.33E+06	(95)	15	537	111	9.9	6.2	15.3
94	4.20E+06	(42)	3.10E+06	(31)	10	263	94	46.8	28.8	77.0
95	5.00E+06	(30)	1.67E+06	(10)	6	141	87	102.2	49.3	234.7
96	5.00E+06	(40)	4.63E+06	(37)	8	392	129	37.4	23.3	60.2
97	3.46E+06	(97)	5.32E+06	(149)	28	451	75	22.6	17.0	30.0
98	3.00E+06	(24)	7.63E+06	(61)	8	646	166	13.7	8.1	22.2
99	2.96E+06	(80)	2.15E+06	(58)	27	182	48	47.7	33.6	68.1
100	2.67E+06	(32)	2.33E+06	(28)	12	198	74	39.5	23.1	68.1
101	4.50E+06	(36)	9.88E+06	(79)	8	837	190	15.8	10.3	23.7
102	3.28E+06	(59)	5.89E+06	(106)	18	499	98	19.3	13.8	26.8
103	3.50E+06	(42)	2.83E+06	(34)	12	240	82	42.7	26.6	69.2
104	3.00E+06	(81)	5.15E+06	(139)	27	436	75	20.2	15.1	26.8
105	1.83E+06	(22)	1.58E+06	(19)	12	134	61	40.0	20.7	78.1

YAKD43 (Alaska), modern sand
EFFECTIVE TRACK DENSITY FOR FLUENCE MONITOR (tracks/cm^2): 5.900E+05
RELATIVE ERROR (%): 1.58
EFFECTIVE URANIUM CONTENT OF MONITOR (ppm): 50.00
ZETA FACTOR AND STANDARD ERROR (yr cm^2): 117.70 7.10
SIZE OF COUNTER SQUARE (cm^2): 1.000E-06

Grain no.	**RhoS (cm^-2)**	**(Ns)**	**RhoI (cm^-2)**	**(Ni)**	**Squares**	**U+/-2s**		**Grain Age**	**Age (Ma) --95% CI--**	
1	5.13E+06	(41)	2.75E+06	(22)	8	233	99	64.2	37.5	113.2
2	4.33E+06	(91)	2.67E+06	(56)	21	226	61	56.1	39.8	79.8
3	2.69E+06	(43)	2.06E+06	(33)	16	175	61	45.0	28.0	73.2
4	3.00E+06	(48)	2.69E+06	(43)	16	228	69	38.6	25.1	59.7
5	6.50E+06	(39)	5.83E+06	(35)	6	494	167	38.6	23.8	62.7
6	5.25E+06	(42)	4.88E+06	(39)	8	413	132	37.3	23.5	59.2
7	9.50E+06	(38)	4.75E+06	(19)	4	403	183	68.8	38.9	126.4
8	1.08E+07	(43)	4.50E+06	(18)	4	381	178	82.0	46.6	151.2
9	2.11E+06	(19)	1.44E+06	(13)	9	122	67	50.4	23.7	110.9
10	3.83E+06	(23)	4.83E+06	(29)	6	410	151	27.5	15.2	49.2
11	8.22E+06	(148)	8.67E+06	(156)	18	734	120	32.9	25.5	42.4
12	4.00E+06	(108)	3.74E+06	(101)	27	317	64	37.0	27.9	49.1
13	7.50E+06	(45)	3.83E+06	(23)	6	325	134	67.4	40.1	116.7
14	8.75E+06	(35)	1.10E+07	(44)	4	932	281	27.6	17.2	44.0

15	1.05E+07	(42)	1.68E+07	(67)	4	1419	348	21.8	14.4	32.5
16	9.00E+06	(72)	6.38E+06	(51)	8	540	152	48.8	33.6	71.3
17	1.18E+07	(59)	1.62E+07	(81)	5	1373	307	25.3	17.7	35.8
18	7.38E+06	(59)	4.75E+06	(38)	8	403	130	53.6	35.1	82.9
19	2.40E+06	(12)	1.20E+06	(6)	5	102	80	68.2	24.1	221.8
20	5.00E+06	(30)	4.17E+06	(25)	6	353	140	41.5	23.6	73.5
21	7.67E+06	(46)	2.83E+06	(17)	6	240	115	92.7	52.6	172.7
22	5.67E+06	(34)	3.83E+06	(23)	6	325	134	51.0	29.3	90.7
23	5.38E+06	(43)	4.13E+06	(33)	8	350	121	45.0	28.0	73.2
24	5.25E+06	(42)	1.50E+06	(12)	8	127	72	119.3	62.5	248.9
25	6.20E+06	(31)	6.00E+06	(30)	5	508	185	35.8	21.0	61.1
26	3.29E+06	(46)	3.64E+06	(51)	14	309	87	31.3	20.5	47.5
27	2.43E+06	(68)	1.68E+06	(47)	28	142	42	50.0	34.0	74.2
28	5.00E+06	(20)	2.50E+06	(10)	4	212	131	68.5	30.9	164.2
29	3.00E+06	(21)	2.43E+06	(17)	7	206	99	42.7	21.5	86.1
30	5.83E+06	(175)	5.37E+06	(161)	30	455	73	37.6	29.4	48.1
31	6.90E+06	(69)	5.00E+06	(50)	10	424	120	47.7	32.7	70.1
32	1.89E+06	(34)	2.72E+06	(49)	18	231	66	24.1	15.1	38.0
33	5.83E+06	(35)	2.83E+06	(17)	6	240	115	70.8	38.8	134.8
34	5.27E+06	(79)	2.40E+06	(36)	15	203	68	75.6	50.5	115.5
35	6.17E+06	(37)	2.67E+06	(16)	6	226	111	79.4	43.4	152.9
36	3.25E+06	(39)	1.25E+06	(15)	12	106	54	89.1	48.4	174.1
37	4.25E+06	(51)	4.25E+06	(51)	12	360	101	34.6	23.0	52.1
38	2.40E+06	(24)	4.30E+06	(43)	10	364	111	19.4	11.2	32.6
39	1.19E+07	(131)	6.09E+06	(67)	11	516	127	67.5	49.9	92.1
40	5.69E+06	(91)	5.44E+06	(87)	16	461	100	36.2	26.7	49.2
41	3.38E+06	(27)	4.38E+06	(35)	8	371	125	26.8	15.6	45.4
42	7.13E+06	(107)	6.80E+06	(102)	15	576	115	36.3	27.4	48.2
43	6.79E+06	(95)	4.43E+06	(62)	14	375	96	52.9	38.1	74.2
44	5.63E+06	(90)	3.44E+06	(55)	16	291	79	56.5	40.0	80.6
45	5.38E+06	(113)	6.24E+06	(131)	21	529	94	29.9	22.6	39.5
46	3.50E+06	(28)	2.63E+06	(21)	8	222	96	46.0	25.3	85.3
47	7.60E+06	(38)	7.60E+06	(38)	5	644	209	34.6	21.5	55.8
48	3.50E+06	(35)	3.50E+06	(35)	10	297	100	34.6	21.0	57.0
49	5.83E+06	(35)	9.83E+06	(59)	6	833	218	20.6	13.1	31.8
50	5.44E+06	(49)	9.22E+06	(83)	9	782	173	20.5	14.1	29.5
51	8.00E+06	(32)	5.25E+06	(21)	4	445	192	52.6	29.5	95.9
52	7.00E+06	(98)	6.64E+06	(93)	14	563	118	36.5	27.2	49.0
53	4.50E+06	(36)	2.88E+06	(23)	8	244	101	54.0	31.2	95.5
54	7.10E+06	(142)	3.85E+06	(77)	20	326	75	63.7	47.9	85.2
55	5.76E+06	(98)	2.71E+06	(46)	17	229	68	73.4	51.3	106.7
56	5.93E+06	(83)	3.50E+06	(49)	14	297	85	58.5	40.6	85.1
57	2.67E+06	(16)	2.00E+06	(12)	6	169	96	46.0	20.5	106.4
58	4.63E+06	(37)	3.38E+06	(27)	8	286	109	47.3	28.1	80.8
59	6.90E+06	(69)	5.30E+06	(53)	10	449	124	45.0	31.0	65.7
60	8.43E+06	(118)	3.71E+06	(52)	14	315	87	78.2	56.1	110.6
61	5.83E+06	(105)	3.94E+06	(71)	18	334	80	51.1	37.5	70.2
62	5.14E+06	(108)	3.86E+06	(81)	21	327	73	46.1	34.2	62.4
63	9.75E+06	(39)	1.00E+07	(40)	4	847	268	33.8	21.2	53.8
64	4.00E+06	(36)	2.67E+06	(24)	9	226	92	51.8	30.1	90.7
65	7.67E+06	(46)	5.33E+06	(32)	6	452	159	49.7	31.0	80.6
66	7.88E+06	(63)	5.13E+06	(41)	8	434	136	53.1	35.3	80.7
67	9.13E+06	(73)	6.50E+06	(52)	8	551	153	48.5	33.6	70.7
68	4.00E+06	(24)	1.83E+06	(11)	6	155	92	74.7	35.6	169.2
69	4.78E+06	(43)	1.67E+06	(15)	9	141	72	98.1	53.9	190.2
70	7.93E+06	(111)	4.86E+06	(68)	14	412	100	56.4	41.3	77.5

71	7.00E+06	(35)	1.34E+07	(67)	5	1136	279	18.2	11.7	27.7
72	4.90E+06	(98)	5.40E+06	(108)	20	458	89	31.4	23.6	41.8
73	1.31E+07	(105)	8.38E+06	(67)	8	710	174	54.1	39.5	74.8
74	6.22E+06	(56)	3.67E+06	(33)	9	311	108	58.5	37.5	93.0
75	6.63E+06	(53)	3.38E+06	(27)	8	286	109	67.6	41.9	111.9
76	6.00E+06	(48)	3.75E+06	(30)	8	318	116	55.2	34.4	90.3
77	5.13E+06	(41)	4.38E+06	(35)	8	371	125	40.5	25.2	65.5
78	4.92E+06	(59)	2.58E+06	(31)	12	219	78	65.6	41.9	104.9
79	1.06E+07	(53)	5.80E+06	(29)	5	492	182	63.0	39.5	102.8
80	1.33E+06	(8)	1.50E+06	(9)	6	127	83	30.9	10.3	89.6
81	7.33E+06	(44)	4.83E+06	(29)	6	410	151	52.4	32.1	86.8
82	5.38E+06	(43)	3.25E+06	(26)	8	275	107	57.0	34.4	96.7
83	9.50E+06	(76)	4.63E+06	(37)	8	392	129	70.8	47.3	107.9
84	8.00E+06	(64)	3.38E+06	(27)	8	286	109	81.5	51.5	133.0
85	1.18E+07	(47)	6.00E+06	(24)	4	508	206	67.4	40.6	115.4
86	9.75E+06	(39)	1.00E+07	(40)	4	847	268	33.8	21.2	53.8
87	4.88E+06	(39)	3.63E+06	(29)	8	307	114	46.5	28.1	77.9
88	5.63E+05	(9)	1.44E+06	(23)	16	122	50	13.7	5.5	30.4
89	4.88E+06	(78)	3.94E+06	(63)	16	334	84	42.8	30.3	60.7
90	3.53E+06	(141)	1.75E+06	(70)	40	148	36	69.5	51.9	94.0
91	1.00E+07	(60)	6.17E+06	(37)	6	523	171	56.0	36.6	86.8
92	5.29E+06	(37)	3.14E+06	(22)	7	266	113	58.0	33.4	103.2
93	6.67E+05	(4)	8.33E+05	(5)	6	71	60	27.9	5.5	127.9
94	5.63E+06	(45)	1.88E+06	(15)	8	159	81	102.6	56.7	198.3
95	4.00E+06	(24)	2.17E+06	(13)	6	184	100	63.4	31.3	135.8
96	8.67E+06	(52)	8.67E+06	(52)	6	734	204	34.6	23.1	51.9
97	4.50E+06	(27)	4.00E+06	(24)	6	339	137	38.9	21.6	70.4
98	7.75E+06	(31)	4.00E+06	(16)	4	339	167	66.6	35.6	130.5
99	3.17E+06	(57)	1.78E+06	(32)	18	151	53	61.4	39.3	97.9
100	9.60E+06	(48)	1.02E+07	(51)	5	864	242	32.6	21.5	49.3
101	4.50E+06	(45)	2.60E+06	(26)	10	220	86	59.7	36.2	100.8
102	6.78E+06	(61)	5.11E+06	(46)	9	433	128	45.8	30.8	68.8
103	5.50E+06	(66)	9.08E+06	(109)	12	770	149	21.0	15.2	28.8
104	4.50E+06	(36)	3.25E+06	(26)	8	275	107	47.8	28.1	82.5
105	5.83E+06	(140)	3.71E+06	(89)	24	314	67	54.3	40.6	72.6

YAKD44 (Alaska), modern sand

EFFECTIVE TRACK DENSITY FOR FLUENCE MONITOR (tracks/cm^2): 5.900E+05
RELATIVE ERROR (%): 1.58
EFFECTIVE URANIUM CONTENT OF MONITOR (ppm): 50.00
ZETA FACTOR AND STANDARD ERROR (yr cm^2): 117.70 7.10
SIZE OF COUNTER SQUARE (cm^2): 1.000E-06

Grain no.	**RhoS (cm^-2)**	**(Ns)**	**RhoI (cm^-2)**	**(Ni)**	**Squares**	**U**	**+/-2s**	**Grain Age**	**Age (Ma) --95% CI--**	
1	9.50E+06	(57)	8.17E+06	(49)	6	692	198	40.3	27.0	60.2
2	3.00E+06	(27)	2.56E+06	(23)	9	217	90	40.6	22.4	74.1
3	1.22E+07	(73)	6.00E+06	(36)	6	508	169	69.9	46.4	107.3
4	4.17E+06	(25)	2.67E+06	(16)	6	226	111	53.8	27.8	107.9
5	1.03E+07	(124)	5.25E+06	(63)	12	445	113	67.9	49.8	93.6
6	4.90E+06	(49)	3.70E+06	(37)	10	314	103	45.8	29.3	72.2
7	8.90E+06	(89)	3.20E+06	(32)	10	271	96	95.6	63.4	148.0
8	4.75E+06	(38)	4.38E+06	(35)	8	371	125	37.6	23.1	61.2
9	3.97E+06	(143)	3.19E+06	(115)	36	271	51	43.0	32.7	56.5
10	9.80E+06	(49)	6.60E+06	(33)	5	559	194	51.3	32.4	82.3
11	1.58E+06	(19)	2.25E+06	(27)	12	191	73	24.5	12.8	45.5
12	7.83E+06	(47)	6.33E+06	(38)	6	537	174	42.8	27.3	67.4

13	5.56E+06 (89)	4.25E+06 (68)	16	360	88	45.3	32.6	63.1
14	2.89E+06 (26)	2.00E+06 (18)	9	169	79	49.8	26.4	96.5
15	6.71E+06 (47)	2.14E+06 (15)	7	182	92	107.1	59.4	206.3
16	2.90E+06 (116)	2.58E+06 (103)	40	218	43	39.0	29.1	52.1
17	5.88E+06 (47)	2.38E+06 (19)	8	201	91	84.9	49.2	153.3
18	6.00E+06 (30)	4.80E+06 (24)	5	407	165	43.2	24.5	77.2
19	5.50E+06 (88)	5.56E+06 (89)	16	471	101	34.2	25.2	46.5
20	1.34E+07 (67)	4.40E+06 (22)	5	373	158	104.4	64.1	177.5
21	3.20E+06 (32)	2.20E+06 (22)	10	186	79	50.2	28.4	90.7
22	1.01E+07 (111)	6.09E+06 (67)	11	516	127	57.2	41.9	78.8
23	2.27E+06 (34)	1.47E+06 (22)	15	124	53	53.3	30.4	95.7
24	1.30E+07 (117)	8.00E+06 (72)	9	678	161	56.1	41.5	76.5
25	6.25E+06 (50)	7.63E+06 (61)	8	646	166	28.4	19.1	42.0
26	5.19E+06 (109)	4.43E+06 (93)	21	375	79	40.6	30.5	54.1
27	9.25E+06 (37)	7.00E+06 (28)	4	593	223	45.7	27.2	77.5
28	5.00E+06 (80)	2.94E+06 (47)	16	249	73	58.8	40.5	86.2
29	4.00E+06 (48)	3.00E+06 (36)	12	254	85	46.1	29.3	73.1
30	4.75E+06 (19)	3.75E+06 (15)	4	318	162	43.7	21.1	92.4
31	4.50E+06 (27)	5.67E+06 (34)	6	480	164	27.6	16.0	47.0
32	1.33E+07 (53)	3.25E+06 (13)	4	275	150	138.7	75.6	277.3
33	2.35E+06 (47)	3.40E+06 (68)	20	288	70	24.0	16.1	35.3
34	5.93E+06 (160)	4.74E+06 (128)	27	402	72	43.2	33.3	56.1
35	6.25E+06 (75)	4.83E+06 (58)	12	410	108	44.7	31.3	64.2
36	3.13E+06 (47)	3.33E+06 (50)	15	282	80	32.6	21.4	49.5
37	2.75E+06 (44)	3.25E+06 (52)	16	275	77	29.3	19.2	44.7
38	7.13E+06 (57)	1.63E+06 (13)	8	138	75	149.1	81.7	296.5
39	3.00E+06 (36)	2.42E+06 (29)	12	205	76	42.9	25.6	72.6
40	9.56E+06 (86)	4.00E+06 (36)	9	339	113	82.2	55.3	125.0
41	5.30E+06 (53)	3.40E+06 (34)	10	288	99	53.8	34.4	85.4
42	5.40E+06 (54)	2.80E+06 (28)	10	237	89	66.4	41.5	109.0
43	1.02E+07 (61)	6.00E+06 (36)	6	508	169	58.5	38.2	90.9
44	4.19E+06 (67)	3.50E+06 (56)	16	297	79	41.4	28.6	60.2
45	1.60E+06 (24)	8.67E+05 (13)	15	73	40	63.4	31.3	135.8
46	6.17E+06 (37)	5.50E+06 (33)	6	466	162	38.8	23.6	64.0
47	7.70E+06 (77)	2.00E+06 (20)	10	169	75	131.5	80.3	227.1
48	2.75E+06 (33)	1.83E+06 (22)	12	155	66	51.8	29.4	93.2
49	5.08E+06 (61)	4.50E+06 (54)	12	381	104	39.1	26.7	57.5
50	7.33E+06 (88)	4.58E+06 (55)	12	388	105	55.3	39.0	78.9
51	7.69E+06 (123)	3.81E+06 (61)	16	323	83	69.6	50.8	96.2
52	3.00E+06 (18)	3.17E+06 (19)	6	268	122	32.8	16.2	65.9
53	7.44E+06 (67)	3.00E+06 (27)	9	254	97	85.3	54.1	138.8
54	4.25E+06 (34)	1.38E+06 (11)	8	117	69	105.4	52.8	230.8
55	7.11E+06 (64)	7.22E+06 (65)	9	612	152	34.1	23.8	48.9
56	1.13E+07 (68)	1.12E+07 (67)	6	946	232	35.1	24.7	50.0
57	4.60E+06 (92)	2.00E+06 (40)	20	169	54	79.2	54.2	117.9
58	4.13E+06 (33)	3.13E+06 (25)	8	265	105	45.6	26.4	80.0
59	7.33E+06 (44)	3.17E+06 (19)	6	268	122	79.5	45.8	144.4
60	3.89E+06 (35)	3.56E+06 (32)	9	301	106	37.9	22.8	63.1
61	4.21E+06 (59)	2.64E+06 (37)	14	224	73	55.0	36.0	85.5
62	9.11E+06 (82)	5.89E+06 (53)	9	499	137	53.4	37.4	77.0
63	9.20E+06 (138)	5.40E+06 (81)	15	458	102	58.8	44.4	78.5
64	2.81E+06 (59)	3.24E+06 (68)	21	274	67	30.1	20.8	43.3
65	7.33E+06 (44)	5.00E+06 (30)	6	424	154	50.6	31.2	83.5
66	5.33E+06 (64)	6.08E+06 (73)	12	516	121	30.4	21.4	43.1
67	7.75E+06 (31)	2.00E+06 (8)	4	169	116	131.2	60.2	330.4
68	5.00E+06 (20)	4.50E+06 (18)	4	381	178	38.4	19.3	77.0

69	2.80E+06	(28)	2.00E+06	(20)	10	169	75	48.3	26.3	90.5
70	9.38E+06	(75)	9.75E+06	(78)	8	826	188	33.3	23.9	46.4
71	5.81E+06	(93)	4.63E+06	(74)	16	392	92	43.5	31.7	59.9
72	1.06E+07	(53)	4.20E+06	(21)	5	356	154	86.6	51.7	151.3
73	4.83E+06	(58)	2.08E+06	(25)	12	177	70	79.8	49.4	133.2
74	3.60E+06	(90)	1.96E+06	(49)	25	166	48	63.4	44.3	91.7
75	5.20E+06	(26)	2.80E+06	(14)	5	237	125	63.8	32.4	132.4
76	1.43E+06	(30)	8.57E+05	(18)	21	73	34	57.4	31.1	109.4
77	4.00E+06	(64)	3.31E+06	(53)	16	281	77	41.8	28.6	61.3
78	2.37E+06	(64)	3.07E+06	(83)	27	261	58	26.7	19.0	37.5
79	5.22E+06	(47)	1.33E+06	(12)	9	113	64	133.3	70.6	275.9
80	4.60E+06	(46)	4.00E+06	(40)	10	339	107	39.8	25.5	62.4
81	6.67E+06	(100)	4.60E+06	(69)	15	390	94	50.1	36.5	69.2
82	6.50E+06	(78)	4.67E+06	(56)	12	395	106	48.1	33.7	69.2
83	6.58E+06	(79)	3.17E+06	(38)	12	268	87	71.6	48.2	108.5
84	2.90E+06	(29)	1.90E+06	(19)	10	161	73	52.6	28.6	99.3
85	2.00E+06	(42)	1.76E+06	(37)	21	149	49	39.3	24.7	62.8
86	7.33E+06	(88)	4.42E+06	(53)	12	374	103	57.3	40.4	82.3
87	3.89E+06	(35)	2.22E+06	(20)	9	188	83	60.3	34.0	110.3
88	5.67E+06	(34)	3.67E+06	(22)	6	311	131	53.3	30.4	95.7
89	3.40E+06	(51)	1.20E+06	(18)	15	102	47	97.1	56.2	176.7
90	6.50E+06	(52)	7.13E+06	(57)	8	604	160	31.6	21.3	46.9
91	4.11E+06	(74)	2.61E+06	(47)	18	221	65	54.4	37.3	80.2
92	3.83E+06	(46)	3.00E+06	(36)	12	254	85	44.2	28.0	70.3
93	3.30E+06	(33)	4.10E+06	(41)	10	347	108	27.9	17.1	45.2
94	2.53E+06	(38)	5.33E+06	(80)	15	452	102	16.5	10.9	24.6
95	3.75E+06	(45)	1.67E+06	(20)	12	141	63	77.3	45.0	138.3
96	5.20E+06	(26)	3.80E+06	(19)	5	322	146	47.2	25.2	90.3
97	3.78E+06	(34)	2.00E+06	(18)	9	169	79	65.0	35.9	122.3
98	5.33E+06	(32)	1.83E+06	(11)	6	155	92	99.3	49.4	218.6
99	4.78E+06	(43)	3.56E+06	(32)	9	301	106	46.4	28.8	75.8
100	7.00E+06	(42)	4.50E+06	(27)	6	381	146	53.7	32.4	90.6
101	9.83E+06	(59)	7.17E+06	(43)	6	607	185	47.4	31.5	72.0
102	1.42E+06	(34)	9.58E+05	(23)	24	81	34	51.0	29.3	90.7
103	4.00E+06	(16)	1.50E+06	(6)	4	127	100	90.4	34.3	282.8
104	9.13E+06	(73)	5.38E+06	(43)	8	456	139	58.6	39.7	87.6
105	3.30E+06	(33)	2.00E+06	(20)	10	169	75	56.9	31.8	104.6

YAKD45 (Alaska), modern sand

EFFECTIVE TRACK DENSITY FOR FLUENCE MONITOR (tracks/cm^2): 5.900E+05
RELATIVE ERROR (%): 1.58
EFFECTIVE URANIUM CONTENT OF MONITOR (ppm): 50.00
ZETA FACTOR AND STANDARD ERROR (yr cm^2): 117.70 7.10
SIZE OF COUNTER SQUARE (cm^2): 1.000E-06

Grain no.	**RhoS (cm^-2)**	**(Ns)**	**RhoI (cm^-2)**	**(Ni)**	**Squares**	**U**	**+/-2s**	**Grain Age**	**Age (Ma) --95%**	**CI--**
1	5.55E+06	(111)	3.25E+06	(65)	20	275	69	59.0	43.1	81.4
2	7.08E+06	(85)	3.17E+06	(38)	12	268	87	77.0	52.1	116.2
3	4.69E+06	(75)	1.50E+06	(24)	16	127	52	107.1	67.3	177.5
4	5.89E+06	(53)	4.22E+06	(38)	9	358	116	48.2	31.2	75.2
5	5.33E+06	(48)	2.33E+06	(21)	9	198	86	78.5	46.4	138.2
6	5.33E+06	(32)	1.83E+06	(11)	6	155	92	99.3	49.4	218.6
7	3.44E+06	(55)	1.00E+06	(16)	16	85	42	117.4	67.0	219.6
8	7.00E+06	(28)	5.00E+06	(20)	4	424	188	48.3	26.3	90.5
9	5.54E+06	(72)	2.77E+06	(36)	13	235	78	68.9	45.7	106.0
10	8.89E+06	(80)	4.11E+06	(37)	9	348	114	74.5	50.0	113.2

11	6.00E+06	(84)	3.21E+06	(45)	14	272	81	64.4	44.4	94.7
12	3.63E+06	(29)	2.38E+06	(19)	8	201	91	52.6	28.6	99.3
13	5.80E+06	(87)	4.33E+06	(65)	15	367	91	46.3	33.2	64.9
14	1.64E+06	(23)	1.57E+06	(22)	14	133	56	36.2	19.3	68.0
15	5.86E+06	(41)	7.57E+06	(53)	7	642	177	26.8	17.4	41.1
16	1.27E+07	(76)	3.83E+06	(23)	6	325	134	113.2	70.7	189.1
17	7.20E+06	(36)	9.80E+06	(49)	5	831	238	25.5	16.1	40.0
18	5.86E+06	(82)	4.86E+06	(68)	14	412	100	41.7	29.9	58.5
19	2.67E+06	(40)	2.20E+06	(33)	15	186	65	41.9	25.8	68.6
20	5.68E+06	(142)	2.12E+06	(53)	25	180	49	92.2	67.0	129.0
21	1.45E+07	(87)	5.00E+06	(30)	6	424	154	99.6	65.4	156.3
22	6.83E+06	(41)	3.17E+06	(19)	6	268	122	74.2	42.3	135.4
23	7.78E+06	(70)	3.78E+06	(34)	9	320	109	70.9	46.6	110.3
24	7.33E+06	(88)	2.50E+06	(30)	12	212	77	100.7	66.2	158.0
25	8.06E+06	(129)	1.69E+06	(27)	16	143	55	163.0	107.9	256.5
26	1.20E+06	(30)	1.24E+06	(31)	25	105	38	33.5	19.6	57.2
27	6.25E+06	(75)	5.83E+06	(70)	12	494	119	37.1	26.4	52.2
28	6.07E+06	(85)	2.64E+06	(37)	14	224	73	79.1	53.3	119.8
29	4.50E+06	(36)	3.25E+06	(26)	8	275	107	47.8	28.1	82.5
30	7.60E+06	(76)	2.00E+06	(20)	10	169	75	129.8	79.2	224.3
31	6.40E+06	(32)	4.80E+06	(24)	5	407	165	46.1	26.3	81.7
32	5.67E+06	(34)	2.67E+06	(16)	6	226	111	73.0	39.5	141.7
33	1.44E+06	(13)	2.11E+06	(19)	9	179	81	23.8	10.8	50.6
34	4.50E+06	(108)	2.42E+06	(58)	24	205	54	64.3	46.3	90.1
35	9.72E+06	(175)	4.00E+06	(72)	18	339	80	83.7	63.4	111.9
36	4.38E+06	(35)	5.00E+06	(40)	8	424	134	30.3	18.7	48.9
37	6.92E+06	(83)	4.00E+06	(48)	12	339	98	59.7	41.4	87.1
38	1.01E+07	(202)	2.70E+06	(54)	20	229	62	128.3	94.9	176.7
39	5.50E+06	(55)	2.70E+06	(27)	10	229	88	70.1	43.7	115.7
40	6.71E+06	(161)	3.33E+06	(80)	24	282	64	69.4	52.8	92.1
41	3.96E+06	(99)	2.32E+06	(58)	25	197	52	58.9	42.2	83.0
42	6.13E+06	(49)	2.00E+06	(16)	8	169	84	104.8	59.1	197.5
43	4.30E+06	(43)	1.70E+06	(17)	10	144	69	86.7	48.8	162.4
44	2.33E+06	(49)	1.71E+06	(36)	21	145	48	47.0	30.0	74.5
45	3.74E+06	(101)	1.70E+06	(46)	27	144	43	75.7	53.0	109.8
46	4.10E+06	(123)	2.23E+06	(67)	30	189	46	63.4	46.7	86.7
47	2.89E+06	(78)	1.89E+06	(51)	27	160	45	52.8	36.7	76.8
48	5.80E+06	(116)	1.85E+06	(37)	20	157	51	107.6	74.1	160.4
49	2.69E+06	(43)	6.88E+05	(11)	16	58	34	132.9	68.4	285.7
50	7.86E+05	(33)	6.67E+05	(28)	42	56	21	40.8	23.9	70.0
51	7.04E+06	(169)	6.75E+06	(162)	24	572	92	36.1	28.2	46.2
52	4.40E+06	(44)	4.60E+06	(46)	10	390	115	33.1	21.4	51.2
53	3.67E+06	(88)	1.46E+06	(35)	24	124	42	86.5	58.1	131.9
54	5.00E+06	(160)	2.94E+06	(94)	32	249	52	58.7	44.3	77.7
55	3.75E+06	(45)	3.00E+06	(36)	12	254	85	43.2	27.3	69.0
56	7.67E+06	(115)	1.53E+06	(23)	15	130	54	170.4	109.2	279.0
57	6.22E+06	(56)	2.11E+06	(19)	9	179	81	101.0	59.6	180.0
58	2.94E+06	(106)	2.19E+06	(79)	36	186	42	46.4	34.3	63.0
59	5.50E+06	(55)	6.30E+06	(63)	10	534	135	30.3	20.7	44.1
60	2.79E+06	(78)	1.93E+06	(54)	28	163	45	49.9	34.9	72.0
61	4.43E+06	(62)	2.36E+06	(33)	14	200	69	64.8	41.9	102.1
62	6.13E+06	(98)	6.69E+06	(107)	16	567	111	31.7	23.8	42.2
63	4.00E+06	(84)	2.67E+06	(56)	21	226	61	51.8	36.5	74.1
64	4.08E+06	(49)	2.08E+06	(25)	12	177	70	67.5	41.1	114.1
65	3.95E+06	(79)	3.70E+06	(74)	20	314	73	37.0	26.6	51.5
66	9.00E+05	(27)	1.67E+06	(50)	30	141	40	18.8	11.3	30.5

67	3.00E+06	(63)	2.62E+06	(55)	21	222	60	39.6	27.2	58.0
68	5.00E+06	(40)	3.00E+06	(24)	8	254	103	57.5	33.9	99.7
69	4.13E+06	(66)	2.50E+06	(40)	16	212	67	57.0	38.0	86.6
70	4.75E+06	(19)	2.50E+06	(10)	4	212	131	65.1	29.1	157.0
71	7.50E+06	(90)	3.42E+06	(41)	12	290	90	75.6	51.9	112.3
72	7.00E+06	(42)	2.33E+06	(14)	6	198	104	102.6	55.5	203.5
73	2.94E+06	(47)	2.31E+06	(37)	16	196	64	43.9	28.0	69.5
74	7.75E+06	(31)	4.00E+06	(16)	4	339	167	66.6	35.6	130.5
75	2.64E+06	(66)	1.16E+06	(29)	25	98	36	78.3	50.1	125.8
76	8.56E+06	(77)	3.78E+06	(34)	9	320	109	78.0	51.6	120.5
77	1.30E+06	(26)	8.50E+05	(17)	20	72	35	52.7	27.7	103.6
78	5.55E+06	(111)	3.40E+06	(68)	20	288	70	56.4	41.3	77.5
79	1.10E+07	(66)	3.33E+06	(20)	6	282	125	112.9	68.2	196.7
80	8.60E+06	(43)	4.60E+06	(23)	5	390	161	64.4	38.1	112.0
81	6.00E+06	(36)	3.50E+06	(21)	6	297	128	59.1	33.7	106.5
82	7.33E+06	(132)	2.22E+06	(40)	18	188	59	113.3	79.3	165.7
83	2.42E+06	(29)	8.33E+05	(10)	12	71	44	98.9	47.5	227.7
84	3.38E+06	(27)	3.75E+06	(30)	8	318	116	31.2	17.8	54.2
85	2.43E+06	(34)	1.57E+06	(22)	14	133	56	53.3	30.4	95.7
86	9.33E+06	(56)	5.83E+06	(35)	6	494	167	55.2	35.6	86.9
87	7.13E+06	(57)	3.75E+06	(30)	8	318	116	65.5	41.5	105.6
88	7.60E+06	(76)	4.00E+06	(40)	10	339	107	65.5	44.2	98.7
89	1.05E+07	(63)	2.83E+06	(17)	6	240	115	126.5	73.9	230.6
90	1.30E+07	(104)	5.00E+06	(40)	8	424	134	89.4	61.8	132.3
91	6.94E+06	(222)	3.38E+06	(108)	32	286	56	70.8	54.7	91.7
92	1.42E+06	(34)	7.92E+05	(19)	24	67	30	61.6	34.3	114.4
93	3.70E+06	(37)	5.20E+06	(52)	10	441	122	24.7	15.7	38.3
94	1.67E+06	(20)	1.17E+06	(14)	12	99	52	49.2	23.8	105.4
95	5.00E+06	(35)	5.29E+06	(37)	7	448	147	32.8	20.0	53.5
96	5.59E+06	(179)	3.19E+06	(102)	32	270	54	60.5	46.2	79.3
97	5.79E+06	(81)	3.29E+06	(46)	14	278	82	60.8	41.9	89.3
98	9.19E+06	(147)	5.25E+06	(84)	16	445	98	60.4	45.9	80.1
99	4.60E+06	(46)	3.40E+06	(34)	10	288	99	46.8	29.4	75.1
100	3.83E+06	(23)	3.17E+06	(19)	6	268	122	41.8	21.8	81.2
101	5.67E+06	(51)	2.00E+06	(18)	9	169	79	97.1	56.2	176.7
102	5.07E+06	(71)	2.43E+06	(34)	14	206	70	71.9	47.3	111.7
103	4.10E+06	(86)	3.62E+06	(76)	21	307	71	39.2	28.4	54.1
104	3.88E+06	(31)	2.25E+06	(18)	8	191	89	59.3	32.3	112.6

YAKD46 (Alaska), modern sand

EFFECTIVE TRACK DENSITY FOR FLUENCE MONITOR (tracks/cm^2): 5.900E+05
RELATIVE ERROR (%): 1.58
EFFECTIVE URANIUM CONTENT OF MONITOR (ppm): 50.00
ZETA FACTOR AND STANDARD ERROR (yr cm^2): 117.70 7.10
SIZE OF COUNTER SQUARE (cm^2): 1.000E-06

Grain no.	**RhoS (cm^-2)**	**(Ns)**	**RhoI (cm^-2)**	**(Ni)**	**Squares**	**U**	**+/-2s**	**Grain Age**	**Age (Ma) --95% CI--**	
1	4.17E+06	(25)	2.33E+06	(14)	6	198	104	61.4	30.9	127.9
2	3.42E+06	(82)	6.25E+06	(150)	24	530	88	19.0	14.3	25.0
3	5.58E+06	(67)	1.26E+07	(151)	12	1066	177	15.4	11.4	20.7
4	7.00E+06	(28)	6.75E+06	(27)	4	572	219	35.9	20.4	63.3
5	3.50E+06	(14)	2.00E+06	(8)	4	169	116	60.0	23.7	165.2
6	3.25E+06	(26)	2.50E+06	(20)	8	212	94	44.9	24.2	84.8
7	8.00E+06	(32)	3.00E+06	(12)	4	254	144	91.2	46.2	194.6
8	4.28E+06	(77)	4.44E+06	(80)	18	377	85	33.3	24.0	46.2
9	3.13E+06	(50)	2.81E+06	(45)	16	238	71	38.5	25.2	58.9

10	3.31E+06	(53)	2.44E+06	(39)	16	207	66	47.0	30.5	73.0
11	9.50E+06	(57)	6.50E+06	(39)	6	551	176	50.5	33.1	78.0
12	4.30E+06	(43)	6.80E+06	(68)	10	576	140	22.0	14.6	32.6
13	2.25E+05	(9)	1.55E+06	(62)	40	131	33	5.1	2.2	10.2
14	2.50E+06	(50)	3.70E+06	(74)	20	314	73	23.4	16.0	34.0
15	3.50E+06	(42)	3.33E+06	(40)	12	282	89	36.4	23.0	57.5
16	8.75E+06	(70)	3.75E+06	(30)	8	318	116	80.3	51.9	127.6
17	4.43E+06	(62)	1.50E+06	(21)	14	127	55	101.2	61.3	174.9
18	1.11E+06	(20)	6.22E+06	(112)	18	527	101	6.2	3.6	10.0
19	1.43E+05	(2)	5.00E+05	(7)	14	42	31	10.4	1.0	51.9
20	3.75E+06	(45)	2.25E+06	(27)	12	191	73	57.5	35.0	96.4
21	4.21E+06	(101)	4.50E+06	(108)	24	381	74	32.4	24.4	42.9
22	7.00E+06	(56)	2.13E+06	(17)	8	180	86	112.6	65.1	206.8
23	3.92E+06	(47)	2.17E+06	(26)	12	184	72	62.3	37.9	104.8
24	4.00E+06	(36)	1.11E+06	(10)	9	94	58	122.4	60.4	276.6
25	1.83E+06	(11)	6.67E+05	(4)	6	56	53	92.5	28.2	398.8
26	4.38E+06	(35)	3.38E+06	(27)	8	286	109	44.8	26.4	76.9
27	2.17E+06	(26)	2.42E+06	(29)	12	205	76	31.1	17.6	54.6
28	4.14E+06	(58)	3.64E+06	(51)	14	309	87	39.4	26.5	58.5
29	4.00E+06	(48)	5.25E+06	(63)	12	445	113	26.4	17.7	39.1
30	4.17E+06	(25)	3.00E+06	(18)	6	254	118	47.9	25.2	93.2
31	4.25E+06	(34)	4.13E+06	(33)	8	350	121	35.7	21.4	59.4
32	7.60E+06	(76)	2.00E+06	(20)	10	169	75	129.8	79.2	224.3
33	1.60E+06	(24)	6.33E+06	(95)	15	537	111	8.8	5.4	13.9
34	4.50E+06	(45)	2.70E+06	(27)	10	229	88	57.5	35.0	96.4
35	3.57E+05	(5)	5.57E+06	(78)	14	472	108	2.3	0.7	5.4
36	3.75E+06	(45)	9.42E+06	(113)	12	798	152	13.8	9.5	19.7
37	3.20E+06	(48)	2.00E+06	(30)	15	169	62	55.2	34.4	90.3
38	5.93E+06	(83)	1.43E+06	(20)	14	121	54	141.6	86.9	243.6
39	9.17E+05	(11)	1.92E+06	(23)	12	162	67	16.7	7.3	35.4
40	7.63E+06	(61)	5.25E+06	(42)	8	445	137	50.2	33.4	76.2
41	4.42E+06	(53)	2.17E+06	(26)	12	184	72	70.2	43.3	117.0
42	6.50E+06	(104)	1.56E+06	(25)	16	132	53	142.2	91.9	229.5
43	3.00E+06	(36)	2.58E+06	(31)	12	219	78	40.2	24.2	67.1
44	6.13E+06	(49)	7.50E+06	(60)	8	636	165	28.3	19.0	42.0
45	6.25E+06	(25)	2.50E+06	(10)	4	212	131	85.4	40.1	199.6
46	4.38E+05	(7)	1.56E+06	(25)	16	132	53	9.9	3.5	23.1
47	5.75E+06	(46)	1.03E+07	(82)	8	869	193	19.5	13.2	28.3
48	5.11E+06	(46)	6.44E+06	(58)	9	546	144	27.5	18.2	41.2
49	4.25E+06	(51)	5.83E+06	(70)	12	494	119	25.3	17.2	36.8
50	5.00E+06	(30)	4.17E+06	(25)	6	353	140	41.5	23.6	73.5
51	1.67E+06	(45)	3.63E+06	(98)	27	308	63	16.0	10.9	22.9
52	4.80E+06	(48)	6.00E+06	(60)	10	508	132	27.7	18.6	41.2
53	8.50E+06	(34)	1.25E+07	(50)	4	1059	300	23.6	14.8	37.2
54	8.67E+06	(52)	3.00E+06	(18)	6	254	118	99.0	57.4	179.9
55	4.83E+06	(58)	6.17E+06	(74)	12	523	122	27.2	18.9	38.9
56	2.58E+06	(31)	3.50E+06	(42)	12	297	91	25.6	15.5	41.7
57	4.43E+06	(62)	3.14E+06	(44)	14	266	80	48.7	32.6	73.4
58	4.00E+06	(24)	2.33E+06	(14)	6	198	104	59.0	29.5	123.4
59	5.44E+06	(98)	7.11E+06	(128)	18	603	108	26.6	19.9	35.5
60	4.25E+06	(51)	3.58E+06	(43)	12	304	93	41.0	26.8	63.1
61	4.88E+06	(39)	2.50E+06	(20)	8	212	94	67.1	38.4	121.5
62	3.42E+06	(41)	1.67E+06	(20)	12	141	63	70.5	40.6	127.1
63	5.67E+06	(51)	4.33E+06	(39)	9	367	117	45.2	29.2	70.5
64	3.89E+06	(35)	4.89E+06	(44)	9	414	125	27.6	17.2	44.0
65	2.67E+06	(24)	5.89E+06	(53)	9	499	137	15.8	9.3	25.9

66	5.33E+06	(128)	1.34E+07	(321)	24	1133	131	13.9	10.9	17.6
67	2.37E+06	(71)	3.07E+06	(92)	30	260	55	26.8	19.3	36.9
68	3.16E+06	(101)	2.56E+06	(82)	32	217	48	42.6	31.5	57.8
69	1.33E+06	(48)	1.36E+06	(49)	36	115	33	33.9	22.3	51.6
70	3.47E+06	(52)	5.73E+06	(86)	15	486	106	21.0	14.6	29.9
71	2.14E+06	(62)	1.86E+06	(54)	29	158	43	39.7	27.1	58.3
72	5.00E+06	(60)	2.67E+06	(32)	12	226	80	64.6	41.5	102.7
73	4.56E+06	(73)	6.06E+06	(97)	16	514	105	26.1	19.0	35.7
74	1.20E+06	(54)	9.56E+05	(43)	45	81	25	43.4	28.6	66.4
75	4.00E+06	(48)	3.42E+06	(41)	12	290	90	40.5	26.2	63.0
76	4.75E+06	(57)	3.50E+06	(42)	12	297	91	46.9	31.0	71.7
77	3.75E+06	(30)	3.88E+06	(31)	8	328	117	33.5	19.6	57.2
78	3.89E+06	(35)	5.67E+06	(51)	9	480	135	23.8	15.0	37.3
79	1.10E+06	(44)	3.85E+06	(154)	40	326	54	9.9	6.9	14.0
80	4.56E+06	(82)	4.22E+06	(76)	18	358	83	37.4	27.0	51.8
81	5.04E+06	(136)	4.48E+06	(121)	27	380	70	38.9	29.6	51.1
82	5.67E+06	(51)	1.00E+07	(90)	9	847	180	19.7	13.6	28.0
83	2.70E+06	(54)	6.05E+06	(121)	20	513	94	15.5	11.0	21.5
84	7.78E+05	(14)	1.33E+06	(24)	18	113	46	20.3	9.7	40.7
85	5.58E+06	(67)	5.67E+06	(68)	12	480	117	34.1	24.0	48.6
86	8.33E+06	(100)	2.25E+06	(27)	12	191	73	126.8	82.7	201.8
87	2.89E+06	(52)	1.56E+06	(28)	18	132	50	64.0	39.8	105.3
88	2.20E+06	(22)	2.20E+06	(22)	10	186	79	34.6	18.3	65.5
89	7.50E+06	(90)	1.06E+07	(127)	12	897	161	24.6	18.5	32.5
90	3.04E+06	(76)	2.76E+06	(69)	25	234	57	38.1	27.1	53.6
91	4.50E+06	(27)	4.50E+06	(27)	6	381	146	34.6	19.6	61.3
92	8.83E+06	(53)	1.33E+07	(80)	6	1130	254	23.0	15.9	32.9
93	4.83E+06	(29)	5.83E+06	(35)	6	494	167	28.7	16.9	48.3
94	3.73E+06	(112)	1.10E+06	(33)	30	93	32	116.4	78.7	177.2
95	2.81E+06	(45)	1.25E+06	(20)	16	106	47	77.3	45.0	138.3
96	3.08E+06	(37)	1.33E+06	(16)	12	113	56	79.4	43.4	152.9
97	4.58E+06	(55)	2.08E+06	(25)	12	177	70	75.7	46.6	126.8
98	2.93E+06	(85)	4.14E+06	(120)	29	351	65	24.6	18.3	32.7
99	2.94E+06	(47)	3.19E+06	(51)	16	270	76	31.9	21.0	48.4
100	2.08E+06	(25)	3.17E+06	(38)	12	268	87	22.9	13.2	38.8
101	5.83E+06	(70)	6.75E+06	(81)	12	572	128	30.0	21.4	41.8
102	3.67E+06	(55)	3.47E+06	(52)	15	294	82	36.6	24.6	54.6
103	3.75E+06	(45)	2.92E+06	(35)	12	247	83	44.4	28.0	71.2
104	4.29E+06	(60)	4.64E+06	(65)	14	393	98	32.0	22.1	46.2
105	3.50E+06	(35)	4.60E+06	(46)	10	390	115	26.4	16.5	41.8

YAKD55 (Alaska), modern sand

EFFECTIVE TRACK DENSITY FOR FLUENCE MONITOR (tracks/cm^2): 5.890E+05
RELATIVE ERROR (%): 1.58
EFFECTIVE URANIUM CONTENT OF MONITOR (ppm): 50.00
ZETA FACTOR AND STANDARD ERROR (yr cm^2): 117.70 7.10
SIZE OF COUNTER SQUARE (cm^2): 1.000E-06

Grain no.	**RhoS (cm^-2)**	**(Ns)**	**RhoI (cm^-2)**	**(Ni)**	**Squares**	**U+/-2s**		**Grain Age**	**Age (Ma) --95%**	**CI--**
1	4.92E+06	(59)	1.03E+07	(123)	12	870	159	16.6	11.9	22.9
2	3.82E+06	(172)	5.38E+06	(242)	45	457	60	24.6	19.6	31.0
3	6.59E+06	(211)	8.22E+06	(263)	32	698	89	27.8	22.3	34.5
4	4.08E+06	(49)	4.33E+06	(52)	12	368	102	32.6	21.6	49.1
5	2.75E+06	(44)	3.75E+06	(60)	16	318	82	25.4	16.8	38.1
6	2.70E+06	(81)	2.47E+06	(74)	30	209	49	37.8	27.2	52.6
7	2.33E+06	(21)	3.11E+06	(28)	9	264	99	26.0	14.0	47.3

8	5.70E+06	(57)	1.36E+07	(136)	10	1154	201	14.5	10.4	19.9
9	4.73E+06	(142)	6.47E+06	(194)	30	549	81	25.3	19.8	32.5
10	2.83E+06	(34)	4.25E+06	(51)	12	361	101	23.1	14.5	36.3
11	3.02E+06	(136)	4.07E+06	(183)	45	345	52	25.7	20.0	33.1
12	2.87E+06	(43)	4.20E+06	(63)	15	357	90	23.6	15.6	35.4
13	2.57E+06	(18)	3.71E+06	(26)	7	315	123	24.0	12.4	45.4
14	5.17E+06	(93)	5.50E+06	(99)	18	467	95	32.5	24.2	43.6
15	7.53E+06	(113)	7.40E+06	(111)	15	628	121	35.2	26.4	46.9
16	4.25E+06	(85)	4.90E+06	(98)	20	416	85	30.0	22.1	40.6
17	2.50E+06	(45)	4.78E+06	(86)	18	406	88	18.1	12.3	26.3
18	2.37E+06	(71)	2.77E+06	(83)	30	235	52	29.6	21.2	41.1
19	5.10E+06	(102)	4.15E+06	(83)	20	352	78	42.4	31.4	57.5
20	3.13E+06	(75)	3.38E+06	(81)	24	287	64	32.0	23.1	44.4
21	4.47E+06	(67)	2.93E+06	(44)	15	249	75	52.5	35.4	78.7
22	2.60E+06	(104)	3.30E+06	(132)	40	280	49	27.3	20.5	36.2
23	3.00E+06	(48)	3.25E+06	(52)	16	276	77	31.9	21.1	48.2
24	2.94E+06	(47)	2.63E+06	(42)	16	223	69	38.7	25.0	60.1
25	4.00E+06	(80)	5.00E+06	(100)	20	424	86	27.7	20.3	37.5
26	6.42E+06	(77)	1.26E+07	(151)	12	1068	177	17.7	13.2	23.4
27	2.75E+06	(22)	2.00E+06	(16)	8	170	84	47.4	23.8	96.5
28	3.33E+06	(30)	2.56E+06	(23)	9	217	90	45.0	25.3	81.1
29	2.35E+06	(47)	2.85E+06	(57)	20	242	64	28.5	19.0	42.7
30	3.50E+06	(35)	4.20E+06	(42)	10	357	110	28.8	17.9	46.2
31	1.45E+06	(29)	1.35E+06	(27)	20	115	44	37.1	21.2	65.1
32	1.80E+06	(27)	2.53E+06	(38)	15	215	70	24.6	14.4	41.3
33	1.75E+06	(28)	2.81E+06	(45)	16	239	71	21.6	12.9	35.3
34	3.00E+06	(48)	2.88E+06	(46)	16	244	72	36.1	23.6	55.3
35	3.32E+06	(83)	4.32E+06	(108)	25	367	71	26.6	19.7	35.8
36	3.00E+06	(24)	6.63E+06	(53)	8	562	155	15.7	9.3	25.9
37	4.25E+06	(51)	7.00E+06	(84)	12	594	131	21.0	14.5	30.1
38	2.57E+06	(72)	2.79E+06	(78)	28	236	54	31.9	22.8	44.6
39	3.13E+06	(50)	2.63E+06	(42)	16	223	69	41.1	26.7	63.5
40	3.22E+06	(87)	2.96E+06	(80)	27	252	57	37.6	27.4	51.6
41	2.93E+06	(41)	2.71E+06	(38)	14	230	75	37.3	23.4	59.6
42	2.09E+06	(67)	2.22E+06	(71)	32	188	45	32.6	23.0	46.2
43	7.19E+06	(115)	5.38E+06	(86)	16	456	99	46.2	34.6	61.9
44	2.41E+06	(77)	2.75E+06	(88)	32	233	50	30.3	22.0	41.6
45	2.17E+06	(52)	1.96E+06	(47)	24	166	49	38.2	25.3	58.0
46	7.70E+06	(77)	6.20E+06	(62)	10	526	134	42.9	30.3	61.0
47	2.44E+06	(44)	3.50E+06	(63)	18	297	75	24.2	16.0	36.1
48	3.05E+06	(61)	3.30E+06	(66)	20	280	69	32.0	22.2	46.0
49	2.67E+06	(48)	2.39E+06	(43)	18	203	62	38.6	25.0	59.6
50	3.13E+06	(50)	6.25E+06	(100)	16	531	107	17.3	12.1	24.6
51	2.44E+06	(44)	1.50E+06	(27)	18	127	49	56.1	34.1	94.3
52	2.87E+06	(86)	3.17E+06	(95)	30	269	56	31.3	23.1	42.4
53	6.58E+06	(79)	6.25E+06	(75)	12	531	123	36.4	26.2	50.7
54	2.39E+06	(43)	3.67E+06	(66)	18	311	77	22.6	15.0	33.6
55	1.50E+06	(27)	2.33E+06	(42)	18	198	61	22.3	13.2	36.9
56	2.87E+06	(86)	3.83E+06	(115)	30	325	61	25.9	19.3	34.6
57	4.13E+06	(33)	6.13E+06	(49)	8	520	149	23.3	14.5	37.0
58	3.00E+06	(48)	3.13E+06	(50)	16	265	75	33.2	21.9	50.3
59	3.05E+06	(122)	3.43E+06	(137)	40	291	50	30.8	23.5	40.4
60	2.75E+06	(44)	2.44E+06	(39)	16	207	66	39.0	24.8	61.6
61	4.83E+06	(29)	5.00E+06	(30)	6	424	154	33.4	19.4	57.6
62	2.43E+06	(51)	3.24E+06	(68)	21	275	67	26.0	17.7	37.9
63	4.14E+06	(58)	4.50E+06	(63)	14	382	97	31.8	21.9	46.2

64	1.89E+06	(17)	1.89E+06	(17)	9	160	77	34.6	16.6	71.9
65	2.09E+06	(46)	1.91E+06	(42)	22	162	50	37.8	24.4	58.9
66	2.79E+06	(67)	3.25E+06	(78)	24	276	63	29.7	21.1	41.7
67	2.80E+06	(28)	2.50E+06	(25)	10	212	84	38.7	21.8	69.1
68	4.14E+06	(87)	4.19E+06	(88)	21	356	76	34.2	25.1	46.5
69	2.63E+06	(63)	1.67E+06	(40)	24	141	45	54.3	36.0	82.9
70	1.72E+06	(31)	2.00E+06	(36)	18	170	56	29.8	17.8	49.5
71	1.58E+06	(19)	2.83E+06	(34)	12	241	82	19.4	10.4	34.9
72	2.93E+06	(44)	3.53E+06	(53)	15	300	83	28.7	18.8	43.7
73	3.00E+06	(30)	4.30E+06	(43)	10	365	111	24.2	14.6	39.4
74	6.64E+06	(93)	5.07E+06	(71)	14	431	103	45.2	32.8	62.5
75	3.94E+06	(71)	4.67E+06	(84)	18	396	87	29.2	21.0	40.6
76	3.55E+06	(71)	3.45E+06	(69)	20	293	71	35.6	25.2	50.3
77	5.00E+05	(3)	6.67E+05	(4)	6	57	53	26.3	3.8	151.9
78	4.25E+06	(17)	4.25E+06	(17)	4	361	173	34.6	16.6	71.9
79	1.60E+06	(32)	2.25E+06	(45)	20	191	57	24.6	15.1	39.6
80	1.80E+06	(54)	8.33E+05	(25)	30	71	28	74.2	45.6	124.5
81	2.60E+06	(39)	2.07E+06	(31)	15	175	63	43.4	26.4	72.0
82	1.95E+06	(41)	2.71E+06	(57)	21	230	61	24.9	16.2	37.9
83	2.67E+06	(32)	2.83E+06	(34)	12	241	82	32.6	19.4	54.3
84	3.17E+06	(57)	4.39E+06	(79)	18	373	84	25.0	17.4	35.6
85	2.44E+06	(39)	3.63E+06	(58)	16	308	81	23.3	15.1	35.5
86	3.80E+06	(19)	2.20E+06	(11)	5	187	110	59.2	27.0	137.9
87	3.25E+06	(52)	3.75E+06	(60)	16	318	82	30.0	20.3	44.2
88	1.08E+07	(65)	5.33E+06	(32)	6	453	159	69.9	45.2	110.3
89	2.93E+06	(41)	3.79E+06	(53)	14	321	88	26.8	17.3	41.0
90	2.30E+06	(23)	3.60E+06	(36)	10	306	102	22.2	12.5	38.3
91	2.00E+06	(34)	2.82E+06	(48)	17	240	69	24.5	15.3	38.8
92	3.40E+06	(34)	2.80E+06	(28)	10	238	89	41.9	24.7	71.7
93	3.58E+06	(43)	2.67E+06	(32)	12	226	80	46.4	28.7	75.7
94	3.96E+06	(95)	2.92E+06	(70)	24	248	59	46.9	34.0	64.8
95	3.13E+06	(50)	2.81E+06	(45)	16	239	71	38.4	25.2	58.8
96	3.33E+06	(60)	3.83E+06	(69)	18	325	79	30.1	20.9	43.2
97	1.85E+06	(37)	2.90E+06	(58)	20	246	65	22.1	14.2	33.9
98	3.00E+06	(45)	4.00E+06	(60)	15	340	88	26.0	17.2	38.9
99	3.33E+05	(2)	1.17E+06	(7)	6	99	72	10.4	1.0	51.8
100	3.19E+06	(51)	3.94E+06	(63)	16	334	85	28.0	19.0	41.2
101	3.33E+06	(30)	5.44E+06	(49)	9	462	132	21.2	13.0	34.1
102	4.25E+06	(68)	5.13E+06	(82)	16	435	97	28.7	20.5	40.1
103	3.70E+06	(37)	3.30E+06	(33)	10	280	97	38.7	23.6	63.9
104	3.13E+06	(25)	3.75E+06	(30)	8	318	116	28.9	16.3	50.7
105	2.80E+06	(42)	2.13E+06	(32)	15	181	64	45.3	28.0	74.1

YAKD57 (Alaska), modern sand

EFFECTIVE TRACK DENSITY FOR FLUENCE MONITOR (tracks/cm^2): 5.900E+05
RELATIVE ERROR (%): 1.58
EFFECTIVE URANIUM CONTENT OF MONITOR (ppm): 50.00
ZETA FACTOR AND STANDARD ERROR (yr cm^2): 117.70 7.10
SIZE OF COUNTER SQUARE (cm^2): 1.000E-06

Grain no.	**RhoS (cm^-2)**	**(Ns)**	**RhoI (cm^-2)**	**(Ni)**	**Squares**	**U+/-2s**		**Grain Age**	**Age (Ma) --95% CI--**	
1	2.70E+06	(27)	1.00E+06	(10)	10	85	52	92.1	43.8	213.7
2	3.20E+05	(8)	8.80E+05	(22)	25	75	32	12.8	4.9	29.4
3	1.14E+05	(8)	4.43E+05	(31)	70	38	13	9.1	3.6	19.9
4	1.50E+05	(6)	4.25E+05	(17)	40	36	17	12.5	4.0	32.5
5	1.11E+05	(4)	6.11E+05	(22)	36	52	22	6.5	1.6	18.6

6	4.54E+06 (109)	1.29E+06 (31)	24	109	39	120.5	80.7	185.9
7	1.75E+06 (84)	5.85E+06 (281)	48	496	61	10.4	7.9	13.7
8	1.07E+06 (48)	2.78E+06 (125)	45	235	43	13.4	9.3	18.7
9	1.17E+06 (14)	1.08E+06 (13)	12	92	50	37.3	16.3	85.9
10	5.30E+06 (106)	5.15E+06 (103)	20	436	87	35.6	26.9	47.3
11	5.33E+05 (8)	1.40E+06 (21)	15	119	51	13.4	5.1	31.0
12	1.27E+06 (19)	8.00E+05 (12)	15	68	38	54.5	25.3	123.1
13	0.00E+00 (0)	3.33E+04 (1)	30	3	5	34.6	0.9	1229.5
14	1.11E+06 (31)	8.21E+05 (23)	28	70	29	46.6	26.3	83.6
15	8.50E+05 (17)	3.75E+06 (75)	20	318	74	7.9	4.4	13.5
16	2.00E+05 (5)	6.80E+05 (17)	25	58	28	10.4	2.9	28.8
17	1.63E+06 (13)	1.13E+06 (9)	8	95	62	49.7	19.8	131.7
18	1.00E+06 (9)	1.89E+06 (17)	9	160	77	18.5	7.2	43.5
19	2.82E+06 (79)	1.86E+06 (52)	28	157	44	52.5	36.6	76.0
20	6.67E+05 (8)	2.75E+06 (33)	12	233	81	8.5	3.4	18.6
21	5.00E+05 (9)	4.44E+05 (8)	18	38	26	38.9	13.4	115.4
22	1.20E+06 (18)	2.07E+06 (31)	15	175	63	20.2	10.6	37.1
23	1.67E+05 (3)	6.67E+05 (12)	18	56	32	9.0	1.6	32.1
24	2.33E+06 (70)	1.58E+07 (474)	30	1339	130	5.2	3.9	6.8
25	2.00E+05 (8)	6.75E+05 (27)	40	57	22	10.4	4.0	23.3
26	2.05E+06 (39)	1.47E+06 (28)	19	125	47	48.1	28.9	81.2
27	4.25E+05 (17)	1.10E+06 (44)	40	93	28	13.5	7.2	23.9
28	6.13E+05 (19)	2.68E+06 (83)	31	227	50	8.0	4.6	13.2
29	5.00E+05 (20)	1.53E+06 (61)	40	129	33	11.4	6.5	19.1
30	5.00E+05 (12)	1.29E+06 (31)	24	109	39	13.5	6.3	26.9
31	3.89E+05 (7)	8.89E+05 (16)	18	75	37	15.4	5.3	38.9
32	2.19E+05 (14)	7.97E+05 (51)	64	68	19	9.6	4.9	17.5
33	1.54E+06 (54)	9.43E+05 (33)	35	80	28	56.5	36.0	89.9
34	5.25E+06 (42)	7.38E+06 (59)	8	625	163	24.7	16.2	37.3
35	2.33E+06 (63)	4.19E+06 (113)	27	355	68	19.4	14.0	26.6
36	4.44E+05 (8)	2.00E+06 (36)	18	169	56	7.8	3.1	16.9
37	1.04E+05 (5)	6.67E+05 (32)	48	56	20	5.6	1.6	14.0
38	1.00E+06 (27)	2.26E+06 (61)	27	191	49	15.4	9.4	24.5
39	1.13E+06 (27)	6.63E+06 (159)	24	561	91	5.9	3.8	8.9
40	9.47E+05 (18)	6.32E+05 (12)	19	54	30	51.6	23.7	117.6
41	2.25E+06 (63)	1.46E+06 (41)	28	124	39	53.1	35.3	80.7
42	0.00E+00 (0)	2.00E+04 (2)	100	2	2	14.4	0.4	182.3
43	1.25E+06 (15)	6.08E+06 (73)	12	516	121	7.2	3.8	12.6
44	7.08E+05 (17)	4.58E+05 (11)	24	39	23	53.2	23.7	125.6
45	2.22E+05 (4)	7.22E+05 (13)	18	61	33	11.0	2.5	34.5
46	3.00E+05 (12)	1.13E+06 (45)	40	95	28	9.3	4.5	17.8
47	4.60E+06 (46)	3.40E+06 (34)	10	288	99	46.8	29.4	75.1
48	1.00E+06 (20)	5.70E+06 (114)	20	483	92	6.1	3.6	9.9
49	1.87E+06 (56)	2.73E+06 (82)	30	232	52	23.7	16.5	33.7
50	6.30E+05 (17)	3.19E+06 (86)	27	270	59	6.9	3.8	11.6
51	9.50E+05 (57)	1.10E+06 (66)	60	93	23	29.9	20.6	43.3
52	3.75E+05 (15)	7.75E+05 (31)	40	66	23	16.9	8.4	32.0
53	2.04E+06 (92)	4.02E+06 (181)	45	341	52	17.7	13.4	23.3
54	2.44E+06 (78)	2.13E+06 (68)	32	180	44	39.7	28.3	55.8
55	4.00E+05 (8)	1.35E+06 (27)	20	114	44	10.4	4.0	23.3
56	2.00E+06 (22)	2.91E+06 (32)	11	247	87	23.9	13.2	42.3
57	5.33E+05 (16)	1.83E+06 (55)	30	155	42	10.2	5.4	17.9
58	4.00E+06 (32)	2.38E+06 (19)	8	201	91	58.0	32.0	108.4
59	1.25E+06 (50)	2.23E+06 (89)	40	189	40	19.5	13.5	27.9
60	9.00E+05 (9)	1.10E+06 (11)	10	93	55	28.4	10.4	75.0
61	4.44E+05 (16)	1.58E+06 (57)	36	134	36	9.8	5.2	17.2

62	5.00E+05	(21)	8.81E+05	(37)	42	75	24	19.7	10.9	34.5
63	1.42E+06	(34)	1.83E+06	(44)	24	155	47	26.8	16.6	42.9
64	9.29E+05	(26)	1.93E+06	(54)	28	163	45	16.8	10.0	27.1
65	1.25E+05	(6)	9.17E+05	(44)	48	78	23	4.8	1.6	11.2
66	1.36E+06	(57)	7.62E+05	(32)	42	65	23	61.4	39.3	97.9
67	7.50E+05	(45)	5.13E+06	(308)	60	435	51	5.1	3.6	7.0
68	1.20E+05	(6)	1.22E+06	(61)	50	103	27	3.5	1.2	7.9
69	1.27E+05	(8)	4.29E+05	(27)	63	36	14	10.4	4.0	23.3
70	5.67E+06	(85)	1.47E+06	(22)	15	124	53	132.1	82.5	221.6
71	1.33E+06	(32)	2.50E+06	(60)	24	212	55	18.5	11.6	28.9
72	1.26E+06	(53)	8.33E+05	(35)	42	71	24	52.3	33.5	82.6
73	2.06E+05	(13)	8.25E+05	(52)	63	70	19	8.8	4.3	16.2
74	2.78E+05	(5)	1.83E+06	(33)	18	155	54	5.4	1.6	13.6
75	5.44E+06	(87)	2.69E+06	(43)	16	228	69	69.7	48.0	103.1
76	1.67E+05	(8)	1.25E+05	(6)	48	11	8	45.8	14.1	160.0
77	8.89E+04	(4)	4.22E+05	(19)	45	36	16	7.5	1.8	22.0
78	5.00E+05	(12)	7.08E+05	(17)	24	60	29	24.6	10.7	54.3
79	9.20E+05	(23)	2.88E+06	(72)	25	244	58	11.1	6.6	18.0
80	6.67E+05	(14)	5.71E+05	(12)	21	48	27	40.3	17.4	95.2
81	1.11E+05	(3)	1.48E+05	(4)	27	13	12	26.3	3.8	152.2
82	5.56E+05	(5)	1.11E+06	(10)	9	94	58	17.6	4.7	55.5
83	2.63E+06	(79)	3.33E+06	(100)	30	282	57	27.4	20.1	37.2
84	1.56E+05	(10)	1.56E+06	(100)	64	132	27	3.5	1.6	6.7
85	2.71E+05	(19)	8.14E+05	(57)	70	69	18	11.6	6.5	19.7
86	1.21E+06	(51)	2.60E+06	(109)	42	220	43	16.3	11.4	22.9
87	2.78E+05	(5)	4.44E+05	(8)	18	38	26	21.9	5.6	74.9
88	2.17E+06	(39)	3.50E+06	(63)	18	297	75	21.5	14.0	32.5
89	3.44E+05	(22)	1.44E+06	(92)	64	122	26	8.3	5.0	13.3
90	1.38E+06	(29)	1.19E+06	(25)	21	101	40	40.1	22.7	71.4
91	3.17E+06	(19)	5.00E+06	(30)	6	424	154	22.0	11.7	40.3
92	3.25E+06	(26)	3.00E+06	(24)	8	254	103	37.5	20.7	68.1
93	2.55E+06	(56)	6.82E+05	(15)	22	58	29	127.3	71.8	242.4
94	3.50E+05	(14)	2.03E+06	(81)	40	172	38	6.1	3.1	10.7
95	1.00E+05	(3)	5.00E+05	(15)	30	42	22	7.2	1.3	24.5
96	8.67E+05	(13)	7.80E+06	(117)	15	661	124	3.9	2.0	6.9
97	2.50E+06	(15)	4.00E+06	(24)	6	339	137	21.8	10.6	43.0
98	4.25E+05	(17)	1.20E+06	(48)	40	102	29	12.4	6.6	21.8
99	3.33E+06	(40)	1.75E+06	(21)	12	148	64	65.6	37.9	117.1
100	3.56E+05	(16)	9.56E+05	(43)	45	81	25	13.0	6.8	23.4
101	2.22E+06	(20)	1.33E+06	(12)	9	113	64	57.3	26.9	128.7
102	1.37E+06	(41)	1.67E+06	(50)	30	141	40	28.4	18.3	43.8
103	1.07E+05	(6)	8.93E+05	(50)	56	76	21	4.3	1.5	9.7
104	3.92E+06	(47)	8.33E+05	(10)	12	71	44	159.2	80.8	352.7
105	4.17E+05	(15)	5.61E+06	(202)	36	476	69	2.6	1.4	4.4

YAKD60 (Alaska), modern sand

EFFECTIVE TRACK DENSITY FOR FLUENCE MONITOR (tracks/cm^2): 5.910E+05

RELATIVE ERROR (%): 1.58

EFFECTIVE URANIUM CONTENT OF MONITOR (ppm): 50.00

ZETA FACTOR AND STANDARD ERROR (yr cm^2): 117.70 7.10

SIZE OF COUNTER SQUARE (cm^2): 1.000E-06

Grain no.	**RhoS (cm^-2)**	**(Ns)**	**RhoI (cm^-2)**	**(Ni)**	**Squares**	**U**	**+/-2s**	**Grain Age**	**Age (Ma) --95% CI--**	
1	1.07E+06	(16)	9.87E+06	(148)	15	835	140	3.8	2.1	6.3
2	4.00E+05	(8)	4.95E+06	(99)	20	419	85	2.9	1.2	5.8
3	2.38E+06	(19)	1.20E+07	(96)	8	1015	209	6.9	4.0	11.3

4	1.85E+06	(48)	1.17E+07	(303)	26	986	117	5.5	4.0	7.5
5	6.25E+05	(5)	6.50E+06	(52)	8	550	153	3.4	1.0	8.3
6	3.44E+05	(11)	4.22E+06	(135)	32	357	62	2.9	1.4	5.2
7	5.63E+05	(18)	4.03E+06	(129)	32	341	61	4.9	2.8	8.0
8	4.38E+05	(7)	4.00E+06	(64)	16	338	85	3.9	1.5	8.3
9	1.14E+06	(32)	7.68E+06	(215)	28	650	91	5.2	3.4	7.5
10	1.40E+06	(14)	5.90E+06	(59)	10	499	130	8.3	4.3	15.0
11	4.00E+05	(12)	3.40E+06	(102)	30	288	58	4.1	2.0	7.5
12	1.42E+06	(44)	8.19E+06	(254)	31	693	90	6.0	4.3	8.3
13	1.00E+06	(36)	8.47E+06	(305)	36	717	85	4.1	2.8	5.8
14	2.22E+06	(40)	1.56E+07	(280)	18	1316	163	5.0	3.5	6.9
15	1.81E+06	(29)	1.08E+07	(173)	16	915	142	5.9	3.8	8.7
16	6.25E+05	(25)	3.75E+06	(150)	40	317	53	5.8	3.6	8.9
17	1.08E+06	(13)	9.50E+06	(114)	12	804	152	4.0	2.0	7.1
18	2.00E+06	(40)	1.45E+07	(290)	20	1227	149	4.8	3.4	6.7
19	3.75E+05	(6)	6.56E+06	(105)	16	555	110	2.0	0.7	4.5
20	4.00E+05	(14)	6.06E+06	(212)	35	512	72	2.3	1.2	3.9
21	6.33E+05	(19)	8.00E+06	(240)	30	677	90	2.8	1.6	4.4
22	1.41E+06	(31)	1.18E+07	(260)	22	1000	128	4.2	2.8	6.0
23	1.58E+06	(63)	8.48E+06	(339)	40	717	81	6.5	4.8	8.5
24	6.88E+05	(11)	8.00E+06	(128)	16	677	121	3.0	1.5	5.5
25	3.06E+05	(11)	6.89E+06	(248)	36	583	76	1.6	0.8	2.8
26	1.55E+06	(34)	1.32E+07	(290)	22	1115	136	4.1	2.8	5.8
27	7.67E+05	(23)	6.03E+06	(181)	30	510	77	4.4	2.7	6.8
28	3.20E+05	(8)	4.08E+06	(102)	25	345	69	2.8	1.1	5.6
29	2.67E+05	(4)	5.07E+06	(76)	15	429	99	1.9	0.5	4.9
30	1.61E+06	(29)	1.18E+07	(212)	18	996	140	4.8	3.1	7.0
31	4.40E+05	(11)	5.72E+06	(143)	25	484	82	2.7	1.3	4.9
32	8.33E+05	(15)	1.11E+07	(199)	18	935	136	2.6	1.4	4.4
33	6.67E+05	(6)	4.00E+06	(36)	9	338	113	5.9	2.0	13.9
34	1.43E+05	(5)	1.86E+06	(65)	35	157	39	2.8	0.8	6.6
35	2.50E+05	(10)	2.53E+06	(101)	40	214	43	3.5	1.6	6.6
36	9.33E+05	(28)	1.27E+07	(381)	30	1074	115	2.6	1.7	3.8
37	1.11E+05	(4)	1.75E+06	(63)	36	148	37	2.3	0.6	5.9
38	7.64E+05	(55)	7.69E+06	(554)	72	651	59	3.5	2.6	4.6
39	5.00E+05	(6)	2.92E+06	(35)	12	247	83	6.1	2.0	14.3
40	4.13E+05	(33)	4.51E+06	(361)	80	382	42	3.2	2.2	4.6
41	9.17E+05	(11)	6.42E+06	(77)	12	543	125	5.0	2.4	9.4
42	1.58E+06	(19)	9.33E+06	(112)	12	790	151	5.9	3.4	9.7
43	1.06E+06	(19)	1.50E+07	(270)	18	1269	159	2.5	1.4	3.9
44	2.33E+06	(21)	9.56E+06	(86)	9	808	176	8.5	5.0	13.8
45	5.67E+05	(17)	4.93E+06	(148)	30	417	70	4.0	2.3	6.6
46	3.75E+06	(30)	2.28E+07	(182)	8	1925	291	5.8	3.8	8.5
47	1.13E+06	(9)	4.50E+06	(36)	8	381	127	8.8	3.7	18.4
48	2.00E+06	(36)	1.20E+07	(216)	18	1015	142	5.8	3.9	8.3
49	1.00E+06	(10)	1.23E+07	(123)	10	1041	190	2.9	1.3	5.4
50	5.00E+05	(12)	4.46E+06	(107)	24	377	74	3.9	2.0	7.1
51	6.50E+05	(26)	7.23E+06	(289)	40	611	74	3.1	2.0	4.7
52	5.56E+05	(5)	5.11E+06	(46)	9	432	128	3.9	1.2	9.5
53	1.75E+06	(21)	1.32E+07	(158)	12	1114	180	4.7	2.8	7.3
54	2.86E+05	(10)	5.97E+06	(209)	35	505	72	1.7	0.8	3.1
55	1.67E+05	(2)	2.75E+06	(33)	12	233	81	2.3	0.2	8.2
56	1.00E+05	(10)	7.80E+05	(78)	100	66	15	4.5	2.1	8.6
57	7.50E+05	(15)	7.30E+06	(146)	20	618	104	3.6	1.9	6.1
58	2.50E+06	(10)	1.50E+07	(60)	4	1269	329	5.9	2.6	11.4
59	6.67E+05	(4)	4.17E+06	(25)	6	353	140	5.8	1.4	16.1

60	6.94E+05 (25)	7.86E+06 (283)	36	665	82	3.1	2.0	4.6
61	1.50E+06 (45)	1.08E+07 (323)	30	911	105	4.9	3.5	6.6
62	6.20E+05 (31)	5.44E+06 (272)	50	460	58	4.0	2.6	5.8
63	1.22E+06 (22)	1.43E+07 (257)	18	1208	155	3.0	1.8	4.6
64	9.58E+05 (23)	6.79E+06 (163)	24	575	92	4.9	3.0	7.6
65	9.33E+05 (14)	8.20E+06 (123)	15	694	127	4.0	2.1	6.9
66	4.00E+05 (8)	4.30E+06 (86)	20	364	79	3.3	1.4	6.7
67	1.75E+06 (14)	1.76E+07 (141)	8	1491	255	3.5	1.8	6.0
68	8.89E+05 (16)	5.83E+06 (105)	18	494	97	5.3	2.9	9.0
69	9.00E+05 (18)	7.05E+06 (141)	20	596	102	4.5	2.6	7.3
70	4.29E+05 (6)	7.36E+06 (103)	14	622	124	2.1	0.7	4.6
71	6.50E+05 (13)	3.95E+06 (79)	20	334	76	5.8	2.9	10.4
72	1.40E+05 (14)	2.19E+06 (219)	100	185	26	2.2	1.2	3.8
73	1.00E+06 (18)	9.17E+06 (165)	18	776	123	3.8	2.2	6.2
74	1.10E+06 (11)	1.04E+07 (104)	10	880	174	3.7	1.8	6.9
75	9.17E+05 (11)	9.17E+06 (110)	12	776	150	3.5	1.7	6.5
76	1.22E+06 (22)	8.78E+06 (158)	18	743	120	4.9	2.9	7.6
77	2.25E+06 (18)	1.14E+07 (91)	8	962	203	6.9	3.9	11.5
78	3.00E+06 (27)	1.28E+07 (115)	9	1081	204	8.2	5.2	12.5
79	4.80E+05 (24)	5.08E+06 (254)	50	430	56	3.3	2.1	5.0
80	7.50E+05 (9)	4.75E+06 (57)	12	402	107	5.6	2.4	11.2
81	8.00E+05 (8)	3.90E+06 (39)	10	330	106	7.2	2.9	15.5
82	1.10E+06 (11)	5.60E+06 (56)	10	474	127	6.9	3.2	13.2
83	7.67E+05 (23)	9.37E+06 (281)	30	792	98	2.9	1.8	4.4
84	3.33E+06 (20)	1.22E+07 (73)	6	1029	242	9.6	5.5	15.8
85	1.33E+06 (8)	1.62E+07 (97)	6	1368	280	2.9	1.2	5.9
86	2.50E+05 (4)	5.75E+06 (92)	16	486	102	1.6	0.4	4.0
87	1.60E+06 (24)	8.40E+06 (126)	15	711	128	6.7	4.1	10.3
88	1.00E+06 (10)	1.06E+07 (106)	10	897	176	3.3	1.5	6.3
89	3.11E+06 (28)	9.44E+06 (85)	9	799	175	11.5	7.2	17.7
90	8.64E+05 (19)	1.02E+07 (225)	22	865	118	3.0	1.7	4.7
91	5.00E+05 (3)	6.83E+06 (41)	6	578	180	2.7	0.5	8.0
92	2.00E+06 (12)	1.42E+07 (85)	6	1199	262	5.0	2.4	9.0
93	2.14E+05 (6)	5.43E+06 (152)	28	459	76	1.4	0.5	3.1
94	6.00E+05 (18)	1.02E+07 (307)	30	866	102	2.1	1.2	3.3
95	1.08E+06 (39)	8.89E+06 (320)	36	752	87	4.3	3.0	5.9
96	1.54E+06 (43)	1.14E+07 (319)	28	964	112	4.7	3.3	6.5
97	1.80E+06 (36)	6.90E+06 (138)	20	584	101	9.1	6.1	13.2
98	1.19E+06 (19)	1.38E+07 (221)	16	1169	161	3.0	1.8	4.8
99	1.50E+06 (24)	9.44E+06 (151)	16	798	132	5.6	3.4	8.5
100	5.00E+05 (7)	6.64E+06 (93)	14	562	118	2.7	1.0	5.6
101	2.33E+06 (56)	1.30E+07 (311)	24	1096	129	6.3	4.6	8.4
102	5.36E+05 (15)	4.46E+06 (125)	28	378	68	4.2	2.3	7.2
103	6.33E+05 (19)	6.00E+06 (180)	30	508	77	3.7	2.2	5.9
104	7.65E+05 (13)	8.76E+06 (149)	17	742	124	3.1	1.6	5.4
105	1.25E+06 (20)	9.81E+06 (157)	16	830	135	4.5	2.6	7.1

Dataset B2. Analytical data of 40Ar/39Ar measurements of cobbles and bedrock samples

Sample: HUB_2_2
Project: Alaska
Owner: Falkowski_Enkelmann
Exp-Nr: 5858
Material: 2.72 mg Bt

Irradiation: FGA014P7H4 (End date: 2013-07-31 15:39:00.0)
Measurement Date: 2014-01-19 14:16:49.0
Device: CO2-Laser
Air: 298.6
J-Value: 0.0031998 f-value: 0.994011
J-Value Error: 0.0000100 f-value Error: 0.000211
Reference Standard(s): FCT01 - 28.305 +/- 0.036 Ma, FCT01 - 28.305 +/- 0.036 Ma,
Total gas age: 49.78 +/- 0.31 Ma

Interfering isotope production ratios:
ca3637 = 0.000205 +/- 0.000012
ca3937 = 0.000932 +/- 0.000035
k3839 = 0.01211 +/- 0.00061
k4039 = 0.00183 +/- 0.00009

Decay constants:
lambda40 = 5.5492e-010 +/- 9.3000e-013 1/a
lambda39 = 0.002577 +/- 0.000026 1/a
lambda37 = 7.2438 +/- 0.0214 1/a

ALF ARGONLAB FREIBERG

Fit model: linear **All errors are 1s!**

Nr.	Step	39Ar(K) (V)	39Ar(K) (%)	39Ar (10e-14 mol)	40Ar* (V)	36Ar_atm (V)	40Ar* (%)	40Ar/36Ar	37Ar/36Ar	37Ar/39Ar	K/Ca	K/Ca Error	40Ar*/39Ar(K)	40Ar*/39Ar(K) Error	Age (Ma)	Age Error(Ma)
1	3.0%	0.0215	0.81	0.725	0.155	0.00102	33.7	450.6	0.02	0.0009	18.923	65.726	7.23	0.95	41.20	5.38
2	3.8%	0.1238	4.65	4.175	1.053	0.00136	72.2	1074.4	0.05	0.0005	32.839	36.577	8.50	0.19	48.37	1.08
3	4.3%	0.1536	5.76	5.178	1.316	0.00087	83.5	1808.4	0.09	0.0005	32.737	30.109	8.57	0.16	48.73	0.90
4	5.0%	0.1504	5.64	5.071	1.319	0.00047	90.3	3087.7	0.09	0.0003	59.740	116.122	8.77	0.16	49.86	0.90
5	5.8%	0.1603	6.01	5.405	1.394	0.00025	95.0	5927.5	0.32	0.0005	34.190	28.552	8.69	0.13	49.45	0.78
6	6.7%	0.1628	6.11	5.489	1.427	0.00016	96.8	9398.8	0.50	0.0005	35.800	33.278	8.77	0.15	49.85	0.86
7	7.7%	0.1652	6.20	5.569	1.454	0.00014	97.1	10409.9	1.01	0.0009	19.446	9.660	8.80	0.15	50.06	0.84
8	8.7%	0.1930	7.24	6.509	1.697	0.00017	97.1	10071.8	3.73	0.0034	5.121	0.567	8.79	0.14	49.98	0.83
9	9.7%	0.2544	9.54	8.577	2.250	0.00012	98.4	17893.3	8.64	0.0043	3.951	0.267	8.84	0.12	50.29	0.68
10	10.7%	0.3464	13.00	11.679	3.034	0.00021	97.9	14309.6	3.00	0.0019	9.151	1.027	8.76	0.11	49.82	0.64
11	11.5%	0.2522	9.46	8.505	2.220	0.00012	98.4	18970.8	2.08	0.0010	17.529	4.811	8.80	0.15	50.05	0.83
12	12.4%	0.2196	8.24	7.404	1.927	0.00009	98.6	21799.2	3.00	0.0012	14.028	3.492	8.77	0.29	49.89	1.66
13	13.4%	0.1813	6.80	6.113	1.596	0.00006	98.8	25483.9	5.16	0.0018	9.520	1.911	8.80	0.18	50.06	1.05
14	14.8%	0.1415	5.31	4.770	1.257	0.00001	99.8	128166.2	36.61	0.0025	6.746	1.303	8.88	0.25	50.51	1.42
15	16.3%	0.0801	3.01	2.701	0.710	0.00002	99.0	29355.4	10.04	0.0031	5.601	1.642	8.86	0.29	50.40	1.64
16	18.3%	0.0438	1.64	1.478	0.384	0.00002	98.4	18114.7	10.50	0.0052	3.331	1.204	8.75	0.64	49.75	3.60
17	20.3%	0.0154	0.58	0.519	0.137	0.00000	100.0	Inf	Inf	0.0027	6.317	10.708	8.93	1.24	50.76	6.96

J - value = 0.0031998
J-error [%] = 0.31

Plateau Data				Isochron Data				Inverse Isochron Data			
Nr.	39Ar%	Age (Ma)	Age_err (Ma)	39/36	err	40/36	err	39/40	err	36/40	err
								0.000000	0.000010	0.003384	0.000010
1	0.8	41.20	5.38	21.039	1.414	450.66	30.23	0.046685	0.000300	0.002219	0.000149
2	4.6	48.37	1.08	91.256	5.079	1074.54	59.82	0.084925	0.000443	0.000931	0.000052
3	5.8	48.73	0.90	176.340	14.789	1809.13	151.72	0.097472	0.000728	0.000553	0.000046
4	5.6	49.86	0.90	318.224	49.189	3088.88	477.48	0.103022	0.000704	0.000324	0.000050
5	6.0	49.45	0.78	648.678	177.722	5938.30	1626.91	0.109236	0.000581	0.000168	0.000046
6	6.1	49.85	0.86	1041.288	478.351	9426.08	4330.24	0.110469	0.000911	0.000106	0.000049
7	6.2	50.06	0.84	1155.791	533.956	10473.75	4838.77	0.110351	0.001043	0.000095	0.000044
8	7.2	49.98	0.83	1138.879	463.924	10308.47	4199.08	0.110480	0.001209	0.000097	0.000040
9	9.5	50.29	0.68	2103.850	1117.507	18905.22	10042.05	0.111284	0.001123	0.000053	0.000028
10	13.0	49.82	0.64	1629.983	518.576	14578.30	4638.31	0.111809	0.001167	0.000069	0.000022
11	9.5	50.05	0.83	2149.000	1215.838	19214.80	10871.08	0.111841	0.001538	0.000052	0.000029
12	8.2	49.89	1.66	2497.345	1809.718	22208.35	16094.44	0.112451	0.003569	0.000045	0.000033
13	6.8	50.06	1.05	2956.284	3364.524	26322.07	29957.07	0.112312	0.001821	0.000038	0.000043
14	5.3	50.51	1.42	18640.970	143443.600	165887.90	1276520.00	0.112371	0.002765	0.000006	0.000046
15	3.0	50.40	1.64	3497.497	10555.460	31302.95	94472.48	0.111731	0.001693	0.000032	0.000096
16	1.6	49.75	3.60	2180.621	8489.669	19374.97	75431.79	0.112548	0.004521	0.000052	0.000201
17	0.6	50.76	6.96	-59255.170	14351140.000	-528754.20	128060100.00	0.112066	0.002837	-0.000002	0.000458

Blank intercepts:

exp.#	Step	36Ar (V)	$\pm\sigma_{36}$ (V)	37Ar (V)	$\pm\sigma_{37}$ (V)	38Ar (V)	$\pm\sigma_{38}$ (V)	39Ar (V)	$\pm\sigma_{39}$ (V)	40Ar (V)	$\pm\sigma_{40}$ (V)
5857	0.0%	-0.004549	0.000049	-0.002267	0.000045	-0.00248	0.000058	0.03065	0.000067	0.001708	0.000147

Blank corrected intensity intercepts:

Nr.	Step	36Ar (V)	$\pm\sigma_{36}$ (V)	37Ar (V)	$\pm\sigma_{37}$ (V)	38Ar (V)	$\pm\sigma_{38}$ (V)	39Ar (V)	$\pm\sigma_{39}$ (V)	40Ar (V)	$\pm\sigma_{40}$ (V)
1	3.0%	0.000998	0.000067	0.000019	0.000066	0.00044	0.000077	0.02134	0.000118	0.460506	0.001511
2	3.8%	0.001325	0.000074	0.000064	0.000071	0.00149	0.000073	0.12292	0.000440	1.458109	0.005519
3	4.3%	0.000851	0.000071	0.000079	0.000073	0.00172	0.000075	0.15247	0.000807	1.575848	0.008293
4	5.0%	0.000462	0.000071	0.000042	0.000082	0.00162	0.000079	0.14930	0.000707	1.459980	0.007175
5	5.8%	0.000242	0.000066	0.000079	0.000066	0.00170	0.000075	0.15914	0.000633	1.467673	0.005169
6	6.7%	0.000153	0.000070	0.000077	0.000071	0.00163	0.000073	0.16162	0.000904	1.473916	0.008921
7	7.7%	0.000140	0.000064	0.000143	0.000071	0.00176	0.000075	0.16397	0.001054	1.496953	0.010372
8	8.7%	0.000169	0.000067	0.000635	0.000070	0.00205	0.000085	0.19166	0.001522	1.747514	0.013150
9	9.7%	0.000125	0.000063	0.001085	0.000072	0.00267	0.000086	0.25256	0.001743	2.286121	0.016806
10	10.7%	0.000211	0.000066	0.000638	0.000071	0.00356	0.000078	0.34390	0.002403	3.098580	0.024003
11	11.5%	0.000116	0.000065	0.000242	0.000066	0.00263	0.000080	0.25043	0.002455	2.255747	0.021739
12	12.4%	0.000087	0.000062	0.000264	0.000065	0.00229	0.000086	0.21802	0.004731	1.953161	0.045228
13	13.4%	0.000062	0.000068	0.000321	0.000064	0.00189	0.000077	0.18001	0.002021	1.614619	0.018885
14	14.8%	0.000010	0.000057	0.000353	0.000068	0.00146	0.000080	0.14045	0.002277	1.259132	0.023310
15	16.3%	0.000024	0.000067	0.000241	0.000071	0.00089	0.000072	0.07952	0.000822	0.716997	0.007941
16	18.3%	0.000021	0.000076	0.000222	0.000080	0.00049	0.000078	0.04353	0.001158	0.389601	0.011717
17	20.3%	0.000000	0.000061	0.000041	0.000070	0.00019	0.000075	0.01527	0.000247	0.137267	0.002674

Sample: HUB_2_8
Project: Alaska
Owner: Falkowski_Enkelmann
Exp-Nr: 5861
Material: 2.78 mg Bt

Irradiation: FGA014P7H5 (End date: 2013-07-31 15:39:00.0)
Measurement Date: 2014-01-20 04:32:47.0
Device: CO2-Laser
Air: 298.6
J-Value: 0.0031998 f-value: 0.994011
J-Value Error: 0.0000100 f-value Error: 0.000211
Reference Standard(s): FCT01 - 28.305 +/- 0.036 Ma, FCT01 - 28.305 +/- 0.036 Ma,
Total gas age: 49.70 +/- 0.45 Ma

Interfering isotope production ratios:
ca3637 = 0.000205 +/- 0.000012
ca3937 = 0.000932 +/- 0.000035
k3839 = 0.01211 +/- 0.00061
k4039 = 0.00183 +/- 0.00009

Decay constants:
lambda40 = 5.5492e-010 +/- 9.3000e-013 1/a
lambda39 = 0.002577 +/- 0.000026 1/a
lambda37 = 7.2438 +/- 0.0214 1/a

ALF ARGONLAB FREIBERG

Fit model: linear **All errors are 1s!**

Nr.	Step	39Ar(K) (V)	39Ar(K) (%)	39Ar (10e-14 mol)	40Ar* (V)	36Ar_atm (V)	40Ar* (%)	40Ar/36Ar	37Ar/36Ar	37Ar/39Ar	K/Ca	K/Ca Error	40Ar*/39Ar(K)	40Ar*/39Ar(K) Error	Age (Ma)	Age Error(Ma)
1	3.0%	0.0175	0.56	0.589	0.142	0.00028	62.8	804.0	0.00	0.0000	Inf	Inf	8.16	1.25	46.44	7.05
2	4.0%	0.1472	4.74	4.963	1.242	0.00086	82.9	1748.3	0.00	0.0000	Inf	Inf	8.44	0.22	48.02	1.27
3	4.7%	0.1524	4.91	5.138	1.316	0.00044	91.0	3323.4	0.00	0.0000	Inf	Inf	8.64	0.16	49.13	0.92
4	5.4%	0.1689	5.44	5.697	1.473	0.00031	94.1	5067.1	0.00	0.0000	Inf	Inf	8.72	0.18	49.59	1.01
5	6.1%	0.1356	4.37	4.573	1.190	0.00014	96.5	8618.9	0.00	0.0000	Inf	Inf	8.78	0.20	49.90	1.16
6	7.0%	0.1627	5.24	5.485	1.421	0.00013	97.4	11633.0	0.00	0.0000	Inf	Inf	8.74	0.18	49.70	1.02
7	7.9%	0.2136	6.88	7.201	1.872	0.00010	98.4	18848.9	0.00	0.0000	Inf	Inf	8.77	0.15	49.85	0.85
8	8.8%	0.1913	6.17	6.451	1.671	0.00010	98.3	17406.5	0.04	0.0000	830.393	13810.150	8.73	0.18	49.66	1.05
9	9.7%	0.1890	6.09	6.374	1.657	0.00009	98.4	19156.6	0.00	0.0000	Inf	Inf	8.77	0.12	49.85	0.71
10	10.6%	0.1783	5.75	6.012	1.567	0.00007	98.8	24373.0	0.00	0.0000	Inf	Inf	8.79	0.22	49.99	1.26
11	11.5%	0.1754	5.65	5.913	1.530	0.00010	98.1	15807.2	0.00	0.0000	Inf	Inf	8.73	0.29	49.62	1.65
12	12.4%	0.1774	5.72	5.980	1.559	0.00006	98.9	28316.3	0.00	0.0000	Inf	Inf	8.79	0.30	49.97	1.66
13	13.3%	0.1687	5.43	5.687	1.479	0.00004	99.1	34855.7	0.28	0.0001	235.238	1264.055	8.77	0.17	49.87	0.98
14	14.3%	0.1247	4.02	4.203	1.092	0.00004	99.0	29088.2	0.00	0.0000	Inf	Inf	8.76	0.22	49.83	1.22
15	15.8%	0.1494	4.82	5.039	1.312	0.00002	99.5	57627.8	0.00	0.0000	Inf	Inf	8.78	0.33	49.92	1.86
16	17.3%	0.1380	4.45	4.654	1.210	0.00004	99.0	32004.1	0.00	0.0000	Inf	Inf	8.76	0.33	49.84	1.84
17	18.8%	0.1114	3.59	3.758	0.976	0.00003	99.0	30946.9	0.46	0.0001	129.398	571.398	8.75	0.24	49.78	1.35
18	20.8%	0.1202	3.87	4.054	1.062	0.00001	99.6	80030.1	0.00	0.0000	Inf	Inf	8.83	0.26	50.22	1.48
19	22.8%	0.3475	11.20	11.717	3.047	0.00010	99.1	32270.5	0.31	0.0001	201.087	443.268	8.77	0.40	49.86	2.28
20	23.8%	0.0272	0.88	0.916	0.238	0.00000	100.0	Inf	NaN	0.0000	Inf	Inf	8.76	1.02	49.84	5.71
21	26.0%	0.0068	0.22	0.229	0.061	0.00000	100.0	Inf	NaN	0.0000	Inf	Inf	8.96	2.55	50.93	14.30

J - value = 0.0031998
J-error [%] = 0.31

Plateau Data				Isochron Data				Inverse Isochron Data			
Nr.	39Ar%	Age (Ma)	Age_err (Ma)	39/36	err	40/36	err	39/40	err	36/40	err
								0.000000	0.000010	0.003384	0.000010
1	0.6	46.44	7.05	61.932	15.842	803.89	205.62	0.077040	0.001725	0.001244	0.000318
2	4.7	48.02	1.27	171.745	14.855	1747.99	151.35	0.098253	0.001755	0.000572	0.000050
3	4.9	49.13	0.92	350.113	55.480	3322.79	526.53	0.105367	0.001020	0.000301	0.000048
4	5.4	49.59	1.01	546.757	107.595	5066.07	997.01	0.107925	0.001704	0.000197	0.000039
5	4.4	49.90	1.16	947.973	365.896	8617.14	3326.18	0.110010	0.002011	0.000116	0.000045
6	5.2	49.70	1.02	1296.734	659.248	11630.58	5913.07	0.111494	0.001704	0.000086	0.000044
7	6.9	49.85	0.85	2115.900	1187.997	18845.01	10580.79	0.112279	0.001593	0.000053	0.000030
8	6.2	49.66	1.05	1959.393	1129.125	17407.25	10031.39	0.112562	0.002068	0.000057	0.000033
9	6.1	49.85	0.71	2150.737	1482.236	19152.62	13199.59	0.112295	0.000977	0.000052	0.000036
10	5.7	49.99	1.26	2738.075	2397.787	24367.95	21340.15	0.112364	0.002551	0.000041	0.000036
11	5.7	49.62	1.65	1777.011	1020.207	15803.97	9074.17	0.112441	0.003517	0.000063	0.000036
12	5.7	49.97	1.66	3187.659	3513.162	28310.48	31202.05	0.112596	0.003522	0.000035	0.000039
13	5.4	49.87	0.98	3947.186	5767.757	34910.87	51013.16	0.113065	0.001678	0.000029	0.000042
14	4.0	49.83	1.22	3284.998	4929.815	29082.17	43644.17	0.112956	0.002140	0.000034	0.000052
15	4.8	49.92	1.86	6529.683	16585.250	57615.90	146343.60	0.113331	0.003991	0.000017	0.000044
16	4.4	49.84	1.84	3616.913	5332.540	31997.50	47174.54	0.113037	0.003888	0.000031	0.000046
17	3.6	49.78	1.35	3510.834	6925.018	31029.94	61205.93	0.113144	0.002183	0.000032	0.000064
18	3.9	50.22	1.48	9026.153	41323.610	80013.53	366318.40	0.112808	0.002733	0.000012	0.000057
19	11.2	49.86	2.28	3653.150	2236.518	32326.30	19792.60	0.113009	0.005152	0.000031	0.000019
20	0.9	49.84	5.71	Inf	Inf	Inf	Inf	0.114104	0.009980	0.000000	0.000256
21	0.2	50.93	14.30	Inf	Inf	Inf	Inf	0.111629	0.004361	0.000000	0.000945

Blank intercepts:

exp.#	Step	36Ar (V)	$\pm\sigma_{36}$ (V)	37Ar (V)	$\pm\sigma_{37}$ (V)	38Ar (V)	$\pm\sigma_{38}$ (V)	39Ar (V)	$\pm\sigma_{39}$ (V)	40Ar (V)	$\pm\sigma_{40}$ (V)
5860	0.0%	-0.004556	0.000046	-0.002260	0.000047	-0.00248	0.000047	0.03077	0.000048	0.001996	0.000454

Blank corrected intensity intercepts:

Nr.	Step	36Ar (V)	$\pm\sigma_{36}$ (V)	37Ar (V)	$\pm\sigma_{37}$ (V)	38Ar (V)	$\pm\sigma_{38}$ (V)	39Ar (V)	$\pm\sigma_{39}$ (V)	40Ar (V)	$\pm\sigma_{40}$ (V)
1	3.0%	0.000275	0.000070	0.000000	0.000076	0.00025	0.000061	0.01733	0.000276	0.226660	0.003563
2	4.0%	0.000837	0.000072	0.000000	0.000074	0.00162	0.000071	0.14614	0.001799	1.498459	0.019376
3	4.7%	0.000425	0.000067	0.000000	0.000070	0.00162	0.000065	0.15128	0.001038	1.446425	0.009857
4	5.4%	0.000302	0.000059	0.000000	0.000063	0.00178	0.000062	0.16773	0.001850	1.565682	0.017684
5	6.1%	0.000140	0.000054	0.000000	0.000066	0.00144	0.000064	0.13465	0.001704	1.233098	0.016269
6	7.0%	0.000122	0.000062	0.000000	0.000065	0.00169	0.000064	0.16149	0.001680	1.459180	0.016321
7	7.9%	0.000099	0.000055	0.000000	0.000064	0.00223	0.000068	0.21202	0.002115	1.902435	0.019183
8	8.8%	0.000095	0.000055	0.000004	0.000064	0.00196	0.000065	0.18994	0.002408	1.700027	0.022593
9	9.7%	0.000086	0.000059	0.000000	0.000070	0.00196	0.000058	0.18766	0.001114	1.683642	0.010703
10	10.6%	0.000064	0.000056	0.000000	0.000066	0.00185	0.000070	0.17700	0.002710	1.586990	0.026600
11	11.5%	0.000096	0.000055	0.000000	0.000065	0.00179	0.000074	0.17411	0.003722	1.559999	0.035611
12	12.4%	0.000054	0.000060	0.000000	0.000064	0.00185	0.000070	0.17608	0.003788	1.575489	0.035777
13	13.3%	0.000042	0.000061	0.000012	0.000064	0.00177	0.000068	0.16744	0.001671	1.491935	0.016382
14	14.3%	0.000037	0.000056	0.000000	0.000060	0.00129	0.000064	0.12376	0.001562	1.103816	0.015589
15	15.8%	0.000022	0.000057	0.000000	0.000068	0.00156	0.000074	0.14837	0.003638	1.318947	0.033330
16	17.3%	0.000037	0.000055	0.000000	0.000065	0.00142	0.000080	0.13702	0.003392	1.221228	0.029147
17	18.8%	0.000031	0.000061	0.000014	0.000063	0.00113	0.000063	0.11064	0.001432	0.985185	0.014095
18	20.8%	0.000013	0.000060	0.000000	0.000064	0.00122	0.000069	0.11935	0.002087	1.065917	0.017863
19	22.8%	0.000093	0.000057	0.000029	0.000063	0.00355	0.000127	0.34500	0.010926	3.075616	0.100835
20	23.8%	0.000000	0.000059	0.000000	0.000065	0.00030	0.000069	0.02696	0.001571	0.238075	0.015529
21	26.0%	0.000000	0.000056	0.000000	0.000064	0.00009	0.000060	0.00675	0.000167	0.060932	0.001841

Sample: MAL_2_10
Project: Alaska
Owner: Falkowski_Enkelmann
Exp-Nr: 5712
Material: 2.78 mg Bt

Irradiation: FGA014P6H10 (End date: 2013-07-31 15:39:00.0)
Measurement Date: 2013-12-04 08:20:42.0
Device: CO2-Laser
Air: 298.6
J-Value: 0.0032477 f-value: 0.993844
J-Value Error: 0.0000090 f-value Error: 0.000235
Reference Standard(s): FCT01 - 28.305 +/- 0.036 Ma,
Total gas age: 50.24 +/- 0.20 Ma

Interfering isotope production ratios:
ca3637 = 0.000205 +/- 0.000012
ca3937 = 0.000932 +/- 0.000035
k3839 = 0.01211 +/- 0.00061
k4039 = 0.00183 +/- 0.00009

Decay constants:
lambda40 = 5.5492e-010 +/- 9.3000e-013 1/a
lambda39 = 0.002577 +/- 0.000026 1/a
lambda37 = 7.2438 +/- 0.0214 1/a

ALF ARGONLAB FREIBERG

Fit model: linear **All errors are 1s!**

Nr.	Step	39Ar(K) (V)	39Ar(K) (%)	39Ar (10e-14 mol)	40Ar* (V)	36Ar_atm (V)	40Ar* (%)	40Ar/36Ar	37Ar/36Ar	37Ar/39Ar	K/Ca	K/Ca Error	40Ar*/39Ar(K)	40Ar*/39Ar(K) Error	Age (Ma)	Age Error(Ma)
1	3.0%	0.0117	0.38	0.394	0.064	0.00096	18.4	366.1	0.00	0.0000	Inf	Inf	5.52	1.75	32.00	10.04
2	3.8%	0.0859	2.78	2.896	0.703	0.00116	66.9	903.0	0.00	0.0000	Inf	Inf	8.19	0.26	47.29	1.49
3	4.2%	0.1374	4.45	4.632	1.180	0.00066	85.8	2100.6	0.00	0.0000	Inf	Inf	8.59	0.16	49.60	0.93
4	4.6%	0.1418	4.60	4.783	1.223	0.00047	89.7	2906.0	0.00	0.0000	Inf	Inf	8.63	0.14	49.79	0.80
5	5.1%	0.1529	4.96	5.156	1.332	0.00032	93.4	4524.6	0.00	0.0000	Inf	Inf	8.71	0.14	50.28	0.81
6	5.8%	0.1585	5.14	5.345	1.383	0.00027	94.4	5370.6	0.00	0.0000	Inf	Inf	8.72	0.12	50.34	0.72
7	6.6%	0.1800	5.83	6.069	1.576	0.00020	96.3	8178.4	0.00	0.0000	Inf	Inf	8.75	0.12	50.51	0.69
8	7.4%	0.2017	6.54	6.802	1.760	0.00021	96.5	8501.5	0.00	0.0000	Inf	Inf	8.73	0.12	50.37	0.68
9	8.2%	0.1964	6.37	6.623	1.713	0.00015	97.5	11849.1	0.21	0.0002	274.246	748.946	8.72	0.12	50.34	0.68
10	9.0%	0.1723	5.58	5.810	1.509	0.00015	97.1	10332.8	0.44	0.0004	112.141	145.665	8.76	0.14	50.54	0.80
11	9.8%	0.2218	7.19	7.478	1.949	0.00021	96.8	9383.4	0.10	0.0001	440.397	1988.447	8.79	0.13	50.72	0.74
12	10.5%	0.2629	8.52	8.866	2.309	0.00023	97.1	10417.7	0.12	0.0001	407.749	1097.345	8.78	0.08	50.67	0.50
13	11.0%	0.1894	6.14	6.387	1.659	0.00016	97.2	10909.7	0.26	0.0002	201.348	417.303	8.76	0.12	50.53	0.67
14	11.8%	0.1960	6.35	6.610	1.719	0.00015	97.5	11922.9	0.24	0.0002	235.852	486.254	8.77	0.11	50.60	0.66
15	12.8%	0.2362	7.66	7.964	2.048	0.00022	96.9	9623.8	0.18	0.0002	253.967	447.340	8.67	0.10	50.06	0.57
16	13.8%	0.1612	5.22	5.435	1.412	0.00011	97.7	12990.6	0.44	0.0003	142.451	252.397	8.76	0.14	50.57	0.81
17	14.8%	0.1141	3.70	3.849	1.001	0.00008	97.6	12478.4	1.08	0.0008	55.144	72.734	8.77	0.30	50.59	1.72
18	16.3%	0.1234	4.00	4.161	1.078	0.00010	97.3	11239.4	1.88	0.0015	28.566	13.436	8.74	0.18	50.42	1.06
19	18.3%	0.0908	2.94	3.063	0.789	0.00009	96.5	8654.0	2.06	0.0021	20.006	8.058	8.68	0.26	50.12	1.48
20	21.3%	0.0506	1.64	1.707	0.448	0.00003	97.9	14609.0	2.67	0.0017	26.025	23.288	8.84	0.47	51.00	2.70

J - value = 0.0032477
J-error [%] = 0.28

Plateau Data				Isochron Data				Inverse Isochron Data			
Nr.	39Ar%	Age (Ma)	Age_err (Ma)	39/36	err	40/36	err	39/40	err	36/40	err
								0.000000	0.000010	0.003384	0.000010
1	0.4	32.00	10.04	12.228	0.879	366.06	26.17	0.033406	0.000247	0.002732	0.000195
2	2.8	47.29	1.49	73.806	4.734	902.84	57.91	0.081748	0.000120	0.001108	0.000071
3	4.5	49.60	0.93	209.685	23.615	2100.19	236.52	0.099841	0.000135	0.000476	0.000054
4	4.6	49.79	0.80	302.233	41.974	2905.45	403.50	0.104023	0.000126	0.000344	0.000048
5	5.0	50.28	0.81	484.971	109.538	4523.75	1021.75	0.107206	0.000155	0.000221	0.000050
6	5.1	50.34	0.72	581.410	138.608	5369.58	1280.10	0.108278	0.000143	0.000186	0.000044
7	5.8	50.51	0.69	900.018	321.151	8176.80	2917.71	0.110070	0.000112	0.000122	0.000044
8	6.5	50.37	0.68	939.693	344.376	8499.77	3114.97	0.110555	0.000127	0.000118	0.000043
9	6.4	50.34	0.68	1324.638	673.494	11852.74	6026.36	0.111758	0.000158	0.000084	0.000043
10	5.6	50.54	0.80	1146.767	602.533	10341.95	5433.85	0.110885	0.000112	0.000097	0.000051
11	7.2	50.72	0.74	1033.747	452.252	9383.88	4105.33	0.110162	0.000120	0.000107	0.000047
12	8.5	50.67	0.50	1152.455	364.034	10418.68	3291.02	0.110614	0.000116	0.000096	0.000030
13	6.1	50.53	0.67	1212.296	564.335	10914.46	5080.78	0.111072	0.000120	0.000092	0.000043
14	6.4	50.60	0.66	1326.227	662.755	11927.57	5960.57	0.111190	0.000117	0.000084	0.000042
15	7.7	50.06	0.57	1075.503	367.728	9626.19	3291.31	0.111727	0.000103	0.000104	0.000036
16	5.2	50.57	0.81	1449.698	974.806	13002.02	8742.81	0.111498	0.000167	0.000077	0.000052
17	3.7	50.59	1.72	1392.991	1951.003	12509.42	17520.52	0.111355	0.000165	0.000080	0.000112
18	4.0	50.42	1.06	1258.048	975.365	11289.84	8753.01	0.111432	0.000147	0.000089	0.000069
19	2.9	50.12	1.48	967.158	807.665	8696.83	7262.64	0.111208	0.000153	0.000115	0.000096
20	1.6	51.00	2.70	1629.921	4212.948	14703.50	38004.94	0.110853	0.000247	0.000068	0.000176

Blank intercepts:

exp.#	Step	36Ar (V)	$\pm\sigma_{36}$ (V)	37Ar (V)	$\pm\sigma_{37}$ (V)	38Ar (V)	$\pm\sigma_{38}$ (V)	39Ar (V)	$\pm\sigma_{39}$ (V)	40Ar (V)	$\pm\sigma_{40}$ (V)
5711	0.0%	-0.004548	0.000053	-0.002236	0.000053	-0.00245	0.000058	0.03070	0.000053	0.015429	0.000174

Blank corrected intensity intercepts:

Nr.	Step	36Ar (V)	$\pm\sigma_{36}$ (V)	37Ar (V)	$\pm\sigma_{37}$ (V)	38Ar (V)	$\pm\sigma_{38}$ (V)	39Ar (V)	$\pm\sigma_{39}$ (V)	40Ar (V)	$\pm\sigma_{40}$ (V)
1	3.0%	0.000932	0.000067	0.000000	0.000063	0.00030	0.000074	0.01160	0.000085	0.349656	0.000404
2	3.8%	0.001135	0.000073	0.000000	0.000075	0.00116	0.000079	0.08527	0.000106	1.050632	0.000771
3	4.2%	0.000639	0.000072	0.000000	0.000069	0.00161	0.000078	0.13641	0.000145	1.376224	0.001096
4	4.6%	0.000458	0.000064	0.000000	0.000067	0.00164	0.000077	0.14085	0.000131	1.363851	0.001020
5	5.1%	0.000308	0.000069	0.000000	0.000071	0.00171	0.000078	0.15183	0.000169	1.426544	0.001266
6	5.8%	0.000266	0.000063	0.000000	0.000068	0.00176	0.000074	0.15741	0.000162	1.464352	0.001165
7	6.6%	0.000195	0.000070	0.000000	0.000073	0.00193	0.000075	0.17873	0.000146	1.635615	0.000910
8	7.4%	0.000209	0.000077	0.000000	0.000074	0.00222	0.000080	0.20030	0.000185	1.824945	0.001166
9	8.2%	0.000145	0.000074	0.000030	0.000082	0.00212	0.000082	0.19503	0.000215	1.757866	0.001512
10	9.0%	0.000147	0.000077	0.000065	0.000084	0.00186	0.000076	0.17109	0.000129	1.554151	0.000968
11	9.8%	0.000209	0.000092	0.000021	0.000096	0.00242	0.000103	0.22021	0.000199	2.013507	0.001111
12	10.5%	0.000223	0.000070	0.000027	0.000073	0.00284	0.000081	0.26109	0.000189	2.377550	0.001704
13	11.0%	0.000153	0.000071	0.000040	0.000082	0.00205	0.000079	0.18810	0.000153	1.705846	0.001144
14	11.8%	0.000144	0.000072	0.000035	0.000072	0.00211	0.000072	0.19466	0.000139	1.763435	0.001305
15	12.8%	0.000214	0.000073	0.000039	0.000069	0.00258	0.000080	0.23452	0.000159	2.114330	0.001224
16	13.8%	0.000109	0.000073	0.000048	0.000084	0.00170	0.000086	0.16005	0.000181	1.445943	0.001377
17	14.8%	0.000080	0.000112	0.000087	0.000115	0.00125	0.000110	0.11334	0.000151	1.025221	0.000634
18	16.3%	0.000096	0.000074	0.000182	0.000086	0.00132	0.000080	0.12255	0.000134	1.107751	0.000772
19	18.3%	0.000092	0.000077	0.000191	0.000077	0.00096	0.000079	0.09021	0.000104	0.817079	0.000572
20	21.3%	0.000031	0.000078	0.000082	0.000073	0.00054	0.000082	0.05028	0.000103	0.456877	0.000375

Sample: MAL2_16
Project: Alaska
Owner: Falkowski_Enkelmann
Exp-Nr: 5843
Material: 2.74 mg Bt

Irradiation: FGA014P7H1 (End date: 2013-07-31 15:39:00.0)
Measurement Date: 2014-01-15 22:36:04.0
Device: CO2-Laser
Air: 298.6
J-Value: 0.0031998 f-value: 0.993789
J-Value Error: 0.0000100 f-value Error: 0.000169
Reference Standard(s): FCT01 - 28.305 +/- 0.036 Ma, FCT01 - 28.305 +/- 0.036 Ma,
Total gas age: 47.89 +/- 0.20 Ma

Interfering isotope production ratios:
ca3637 = 0.000205 +/- 0.000012
ca3937 = 0.000932 +/- 0.000035
k3839 = 0.01211 +/- 0.00061
k4039 = 0.00183 +/- 0.00009

Decay constants:
lambda40 = 5.5492e-010 +/- 9.3000e-013 1/a
lambda39 = 0.002577 +/- 0.000026 1/a
lambda37 = 7.2438 +/- 0.0214 1/a

ALF ARGONLAB FREIBERG

Fit model: linear **All errors are 1s!**

Nr.	Step	39Ar(K) (V)	39Ar(K) (%)	39Ar (10e-14 mol)	40Ar* (V)	36Ar_atm (V)	40Ar* (%)	40Ar/36Ar	37Ar/36Ar	37Ar/39Ar	K/Ca	K/Ca Error	40Ar*/39Ar(K)	40Ar*/39Ar(K) Error	Age (Ma)	Age Error(Ma)
1	3.0%	0.0080	0.35	0.271	0.059	0.00031	39.4	493.1	0.02	0.0007	27.543	374.139	7.38	1.83	42.08	10.31
2	4.0%	0.0375	1.61	1.264	0.302	0.00056	64.3	835.4	0.05	0.0008	22.939	49.228	8.05	0.42	45.84	2.39
3	4.9%	0.0470	2.02	1.583	0.380	0.00053	70.6	1014.8	0.00	0.0000	Inf	Inf	8.10	0.33	46.14	1.86
4	5.8%	0.0385	1.66	1.299	0.315	0.00037	74.1	1153.3	0.11	0.0010	18.150	32.640	8.17	0.41	46.50	2.30
5	9.3%	0.2489	10.72	8.394	2.108	0.00088	88.9	2705.9	0.04	0.0001	130.953	319.023	8.47	0.09	48.18	0.53
6	10.1%	0.2823	12.15	9.519	2.397	0.00077	91.3	3428.4	0.09	0.0003	72.655	89.268	8.49	0.09	48.30	0.53
7	10.6%	0.2259	9.73	7.619	1.904	0.00054	92.2	3816.7	0.10	0.0002	77.171	106.794	8.43	0.09	47.96	0.51
8	11.2%	0.1570	6.76	5.294	1.337	0.00030	93.7	4763.3	0.11	0.0002	90.669	209.565	8.51	0.12	48.43	0.69
9	12.0%	0.1734	7.47	5.848	1.467	0.00036	93.1	4356.5	0.11	0.0002	80.022	149.729	8.46	0.11	48.12	0.65
10	13.0%	0.1683	7.24	5.675	1.423	0.00042	91.9	3680.5	0.15	0.0004	48.575	53.512	8.45	0.13	48.10	0.76
11	14.5%	0.2194	9.45	7.399	1.843	0.00056	91.7	3608.4	0.25	0.0006	29.189	16.576	8.40	0.10	47.79	0.59
12	16.0%	0.2825	12.16	9.525	2.374	0.00065	92.4	3930.3	0.38	0.0009	20.756	6.143	8.41	0.07	47.83	0.41
13	17.0%	0.1733	7.46	5.842	1.464	0.00032	93.8	4832.5	0.37	0.0007	26.447	17.016	8.45	0.12	48.08	0.69
14	18.5%	0.1390	5.98	4.688	1.165	0.00022	94.6	5509.5	1.15	0.0019	9.957	3.006	8.38	0.15	47.70	0.86
15	20.5%	0.0554	2.38	1.867	0.459	0.00012	92.8	4126.1	0.92	0.0020	9.263	7.775	8.29	0.40	47.18	2.24

J - value = 0.0031998
J-error [%] = 0.31

Plateau Data				Isochron Data				Inverse Isochron Data			
Nr.	39Ar%	Age (Ma)	Age_err (Ma)	39/36	err	40/36	err	39/40	err	36/40	err
								0.000000	0.000010	0.003384	0.000010
1	0.3	42.08	10.31	26.340	4.257	493.08	79.57	0.053420	0.000489	0.002028	0.000327
2	1.6	45.84	2.39	66.686	6.308	835.55	79.02	0.079811	0.000240	0.001197	0.000113
3	2.0	46.14	1.86	88.348	8.599	1014.59	98.73	0.087078	0.000198	0.000986	0.000096
4	1.7	46.50	2.30	104.680	14.968	1153.78	164.96	0.090728	0.000269	0.000867	0.000124
5	10.7	48.18	0.53	284.263	23.496	2706.01	223.67	0.105049	0.000232	0.000370	0.000031
6	12.2	48.30	0.53	368.804	39.537	3429.61	367.67	0.107535	0.000261	0.000292	0.000031
7	9.7	47.96	0.51	417.568	49.315	3818.18	450.93	0.109363	0.000160	0.000262	0.000031
8	6.8	48.43	0.69	524.708	107.835	4765.29	979.34	0.110110	0.000222	0.000210	0.000043
9	7.5	48.12	0.65	480.013	85.261	4358.36	774.14	0.110136	0.000179	0.000229	0.000041
10	7.2	48.10	0.76	400.311	69.575	3682.96	640.10	0.108693	0.000247	0.000272	0.000047
11	9.4	47.79	0.59	394.619	51.621	3612.92	472.61	0.109224	0.000160	0.000277	0.000036
12	12.2	47.83	0.41	432.980	39.314	3938.22	357.56	0.109943	0.000304	0.000254	0.000023
13	7.5	48.08	0.69	537.647	111.370	4842.03	1003.00	0.111037	0.000372	0.000207	0.000043
14	6.0	47.70	0.86	625.934	193.680	5545.31	1715.87	0.112876	0.000379	0.000180	0.000056
15	2.4	47.18	2.24	464.226	286.477	4147.29	2559.31	0.111935	0.000249	0.000241	0.000149

Blank intercepts:

exp.#	Step	36Ar (V)	$\pm\sigma_{36}$ (V)	37Ar (V)	$\pm\sigma_{37}$ (V)	38Ar (V)	$\pm\sigma_{38}$ (V)	39Ar (V)	$\pm\sigma_{39}$ (V)	40Ar (V)	$\pm\sigma_{40}$ (V)
5842	0.0%	-0.004572	0.000037	-0.002292	0.000046	-0.00251	0.000044	0.03073	0.000042	0.005973	0.000093

Blank corrected intensity intercepts:

Nr.	Step	36Ar (V)	$\pm\sigma_{36}$ (V)	37Ar (V)	$\pm\sigma_{37}$ (V)	38Ar (V)	$\pm\sigma_{38}$ (V)	39Ar (V)	$\pm\sigma_{39}$ (V)	40Ar (V)	$\pm\sigma_{40}$ (V)
1	3.0%	0.000298	0.000048	0.000005	0.000072	0.00022	0.000064	0.00798	0.000071	0.150557	0.000325
2	4.0%	0.000549	0.000052	0.000030	0.000063	0.00074	0.000055	0.03721	0.000095	0.469787	0.000740
3	4.9%	0.000518	0.000050	0.000000	0.000059	0.00083	0.000060	0.04660	0.000098	0.539266	0.000460
4	5.8%	0.000359	0.000051	0.000038	0.000069	0.00072	0.000061	0.03823	0.000097	0.424559	0.000636
5	9.3%	0.000855	0.000071	0.000034	0.000084	0.00410	0.000080	0.24710	0.000393	2.370195	0.003619
6	10.1%	0.000747	0.000080	0.000070	0.000086	0.00460	0.000075	0.28023	0.000468	2.625848	0.004593
7	10.6%	0.000528	0.000062	0.000053	0.000073	0.00369	0.000069	0.22428	0.000235	2.066424	0.002089
8	11.2%	0.000292	0.000060	0.000031	0.000072	0.00253	0.000064	0.15585	0.000210	1.426239	0.002121
9	12.0%	0.000353	0.000063	0.000039	0.000073	0.00284	0.000074	0.17215	0.000207	1.575042	0.001689
10	13.0%	0.000411	0.000071	0.000063	0.000069	0.00279	0.000066	0.16706	0.000288	1.548692	0.002291
11	14.5%	0.000543	0.000071	0.000136	0.000077	0.00352	0.000075	0.21782	0.000225	2.009495	0.002056
12	16.0%	0.000638	0.000058	0.000246	0.000073	0.00459	0.000072	0.28039	0.000593	2.569807	0.004575
13	17.0%	0.000315	0.000065	0.000119	0.000076	0.00284	0.000068	0.17198	0.000396	1.560650	0.003786
14	18.5%	0.000218	0.000067	0.000253	0.000076	0.00227	0.000072	0.13802	0.000323	1.232017	0.002953
15	20.5%	0.000117	0.000072	0.000108	0.000091	0.00091	0.000083	0.05495	0.000105	0.494653	0.000554

Nr.	Step	39Ar(K) (V)	39Ar(K) (%)	39Ar (10e-14 mol)	40Ar* (V)	36Ar_atm (V)	40Ar* (%)	40Ar/36Ar	37Ar/36Ar	37Ar/39Ar	K/Ca	K/Ca Error	40Ar*/39Ar(K)	40Ar*/39Ar(K) Error	Age (Ma)	Age Error(Ma)
16	24.0%	0.0667	2.87	2.248	0.554	0.00013	93.5	4572.0	1.11	0.0022	8.577	4.968	8.31	0.30	47.31	1.69

Nr.	39Ar%	Age (Ma)	Age_err (Ma)	39/36	err	40/36	err	39/40	err	36/40	err
16	2.9	47.31	1.69	517.488	266.912	4600.49	2372.86	0.112485	0.000439	0.000217	0.000112

Nr.	Step	36Ar (V)	$\pm\sigma_{36}$ (V)	37Ar (V)	$\pm\sigma_{37}$ (V)	38Ar (V)	$\pm\sigma_{38}$ (V)	39Ar (V)	$\pm\sigma_{39}$ (V)	40Ar (V)	$\pm\sigma_{40}$ (V)
16	24.0%	0.000127	0.000065	0.000141	0.000081	0.00113	0.000081	0.06619	0.000184	0.592914	0.001619

Sample: MAL_3_8
Project: Alaska
Owner: Falkowski_Enkelmann

Exp-Nr: 5846
Material: 2.72 mg Bt

Irradiation: FGA014P7H2 (End date: 2013-07-31 15:39:00.0)
Measurement Date: 2014-01-17 02:38:29.0
Device: CO2-Laser
Air: 298.6
J-Value: **0.0031998** f-value: 0.993892
J-Value Error: **0.0000100** f-value Error: 0.000180
Reference Standard(s): FCT01 - 28.305 +/- 0.036 Ma, FCT01 - 28.305 +/- 0.036 Ma,
Total gas age: 41.38 +/- 0.21 Ma

Interfering isotope production ratios:
ca3637 = 0.000205 +/- 0.000012
ca3937 = 0.000932 +/- 0.000035
k3839 = 0.01211 +/- 0.00061
k4039 = 0.00183 +/- 0.00009

Decay constants:
lambda40 = 5.5492e-010 +/- 9.3000e-013 1/a
lambda39 = 0.002577 +/- 0.000026 1/a
lambda37 = 7.2438 +/- 0.0214 1/a

ALF ARGONLAB FREIBERG

Fit model: linear **All errors are 1s!**

Nr.	Step	39Ar(K) (V)	39Ar(K) (%)	39Ar (10e-14 mol)	40Ar* (V)	36Ar_atm (V)	40Ar* (%)	40Ar/36Ar	37Ar/36Ar	37Ar/39Ar	K/Ca	K/Ca Error	40Ar*/39Ar(K)	40Ar*/39Ar(K) Error	Age (Ma)	Age Error(Ma)
1	3.0%	0.0189	0.61	0.639	0.105	0.00054	39.4	492.5	0.07	0.0020	8.852	18.216	5.52	1.40	31.56	7.92
2	4.0%	0.1045	3.36	3.523	0.692	0.00106	68.5	948.9	0.03	0.0003	53.826	121.090	6.62	0.23	37.79	1.33
3	4.5%	0.1062	3.41	3.580	0.740	0.00052	82.5	1709.2	0.06	0.0003	65.110	172.655	6.97	0.24	39.73	1.35
4	5.2%	0.1671	5.37	5.635	1.188	0.00050	88.7	2656.9	0.05	0.0002	108.657	300.179	7.11	0.14	40.54	0.82
5	6.0%	0.1785	5.73	6.018	1.274	0.00035	92.3	3903.1	0.07	0.0001	130.667	445.972	7.14	0.13	40.72	0.76
6	6.8%	0.2060	6.62	6.945	1.479	0.00030	94.2	5188.3	0.11	0.0002	115.483	283.377	7.18	0.12	40.95	0.67
7	7.6%	0.1997	6.42	6.733	1.473	0.00016	96.8	9404.3	0.10	0.0001	212.357	1050.152	7.38	0.13	42.04	0.75
8	8.5%	0.2294	7.37	7.734	1.669	0.00019	96.6	8835.1	0.46	0.0004	45.683	37.683	7.28	0.11	41.47	0.65
9	9.4%	0.2023	6.50	6.821	1.493	0.00016	97.0	9843.7	0.58	0.0004	40.225	36.697	7.38	0.13	42.06	0.73
10	10.3%	0.1939	6.23	6.538	1.422	0.00018	96.4	8367.7	0.87	0.0008	22.769	12.877	7.33	0.14	41.79	0.78
11	11.2%	0.1905	6.12	6.423	1.397	0.00017	96.5	8516.2	1.47	0.0013	13.710	4.328	7.33	0.14	41.79	0.81
12	12.1%	0.2425	7.79	8.176	1.785	0.00017	97.2	10552.2	1.99	0.0014	12.594	2.724	7.36	0.11	41.96	0.66
13	12.8%	0.2191	7.04	7.388	1.594	0.00020	96.4	8374.7	0.93	0.0008	21.545	9.508	7.27	0.12	41.46	0.70
14	13.6%	0.1879	6.03	6.334	1.376	0.00014	97.0	9917.2	1.13	0.0009	20.904	10.202	7.32	0.16	41.75	0.89
15	14.6%	0.2047	6.57	6.901	1.497	0.00031	94.1	5090.7	0.70	0.0011	16.791	7.527	7.32	0.14	41.70	0.80
16	16.0%	0.2197	7.06	7.407	1.624	0.00014	97.5	11956.8	1.29	0.0008	22.099	10.168	7.39	0.12	42.12	0.71
17	17.5%	0.1079	3.47	3.638	0.801	0.00009	96.8	9310.9	1.98	0.0016	11.019	4.939	7.43	0.23	42.34	1.28
18	20.0%	0.0761	2.44	2.565	0.564	0.00006	96.7	8907.8	1.63	0.0014	12.879	10.709	7.41	0.35	42.21	1.96
19	23.0%	0.0582	1.87	1.962	0.422	0.00007	95.1	6132.1	0.83	0.0010	17.462	22.929	7.26	0.43	41.39	2.40

J - value = 0.0031998
J-error [%] = 0.31

Plateau Data				Isochron Data				Inverse Isochron Data			
Nr.	39Ar%	Age (Ma)	Age_err (Ma)	39/36	err	40/36	err	39/40 (0.000000)	err (0.000010)	36/40 (0.003384)	err (0.000010)
1	0.6	31.56	7.92	35.142	5.780	492.61	80.99	0.071339	0.000374	0.002030	0.000334
2	3.4	37.79	1.33	98.194	7.551	948.93	72.97	0.103479	0.000276	0.001054	0.000081
3	3.4	39.73	1.35	202.483	32.525	1709.37	274.58	0.118455	0.000321	0.000585	0.000094
4	5.4	40.54	0.82	331.733	52.203	2657.17	418.14	0.124844	0.000347	0.000376	0.000059
5	5.7	40.72	0.76	504.832	111.485	3903.78	862.10	0.129319	0.000397	0.000256	0.000057
6	6.6	40.95	0.67	681.057	171.992	5190.36	1310.73	0.131216	0.000567	0.000193	0.000049
7	6.4	42.04	0.75	1234.872	648.699	9407.89	4942.11	0.131259	0.000556	0.000106	0.000056
8	7.4	41.47	0.65	1176.285	506.053	8857.16	3810.45	0.132806	0.000413	0.000113	0.000049
9	6.5	42.06	0.73	1297.570	699.032	9875.13	5319.96	0.131398	0.000446	0.000101	0.000055
10	6.2	41.79	0.78	1106.157	553.707	8409.02	4209.29	0.131544	0.000351	0.000119	0.000060
11	6.1	41.79	0.81	1130.757	592.614	8589.03	4501.37	0.131651	0.000489	0.000116	0.000061
12	7.8	41.96	0.66	1409.340	712.727	10675.51	5398.77	0.132016	0.000657	0.000094	0.000047
13	7.0	41.46	0.70	1116.531	484.019	8418.92	3649.66	0.132622	0.000646	0.000119	0.000051
14	6.0	41.75	0.89	1321.931	904.889	9981.62	6832.63	0.132437	0.000447	0.000100	0.000069
15	6.6	41.70	0.80	657.687	197.138	5110.77	1531.92	0.128687	0.000571	0.000196	0.000059
16	7.1	42.12	0.71	1589.259	965.008	12045.52	7314.13	0.131938	0.000810	0.000083	0.000050
17	3.5	42.34	1.28	1227.729	1135.956	9419.24	8715.15	0.130343	0.000455	0.000106	0.000098
18	2.4	42.21	1.96	1173.756	1590.541	8992.17	12185.18	0.130531	0.000761	0.000111	0.000151
19	1.9	41.39	2.40	807.433	927.758	6160.86	7078.96	0.131059	0.000398	0.000162	0.000187

Blank intercepts:

exp.#	Step	36Ar (V)	$\pm\sigma_{36}$ (V)	37Ar (V)	$\pm\sigma_{37}$ (V)	38Ar (V)	$\pm\sigma_{38}$ (V)	39Ar (V)	$\pm\sigma_{39}$ (V)	40Ar (V)	$\pm\sigma_{40}$ (V)
5845	0.0%	-0.004564	0.000063	-0.002292	0.000055	-0.00246	0.000064	0.03068	0.000063	0.006618	0.000119

Blank corrected intensity intercepts:

Nr.	Step	36Ar (V)	$\pm\sigma_{36}$ (V)	37Ar (V)	$\pm\sigma_{37}$ (V)	38Ar (V)	$\pm\sigma_{38}$ (V)	39Ar (V)	$\pm\sigma_{39}$ (V)	40Ar (V)	$\pm\sigma_{40}$ (V)
1	3.0%	0.000526	0.000086	0.000038	0.000078	0.00034	0.000089	0.01880	0.000094	0.265481	0.000438
2	4.0%	0.001039	0.000080	0.000034	0.000077	0.00139	0.000078	0.10373	0.000198	1.009958	0.001869
3	4.5%	0.000512	0.000082	0.000029	0.000077	0.00133	0.000081	0.10541	0.000196	0.896563	0.001752
4	5.2%	0.000492	0.000077	0.000027	0.000075	0.00200	0.000082	0.16590	0.000334	1.338932	0.002544
5	6.0%	0.000345	0.000076	0.000024	0.000082	0.00213	0.000082	0.17716	0.000381	1.380356	0.003011
6	6.8%	0.000295	0.000075	0.000032	0.000077	0.00238	0.000078	0.20446	0.000667	1.570041	0.004436
7	7.6%	0.000158	0.000083	0.000017	0.000082	0.00230	0.000079	0.19824	0.000622	1.521725	0.004321
8	8.5%	0.000191	0.000082	0.000089	0.000073	0.00265	0.000082	0.22768	0.000536	1.727409	0.003496
9	9.4%	0.000153	0.000082	0.000089	0.000081	0.00238	0.000082	0.20082	0.000511	1.539905	0.003450
10	10.3%	0.000172	0.000086	0.000151	0.000085	0.00228	0.000089	0.19250	0.000332	1.474451	0.002992
11	11.2%	0.000166	0.000086	0.000246	0.000078	0.00227	0.000083	0.18910	0.000525	1.447255	0.003562
12	12.1%	0.000170	0.000085	0.000341	0.000074	0.00280	0.000085	0.24072	0.000868	1.837173	0.006287
13	12.8%	0.000193	0.000083	0.000180	0.000079	0.00255	0.000086	0.21752	0.000682	1.652559	0.006152
14	13.6%	0.000140	0.000095	0.000159	0.000078	0.00215	0.000075	0.18649	0.000425	1.418804	0.003518
15	14.6%	0.000305	0.000091	0.000216	0.000097	0.00240	0.000087	0.20318	0.000631	1.590780	0.005043
16	16.0%	0.000136	0.000082	0.000176	0.000081	0.00255	0.000082	0.21807	0.000915	1.665345	0.007449
17	17.5%	0.000087	0.000079	0.000173	0.000078	0.00123	0.000076	0.10710	0.000263	0.827866	0.002042
18	20.0%	0.000064	0.000086	0.000105	0.000087	0.00087	0.000090	0.07553	0.000279	0.583024	0.002629
19	23.0%	0.000071	0.000081	0.000059	0.000077	0.00070	0.000080	0.05776	0.000139	0.444078	0.000822

Sample: MAL_6_23
Project: Alaska
Owner: Falkowski_Enkelmann

Exp-Nr: 5709
Material: 2.87 mg Bt

Irradiation: FGA014P5H10 (End date: 2013-07-31 15:39:00.0)
Measurement Date: 2013-12-03 08:50:10.0
Device: CO2-Laser
Air: 298.6
J-Value: **0.0032573** f-value: 0.993558
J-Value Error: **0.0000104** f-value Error: 0.000221
Reference Standard(s): FCT01 - 28.305 +/- 0.036 Ma,
Total gas age: 48.44 +/- 0.14 Ma

Interfering isotope production ratios:
ca3637 = 0.000205 +/- 0.000012
ca3937 = 0.000932 +/- 0.000035
k3839 = 0.01211 +/- 0.00061
k4039 = 0.00183 +/- 0.00009

Decay constants:
lambda40 = 5.5492e-010 +/- 9.3000e-013 1/a
lambda39 = 0.002577 +/- 0.000026 1/a
lambda37 = 7.2438 +/- 0.0214 1/a

ALF ARGONLAB FREIBERG

Fit model: linear **All errors are 1s!**

Nr.	Step	39Ar(K) (V)	39Ar(K) (%)	39Ar (10e-14 mol)	40Ar* (V)	36Ar_atm (V)	40Ar* (%)	40Ar/36Ar	37Ar/36Ar	37Ar/39Ar	K/Ca	K/Ca Error	40Ar*/39Ar(K)	40Ar*/39Ar(K) Error	Age (Ma)	Age Error(Ma)
1	3.0%	0.0148	0.45	0.500	0.086	0.00101	22.1	383.4	0.08	0.0057	7.725	5.216	5.79	1.14	33.65	6.59
2	3.8%	0.0885	2.70	2.984	0.662	0.00200	52.5	629.0	0.05	0.0012	36.267	22.038	7.48	0.19	43.40	1.08
3	4.2%	0.1144	3.49	3.857	0.924	0.00137	69.3	973.0	0.03	0.0004	106.908	153.213	8.08	0.16	46.81	0.91
4	4.6%	0.1353	4.13	4.563	1.121	0.00113	76.9	1292.1	0.05	0.0004	109.985	147.242	8.28	0.12	47.98	0.73
5	5.1%	0.1673	5.10	5.643	1.396	0.00092	83.6	1816.9	0.07	0.0004	119.260	110.204	8.35	0.10	48.33	0.61
6	5.8%	0.1850	5.64	6.239	1.552	0.00065	88.9	2697.8	0.09	0.0003	132.060	139.836	8.39	0.09	48.58	0.56
7	6.5%	0.1880	5.73	6.339	1.584	0.00045	92.1	3790.0	0.20	0.0005	90.609	64.026	8.43	0.10	48.80	0.59
8	7.3%	0.1894	5.77	6.387	1.592	0.00041	92.8	4165.4	0.17	0.0004	118.383	101.763	8.40	0.09	48.67	0.52
9	8.2%	0.1934	5.90	6.523	1.618	0.00049	91.6	3582.5	0.19	0.0005	88.767	61.038	8.37	0.08	48.45	0.50
10	9.1%	0.1670	5.09	5.631	1.404	0.00055	89.5	2845.0	0.13	0.0004	100.305	80.875	8.41	0.09	48.69	0.54
11	10.1%	0.2021	6.16	6.813	1.695	0.00090	86.3	2179.7	0.14	0.0006	69.971	35.065	8.39	0.08	48.59	0.51
12	10.8%	0.2002	6.10	6.749	1.690	0.00070	89.0	2726.3	0.19	0.0007	66.608	29.213	8.45	0.08	48.90	0.47
13	11.6%	0.1870	5.70	6.304	1.572	0.00052	91.0	3323.8	0.46	0.0013	34.333	10.004	8.41	0.09	48.69	0.57
14	12.5%	0.1795	5.47	6.054	1.509	0.00041	92.5	3974.0	1.01	0.0023	18.890	2.771	8.41	0.10	48.68	0.58
15	13.5%	0.1742	5.31	5.874	1.472	0.00029	94.5	5391.6	2.02	0.0033	13.083	1.218	8.45	0.09	48.93	0.55
16	14.7%	0.1802	5.49	6.077	1.529	0.00025	95.4	6447.8	1.32	0.0018	23.983	4.468	8.48	0.09	49.13	0.54
17	16.2%	0.1913	5.83	6.451	1.619	0.00026	95.5	6616.5	0.67	0.0009	48.489	16.268	8.46	0.09	49.01	0.52
18	18.0%	0.1672	5.10	5.638	1.411	0.00023	95.2	6292.9	0.71	0.0010	43.669	15.767	8.44	0.12	48.85	0.69
19	20.0%	0.1505	4.59	5.076	1.271	0.00020	95.4	6525.1	1.73	0.0023	18.641	3.735	8.44	0.12	48.89	0.72
20	22.5%	0.1947	5.94	6.565	1.647	0.00023	96.0	7420.1	1.79	0.0021	20.546	3.227	8.46	0.08	48.99	0.49
21	28.5%	0.0098	0.30	0.331	0.078	0.00005	84.8	1965.4	1.39	0.0067	6.560	8.020	7.98	2.07	46.23	11.83

J - value = 0.0032573
J-error [%] = 0.32

Plateau Data				Isochron Data				Inverse Isochron Data			
Nr.	39Ar%	Age (Ma)	Age_err (Ma)	39/36	err	40/36	err	39/40 (0.000000)	err (0.000010)	36/40 (0.003384)	err (0.000010)
1	0.5	33.65	6.59	14.662	0.825	383.43	21.51	0.038238	0.000167	0.002608	0.000146
2	2.7	43.40	1.08	44.140	1.218	628.95	17.35	0.070180	0.000095	0.001590	0.000044
3	3.5	46.81	0.91	83.471	3.638	972.96	42.40	0.085791	0.000134	0.001028	0.000045
4	4.1	47.98	0.73	119.916	5.972	1291.98	64.35	0.092816	0.000117	0.000774	0.000039
5	5.1	48.33	0.61	181.936	11.182	1816.90	111.67	0.100136	0.000173	0.000550	0.000034
6	5.6	48.58	0.56	286.023	25.434	2697.88	239.90	0.106018	0.000170	0.000371	0.000033
7	5.7	48.80	0.59	414.432	56.152	3791.06	513.65	0.109319	0.000122	0.000264	0.000036
8	5.8	48.67	0.52	460.165	61.061	4166.25	552.83	0.110451	0.000107	0.000240	0.000032
9	5.9	48.45	0.50	392.613	41.966	3583.50	383.03	0.109562	0.000158	0.000279	0.000030
10	5.1	48.69	0.54	302.927	27.566	2845.37	258.92	0.106463	0.000101	0.000351	0.000032
11	6.2	48.59	0.51	224.257	13.995	2180.05	136.05	0.102868	0.000115	0.000459	0.000029
12	6.1	48.90	0.47	287.535	21.083	2726.98	199.95	0.105441	0.000160	0.000367	0.000027
13	5.7	48.69	0.57	360.156	40.769	3326.89	376.60	0.108256	0.000130	0.000301	0.000034
14	5.5	48.68	0.58	438.305	61.614	3982.98	559.90	0.110045	0.000169	0.000251	0.000035
15	5.3	48.93	0.55	605.711	110.534	5417.06	988.54	0.111816	0.000118	0.000185	0.000034
16	5.5	49.13	0.54	727.016	158.954	6467.29	1413.99	0.112414	0.000111	0.000155	0.000034
17	5.8	49.01	0.52	747.617	158.299	6625.98	1402.97	0.112831	0.000128	0.000151	0.000032
18	5.1	48.85	0.69	711.681	195.719	6302.56	1733.26	0.112919	0.000182	0.000159	0.000044
19	4.6	48.89	0.72	740.547	222.875	6551.37	1971.69	0.113037	0.000167	0.000153	0.000046
20	5.9	48.99	0.49	845.349	190.002	7451.08	1674.71	0.113453	0.000133	0.000134	0.000030
21	0.3	46.23	11.83	209.738	304.601	1971.73	2863.50	0.106373	0.000761	0.000507	0.000737

Blank intercepts:

exp.#	Step	36Ar (V)	$\pm\sigma_{36}$ (V)	37Ar (V)	$\pm\sigma_{37}$ (V)	38Ar (V)	$\pm\sigma_{38}$ (V)	39Ar (V)	$\pm\sigma_{39}$ (V)	40Ar (V)	$\pm\sigma_{40}$ (V)
5708	0.0%	-0.004528	0.000037	-0.002297	0.000040	-0.00249	0.000047	0.03064	0.000037	0.019952	0.000143

Blank corrected intensity intercepts:

Nr.	Step	36Ar (V)	$\pm\sigma_{36}$ (V)	37Ar (V)	$\pm\sigma_{37}$ (V)	38Ar (V)	$\pm\sigma_{38}$ (V)	39Ar (V)	$\pm\sigma_{39}$ (V)	40Ar (V)	$\pm\sigma_{40}$ (V)
1	3.0%	0.000986	0.000055	0.000082	0.000056	0.00036	0.000061	0.01471	0.000063	0.387629	0.000331
2	3.8%	0.001954	0.000054	0.000105	0.000064	0.00138	0.000065	0.08784	0.000091	1.260995	0.001061
3	4.2%	0.001336	0.000058	0.000046	0.000066	0.00153	0.000070	0.11356	0.000139	1.333595	0.001260
4	4.6%	0.001100	0.000055	0.000053	0.000071	0.00173	0.000065	0.13432	0.000115	1.458093	0.001302
5	5.1%	0.000897	0.000055	0.000060	0.000056	0.00209	0.000060	0.16612	0.000199	1.671451	0.002045
6	5.8%	0.000631	0.000056	0.000060	0.000064	0.00225	0.000068	0.18369	0.000214	1.745723	0.001870
7	6.5%	0.000442	0.000060	0.000089	0.000063	0.00221	0.000065	0.18663	0.000150	1.720149	0.001271
8	7.3%	0.000401	0.000053	0.000069	0.000059	0.00224	0.000058	0.18803	0.000126	1.715288	0.001129
9	8.2%	0.000480	0.000051	0.000094	0.000064	0.00227	0.000064	0.19203	0.000209	1.765954	0.001626
10	9.1%	0.000538	0.000049	0.000071	0.000058	0.00203	0.000064	0.16577	0.000113	1.568860	0.000967
11	10.1%	0.000879	0.000055	0.000124	0.000062	0.00247	0.000064	0.20059	0.000143	1.964699	0.001648
12	10.8%	0.000679	0.000050	0.000129	0.000057	0.00240	0.000065	0.19869	0.000212	1.898641	0.002007
13	11.6%	0.000507	0.000057	0.000234	0.000068	0.00220	0.000066	0.18559	0.000162	1.727303	0.001358
14	12.5%	0.000400	0.000056	0.000408	0.000060	0.00209	0.000062	0.17824	0.000176	1.631909	0.001874
15	13.5%	0.000282	0.000051	0.000572	0.000053	0.00202	0.000061	0.17293	0.000130	1.558198	0.001104
16	14.7%	0.000242	0.000053	0.000323	0.000060	0.00210	0.000065	0.17892	0.000138	1.603627	0.000919
17	16.2%	0.000250	0.000053	0.000169	0.000057	0.00221	0.000064	0.18991	0.000158	1.695834	0.001249
18	18.0%	0.000229	0.000063	0.000164	0.000059	0.00197	0.000062	0.16599	0.000200	1.481079	0.001546
19	20.0%	0.000199	0.000060	0.000347	0.000069	0.00177	0.000062	0.14944	0.000167	1.332013	0.001260
20	22.5%	0.000225	0.000050	0.000407	0.000064	0.00232	0.000069	0.19328	0.000167	1.716519	0.001304
21	28.5%	0.000046	0.000066	0.000064	0.000078	0.00013	0.000079	0.00974	0.000067	0.092207	0.000182

Sample: MAL_6_24
Project: Alaska
Owner: Falkowski_Enkelmann

Exp-Nr: 5855
Material: 2.47 mg Bt

Irradiation: FGA014P7H3 (End date: 2013-07-31 15:39:00.0)
Measurement Date: 2014-01-18 17:46:46.0
Device: CO2-Laser
Air: 298.6
J-Value: **0.0031998** f-value: 0.994011
J-Value Error: **0.0000100** f-value Error: 0.000211
Reference Standard(s): FCT01 - 28.305 +/- 0.036 Ma, FCT01 - 28.305 +/- 0.036 Ma,
Total gas age: 48.51 +/- 0.18 Ma

Interfering isotope production ratios:
ca3637 = 0.000205 +/- 0.000012
ca3937 = 0.000932 +/- 0.000035
k3839 = 0.01211 +/- 0.00061
k4039 = 0.00183 +/- 0.00009

Decay constants:
lambda40 = 5.5492e-010 +/- 9.3000e-013 1/a
lambda39 = 0.002577 +/- 0.000026 1/a
lambda37 = 7.2438 +/- 0.0214 1/a

ALF ARGONLAB FREIBERG

Fit model: linear **All errors are 1s!**

Nr.	Step	39Ar(K) (V)	39Ar(K) (%)	39Ar (10e-14 mol)	40Ar* (V)	36Ar_atm (V)	40Ar* (%)	40Ar/36Ar	37Ar/36Ar	37Ar/39Ar	K/Ca	K/Ca Error	40Ar*/39Ar(K)	40Ar*/39Ar(K) Error	Age (Ma)	Age Error(Ma)
1	3.0%	0.0131	0.42	0.443	0.096	0.00140	18.6	366.9	0.02	0.0026	6.754	17.051	7.30	1.54	41.59	8.69
2	3.8%	0.0686	2.20	2.313	0.525	0.00231	43.2	525.6	0.01	0.0004	42.101	128.639	7.66	0.32	43.62	1.80
3	4.3%	0.0714	2.29	2.407	0.590	0.00142	58.2	713.8	0.00	0.0000	Inf	Inf	8.27	0.32	47.09	1.82
4	5.0%	0.1404	4.51	4.734	1.164	0.00176	68.8	958.6	0.01	0.0001	240.494	2165.677	8.29	0.15	47.18	0.86
5	5.7%	0.1674	5.38	5.644	1.398	0.00150	75.7	1228.5	0.09	0.0008	20.988	12.458	8.35	0.13	47.52	0.73
6	6.4%	0.2153	6.92	7.259	1.827	0.00148	80.5	1534.9	0.03	0.0002	74.816	120.804	8.49	0.09	48.28	0.56
7	7.0%	0.2365	7.60	7.976	2.025	0.00093	87.9	2472.4	0.05	0.0002	87.563	153.851	8.56	0.08	48.71	0.50
8	7.6%	0.2548	8.19	8.591	2.190	0.00058	92.6	4061.9	0.02	0.0000	360.576	2443.964	8.60	0.07	48.89	0.42
9	8.2%	0.2013	6.47	6.788	1.733	0.00034	94.4	5360.4	0.27	0.0005	38.622	40.990	8.61	0.11	48.97	0.64
10	9.0%	0.1661	5.34	5.601	1.429	0.00029	94.2	5162.3	0.02	0.0000	449.696	6398.940	8.61	0.12	48.95	0.69
11	10.0%	0.1405	4.52	4.737	1.209	0.00037	91.7	3589.4	0.01	0.0000	1289.676	59314.990	8.61	0.15	48.97	0.85
12	11.0%	0.1658	5.33	5.591	1.407	0.00053	89.9	2960.6	0.04	0.0001	148.858	635.293	8.49	0.12	48.29	0.69
13	12.0%	0.1867	6.00	6.296	1.608	0.00054	90.9	3282.7	0.03	0.0001	184.492	959.714	8.61	0.11	48.98	0.64
14	13.2%	0.2462	7.91	8.301	2.110	0.00070	91.0	3315.8	0.06	0.0002	98.377	207.808	8.57	0.10	48.75	0.59
15	14.4%	0.2210	7.10	7.450	1.906	0.00052	92.5	3988.8	0.00	0.0000	Inf	Inf	8.63	0.11	49.07	0.65
16	15.6%	0.1757	5.65	5.926	1.514	0.00041	92.5	3993.3	0.04	0.0001	177.656	871.784	8.61	0.13	48.99	0.74
17	17.1%	0.1791	5.76	6.037	1.525	0.00044	92.0	3762.9	0.00	0.0000	Inf	Inf	8.52	0.13	48.46	0.75
18	18.6%	0.1043	3.35	3.517	0.900	0.00024	92.5	4003.1	0.00	0.0000	Inf	Inf	8.63	0.21	49.08	1.18
19	20.6%	0.1341	4.31	4.521	1.165	0.00027	93.5	4619.9	0.00	0.0000	3035.127	322940.100	8.69	0.14	49.41	0.81
20	23.0%	0.0229	0.73	0.771	0.207	0.00003	95.5	6687.9	0.54	0.0008	22.922	117.444	9.06	0.87	51.50	4.90

J - value = 0.0031998
J-error [%] = 0.31

Plateau Data				Isochron Data				Inverse Isochron Data			
Nr.	39Ar%	Age (Ma)	Age_err (Ma)	39/36	err	40/36	err	39/40 (0.000000)	err (0.000010)	36/40 (0.003384)	err (0.000010)
1	0.4	41.59	8.69	9.370	0.458	366.96	17.75	0.025533	0.000184	0.002725	0.000132
2	2.2	43.62	1.80	29.643	0.936	525.57	16.57	0.056402	0.000092	0.001903	0.000060
3	2.3	47.09	1.82	50.179	2.723	713.74	38.72	0.070304	0.000111	0.001401	0.000076
4	4.5	47.18	0.86	79.590	3.190	958.48	38.41	0.083037	0.000084	0.001043	0.000042
5	5.4	47.52	0.73	111.411	5.282	1229.00	58.26	0.090652	0.000101	0.000814	0.000039
6	6.9	48.28	0.56	145.698	6.673	1534.97	70.30	0.094919	0.000109	0.000651	0.000030
7	7.6	48.71	0.50	253.908	17.895	2472.74	174.27	0.102683	0.000142	0.000404	0.000029
8	8.2	48.89	0.42	437.793	44.096	4061.67	409.10	0.107787	0.000108	0.000246	0.000025
9	6.5	48.97	0.64	588.817	127.423	5368.08	1161.67	0.109689	0.000180	0.000186	0.000040
10	5.3	48.95	0.69	565.111	122.779	5161.97	1121.49	0.109476	0.000354	0.000194	0.000042
11	4.5	48.97	0.85	382.171	71.609	3588.78	672.43	0.106491	0.000273	0.000279	0.000052
12	5.3	48.29	0.69	313.623	35.999	2960.67	339.83	0.105930	0.000561	0.000338	0.000039
13	6.0	48.98	0.64	346.526	41.160	3282.74	389.97	0.105560	0.000488	0.000305	0.000036
14	7.9	48.75	0.59	352.161	37.988	3316.40	357.73	0.106188	0.000488	0.000302	0.000033
15	7.1	49.07	0.65	427.666	59.953	3988.03	559.10	0.107238	0.000655	0.000251	0.000035
16	5.6	48.99	0.74	429.003	66.257	3993.51	616.83	0.107425	0.000826	0.000250	0.000039
17	5.8	48.46	0.75	406.586	63.608	3762.16	588.59	0.108072	0.000721	0.000266	0.000042
18	3.4	49.08	1.18	429.228	122.248	4002.31	1139.87	0.107245	0.000735	0.000250	0.000071
19	4.3	49.41	0.81	497.347	111.516	4619.10	1035.71	0.107672	0.000511	0.000216	0.000049
20	0.7	51.50	4.90	707.557	1458.953	6708.62	13832.90	0.105470	0.000943	0.000149	0.000307

Blank intercepts:

exp.#	Step	36Ar (V)	$\pm\sigma_{36}$ (V)	37Ar (V)	$\pm\sigma_{37}$ (V)	38Ar (V)	$\pm\sigma_{38}$ (V)	39Ar (V)	$\pm\sigma_{39}$ (V)	40Ar (V)	$\pm\sigma_{40}$ (V)
5854	0.0%	-0.004558	0.000047	-0.002276	0.000064	-0.00248	0.000051	0.03058	0.000059	0.001627	0.000147

Blank corrected intensity intercepts:

Nr.	Step	36Ar (V)	$\pm\sigma_{36}$ (V)	37Ar (V)	$\pm\sigma_{37}$ (V)	38Ar (V)	$\pm\sigma_{38}$ (V)	39Ar (V)	$\pm\sigma_{39}$ (V)	40Ar (V)	$\pm\sigma_{40}$ (V)
1	3.0%	0.001370	0.000066	0.000033	0.000084	0.00046	0.000066	0.01305	0.000093	0.514942	0.000619
2	3.8%	0.002260	0.000071	0.000028	0.000085	0.00139	0.000071	0.06811	0.000106	1.216363	0.000504
3	4.3%	0.001389	0.000075	0.000000	0.000092	0.00129	0.000085	0.07086	0.000105	1.015352	0.000518
4	5.0%	0.001723	0.000069	0.000010	0.000090	0.00234	0.000079	0.13939	0.000119	1.691077	0.000853
5	5.7%	0.001468	0.000070	0.000137	0.000081	0.00262	0.000070	0.16619	0.000154	1.846800	0.001077
6	6.4%	0.001443	0.000066	0.000049	0.000080	0.00330	0.000075	0.21373	0.000182	2.268437	0.001674
7	7.0%	0.000910	0.000064	0.000046	0.000081	0.00355	0.000082	0.23483	0.000229	2.303945	0.002206
8	7.6%	0.000568	0.000057	0.000012	0.000082	0.00375	0.000073	0.25295	0.000194	2.364183	0.001437
9	8.2%	0.000334	0.000072	0.000089	0.000095	0.00294	0.000075	0.19986	0.000248	1.835606	0.001939
10	9.0%	0.000287	0.000062	0.000006	0.000090	0.00241	0.000073	0.16490	0.000410	1.517486	0.003107
11	10.0%	0.000359	0.000067	0.000002	0.000086	0.00209	0.000069	0.13947	0.000269	1.319468	0.002217
12	11.0%	0.000516	0.000059	0.000019	0.000081	0.00248	0.000070	0.16462	0.000623	1.565566	0.005784
13	12.0%	0.000526	0.000062	0.000017	0.000090	0.00276	0.000070	0.18539	0.000552	1.769319	0.006249
14	13.2%	0.000683	0.000074	0.000043	0.000091	0.00364	0.000089	0.24441	0.000814	2.318770	0.007319
15	14.4%	0.000505	0.000071	0.000000	0.000076	0.00325	0.000069	0.21937	0.000919	2.060860	0.009162
16	15.6%	0.000400	0.000062	0.000017	0.000083	0.00258	0.000070	0.17448	0.000915	1.636294	0.009200
17	17.1%	0.000430	0.000067	0.000000	0.000079	0.00270	0.000078	0.17776	0.000815	1.657087	0.008015
18	18.6%	0.000237	0.000068	0.000000	0.000083	0.00151	0.000066	0.10355	0.000517	0.972694	0.004568
19	20.6%	0.000263	0.000059	0.000001	0.000081	0.00195	0.000062	0.13311	0.000439	1.245443	0.004247
20	23.0%	0.000032	0.000065	0.000017	0.000088	0.00035	0.000077	0.02270	0.000143	0.216785	0.001373

Sample:	HUB_2_3
Project:	Alaska
Owner:	Falkowski_Enkelmann
Exp-Nr:	5687.00
Material:	101.24 mg Hbl

Nr.	Step	39Ar(K) (V)	39Ar(K) (%)	39Ar (10e-14 mol)	40Ar* (V)	36Ar_atm (V)	40Ar* (%)	40Ar/36Ar	37Ar/36Ar	37Ar/39Ar	K/Ca	K/Ca Error	40Ar*/39Ar(K)	40Ar*/39Ar(K) Error	Age (Ma)	Age Error(Ma)
23.00	1335°C	0.6243	6.0	21.05	31.149	0.0033	96.9	8153.8	68.92	0.434	0.111	0.001	49.90	0.06	271.51	0.95
24.00	1350°C	0.8917	8.6	30.07	44.799	0.0049	96.8	8067.4	66.25	0.425	0.113	0.001	50.24	0.06	273.23	0.96
25.00	1358°C	1.0424	10.1	35.15	52.939	0.0059	96.8	7995.5	62.97	0.412	0.117	0.001	50.78	0.06	275.98	0.97
26.00	1366°C	0.2122	2.1	7.16	10.791	0.0031	92.2	3597.3	26.65	0.407	0.118	0.001	50.85	0.09	276.33	1.03
27.00	1381°C	0.0352	0.3	1.19	1.800	0.0015	79.7	1437.4	9.73	0.433	0.111	0.001	51.15	0.45	277.84	2.47
28.00	1410°C	0.0315	0.3	1.06	1.615	0.0017	75.6	1200.3	7.83	0.441	0.109	0.001	51.31	0.55	278.61	2.90

J - value =	0.0032588
J-error [%] =	0.31

Plateau Data · **Isochron Data** · **Inverse Isochron Data**

Nr.	39Ar%	Age (Ma)	Age_err (Ma)	39/36	err	40/36	err	39/40 (0.000000)	err (0.000010)	36/40 (0.003384)	err (0.000010)
1	0.6	138.65	1.33	7.942	0.048	493.51	2.94	0.016093	0.000024	0.002026	0.000012
2	0.5	150.19	1.50	8.761	0.067	532.26	4.03	0.016460	0.000023	0.001879	0.000014
3	0.6	194.19	1.55	10.339	0.095	659.58	5.99	0.015675	0.000021	0.001516	0.000014
4	0.7	160.32	1.12	15.866	0.152	751.58	7.13	0.021110	0.000023	0.001331	0.000013
5	0.6	148.86	1.33	41.799	1.306	1403.11	43.82	0.029790	0.000043	0.000713	0.000022
6	0.6	152.48	1.25	55.420	2.126	1800.23	69.02	0.030785	0.000038	0.000555	0.000021
7	1.2	172.69	0.81	69.066	1.575	2430.13	55.37	0.028421	0.000030	0.000412	0.000009
8	2.2	191.49	0.78	97.395	1.801	3649.24	67.42	0.026689	0.000042	0.000274	0.000005
9	3.0	197.33	0.72	153.275	3.290	5741.49	123.16	0.026696	0.000020	0.000174	0.000004
10	3.7	210.33	0.76	194.854	4.402	7700.98	173.92	0.025302	0.000026	0.000130	0.000003
11	4.9	222.31	0.84	232.957	5.955	9684.44	247.56	0.024055	0.000037	0.000103	0.000003
12	5.6	230.82	0.82	273.921	6.648	11785.12	285.92	0.023243	0.000022	0.000085	0.000002
13	6.0	237.84	0.83	310.825	8.301	13755.40	367.23	0.022597	0.000017	0.000073	0.000002
14	5.5	242.92	0.85	340.151	9.860	15361.64	445.15	0.022143	0.000018	0.000065	0.000002
15	4.9	247.08	0.87	358.155	11.724	16449.12	538.35	0.021774	0.000020	0.000061	0.000002
16	4.4	251.03	0.88	388.711	16.199	18127.89	755.35	0.021443	0.000018	0.000055	0.000002
17	3.7	254.06	1.07	407.695	19.696	19240.20	929.62	0.021190	0.000054	0.000052	0.000003
18	4.0	258.14	0.92	435.752	19.218	20892.66	921.32	0.020857	0.000023	0.000048	0.000002
19	4.1	262.13	0.94	443.546	23.918	21609.54	1165.17	0.020525	0.000024	0.000046	0.000002
20	4.5	265.28	1.06	409.540	17.615	20229.73	869.99	0.020244	0.000046	0.000049	0.000002
21	4.9	267.82	0.97	304.457	11.487	15268.52	576.01	0.019940	0.000025	0.000065	0.000002
22	6.5	269.48	0.94	226.415	4.804	11505.36	243.99	0.019679	0.000017	0.000087	0.000002
23	6.0	271.51	0.95	186.764	3.806	9617.73	195.88	0.019419	0.000018	0.000104	0.000002
24	8.6	273.23	0.96	182.157	2.571	9450.10	133.23	0.019276	0.000019	0.000106	0.000001
25	10.1	275.98	0.97	176.992	2.295	9286.96	120.28	0.019058	0.000020	0.000108	0.000001
26	2.1	276.33	1.03	69.289	1.139	3822.24	62.75	0.018128	0.000021	0.000262	0.000004
27	0.3	277.84	2.47	22.879	0.776	1468.97	49.74	0.015575	0.000032	0.000681	0.000023
28	0.3	278.61	2.90	17.986	0.572	1221.40	38.68	0.014725	0.000042	0.000819	0.000026

Blank intercepts:

exp.#	Step	36Ar (V)	±σ36 (V)	37Ar (V)	±σ37 (V)	38Ar (V)	±σ38 (V)	39Ar (V)	±σ39 (V)	40Ar (V)	±σ40 (V)
5686	(1450°C)	-0.004488	0.000038	-0.002304	0.000040	-0.002507	0.000040	0.030637	0.000040	0.030743	0.000152
5685	(1200°C)	-0.004507	0.000034	-0.002301	0.000024	-0.002445	0.000039	0.030677	0.000047	0.030610	0.000103
5684	(950°C)	-0.004506	0.000035	-0.002280	0.000030	-0.002491	0.000038	0.030664	0.000035	0.031270	0.000111

Blank corrected intensity intercepts:

Nr.	Step	36Ar (V)	±σ36 (V)	37Ar (V)	±σ37 (V)	38Ar (V)	±σ38 (V)	39Ar (V)	±σ39 (V)	40Ar (V)	±σ40 (V)
1	900°C	0.007496	0.000040	0.006509	0.000044	0.006585	0.000052	0.060449	0.000070	3.776752	0.002663
2	950°C	0.006092	0.000043	0.004900	0.000061	0.004913	0.000045	0.054189	0.000066	3.310742	0.000720
3	1000°C	0.005563	0.000048	0.006365	0.000052	0.004768	0.000050	0.058362	0.000067	3.743588	0.001127
4	1050°C	0.004426	0.000040	0.006427	0.000052	0.004578	0.000039	0.071199	0.000061	3.391910	0.000477
5	1080°C	0.001408	0.000043	0.004732	0.000046	0.003066	0.000041	0.059399	0.000073	2.005447	0.000809
6	1120°C	0.001136	0.000043	0.010023	0.000045	0.004258	0.000044	0.062816	0.000062	2.050642	0.000872
7	1160°C	0.001771	0.000038	0.041260	0.000076	0.016437	0.000045	0.118333	0.000094	4.176266	0.001116
8	1190°C	0.002504	0.000040	0.096954	0.000100	0.042576	0.000067	0.227762	0.000243	8.553100	0.008230
9	1205°C	0.002261	0.000037	0.137948	0.000075	0.063634	0.000068	0.306375	0.000095	11.499430	0.001442
10	1215°C	0.002318	0.000037	0.174819	0.000118	0.083370	0.000071	0.384707	0.000222	15.234090	0.008646
11	1225°C	0.002623	0.000044	0.228027	0.000249	0.112093	0.000122	0.504560	0.000447	21.017010	0.021991
12	1233°C	0.002624	0.000036	0.257935	0.000178	0.129430	0.000113	0.575340	0.000291	24.803200	0.011967
13	1241°C	0.002571	0.000037	0.276786	0.000158	0.141717	0.000080	0.622966	0.000148	27.625660	0.006993
14	1246°C	0.002181	0.000033	0.249756	0.000106	0.130030	0.000067	0.566603	0.000199	25.641980	0.008031
15	1251°C	0.001857	0.000034	0.219583	0.000138	0.116195	0.000090	0.502464	0.000238	23.125990	0.011125
16	1256°C	0.001562	0.000039	0.195110	0.000089	0.104835	0.000082	0.449608	0.000191	21.013150	0.006739
17	1261°C	0.001261	0.000038	0.161642	0.000283	0.088555	0.000164	0.377140	0.000607	17.837640	0.033530
18	1270°C	0.001303	0.000033	0.173842	0.000098	0.097277	0.000079	0.409592	0.000272	19.682670	0.011412
19	1280°C	0.001323	0.000044	0.177617	0.000113	0.101539	0.000104	0.422417	0.000288	20.627340	0.013379
20	1295°C	0.001530	0.000040	0.192980	0.000264	0.112327	0.000176	0.462427	0.000718	22.895330	0.034843
21	1310°C	0.002070	0.000054	0.210760	0.000134	0.122132	0.000094	0.499440	0.000365	25.103980	0.018584
22	1325°C	0.003519	0.000047	0.285622	0.000136	0.164308	0.000113	0.668253	0.000269	34.032940	0.011967
23	1335°C	0.003855	0.000055	0.267158	0.000138	0.154208	0.000102	0.622901	0.000280	32.148140	0.014430
24	1350°C	0.005607	0.000044	0.373538	0.000177	0.220691	0.000142	0.889695	0.000496	46.262380	0.024677
25	1358°C	0.006689	0.000046	0.423534	0.000201	0.260156	0.000172	1.039950	0.000581	54.699780	0.030575
26	1366°C	0.003182	0.000047	0.085278	0.000086	0.053093	0.000080	0.211685	0.000177	11.706220	0.005274
27	1381°C	0.001537	0.000051	0.015040	0.000070	0.008766	0.000048	0.035120	0.000065	2.259843	0.001377
28	1410°C	0.001741	0.000054	0.013709	0.000071	0.007928	0.000064	0.031405	0.000086	2.137246	0.000629

Sample:	HUB_2_5		
Project:	Alaska		
Owner:	Falkowski_Enkelmann		
Exp-Nr:	5692.00		
Material:	150.63 mg Hbl		
Irradiation:	FGA014P5H1 (End date: 2013-07-31 15:39:00.0)		
Measurement Date:	2013-11-30 08:42:00.0		
Device:	HTC		
Air:	298.6		
J-Value:	0.0032573	f-value:	0.993342
J-Value Error:	0.0000104	f-value Error:	0.000478

Reference Standard(s): FCT01 - 28.305 +/- 0.036 Ma,

Total gas age: 148.67 +/- 0.18 Ma

Interfering isotope production ratios:

ca3637 = 0.000205 +/- 0.000012
ca3937 = 0.000932 +/- 0.000035
k3839 = 0.01211 +/- 0.00061
k4039 = 0.00183 +/- 0.00009

Decay constants:

lambda40 = 5.5492e-010 +/- 9.3000e-013 1/a
lambda39 = 0.002577 +/- 0.000026 1/a
lambda37 = 7.2438 +/- 0.0214 1/a

ALF ARGONLAB FREIBERG

Fit model: linear All errors are 1s!

Nr.	Step	39Ar(K) (V)	39Ar(K) (%)	39Ar (10e-14 mol)	40Ar* (V)	36Ar_atm (V)	40Ar* (%)	40Ar/36Ar	37Ar/36Ar	37Ar/39Ar	K/Ca	K/Ca Error	40Ar*/39Ar(K)	40Ar*/39Ar(K) Error	Age (Ma)	Age Error(Ma)
1.00	900°C	0.0069	0.1	0.23	0.274	0.0044	17.1	357.2	3.62	2.292	0.020	0.000	39.60	2.07	218.62	10.81
2.00	950°C	0.0047	0.1	0.16	0.109	0.0017	17.4	358.4	3.78	1.381	0.033	0.001	23.10	3.55	130.73	19.37
3.00	1000°C	0.0069	0.1	0.23	0.214	0.0020	26.6	403.9	3.35	0.950	0.048	0.001	30.84	2.08	172.48	11.10
4.00	1050°C	0.0095	0.2	0.32	0.392	0.0032	29.1	418.1	3.38	1.127	0.041	0.000	41.05	1.67	226.15	8.66
5.00	1100°C	0.0140	0.2	0.47	0.322	0.0017	38.7	476.4	9.57	1.184	0.039	0.000	23.07	0.96	130.58	5.26
6.00	1150°C	0.0294	0.5	0.99	0.491	0.0009	63.8	730.9	50.23	1.762	0.026	0.000	16.67	0.52	95.26	2.90
7.00	1200°C	0.0970	1.6	3.27	1.977	0.0014	82.5	1383.5	82.30	1.450	0.032	0.000	20.39	0.15	115.88	0.94
8.00	1230°C	0.6620	10.8	22.32	16.883	0.0038	93.8	3444.6	122.19	0.956	0.048	0.000	25.50	0.05	143.81	0.58
9.00	1240°C	0.5224	8.6	17.62	13.826	0.0026	94.7	3916.3	132.56	0.938	0.049	0.000	26.46	0.06	149.01	0.60
10.00	1248°C	0.2841	4.7	9.58	7.511	0.0015	94.3	3708.9	125.46	0.940	0.049	0.000	26.44	0.07	148.86	0.65
11.00	1256°C	0.1683	2.8	5.68	4.435	0.0009	94.4	3740.9	127.81	0.945	0.049	0.000	26.35	0.09	148.38	0.71
12.00	1266°C	0.1422	2.3	4.80	3.765	0.0008	94.4	3750.1	128.19	0.950	0.048	0.000	26.47	0.10	149.05	0.75
13.00	1278°C	0.1040	1.7	3.51	2.751	0.0006	94.3	3706.4	130.02	0.975	0.047	0.000	26.46	0.15	148.97	0.96
14.00	1293°C	0.1024	1.7	3.45	2.657	0.0006	93.7	3373.4	125.45	1.019	0.045	0.000	25.94	0.13	146.16	0.89
15.00	1313°C	0.2447	4.0	8.25	6.341	0.0013	94.1	3560.6	130.00	0.996	0.046	0.000	25.91	0.08	146.03	0.66
16.00	1325°C	0.3559	5.8	12.00	9.400	0.0020	94.0	3581.8	123.19	0.957	0.048	0.000	26.41	0.09	148.73	0.69
17.00	1335°C	0.4389	7.2	14.80	11.675	0.0023	94.4	3764.7	126.80	0.941	0.049	0.000	26.60	0.06	149.73	0.60
18.00	1345°C	0.6563	10.7	22.13	17.529	0.0032	94.8	3992.8	132.38	0.926	0.050	0.000	26.71	0.05	150.34	0.60
19.00	1350°C	0.6320	10.4	21.31	16.949	0.0032	94.7	3937.9	128.87	0.919	0.050	0.000	26.82	0.05	150.93	0.59
20.00	1355°C	0.5960	9.8	20.10	16.012	0.0028	95.0	4125.5	134.77	0.916	0.050	0.000	26.87	0.05	151.18	0.60
21.00	1365°C	0.7994	13.1	26.96	21.515	0.0038	95.0	4125.1	133.76	0.911	0.051	0.000	26.91	0.05	151.43	0.59
22.00	1375°C	0.1287	2.1	4.34	3.473	0.0013	89.9	2445.0	74.82	0.910	0.051	0.000	26.98	0.11	151.78	0.79
23.00	1390°C	0.0319	0.5	1.08	0.860	0.0009	77.0	1205.9	31.80	0.914	0.050	0.000	26.95	0.54	151.63	2.94
24.00	1410°C	0.0549	0.9	1.85	1.500	0.0022	69.7	934.1	22.16	0.922	0.050	0.000	27.31	0.29	153.59	1.68
25.00	1450°C	0.0128	0.2	0.43	0.351	0.0007	64.3	802.3	17.27	0.915	0.050	0.001	27.56	1.23	154.93	6.62

J - value =	0.0032573
J-error [%] =	0.32

Plateau Data · **Isochron Data** · **Inverse Isochron Data**

Nr.	39Ar%	Age (Ma)	Age_err (Ma)	39/36	err	40/36	err	39/40 (0.000000)	err (0.000010)	36/40 (0.003384)	err (0.000010)
1	0.1	218.62	10.81	1.555	0.022	360.17	3.83	0.004317	0.000041	0.002776	0.000029
2	0.1	130.73	19.37	2.726	0.096	361.57	11.65	0.007539	0.000111	0.002766	0.000089
3	0.1	172.48	11.10	3.516	0.092	407.01	9.85	0.008638	0.000084	0.002457	0.000059
4	0.2	226.15	8.66	2.991	0.052	421.39	6.95	0.007099	0.000043	0.002373	0.000039
5	0.2	130.58	5.26	8.170	0.216	487.11	12.74	0.016773	0.000061	0.002053	0.000054
6	0.5	95.26	2.90	31.652	1.733	826.09	45.19	0.038316	0.000100	0.001211	0.000066
7	1.6	115.88	0.94	68.997	2.406	1705.47	59.45	0.040456	0.000052	0.000586	0.000020
8	10.8	143.81	0.58	175.979	4.729	4786.68	128.59	0.036764	0.000041	0.000209	0.000006
9	8.6	149.01	0.60	201.385	6.452	5628.22	180.27	0.035781	0.000038	0.000178	0.000006
10	4.7	148.86	0.65	185.710	7.867	5208.29	220.60	0.035657	0.000031	0.000192	0.000008
11	2.8	148.38	0.71	189.565	10.536	5293.16	294.18	0.035813	0.000030	0.000189	0.000010
12	2.3	149.05	0.75	189.421	11.604	5312.95	325.46	0.035653	0.000036	0.000188	0.000012
13	1.7	148.97	0.96	188.369	17.555	5282.39	492.27	0.035660	0.000038	0.000189	0.000018
14	1.7	146.16	0.89	171.117	12.785	4737.06	353.90	0.036123	0.000042	0.000211	0.000016
15	4.0	146.03	0.66	184.294	8.322	5074.29	229.11	0.036319	0.000035	0.000197	0.000009
16	5.8	148.73	0.69	177.745	5.843	4993.25	164.14	0.035597	0.000085	0.000200	0.000007
17	7.2	149.73	0.60	188.388	5.881	5309.47	165.69	0.035482	0.000034	0.000188	0.000006
18	10.7	150.34	0.60	203.529	6.285	5734.97	177.06	0.035489	0.000034	0.000174	0.000005
19	10.4	150.93	0.59	197.346	5.752	5591.39	162.92	0.035295	0.000026	0.000179	0.000005
20	9.8	151.18	0.60	211.188	6.535	5972.36	184.76	0.035361	0.000041	0.000167	0.000005
21	13.1	151.43	0.59	210.065	6.240	5951.91	176.75	0.035294	0.000034	0.000168	0.000005
22	2.1	151.78	0.79	98.346	3.444	2951.68	103.34	0.033319	0.000032	0.000339	0.000012
23	0.5	151.63	2.94	37.184	2.462	1300.73	86.06	0.028587	0.000069	0.000769	0.000051
24	0.9	153.59	1.68	25.096	0.617	984.07	24.14	0.025502	0.000039	0.001016	0.000025
25	0.2	154.93	6.62	19.473	1.553	835.34	66.53	0.023312	0.000086	0.001197	0.000095

Blank intercepts:

exp.#	Step	36Ar (V)	±σ36 (V)	37Ar (V)	±σ37 (V)	38Ar (V)	±σ38 (V)	39Ar (V)	±σ39 (V)	40Ar (V)	±σ40 (V)
5691	(1450°C)	-0.004527	0.000035	-0.002264	0.000039	-0.002499	0.000046	0.030603	0.000040	0.028597	0.000140
5690	(1200°C)	-0.004516	0.000042	-0.002272	0.000050	-0.002454	0.000051	0.030671	0.000053	0.025170	0.000141
5689	(950°C)	-0.004526	0.000046	-0.002264	0.000053	-0.002506	0.000042	0.030669	0.000045	0.025914	0.000125

Blank corrected intensity intercepts:

Nr.	Step	36Ar (V)	±σ36 (V)	37Ar (V)	±σ37 (V)	38Ar (V)	±σ38 (V)	39Ar (V)	±σ39 (V)	40Ar (V)	±σ40 (V)
1	900°C	0.004365	0.000045	0.015891	0.000062	0.002190	0.000049	0.007027	0.000064	1.600856	0.000843
2	950°C	0.001704	0.000054	0.006488	0.000059	0.000796	0.000043	0.004761	0.000069	0.627083	0.000726
3	1000°C	0.001939	0.000046	0.006529	0.000055	0.001032	0.000055	0.006962	0.000067	0.804014	0.000556
4	1050°C	0.003132	0.000051	0.010662	0.000065	0.001603	0.000043	0.009585	0.000056	1.344572	0.000968
5	1100°C	0.001702	0.000043	0.016400	0.000064	0.001510	0.000053	0.014034	0.000049	0.832639	0.000610
6	1150°C	0.001024	0.000049	0.051764	0.000073	0.002457	0.000058	0.029768	0.000069	0.768463	0.000495
7	1200°C	0.001687	0.000044	0.139760	0.000083	0.009762	0.000046	0.097702	0.000092	2.396692	0.000915
8	1230°C	0.005091	0.000046	0.626215	0.000388	0.079136	0.000092	0.663650	0.000459	18.007950	0.011380
9	1240°C	0.003631	0.000045	0.484481	0.000270	0.059919	0.000067	0.523616	0.000338	14.601380	0.008598
10	1248°C	0.002092	0.000051	0.264219	0.000108	0.030915	0.000059	0.284745	0.000134	7.967847	0.003085
11	1256°C	0.001224	0.000043	0.157427	0.000106	0.018247	0.000062	0.168730	0.000091	4.700562	0.000866
12	1266°C	0.001036	0.000041	0.133680	0.000098	0.014820	0.000061	0.142565	0.000097	3.989343	0.001707
13	1278°C	0.000766	0.000048	0.100269	0.000077	0.010678	0.000048	0.104245	0.000087	2.915689	0.000680
14	1293°C	0.000819	0.000041	0.103392	0.000080	0.010452	0.000052	0.102768	0.000094	2.836183	0.000914
15	1313°C	0.001843	0.000048	0.241161	0.000146	0.028560	0.000060	0.245403	0.000146	6.737758	0.002758
16	1325°C	0.002718	0.000044	0.337075	0.000526	0.041827	0.000095	0.356764	0.000552	9.998003	0.017094
17	1335°C	0.003200	0.000043	0.408482	0.000188	0.051255	0.000079	0.439956	0.000249	12.371690	0.005853
18	1345°C	0.004511	0.000050	0.601063	0.000384	0.075779	0.000072	0.657684	0.000338	18.493190	0.009801
19	1350°C	0.004428	0.000044	0.574461	0.000173	0.073236	0.000080	0.633283	0.000192	17.906430	0.004395
20	1355°C	0.003979	0.000040	0.539760	0.000345	0.068182	0.000082	0.597216	0.000412	16.855590	0.011907
21	1365°C	0.005348	0.000047	0.720019	0.000490	0.090872	0.000096	0.801044	0.000419	22.652620	0.011933
22	1375°C	0.001539	0.000042	0.115915	0.000089	0.014512	0.000060	0.129005	0.000083	3.864363	0.001338
23	1390°C	0.000901	0.000055	0.028845	0.000072	0.003700	0.000049	0.031965	0.000073	1.115933	0.000402
24	1410°C	0.002245	0.000052	0.050085	0.000081	0.006580	0.000057	0.055028	0.000075	2.153288	0.000503
25	1450°C	0.000664	0.000051	0.011543	0.000067	0.001561	0.000051	0.012777	0.000046	0.546999	0.000257

Sample:	HUB_2_7
Project:	Alaska
Owner:	Falkowski_Enkelmann
Irradiation:	FGA014P4H6 (End date: 2013-07-31 15:39:00.0)
Measurement Date:	2013-12-01 16:46:15.0
Device:	HTC
Air:	298.6

Interfering isotope production ratios:

ca3637 = 0.000205 +/- 0.000012
ca3937 = 0.000932 +/- 0.000035

Decay constants:

lambda40 = 5.5492e-010 +/- 9.3000e-013 1/a
lambda39 = 0.002577 +/- 0.000026 1/a

J - value =	0.0032588

Blank intercepts:

exp.#	Step	36Ar (V)	±σ36 (V)	37Ar (V)	±σ37 (V)	38Ar (V)	±σ38 (V)	39Ar (V)	±σ39 (V)	40Ar (V)	±σ40 (V)
5695	(1450°C)	-0.004494	0.000036	-0.002298	0.000033	-0.002437	0.000032	0.030661	0.000045	0.028349	0.000135

Nr.	Step	39Ar(K) (V)	39Ar(K) (%)	39Ar (10e-14 mol)	40Ar* (V)	36Ar_atm (V)	40Ar* (%)	40Ar/36Ar	37Ar/36Ar	37Ar/39Ar	K/Ca	K/Ca Error	40Ar*/39Ar(K)	40Ar*/39Ar(K) Error	Age (Ma)	Age Error(Ma)
14.00	1340°C	0.0518	5.3	1.74	2.628	0.0022	79.7	1131.0	76.41	4.066	0.008	0.000	50.78	0.44	275.84	2.41
15.00	1360°C	0.1150	11.7	3.88	8.540	0.0043	87.0	1697.9	85.71	4.070	0.008	0.000	74.25	0.37	390.32	2.17
16.00	1375°C	0.0856	8.7	2.89	9.815	0.0032	91.1	2483.3	84.61	4.054	0.008	0.000	114.67	0.44	571.91	2.63
17.00	1390°C	0.0973	9.9	3.28	9.333	0.0029	91.4	2433.1	99.12	4.042	0.008	0.000	95.96	0.36	490.16	2.28
18.00	1405°C	0.0278	2.8	0.94	1.998	0.0007	90.1	2018.3	108.10	4.038	0.008	0.000	71.85	0.84	378.95	4.18
19.00	1430°C	0.0108	1.1	0.36	0.706	0.0003	89.5	1881.3	110.56	4.070	0.008	0.000	65.57	1.50	348.85	7.33

Nr.	39Ar%	Age (Ma)	Age_err (Ma)	39/36	err	40/36	err	39/40	err	36/40	err
14	5.3	275.84	2.41	23.123	0.739	1472.81	46.86	0.015700	0.000049	0.000679	0.000022
15	11.7	390.32	2.17	26.897	0.669	2295.64	56.82	0.011717	0.000037	0.000436	0.000011
16	8.7	571.91	2.63	26.545	0.705	3342.44	88.42	0.007942	0.000022	0.000299	0.000008
17	9.9	490.16	2.28	33.167	1.016	3481.45	106.32	0.009527	0.000024	0.000287	0.000009
18	2.8	378.95	4.18	37.670	3.752	3005.17	299.10	0.012535	0.000049	0.000333	0.000033
19	1.1	348.85	7.33	38.645	7.066	2832.70	517.47	0.013642	0.000104	0.000353	0.000064

Nr.	Step	36Ar (V)	±σ36 (V)	37Ar (V)	±σ37 (V)	38Ar (V)	±σ38 (V)	39Ar (V)	±σ39 (V)	40Ar (V)	±σ40 (V)
14	1340°C	0.002850	0.000057	0.218972	0.000235	0.001747	0.000051	0.054465	0.000095	3.296334	0.003264
15	1360°C	0.005653	0.000052	0.487251	0.000707	0.003381	0.000052	0.121064	0.000192	9.817437	0.014420
16	1375°C	0.004243	0.000051	0.361041	0.000380	0.002733	0.000057	0.090067	0.000111	10.777990	0.010382
17	1390°C	0.004102	0.000045	0.408911	0.000240	0.002710	0.000052	0.102320	0.000079	10.209030	0.005394
18	1405°C	0.001075	0.000069	0.116808	0.000096	0.000679	0.000056	0.029252	0.000084	2.218258	0.001578
19	1430°C	0.000410	0.000049	0.045628	0.000081	0.000304	0.000060	0.011338	0.000077	0.789649	0.000585

Sample:	**MAL_6_23**				
Project:	Alaska	Irradiation:	FGA014P5H7 (End date: 2013-07-31 15:39:00.0)	Interfering isotope production ratios:	Decay constants:
Owner:	Falkowski_Enkelmann	Measurement Date:	2013-12-17 16:48:34.0		
		Device:	HTC	ca3637 = 0.000205 +/- 0.000012	lambda40 = 5.5492e-010 +/- 9.3000e-013 1/a
		Air:	298.6	ca3937 = 0.000932 +/- 0.000035	lambda39 = 0.002577 +/- 0.000026 1/a
Exp-Nr:	**5763.00**	**J-Value:**	**0.0032573** f-value: 0.995004	k3839 = 0.01211 +/- 0.00061	lambda37 = 7.2438 +/- 0.0214 1/a
Material:	152.30 mg Hbl	**J-Value Error:**	**0.0000104** f-value Error: 0.000176	k4039 = 0.00183 +/- 0.00009	
		Reference Standard(s): FCT01 - 28.305 +/- 0.036 Ma,			
		Total gas age: 50.89 +/- 0.11 Ma			**Fit model: linear** All errors are 1s!

Nr.	Step	39Ar(K) (V)	39Ar(K) (%)	39Ar (10e-14 mol)	40Ar* (V)	36Ar_atm (V)	40Ar* (%)	40Ar/36Ar	37Ar/36Ar	37Ar/39Ar	K/Ca	K/Ca Error	40Ar*/39Ar(K)	40Ar*/39Ar(K) Error	Age (Ma)	Age Error(Ma)
1.00	900°C	0.0069	0.1	0.23	0.051	0.0053	3.1	307.6	0.53	0.403	0.081	0.002	7.33	2.18	42.51	12.53
2.00	950°C	0.0097	0.1	0.33	0.050	0.0018	8.4	325.1	0.81	0.155	0.213	0.009	5.19	1.63	30.20	9.43
3.00	1000°C	0.0173	0.3	0.58	0.101	0.0019	15.0	349.8	1.44	0.160	0.205	0.005	5.84	0.89	33.94	5.16
4.00	1050°C	0.0251	0.4	0.85	0.159	0.0023	18.6	364.2	2.39	0.222	0.148	0.002	6.34	0.62	36.86	3.58
5.00	1100°C	0.0379	0.6	1.28	0.256	0.0016	34.7	445.4	7.95	0.347	0.095	0.001	6.77	0.46	39.29	2.66
6.00	1150°C	0.0591	0.9	1.99	0.462	0.0016	49.7	560.2	17.37	0.485	0.067	0.001	7.82	0.28	45.34	1.64
7.00	1190°C	0.1350	2.0	4.55	1.173	0.0030	57.1	618.7	34.47	0.838	0.039	0.000	8.69	0.14	50.31	0.80
8.00	1210°C	1.0101	14.9	34.06	8.904	0.0080	78.9	1067.7	75.79	0.785	0.042	0.000	8.82	0.05	51.02	0.34
9.00	1217°C	0.6168	9.1	20.80	5.434	0.0035	83.9	1329.2	88.45	0.692	0.047	0.000	8.81	0.05	50.98	0.34
10.00	1224°C	0.5609	8.3	18.91	4.941	0.0028	85.7	1467.5	92.19	0.640	0.051	0.000	8.81	0.05	50.98	0.33
11.00	1233°C	0.5569	8.2	18.78	4.928	0.0024	87.5	1634.1	97.85	0.601	0.054	0.000	8.85	0.05	51.21	0.35
12.00	1243°C	0.6726	9.9	22.68	5.956	0.0024	89.1	1829.7	103.57	0.558	0.059	0.000	8.85	0.04	51.24	0.31
13.00	1252°C	0.3815	5.6	12.86	3.385	0.0013	89.9	1958.1	104.69	0.524	0.062	0.001	8.87	0.05	51.34	0.36
14.00	1262°C	0.2663	3.9	8.98	2.363	0.0009	90.1	2006.0	104.25	0.508	0.064	0.001	8.87	0.07	51.33	0.41
15.00	1279°C	0.2246	3.3	7.57	1.987	0.0007	90.0	1971.2	105.30	0.522	0.063	0.001	8.85	0.09	51.19	0.54
16.00	1295°C	0.1646	2.4	5.55	1.449	0.0006	88.2	1684.0	103.94	0.611	0.053	0.000	8.80	0.11	50.95	0.63
17.00	1310°C	0.2053	3.0	6.92	1.810	0.0008	88.8	1681.9	114.28	0.669	0.049	0.000	8.82	0.10	51.02	0.61
18.00	1320°C	0.2518	3.7	8.49	2.214	0.0008	89.7	1759.1	122.36	0.676	0.048	0.000	8.79	0.07	50.89	0.46
19.00	1330°C	0.2919	4.3	9.84	2.575	0.0009	90.9	1900.3	130.24	0.659	0.050	0.000	8.82	0.07	51.05	0.43
20.00	1340°C	0.3018	4.4	10.18	2.663	0.0009	90.9	1932.1	127.54	0.635	0.051	0.000	8.82	0.07	51.06	0.44
21.00	1350°C	0.2755	4.1	9.29	2.446	0.0008	90.7	1953.3	122.15	0.607	0.054	0.000	8.88	0.08	51.38	0.47
22.00	1360°C	0.2547	3.7	8.59	2.265	0.0009	89.8	1880.7	111.37	0.582	0.056	0.000	8.89	0.07	51.46	0.45
23.00	1372°C	0.2003	2.9	6.76	1.788	0.0008	88.6	1782.1	99.68	0.559	0.058	0.001	8.93	0.09	51.65	0.54
24.00	1400°C	0.1678	2.5	5.66	1.497	0.0008	85.9	1561.0	81.89	0.541	0.060	0.001	8.92	0.11	51.62	0.65
25.00	1500°C	0.1035	1.5	3.49	0.922	0.0005	84.9	1463.5	80.14	0.570	0.057	0.000	8.91	0.21	51.54	1.24

J - value =	0.0032573
J-error [%] =	0.32

Plateau Data				Isochron Data				Inverse Isochron Data			
Nr.	39Ar%	Age (Ma)	Age_err (Ma)	39/36	err	40/36	err	39/40	err	36/40	err
								0.000000	0.000010	0.003384	0.000010
1	0.1	42.51	12.53	1.304	0.015	308.16	2.94	0.004233	0.000030	0.003245	0.000031
2	0.1	30.20	9.43	5.266	0.156	325.92	9.39	0.016156	0.000113	0.003068	0.000088
3	0.3	33.94	5.16	9.046	0.247	351.40	9.52	0.025743	0.000092	0.002846	0.000077
4	0.4	36.86	3.58	10.788	0.244	367.04	8.23	0.029393	0.000085	0.002724	0.000061
5	0.6	39.29	2.66	23.435	0.852	457.16	16.59	0.051261	0.000102	0.002187	0.000079
6	0.9	45.34	1.64	37.698	1.354	593.49	21.30	0.063518	0.000123	0.001685	0.000060
7	2.0	50.31	0.80	45.752	0.940	696.29	14.29	0.065708	0.000137	0.001436	0.000029
8	14.9	51.02	0.34	126.588	2.611	1414.54	29.17	0.089490	0.000117	0.000707	0.000015
9	9.1	50.98	0.34	177.473	5.124	1862.10	53.76	0.095308	0.000137	0.000537	0.000016
10	8.3	50.98	0.33	203.497	6.572	2091.18	67.52	0.097312	0.000124	0.000478	0.000015
11	8.2	51.21	0.35	236.481	8.719	2391.14	88.17	0.098899	0.000238	0.000418	0.000015
12	9.9	51.24	0.31	277.059	10.841	2751.78	107.67	0.100684	0.000129	0.000363	0.000014
13	5.6	51.34	0.36	300.075	15.458	2961.13	152.54	0.101338	0.000180	0.000338	0.000017
14	3.9	51.33	0.41	307.564	20.424	3027.01	201.00	0.101607	0.000098	0.000330	0.000022
15	3.3	51.19	0.54	304.262	25.936	2989.89	254.87	0.101763	0.000333	0.000334	0.000029
16	2.4	50.95	0.63	254.306	22.669	2537.28	226.17	0.100228	0.000155	0.000394	0.000035
17	3.0	51.02	0.61	268.833	24.324	2668.65	241.45	0.100738	0.000167	0.000375	0.000034
18	3.7	50.89	0.46	297.251	21.694	2912.24	212.54	0.102069	0.000139	0.000343	0.000025
19	4.3	51.05	0.43	338.492	25.996	3284.67	252.26	0.103052	0.000124	0.000304	0.000023
20	4.4	51.06	0.44	339.040	26.203	3289.79	254.26	0.103058	0.000152	0.000304	0.000023
21	4.1	51.38	0.47	330.134	27.188	3229.85	265.99	0.102213	0.000165	0.000310	0.000025
22	3.7	51.46	0.45	297.027	20.455	2940.31	202.48	0.101019	0.000207	0.000340	0.000023
23	2.9	51.65	0.54	261.224	18.920	2630.38	190.51	0.099310	0.000349	0.000380	0.000028
24	2.5	51.62	0.65	204.577	15.173	2123.58	157.50	0.096336	0.000180	0.000471	0.000035
25	1.5	51.54	1.24	188.299	25.401	1975.82	266.53	0.095302	0.000122	0.000506	0.000068

Blank intercepts:

exp.#	Step	36Ar (V)	±σ36 (V)	37Ar (V)	±σ37 (V)	38Ar (V)	±σ38 (V)	39Ar (V)	±σ39 (V)	40Ar (V)	±σ40 (V)
5762	(1450°C)	-0.004526	0.000056	-0.002224	0.000058	-0.002498	0.000052	0.030436	0.000050	0.014851	0.000139
5761	(1200°C)	-0.004522	0.000046	-0.002211	0.000051	-0.002463	0.000040	0.030477	0.000052	0.012834	0.000107
5760	(950°C)	-0.004544	0.000042	-0.002265	0.000060	-0.002453	0.000047	0.030542	0.000053	0.013494	0.000135

Blank corrected intensity intercepts:

Nr.	Step	36Ar (V)	±σ36 (V)	37Ar (V)	±σ37 (V)	38Ar (V)	±σ38 (V)	39Ar (V)	±σ39 (V)	40Ar (V)	±σ40 (V)
1	900°C	0.005217	0.000049	0.002765	0.000067	0.001555	0.000053	0.006929	0.000049	1.637046	0.000962
2	950°C	0.001807	0.000052	0.001477	0.000058	0.000563	0.000053	0.009646	0.000067	0.599254	0.000453
3	1000°C	0.001887	0.000051	0.002737	0.000059	0.000720	0.000057	0.017271	0.000060	0.673368	0.000471
4	1050°C	0.002296	0.000054	0.005505	0.000076	0.001018	0.000054	0.025009	0.000070	0.853216	0.000582
5	1100°C	0.001627	0.000057	0.012996	0.000069	0.001234	0.000058	0.037870	0.000070	0.739487	0.000447
6	1150°C	0.001628	0.000055	0.028423	0.000083	0.001938	0.000060	0.059159	0.000099	0.930387	0.000810
7	1190°C	0.003255	0.000055	0.112765	0.000174	0.006466	0.000063	0.135845	0.000199	2.054440	0.002806
8	1210°C	0.010365	0.000047	0.789471	0.000715	0.056167	0.000079	1.015773	0.000826	11.288910	0.010047
9	1217°C	0.004774	0.000053	0.424371	0.000436	0.035885	0.000066	0.619454	0.000567	6.473161	0.006550
10	1224°C	0.003851	0.000053	0.356786	0.000342	0.033528	0.000068	0.562862	0.000514	5.765116	0.004539
11	1233°C	0.003379	0.000055	0.332254	0.000533	0.033739	0.000082	0.558509	0.000881	5.632044	0.009900
12	1243°C	0.003580	0.000058	0.372612	0.000384	0.041441	0.000083	0.674149	0.000539	6.681895	0.006216
13	1252°C	0.001885	0.000051	0.198320	0.000245	0.023847	0.000070	0.382162	0.000438	3.765279	0.004906
14	1262°C	0.001281	0.000050	0.134217	0.000125	0.016635	0.000065	0.266727	0.000185	2.621623	0.001477
15	1279°C	0.001098	0.000057	0.116177	0.000300	0.014018	0.000079	0.224989	0.000507	2.207544	0.005143
16	1295°C	0.000956	0.000053	0.099854	0.000136	0.009672	0.000065	0.165063	0.000183	1.642194	0.001632
17	1310°C	0.001188	0.000062	0.136445	0.000180	0.011534	0.000065	0.206105	0.000233	2.038388	0.002302
18	1320°C	0.001375	0.000051	0.169067	0.000182	0.014249	0.000061	0.252784	0.000230	2.467190	0.002267
19	1330°C	0.001462	0.000053	0.191313	0.000186	0.016920	0.000067	0.293025	0.000236	2.833344	0.002232
20	1340°C	0.001486	0.000056	0.190515	0.000202	0.018112	0.000062	0.302876	0.000281	2.929481	0.003117
21	1350°C	0.001353	0.000059	0.166088	0.000217	0.016945	0.000063	0.276332	0.000305	2.695959	0.002975
22	1360°C	0.001315	0.000050	0.147125	0.000203	0.015836	0.000063	0.255381	0.000352	2.521944	0.003684
23	1372°C	0.001110	0.000050	0.111177	0.000283	0.012672	0.000067	0.200790	0.000488	2.017634	0.005031
24	1400°C	0.001094	0.000057	0.090046	0.000136	0.010678	0.000056	0.168143	0.000219	1.742219	0.002237
25	1500°C	0.000728	0.000072	0.058604	0.000087	0.006601	0.000069	0.103764	0.000105	1.086336	0.000733

Sample:	**MAL_7_2**				
Project:	Alaska	Irradiation:	FGA014P6H4 (End date: 2013-07-31 15:39:00.0)	Interfering isotope production ratios:	Decay constants:
Owner:	Falkowski_Enkelmann	Measurement Date:	2013-12-22 13:56:01.0		
		Device:	HTC	ca3637 = 0.000205 +/- 0.000012	lambda40 = 5.5492e-010 +/- 9.3000e-013 1/a
		Air:	298.6	ca3937 = 0.000932 +/- 0.000035	lambda39 = 0.002577 +/- 0.000026 1/a
Exp-Nr:	**5776.00**	**J-Value:**	**0.0032477** f-value: 0.995004	k3839 = 0.01211 +/- 0.00061	lambda37 = 7.2438 +/- 0.0214 1/a
Material:	98.30 mg Hbl	**J-Value Error:**	**0.0000090** f-value Error: 0.000176	k4039 = 0.00183 +/- 0.00009	
		Reference Standard(s): FCT01 - 28.305 +/- 0.036 Ma,			
		Total gas age: 62.42 +/- 0.18 Ma			**Fit model: linear** All errors are 1s!

Nr.	Step	39Ar(K) (V)	39Ar(K) (%)	39Ar (10e-14 mol)	40Ar* (V)	36Ar_atm (V)	40Ar* (%)	40Ar/36Ar	37Ar/36Ar	37Ar/39Ar	K/Ca	K/Ca Error	40Ar*/39Ar(K)	40Ar*/39Ar(K) Error	Age (Ma)	Age Error(Ma)
1.00	950°C	0.0274	0.9	0.92	1.095	0.0388	8.6	326.1	0.68	0.945	0.031	0.000	40.00	1.35	220.11	7.01
2.00	1000°C	0.0188	0.6	0.63	0.190	0.0090	6.6	318.5	0.95	0.458	0.065	0.001	10.09	0.76	58.13	4.30
3.00	1050°C	0.0275	0.9	0.93	0.166	0.0069	7.4	320.3	1.90	0.481	0.062	0.001	6.04	0.68	34.99	3.90
4.00	1100°C	0.0534	1.8	1.80	0.372	0.0058	17.7	355.2	6.01	0.659	0.045	0.000	6.97	0.36	40.32	2.08
5.00	1140°C	0.2137	7.0	7.21	2.223	0.0091	45.1	507.7	18.68	0.838	0.035	0.000	10.40	0.10	59.87	0.61
6.00	1160°C	0.4267	14.0	14.39	4.625	0.0091	62.9	720.0	29.59	0.701	0.042	0.000	10.84	0.08	62.35	0.48
7.00	1170°C	0.4365	14.3	14.72	4.609	0.0069	69.2	855.1	32.88	0.582	0.051	0.000	10.56	0.07	60.76	0.42
8.00	1180°C	0.3785	12.4	12.76	3.915	0.0052	71.8	927.7	34.49	0.532	0.056	0.000	10.34	0.07	59.54	0.42
9.00	1190°C	0.3056	10.0	10.31	3.127	0.0040	72.3	944.5	34.67	0.516	0.058	0.000	10.23	0.06	58.90	0.39
10.00	1203°C	0.2584	8.5	8.71	2.623	0.0033	72.5	947.4	35.68	0.524	0.057	0.000	10.15	0.07	58.46	0.44
11.00	1226°C	0.2605	8.5	8.78	2.580	0.0032	72.9	949.0	38.88	0.552	0.054	0.000	9.91	0.07	57.06	0.46
12.00	1255°C	0.1937	6.3	6.53	1.827	0.0023	72.6	931.5	40.45	0.560	0.053	0.000	9.43	0.09	54.37	0.57
13.00	1285°C	0.1013	3.3	3.42	0.952	0.0019	62.4	709.7	29.82	0.627	0.047	0.000	9.40	0.15	54.19	0.86
14.00	1305°C	0.0671	2.2	2.26	0.723	0.0024	50.2	555.9	20.64	0.786	0.038	0.000	10.77	0.20	61.93	1.16
15.00	1325°C	0.0834	2.7	2.81	1.047	0.0040	46.8	526.2	17.36	0.874	0.034	0.000	12.55	0.19	71.99	1.10
16.00	1335°C	0.0591	1.9	1.99	0.786	0.0031	45.6	516.9	16.42	0.914	0.032	0.000	13.30	0.27	76.18	1.53
17.00	1345°C	0.0723	2.4	2.44	1.092	0.0049	43.0	494.9	15.47	1.081	0.027	0.000	15.11	0.22	86.35	1.25
18.00	1360°C	0.0399	1.3	1.35	0.693	0.0039	37.5	456.6	12.48	1.242	0.024	0.000	17.37	0.32	98.90	1.82
19.00	1390°C	0.0226	0.7	0.76	0.433	0.0025	36.6	451.3	11.94	1.354	0.022	0.000	19.16	0.70	108.77	3.88
20.00	1430°C	0.0049	0.2	0.17	0.085	0.0009	24.3	384.7	7.11	1.288	0.023	0.000	17.30	4.00	98.51	22.17

J - value =	0.0032477
J-error [%] =	0.28

Plateau Data				Isochron Data				Inverse Isochron Data			
Nr.	39Ar%	Age (Ma)	Age_err (Ma)	39/36	err	40/36	err	39/40	err	36/40	err
								0.000000	0.000010	0.003384	0.000010
1	0.9	220.11	7.01	0.706	0.003	326.84	1.01	0.002160	0.000007	0.003060	0.000009
2	0.6	58.13	4.30	2.076	0.013	319.56	1.68	0.006497	0.000024	0.003129	0.000016
3	0.9	34.99	3.90	3.952	0.037	322.46	2.88	0.012257	0.000054	0.003101	0.000028
4	1.8	40.32	2.08	9.240	0.104	362.98	4.05	0.025456	0.000078	0.002755	0.000031
5	7.0	59.87	0.61	23.579	0.177	543.86	4.05	0.043354	0.000109	0.001839	0.000014
6	14.0	62.35	0.48	46.708	0.466	804.89	8.03	0.058030	0.000191	0.001242	0.000012
7	14.3	60.76	0.42	63.449	0.788	968.49	12.03	0.065513	0.000148	0.001033	0.000013
8	12.4	59.54	0.42	73.393	1.132	1057.70	16.31	0.069390	0.000125	0.000945	0.000015
9	10.0	58.90	0.39	76.154	1.128	1077.62	15.95	0.070669	0.000099	0.000928	0.000014
10	8.5	58.46	0.44	77.492	1.341	1085.40	18.77	0.071395	0.000126	0.000921	0.000016
11	8.5	57.06	0.46	81.071	1.580	1101.63	21.46	0.073592	0.000112	0.000908	0.000018
12	6.3	54.37	0.57	83.734	2.197	1088.30	28.55	0.076941	0.000110	0.000919	0.000024
13	3.3	54.19	0.86	52.707	1.371	794.06	20.64	0.066377	0.000098	0.001259	0.000033
14	2.2	61.93	1.16	27.996	0.527	600.01	11.26	0.046659	0.000107	0.001667	0.000031
15	2.7	71.99	1.10	20.894	0.278	560.83	7.44	0.037256	0.000061	0.001783	0.000024
16	1.9	76.18	1.53	18.832	0.317	548.99	9.20	0.034303	0.000083	0.001822	0.000031
17	2.4	86.35	1.25	14.901	0.161	523.80	5.62	0.028447	0.000052	0.001909	0.000020
18	1.3	98.90	1.82	10.319	0.116	477.85	5.30	0.021595	0.000048	0.002093	0.000023
19	0.7	108.77	3.88	9.015	0.192	471.30	9.93	0.019127	0.000058	0.002122	0.000045
20	0.2	98.51	22.17	5.555	0.419	394.70	29.33	0.014073	0.000184	0.002534	0.000188

Blank intercepts:

exp.#	Step	36Ar (V)	±σ36 (V)	37Ar (V)	±σ37 (V)	38Ar (V)	±σ38 (V)	39Ar (V)	±σ39 (V)	40Ar (V)	±σ40 (V)
5775	(1450°C)	-0.004508	0.000044	-0.002248	0.000061	-0.002469	0.000051	0.030613	0.000049	0.014226	0.000115
5774	(1200°C)	-0.004550	0.000045	-0.002249	0.000051	-0.002499	0.000045	0.030560	0.000056	0.011294	0.000118
5773	(950°C)	-0.004544	0.000041	-0.002241	0.000055	-0.002468	0.000042	0.030530	0.000046	0.011536	0.000124

Blank corrected intensity intercepts:

Nr.	Step	36Ar (V)	±σ36 (V)	37Ar (V)	±σ37 (V)	38Ar (V)	±σ38 (V)	39Ar (V)	±σ39 (V)	40Ar (V)	±σ40 (V)
1	950°C	0.038107	0.000096	0.025852	0.000090	0.025356	0.000071	0.027634	0.000076	12.674560	0.020653
2	1000°C	0.008899	0.000045	0.008520	0.000049	0.010329	0.000059	0.018808	0.000064	2.890970	0.003347
3	1050°C	0.006857	0.000058	0.013105	0.000067	0.016781	0.000069	0.027506	0.000102	2.240110	0.005239
4	1100°C	0.005792	0.000062	0.034998	0.000092	0.043009	0.000107	0.053674	0.000127	2.098699	0.003879
5	1140°C	0.009521	0.000051	0.178728	0.000316	0.324268	0.000558	0.215378	0.000390	4.930477	0.008068
6	1160°C	0.010011	0.000058	0.297684	0.000618	0.736407	0.001654	0.428963	0.000957	7.353125	0.017236
7	1170°C	0.007640	0.000063	0.252413	0.000358	0.745592	0.001120	0.438010	0.000653	6.663653	0.010872
8	1180°C	0.005765	0.000065	0.199812	0.000236	0.615645	0.000750	0.379523	0.000472	5.455808	0.006731
9	1190°C	0.004490	0.000047	0.156417	0.000169	0.455670	0.000440	0.306370	0.000281	4.325643	0.004229
10	1203°C	0.003745	0.000048	0.134288	0.000175	0.326132	0.000367	0.259014	0.000325	3.619359	0.004245
11	1226°C	0.003657	0.000053	0.142890	0.000151	0.227735	0.000225	0.261259	0.000275	3.540087	0.003601
12	1255°C	0.002650	0.000055	0.107740	0.000129	0.130360	0.000128	0.194327	0.000187	2.518237	0.002418
13	1285°C	0.002109	0.000048	0.063185	0.000098	0.096070	0.000105	0.101746	0.000113	1.526641	0.001289
14	1305°C	0.002537	0.000042	0.052618	0.000094	0.076272	0.000116	0.067572	0.000122	1.438528	0.001862
15	1325°C	0.004174	0.000049	0.072799	0.000095	0.102757	0.000126	0.084138	0.000106	2.240007	0.001911
16	1335°C	0.003268	0.000050	0.053935	0.000133	0.072306	0.000134	0.059631	0.000112	1.723072	0.002366
17	1345°C	0.005032	0.000048	0.078233	0.000102	0.075187	0.000085	0.073116	0.000102	2.540652	0.002297
18	1360°C	0.003969	0.000040	0.049781	0.000092	0.036412	0.000081	0.040494	0.000077	1.848669	0.001297
19	1390°C	0.002565	0.000051	0.030773	0.000067	0.020669	0.000058	0.022946	0.000063	1.180472	0.000874
20	1430°C	0.000891	0.000065	0.006369	0.000063	0.004718	0.000047	0.004996	0.000063	0.349677	0.000413

Sample:	**MAL_7_3**				
Project:	Alaska	Irradiation:	FGA014P6H6 (End date: 2013-07-31 15:39:00.0)	Interfering isotope production ratios:	Decay constants:
Owner:	Falkowski_Enkelmann	Measurement Date:	2014-01-03 21:58:24.0		
		Device:	HTC	ca3637 = 0.000205 +/- 0.000012	lambda40 = 5.5492e-010 +/- 9.3000e-013 1/a
		Air:	298.6	ca3937 = 0.000932 +/- 0.000035	lambda39 = 0.002577 +/- 0.000026 1/a

Blank intercepts:

exp.#	Step	36Ar (V)	±σ36 (V)	37Ar (V)	±σ37 (V)	38Ar (V)	±σ38 (V)	39Ar (V)	±σ39 (V)	40Ar (V)	±σ40 (V)
5784	(1450°C)	-0.004502	0.000058	-0.002230	0.000063	-0.002472	0.000051	0.030590	0.000067	0.010448	0.000174

J - value =	0.0032477

03PH305A

Procedure Blanks		36Ar	1s	37Ar	1s	38Ar	1s	39Ar	1s	40Ar	1s
LU1367-001	600 °C	11.447247	1.144725	2.604866	3.224383	3.179280	1.276585	2.028167	1.718632	3427.863534	342.786353
LU1367-002	660 °C	11.356683	1.135668	2.604866	3.224383	2.799928	1.276585	0.238958	1.718632	3224.618678	322.461868
LU1367-003	710 °C	11.404452	1.140445	2.604866	3.224383	2.570960	1.276585	0.238958	1.718632	3123.099693	312.309969
LU1367-004	780 °C	11.659548	1.165955	2.604866	3.224383	2.383521	1.276585	0.238958	1.718632	3084.601206	308.460121
LU1367-005	860 °C	12.219972	1.221997	2.604866	3.224383	2.359469	1.276585	0.238958	1.718632	3188.643069	318.864307
LU1367-006	950 °C	13.193277	1.319328	2.604866	3.224383	2.574872	1.276585	0.238958	1.718632	3494.441335	349.444134
LU1367-007	1010 °C	14.043811	1.404381	2.604866	3.224383	2.861098	1.276585	0.238958	1.718632	3809.336946	380.933695
LU1367-008	1060 °C	14.875828	1.487583	2.604866	3.224383	3.186778	1.276585	0.117525	1.718632	4139.601683	413.960168
LU1367-009	1100 °C	15.622108	1.562211	2.604866	3.224383	3.504372	1.276585	1.234712	1.718632	4448.225512	444.822551
LU1367-010	1130 °C	16.228872	1.622887	2.604866	3.224383	3.775846	1.276585	2.207351	1.718632	4705.600407	470.560041
LU1367-011	1160 °C	16.875970	1.687597	2.604866	3.224383	4.075845	1.276585	3.295490	1.718632	4985.181323	498.518132
LU1367-012	1200 °C	17.801506	1.780151	2.604866	3.224383	4.520215	1.276585	4.926008	1.718632	5392.498574	539.249857
LU1367-013	1300 °C	20.429046	2.042905	2.604866	3.224383	5.853001	1.276585	9.900634	1.718632	6583.505192	658.350519

Intercept Values		36Ar	1s	r2		37Ar	1s	r2		38Ar	1s	r2		39Ar	1s	r2		40Ar	1s	r2	
LU1367-001	600 °C	650.508507	4.344492	0.7779	LIN #	0.103977	0.674438	0.8403	EXP # 2 6	475.255042	12.329988	0.2269	LIN #	6266.211065	27.858585	0.8306	EXP #	242601.424389	140.603240	0.9968	EXP #
LU1367-002	660 °C	459.638926	4.029993	0.7383	LIN #	0.480381	4.106693	0.1134	LIN #	1398.926899	19.407704	0.5182	LIN #	32228.663352	59.545800	0.9801	EXP #	566906.467479	354.739388	0.9972	EXP #
LU1367-003	710 °C	247.412705	5.377707	0.0000	LIN #	9.381276	5.649539		AVE #	2272.589021	12.373932	0.8053	LIN #	55052.668939	94.879914	0.9847	EXP #	822464.328359	231.863069	0.9995	EXP #
LU1367-004	780 °C	178.119537	0.552107	0.2475	LIN # 6	0.220654	3.175236	0.0373	LIN #	2163.494633	18.542797	0.8112	LIN #	51658.583989	54.972161	0.9948	EXP #	751824.052447	258.315774	0.9993	EXP #
LU1367-005	860 °C	194.507970	4.020236	0.2535	LIN #	0.250002	1.767773		AVE # 5 6 7	1296.798438	14.987061	0.4742	LIN #	33022.183271	39.198611	0.9918	EXP #	490075.778833	219.380126	0.9987	EXP #
LU1367-006	950 °C	83.932714	1.715972	0.0005	LIN #	0.994925	2.477610	0.2629	LIN # 2	676.066225	5.876095	0.8142	LIN #	16524.072698	55.912564	0.9382	EXP #	253739.266959	127.354602	0.9983	EXP #
LU1367-007	1010 °C	126.440186	2.885390	0.0025	LIN #	9.293779	4.448966		AVE #	1952.906814	16.549006	0.6792	LIN #	47846.843249	29.730627	0.9979	EXP #	695689.698681	327.866422	0.9985	EXP #
LU1367-008	1060 °C	81.332138	2.294403	0.0102	LIN #	0.836217	1.749283	0.6415	LIN # 1 4	1134.838110	10.101854	0.7152	LIN #	27490.603699	36.025520	0.9906	EXP #	396373.125179	247.338926	0.9973	EXP #
LU1367-009	1100 °C	44.548665	1.641915	0.4252	LIN #	1.950535	3.313174	0.3548	LIN # 7 8	656.307560	6.152251	0.4385	LIN #	16250.233490	39.369670	0.9647	EXP #	232883.743767	171.561547	0.9963	EXP #
LU1367-010	1130 °C	180.842491	1.872117	0.4750	LIN #	3.822589	2.726108	0.5723	LIN # 2	1702.421780	20.494402	0.6678	LIN #	40581.006106	118.365642	0.9589	EXP #	601872.877538	240.639191	0.9989	EXP #
LU1367-011	1160 °C	93.666037	2.739810	0.1252	LIN #	1.293328	8.451122	0.2306	LIN # 1 2 3 5	979.518164	18.428020	0.5074	LIN #	23812.389791	79.352881	0.9285	EXP #	337305.831442	308.521309	0.9934	EXP #
LU1367-012	1200 °C	82.113644	1.980760	0.0054	LIN #	4.732686	1.594257	0.6838	LIN #	910.276823	10.400207	0.1050	LIN #	23527.037243	34.401665	0.9859	EXP #	329754.905493	265.206461	0.9952	EXP #
LU1367-013	1300 °C	89.933162	4.476200	0.0111	LIN #	1.963403	2.843051	0.0605	LIN #	1098.104677	19.451864	0.4532	LIN #	27505.928960	73.383920	0.9572	EXP #	397003.551322	198.462789	0.9982	EXP #

Sample Parameters		Sample	Material	Location	Analyst	Temp	Standard (in Ma)	%1s	J	%1s	MDF	%1s	Volume Ratio	Sensitivity (mol/vol)	Day	Month	Year	Hour	Min	Resi	Irradiation	Project	Standard Name
LU1367-001	600 °C	03PH305A	Biotite	03PH305A biotite, Alaska (Enkelmann-Spotila), I47, pkt B) 10m gettering	Zeitler	600	98.79	0.55	0.001915	0.5	1.000564	0.18	23.4192	1.154E-19	09	02	2009	13	33	001	I47	Alaska Micas 09	GA-1550
LU1367-002	660 °C	03PH305A	Biotite	03PH305A biotite, Alaska (Enkelmann-Spotila), I47, pkt B) 10m gettering	Zeitler	660	98.79	0.55	0.001915	0.5	1.000564	0.18	4.3497	1.154E-19	09	02	2009	15	16	001	I47	Alaska Micas 09	GA-1550
LU1367-003	710 °C	03PH305A	Biotite	03PH305A biotite, Alaska (Enkelmann-Spotila), I47, pkt B) 10m gettering	Zeitler	710	98.79	0.55	0.001915	0.5	1.000564	0.18	4.3497	1.154E-19	09	02	2009	15	56	001	I47	Alaska Micas 09	GA-1550
LU1367-004	780 °C	03PH305A	Biotite	03PH305A biotite, Alaska (Enkelmann-Spotila), I47, pkt B) 10m gettering	Zeitler	780	98.79	0.55	0.001915	0.5	1.000564	0.18	4.3497	1.154E-19	09	02	2009	16	35	001	I47	Alaska Micas 09	GA-1550
LU1367-005	860 °C	03PH305A	Biotite	03PH305A biotite, Alaska (Enkelmann-Spotila), I47, pkt B) 10m gettering	Zeitler	860	98.79	0.55	0.001915	0.5	1.000564	0.18	4.3497	1.154E-19	09	02	2009	17	14	001	I47	Alaska Micas 09	GA-1550
LU1367-006	950 °C	03PH305A	Biotite	03PH305A biotite, Alaska (Enkelmann-Spotila), I47, pkt B) 10m gettering	Zeitler	950	98.79	0.55	0.001915	0.5	1.000564	0.18	23.4192	1.154E-19	09	02	2009	17	49	001	I47	Alaska Micas 09	GA-1550
LU1367-007	1010 °C	03PH305A	Biotite	03PH305A biotite, Alaska (Enkelmann-Spotila), I47, pkt B) 10m gettering	Zeitler	1010	98.79	0.55	0.001915	0.5	1.000564	0.18	4.3497	1.154E-19	09	02	2009	18	28	001	I47	Alaska Micas 09	GA-1550
LU1367-008	1060 °C	03PH305A	Biotite	03PH305A biotite, Alaska (Enkelmann-Spotila), I47, pkt B) 10m gettering	Zeitler	1060	98.79	0.55	0.001915	0.5	1.000564	0.18	4.3497	1.154E-19	09	02	2009	19	07	001	I47	Alaska Micas 09	GA-1550
LU1367-009	1100 °C	03PH305A	Biotite	03PH305A biotite, Alaska (Enkelmann-Spotila), I47, pkt B) 10m gettering	Zeitler	1100	98.79	0.55	0.001915	0.5	1.000564	0.18	4.3497	1.154E-19	09	02	2009	19	47	001	I47	Alaska Micas 09	GA-1550
LU1367-010	1130 °C	03PH305A	Biotite	03PH305A biotite, Alaska (Enkelmann-Spotila), I47, pkt B) 10m gettering	Zeitler	1130	98.79	0.55	0.001915	0.5	1.000564	0.18	1	1.154E-19	09	02	2009	20	21	001	I47	Alaska Micas 09	GA-1550
LU1367-011	1160 °C	03PH305A	Biotite	03PH305A biotite, Alaska (Enkelmann-Spotila), I47, pkt B) 10m gettering	Zeitler	1160	98.79	0.55	0.001915	0.5	1.000564	0.18	1	1.154E-19	09	02	2009	20	56	001	I47	Alaska Micas 09	GA-1550
LU1367-012	1200 °C	03PH305A	Biotite	03PH305A biotite, Alaska (Enkelmann-Spotila), I47, pkt B) 10m gettering	Zeitler	1200	98.79	0.55	0.001915	0.5	1.000564	0.18	1	1.154E-19	09	02	2009	21	31	001	I47	Alaska Micas 09	GA-1550
LU1367-013	1300 °C	03PH305A	Biotite	03PH305A biotite, Alaska (Enkelmann-Spotila), I47, pkt B) 10m gettering	Zeitler	1300	98.79	0.55	0.001915	0.5	1.000564	0.18	1	1.154E-19	09	02	2009	22	06	001	I47	Alaska Micas 09	GA-1550

Irradiation Constants		40/36(a)	%1s	40/36(c)	%1s	38/36(a)	%1s	38/36(c)	%1s	39/37(ca)	%1s	38/37(ca)	%1s	36/37(ca)	%1s	40/39(k)	%1s	38/39(k)	%1s	36/38(cl)	%1s	K/Ca	%1s	K/Cl	%1s	Ca/Cl	%1s
LU1367-001	600 °C	295.5	0	0.018	35	0.1869	0	1.493	3	0.0006959	4.8	0.00028	9.1	0.000264	0	0.0258	3	0.01138	0	0	0	0.43	0	0	0	0	0
LU1367-002	660 °C	295.5	0	0.018	35	0.1869	0	1.493	3	0.0006959	4.8	0.00028	9.1	0.000264	0	0.0258	3	0.01138	0	0	0	0.43	0	0	0	0	0
LU1367-003	710 °C	295.5	0	0.018	35	0.1869	0	1.493	3	0.0006959	4.8	0.00028	9.1	0.000264	0	0.0258	3	0.01138	0	0	0	0.43	0	0	0	0	0
LU1367-004	780 °C	295.5	0	0.018	35	0.1869	0	1.493	3	0.0006959	4.8	0.00028	9.1	0.000264	0	0.0258	3	0.01138	0	0	0	0.43	0	0	0	0	0
LU1367-005	860 °C	295.5	0	0.018	35	0.1869	0	1.493	3	0.0006959	4.8	0.00028	9.1	0.000264	0	0.0258	3	0.01138	0	0	0	0.43	0	0	0	0	0
LU1367-006	950 °C	295.5	0	0.018	35	0.1869	0	1.493	3	0.0006959	4.8	0.00028	9.1	0.000264	0	0.0258	3	0.01138	0	0	0	0.43	0	0	0	0	0
LU1367-007	1010 °C	295.5	0	0.018	35	0.1869	0	1.493	3	0.0006959	4.8	0.00028	9.1	0.000264	0	0.0258	3	0.01138	0	0	0	0.43	0	0	0	0	0
LU1367-008	1060 °C	295.5	0	0.018	35	0.1869	0	1.493	3	0.0006959	4.8	0.00028	9.1	0.000264	0	0.0258	3	0.01138	0	0	0	0.43	0	0	0	0	0
LU1367-009	1100 °C	295.5	0	0.018	35	0.1869	0	1.493	3	0.0006959	4.8	0.00028	9.1	0.000264	0	0.0258	3	0.01138	0	0	0	0.43	0	0	0	0	0
LU1367-010	1130 °C	295.5	0	0.018	35	0.1869	0	1.493	3	0.0006959	4.8	0.00028	9.1	0.000264	0	0.0258	3	0.01138	0	0	0	0.43	0	0	0	0	0
LU1367-011	1160 °C	295.5	0	0.018	35	0.1869	0	1.493	3	0.0006959	4.8	0.00028	9.1	0.000264	0	0.0258	3	0.01138	0	0	0	0.43	0	0	0	0	0
LU1367-012	1200 °C	295.5	0	0.018	35	0.1869	0	1.493	3	0.0006959	4.8	0.00028	9.1	0.000264	0	0.0258	3	0.01138	0	0	0	0.43	0	0	0	0	0
LU1367-013	1300 °C	295.5	0	0.018	35	0.1869	0	1.493	3	0.0006959	4.8	0.00028	9.1	0.000264	0	0.0258	3	0.01138	0	0	0	0.43	0	0	0	0	0

Incremental Heating			36Ar(a)	37Ar(ca)	38Ar(cl)	39Ar(k)	40Ar(r)	Age ± 2s (Ma)	40Ar(r) (%)	39Ar(k) (%)	K/Ca ± 2s
LU1367-001	600 °C		15188.675930	0.000000	6596.671584	147534.400353	1186043.289715	27.56 ± 2.05	20.89	8.17	
LU1367-002	660 °C		1983.460069	0.000000	4100.694124	140936.441223	1872899.832402	45.34 ± 0.40	76.05	7.81	
LU1367-003	710 °C	4	1062.359816	38.136342	6933.115289	240746.359971	3254211.407636	46.11 ± 0.31	91.04	13.34	2714.496 ± 3522.437
LU1367-004	780 °C	4	761.389306	0.000000	6684.477265	225904.015709	3036305.616120	45.85 ± 0.20	92.94	12.51	
LU1367-005	860 °C	4	831.954455	0.000000	3833.132376	144406.605460	1878925.740349	44.40 ± 0.32	88.27	8.00	
LU1367-006	950 °C	4	1948.043492	20.660523	11020.971257	389055.569234	5353191.713928	46.92 ± 0.42	90.14	21.55	8097.273 ± 45474.604
LU1367-007	1010 °C	4	534.716754	37.756398	6001.083330	209235.269455	2858825.074739	46.60 ± 0.22	94.59	11.59	2382.938 ± 2472.345
LU1367-008	1060 °C	4	338.131477	1.030681	3496.193219	120217.055504	1616945.129422	45.88 ± 0.27	94.01	6.66	50154.539 ± 802906.097
LU1367-009	1100 °C	4	177.748667	5.869446	2006.121409	71061.491416	954168.077256	45.80 ± 0.35	94.61	3.94	5206.018 ± 26152.675
LU1367-010	1130 °C	4	164.242765	1.215666	1201.771218	40796.440203	547580.991865	45.79 ± 0.35	91.70	2.26	14430.336 ± 100072.270
LU1367-011	1160 °C		76.617219	0.000000	687.622748	23936.797256	309062.692571	44.06 ± 0.46	93.00	1.33	
LU1367-012	1200 °C		64.166816	2.124226	623.625295	23648.277499	304790.987364	43.99 ± 0.35	93.97	1.31	4787.042 ± 16184.658
LU1367-013	1300 °C		69.347668	0.000000	763.476712	27643.516078	369214.607558	45.56 ± 0.49	94.57	1.53	
		S	23200.854432	106.793283	53948.955826	1805122.239360	23542165.160924				

Normal Isochron			39(k)/36(a) ± 2s	40(a+r)/36(a) ± 2s	r.i.
LU1367-001	600 °C		9.7 ± 0.2	373.6 ± 7.3	0.8969
LU1367-002	660 °C		71.1 ± 1.7	1239.8 ± 28.3	0.9737
LU1367-003	710 °C	4	226.6 ± 10.5	3358.7 ± 155.5	0.9942
LU1367-004	780 °C	4	296.7 ± 4.9	4283.3 ± 68.6	0.9664
LU1367-005	860 °C	4	173.6 ± 7.7	2553.9 ± 113.5	0.9951
LU1367-006	950 °C	4	199.7 ± 8.8	3043.5 ± 132.8	0.9846
LU1367-007	1010 °C	4	391.3 ± 19.3	5641.9 ± 278.1	0.9968
LU1367-008	1060 °C	4	355.5 ± 21.8	5077.5 ± 311.1	0.9971
LU1367-009	1100 °C	4	399.8 ± 33.4	5663.6 ± 472.0	0.9972
LU1367-010	1130 °C	4	248.4 ± 8.5	3629.5 ± 121.2	0.9781
LU1367-011	1160 °C		312.4 ± 26.7	4329.4 ± 368.5	0.9952
LU1367-012	1200 °C		368.5 ± 31.0	5045.5 ± 424.5	0.9975
LU1367-013	1300 °C		398.6 ± 56.8	5619.6 ± 800.0	0.9987

Inverse Isochron			39(k)/40(a+r) ± 2s	36(a)/40(a+r) ± 2s	r.i.
LU1367-001	600 °C		0.026000 ± 0.000251	0.002677 ± 0.000053	0.0072
LU1367-002	660 °C		0.057314 ± 0.000305	0.000807 ± 0.000018	0.0136
LU1367-003	710 °C	4	0.067471 ± 0.000339	0.000298 ± 0.000014	0.0016
LU1367-004	780 °C	4	0.069268 ± 0.000294	0.000233 ± 0.000004	0.0077
LU1367-005	860 °C	4	0.067963 ± 0.000300	0.000392 ± 0.000017	0.0046
LU1367-006	950 °C	4	0.065621 ± 0.000507	0.000329 ± 0.000014	0.0031
LU1367-007	1010 °C	4	0.069356 ± 0.000273	0.000177 ± 0.000009	0.0050
LU1367-008	1060 °C	4	0.070021 ± 0.000326	0.000197 ± 0.000012	0.0064
LU1367-009	1100 °C	4	0.070589 ± 0.000443	0.000177 ± 0.000015	0.0057
LU1367-010	1130 °C	4	0.068437 ± 0.000485	0.000276 ± 0.000009	0.0133
LU1367-011	1160 °C		0.072163 ± 0.000603	0.000231 ± 0.000020	0.0176
LU1367-012	1200 °C		0.073044 ± 0.000434	0.000198 ± 0.000017	0.0276
LU1367-013	1300 °C		0.070934 ± 0.000521	0.000178 ± 0.000025	0.0119

Information on Analysis

03PH305A
Biotite
03PH305A biotite, Alaska (Enkelmann-Spotil
Zeitler

Project = Alaska Micas 09
Irradiation = I47
J = 0.0019150 ± 0.0000096
GA-1550 = 98.790 ± 0.543 Ma

Results	40(r)/39(k) ± 2s	Age ± 2s (Ma)	MSWD	39Ar(k) (%,n)	K/Ca ± 2s
Error Plateau	13.4692 ± 0.1379 ± 1.02%	45.94 ± 0.65 ± 1.41% External Error ± 0.67 Analytical Error ± 0.46	21.84 2.36 4.6736	79.85 8 Statistical T Ratio Error Magnification	0.001 ± 1.155
Total Fusion Age	13.0419 ± 0.0602 ± 0.46%	44.50 ± 0.48 ± 1.09% External Error ± 0.51 Analytical Error ± 0.20		13	192.356 ± 270.414

Results	40(a)/36(a) ± 2s	40(r)/39(k) ± 2s	Age ± 2s (Ma)	MSWD
No Convergence	213.1099 ± 116.6501 ± 54.74%	13.7341 ± 0.4421 ± 3.22%	46.84 ± 1.56 ± 3.33% External Error ± 1.57 Analytical Error ± 1.49	21.85

Statistics

Statistical F Ratio	2.10	Convergence		0.0006046106
Error Magnification	4.6739	Number of Iterations		100
n	8	Calculated Line		Weighted York-2

Results	40(a)/36(a) ± 2s	40(r)/39(k) ± 2s	Age ± 2s (Ma)	MSV
Error Chron	214.3417 ± 107.7623 ± 50.28%	13.7561 ± 0.4472 ± 3.25%	46.91 ± 1.58 ± 3.36% External Error ± 1.58 Analytical Error ± 1.51	21.83

Statistics				
	Statistical F Ratio	2.10	Convergence	0.0000007777
	Error Magnification	4.6726	Number of Iterations	11
	n	8	Calculated Line	Weighted York-2

Degassing Patterns			36Ar(a)	36Ar(c)	36Ar(ca)	36Ar(cl)	37Ar(ca)	38Ar(a)	38Ar(c)	38Ar(k)	38Ar(ca)	38Ar(cl)	39Ar(k)	39Ar(ca)	40Ar(r)	40Ar(a)	40Ar(c)	40Ar(k)
LU1367-001	600 °C		15188.675930	0.000000	0.000000	0.000000	0.000000	2838.763531	0.000000	1678.941476	0.000000	6596.671584	147534.400353	0.000000	1186043.289715	4488253.737283	0.000000	3806.387529
LU1367-002	660 °C		1983.460069	0.000000	0.000000	0.000000	0.000000	370.708687	0.000000	1603.856701	0.000000	4100.694124	140936.441223	0.000000	1872899.832402	586112.450329	0.000000	3636.160184
LU1367-003	710 °C	4	1062.359816	0.000000	0.010068	0.000000	38.136342	198.555050	0.000000	2739.693576	0.010678	6933.115289	240746.359971	0.026539	3254211.407636	313927.325647	0.000000	6211.256087
LU1367-004	780 °C	4	761.389306	0.000000	0.000000	0.000000	0.000000	142.303661	0.000000	2570.787699	0.000000	6684.477265	225904.015709	0.000000	3036305.616120	224990.539997	0.000000	5828.323605
LU1367-005	860 °C	4	831.954455	0.000000	0.000000	0.000000	0.000000	155.492288	0.000000	1643.347170	0.000000	3833.132376	144406.605460	0.000000	1878925.740349	245842.541350	0.000000	3725.690421
LU1367-006	950 °C	4	1948.043492	0.000000	0.005454	0.000000	20.660523	364.089329	0.000000	4427.452378	0.005785	11020.971257	389055.569234	0.014378	5353191.713928	575646.851817	0.000000	10037.633686
LU1367-007	1010 °C	4	534.716754	0.000000	0.009968	0.000000	37.756398	99.938561	0.000000	2381.097366	0.010572	6001.083330	209235.269455	0.026275	2858825.074739	158008.800718	0.000000	5398.269952
LU1367-008	1060 °C	4	338.131477	0.000000	0.000272	0.000000	1.030681	63.196773	0.000000	1368.070092	0.000289	3496.193219	120217.055504	0.000717	1616945.129422	99917.851454	0.000000	3101.600032
LU1367-009	1100 °C	4	177.748667	0.000000	0.001550	0.000000	5.869446	33.221226	0.000000	808.679772	0.001643	2006.121409	71061.491416	0.004085	954168.077256	52524.731018	0.000000	1833.386479
LU1367-010	1130 °C	4	164.242765	0.000000	0.000321	0.000000	1.215666	30.696973	0.000000	464.263490	0.000340	1201.771218	40796.440203	0.000846	547580.991865	48533.737108	0.000000	1052.548157
LU1367-011	1160 °C		76.617219	0.000000	0.000000	0.000000	0.000000	14.319758	0.000000	272.400753	0.000000	687.622748	23936.797256	0.000000	309062.692571	22640.388179	0.000000	617.569369
LU1367-012	1200 °C		64.166816	0.000000	0.000561	0.000000	2.124226	11.992778	0.000000	269.117398	0.000595	623.625295	23648.277499	0.001478	304790.987364	18961.293995	0.000000	610.125559
LU1367-013	1300 °C		69.347668	0.000000	0.000000	0.000000	0.000000	12.961079	0.000000	314.583213	0.000000	763.476712	27643.516078	0.000000	369214.607558	20492.235858	0.000000	713.202715
		S	23200.854432	0.000000	0.028193	0.000000	106.793283	4336.239693	0.000000	20542.291084	0.029902	53948.955826	1805122.239360	0.074317	23542165.160924	6855852.484753	0.000000	46572.153775
		S				23200.882626	106.793283					78827.516506		1805122.313678				30444589.799452

Additional Parameters			40(r)/39(k)	1s	40(r+a)	1s	40Ar/39Ar	1s	37Ar/39Ar	1s	36Ar/39Ar	1s	37Ar (decay)	39Ar (decay)	40Ar (moles)
LU1367-001	600 °C		8.039097	0.30192	5674297.02700	3312.62869	38.48664	0.18597	0.00000	0.00011	0.10295	0.00112	1.00000000	1.00592846	6.553E-13
LU1367-002	660 °C		13.288968	0.05954	2459012.28273	1580.14201	17.47347	0.04645	0.00000	0.00013	0.01407	0.00016	1.00000000	1.00592897	2.842E-13
LU1367-003	710 °C	4	13.517178	0.04545	3568138.73328	1072.21332	14.84695	0.03727	0.00016	0.00010	0.00441	0.00010	1.00000000	1.00592917	4.125E-13
LU1367-004	780 °C	4	13.440689	0.02968	3261296.15612	1178.27712	14.46245	0.03069	0.00001	0.00006	0.00337	0.00003	1.00000000	1.00592936	3.770E-13
LU1367-005	860 °C	4	13.011356	0.04762	2124768.28170	1012.32474	14.73959	0.03255	0.00001	0.00006	0.00576	0.00013	1.00000000	1.00592955	2.456E-13
LU1367-006	950 °C	4	13.759453	0.06232	5928838.56575	3018.24990	15.26485	0.05902	0.00005	0.00015	0.00501	0.00011	1.00000000	1.00592972	6.853E-13
LU1367-007	1010 °C	4	13.663208	0.03277	3016833.87546	1485.01291	14.44418	0.02841	0.00018	0.00009	0.00256	0.00006	1.00000000	1.00592992	3.488E-13
LU1367-008	1060 °C	4	13.450214	0.04047	1716862.98088	1156.51293	14.30716	0.03328	0.00001	0.00007	0.00281	0.00009	1.00000000	1.00593011	1.985E-13
LU1367-009	1100 °C	4	13.427358	0.05236	1006692.80827	870.51647	14.19230	0.04456	0.00008	0.00021	0.00250	0.00010	1.00000000	1.00593031	1.164E-13
LU1367-010	1130 °C	4	13.422274	0.05177	596114.72897	529.47527	14.63773	0.05183	0.00003	0.00010	0.00403	0.00007	1.00000000	1.00593047	6.891E-14
LU1367-011	1160 °C		12.911614	0.06790	331703.08075	586.56155	13.88325	0.05803	0.00005	0.00038	0.00320	0.00014	1.00000000	1.00593065	3.835E-14
LU1367-012	1200 °C		12.888507	0.05174	323752.28136	601.21702	13.71611	0.04074	0.00009	0.00015	0.00271	0.00011	1.00000000	1.00593082	3.743E-14
LU1367-013	1300 °C		13.356282	0.07247	389706.84342	687.95054	14.12339	0.05184	0.00002	0.00016	0.00251	0.00018	1.00000000	1.00593099	4.505E-14

03PH307A

Procedure Blanks		36Ar	1s	37Ar	1s	38Ar	1s	39Ar	1s	40Ar	1s
LU1368-001	600 °C	11.503445	1.150344	0.000000	3.498678	2.847958	1.216228	0.000000	1.993537	3483.497516	348.349752
LU1368-002	660 °C	11.062095	1.106210	0.000000	3.498678	2.862404	1.216228	0.000000	1.993537	3335.187753	333.518775
LU1368-003	720 °C	10.863082	1.086308	0.000000	3.498678	2.876851	1.216228	0.000000	1.993537	3255.798440	325.579844
LU1368-004	780 °C	10.906404	1.090640	0.000000	3.498678	2.891297	1.216228	0.750016	1.993537	3245.329579	324.532958
LU1368-005	860 °C	11.341134	1.134113	0.000000	3.498678	2.910559	1.216228	1.975769	1.993537	3338.580688	333.858069
LU1368-006	940 °C	12.206683	1.220668	0.000000	3.498678	2.929821	1.216228	3.201522	1.993537	3554.357044	355.435704
LU1368-007	1000 °C	13.138570	1.313857	0.000000	3.498678	2.944268	1.216228	4.120837	1.993537	3796.596504	379.659650
LU1368-008	1050 °C	14.100260	1.410026	0.000000	3.498678	2.956306	1.216228	4.886933	1.993537	4051.110287	405.111029
LU1368-009	1090 °C	14.990780	1.499078	0.000000	3.498678	2.965937	1.216228	5.499810	1.993537	4289.181539	428.918154
LU1368-010	1120 °C	15.729352	1.572935	0.000000	3.498678	2.973161	1.216228	5.959467	1.993537	4487.836776	448.783678
LU1368-011	1160 °C	16.808355	1.680835	0.000000	3.498678	2.982792	1.216228	6.572344	1.993537	4779.512824	477.951282
LU1368-012	1200 °C	17.995063	1.799506	0.000000	3.498678	2.992423	1.216228	7.185220	1.993537	5101.820183	510.182018
LU1368-013	1300 °C	21.433042	2.143304	0.000000	3.498678	3.016500	1.216228	8.717412	1.993537	6041.600569	604.160057

Intercept Values		36Ar	1s	r2		37Ar	1s	r2		38Ar	1s	r2		39Ar	1s	r2		40Ar	1s	r2	
LU1368-001	600 °C	1968.140817	9.959616	0.8586	LIN #	0.000000	2.680407	0.1748	LIN # 1	2733.402650	26.456819	0.7118	LIN #	18191.633812	38.119930	0.9653	EXP #	681354.040167	684.143575	0.9918	EXP #
LU1368-002	660 °C	927.907612	10.809317	0.7509	LIN #	0.000000	3.945164	0.1165	LIN #	2560.845502	17.165074	0.8441	LIN #	28581.720453	42.773044	0.9875	EXP #	582361.202508	414.439578	0.9967	EXP #
LU1368-003	720 °C	152.047448	2.764796	0.3323	LIN # 3	0.000000	3.407976		AVE #	1570.445111	11.777690	0.7591	LIN #	20419.542854	58.438868	0.9611	EXP #	296833.739077	108.616728	0.9991	EXP #
LU1368-004	780 °C	101.905941	3.121019	0.0015	LIN #	0.000000	10.307407	0.3496	LIN # 1 2 3 6	2556.610544	10.761272	0.9442	LIN #	33148.153832	30.470353	0.9959	EXP #	456742.327348	215.163888	0.9987	EXP #
LU1368-005	860 °C	162.043282	2.376839	0.1911	LIN #	0.000000	2.362000	0.3551	LIN #	2218.769081	23.650630	0.5390	LIN #	28397.670470	68.997679	0.9705	EXP #	415842.826643	263.867693	0.9975	EXP #
LU1368-006	940 °C	154.879797	2.939066	0.1583	LIN #	0.000000	6.363357	0.3136	LIN # 1 2 8	2363.165594	25.098523	0.7704	LIN #	29610.415343	38.869047	0.9905	EXP #	431186.713501	199.021430	0.9985	EXP #
LU1368-007	1000 °C	219.448833	3.382091	0.1141	LIN #	0.000000	3.229561	0.1236	LIN #	3324.649595	25.655154	0.5648	LIN #	41637.155683	66.630119	0.9859	EXP #	587737.469999	247.263430	0.9989	EXP #
LU1368-008	1050 °C	86.925219	1.633283	0.0371	LIN #	0.000000	3.710608	0.0000	LIN #	4589.137855	34.671612	0.8193	LIN #	51682.475015	80.161692	0.9856	EXP #	675016.819121	330.407517	0.9985	EXP #
LU1368-009	1090 °C	76.786455	2.914019	0.1046	LIN #	0.000000	2.589767	0.4412	LIN #	5623.320940	27.396087	0.8205	LIN #	65919.939391	128.853558	0.9809	EXP #	849915.855714	372.187524	0.9988	EXP #
LU1368-010	1120 °C	47.602289	2.313861	0.0124	LIN #	0.000000	2.673755	0.2589	LIN # 1	3380.378549	23.341014	0.8515	LIN #	44271.530690	68.057118	0.9892	EXP #	590652.706052	245.734658	0.9989	EXP #
LU1368-011	1160 °C	36.264189	2.253629	0.2751	LIN #	0.000000	4.996367	0.0167	LIN #	3210.707179	26.117061	0.7760	LIN #	41457.065618	56.699211	0.9895	EXP #	574644.586561	189.283957	0.9993	EXP #
LU1368-012	1200 °C	26.512023	1.475216	0.2564	LIN #	0.000000	1.740880	0.0671	LIN # 7 8	2521.023775	21.557283	0.5542	LIN #	31884.435077	62.835372	0.9688	EXP #	464224.039180	414.329680	0.9945	EXP #
LU1368-013	1300 °C	38.727816	0.910620	0.7608	LIN #	0.000000	4.396720	0.0074	LIN # 3 8	2361.539325	12.144895	0.9074	LIN #	30275.023767	80.366552	0.9606	EXP #	436175.469531	254.340107	0.9975	EXP #

Sample Parameters		Sample	Material	Location	Analyst	Tem	Standard (in Ma)	%1s	J	%1s	MDF	%1s	Volume Ratio	Sensitivity (mol/vol)	Day	Mon	Year	Hou	Min	Resi	Irradiation	Project	Standard Name
LU1368-001	600 °C	03PH307A	Biotite	03PH307A biotite, Alaska (Enkelmann-Spotila), I47, pkt C) 10m gettering	Zeitler	600	98.79	0.55	0.001922	0.5	1.000564	0.18	4.3497	1.154E-19	06	02	2009	12	01	001	I47	Alaska Micas 09	GA-1550
LU1368-002	660 °C	03PH307A	Biotite	03PH307A biotite, Alaska (Enkelmann-Spotila), I47, pkt C) 10m gettering	Zeitler	660	98.79	0.55	0.001922	0.5	1.000564	0.18	4.3497	1.154E-19	06	02	2009	12	40	001	I47	Alaska Micas 09	GA-1550
LU1368-003	720 °C	03PH307A	Biotite	03PH307A biotite, Alaska (Enkelmann-Spotila), I47, pkt C) 10m gettering	Zeitler	720	98.79	0.55	0.001922	0.5	1.000564	0.18	23.4192	1.154E-19	06	02	2009	13	15	001	I47	Alaska Micas 09	GA-1550
LU1368-004	780 °C	03PH307A	Biotite	03PH307A biotite, Alaska (Enkelmann-Spotila), I47, pkt C) 10m gettering	Zeitler	780	98.79	0.55	0.001922	0.5	1.000564	0.18	23.4192	1.154E-19	06	02	2009	13	50	001	I47	Alaska Micas 09	GA-1550
LU1368-005	860 °C	03PH307A	Biotite	03PH307A biotite, Alaska (Enkelmann-Spotila), I47, pkt C) 10m gettering	Zeitler	860	98.79	0.55	0.001922	0.5	1.000564	0.18	23.4192	1.154E-19	06	02	2009	14	25	001	I47	Alaska Micas 09	GA-1550
LU1368-006	940 °C	03PH307A	Biotite	03PH307A biotite, Alaska (Enkelmann-Spotila), I47, pkt C) 10m gettering	Zeitler	940	98.79	0.55	0.001922	0.5	1.000564	0.18	23.4192	1.154E-19	06	02	2009	15	00	001	I47	Alaska Micas 09	GA-1550
LU1368-007	1000 °C	03PH307A	Biotite	03PH307A biotite, Alaska (Enkelmann-Spotila), I47, pkt C) 10m gettering	Zeitler	1000	98.79	0.55	0.001922	0.5	1.000564	0.18	23.4192	1.154E-19	06	02	2009	15	35	001	I47	Alaska Micas 09	GA-1550
LU1368-008	1050 °C	03PH307A	Biotite	03PH307A biotite, Alaska (Enkelmann-Spotila), I47, pkt C) 10m gettering	Zeitler	1050	98.79	0.55	0.001922	0.5	1.000564	0.18	23.4192	1.154E-19	06	02	2009	16	09	001	I47	Alaska Micas 09	GA-1550
LU1368-009	1090 °C	03PH307A	Biotite	03PH307A biotite, Alaska (Enkelmann-Spotila), I47, pkt C) 10m gettering	Zeitler	1090	98.79	0.55	0.001922	0.5	1.000564	0.18	23.4192	1.154E-19	06	02	2009	16	44	001	I47	Alaska Micas 09	GA-1550
LU1368-010	1120 °C	03PH307A	Biotite	03PH307A biotite, Alaska (Enkelmann-Spotila), I47, pkt C) 10m gettering	Zeitler	1120	98.79	0.55	0.001922	0.5	1.000564	0.18	23.4192	1.154E-19	06	02	2009	17	19	001	I47	Alaska Micas 09	GA-1550
LU1368-011	1160 °C	03PH307A	Biotite	03PH307A biotite, Alaska (Enkelmann-Spotila), I47, pkt C) 10m gettering	Zeitler	1160	98.79	0.55	0.001922	0.5	1.000564	0.18	23.4192	1.154E-19	06	02	2009	17	54	001	I47	Alaska Micas 09	GA-1550
LU1368-012	1200 °C	03PH307A	Biotite	03PH307A biotite, Alaska (Enkelmann-Spotila), I47, pkt C) 10m gettering	Zeitler	1200	98.79	0.55	0.001922	0.5	1.000564	0.18	23.4192	1.154E-19	06	02	2009	18	28	001	I47	Alaska Micas 09	GA-1550
LU1368-013	1300 °C	03PH307A	Biotite	03PH307A biotite, Alaska (Enkelmann-Spotila), I47, pkt C) 10m gettering	Zeitler	1300	98.79	0.55	0.001922	0.5	1.000564	0.18	4.3497	1.154E-19	06	02	2009	19	08	001	I47	Alaska Micas 09	GA-1550

Irradiation Constants		40/36(a)	%1s	40/36(c)	%1s	38/36(a)	%1s	38/36(c)	%1s	39/37(ca)	%1s	38/37(ca)	%1s	36/37(ca)	%1s	40/39(k)	%1s	38/39(k)	%1s	36/38(cl)	%1s	K/Ca	%1s	K/Cl	%1s	Ca/Cl	%1s
LU1368-001	600 °C	295.5	0	0.018	35	0.1869	0	1.493	3	0.0006959	4.8	0.00028	9.1	0.000264	0	0.0258	3	0.01138	0	0	0	0.43	0	0	0	0	0
LU1368-002	660 °C	295.5	0	0.018	35	0.1869	0	1.493	3	0.0006959	4.8	0.00028	9.1	0.000264	0	0.0258	3	0.01138	0	0	0	0.43	0	0	0	0	0
LU1368-003	720 °C	295.5	0	0.018	35	0.1869	0	1.493	3	0.0006959	4.8	0.00028	9.1	0.000264	0	0.0258	3	0.01138	0	0	0	0.43	0	0	0	0	0
LU1368-004	780 °C	295.5	0	0.018	35	0.1869	0	1.493	3	0.0006959	4.8	0.00028	9.1	0.000264	0	0.0258	3	0.01138	0	0	0	0.43	0	0	0	0	0
LU1368-005	860 °C	295.5	0	0.018	35	0.1869	0	1.493	3	0.0006959	4.8	0.00028	9.1	0.000264	0	0.0258	3	0.01138	0	0	0	0.43	0	0	0	0	0
LU1368-006	940 °C	295.5	0	0.018	35	0.1869	0	1.493	3	0.0006959	4.8	0.00028	9.1	0.000264	0	0.0258	3	0.01138	0	0	0	0.43	0	0	0	0	0
LU1368-007	1000 °C	295.5	0	0.018	35	0.1869	0	1.493	3	0.0006959	4.8	0.00028	9.1	0.000264	0	0.0258	3	0.01138	0	0	0	0.43	0	0	0	0	0
LU1368-008	1050 °C	295.5	0	0.018	35	0.1869	0	1.493	3	0.0006959	4.8	0.00028	9.1	0.000264	0	0.0258	3	0.01138	0	0	0	0.43	0	0	0	0	0
LU1368-009	1090 °C	295.5	0	0.018	35	0.1869	0	1.493	3	0.0006959	4.8	0.00028	9.1	0.000264	0	0.0258	3	0.01138	0	0	0	0.43	0	0	0	0	0
LU1368-010	1120 °C	295.5	0	0.018	35	0.1869	0	1.493	3	0.0006959	4.8	0.00028	9.1	0.000264	0	0.0258	3	0.01138	0	0	0	0.43	0	0	0	0	0

LU1368-011	1160 °C	295.5	0	0.018	35	0.1869	0	1.493	3	0.0006959	4.8	0.00028	9.1	0.000264	0	0.0258	3	0.01138	0	0	0	0.43	0	0	0	0	0
LU1368-012	1200 °C	295.5	0	0.018	35	0.1869	0	1.493	3	0.0006959	4.8	0.00028	9.1	0.000264	0	0.0258	3	0.01138	0	0	0	0.43	0	0	0	0	0
LU1368-013	1300 °C	295.5	0	0.018	35	0.1869	0	1.493	3	0.0006959	4.8	0.00028	9.1	0.000264	0	0.0258	3	0.01138	0	0	0	0.43	0	0	0	0	0

Incremental Heating			36Ar(a)	37Ar(ca)	38Ar(cl)	39Ar(k)	40Ar(r)	Age ± 2s (Ma)	40Ar(r) (%)	39Ar(k) (%)	K/Ca ± 2s
LU1368-001	600 °C		8530.074820	0.000000	9373.682921	79550.670494	437512.654495	18.97 ± 1.93	14.78	0.84	1.02E+103 ± 0.000
LU1368-002	660 °C		4015.997552	0.000000	8950.571898	124985.775539	1339809.425187	36.79 ± 0.91	52.96	1.32	1.61E+103 ± 0.000
LU1368-003	720 °C		3541.975807	0.000000	30601.176515	480763.028780	5889295.366728	41.98 ± 0.40	84.76	5.07	9.24E+102 ± 0.000
LU1368-004	780 °C	4	2370.301797	0.000000	50478.914898	780448.136600	9972734.839975	43.77 ± 0.26	93.26	8.23	1.50E+103 ± 0.000
LU1368-005	860 °C	4	3775.066355	0.000000	43586.110442	668600.383751	8602585.747162	44.07 ± 0.33	88.36	7.05	1.28E+103 ± 0.000
LU1368-006	940 °C	4	3606.817271	0.000000	46670.454934	697152.461568	9010692.486773	44.27 ± 0.29	89.26	7.35	1.34E+103 ± 0.000
LU1368-007	1000 °C	4	5114.638921	0.000000	65658.082124	980312.554286	12223876.895753	42.73 ± 0.27	88.83	10.34	1.88E+103 ± 0.000
LU1368-008	1050 °C	4	2017.068327	0.000000	93125.468572	1216821.760544	15176865.087940	42.74 ± 0.22	96.03	12.83	2.34E+103 ± 0.000
LU1368-009	1090 °C	4	1779.272517	0.000000	113547.658913	1552032.261298	19334242.765601	42.69 ± 0.24	97.16	16.37	2.98E+103 ± 0.000
LU1368-010	1120 °C		1096.604236	0.000000	67006.857655	1042335.690006	13477187.204377	44.29 ± 0.24	97.46	10.99	2.00E+103 ± 0.000
LU1368-011	1160 °C		830.596107	0.000000	63841.570337	976070.664239	13182313.216157	46.23 ± 0.24	97.99	10.29	1.88E+103 ± 0.000
LU1368-012	1200 °C		601.538231	0.000000	50315.576027	750689.361410	10669531.465302	48.62 ± 0.29	98.19	7.92	1.44E+103 ± 0.000
LU1368-013	1300 °C		146.690408	0.000000	8723.477671	132381.954952	1844428.369287	47.67 ± 0.32	97.53	1.40	1.70E+103 ± 0.000
		S	37426.642348	0.000000	651879.602907	9482144.703466	121161075.524737				

Normal Isochron			39(k)/36(a) ± 2s	40(a+r)/36(a) ± 2s	r.i.
LU1368-001	600 °C		9.3 ± 0.2	346.8 ± 6.1	0.9478
LU1368-002	660 °C		31.1 ± 0.9	629.1 ± 17.3	0.9844
LU1368-003	720 °C		135.7 ± 5.4	1958.2 ± 76.8	0.9853
LU1368-004	780 °C	4	329.3 ± 20.9	4502.9 ± 284.6	0.9978
LU1368-005	860 °C	4	177.1 ± 5.9	2574.3 ± 84.4	0.9826
LU1368-006	940 °C	4	193.3 ± 7.9	2793.7 ± 113.8	0.9938
LU1368-007	1000 °C	4	191.7 ± 6.6	2685.5 ± 91.6	0.9898
LU1368-008	1050 °C	4	603.3 ± 24.6	7819.7 ± 316.8	0.9929
LU1368-009	1090 °C	4	872.3 ± 68.1	11161.9 ± 869.5	0.9976
LU1368-010	1120 °C		950.5 ± 94.9	12585.4 ± 1254.7	0.9988
LU1368-011	1160 °C		1175.1 ± 150.1	16166.4 ± 2064.1	0.9994
LU1368-012	1200 °C		1247.9 ± 144.5	18032.6 ± 2085.9	0.9988
LU1368-013	1300 °C		902.5 ± 57.1	12869.1 ± 810.0	0.9946

Inverse Isochron			39(k)/40(a+r) ± 2s	36(a)/40(a+r) ± 2s	r.i.
LU1368-001	600 °C		0.026892 ± 0.000158	0.002884 ± 0.000051	0.0394
LU1368-002	660 °C		0.049469 ± 0.000243	0.001590 ± 0.000044	0.0157
LU1368-003	720 °C		0.069315 ± 0.000472	0.000511 ± 0.000020	0.0021
LU1368-004	780 °C	4	0.073123 ± 0.000304	0.000222 ± 0.000014	0.0035
LU1368-005	860 °C	4	0.068799 ± 0.000425	0.000388 ± 0.000013	0.0081
LU1368-006	940 °C	4	0.069186 ± 0.000315	0.000358 ± 0.000015	0.0047
LU1368-007	1000 °C	4	0.071372 ± 0.000349	0.000372 ± 0.000013	0.0044
LU1368-008	1050 °C	4	0.077146 ± 0.000375	0.000128 ± 0.000005	0.0050
LU1368-009	1090 °C	4	0.078149 ± 0.000421	0.000090 ± 0.000007	0.0019
LU1368-010	1120 °C		0.075525 ± 0.000363	0.000079 ± 0.000008	0.0015
LU1368-011	1160 °C		0.072691 ± 0.000332	0.000062 ± 0.000008	0.0008
LU1368-012	1200 °C		0.069205 ± 0.000390	0.000055 ± 0.000006	0.0049
LU1368-013	1300 °C		0.070126 ± 0.000460	0.000078 ± 0.000005	0.0044

Degassing Patterns			36Ar(a)	36Ar(c)	36Ar(ca)	36Ar(cl)	37Ar(ca)	38Ar(a)	38Ar(c)	38Ar(k)	38Ar(ca)	38Ar(cl)	39Ar(k)	39Ar(ca)	40Ar(r)	40Ar(a)	40Ar(c)	40Ar(k)
LU1368-001	600 °C		8530.074820	0.000000	0.000000	0.000000	0.000000	1594.270984	0.000000	905.286630	0.000000	9373.682921	79550.670494	0.000000	437512.654495	2520637.109206	0.000000	2052.407299
LU1368-002	660 °C		4015.997552	0.000000	0.000000	0.000000	0.000000	750.589942	0.000000	1422.338126	0.000000	8950.571898	124985.775539	0.000000	1339809.425187	1186727.276599	0.000000	3224.633009
LU1368-003	720 °C		3541.975807	0.000000	0.000000	0.000000	0.000000	661.995278	0.000000	5471.083268	0.000000	30601.176515	480763.028780	0.000000	5889295.366728	1046653.850875	0.000000	12403.686143
LU1368-004	780 °C	4	2370.301797	0.000000	0.000000	0.000000	0.000000	443.009406	0.000000	8881.499795	0.000000	50478.914898	780448.136600	0.000000	9972734.839975	700424.181149	0.000000	20135.561924
LU1368-005	860 °C	4	3775.066355	0.000000	0.000000	0.000000	0.000000	705.559902	0.000000	7608.672367	0.000000	43586.110442	668600.383751	0.000000	8602585.747162	1115532.107957	0.000000	17249.889901
LU1368-006	940 °C	4	3606.817271	0.000000	0.000000	0.000000	0.000000	674.114148	0.000000	7933.595013	0.000000	46670.454934	697152.461568	0.000000	9010692.486773	1065814.503508	0.000000	17986.533508
LU1368-007	1000 °C	4	5114.638921	0.000000	0.000000	0.000000	0.000000	955.926014	0.000000	11155.956868	0.000000	65658.082124	980312.554286	0.000000	12223876.895753	1511375.801240	0.000000	25292.063901
LU1368-008	1050 °C	4	2017.068327	0.000000	0.000000	0.000000	0.000000	376.990070	0.000000	13847.431635	0.000000	93125.468572	1216821.760544	0.000000	15176865.087940	596043.690703	0.000000	31394.001422
LU1368-009	1090 °C	4	1779.272517	0.000000	0.000000	0.000000	0.000000	332.546033	0.000000	17662.127134	0.000000	113547.658913	1552032.261298	0.000000	19334242.765601	525775.028662	0.000000	40042.432341
LU1368-010	1120 °C		1096.604236	0.000000	0.000000	0.000000	0.000000	204.955332	0.000000	11861.780152	0.000000	67006.857655	1042335.690006	0.000000	13477187.204377	324046.551621	0.000000	26892.260802
LU1368-011	1160 °C		830.596107	0.000000	0.000000	0.000000	0.000000	155.238412	0.000000	11107.684159	0.000000	63841.570337	976070.664239	0.000000	13182313.216157	245441.149471	0.000000	25182.623137
LU1368-012	1200 °C		601.538231	0.000000	0.000000	0.000000	0.000000	112.427495	0.000000	8542.844933	0.000000	50315.576027	750689.361410	0.000000	10669531.465302	177754.547360	0.000000	19367.785524
LU1368-013	1300 °C		146.690408	0.000000	0.000000	0.000000	0.000000	27.416437	0.000000	1506.506647	0.000000	8723.477671	132381.954952	0.000000	1844428.369287	43347.015528	0.000000	3415.454438
		S	37426.642348	0.000000	0.000000	0.000000	0.000000	6995.039455	0.000000	107906.806725	0.000000	651879.602907	9482144.703466	0.000000	121161075.524737	11059572.813881	0.000000	244639.333349
		S				37426.642348	0.000000					766781.449087		9482144.703466				132465287.671967

Additional Parameters			40(r)/39(k)	1s	40(r+a)	1s	40Ar/39Ar	1s	37Ar/39Ar	1s	36Ar/39Ar	1s	37Ar (decay)	39Ar (decay)	40Ar (moles)
LU1368-001	600 °C		5.499798	0.28164	2958149.76370	2996.77684	37.21153	0.10950	0.00000	0.00015	0.10723	0.00099	1.00000000	1.00590672	3.416E-13
LU1368-002	660 °C		10.719695	0.13346	2526536.70179	1835.84685	20.24039	0.04961	0.00000	0.00014	0.03213	0.00045	1.00000000	1.00590691	2.919E-13
LU1368-003	720 °C		12.249892	0.05972	6935949.21760	2591.66419	14.45276	0.04916	0.00000	0.00017	0.00737	0.00015	1.00000000	1.00590708	8.018E-13
LU1368-004	780 °C	4	12.778216	0.03891	10673159.02112	5085.57329	13.70148	0.02845	0.00000	0.00031	0.00304	0.00010	1.00000000	1.00590725	1.234E-12
LU1368-005	860 °C	4	12.866558	0.04845	9718117.85512	6210.40051	14.56082	0.04500	0.00000	0.00008	0.00565	0.00009	1.00000000	1.00590743	1.123E-12
LU1368-006	940 °C	4	12.924996	0.04294	10076506.99028	4705.66736	14.47961	0.03296	0.00000	0.00021	0.00517	0.00011	1.00000000	1.00590760	1.165E-12
LU1368-007	1000 °C	4	12.469367	0.04036	13735252.69699	5852.85539	14.03690	0.03433	0.00000	0.00008	0.00522	0.00009	1.00000000	1.00590777	1.588E-12
LU1368-008	1050 °C	4	12.472546	0.03191	15772908.77864	7805.86256	12.98818	0.03152	0.00000	0.00007	0.00166	0.00003	1.00000000	1.00590794	1.824E-12
LU1368-009	1090 °C	4	12.457372	0.03609	19860017.79426	8809.81463	12.82194	0.03454	0.00000	0.00004	0.00115	0.00004	1.00000000	1.00590811	2.296E-12
LU1368-010	1120 °C		12.929795	0.03477	13801233.75600	5828.83476	13.26648	0.03190	0.00000	0.00006	0.00105	0.00005	1.00000000	1.00590828	1.596E-12
LU1368-011	1160 °C		13.505491	0.03481	13427754.36563	4522.48201	13.78275	0.03150	0.00000	0.00012	0.00085	0.00005	1.00000000	1.00590846	1.552E-12
LU1368-012	1200 °C		14.212978	0.04237	10847286.01266	9734.16669	14.47557	0.04076	0.00000	0.00005	0.00080	0.00005	1.00000000	1.00590862	1.254E-12
LU1368-013	1300 °C		13.932627	0.04685	1887775.38481	1264.72721	14.28587	0.04681	0.00000	0.00015	0.00111	0.00004	1.00000000	1.00590882	2.182E-13

Information on Analysis

03PH307A
Biotite
03PH307A biotite, Alaska (Enkelmann-Spotil
Zeitler

Project = Alaska Micas 09
Irradiation = I47
J = 0.0019220 ± 0.0000096
GA-1550 = 98.790 ± 0.543 Ma

Results	40(r)/39(k) ± 2s	Age ± 2s (Ma)	MSWD	39Ar(k) (%,n)	K/Ca ± 2s
Error Plateau	12.6232 ± 0.1725 ± 1.37%	43.25 ± 0.72 ± 1.67% External Error ± 0.74 Analytical Error ± 0.58	29.69 2.57 5.4485	62.17 6 Statistical T Ratio Error Magnification	1.89E+103 ± 0.816
Total Fusion Age	12.7778 ± 0.0251 ± 0.20%	43.77 ± 0.44 ± 1.01% External Error ± 0.47 Analytical Error ± 0.09		13	4.61E+101 ± 0.000

Results	40(a)/36(a) ± 2s	40(r)/39(k) ± 2s	Age ± 2s (Ma)	MSWD
No Convergence	366.2205 ± 81.7026 ± 22.31%	12.3683 ± 0.2970 ± 2.40%	42.38 ± 1.09 ± 2.57% External Error ± 1.10 Analytical Error ± 1.01	18.95
Statistics	Statistical F Ratio 2.37 Error Magnification 4.3534 n 6	Convergence 0.0000507150 Number of Iterations 100 Calculated Line Weighted York-2		

Results	40(a)/36(a) ± 2s	40(r)/39(k) ± 2s	Age ± 2s (Ma)	MSWD
Error Chron	374.0257 ± 81.2267 ± 21.72%	12.3676 ± 0.2913 ± 2.36%	42.38 ± 1.07 ± 2.53% External Error ± 1.08 Analytical Error ± 0.99	18.32
Statistics	Statistical F Ratio 2.37 Error Magnification 4.2803 n 6	Convergence 0.0000000427 Number of Iterations 5 Calculated Line Weighted York-2		

03PH3011A

Procedure Blanks		36Ar	1s	37Ar	1s	38Ar	1s	39Ar	1s	40Ar	1s
LU1366-001	600 °C	7.872147	1.028312	0.000000	3.037310	4.664651	1.151422	6.816992	1.410495	3149.861654	314.986165
LU1366-002	660 °C	8.854639	1.028312	0.000000	3.037310	4.528112	1.151422	6.816992	1.410495	3188.013579	318.801358

LU1366-003	710 °C	9.673383	1.028312	0.000000	3.037310	4.414330	1.151422	6.816992	1.410495	3240.683002	324.068300
LU1366-004	780 °C	10.819624	1.081962	0.000000	3.037310	4.255034	1.151422	6.816992	1.410495	3346.303771	334.630377
LU1366-005	860 °C	12.129614	1.212961	0.000000	3.037310	4.072982	1.151422	6.816992	1.410495	3512.561190	351.256119
LU1366-006	950 °C	13.603352	1.360335	0.000000	3.037310	3.868174	1.151422	6.816992	1.410495	3757.674445	375.767445
LU1366-007	1010 °C	14.585844	1.458584	0.000000	3.037310	3.731635	1.151422	6.816992	1.410495	3955.244258	395.524426
LU1366-008	1060 °C	15.404588	1.540459	0.000000	3.037310	3.617852	1.151422	6.816992	1.410495	4140.761921	414.076192
LU1366-009	1100 °C	16.059583	1.605958	0.000000	3.037310	3.526826	1.151422	6.816992	1.410495	4302.840441	430.284044
LU1366-010	1130 °C	16.550829	1.655083	0.000000	3.037310	3.458557	1.151422	6.816992	1.410495	4432.370226	443.237023
LU1366-011	1160 °C	17.042075	1.704208	0.000000	3.037310	3.390287	1.151422	6.816992	1.410495	4568.732206	456.873221
LU1366-012	1200 °C	17.697070	1.769707	0.000000	3.037310	3.299261	1.151422	6.816992	1.410495	4761.176039	476.117604
LU1366-013	1300 °C	19.334557	1.933456	0.000000	3.037310	3.071696	1.151422	6.816992	1.410495	5295.424916	529.542492

Intercept Values		36Ar	1s	r2		37Ar	1s	r2		38Ar	1s	r2		39Ar	1s	r2		40Ar	1s	r2	
LU1366-001	600 °C	2183.370595	15.232432	0.8227	LIN #	0.000000	1.775364	0.5313	LIN #	1196.322441	10.954012	0.6569	LIN #	7423.549117	36.565688	0.8607	EXP #	693099.002555	506.459905	0.9958	EXP #
LU1366-002	660 °C	1653.818120	12.660937	0.8223	LIN #	0.000000	2.374962	0.0324	LIN #	551.125592	13.129091	0.0466	LIN #	12435.215385	42.476452	0.9039	EXP #	607425.307626	315.151157	0.9981	EXP #
LU1366-003	710 °C	1046.859311	11.766660	0.6950	LIN #	0.000000	2.726365	0.1279	LIN #	505.111393	7.146228	0.0540	LIN #	17183.983869	64.651987	0.9252	EXP #	485771.988370	463.869935	0.9942	EXP #
LU1366-004	780 °C	934.677191	5.935757	0.8845	LIN #	0.000000	2.475993	0.0128	LIN #	605.898495	11.932865	0.0278	LIN #	24146.955763	74.604001	0.9469	EXP #	527124.048736	269.731853	0.9982	EXP #
LU1366-005	860 °C	802.817234	3.898289	0.9420	LIN #	0.000000	2.563826	0.1122	LIN #	607.706329	11.310354	0.2941	LIN #	24828.280436	57.366295	0.9645	LIN #	492135.602959	355.006578	0.9965	EXP #
LU1366-006	950 °C	669.019227	6.870727	0.6513	LIN #	0.000000	4.335241	0.0475	LIN #	629.856701	7.426341	0.1677	LIN #	29500.806353	29.573801	0.9933	EXP #	499256.395142	355.701153	0.9966	EXP #
LU1366-007	1010 °C	308.433211	5.633273	0.0131	LIN #	0.000000	3.667440	0.1835	LIN #	518.845072	2.240472	0.0013	LIN # 7 8	27431.093400	38.429271	0.9898	EXP #	376006.752604	244.432895	0.9971	EXP #
LU1366-008	1060 °C	179.619713	5.855544	0.0020	LIN # 3	0.000000	3.404875	0.1028	LIN # 3	462.874037	6.552184	0.0872	LIN # 3	24736.945965	65.961959	0.9588	EXP #	310745.888588	143.276377	0.9985	EXP #
LU1366-009	1100 °C	277.864655	5.933473	0.2419	LIN #	0.000000	3.097959	0.0092	LIN #	457.156861	7.994885	0.2941	LIN #	24516.603481	26.422411	0.9925	EXP #	340758.751708	194.774663	0.9977	EXP #
LU1366-010	1130 °C	280.195976	3.181970	0.6066	LIN #	0.000000	2.821993	0.2036	LIN # 7	394.411714	11.475774	0.4950	LIN #	19176.922159	44.568880	0.9698	EXP #	289826.921003	185.284776	0.9969	EXP #
LU1366-011	1160 °C	368.070407	2.274864	0.8640	LIN #	0.000000	4.970712	0.0027	LIN #	568.944758	6.445359	0.4788	LIN #	29032.049118	49.762060	0.9836	LIN #	426950.150849	152.520701	0.9991	LIN #
LU1366-012	1200 °C	163.150218	1.767357	0.8366	LIN #	0.000000	2.567744	0.0934	LIN #	254.664791	7.737823	0.1531	LIN #	11382.180776	54.938032	0.8800	EXP #	170909.371461	146.015350	0.9936	EXP #
LU1366-013	1300 °C	92.175204	1.759513	0.1172	LIN #	0.000000	2.949932	0.3034	LIN #	109.399313	2.972393	0.0005	LIN #	5685.977384	45.167283	0.8197	LIN #	90316.595308	79.578799	0.9915	LIN #

Sample Parameters		Sample	Material	Location	Analyst	Temp	Standard (in Ma)	%1s	J	%1s	MDF	%1s	Volume Ratio	Sensitivity (mol/vol)	Day	Mont	Year	Hour	Min	Resi	Irradiation	Project	Standard Name
LU1366-001	600 °C	03PH311A	Biotite	03PH311A biotite, Alaska (Enkelmann-Spotila), I47, pkt A) 10m gettering	Zeitler	600	98.79	0.55	0.001915	0.5	1.000564	0.18	4.3497	1.130E-19	10	02	2009	12	30	001	I47	Eva-Alaska Biotites	GA-1550
LU1366-002	660 °C	03PH311A	Biotite	03PH311A biotite, Alaska (Enkelmann-Spotila), I47, pkt A) 10m gettering	Zeitler	660	98.79	0.55	0.001915	0.5	1.000564	0.18	4.3497	1.130E-19	10	02	2009	13	09	001	I47	Eva-Alaska Biotites	GA-1550
LU1366-003	710 °C	03PH311A	Biotite	03PH311A biotite, Alaska (Enkelmann-Spotila), I47, pkt A) 10m gettering	Zeitler	710	98.79	0.55	0.001915	0.5	1.000564	0.18	4.3497	1.130E-19	10	02	2009	13	48	001	I47	Eva-Alaska Biotites	GA-1550
LU1366-004	780 °C	03PH311A	Biotite	03PH311A biotite, Alaska (Enkelmann-Spotila), I47, pkt A) 10m gettering	Zeitler	780	98.79	0.55	0.001915	0.5	1.000564	0.18	4.3497	1.130E-19	10	02	2009	14	28	001	I47	Eva-Alaska Biotites	GA-1550
LU1366-005	860 °C	03PH311A	Biotite	03PH311A biotite, Alaska (Enkelmann-Spotila), I47, pkt A) 10m gettering	Zeitler	860	98.79	0.55	0.001915	0.5	1.000564	0.18	4.3497	1.130E-19	10	02	2009	15	07	001	I47	Eva-Alaska Biotites	GA-1550
LU1366-006	950 °C	03PH311A	Biotite	03PH311A biotite, Alaska (Enkelmann-Spotila), I47, pkt A) 10m gettering	Zeitler	950	98.79	0.55	0.001915	0.5	1.000564	0.18	4.3497	1.130E-19	10	02	2009	15	46	001	I47	Eva-Alaska Biotites	GA-1550
LU1366-007	1010 °C	03PH311A	Biotite	03PH311A biotite, Alaska (Enkelmann-Spotila), I47, pkt A) 10m gettering	Zeitler	1010	98.79	0.55	0.001915	0.5	1.000564	0.18	4.3497	1.130E-19	10	02	2009	16	25	001	I47	Eva-Alaska Biotites	GA-1550
LU1366-008	1060 °C	03PH311A	Biotite	03PH311A biotite, Alaska (Enkelmann-Spotila), I47, pkt A) 10m gettering	Zeitler	1060	98.79	0.55	0.001915	0.5	1.000564	0.18	4.3497	1.130E-19	10	02	2009	17	05	001	I47	Eva-Alaska Biotites	GA-1550
LU1366-009	1100 °C	03PH311A	Biotite	03PH311A biotite, Alaska (Enkelmann-Spotila), I47, pkt A) 10m gettering	Zeitler	1100	98.79	0.55	0.001915	0.5	1.000564	0.18	4.3497	1.130E-19	10	02	2009	17	44	001	I47	Eva-Alaska Biotites	GA-1550
LU1366-010	1130 °C	03PH311A	Biotite	03PH311A biotite, Alaska (Enkelmann-Spotila), I47, pkt A) 10m gettering	Zeitler	1130	98.79	0.55	0.001915	0.5	1.000564	0.18	4.3497	1.130E-19	10	02	2009	18	23	001	I47	Eva-Alaska Biotites	GA-1550
LU1366-011	1160 °C	03PH311A	Biotite	03PH311A biotite, Alaska (Enkelmann-Spotila), I47, pkt A) 10m gettering	Zeitler	1160	98.79	0.55	0.001915	0.5	1.000564	0.18	1	1.130E-19	10	02	2009	18	58	001	I47	Eva-Alaska Biotites	GA-1550
LU1366-012	1200 °C	03PH311A	Biotite	03PH311A biotite, Alaska (Enkelmann-Spotila), I47, pkt A) 10m gettering	Zeitler	1200	98.79	0.55	0.001915	0.5	1.000564	0.18	1	1.130E-19	10	02	2009	19	33	001	I47	Eva-Alaska Biotites	GA-1550
LU1366-013	1300 °C	03PH311A	Biotite	03PH311A biotite, Alaska (Enkelmann-Spotila), I47, pkt A) 10m gettering	Zeitler	1300	98.79	0.55	0.001915	0.5	1.000564	0.18	1	1.130E-19	10	02	2009	20	07	001	I47	Eva-Alaska Biotites	GA-1550

Irradiation Constants		40/36(a)	%1s	40/36(c)	%1s	38/36(a)	%1s	38/36(c)	%1s	39/37(ca)	%1s	38/37(ca)	%1s	36/37(ca)	%1s	40/39(k)	%1s	38/39(k)	%1s	36/38(cl)	%1s	K/Ca	%1s	K/Cl	%1s	Ca/Cl	%1s
LU1366-001	600 °C	295.5	0	0.018	35	0.1869	0	1.493	3	0.0006959	4.8	0.00028	9.1	0.000264	0	0.0258	3	0.01138	0	0	0	0.43	0	0	0	0	0
LU1366-002	660 °C	295.5	0	0.018	35	0.1869	0	1.493	3	0.0006959	4.8	0.00028	9.1	0.000264	0	0.0258	3	0.01138	0	0	0	0.43	0	0	0	0	0
LU1366-003	710 °C	295.5	0	0.018	35	0.1869	0	1.493	3	0.0006959	4.8	0.00028	9.1	0.000264	0	0.0258	3	0.01138	0	0	0	0.43	0	0	0	0	0
LU1366-004	780 °C	295.5	0	0.018	35	0.1869	0	1.493	3	0.0006959	4.8	0.00028	9.1	0.000264	0	0.0258	3	0.01138	0	0	0	0.43	0	0	0	0	0
LU1366-005	860 °C	295.5	0	0.018	35	0.1869	0	1.493	3	0.0006959	4.8	0.00028	9.1	0.000264	0	0.0258	3	0.01138	0	0	0	0.43	0	0	0	0	0
LU1366-006	950 °C	295.5	0	0.018	35	0.1869	0	1.493	3	0.0006959	4.8	0.00028	9.1	0.000264	0	0.0258	3	0.01138	0	0	0	0.43	0	0	0	0	0
LU1366-007	1010 °C	295.5	0	0.018	35	0.1869	0	1.493	3	0.0006959	4.8	0.00028	9.1	0.000264	0	0.0258	3	0.01138	0	0	0	0.43	0	0	0	0	0
LU1366-008	1060 °C	295.5	0	0.018	35	0.1869	0	1.493	3	0.0006959	4.8	0.00028	9.1	0.000264	0	0.0258	3	0.01138	0	0	0	0.43	0	0	0	0	0
LU1366-009	1100 °C	295.5	0	0.018	35	0.1869	0	1.493	3	0.0006959	4.8	0.00028	9.1	0.000264	0	0.0258	3	0.01138	0	0	0	0.43	0	0	0	0	0
LU1366-010	1130 °C	295.5	0	0.018	35	0.1869	0	1.493	3	0.0006959	4.8	0.00028	9.1	0.000264	0	0.0258	3	0.01138	0	0	0	0.43	0	0	0	0	0
LU1366-011	1160 °C	295.5	0	0.018	35	0.1869	0	1.493	3	0.0006959	4.8	0.00028	9.1	0.000264	0	0.0258	3	0.01138	0	0	0	0.43	0	0	0	0	0
LU1366-012	1200 °C	295.5	0	0.018	35	0.1869	0	1.493	3	0.0006959	4.8	0.00028	9.1	0.000264	0	0.0258	3	0.01138	0	0	0	0.43	0	0	0	0	0
LU1366-013	1300 °C	295.5	0	0.018	35	0.1869	0	1.493	3	0.0006959	4.8	0.00028	9.1	0.000264	0	0.0258	3	0.01138	0	0	0	0.43	0	0	0	0	0

Incremental Heating			36Ar(a)	37Ar(ca)	38Ar(cl)	39Ar(k)	40Ar(r)	Age ± 2s (Ma)	40Ar(r) (%)	39Ar(k) (%)	K/Ca ± 2s
LU1366-001	600 °C		9467.775629	0.000000	3054.236728	32456.699033	213057.788461	22.54 ± 5.92	7.07	3.34	4.17E+102 ± 0.000
LU1366-002	660 °C		7168.585709	0.000000	431.433795	54372.977372	519209.947170	32.69 ± 2.79	19.68	5.60	6.99E+102 ± 0.000
LU1366-003	710 °C	4	4533.622709	0.000000	487.775437	75139.598456	768097.622793	34.97 ± 1.65	36.41	7.74	9.66E+102 ± 0.000
LU1366-004	780 °C	4	4045.618836	0.000000	670.527358	105589.056111	1091280.607413	35.36 ± 0.78	47.66	10.88	1.36E+103 ± 0.000
LU1366-005	860 °C	4	3472.051562	0.000000	751.857011	108568.545550	1108337.365812	34.93 ± 0.60	51.86	11.19	1.40E+103 ± 0.000
LU1366-006	950 °C	4	2889.912114	0.000000	724.572204	129001.776109	1310560.591869	34.76 ± 0.59	60.45	13.29	1.66E+103 ± 0.000
LU1366-007	1010 °C	4	1324.019108	0.000000	638.050517	119950.831790	1237218.949625	35.29 ± 0.47	75.83	12.36	1.54E+103 ± 0.000
LU1366-008	1060 °C	4	764.163324	0.000000	633.693313	108169.197561	1118909.602074	35.39 ± 0.53	83.04	11.14	1.39E+103 ± 0.000
LU1366-009	1100 °C	4	1189.883929	0.000000	540.342270	107205.648018	1123518.895003	35.85 ± 0.53	76.02	11.04	1.38E+103 ± 0.000
LU1366-010	1130 °C		1199.511508	0.000000	531.727138	83854.933882	899608.680172	36.69 ± 0.45	71.61	8.64	1.08E+103 ± 0.000
LU1366-011	1160 °C		350.238194	0.000000	167.376791	29181.101495	318133.159806	37.28 ± 0.34	75.32	3.01	9.58E-04 ± 0.000
LU1366-012	1200 °C		145.125744	0.000000	93.811473	11436.452967	122968.477533	36.77 ± 0.67	74.01	1.18	1.93E-04 ± 0.000
LU1366-013	1300 °C		72.676688	0.000000	27.648609	5709.660171	63397.899868	37.96 ± 1.28	74.57	0.59	0.00E+00 ± 0.000
		S	36623.185056	0.000000	8753.052644	970636.478514	9894299.587599				

Normal Isochron			39(k)/36(a) ± 2s	40(a+r)/36(a) ± 2s	r.i.
LU1366-001	600 °C		3.4 ± 0.1	318.0 ± 6.4	0.8836
LU1366-002	660 °C		7.6 ± 0.2	367.9 ± 7.7	0.9374
LU1366-003	710 °C	4	16.6 ± 0.5	464.9 ± 12.5	0.9521
LU1366-004	780 °C	4	26.1 ± 0.5	565.2 ± 10.9	0.9357
LU1366-005	860 °C	4	31.3 ± 0.6	614.7 ± 10.7	0.9442
LU1366-006	950 °C	4	44.6 ± 1.1	749.0 ± 18.9	0.9852
LU1366-007	1010 °C	4	90.6 ± 3.6	1229.9 ± 48.8	0.9928
LU1366-008	1060 °C	4	141.6 ± 9.7	1759.7 ± 120.0	0.9954
LU1366-009	1100 °C	4	90.1 ± 4.1	1239.7 ± 56.7	0.9954
LU1366-010	1130 °C		69.9 ± 2.0	1045.5 ± 28.6	0.9761
LU1366-011	1160 °C		83.3 ± 1.9	1203.8 ± 26.2	0.9692
LU1366-012	1200 °C		78.8 ± 3.0	1142.8 ± 43.1	0.9515
LU1366-013	1300 °C		78.6 ± 5.9	1167.8 ± 86.8	0.9619

Inverse Isochron			39(k)/40(a+r) ± 2s	36(a)/40(a+r) ± 2s	r.i.
LU1366-001	600 °C		0.010780 ± 0.000114	0.003145 ± 0.000063	0.0103
LU1366-002	660 °C		0.020615 ± 0.000161	0.002718 ± 0.000057	0.0069
LU1366-003	710 °C	4	0.035649 ± 0.000305	0.002151 ± 0.000058	0.0164
LU1366-004	780 °C	4	0.046174 ± 0.000334	0.001769 ± 0.000034	0.0082
LU1366-005	860 °C	4	0.050868 ± 0.000307	0.001627 ± 0.000028	0.0209
LU1366-006	950 °C	4	0.059598 ± 0.000261	0.001335 ± 0.000034	0.0197
LU1366-007	1010 °C	4	0.073659 ± 0.000352	0.000813 ± 0.000032	0.0103
LU1366-008	1060 °C	4	0.080440 ± 0.000525	0.000568 ± 0.000039	0.0028
LU1366-009	1100 °C	4	0.072675 ± 0.000319	0.000807 ± 0.000037	0.0083
LU1366-010	1130 °C		0.066867 ± 0.000405	0.000956 ± 0.000026	0.0131
LU1366-011	1160 °C		0.069210 ± 0.000379	0.000831 ± 0.000018	0.0439
LU1366-012	1200 °C		0.068955 ± 0.000823	0.000875 ± 0.000033	0.0801
LU1366-013	1300 °C		0.067272 ± 0.001388	0.000856 ± 0.000064	0.1039

Degassing Patterns			36Ar(a)	36Ar(c)	36Ar(ca)	36Ar(cl)	37Ar(ca)	38Ar(a)	38Ar(c)	38Ar(k)	38Ar(ca)	38Ar(cl)	39Ar(k)	39Ar(ca)	40Ar(r)	40Ar(a)	40Ar(c)	40Ar(k)
LU1366-001	600 °C		9467.775629	0.000000	0.000000	0.000000	0.000000	1769.527265	0.000000	369.357235	0.000000	3054.236728	32456.699033	0.000000	213057.788461	2797727.698463	0.000000	837.382835
LU1366-002	660 °C		7168.585709	0.000000	0.000000	0.000000	0.000000	1339.808669	0.000000	618.764482	0.000000	431.433795	54372.977372	0.000000	519209.947170	2118317.077014	0.000000	1402.822816
LU1366-003	710 °C	4	4533.622709	0.000000	0.000000	0.000000	0.000000	847.334084	0.000000	855.088630	0.000000	487.775437	75139.598456	0.000000	768097.622793	1339685.510380	0.000000	1938.601640
LU1366-004	780 °C	4	4045.618836	0.000000	0.000000	0.000000	0.000000	756.126160	0.000000	1201.603459	0.000000	670.527358	105589.056111	0.000000	1091280.607413	1195480.365954	0.000000	2724.197648
LU1366-005	860 °C	4	3472.051562	0.000000	0.000000	0.000000	0.000000	648.926437	0.000000	1235.510048	0.000000	751.857011	108568.545550	0.000000	1108337.365812	1025991.236716	0.000000	2801.068475
LU1366-006	950 °C	4	2889.912114	0.000000	0.000000	0.000000	0.000000	540.124574	0.000000	1468.040212	0.000000	724.572204	129001.776109	0.000000	1310560.591869	853969.029810	0.000000	3328.245824
LU1366-007	1010 °C	4	1324.019108	0.000000	0.000000	0.000000	0.000000	247.459171	0.000000	1365.040466	0.000000	638.050517	119950.831790	0.000000	1237218.949625	391247.646460	0.000000	3094.731460
LU1366-008	1060 °C	4	764.163324	0.000000	0.000000	0.000000	0.000000	142.822125	0.000000	1230.965468	0.000000	633.693313	108169.197561	0.000000	1118909.602074	225810.262301	0.000000	2790.765297
LU1366-009	1100 °C	4	1189.883929	0.000000	0.000000	0.000000	0.000000	222.389306	0.000000	1220.000274	0.000000	540.342270	107205.648018	0.000000	1123518.895003	351610.701139	0.000000	2765.905719
LU1366-010	1130 °C		1199.511508	0.000000	0.000000	0.000000	0.000000	224.188701	0.000000	954.269148	0.000000	531.727138	83854.933882	0.000000	899608.680172	354455.650595	0.000000	2163.457294
LU1366-011	1160 °C		350.238194	0.000000	0.000000	0.000000	0.000000	65.459519	0.000000	332.080935	0.000000	167.376791	29181.101495	0.000000	318133.159806	103495.386419	0.000000	752.872419
LU1366-012	1200 °C		145.125744	0.000000	0.000000	0.000000	0.000000	27.124002	0.000000	130.146835	0.000000	93.811473	11436.452967	0.000000	122968.477533	42884.657403	0.000000	295.060487

LU1366-013	1300 °C		72.676688	0.000000	0.000000	0.000000	0.000000	13.583273	0.000000	64.975933	0.000000	27.648609	5709.660171	0.000000	63397.899868	21475.961292	0.000000	147.309232
		S	36623.185056	0.000000	0.000000	0.000000	0.000000	6844.873287	0.000000	11045.843125	0.000000	8753.052644	970636.478514	0.000000	9894299.587599	10822151.183945	0.000000	25042.421146
		S				36623.185056	0.000000					26643.769057		970636.478514				20741493.192690

Additional Parameters			40(r)/39(k)	1s	40(r+a)	1s	40Ar/39Ar	1s	37Ar/39Ar	1s	36Ar/39Ar	1s	37Ar (decay)	39Ar (decay)	40Ar (moles)
LU1366-001	600 °C		6.564370	0.86724	3010785.48692	2225.49981	92.78895	0.49155	0.00000	0.00026	0.29170	0.00330	1.00000000	1.00593525	3.403E-13
LU1366-002	660 °C		9.549044	0.41189	2637527.02418	1408.03517	48.53385	0.18922	0.00000	0.00020	0.13184	0.00148	1.00000000	1.00593544	2.982E-13
LU1366-003	710 °C	4	10.222275	0.24358	2107783.13317	2044.39756	28.07736	0.12024	0.00000	0.00016	0.06034	0.00084	1.00000000	1.00593563	2.384E-13
LU1366-004	780 °C	4	10.335168	0.11545	2286760.97337	1222.81368	21.68298	0.07840	0.00000	0.00011	0.03831	0.00039	1.00000000	1.00593583	2.587E-13
LU1366-005	860 °C	4	10.208642	0.08862	2134328.60253	1585.86793	19.68461	0.05949	0.00000	0.00011	0.03198	0.00029	1.00000000	1.00593602	2.415E-13
LU1366-006	950 °C	4	10.159245	0.08678	2164529.62168	1595.31340	16.80487	0.03677	0.00000	0.00015	0.02240	0.00029	1.00000000	1.00593622	2.450E-13
LU1366-007	1010 °C	4	10.314384	0.06953	1628466.59609	1138.21091	13.60192	0.03245	0.00000	0.00014	0.01104	0.00022	1.00000000	1.00593641	1.844E-13
LU1366-008	1060 °C	4	10.344069	0.07886	1344719.86437	752.95355	12.45743	0.04068	0.00000	0.00014	0.00706	0.00024	1.00000000	1.00593661	1.523E-13
LU1366-009	1100 °C	4	10.480035	0.07859	1475129.59614	953.85027	13.78561	0.03026	0.00000	0.00013	0.01110	0.00025	1.00000000	1.00593680	1.670E-13
LU1366-010	1130 °C		10.728154	0.06664	1254064.33077	922.08477	14.98096	0.04540	0.00000	0.00015	0.01430	0.00020	1.00000000	1.00593699	1.420E-13
LU1366-011	1160 °C		10.902027	0.04983	421628.54622	482.19223	14.47449	0.03960	0.00000	0.00020	0.01200	0.00013	1.00000000	1.00593716	4.773E-14
LU1366-012	1200 °C		10.752327	0.09927	165853.13494	498.08546	14.52795	0.08664	0.00000	0.00035	0.01269	0.00025	1.00000000	1.00593733	1.877E-14
LU1366-013	1300 °C		11.103621	0.18962	84873.86116	535.50818	14.89076	0.15347	0.00000	0.00074	0.01273	0.00048	1.00000000	1.00593750	9.607E-15

Information on Analysis

03PH311A
Biotite
03PH311A biotite, Alaska (Enkelmann-Spotil
Zeitler

Project = Eva-Alaska Biotites
Irradiation = I47
J = 0.0019150 ± 0.0000096
GA-1550 = 98.790 ± 0.543 Ma

Results	40(r)/39(k) ± 2s	Age ± 2s (Ma)	MSWD	39Ar(k) (%,n)	K/Ca ± 2s
Weighted Plateau	10.3116 ± 0.0842 ± 0.82%	35.28 ± 0.45 ± 1.28% External Error ± 0.47 Analytical Error ± 0.29	1.56 2.45 1.2499	77.64 7 Statistical T Ratio Error Magnification	1.38E+103 ± 0.756
Total Fusion Age	10.1936 ± 0.0976 ± 0.96%	34.88 ± 0.48 ± 1.37% External Error ± 0.49 Analytical Error ± 0.33		13	3.30E+101 ± 0.000

Results	40(a)/36(a) ± 2s	40(r)/39(k) ± 2s	Age ± 2s (Ma)	MSWD
No Convergence	291.3553 ± 6.6187 ± 2.27%	10.3832 ± 0.1450 ± 1.40%	35.52 ± 0.60 ± 1.70% External Error ± 0.62 Analytical Error ± 0.49	1.40

Statistics				
Statistics	Statistical F Ratio Error Magnification n	2.21 1.1820 7	Convergence Number of Iterations Calculated Line	0.0000009865 100 Weighted York-2

Results	40(a)/36(a) ± 2s	40(r)/39(k) ± 2s	Age ± 2s (Ma)	MSWD
Isochron	291.2859 ± 6.6726 ± 2.29%	10.3890 ± 0.1458 ± 1.40%	35.54 ± 0.61 ± 1.71% External Error ± 0.62 Analytical Error ± 0.49	1.43

Statistics				
Statistics	Statistical F Ratio Error Magnification n	2.21 1.1958 7	Convergence Number of Iterations Calculated Line	0.0000002433 3 Weighted York-2

2000APa45

Procedure Blanks		36Ar	1s	37Ar	1s	38Ar	1s	39Ar	1s	40Ar	1s
LU1369-001	600 °C	11.588091	1.158809	0.000000	2.579125	3.506617	0.906477	0.513287	1.691421	2978.888023	297.888802
LU1369-002	660 °C	11.959356	1.195936	0.000000	2.579125	3.533891	0.906477	0.845496	1.691421	3010.410763	301.041076
LU1369-003	710 °C	12.268744	1.226874	0.000000	2.579125	3.556620	0.906477	1.122337	1.691421	3056.357125	305.635713
LU1369-004	780 °C	12.701888	1.270189	0.000000	2.579125	3.588440	0.906477	1.509914	1.691421	3150.734808	315.073481
LU1369-005	860 °C	13.196908	1.319691	0.000000	2.579125	3.624805	0.906477	1.952860	1.691421	3301.527554	330.152755
LU1369-006	950 °C	13.753807	1.375381	0.000000	2.579125	3.665717	0.906477	2.451173	1.691421	3525.908378	352.590838
LU1369-007	1010 °C	14.125072	1.412507	0.000000	2.579125	3.692991	0.906477	2.783382	1.691421	3707.694996	370.769500
LU1369-008	1060 °C	14.434460	1.443446	0.000000	2.579125	3.715719	0.906477	3.060223	1.691421	3878.861257	387.886126
LU1369-009	1100 °C	14.681971	1.468197	0.000000	2.579125	3.733902	0.906477	3.281696	1.691421	4028.674027	402.867403
LU1369-010	1130 °C	14.867603	1.486760	0.000000	2.579125	3.747539	0.906477	3.447800	1.691421	4148.546798	414.854680
LU1369-011	1160 °C	15.053236	1.505324	0.000000	2.579125	3.761176	0.906477	3.613905	1.691421	4274.859450	427.485945
LU1369-012	1200 °C	15.300747	1.530075	0.000000	2.579125	3.779359	0.906477	3.835377	1.691421	4453.293911	445.329391
LU1369-013	1300 °C	15.919523	1.591952	0.000000	2.579125	3.824816	0.906477	4.389059	1.691421	4949.468022	494.946802

Intercept Values		36Ar	1s	r2		37Ar	1s	r2		38Ar	1s	r2	
LU1369-001	600 °C	2297.701176	10.748386	0.8825	LIN #	0.000000	4.040358	0.3943	LIN #	6553.056459	38.023615	0.8449	LIN #
LU1369-002	660 °C	475.494289	9.945076	0.2427	LIN #	0.000000	3.019613	0.1134	LIN #	7525.862372	39.527258	0.9126	LIN #
LU1369-003	710 °C	255.952761	2.605522	0.4559	LIN #	0.000000	4.417662	0.3238	LIN # 1	10364.944135	35.179982	0.9497	LIN #
LU1369-004	780 °C	151.992823	2.727054	0.2813	LIN #	0.000000	2.804916	0.2045	LIN #	5891.129360	48.941555	0.7327	LIN #
LU1369-005	860 °C	166.547297	3.128375	0.4960	LIN # 6	0.000000	3.290526		AVE # 4	5789.404281	35.972631	0.8152	LIN #
LU1369-006	950 °C	283.551176	4.223647	0.3727	LIN #	0.000000	2.086720	0.4385	LIN #	10726.952602	49.485548	0.8736	LIN #
LU1369-007	1010 °C	167.421683	4.118824	0.6280	LIN #	0.000000	2.170276	0.4250	LIN #	4905.060363	29.622017	0.7354	LIN #
LU1369-008	1060 °C	62.021499	1.606882	0.1442	LIN #	0.000000	1.840439	0.6099	LIN #	1475.997181	17.280545	0.6186	LIN #
LU1369-009	1100 °C	35.549299	1.476266	0.7053	LIN #	0.000000	4.408741	0.0346	LIN #	239.472670	7.651167	0.0524	LIN #
LU1369-010	1130 °C	139.205924	2.212485	0.0005	LIN #	0.000000	5.707641		AVE #	105.258256	5.075825	0.0013	LIN #
LU1369-011	1160 °C	38.463823	2.416891	0.0403	LIN #	0.000000	2.877260	0.0056	LIN #	41.400698	3.780867	0.1807	LIN #
LU1369-012	1200 °C	28.047455	0.752065	0.0214	LIN #	0.000000	2.155479	0.8716	LIN # 1 2 6 8	43.164034	3.652503	0.0383	LIN #
LU1369-013	1300 °C	34.230852	1.027031	0.5563	LIN #	0.000000	2.336939		AVE #	36.656762	2.069058	0.1188	LIN #

Intercept Values		39Ar	1s	r2		40Ar	1s	r2	
LU1369-001	600 °C	92099.758574	105.308116	0.9909	EXP #	838638.943400	870.128589	0.9910	EXP #
LU1369-002	660 °C	155326.487720	188.399359	0.9914	EXP #	347216.619517	285.251965	0.9947	EXP #
LU1369-003	710 °C	197092.742230	220.268609	0.9934	EXP #	327089.349071	136.941401	0.9985	EXP #
LU1369-004	780 °C	105751.159502	142.300751	0.9895	EXP #	195542.787745	213.901892	0.9905	EXP #
LU1369-005	860 °C	117584.615306	131.830697	0.9918	EXP #	220603.528689	255.168961	0.9886	EXP #
LU1369-006	950 °C	219956.887491	221.772705	0.9944	EXP #	391379.218262	245.413786	0.9971	EXP #
LU1369-007	1010 °C	82250.648944	85.386801	0.9946	EXP #	177322.976523	183.736862	0.9916	EXP #
LU1369-008	1060 °C	22600.520080	47.920468	0.9753	EXP #	64735.276234	63.712207	0.9825	EXP #
LU1369-009	1100 °C	4182.602127	12.886818	0.9568	EXP #	28332.326367	33.701668	0.8236	EXP #
LU1369-010	1130 °C	1508.017985	15.214093	0.4498	EXP #	46312.411569	84.426372	0.9287	EXP #
LU1369-011	1160 °C	797.763346	10.315843	0.1613	EXP #	13051.741158	40.440679	0.8613	EXP #
LU1369-012	1200 °C	720.756292	10.455029	0.0784	EXP #	10447.944338	25.898732	0.9683	EXP #
LU1369-013	1300 °C	881.380645	14.355441	0.0428	EXP #	12217.762663	40.856599	0.9208	EXP #

Sample Parameters		Sample	Material	Location	Analyst	Temp	Standard (in Ma)	%1s	J	%1s
LU1369-001	600 °C	2000APa45	Biotite	2000APa45 biotite, Alaska (Enkelmann-Spotila), I47, pkt D) 10m gettering	Zeitler	600	98.79	0.55	0.001925	0.5
LU1369-002	660 °C	2000APa45	Biotite	2000APa45 biotite, Alaska (Enkelmann-Spotila), I47, pkt D) 10m gettering	Zeitler	660	98.79	0.55	0.001925	0.5
LU1369-003	710 °C	2000APa45	Biotite	2000APa45 biotite, Alaska (Enkelmann-Spotila), I47, pkt D) 10m gettering	Zeitler	710	98.79	0.55	0.001925	0.5
LU1369-004	780 °C	2000APa45	Biotite	2000APa45 biotite, Alaska (Enkelmann-Spotila), I47, pkt D) 10m gettering	Zeitler	780	98.79	0.55	0.001925	0.5
LU1369-005	860 °C	2000APa45	Biotite	2000APa45 biotite, Alaska (Enkelmann-Spotila), I47, pkt D) 10m gettering	Zeitler	860	98.79	0.55	0.001925	0.5
LU1369-006	950 °C	2000APa45	Biotite	2000APa45 biotite, Alaska (Enkelmann-Spotila), I47, pkt D) 10m gettering	Zeitler	950	98.79	0.55	0.001925	0.5
LU1369-007	1010 °C	2000APa45	Biotite	2000APa45 biotite, Alaska (Enkelmann-Spotila), I47, pkt D) 10m gettering	Zeitler	1010	98.79	0.55	0.001925	0.5
LU1369-008	1060 °C	2000APa45	Biotite	2000APa45 biotite, Alaska (Enkelmann-Spotila), I47, pkt D) 10m gettering	Zeitler	1060	98.79	0.55	0.001925	0.5
LU1369-009	1100 °C	2000APa45	Biotite	2000APa45 biotite, Alaska (Enkelmann-Spotila), I47, pkt D) 10m gettering	Zeitler	1100	98.79	0.55	0.001925	0.5
LU1369-010	1130 °C	2000APa45	Biotite	2000APa45 biotite, Alaska (Enkelmann-Spotila), I47, pkt D) 10m gettering	Zeitler	1130	98.79	0.55	0.001925	0.5
LU1369-011	1160 °C	2000APa45	Biotite	2000APa45 biotite, Alaska (Enkelmann-Spotila), I47, pkt D) 10m gettering	Zeitler	1160	98.79	0.55	0.001925	0.5
LU1369-012	1200 °C	2000APa45	Biotite	2000APa45 biotite, Alaska (Enkelmann-Spotila), I47, pkt D) 10m gettering	Zeitler	1200	98.79	0.55	0.001925	0.5
LU1369-013	1300 °C	2000APa45	Biotite	2000APa45 biotite, Alaska (Enkelmann-Spotila), I47, pkt D) 10m gettering	Zeitler	1300	98.79	0.55	0.001925	0.5

Sample Parameters		MDF	%1s	Volume Ratio	Sensitivity (mol/vol)	Day	Month	Year	Hour	Min	Resi	Irradiation	Project	Standard Name
LU1369-001	600 °C	1.000564	0.18	1	1.154E-19	11	02	2009	16	52	001	I47	Alaska Micas 09	GA-1550
LU1369-002	660 °C	1.000564	0.18	1	1.154E-19	11	02	2009	17	26	001	I47	Alaska Micas 09	GA-1550
LU1369-003	710 °C	1.000564	0.18	1	1.154E-19	11	02	2009	18	01	001	I47	Alaska Micas 09	GA-1550
LU1369-004	780 °C	1.000564	0.18	1	1.154E-19	11	02	2009	18	36	001	I47	Alaska Micas 09	GA-1550
LU1369-005	860 °C	1.000564	0.18	1	1.154E-19	11	02	2009	19	10	001	I47	Alaska Micas 09	GA-1550
LU1369-006	950 °C	1.000564	0.18	1	1.154E-19	11	02	2009	19	45	001	I47	Alaska Micas 09	GA-1550
LU1369-007	1010 °C	1.000564	0.18	1	1.154E-19	11	02	2009	20	20	001	I47	Alaska Micas 09	GA-1550
LU1369-008	1060 °C	1.000564	0.18	1	1.154E-19	11	02	2009	20	54	001	I47	Alaska Micas 09	GA-1550
LU1369-009	1100 °C	1.000564	0.18	1	1.154E-19	11	02	2009	21	29	001	I47	Alaska Micas 09	GA-1550
LU1369-010	1130 °C	1.000564	0.18	1	1.154E-19	11	02	2009	22	04	001	I47	Alaska Micas 09	GA-1550
LU1369-011	1160 °C	1.000564	0.18	1	1.154E-19	11	02	2009	22	38	001	I47	Alaska Micas 09	GA-1550
LU1369-012	1200 °C	1.000564	0.18	1	1.154E-19	11	02	2009	23	13	001	I47	Alaska Micas 09	GA-1550
LU1369-013	1300 °C	1.000564	0.18	1	1.154E-19	11	02	2009	23	48	001	I47	Alaska Micas 09	GA-1550

Irradiation Constants	40/36(a)	%1s	40/36(c)	%1s	38/36(a)	%1s	38/36(c)	%1s	39/37(ca)	%1s	38/37(ca)	%1s	36/37(ca)	%1s	40/39(k)	%1s	38/39(k)	%1s	36/38(cl)	%1s	K/Ca	%1s	K/Cl	%1s	Ca/Cl	%1s

LU1369-001	600 °C	295.5	0	0.018	35	0.1869	0	1.493	3	0.0006959	4.8	0.00028	9.1	0.000264	0	0.0258	3	0.01138	0	0	0	0.43	0	0	0	0	0
LU1369-002	660 °C	295.5	0	0.018	35	0.1869	0	1.493	3	0.0006959	4.8	0.00028	9.1	0.000264	0	0.0258	3	0.01138	0	0	0	0.43	0	0	0	0	0
LU1369-003	710 °C	295.5	0	0.018	35	0.1869	0	1.493	3	0.0006959	4.8	0.00028	9.1	0.000264	0	0.0258	3	0.01138	0	0	0	0.43	0	0	0	0	0
LU1369-004	780 °C	295.5	0	0.018	35	0.1869	0	1.493	3	0.0006959	4.8	0.00028	9.1	0.000264	0	0.0258	3	0.01138	0	0	0	0.43	0	0	0	0	0
LU1369-005	860 °C	295.5	0	0.018	35	0.1869	0	1.493	3	0.0006959	4.8	0.00028	9.1	0.000264	0	0.0258	3	0.01138	0	0	0	0.43	0	0	0	0	0
LU1369-006	950 °C	295.5	0	0.018	35	0.1869	0	1.493	3	0.0006959	4.8	0.00028	9.1	0.000264	0	0.0258	3	0.01138	0	0	0	0.43	0	0	0	0	0
LU1369-007	1010 °C	295.5	0	0.018	35	0.1869	0	1.493	3	0.0006959	4.8	0.00028	9.1	0.000264	0	0.0258	3	0.01138	0	0	0	0.43	0	0	0	0	0
LU1369-008	1060 °C	295.5	0	0.018	35	0.1869	0	1.493	3	0.0006959	4.8	0.00028	9.1	0.000264	0	0.0258	3	0.01138	0	0	0	0.43	0	0	0	0	0
LU1369-009	1100 °C	295.5	0	0.018	35	0.1869	0	1.493	3	0.0006959	4.8	0.00028	9.1	0.000264	0	0.0258	3	0.01138	0	0	0	0.43	0	0	0	0	0
LU1369-010	1130 °C	295.5	0	0.018	35	0.1869	0	1.493	3	0.0006959	4.8	0.00028	9.1	0.000264	0	0.0258	3	0.01138	0	0	0	0.43	0	0	0	0	0
LU1369-011	1160 °C	295.5	0	0.018	35	0.1869	0	1.493	3	0.0006959	4.8	0.00028	9.1	0.000264	0	0.0258	3	0.01138	0	0	0	0.43	0	0	0	0	0
LU1369-012	1200 °C	295.5	0	0.018	35	0.1869	0	1.493	3	0.0006959	4.8	0.00028	9.1	0.000264	0	0.0258	3	0.01138	0	0	0	0.43	0	0	0	0	0
LU1369-013	1300 °C	295.5	0	0.018	35	0.1869	0	1.493	3	0.0006959	4.8	0.00028	9.1	0.000264	0	0.0258	3	0.01138	0	0	0	0.43	0	0	0	0	0

Incremental Heating			36Ar(a)	37Ar(ca)	38Ar(cl)	39Ar(k)	40Ar(r)	Age ± 2s (Ma)	40Ar(r) (%)	39Ar(k) (%)	K/Ca ± 2s
LU1369-001	600 °C		2280.967223	0.000000	5062.132924	92594.426698	159245.304844	5.96 ± 0.44	19.06	9.20	4147.350 ± 4134.795
LU1369-002	660 °C	4	462.491551	0.000000	5650.303358	156160.793115	203511.006843	4.52 ± 0.14	59.12	15.52	10799.100 ± 13770.944
LU1369-003	710 °C	4	243.135503	0.000000	8049.308411	198151.370994	247074.145364	4.33 ± 0.04	76.25	19.69	82603.188 ± 817911.483
LU1369-004	780 °C	4	138.977402	0.000000	4645.030376	106318.278032	148581.219055	4.85 ± 0.07	77.23	10.57	201751.028 ± 6773698.028
LU1369-005	860 °C	4	153.005209	0.000000	4405.377801	118214.938103	169039.016582	4.96 ± 0.07	77.79	11.75	5886.506 ± 5690.693
LU1369-006	950 °C	4	269.190077	0.000000	8144.351318	221137.232252	302602.301641	4.75 ± 0.05	78.02	21.98	98021.386 ± 669311.330
LU1369-007	1010 °C	4	152.951552	0.000000	3926.244145	82690.164257	126284.691650	5.30 ± 0.12	72.74	8.22	6359.299 ± 7654.894
LU1369-008	1060 °C		47.479924	0.000000	1203.206559	22718.984449	46239.947655	7.05 ± 0.23	75.98	2.26	1884.077 ± 2298.819
LU1369-009	1100 °C		20.820358	0.000000	183.765383	4201.796696	18042.830316	14.85 ± 1.21	74.24	0.42	2449.924 ± 33878.609
LU1369-010	1130 °C		124.058444	0.000000	60.995726	1512.661979	5465.567800	12.50 ± 4.25	12.96	0.15	82.604 ± 131.203
LU1369-011	1160 °C		23.357891	0.000000	24.145495	798.420624	1854.025635	8.05 ± 8.18	21.12	0.08	77.030 ± 133.357
LU1369-012	1200 °C		12.718017	0.000000	28.760861	720.776862	2217.880487	10.65 ± 6.45	37.00	0.07	103.486 ± 231.917
LU1369-013	1300 °C		18.270112	0.000000	19.346426	881.708622	1846.728478	7.26 ± 5.88	25.41	0.09	167.856 ± 516.457
		S	3947.423262	0.000000	41402.968782	1006101.552683	1432004.666351				

Normal Isochron			39(k)/36(a) ± 2s	40(a+r)/36(a) ± 2s	r.i.
LU1369-001	600 °C		40.6 ± 0.7	365.3 ± 6.3	0.9627
LU1369-002	660 °C	4	337.7 ± 15.4	735.5 ± 33.6	0.9939
LU1369-003	710 °C	4	815.0 ± 22.8	1311.7 ± 36.4	0.9850
LU1369-004	780 °C	4	765.0 ± 35.0	1364.6 ± 62.4	0.9911
LU1369-005	860 °C	4	772.6 ± 36.1	1400.3 ± 65.4	0.9922
LU1369-006	950 °C	4	821.5 ± 29.7	1419.6 ± 51.1	0.9912
LU1369-007	1010 °C	4	540.6 ± 31.8	1121.2 ± 65.9	0.9940
LU1369-008	1060 °C		478.5 ± 44.1	1269.4 ± 117.8	0.9882
LU1369-009	1100 °C		201.8 ± 40.4	1162.1 ± 235.7	0.9857
LU1369-010	1130 °C		12.2 ± 0.6	339.6 ± 16.8	0.8311
LU1369-011	1160 °C		34.2 ± 8.4	374.9 ± 98.5	0.9222
LU1369-012	1200 °C		56.7 ± 15.3	469.9 ± 144.1	0.8682
LU1369-013	1300 °C		48.3 ± 10.1	396.6 ± 98.6	0.8238

Inverse Isochron			39(k)/40(a+r) ± 2s	36(a)/40(a+r) ± 2s	r.i.
LU1369-001	600 °C		0.111122 ± 0.000534	0.002737 ± 0.000047	0.0588
LU1369-002	660 °C	4	0.459057 ± 0.002310	0.001360 ± 0.000062	0.0281
LU1369-003	710 °C	4	0.621319 ± 0.003000	0.000762 ± 0.000021	0.0398
LU1369-004	780 °C	4	0.560605 ± 0.003415	0.000733 ± 0.000033	0.0606
LU1369-005	860 °C	4	0.551756 ± 0.003213	0.000714 ± 0.000033	0.0585
LU1369-006	950 °C	4	0.578669 ± 0.002769	0.000704 ± 0.000025	0.0340
LU1369-007	1010 °C	4	0.482209 ± 0.003093	0.000892 ± 0.000052	0.0632
LU1369-008	1060 °C		0.376952 ± 0.005351	0.000788 ± 0.000073	0.1294
LU1369-009	1100 °C		0.173662 ± 0.005936	0.000861 ± 0.000175	0.1611
LU1369-010	1130 °C		0.035909 ± 0.001035	0.002945 ± 0.000146	0.2832
LU1369-011	1160 °C		0.091183 ± 0.009265	0.002668 ± 0.000701	0.3604
LU1369-012	1200 °C		0.120611 ± 0.018360	0.002128 ± 0.000653	0.4774
LU1369-013	1300 °C		0.121690 ± 0.017163	0.002522 ± 0.000627	0.5359

Degassing Patterns			36Ar(a)	36Ar(c)	36Ar(ca)	36Ar(cl)	37Ar(ca)	38Ar(a)	38Ar(c)	38Ar(k)	38Ar(ca)	38Ar(cl)	39Ar(k)	39Ar(ca)	40Ar(r)	40Ar(a)	40Ar(c)	40Ar(k)
LU1369-001	600 °C		2280.967223	0.000000	0.000000	0.000000	0.000000	426.312774	0.000000	1053.724576	0.000000	5062.132924	92594.426698	0.000000	159245.304844	674025.814324	0.000000	2388.936209
LU1369-002	660 °C	4	462.491551	0.000000	0.000000	0.000000	0.000000	86.439671	0.000000	1777.109826	0.000000	5650.303358	156160.793115	0.000000	203511.006843	136666.253449	0.000000	4028.948462
LU1369-003	710 °C	4	243.135503	0.000000	0.000000	0.000000	0.000000	45.442026	0.000000	2254.962602	0.000000	8049.308411	198151.370994	0.000000	247074.145364	71846.541210	0.000000	5112.305372
LU1369-004	780 °C	4	138.977402	0.000000	0.000000	0.000000	0.000000	25.974876	0.000000	1209.902004	0.000000	4645.030376	106318.278032	0.000000	148581.219055	41067.822309	0.000000	2743.011573
LU1369-005	860 °C	4	153.005209	0.000000	0.000000	0.000000	0.000000	28.596673	0.000000	1345.285996	0.000000	4405.377801	118214.938103	0.000000	169039.016582	45213.039149	0.000000	3049.945403
LU1369-006	950 °C	4	269.190077	0.000000	0.000000	0.000000	0.000000	50.311625	0.000000	2516.541703	0.000000	8144.351318	221137.232252	0.000000	302602.301641	79545.667650	0.000000	5705.340592
LU1369-007	1010 °C	4	152.951552	0.000000	0.000000	0.000000	0.000000	28.586645	0.000000	941.014069	0.000000	3926.244145	82690.164257	0.000000	126284.691650	45197.183640	0.000000	2133.406238
LU1369-008	1060 °C		47.479924	0.000000	0.000000	0.000000	0.000000	8.873998	0.000000	258.542043	0.000000	1203.206559	22718.984449	0.000000	46239.947655	14030.317523	0.000000	586.149799
LU1369-009	1100 °C		20.820358	0.000000	0.000000	0.000000	0.000000	3.891325	0.000000	47.816446	0.000000	183.765383	4201.796696	0.000000	18042.830316	6152.415670	0.000000	108.406355
LU1369-010	1130 °C		124.058444	0.000000	0.000000	0.000000	0.000000	23.186523	0.000000	17.214093	0.000000	60.995726	1512.661979	0.000000	5465.567800	36659.270291	0.000000	39.026679
LU1369-011	1160 °C		23.357891	0.000000	0.000000	0.000000	0.000000	4.365590	0.000000	9.086027	0.000000	24.145495	798.420624	0.000000	1854.025635	6902.256821	0.000000	20.599252
LU1369-012	1200 °C		12.718017	0.000000	0.000000	0.000000	0.000000	2.376997	0.000000	8.202441	0.000000	28.760861	720.776862	0.000000	2217.880487	3758.173896	0.000000	18.596043
LU1369-013	1300 °C		18.270112	0.000000	0.000000	0.000000	0.000000	3.414684	0.000000	10.033844	0.000000	19.346426	881.708622	0.000000	1846.728478	5398.818079	0.000000	22.748082
		S	3947.423262	0.000000	0.000000	0.000000	0.000000	737.773408	0.000000	11449.435670	0.000000	41402.968782	1006101.552683	0.000000	1432004.666351	1166463.574013	0.000000	25957.420059
		S				3947.423262	0.000000					53590.177860		1006101.552683				2624425.660424

Additional Parameters			40(r)/39(k)	1s	40(r+a)	1s	40Ar/39Ar	1s	37Ar/39Ar	1s	36Ar/39Ar	1s	37Ar (decay)	39Ar (decay)	40Ar (moles)
LU1369-001	600 °C		1.719815	0.06352	833271.11917	922.50951	9.02495	0.02166	0.00000	0.00005	0.02463	0.00022	1.00000000	1.00594364	9.644E-14
LU1369-002	660 °C	4	1.303214	0.02032	340177.26029	432.06496	2.20418	0.00547	0.00000	0.00003	0.00296	0.00007	1.00000000	1.00594381	3.972E-14
LU1369-003	710 °C	4	1.246896	0.00597	318920.68657	368.51819	1.63528	0.00386	0.00000	0.00003	0.00123	0.00002	1.00000000	1.00594398	3.739E-14
LU1369-004	780 °C	4	1.397513	0.01003	189649.04136	389.66017	1.80959	0.00542	0.00000	0.00004	0.00131	0.00003	1.00000000	1.00594415	2.220E-14
LU1369-005	860 °C	4	1.429929	0.01008	214252.05573	427.23045	1.83819	0.00526	0.00000	0.00004	0.00129	0.00003	1.00000000	1.00594432	2.508E-14
LU1369-006	950 °C	4	1.368391	0.00736	382147.96929	462.58266	1.75390	0.00411	0.00000	0.00001	0.00122	0.00002	1.00000000	1.00594449	4.476E-14
LU1369-007	1010 °C	4	1.527203	0.01709	171481.87529	418.74241	2.09959	0.00664	0.00000	0.00004	0.00185	0.00005	1.00000000	1.00594466	2.004E-14
LU1369-008	1060 °C		2.035300	0.03373	60270.26518	393.48033	2.67866	0.01884	0.00000	0.00014	0.00209	0.00010	1.00000000	1.00594483	7.023E-15
LU1369-009	1100 °C		4.294075	0.17593	24195.24599	404.28786	5.78411	0.09843	0.00000	0.00121	0.00496	0.00050	1.00000000	1.00594500	2.805E-15
LU1369-010	1130 °C		3.613212	0.61645	42124.83809	423.36007	27.87395	0.40159	0.00000	0.00413	0.08201	0.00204	1.00000000	1.00594518	4.866E-15
LU1369-011	1160 °C		2.322116	1.18304	8756.28246	429.39508	10.99280	0.55728	0.00000	0.00483	0.02926	0.00359	1.00000000	1.00594534	1.013E-15
LU1369-012	1200 °C		3.077069	0.93429	5976.05438	446.08228	8.31693	0.63115	0.00000	0.00466	0.01764	0.00238	1.00000000	1.00594552	6.918E-16
LU1369-013	1300 °C		2.094488	0.84955	7245.54656	496.63086	8.24342	0.57960	0.00000	0.00394	0.02072	0.00218	1.00000000	1.00594569	8.388E-16

Information on Analysis

2000APa45
Biotite
2000APa45 biotite, Alaska (Enkelmann-Spot
Zeitler

Project = Alaska Micas 09
Irradiation = I47
J = 0.0019250 ± 0.0000096
GA-1550 = 98.790 ± 0.543 Ma

Results	40(r)/39(k) ± 2s	Age ± 2s (Ma)	MSWD	39Ar(k) (%,n)	K/Ca ± 2s
Error Plateau	1.3389 ± 0.0740 ± 5.53%	4.64 ± 0.26 ± 5.61% External Error ± 0.26 Analytical Error ± 0.26	98.81 2.57 9.9404	87.73 6 Statistical T Ratio Error Magnification	6530.941 ± 4334.654
Total Fusion Age	1.4233 ± 0.0150 ± 1.06%	4.94 ± 0.07 ± 1.45% External Error ± 0.07 Analytical Error ± 0.05		13	205.259 ± 112.146

Results	40(a)/36(a) ± 2s	40(r)/39(k) ± 2s	Age ± 2s (Ma)	MSWD
Error Chron	423.3140 ± 236.4522 ± 55.86%	1.1380 ± 0.3286 ± 28.87%	3.95 ± 1.14 ± 28.86% External Error ± 1.14 Analytical Error ± 1.14	73.89

Statistics				
	Statistical F Ratio	2.37	Convergence	0.0000000902
	Error Magnification	8.5959	Number of Iterations	50
	n	6	Calculated Line	Weighted York-2

Results	40(a)/36(a) ± 2s	40(r)/39(k) ± 2s	Age ± 2s (Ma)	MSWD
Error Chron	531.5752 ± 391.7086 ± 73.69%	1.0250 ± 0.3389 ± 33.06%	3.56 ± 1.18 ± 33.05% External Error ± 1.18 Analytical Error ± 1.17	66.39

Statistics				
	Statistical F Ratio	2.37	Convergence	0.0000470423
	Error Magnification	8.1479	Number of Iterations	9
	n	6	Calculated Line	Weighted York-2

Dataset B-3. Data used in time-temperature plots of Areas 1–4 as presented in Figures 4-5 to 4-9 and Figures A-1–A-4

B-3.1. *Data compilation of samples used in Area 1*

Sample ID	Lat (°)	Long (°)	Elevation (m)	Rock type	Sample type	Zr U/Pb (Ma)	2σ error (Ma)	Am 40Ar/39Ar or K-Ar (Ma)	2σ error (Ma)	Ms 40Ar/39Ar or K-Ar (Ma)	2σ error (Ma)	Bt 40Ar/39Ar (MA) or K-Ar (Ma)	2σ error (Ma)	ZFT (Ma)	2σ error (Ma)	ZHe (Ma)	1σ error (Ma)	AFT (Ma)	2σ error (Ma)	AHe (Ma)	1σ error (Ma)	Reference	Remarks
Tk6	60.6642	-141.5488		Schist	Bedrock	54	± 0.8			49	± 2.8											Gasser et al. 2011	
Tk7	60.6671	-141.5521		Intrusion	Bedrock	53	± 0.7					49.1	± 2.8									Gasser et al. 2011	
Loc4	60.5544	-141.303		Gneiss	Bedrock							47.4	± 2.1	26	± 2.8							Gasser et al. 2011	
91Asn11	60.8236	-144.25		Gneiss	Bedrock	52.8	± 1							30.9	± 8.6							Gasser et al. 2011	sample by V. Sisson
B40	60.8883	-143.2384		Schist	Bedrock							47.6	± 2.3									Gasser et al. 2011	
B21	60.8124	-143.3148		Gneiss	Bedrock							48.4	± 2.1	28.1	± 2.8							Gasser et al. 2011	
KB1	60.7643	-143.2881		Gneiss	Bedrock							50	± 2.2									Gasser et al. 2011	
KB5	60.7381	-143.3015		Gneiss	Bedrock	54	± 0.8					47.3	± 2.1									Gasser et al. 2011	
B1	60.8496	-143.2388		Dike	Bedrock					45.8	± 2.1											Gasser et al. 2011	
B14	60.8233	-143.2777		Intrusion	Bedrock					53.4	± 2.9											Gasser et al. 2011	
T27	60.7146	-142.9147		Gneiss	Bedrock	52.6	± 0.8					49.2	± 2.5									Gasser et al. 2011	
T22	60.7108	-142.9036		Gneiss	Bedrock					46.2	± 2.3	47.3	± 2									Gasser et al. 2011	
T11	60.7013	-142.9004		Gneiss	Bedrock							47.5	± 2.3									Gasser et al. 2011	
T33	60.6856	-142.9034		Fault rock	Bedrock							46.9	± 2.1									Gasser et al. 2011	
T40	60.6828	-142.9238		Gneiss	Bedrock	54	± 0.9					47	± 2	28.9	± 2.4							Gasser et al. 2011	
01-48a	60.7911	-142.6368	1920	Schist	Bedrock									48.4	± 2.6			5	± 2.4	16	± 1.6	Meigs et al. 2008	AHe and ZHe from Spotila et al. 2004
01-49a	60.6793	-142.534	2012	Gneiss	Bedrock													13.3	± 1.3	13	± 1.3	Meigs et al. 2008	AHe and ZHe from Spotila et al. 2004
99-2	60.7203	-142.5435	754	Gneiss	Bedrock									34.4	± 1.8	26	± 2.1	13.8	± 1.4	8.2	± 0.8	Meigs et al. 2008	AHe and ZHe from Spotila et al. 2004
01-45a	60.6572	-142.4146	1783	Granite	Bedrock													14.5	± 1.3	9.7	± 1	Meigs et al. 2008	AHe and ZHe from Spotila et al. 2004
01-47a	60.7672	-142.6065	1494	Schist	Bedrock													27.3	± 2.7	13.3	± 1.3	Meigs et al. 2008	AHe and ZHe from Spotila et al. 2004
06STP13	60.6312	-141.1747	2639	Granitoid	Bedrock															9.64	± 0.24	Spotila and Berger 2010	
06STP15	60.5279	-141.1024	2226	Granitoid	Bedrock															4.95	± 0.33	Spotila and Berger 2010	
06STP69	60.6632	-141.4497	2391	Granitoid	Bedrock															10.8	± 1.39	Spotila and Berger 2010	
06STP51	60.5873	-143.9549	1469	Granitoid	Bedrock															2.04	± 0.11	Spotila and Berger 2010	
06STP52	60.6595	-143.9058	1445	Schist	Bedrock															6.49	± 1.09	Spotila and Berger 2010	
06STP53	60.5851	-143.6721	2094	Metagraywacke	Bedrock															1.6	± 0.17	Spotila and Berger 2010	
06STP60	60.6552	-143.0018	1475	Metaflysch	Bedrock															3.63	± 0.29	Spotila and Berger 2010	
06STP55	60.7496	-143.7488	1652	Gneiss	Bedrock															9.08	± 0.96	Spotila and Berger 2010	
06STP56	60.7849	-143.7299	1630	Gneiss	Bedrock															18.2	± 1.45	Spotila and Berger 2010	
06STP57	60.7095	-143.4223	2180	Granitoid	Bedrock															4.18	± 0.24	Spotila and Berger 2010	
05STP23	60.60122	-142.34093	1432	Schist, meta-sandstone	Bedrock															6.86	± 1.26	Berger et al. 2008	
05STP36	60.55415	-141.74559	2171	Biotite gneiss	Bedrock															9.03	± 0.5	Berger et al. 2008	
06STP41	60.74383	-141.96478	900	Schist	Bedrock															16.9	± 1.15	Berger et al. 2008	
06STP44	60.75363	-141.92648	1732	Quartzite	Bedrock															20.7	± 1.2	Berger et al. 2008	
05STP10	60.8622	-143.3235	1804	Metapelite/schist	Bedrock															22.8	± 1.8	Berger et al. 2008	
05STP7	60.8838	-143.7637	1140	Gneiss	Bedrock															25.1	± 0.87	Berger and Spotila 2008	
01CH22	60.9104	-144.315	1532	Schist	Bedrock															18.9	± 1.2	Berger and Spotila 2008	
01CH25	60.694	-144.3774	320	Phyllite	Bedrock															10.7	± 1.31	Berger and Spotila 2008	
73AH234A	60.68333	-142.933333		(Qz-Hbl) Amphibolite	Bedrock			51.5	± 2													Hudson et al. 1979	K-Ar age
73AH234B	60.68333	-142.933333		Schist	Bedrock							46.7	± 2									Hudson et al. 1979	K-Ar age

B-3.2. *Data compilation of samples used in Area 2*

Sample ID	Lat (º)	Long (º)	Elevation (m)	Rock type	Sample type	Zr U/Pb (Ma)	2σ error (Ma)	Am 40Ar/39Ar or K-Ar (Ma	2σ error (Ma)	Bt Ar/Ar (Ma) or K-Ar (Ma	2σ error (Ma)	ZFT (Ma)	2σ error (Ma)	ZHe (Ma)	1σ error (Ma)	AFT (Ma)	2σ error (Ma)	AHe (Ma)	1σ error (Ma)	Reference	Remarks
5924	60.60333333	-140.515	5924	Granite	Bedrock							43.8	± 2.5			36.0	± 3.0			O'Sullivan and Currie 1996	
5050	60.625	-140.5666667	5050	Granite	Bedrock											36.6	± 3.0	13.30	± 1.07	O'Sullivan and Currie 1996	AHe data from Spotila and Berger 2010
3335	60.61666667	-140.0166667	3335	Granite (King Peak Pluton)	Bedrock							41.2	± 2.0			25.7	± 2.4	7.08	± 0.15	O'Sullivan and Currie 1996	AHe data from Spotila and Berger 2010
1783	60.45	-140.2666667	1783	Granite	Bedrock											4.0	± 0.3			O'Sullivan and Currie 1996	
98ASn106	60.439133	-140.269267	~1750		Bedrock									9.6	± 2.0					Enkelmann et al. 2010	
69APr47C1	60.288333	-140.675		Quartzofeldspathic schist	Bedrock					17.4	± 0.5									Hudson et al. 1977b	K-Ar, metamorphics
69APr47C2	60.288333	-140.675		Amphibolite	Bedrock			23.4	± 0.7											Hudson et al. 1977b	K-Ar, metamorphics
69APr43B3	60.348333	-139.833333		Feldspathic schist	Bedrock			51.0	± 1.5	47.3	± 1.4									Hudson et al. 1977b	K-Ar, metamorphics
72-CAc-74-1	60.41805556	-140.2627778		Tonalite	Detrital moraine sample			51.5	± 3.0	45.4	± 2.4									Dodds and Campbell 1988	K-Ar, upper Seward Glacier
51-Cac-77-1	60.47833333	-140.5166667		Granitoid gneiss	Bedrock					48.7	± 2.7									Dodds and Campbell 1988	K-Ar, N side upper Seward Glacier
69APr-48A	60.31666667	-140.8333333		Gabbro/diorite, moraine sample	Detrital moraine sample			27.4	± 22.9											Dodds and Campbell 1988	K-Ar, Mt Newton sample
45-CAc-77-1	60.63833333	-140.2533333		Qartz diorite	Bedrock			153.0	± 7.0											Dodds and Campbell 1988	K-Ar, Mt. Logan batholith
106-CAc-77-1	60.60416667	-140.865		Tonalite	Detrital moraine sample					50.0	± 2.4									Dodds and Campbell 1988	K-Ar, King Peak Pluton
MAL7-14	59.8669	-140.1084667	61	Granitoid	Cobble-size detrital sample	50.9	± 1.4							2.4	± 0.2					This study	ZHe data from Grbaowski et al. 2013
MAL7-20	59.8669	-140.1084667	61	Granitoid	Cobble-size detrital sample	48.5	± 0.6							2.5	± 0.3					This study	ZHe data from Grbaowski et al. 2013
MAL3-8	59.70058333	-140.4039333	2	Orthogneiss	Cobble-size detrital sample	52.3	± 7.3			41.8	± 0.3			2.6	± 0.3			0.83	± 0.20	This study	ZHe data from Grbaowski et al. 2013
MAL2-4	59.77705	-140.7895167	81	Granitoid	Cobble-size detrital sample	50.8	± 1.0							13.3	± 1.6					This study	ZHe data from Grbaowski et al. 2013
MAL6-24	59.81708333	-140.30245	47	Paragneiss	Cobble-size detrital sample	52.8	± 0.5			48.8	± 0.2			14.5	± 0.8					This study	ZHe data from Grbaowski et al. 2013
MAL2-16	59.77705	-140.7895167	81	Micaschist	Cobble-size detrital sample	72-49				48.0	± 0.2			15.5	± 0.7			4.20	± 0.29	This study	ZHe data from Grbaowski et al. 2013
MAL6-23	59.81708333	-140.30245	47	Gneiss	Cobble-size detrital sample	52.4	± 0.4	51.2	± 0.2	48.7	± 0.2			15.5	± 1.5			3.62	± 0.35	This study	ZHe data from Grbaowski et al. 2013
MAL4-5	59.74943333	-140.4836333	65	Paragneiss	Cobble-size detrital sample	60-48								16.4	± 1.3					This study	ZHe data from Grbaowski et al. 2013
MAL2-10	59.77705	-140.7895167	81	Paragneiss	Cobble-size detrital sample	335-81				50.4	± 0.2			16.7	± 5.6			6.52	± 0.87	This study	ZHe data from Grbaowski et al. 2013
MAL4-16	59.74943333	-140.4836333	65	Paragneiss	Cobble-size detrital sample	279-56								16.8	± 2.6					This study	ZHe data from Grbaowski et al. 2013
MAL7-3	59.8669	-140.1084667	61	Meta-Quartzdiorite	Cobble-size detrital sample	181.6	± 0.8	181.0	± 0.6					3.0	± 0.2			0.64	± 0.03	This study	ZHe data from Grbaowski et al. 2013
MAL3-19	59.70058333	-140.4039333	2	Granitoid	Cobble-size detrital sample	277.1	± 6.7							11.0	± 1.9					This study	ZHe data from Grbaowski et al. 2013
MAL4-9	59.74943333	-140.4836333	65	Orthogneiss	Cobble-size detrital sample	150.0	± 1.0							32.3	± 10.1					This study	ZHe data from Grbaowski et al. 2013
MAL6-5	59.81708333	-140.30245	47	Orthogneiss	Cobble-size detrital sample	151.0	± 0.7							36.9	± 9.9					This study	ZHe data from Grbaowski et al. 2013
MAL4-6	59.74943333	-140.4836333	65	Igneous mylonite	Cobble-size detrital sample	53.3	± 0.3							29.2	± 1.4					This study	ZHe data from Grbaowski et al. 2013
MAL1-14	59.8592	-140.89585		Amphibolite	Cobble-size detrital sample	30.8	± 0.8							2.2	± 0.3					This study	ZHe data from Grbaowski et al. 2013
MAL1-19	59.8592	-140.89585		Aplite	Cobble-size detrital sample	46.4	± 1.0							2.3	± 0.4					This study	ZHe data from Grbaowski et al. 2013
MAL1-8	59.8592	-140.89585		Migmatitic gneiss	Cobble-size detrital sample			15.8	± 0.4					2.4	± 0.5			1.84	± 0.41	This study	ZHe data from Grbaowski et al. 2013
MAL7-2	59.8669	-140.1084667	61	Gabbro	Cobble-size detrital sample	49.4	± 0.4	42	± 2.7					3.2	± 1.03					This study	ZHe data from Grbaowski et al. 2013
MAL4-21	59.74943333	-140.4836333	65	Metasedimentary mylonite	Cobble-size detrital sample	493-58								20.5	± 1.3					This study	ZHe data from Grbaowski et al. 2013

B-3.3. *Data compilation of samples used in Area 3*

Sample ID	Lat (º)	Long (º)	Elevation (m)	Rock type	Sample type	Am 40Ar/39Ar or K-Ar (Ma)	2σ error (Ma)	Ms 40Ar/39Ar or K-Ar (Ma)	2σ error (Ma)	Bt 40Ar/39Ar or K-Ar (Ma)	2σ error (Ma)	ZFT (Ma)	2σ error (Ma)	ZHe (Ma)	1σ error (Ma)	AFT (Ma)	2σ error (Ma)	AHe (Ma)	1σ error (Ma)	Reference	Remarks
69APR32A	60.300278	-139.600278	2499	Granodiorite	Bedrock			46.8	± 1.0	44.6	± 1.0					4.4	± 1.0			O'Sullivan et al. 1997	K-Ar (from Hudson et al. 77)
69APR40A2	60.2175	-139.516667	1524	Granodiorite ?	Bedrock					30.6	± 1.0					1.7	± 0.4			O'Sullivan et al. 1997	K-Ar (from Hudson et al. 77)
81APr5	60.269965	-139.435089	2332	Foliated hornblende diorite	Bedrock	50.9	± 3.9									3.4	± 1.3			O'Sullivan et al. 1997	K-Ar (from Hudson et al. 77)
67APR78A	60.118333	-139.468056	922	Tonalite	Bedrock	18.5	± 1.0	20.9	± 3.0							3.5	± 1.2			O'Sullivan et al. 1997	K-Ar (from Hudson et al. 77)
69APr23A	60.001389	-139.283333			Bedrock	20.0	± 2.0													Hudson et al. 1977a	K-Ar
69APr31C2	60.33611	-139.20167			Bedrock	284.0	± 7.0													Hudson et al. 1977a	K-Ar
69APr31B	60.283889	-139.185833			Bedrock	279.0	± 8.0													Hudson et al. 1977a	K-Ar
69APr37D	60.301667	-139.531667			Bedrock	58.5	± 1.7													Hudson et al. 1977b	K-Ar
118-CAc-77-1	60.97833333	-140.3283333		Granodiorite	Bedrock	149.0	± 14.0			146.0	± 4.0									Dodds and Campbell 1988	K-Ar, Mt. Lucania pluton
90-CAc-77-1	61.00666667	-140.2533333		Diorite	Bedrock	139.0	± 12.0													Dodds and Campbell 1988	K-Ar, Mt. Lucania pluton
164-CAc-77-1	61.025	-140.0483333		Monzonite	Bedrock	147.0	± 10.0			144.0	± 4.0									Dodds and Campbell 1988	K-Ar, Mt. Walsh pluton
112-CAc-77-1	60.79166667	-140.2816667		Granodiorite	Bedrock	159.0	± 11.0													Dodds and Campbell 1988	K-Ar, Logan Glacier pluton
110-CAc-77-1	60.78777778	-140.2341667		Diorite	Bedrock	159.0	± 8.0													Dodds and Campbell 1988	K-Ar, Logan Glacier pluton
16-CAc-77-1	60.71833333	-140.0333333		Granodiorite	Bedrock	150.0	± 11.0			156.0	± 6.0									Dodds and Campbell 1988	K-Ar, Logan Glacier pluton
13-CAc-77-1	60.71	-139.865		Granodiorite	Bedrock	189.0	± 10.0			151.0	± 5.0									Dodds and Campbell 1988	K-Ar, E side Hubbard Glacier
82-CAc-77-1	60.68	-140.1683333		Granodiorite	Bedrock	147.0	± 8.0													Dodds and Campbell 1988	K-Ar, Hubbard Glacier pluton
33-CAc-77-1	60.57166667	-139.8833333		Granodiorite/quartz diorite	Bedrock	132.0	± 9.0													Dodds and Campbell 1988	K-Ar, Hubbard Glacier pluton
45-CAc-77-1	60.63833333	-140.2533333		Quartz diorite	Bedrock	153.0	± 7.0													Dodds and Campbell 1988	K-Ar, Mt. Logan batholith
71-CAc-74-1	60.74138889	-139.7491667		Monzodiorite	Bedrock	281.0	± 12.0													Dodds and Campbell 1988	K-Ar, Divide batholith
66-CAc-74-1	60.51277778	-139.3547222		Monzonite	Bedrock	276.0	± 11.0													Dodds and Campbell 1988	K-Ar, Kaskawulsh Glacier batholith
54-CAc-74-1	60.33138889	-139.2538889		Monzodiorite	Bedrock	297.0	± 20.0													Dodds and Campbell 1988	K-Ar, Mt. Hubbard pluton
111-CAc-77-1	60.745	-140.16		Diorite	Bedrock	154.0	± 12.0													Dodds and Campbell 1988	K-Ar, Logan Glacier pluton
6-CAc-77-1	60.42333333	-139.5283333		Quartz diorite	Bedrock	150.0	± 10.0													Dodds and Campbell 1988	K-Ar, NE side, central Hubbard Glacier
155-CAc-77-1	60.05	-138.76		Monzonite	Bedrock	290.0	± 15.0			270.0	± 9.0									Dodds and Campbell 1988	K-Ar, Fisher pluton
K1	60.571	-139.8902	2316	Granitoid	Bedrock													3.75	± 0.31	Spotila and Berger 2010	multialiquot analysis
K2	60.6633	-139.5177	2225	Granitoid	Bedrock													5.93	± 1.48	Spotila and Berger 2010	multialiquot analysis
K14	60.3963	-138.9317	2233	Metagranite	Bedrock													4.32	± 0.38	Spotila and Berger 2010	multialiquot analysis
03PH311A	60.0225	-139.2058	1610	Granite	Bedrock					35.3	± 0.5	4.5	± 0.3	2.0	± 0.1			0.89	± 0.11	McAleer et al. 2009; This study (Bt 40Ar/39Ar)	
HUB2-2	60.04038333	-139.5425333	16	Granitoid	Cobble-size detritus					50.0	± 0.3			34.8	± 3.0	3.8	± 2.0			This study	
HUB2-3	60.04038333	-139.5425333	16	Meta-quartzdiorite	Cobble-size detritus	276/139*								between ~17 and ~24		17.2	± 1.4			This study	*276 Ma Am 40Ar/39Ar age is minimum crystallization age; 139 Ma is max. age of resetting thermal event
HUB2-5	60.04038333	-139.5425333	16	Granodiorite	Cobble-size detritus	151.2	± 1.1							5.8	± 1.3	4.8	± 1.3			This study	
HUB2-7	60.04038333	-139.5425333	16	Hornblende-gabbro	Cobble-size detritus	25.5	± 0.4									1.6	± 1.0			This study	
HUB2-8	60.04038333	-139.5425333	16	Mylonite	Cobble-size detritus					49.8	± 0.3			4.8	± 0.0					This study	
2000APa45	60.03215	-139.328241	309	Mylonitic tonalite	Bedrock					5-3.5										This study	

B-3.4. *Data compilation of samples used in Area 4*

Sample ID	Lat (º)	Long (º)	Elevation (m)	Rock type	Sample type	Zr U/Pb (Ma)	2σ error (Ma)	Am 40Ar/39Ar or K-Ar (Ma)	2σ error (Ma)	Ms 40Ar/39Ar or K-Ar (Ma)	2σ error (Ma)	Bt 40Ar/39Ar or K-Ar (Ma)	2σ error (Ma)	ZFT (Ma)	2σ error (Ma)	ZHe (Ma)	1σ error (Ma)	AFT (Ma)	2σ error (Ma)	AHe (Ma)	1σ error (Ma)	Reference	Remarks
N9	59.8223	-138.8313		Gneiss	Bedrock	51.3	± 0.7			22.6	± 1.1	15.8	± 0.8									Gasser et al. 2011	
N28	59.8151	-138.8827		Mylonite	Bedrock					20.0	± 1.0											Gasser et al. 2011	
N48	59.821	-138.8783		Gneiss	Bedrock																	Gasser et al. 2011	
N19	59.833	-138.8314		Pegmatite	Bedrock					36.2	± 2.2											Gasser et al. 2011	
94APo9	59.8414	-139.1825		Diorite	Bedrock			53.9	± 0.7													Sisson et al. 2003	
94APo27	59.8503	-139.0258		Amphibolite	Bedrock			20.0	± 0.7													Sisson et al. 2003	
03PH305A	59.1281	-138.0839	88	Tonalite	Bedrock									27.5	± 1.5	2.45	± 0.2			1.82	± 0.49	McAleer et al. 2009	
03PH306A	59.4272	-138.1097	67	Tonalite	Bedrock															5.11	± 0.65	McAleer et al. 2009	
03PH307A	59.4378	-138.2429	243	Granodiorite	Bedrock							42.4	± 1.1	16.5	± 0.8	13	± 0.8			2.34	± 0.33	McAleer et al. 2009; This study (Bt 40Ar/39Ar)	
03PH308A	59.4214	-138.4519			Bedrock									18.8	± 1.2	2.6	± 0.3					McAleer et al. 2009	
03PH309A	59.4044	-138.6967	741	Orthogneiss	Bedrock															2.56	± 0.17	McAleer et al. 2009	
03PH310A	59.9417	-139.2331	926	Granodiorite	Bedrock															1.67	± 0.12	McAleer et al. 2009	
03PH311A	60.0225	-139.2058	1610	Granite	Bedrock							35.3	± 0.5	4.5	± 0.3	1.96	± 0.1			0.89	± 0.11	McAleer et al. 2009; This study (Bt 40Ar/39Ar)	
69APR32A	60.3017	-139.6017	2499	Granodiorite	Bedrock															1.9	± 0.14	McAleer et al. 2009	Sample from O'Sullivan et al. 1997
95APo13	59.6006	-138.5422	914	Tonalite	Bedrock															1.45	± 0.04	McAleer et al. 2009	
95APo21	59.8144	-138.9167	0	Granite	Bedrock															2.5	± 0.51	McAleer et al. 2009	
67APR42A	59.8875	-139.133611	617	Diorite	Bedrock			51.1	± 3.0									2.8	± 0.4			O'Sullivan et al. 1997	
67APR42B	59.751389	-139.100556	712	Adamellite	Bedrock					48.4	± 2.0	42.7	± 2.0					3.1	± 0.8			O'Sullivan et al. 1997	
69APR40A2	60.2175	-139.516667	1524	Granodiorite ?	Bedrock							30.6	± 1.0					1.7	± 0.4			O'Sullivan et al. 1997	
67APR78A	60.118333	-139.468056	922	Tonalite	Bedrock			18.5	± 1.0	20.9	± 3.0							3.5	± 1.2			O'Sullivan et al. 1997	
80APR49A	59.8967	-138.9033	1250	Biotite muscovite tonalite	Bedrock			37.1	± 1.4			36.2	± 1.4					2.7	± 0.7	1.13	± 0.08	O'Sullivan et al. 1997	AHe from McAleer et al. 2009
69APr23A	60.001389	-139.283333			Bedrock			20.0	± 2.0													Hudson et al. 1977a	K-Ar
68APr103B	59.616667	-138.516667			Bedrock			61.0	± 2.0													Hudson et al. 1977a	K-Ar
68AMk108	59.518889	-138.384722			Bedrock							25.3	± 1.0									Hudson et al. 1977a	K-Ar
67APr57B1	59.866944	-138.968889			Bedrock					23.5	± 0.7											Hudson et al. 1977a	K-Ar
69APr30B	59.8525	-138.75			Bedrock			225.0	± 6.0													Hudson et al. 1977a	K-Ar
68APr64B	59.343056	-138.35			Bedrock							24.1	± 3.0									Hudson et al. 1977a	K-Ar
67APr94C	59.418056	-138			Bedrock							165.0	± 5.0									Hudson et al. 1977a	K-Ar
68APr69C	59.8175	-138.735278			Bedrock			136.0	± 4.0													Hudson et al. 1977a	K-Ar
63APr219	59.826667	-139.03			Bedrock			63.8	± 1.9													Hudson et al. 1977b	K-Ar
67APr44B	59.851667	-138.996667			Bedrock			67.2	± 2.0													Hudson et al. 1977b	K-Ar
67APr45B	59.811667	-138.813333			Bedrock							19.4	± 0.6									Hudson et al. 1977b	K-Ar
68APr65B	59.396667	-138.41			Bedrock			65.4	± 2.0													Hudson et al. 1977b	K-Ar
68APr78D1	59.14	-138.003333			Bedrock			18.5	± 0.6													Hudson et al. 1977b	K-Ar
68APr84A	59.37	-138.11			Bedrock							23.3	± 0.7									Hudson et al. 1977b	K-Ar
68APr106A2	59.591667	-138.771667			Bedrock							30.1	± 0.9									Hudson et al. 1977b	K-Ar
68APr106B	59.591667	-138.771667			Bedrock			47.0	± 1.4													Hudson et al. 1977b	K-Ar
68APr57F	59.196667	-138.211667			Bedrock							4.0	± 0.2									Hudson et al. 1977b	K-Ar
63APr205	59.803333	-138.888333			Bedrock			21.9	± 1.0													Hudson et al. 1977b	K-Ar
53-CAc-78-1	59.48166667	-138.1533333		Quartz monzonite/granite	Bedrock							32.0	± 1.9									Dodds and Campbell 1988	K-Ar, Alsek River pluton
49-CAc-78-1	59.4125	-138.025		Quartz monzonite	Bedrock							32.8	± 1.9									Dodds and Campbell 1988	K-Ar, Alsek River pluton
YA-54	59.841483	-139.0606	1	Fine-grained sandstone	Bedrock											5.1	± 1.4			1.88	± 0.69	Enkelmann et al. 2015b	
Y-09	59.84286	-139.1529	1	Fine-grained sandstone	Bedrock															5.13	± 2.8	Enkelmann et al. 2015b	
HUB2-2	60.04038333	-139.5425333	16	Granitoid	Cobble-size detritus							50.0	± 0.3			34.84	± 3.0	3.8	± 2.0			This study	
HUB2-3	60.04038333	-139.5425333	16	Meta-quartzdiorite	Cobble-size detritus			276/139*								between ~17 and ~24		17.2	± 1.4			This study	*276 Ma Am 40Ar/39Ar age is minimum crystallization age; 139 Ma is max. age of resetting thermal event
HUB2-5	60.04038333	-139.5425333	16	Granodiorite	Cobble-size detritus			151.2	± 1.1							5.79	± 1.3	4.8	± 1.3			This study	
HUB2-7	60.04038333	-139.5425333	16	Hornblende-gabbro	Cobble-size detritus			25.5	± 0.4									1.6	± 1.0			This study	
HUB2-8	60.04038333	-139.5425333	16	Mylonite	Cobble-size detritus							49.8	± 0.3			4.82	± 0.0					This study	
2000APa45	60.03215	-139.328241	309	Mylonitic tonalite	Bedrock							5-3.5										This study	

Dataset B-4. Single-grain zircon fission-track ages of KLD samples

==================ZetaAge Program v. 4.8 (Brandon 8/13/02)==================

KLD9 (Yukon), modern sand, TU11z (counted by Sarah Falkowski, April 2014)

EFFECTIVE TRACK DENSITY FOR FLUENCE MONITOR (tracks/cm^2): 6.480E+05

RELATIVE ERROR (%): 1.57

EFFECTIVE URANIUM CONTENT OF MONITOR (ppm): 50.00

ZETA FACTOR AND STANDARD ERROR (yr cm^2): 119.60 5.40

SIZE OF COUNTER SQUARE (cm^2): 1.000E-06

------ GRAIN AGES IN ORIGINAL ORDER ------

Grain no.	RhoS (cm^-2)	(Ns)	RhoI (cm^-2)	(Ni)	Squares	U	+/-2s	Grain Age	Age (Ma) --95% CI--	
1	2.35E+07	(94)	7.25E+06	(29)	4	559	207	123.9	81.4	194.9
2	2.33E+07	(140)	1.47E+07	(88)	6	1132	243	61.2	46.2	81.0
3	1.57E+07	(94)	5.17E+06	(31)	6	399	143	116.0	77.0	180.2
4	1.47E+07	(88)	4.17E+06	(25)	6	322	128	134.4	86.0	218.6
5	1.73E+07	(138)	4.38E+06	(35)	8	338	114	150.5	103.8	224.6
6	1.08E+07	(65)	3.83E+06	(23)	6	296	122	108.1	66.7	182.3
7	1.27E+07	(152)	4.67E+06	(56)	12	360	96	104.1	76.4	144.2
8	1.10E+07	(44)	4.00E+06	(16)	4	309	152	105.0	58.6	199.4
9	1.49E+07	(119)	4.50E+06	(36)	8	347	115	126.4	86.9	189.0
10	8.14E+06	(114)	6.93E+06	(97)	14	535	110	45.3	34.1	60.3
11	1.23E+07	(98)	4.75E+06	(38)	8	367	119	98.9	67.6	147.9
12	9.25E+06	(37)	4.25E+06	(17)	4	328	157	83.4	46.1	157.9
13	1.28E+07	(192)	2.53E+06	(38)	15	195	63	192.2	136.0	279.4
14	2.02E+07	(121)	5.33E+06	(32)	6	412	145	144.4	97.7	220.1
15	7.50E+06	(30)	3.75E+06	(15)	4	289	147	76.6	40.3	153.3
16	1.11E+07	(156)	4.00E+06	(56)	14	309	83	106.9	78.5	147.8
17	1.46E+07	(102)	9.00E+06	(63)	7	694	176	62.4	45.2	86.9
18	1.23E+07	(49)	3.50E+06	(14)	4	270	142	133.1	73.2	260.9
19	1.44E+07	(173)	4.25E+06	(51)	12	328	92	129.8	94.8	181.1
20	9.91E+06	(109)	3.64E+06	(40)	11	281	89	104.5	72.4	154.1
21	8.07E+06	(113)	2.29E+06	(32)	14	176	62	134.9	90.9	206.4
22	9.42E+06	(113)	4.92E+06	(59)	12	379	99	73.7	53.4	102.8
23	1.68E+07	(67)	5.50E+06	(22)	4	424	179	116.4	71.5	197.8
24	1.34E+07	(267)	4.80E+06	(96)	20	370	76	106.5	83.0	136.6
25	1.82E+07	(109)	5.67E+06	(34)	6	437	150	122.7	83.2	185.9
26	1.09E+07	(131)	3.17E+06	(38)	12	244	79	131.8	91.7	194.4
27	1.71E+07	(120)	3.00E+06	(21)	7	231	100	216.3	136.9	360.9
28	1.76E+07	(141)	4.88E+06	(39)	8	376	120	138.2	96.8	202.3
29	1.48E+07	(59)	9.50E+06	(38)	4	733	237	59.8	39.2	92.4
30	8.50E+06	(34)	1.75E+06	(7)	4	135	99	182.2	81.6	484.7
31	1.24E+07	(62)	6.80E+06	(34)	5	525	179	70.1	45.6	109.9
32	1.48E+07	(59)	4.00E+06	(16)	4	309	152	140.3	80.6	260.9
33	1.49E+07	(119)	5.88E+06	(47)	8	453	132	97.2	69.0	139.3
34	1.50E+07	(60)	4.50E+06	(18)	4	347	162	127.1	74.7	228.6
35	1.95E+07	(78)	6.25E+06	(25)	4	482	192	119.3	75.7	195.3
36	1.78E+07	(71)	5.50E+06	(22)	4	424	179	123.2	76.1	208.8
37	1.03E+07	(62)	2.67E+06	(16)	6	206	102	147.3	85.0	273.2
38	1.52E+07	(91)	6.00E+06	(36)	6	463	154	97.0	65.5	146.9
39	1.36E+07	(109)	6.13E+06	(49)	8	473	135	85.5	60.6	122.4
40	1.21E+07	(254)	3.90E+06	(82)	21	301	67	118.4	91.0	154.0
41	1.62E+07	(243)	5.13E+06	(77)	15	396	91	120.6	92.1	157.9
42	1.23E+07	(74)	2.83E+06	(17)	6	219	105	165.3	97.7	298.2
43	1.60E+07	(96)	3.83E+06	(23)	6	296	122	158.9	100.9	262.1
44	9.25E+06	(37)	4.25E+06	(17)	4	328	157	83.4	46.1	157.9
45	1.28E+07	(179)	4.36E+06	(61)	14	336	86	112.5	83.9	153.1

46	1.50E+07	(150)	8.00E+06	(80)	10	617	139	72.0	54.2	95.8
47	1.04E+07	(52)	4.40E+06	(22)	5	340	144	90.6	54.4	156.6
48	1.64E+07	(131)	4.63E+06	(37)	8	357	117	135.3	93.8	200.5
49	1.14E+07	(57)	2.20E+06	(11)	5	170	100	195.4	103.3	411.6
50	1.63E+07	(65)	6.25E+06	(25)	4	482	192	99.6	62.3	164.9
51	1.60E+07	(64)	4.00E+06	(16)	4	309	152	152.0	87.9	281.3
52	1.08E+07	(86)	2.75E+06	(22)	8	212	90	148.9	93.2	249.6
53	1.95E+07	(78)	5.00E+06	(20)	4	386	171	148.5	90.8	256.0
54	1.21E+07	(145)	4.50E+06	(54)	12	347	95	103.0	75.1	143.6
55	1.30E+07	(52)	3.25E+06	(13)	4	251	137	151.8	82.6	303.3
56	9.00E+06	(36)	3.50E+06	(14)	4	270	142	98.2	52.2	197.1
57	1.77E+07	(106)	7.17E+06	(43)	6	553	169	94.6	66.0	138.2
58	1.90E+07	(342)	5.50E+06	(99)	18	424	86	132.0	103.9	167.7
59	8.50E+06	(51)	4.00E+06	(24)	6	309	125	81.5	49.5	138.5
60	1.10E+07	(44)	3.75E+06	(15)	4	289	147	111.9	61.7	216.4
61	1.10E+07	(44)	4.50E+06	(18)	4	347	162	93.5	53.4	172.0
62	1.09E+07	(87)	6.38E+06	(51)	8	492	138	65.7	46.0	94.8
63	7.83E+06	(47)	4.33E+06	(26)	6	334	130	69.5	42.3	116.9
64	1.82E+07	(109)	5.00E+06	(30)	6	386	140	138.7	92.5	215.2
65	1.48E+07	(59)	4.75E+06	(19)	4	367	166	118.5	70.3	210.5
66	1.46E+07	(146)	4.90E+06	(49)	10	378	108	114.2	82.4	161.2
67	9.50E+06	(171)	2.11E+06	(38)	18	163	53	171.5	120.8	250.3
68	1.02E+07	(203)	5.35E+06	(107)	20	413	81	72.9	56.8	93.7
69	1.06E+07	(127)	3.83E+06	(46)	12	296	87	105.9	75.2	151.8
70	9.83E+06	(59)	3.50E+06	(21)	6	270	117	107.4	64.8	186.1
71	1.01E+07	(81)	5.63E+06	(45)	8	434	129	69.3	47.6	102.1
72	1.65E+07	(66)	3.00E+06	(12)	4	231	131	207.4	113.1	419.6
73	1.20E+07	(120)	3.70E+06	(37)	10	285	94	124.1	85.6	184.5
74	1.64E+07	(82)	4.00E+06	(20)	5	309	137	156.0	95.7	268.2
75	1.03E+07	(123)	4.33E+06	(52)	12	334	93	90.9	65.3	128.2
76	1.19E+07	(167)	4.79E+06	(67)	14	369	91	95.7	71.8	129.2
77	1.23E+07	(98)	4.25E+06	(34)	8	328	112	110.4	74.4	168.2
78	1.04E+07	(73)	2.43E+06	(17)	7	187	90	163.1	96.3	294.5
79	6.17E+06	(37)	1.33E+06	(8)	6	103	71	174.0	81.6	431.1
80	1.54E+07	(215)	5.93E+06	(83)	14	457	101	99.2	75.9	129.6
81	1.08E+07	(97)	4.78E+06	(43)	9	369	112	86.7	60.1	127.2
82	1.32E+07	(79)	4.17E+06	(25)	6	322	128	120.8	76.7	197.6
83	7.50E+06	(75)	2.10E+06	(21)	10	162	70	136.2	83.7	232.5
84	1.43E+07	(86)	5.50E+06	(33)	6	424	147	99.9	66.5	154.1
85	1.12E+07	(67)	3.00E+06	(18)	6	231	108	141.7	84.1	253.2
86	1.11E+07	(233)	3.24E+06	(68)	21	250	61	130.8	98.6	173.3
87	1.26E+07	(176)	3.64E+06	(51)	14	281	79	132.1	96.5	184.1
88	1.37E+07	(82)	4.50E+06	(27)	6	347	133	116.2	74.8	186.7
89	1.50E+07	(120)	5.00E+06	(40)	8	386	122	114.9	80.1	168.7
90	6.67E+06	(40)	1.67E+06	(10)	6	129	79	151.3	75.7	338.8
91	6.70E+06	(67)	2.10E+06	(21)	10	162	70	121.8	74.3	209.4
92	1.27E+07	(684)	4.28E+06	(231)	54	330	45	113.6	95.4	135.2
93	7.50E+06	(30)	1.25E+06	(5)	4	96	82	222.6	88.7	725.5
94	9.50E+06	(133)	3.79E+06	(53)	14	292	80	96.3	69.7	135.1
95	1.33E+07	(80)	4.00E+06	(24)	6	309	125	127.3	80.4	210.0
96	1.20E+07	(48)	3.00E+06	(12)	4	231	131	151.6	80.5	313.1
97	6.88E+06	(55)	2.88E+06	(23)	8	222	92	91.6	55.7	156.3
98	1.33E+07	(53)	4.00E+06	(16)	4	309	152	126.2	71.8	236.4
99	7.57E+06	(106)	2.43E+06	(34)	14	187	64	119.3	80.8	181.1
100	1.46E+07	(146)	4.20E+06	(42)	10	324	100	133.0	94.2	192.1
101	9.88E+06	(79)	4.50E+06	(36)	8	347	115	84.3	56.3	128.7
102	1.21E+07	(97)	4.50E+06	(36)	8	347	115	103.3	70.1	155.9

KLD13 (Yukon), modern sand, TU11z (counted by Sarah Falkowski, April 2014)

EFFECTIVE TRACK DENSITY FOR FLUENCE MONITOR (tracks/cm^2): 6.470E+05
RELATIVE ERROR (%): 1.57
EFFECTIVE URANIUM CONTENT OF MONITOR (ppm): 50.00
ZETA FACTOR AND STANDARD ERROR (yr cm^2): 119.60 5.40
SIZE OF COUNTER SQUARE (cm^2): 1.000E-06

------ GRAIN AGES IN ORIGINAL ORDER ------

Grain no.	**RhoS (cm^-2)**	**(Ns)**	**RhoI (cm^-2)**	**(Ni)**	**Squares**	**U+/-2s**		**Grain Age**	**Age (Ma) --95% CI--**	
1	9.20E+06	(138)	4.60E+06	(69)	15	355	86	76.8	57.2	104.2
2	8.17E+06	(98)	4.08E+06	(49)	12	316	90	76.8	54.1	110.6
3	6.44E+05	(29)	3.47E+06	(156)	45	268	44	7.2	4.7	10.8
4	1.06E+07	(95)	3.89E+06	(35)	9	301	101	103.9	70.1	157.8
5	1.45E+07	(58)	7.25E+06	(29)	4	560	207	76.7	48.5	124.3
6	4.17E+06	(25)	1.50E+06	(9)	6	116	75	105.4	48.3	256.7
7	9.05E+05	(19)	3.62E+06	(76)	21	280	65	9.7	5.5	16.2
8	1.70E+07	(68)	9.25E+06	(37)	4	715	235	70.6	46.7	108.4
9	1.08E+07	(54)	6.60E+06	(33)	5	510	177	62.9	40.1	100.1
10	1.02E+07	(409)	3.60E+06	(144)	40	278	47	108.7	88.1	134.1
11	7.33E+06	(88)	3.92E+06	(47)	12	303	88	71.9	50.0	104.8
12	6.25E+06	(50)	2.13E+06	(17)	8	164	79	112.1	64.1	207.3
13	1.53E+07	(92)	5.83E+06	(35)	6	451	152	100.6	67.8	153.1
14	9.17E+06	(110)	2.75E+06	(33)	12	213	74	127.3	86.0	193.8
15	1.13E+07	(68)	6.00E+06	(36)	6	464	154	72.5	47.9	111.9
16	8.13E+06	(130)	2.44E+06	(39)	16	188	60	127.3	88.8	187.0
17	1.63E+07	(98)	5.17E+06	(31)	6	399	143	120.7	80.3	187.1
18	8.00E+06	(80)	4.50E+06	(45)	10	348	104	68.3	46.9	100.8
19	6.25E+06	(125)	1.20E+06	(24)	20	93	38	197.4	128.0	318.6
20	1.03E+07	(257)	3.24E+06	(81)	25	250	56	121.1	93.0	157.6
21	1.35E+07	(54)	4.75E+06	(19)	4	367	167	108.4	63.8	193.7
22	2.14E+07	(193)	4.33E+06	(39)	9	335	107	188.1	133.6	272.1
23	4.38E+06	(35)	1.13E+06	(9)	8	87	56	146.8	70.5	346.7
24	5.03E+06	(181)	2.19E+06	(79)	36	170	38	87.7	66.4	115.8
25	5.24E+06	(110)	1.10E+06	(23)	21	85	35	181.4	116.1	297.4
26	7.33E+06	(88)	2.25E+06	(27)	12	174	67	124.4	80.5	199.1
27	1.43E+07	(57)	5.75E+06	(23)	4	444	184	94.8	57.8	161.2
28	7.12E+06	(171)	3.33E+06	(80)	24	258	58	81.9	61.9	108.2
29	1.38E+07	(55)	5.25E+06	(21)	4	406	175	100.1	60.0	174.2
30	7.67E+06	(138)	2.61E+06	(47)	18	202	59	112.4	80.4	160.0
31	1.43E+07	(57)	6.50E+06	(26)	4	502	196	84.0	52.2	139.2
32	1.11E+07	(89)	3.25E+06	(26)	8	251	98	130.5	84.1	210.4
33	1.03E+07	(62)	5.83E+06	(35)	6	451	152	68.0	44.4	106.2
34	9.83E+06	(59)	1.67E+06	(10)	6	129	80	221.4	114.7	482.4
35	1.25E+07	(200)	3.88E+06	(62)	16	299	76	123.4	92.6	166.9
36	1.41E+07	(141)	4.70E+06	(47)	10	363	106	114.8	82.2	163.3
37	1.10E+07	(88)	3.88E+06	(31)	8	299	107	108.5	71.7	169.1
38	1.00E+05	(1)	1.50E+06	(15)	10	116	59	2.9	0.1	16.8
39	9.75E+06	(39)	5.75E+06	(23)	4	444	184	65.1	38.1	114.2
40	9.80E+06	(98)	4.00E+06	(40)	10	309	98	93.9	64.6	139.3
41	8.29E+06	(141)	2.12E+06	(36)	17	164	54	149.3	103.5	221.5
42	1.05E+07	(295)	2.96E+06	(83)	28	229	51	135.5	104.7	175.2
43	1.00E+07	(60)	6.67E+06	(40)	6	515	163	57.7	38.1	88.4
44	5.00E+06	(105)	1.71E+06	(36)	21	132	44	111.5	76.1	167.7
45	1.29E+07	(168)	5.85E+06	(76)	13	452	104	84.7	63.7	112.4
46	5.07E+06	(152)	1.23E+06	(37)	30	95	31	156.5	109.3	230.4
47	9.56E+06	(86)	5.67E+06	(51)	9	438	123	64.8	45.4	93.6
48	7.70E+06	(231)	1.70E+06	(51)	30	131	37	172.5	127.4	238.2
49	1.46E+07	(234)	4.69E+06	(75)	16	362	84	119.1	90.6	156.4
50	1.63E+07	(65)	4.50E+06	(18)	4	348	162	137.3	81.3	245.8
51	1.13E+06	(9)	1.75E+06	(14)	8	135	71	25.0	9.5	61.5
52	8.25E+06	(231)	2.39E+06	(67)	28	185	45	131.3	98.8	174.4

53	1.65E+07 (132)	4.25E+06 (34)	8	328	112	148.0	101.4	222.4
54	6.50E+06 (195)	1.83E+06 (55)	30	142	38	135.5	100.3	186.2
55	1.06E+07 (127)	2.83E+06 (34)	12	219	75	142.4	97.4	214.4
56	1.30E+07 (78)	2.33E+06 (14)	6	180	95	210.1	119.9	400.1
57	1.17E+07 (176)	3.87E+06 (58)	15	299	79	116.1	86.1	159.1
58	1.22E+07 (73)	3.00E+06 (18)	6	232	108	154.0	91.9	273.7
59	1.01E+07 (201)	3.45E+06 (69)	20	267	65	111.2	83.5	147.9
60	1.03E+07 (41)	4.75E+06 (19)	4	367	167	82.6	47.2	150.7
61	1.54E+07 (123)	4.50E+06 (36)	8	348	116	130.4	89.8	194.7
62	1.77E+07 (106)	4.00E+06 (24)	6	309	125	167.8	107.9	272.9
63	6.88E+06 (55)	2.50E+06 (20)	8	193	86	105.0	62.4	184.9
64	1.24E+07 (261)	4.05E+06 (85)	21	313	68	117.3	90.5	151.9
65	1.05E+07 (42)	2.00E+06 (8)	4	155	106	196.8	93.5	482.7
66	6.83E+06 (82)	2.58E+06 (31)	12	200	71	101.2	66.5	158.4
67	1.27E+07 (76)	4.17E+06 (25)	6	322	128	116.1	73.5	190.3
68	1.23E+07 (49)	5.50E+06 (22)	4	425	180	85.3	50.9	148.1
69	9.95E+06 (199)	1.70E+06 (34)	20	131	45	221.7	154.7	328.1
70	4.56E+06 (41)	1.33E+06 (12)	9	103	58	129.6	67.7	270.8
71	1.28E+07 (77)	4.17E+06 (25)	6	322	128	117.6	74.5	192.7
72	1.18E+07 (47)	4.00E+06 (16)	4	309	153	111.9	62.9	211.4
73	8.75E+06 (35)	2.00E+06 (8)	4	155	106	164.6	76.6	409.4
74	6.25E+06 (75)	1.83E+06 (22)	12	142	60	129.9	80.5	219.3
75	1.58E+07 (63)	4.50E+06 (18)	4	348	162	133.2	78.6	238.8
76	7.50E+06 (180)	1.79E+06 (43)	24	138	42	159.5	114.4	227.8
77	9.50E+06 (76)	2.50E+06 (20)	8	193	86	144.5	88.2	249.5
78	5.20E+06 (52)	1.40E+06 (14)	10	108	57	140.9	77.9	275.1
79	7.78E+05 (7)	3.00E+06 (27)	9	232	89	10.2	3.7	23.6
80	8.72E+06 (279)	2.44E+06 (78)	32	188	43	136.3	104.6	177.5
81	1.34E+07 (67)	3.80E+06 (19)	5	294	133	134.2	80.4	236.4
82	1.01E+07 (91)	3.67E+06 (33)	9	283	98	105.5	70.4	162.2
83	9.00E+06 (36)	3.75E+06 (15)	4	290	147	91.6	49.4	180.2
84	6.73E+06 (74)	2.55E+06 (28)	11	197	74	101.1	65.0	162.2
85	8.75E+06 (35)	4.50E+06 (18)	4	348	162	74.5	41.3	139.7
86	7.71E+06 (108)	2.86E+06 (40)	14	221	70	103.4	71.6	152.6
87	1.00E+07 (60)	2.67E+06 (16)	6	206	102	142.4	81.9	264.6
88	1.25E+07 (50)	4.25E+06 (17)	4	328	157	112.1	64.1	207.3
89	1.88E+06 (15)	2.10E+07 (168)	8	1623	255	3.5	1.9	5.9
90	8.34E+06 (417)	2.46E+06 (123)	50	190	35	129.5	104.0	161.2
91	6.08E+06 (146)	1.75E+06 (42)	24	135	42	132.8	94.0	191.8
92	6.60E+06 (264)	1.83E+06 (73)	40	141	33	137.8	104.9	180.7
93	7.58E+06 (91)	2.92E+06 (35)	12	225	76	99.5	67.0	151.5
94	7.81E+06 (250)	2.19E+06 (70)	32	169	41	136.0	103.0	179.4
95	4.63E+06 (74)	3.25E+06 (52)	16	251	70	54.8	37.9	79.7
96	6.25E+05 (15)	6.17E+06 (148)	24	477	80	4.0	2.1	6.7
97	8.67E+06 (52)	2.17E+06 (13)	6	167	91	151.5	82.5	302.9
98	1.40E+06 (7)	2.60E+06 (13)	5	201	110	21.0	7.0	56.0
99	6.22E+06 (112)	1.78E+06 (32)	18	137	48	133.5	90.0	204.4
100	1.00E+06 (9)	3.56E+06 (32)	9	275	97	11.0	4.6	23.3
101	8.80E+06 (44)	3.40E+06 (17)	5	263	126	98.8	55.8	184.5
102	7.29E+06 (51)	4.14E+06 (29)	7	320	118	67.5	42.1	110.5
103	6.67E+05 (8)	2.42E+06 (29)	12	187	69	10.8	4.2	23.9
104	5.13E+06 (164)	1.66E+06 (53)	32	128	35	118.4	86.6	164.6
105	3.33E+05 (2)	4.00E+06 (24)	6	309	125	3.5	0.4	13.0
106	3.33E+05 (2)	2.17E+06 (13)	6	167	91	6.3	0.7	26.3

KLD17 (Yukon), modern sand, TU11z (counted by Sarah Falkowski, April 2014)

EFFECTIVE TRACK DENSITY FOR FLUENCE MONITOR (tracks/cm^2): 6.460E+05

RELATIVE ERROR (%): 1.57

EFFECTIVE URANIUM CONTENT OF MONITOR (ppm): 50.00

ZETA FACTOR AND STANDARD ERROR (yr cm^2): 119.60 5.40

SIZE OF COUNTER SQUARE (cm^2): 1.000E-06

------ GRAIN AGES IN ORIGINAL ORDER ------

Grain no.	RhoS (cm^-2)	(Ns)	RhoI (cm^-2)	(Ni)	Squares	U+/-2s		Grain Age	Age (Ma) --95% CI--	
1	9.83E+06	(59)	6.17E+06	(37)	6	477	157	61.2	40.0	95.0
2	4.75E+06	(76)	2.13E+06	(34)	16	164	56	85.6	56.6	132.3
3	1.23E+07	(98)	4.00E+06	(32)	8	310	109	116.8	78.1	180.0
4	4.00E+06	(16)	1.50E+06	(6)	4	116	91	100.5	38.2	313.9
5	9.67E+06	(58)	3.33E+06	(20)	6	258	114	110.5	66.0	193.9
6	1.00E+07	(40)	4.75E+06	(19)	4	368	167	80.5	45.8	147.1
7	1.47E+07	(103)	5.43E+06	(38)	7	420	136	103.6	71.0	154.5
8	7.75E+06	(124)	1.44E+06	(23)	16	111	46	203.8	131.2	332.4
9	1.13E+07	(79)	3.29E+06	(23)	7	254	105	130.7	81.9	217.8
10	2.00E+06	(12)	3.50E+06	(21)	6	271	117	22.2	9.9	46.9
11	1.00E+07	(120)	1.25E+06	(15)	12	97	49	299.1	177.4	546.1
12	7.50E+06	(150)	1.50E+06	(30)	20	116	42	189.5	128.4	290.0
13	2.01E+07	(141)	6.14E+06	(43)	7	475	145	125.1	88.7	180.4
14	4.00E+06	(16)	2.00E+06	(8)	4	155	106	76.0	31.1	205.4
15	9.33E+06	(56)	3.17E+06	(19)	6	245	111	112.2	66.2	200.0
16	5.50E+06	(44)	1.88E+06	(15)	8	145	74	111.5	61.5	215.8
17	9.25E+06	(185)	2.75E+06	(55)	20	213	58	128.4	94.8	176.8
18	1.99E+07	(179)	6.11E+06	(55)	9	473	128	124.3	91.7	171.3
19	1.82E+07	(218)	3.00E+06	(36)	12	232	77	228.9	161.6	334.4
20	4.83E+06	(29)	2.17E+06	(13)	6	168	91	85.0	43.2	178.3
21	7.64E+06	(214)	2.43E+06	(68)	28	188	46	119.8	90.1	159.3
22	1.80E+07	(72)	7.00E+06	(28)	4	542	204	98.2	63.0	157.9
23	5.05E+06	(101)	1.05E+06	(21)	20	81	35	182.1	114.1	306.1
24	7.94E+06	(143)	2.94E+06	(53)	18	228	63	103.2	75.0	144.3
25	4.00E+06	(24)	2.00E+06	(12)	6	155	88	76.3	37.0	167.5
26	9.40E+06	(188)	2.95E+06	(59)	20	228	60	121.7	90.6	166.0
27	1.85E+07	(148)	4.13E+06	(33)	8	319	111	170.3	116.9	256.1
28	1.55E+07	(62)	6.00E+06	(24)	4	464	188	98.6	61.0	165.3
29	2.12E+07	(254)	5.17E+06	(62)	12	400	102	155.4	116.4	207.3
30	6.25E+06	(100)	9.38E+05	(15)	16	73	37	250.3	147.1	460.9
31	1.08E+07	(65)	3.33E+06	(20)	6	258	114	123.7	74.6	215.4
32	7.57E+06	(159)	1.52E+06	(32)	21	118	42	188.4	129.2	284.1
33	1.01E+07	(91)	1.78E+06	(16)	9	138	68	214.3	126.9	389.0
34	8.00E+06	(40)	2.40E+06	(12)	5	186	105	126.3	65.8	264.4
35	1.26E+07	(101)	3.38E+06	(27)	8	261	100	142.3	92.9	226.2
36	8.83E+06	(53)	3.83E+06	(23)	6	297	123	88.1	53.3	150.6
37	7.38E+06	(118)	1.69E+06	(27)	16	131	50	165.9	109.3	261.8
38	9.22E+06	(83)	2.56E+06	(23)	9	198	82	137.2	86.3	228.1
39	4.50E+06	(18)	2.25E+06	(9)	4	174	113	76.1	32.9	192.5
40	8.50E+06	(136)	4.75E+06	(76)	16	368	85	68.7	51.5	92.3
41	1.08E+07	(43)	2.25E+06	(9)	4	174	113	179.5	88.1	417.1
42	8.44E+06	(76)	1.89E+06	(17)	9	146	70	169.2	100.2	304.8
43	9.83E+06	(59)	4.17E+06	(25)	6	322	128	90.2	55.9	150.3
44	9.50E+06	(228)	3.71E+06	(89)	24	287	61	97.9	75.5	126.9
45	6.00E+06	(36)	1.83E+06	(11)	6	142	84	123.9	62.6	269.8
46	2.63E+06	(21)	3.75E+05	(3)	8	29	31	253.7	80.2	1280.5
47	7.75E+06	(62)	4.88E+06	(39)	8	377	121	61.0	40.3	93.6
48	1.22E+07	(73)	3.17E+06	(19)	6	245	111	145.8	87.9	255.6
49	1.01E+07	(91)	2.89E+06	(26)	9	224	87	133.2	85.9	214.5
50	7.75E+06	(31)	3.00E+06	(12)	4	232	132	98.2	49.6	210.1
51	9.68E+06	(387)	2.45E+06	(98)	40	190	39	150.2	118.4	190.4
52	3.50E+06	(35)	1.40E+06	(14)	10	108	57	95.2	50.4	191.6

53	8.25E+06 (66)	2.00E+06 (16)	8	155	76	156.2	90.5	288.6
54	6.25E+06 (225)	1.33E+06 (48)	36	103	30	178.1	130.6	248.3
55	1.30E+07 (78)	5.00E+06 (30)	6	387	141	99.3	64.7	156.8
56	1.38E+07 (110)	4.50E+06 (36)	8	348	116	116.6	79.8	175.0
57	9.00E+06 (36)	4.00E+06 (16)	4	310	153	85.9	46.8	165.8
58	1.18E+07 (71)	6.67E+06 (40)	6	516	163	68.1	45.7	103.0
59	1.30E+07 (52)	4.50E+06 (18)	4	348	162	110.0	63.8	199.8
60	7.25E+06 (116)	2.44E+06 (39)	16	189	60	113.6	78.7	167.7
61	4.00E+06 (24)	2.33E+06 (14)	6	181	95	65.6	32.8	137.1
62	9.50E+06 (38)	1.75E+06 (7)	4	135	99	202.6	91.8	534.1
63	1.25E+07 (50)	4.25E+06 (17)	4	329	158	111.9	64.0	207.0
64	7.11E+06 (64)	1.56E+06 (14)	9	120	63	172.7	97.2	332.6
65	1.06E+07 (148)	2.36E+06 (33)	14	182	63	170.3	116.9	256.1
66	4.50E+06 (18)	1.25E+06 (5)	4	97	83	134.5	49.5	462.5
67	6.70E+06 (134)	1.90E+06 (38)	20	147	48	134.4	93.6	198.0
68	8.57E+06 (180)	3.05E+06 (64)	21	236	59	107.6	80.6	145.5
69	1.55E+07 (62)	3.50E+06 (14)	4	271	143	167.4	93.9	323.0
70	8.17E+06 (49)	1.67E+06 (10)	6	129	80	184.2	94.0	406.4
71	7.60E+06 (152)	3.30E+06 (66)	20	255	63	88.2	65.8	119.7
72	9.75E+06 (39)	3.50E+06 (14)	4	271	143	105.9	56.9	211.3
73	9.50E+06 (38)	1.00E+06 (4)	4	77	73	344.9	130.7	1280.3
74	1.32E+07 (263)	3.35E+06 (67)	20	259	64	149.1	112.6	197.1
75	1.82E+07 (109)	5.67E+06 (34)	6	439	150	122.3	82.9	185.3
76	8.50E+06 (51)	1.17E+06 (7)	6	90	66	270.2	125.8	696.6
77	1.03E+07 (123)	3.08E+06 (37)	12	239	78	126.8	87.6	188.3
78	1.33E+07 (80)	4.50E+06 (27)	6	348	133	113.0	72.7	181.9
79	1.40E+07 (56)	6.75E+06 (27)	4	522	200	79.4	49.5	130.8
80	7.60E+06 (38)	5.20E+06 (26)	5	402	157	56.1	33.3	96.2
81	1.75E+07 (105)	3.83E+06 (23)	6	297	123	173.0	110.4	284.3
82	5.04E+06 (121)	1.38E+06 (33)	24	106	37	139.6	94.9	211.7
83	4.50E+06 (72)	1.19E+06 (19)	16	92	42	143.9	86.7	252.3
84	8.25E+06 (33)	2.75E+06 (11)	4	213	126	113.8	56.8	249.5
85	8.38E+06 (67)	2.88E+06 (23)	8	223	92	111.1	68.7	186.9
86	9.81E+06 (157)	3.63E+06 (58)	16	281	74	103.6	76.3	142.5
87	3.50E+06 (14)	5.00E+06 (20)	4	387	171	27.1	12.6	56.1
88	8.06E+06 (129)	2.44E+06 (39)	16	189	60	126.2	88.0	185.4
89	8.10E+06 (81)	3.10E+06 (31)	10	240	86	99.8	65.6	156.3
90	1.14E+07 (57)	1.80E+06 (9)	5	139	91	236.6	119.0	539.4
91	1.28E+07 (51)	2.50E+06 (10)	4	193	120	191.6	98.1	421.5
92	1.18E+07 (71)	2.00E+06 (12)	6	155	88	222.1	121.8	447.6
93	8.11E+06 (73)	2.56E+06 (23)	9	198	82	120.9	75.3	202.4
94	1.00E+07 (40)	2.25E+06 (9)	4	174	113	167.1	81.4	390.6
95	5.13E+06 (41)	1.50E+06 (12)	8	116	66	129.4	67.6	270.4
96	1.03E+07 (72)	3.57E+06 (25)	7	276	110	109.8	69.3	180.7
97	8.00E+06 (32)	3.00E+06 (12)	4	232	132	101.4	51.4	216.2
98	4.50E+06 (27)	5.00E+05 (3)	6	39	41	323.9	106.0	1580.8
99	1.16E+07 (81)	1.14E+06 (8)	7	88	61	373.1	186.5	875.1
100	1.33E+07 (53)	3.00E+06 (12)	4	232	132	166.7	89.3	341.9
101	1.13E+07 (45)	1.50E+06 (6)	4	116	91	277.1	122.0	782.1
102	1.50E+07 (75)	9.20E+06 (46)	5	712	210	62.6	42.9	92.5
103	1.22E+07 (73)	4.33E+06 (26)	6	335	131	107.1	68.0	174.7
104	2.83E+06 (17)	1.00E+06 (6)	6	77	61	106.7	41.0	330.6
105	5.50E+06 (22)	3.75E+06 (15)	4	290	148	56.2	28.0	116.5
106	7.00E+06 (63)	2.22E+06 (20)	9	172	76	119.9	72.1	209.3

KLD18 (Yukon), modern sand, UC2z (counted by Sarah Falkowski, May 2014)

```
EFFECTIVE TRACK DENSITY FOR FLUENCE MONITOR (tracks/cm^2):      4.460E+05
                                       RELATIVE ERROR (%):      1.57
               EFFECTIVE URANIUM CONTENT OF MONITOR (ppm):     50.00
                 ZETA FACTOR AND STANDARD ERROR (yr cm^2):    119.60     5.40
                            SIZE OF COUNTER SQUARE (cm^2):      1.000E-06
```

------ GRAIN AGES IN ORIGINAL ORDER ------

Grain no.	RhoS (cm^-2)	(Ns)	RhoI (cm^-2)	(Ni)	Squares	U+/-2s		Grain Age	Age (Ma) --95% CI--	
1	9.25E+06	(259)	1.39E+06	(39)	28	156	50	174.1	124.7	250.3
2	1.07E+07	(192)	1.83E+06	(33)	18	206	71	152.7	105.8	228.1
3	7.60E+06	(190)	1.36E+06	(34)	25	152	52	146.8	102.1	218.1
4	6.43E+06	(257)	1.15E+06	(46)	40	129	38	146.9	107.5	205.7
5	1.34E+07	(187)	2.86E+06	(40)	14	320	101	123.1	87.5	177.9
6	1.29E+07	(270)	2.24E+06	(47)	21	251	73	151.0	110.9	210.4
7	1.22E+07	(367)	2.27E+06	(68)	30	254	62	141.5	107.8	185.6
8	1.04E+07	(292)	1.75E+06	(49)	28	196	56	156.6	115.9	216.4
9	1.26E+07	(379)	1.87E+06	(56)	30	209	56	177.6	134.4	239.4
10	1.42E+07	(256)	1.83E+06	(33)	18	206	71	202.8	141.8	300.4
11	7.76E+06	(194)	1.68E+06	(42)	25	188	58	121.7	87.1	174.2
12	1.16E+07	(278)	2.08E+06	(50)	24	234	66	146.2	108.3	201.8
13	1.53E+07	(92)	3.00E+06	(18)	6	336	157	133.9	81.0	236.0
14	6.45E+06	(129)	1.50E+06	(30)	20	168	61	113.2	76.0	174.7
15	6.61E+06	(119)	1.33E+06	(24)	18	149	61	130.2	84.1	211.2
16	1.70E+07	(339)	2.85E+06	(57)	20	320	85	156.3	118.2	210.8
17	8.83E+06	(353)	1.43E+06	(57)	40	160	42	162.7	123.2	219.2
18	1.19E+07	(214)	1.72E+06	(31)	18	193	69	180.7	124.5	272.3
19	1.12E+07	(224)	1.90E+06	(38)	20	213	69	154.8	110.0	224.4
20	1.56E+07	(312)	2.25E+06	(45)	20	252	75	181.8	133.3	254.1
21	1.44E+07	(173)	2.83E+06	(34)	12	318	109	133.8	92.7	199.4
22	9.17E+06	(220)	2.13E+06	(51)	24	238	67	113.8	83.8	157.6
23	7.25E+06	(290)	1.80E+06	(72)	40	202	48	106.0	80.8	139.0
24	1.43E+07	(258)	2.44E+06	(44)	18	274	83	154.1	112.1	217.2
25	1.08E+07	(108)	2.40E+06	(24)	10	269	109	118.3	76.0	192.7
26	1.72E+07	(155)	2.56E+06	(23)	9	286	119	176.2	114.4	285.9
27	8.25E+06	(66)	1.38E+06	(11)	8	154	91	156.2	83.3	327.8
28	7.17E+06	(172)	1.08E+06	(26)	24	121	47	173.2	115.2	272.3
29	8.86E+06	(186)	1.67E+06	(35)	21	187	63	139.7	97.5	206.6
30	1.87E+07	(374)	2.85E+06	(57)	20	320	85	171.4	128.3	228.7
31	1.65E+07	(198)	3.00E+06	(36)	12	336	112	144.5	101.5	212.3
32	9.07E+06	(272)	1.73E+06	(52)	30	194	54	137.7	102.4	189.0
33	1.25E+07	(299)	1.33E+06	(32)	24	149	53	243.4	170.2	361.2
34	9.40E+06	(188)	1.55E+06	(31)	20	174	62	159.1	109.1	240.6
35	8.90E+06	(178)	1.45E+06	(29)	20	163	60	160.9	109.0	247.0
36	1.60E+07	(224)	2.43E+06	(34)	14	272	93	172.7	120.8	255.3
37	1.25E+07	(374)	2.10E+06	(63)	30	235	60	155.4	117.6	205.2
38	6.50E+06	(104)	1.19E+06	(19)	16	133	60	143.4	88.2	247.6
39	1.46E+07	(131)	2.89E+06	(26)	9	324	126	132.3	87.0	210.1
40	1.11E+07	(167)	2.07E+06	(31)	15	232	83	141.5	96.6	214.8
41	8.29E+06	(199)	1.08E+06	(26)	24	121	47	199.9	133.7	312.9
42	9.50E+06	(152)	2.13E+06	(34)	16	238	81	117.7	81.1	176.2
43	9.08E+06	(109)	1.83E+06	(22)	12	206	87	130.0	82.4	216.1
44	9.00E+06	(81)	2.00E+06	(18)	9	224	104	118.1	70.9	209.4
45	8.27E+06	(124)	1.80E+06	(27)	15	202	77	120.8	79.7	190.7
46	8.00E+06	(120)	1.40E+06	(21)	15	157	68	149.7	94.5	250.5
47	1.15E+07	(207)	2.17E+06	(39)	18	243	78	139.6	99.2	201.9
48	1.70E+07	(170)	3.00E+06	(30)	10	336	122	148.7	101.1	227.1
49	1.43E+07	(214)	2.20E+06	(33)	15	247	86	170.0	118.2	253.0
50	1.50E+07	(210)	1.50E+06	(21)	14	168	73	259.6	167.6	426.0
51	9.25E+06	(148)	1.56E+06	(25)	16	175	70	155.2	101.9	247.4
52	1.26E+07	(201)	2.56E+06	(41)	16	287	90	129.0	92.3	185.3

53	6.43E+06	(257)	1.48E+06	(59)	40	165	43	114.9	86.5	155.3
54	8.06E+06	(145)	1.83E+06	(33)	18	206	71	115.7	79.2	174.5
55	8.13E+06	(130)	1.06E+06	(17)	16	119	57	199.2	121.3	351.4
56	1.63E+07	(98)	2.67E+06	(16)	6	299	147	160.0	94.9	290.6
57	1.10E+07	(66)	1.50E+06	(9)	6	168	109	189.8	96.2	432.0
58	7.38E+06	(118)	1.81E+06	(29)	16	203	75	107.2	71.3	167.1
59	9.63E+06	(289)	1.90E+06	(57)	30	213	57	133.5	100.5	180.7
60	8.63E+06	(259)	1.50E+06	(45)	30	168	50	151.3	110.4	212.4
61	9.83E+06	(236)	1.46E+06	(35)	24	163	55	176.7	124.3	259.5
62	9.77E+06	(293)	1.27E+06	(38)	30	142	46	201.7	144.5	290.3
63	1.03E+07	(246)	2.04E+06	(49)	24	229	65	132.2	97.3	183.5
64	1.76E+07	(211)	2.92E+06	(35)	12	327	110	158.2	110.9	233.1
65	1.67E+07	(300)	3.06E+06	(55)	18	343	93	143.5	107.7	195.0
66	8.56E+06	(137)	2.13E+06	(34)	16	238	81	106.2	72.9	159.6
67	1.55E+07	(309)	3.30E+06	(66)	20	370	91	122.9	93.0	162.3
68	1.63E+07	(261)	3.44E+06	(55)	16	385	104	125.1	93.5	170.5
69	1.53E+07	(490)	2.22E+06	(71)	32	249	59	180.4	138.8	234.2
70	1.53E+07	(412)	2.37E+06	(64)	27	266	67	168.4	127.8	221.5
71	1.06E+07	(190)	1.61E+06	(29)	18	181	67	171.6	116.6	262.9
72	1.62E+07	(146)	3.22E+06	(29)	9	361	134	132.3	88.9	204.5
73	1.03E+07	(155)	1.80E+06	(27)	15	202	77	150.6	100.4	235.7
74	1.07E+07	(321)	1.80E+06	(54)	30	202	55	156.2	117.2	212.5
75	1.14E+07	(273)	2.00E+06	(48)	24	224	65	149.5	110.2	207.7
76	1.16E+07	(279)	1.96E+06	(47)	24	220	64	156.0	114.7	217.2
77	1.09E+07	(350)	2.59E+06	(83)	32	291	64	111.0	86.1	143.1
78	1.28E+07	(345)	2.63E+06	(71)	27	295	70	127.6	97.5	166.9
79	9.00E+06	(360)	1.40E+06	(56)	40	157	42	168.8	127.6	227.8
80	9.87E+06	(296)	1.80E+06	(54)	30	202	55	144.2	108.0	196.5
81	1.22E+07	(365)	2.47E+06	(74)	30	277	65	129.5	99.5	168.5
82	1.54E+07	(308)	3.10E+06	(62)	20	348	89	130.3	98.0	173.2
83	1.56E+07	(374)	1.92E+06	(46)	24	215	63	212.6	157.1	295.0
84	1.04E+07	(280)	1.89E+06	(51)	27	212	59	144.4	107.2	198.7
85	1.05E+07	(253)	1.92E+06	(46)	24	215	63	144.6	105.8	202.6
86	1.29E+07	(207)	1.94E+06	(31)	16	217	78	174.9	120.4	263.8
87	1.00E+07	(300)	1.77E+06	(53)	30	198	55	148.9	111.3	203.3
88	1.62E+07	(146)	2.22E+06	(20)	9	249	110	190.5	120.3	320.4
89	1.04E+07	(167)	1.13E+06	(18)	16	126	59	240.9	149.9	414.6
90	2.19E+07	(219)	3.70E+06	(37)	10	415	136	155.4	109.9	226.5
91	1.30E+07	(352)	1.96E+06	(53)	27	220	61	174.3	130.8	237.1
92	8.83E+06	(159)	1.83E+06	(33)	18	206	71	126.8	87.2	190.5
93	1.77E+07	(106)	3.83E+06	(23)	6	430	178	121.1	77.2	199.4
94	8.56E+06	(154)	1.06E+06	(19)	18	118	54	211.1	132.3	359.1
95	6.80E+06	(136)	1.45E+06	(29)	20	163	60	123.3	82.6	191.2
96	1.27E+07	(203)	2.31E+06	(37)	16	259	85	144.2	101.7	210.6
97	1.09E+07	(217)	1.60E+06	(32)	20	179	63	177.6	123.0	265.8
98	8.43E+06	(253)	1.27E+06	(38)	30	142	46	174.5	124.5	252.2
99	1.22E+07	(110)	1.78E+06	(16)	9	199	98	179.3	107.0	324.1
100	7.13E+06	(114)	1.19E+06	(19)	16	133	60	157.0	97.1	270.1
101	6.10E+06	(122)	1.50E+06	(30)	20	168	61	107.1	71.8	165.6
102	1.73E+07	(276)	2.38E+06	(38)	16	266	86	190.2	136.0	274.1
103	8.20E+06	(123)	1.33E+06	(20)	15	149	66	160.9	100.8	272.4
104	1.03E+07	(206)	1.35E+06	(27)	20	151	58	199.3	134.3	309.1

KLD20 (Yukon), modern sand, TU11z (counted by Sarah Falkowski, April 2014)

EFFECTIVE TRACK DENSITY FOR FLUENCE MONITOR (tracks/cm^2): 6.450E+05

RELATIVE ERROR (%): 1.57

EFFECTIVE URANIUM CONTENT OF MONITOR (ppm): 50.00

ZETA FACTOR AND STANDARD ERROR (yr cm^2): 119.60 5.40

SIZE OF COUNTER SQUARE (cm^2): 1.000E-06

------ GRAIN AGES IN ORIGINAL ORDER ------

Grain no.	**RhoS (cm^-2)**	**(Ns)**	**RhoI (cm^-2)**	**(Ni)**	**Squares**	**U+/-2s**		**Grain Age**	**Age (Ma) --95% CI--**	
1	4.67E+06	(70)	1.20E+06	(18)	15	93	43	147.3	87.7	262.5
2	9.33E+06	(112)	3.08E+06	(37)	12	239	78	115.4	79.3	172.1
3	1.40E+07	(168)	4.42E+06	(53)	12	342	94	120.9	88.5	167.9
4	1.38E+07	(83)	3.50E+06	(21)	6	271	117	149.8	92.8	254.3
5	3.50E+06	(63)	6.67E+05	(12)	18	52	29	197.2	107.2	400.2
6	1.00E+07	(80)	4.00E+06	(32)	8	310	109	95.4	62.9	148.7
7	8.92E+06	(535)	2.75E+06	(165)	60	213	34	123.6	101.6	150.3
8	8.76E+06	(219)	2.52E+06	(63)	25	195	49	132.5	99.9	178.2
9	1.15E+07	(275)	2.75E+06	(66)	24	213	53	157.8	119.2	208.8
10	8.90E+06	(89)	3.20E+06	(32)	10	248	87	106.1	70.4	164.2
11	7.80E+06	(273)	2.17E+06	(76)	35	168	39	136.4	104.4	178.2
12	1.53E+07	(184)	7.00E+06	(84)	12	543	119	83.7	63.7	109.8
13	9.64E+06	(135)	2.50E+06	(35)	14	194	65	146.6	101.0	219.0
14	7.36E+06	(81)	2.91E+06	(32)	11	226	79	96.6	63.7	150.4
15	1.19E+07	(167)	4.00E+06	(56)	14	310	83	113.8	83.8	156.9
16	7.58E+06	(91)	1.83E+06	(22)	12	142	60	156.7	98.4	261.9
17	1.05E+07	(158)	3.27E+06	(49)	15	253	72	122.9	89.0	173.0
18	1.38E+07	(83)	6.17E+06	(37)	6	478	157	85.7	57.7	130.0
19	3.70E+06	(37)	9.00E+05	(9)	10	70	45	154.6	74.7	363.4
20	9.31E+06	(149)	3.38E+06	(54)	16	262	71	105.4	76.9	146.7
21	1.35E+07	(162)	2.83E+06	(34)	12	220	75	180.5	125.0	269.1
22	5.22E+06	(47)	1.00E+06	(9)	9	78	50	195.5	96.8	451.6
23	5.08E+06	(61)	1.25E+06	(15)	12	97	49	153.7	87.4	290.8
24	4.79E+06	(67)	2.43E+06	(34)	14	188	64	75.4	49.3	117.5
25	7.83E+06	(313)	1.60E+06	(64)	40	124	31	184.8	139.6	244.3
26	9.86E+06	(69)	2.86E+06	(20)	7	221	98	131.0	79.4	227.4
27	6.67E+06	(60)	2.33E+06	(21)	9	181	78	108.7	65.7	188.2
28	6.50E+06	(130)	2.30E+06	(46)	20	178	53	107.9	76.8	154.5
29	1.10E+07	(66)	4.33E+06	(26)	6	336	131	96.8	61.0	158.8
30	6.33E+06	(38)	4.17E+06	(25)	6	323	128	58.2	34.4	100.7
31	1.08E+07	(65)	5.00E+06	(30)	6	388	141	82.8	53.2	132.3
32	9.60E+06	(96)	2.60E+06	(26)	10	202	79	140.2	90.8	225.2
33	8.00E+06	(80)	2.60E+06	(26)	10	202	79	117.1	74.9	189.9
34	6.38E+06	(102)	1.13E+06	(18)	16	87	41	213.4	130.1	372.9
35	4.25E+06	(34)	6.25E+05	(5)	8	48	41	250.4	101.2	806.9
36	1.27E+07	(76)	3.83E+06	(23)	6	297	123	125.6	78.5	209.8
37	1.54E+07	(139)	2.67E+06	(24)	9	207	84	218.4	142.4	351.1
38	9.17E+06	(55)	5.00E+06	(30)	6	388	141	70.2	44.3	113.4
39	6.00E+06	(138)	1.48E+06	(34)	23	115	39	154.1	105.9	231.2
40	7.34E+06	(235)	1.78E+06	(57)	32	138	37	156.8	117.3	213.1
41	4.80E+06	(48)	2.40E+06	(24)	10	186	75	76.4	46.1	130.5
42	7.93E+06	(119)	2.93E+06	(44)	15	227	69	103.2	72.7	149.5
43	5.03E+06	(161)	1.25E+06	(40)	32	97	31	152.9	108.2	221.8
44	9.75E+06	(39)	2.00E+06	(8)	4	155	106	182.4	86.0	450.1
45	8.20E+06	(246)	3.03E+06	(91)	30	235	50	103.1	79.8	133.1
46	8.89E+06	(80)	4.11E+06	(37)	9	319	105	82.7	55.5	125.6
47	1.33E+07	(53)	4.75E+06	(19)	4	368	167	106.1	62.3	189.8
48	6.19E+06	(99)	1.81E+06	(29)	16	141	52	129.8	85.6	203.7
49	9.05E+06	(181)	2.75E+06	(55)	20	213	58	125.5	92.6	172.9
50	9.00E+06	(36)	4.50E+06	(18)	4	349	163	76.3	42.5	142.8
51	1.00E+07	(40)	3.50E+06	(14)	4	271	143	108.5	58.4	215.8
52	8.89E+06	(160)	2.67E+06	(48)	18	207	60	127.0	91.8	179.2

53	4.69E+06	(	150)	2.38E+06	(	76)	32	184	42	75.4	56.5	100.7
54	1.01E+07	(	303)	2.67E+06	(	80)	30	207	47	143.8	110.8	186.4
55	1.16E+07	(	93)	4.13E+06	(	33)	8	320	111	107.5	71.9	165.1
56	8.72E+06	(	157)	2.67E+06	(	48)	18	207	60	124.7	90.0	176.0
57	5.13E+06	(	154)	1.30E+06	(	39)	30	101	32	150.1	105.6	218.9
58	6.38E+06	(	102)	2.00E+06	(	32)	16	155	55	121.4	81.3	186.6
59	1.15E+07	(	69)	5.67E+06	(	34)	6	439	150	77.6	50.9	120.8
60	5.25E+06	(	84)	2.06E+06	(	33)	16	160	55	97.2	64.5	150.1
61	8.71E+06	(	61)	3.43E+06	(	24)	7	266	108	96.9	59.9	162.5
62	3.75E+06	(	60)	1.13E+06	(	18)	16	87	41	126.5	74.4	227.6
63	1.41E+07	(	211)	3.73E+06	(	56)	15	289	78	143.4	106.7	196.1
64	8.52E+06	(	179)	2.43E+06	(	51)	21	188	53	133.7	97.8	186.2
65	8.83E+06	(	53)	2.00E+06	(	12)	6	155	88	166.4	89.2	341.3
66	1.08E+07	(	108)	3.60E+06	(	36)	10	279	93	114.3	78.1	171.7
67	6.00E+06	(	108)	2.50E+06	(	45)	18	194	58	91.7	64.4	133.0
68	1.08E+07	(	227)	3.52E+06	(	74)	21	273	64	116.7	88.6	153.7
69	7.25E+06	(	87)	2.08E+06	(	25)	12	161	64	132.2	84.5	215.3
70	1.63E+07	(	65)	3.75E+06	(	15)	4	291	148	163.7	93.5	308.4
71	1.39E+07	(	111)	4.00E+06	(	32)	8	310	109	132.0	88.9	202.0
72	7.44E+06	(	67)	3.22E+06	(	29)	9	250	92	88.2	56.5	141.5
73	1.58E+07	(	95)	4.17E+06	(	25)	6	323	128	144.2	92.7	233.7
74	9.67E+06	(	58)	2.67E+06	(	16)	6	207	102	137.3	78.7	255.7
75	1.90E+07	(	76)	5.25E+06	(	21)	4	407	176	137.3	84.5	234.3
76	1.06E+07	(	159)	2.87E+06	(	43)	15	222	68	140.7	100.3	201.8
77	1.35E+07	(	81)	4.50E+06	(	27)	6	349	133	114.2	73.5	183.7
78	8.11E+06	(	73)	3.67E+06	(	33)	9	284	99	84.5	55.5	131.7
79	1.14E+07	(	57)	2.60E+06	(	13)	5	202	110	165.4	90.7	328.5
80	7.92E+06	(	95)	2.33E+06	(	28)	12	181	68	129.0	84.4	204.2
81	8.57E+06	(	257)	2.30E+06	(	69)	30	178	43	141.3	107.0	186.6
82	1.10E+07	(	66)	2.33E+06	(	14)	6	181	95	177.7	100.2	341.7
83	6.00E+06	(	60)	1.40E+06	(	14)	10	109	57	161.8	90.6	312.9
84	1.08E+07	(	65)	5.17E+06	(	31)	6	401	143	80.2	51.7	127.3
85	1.18E+07	(	71)	4.83E+06	(	29)	6	375	138	93.4	60.2	149.3
86	1.40E+07	(	84)	3.00E+06	(	18)	6	233	108	176.3	106.3	311.0
87	1.52E+07	(	182)	5.17E+06	(	62)	12	401	102	112.1	83.7	152.1
88	9.64E+06	(	106)	3.00E+06	(	33)	11	233	81	122.3	82.5	186.6
89	1.20E+07	(	144)	4.67E+06	(	56)	12	362	97	98.3	71.8	136.4
90	6.87E+06	(	103)	2.07E+06	(	31)	15	160	57	126.4	84.4	195.4
91	6.50E+06	(	156)	1.75E+06	(	42)	24	136	42	141.3	100.4	203.6
92	7.14E+06	(	157)	2.14E+06	(	47)	22	166	48	127.3	91.7	180.3
93	9.25E+06	(	37)	2.00E+06	(	8)	4	155	106	173.3	81.2	429.2
94	1.48E+07	(	89)	4.17E+06	(	25)	6	323	128	135.2	86.6	219.9
95	5.60E+06	(	28)	3.40E+06	(	17)	5	264	126	63.0	33.5	122.7
96	1.07E+07	(	64)	1.67E+06	(	10)	6	129	80	239.0	124.6	518.3
97	9.00E+06	(	45)	1.60E+06	(	8)	5	124	85	209.9	100.4	512.4
98	7.00E+06	(	28)	1.75E+06	(	7)	4	136	99	149.9	65.5	405.6
99	6.00E+06	(	90)	1.40E+06	(	21)	15	109	47	162.3	101.0	274.3
100	7.13E+06	(	57)	2.13E+06	(	17)	8	165	79	127.2	73.7	233.1
101	1.07E+07	(	107)	2.80E+06	(	28)	10	217	82	145.1	95.6	228.4
102	7.86E+06	(	110)	3.57E+06	(	50)	14	277	78	84.2	59.8	120.1
103	9.00E+06	(	54)	3.50E+06	(	21)	6	271	117	98.0	58.6	170.8

KLD23 (Yukon), modern sand, TU11z (counted by Sarah Falkowski, April 2014)

EFFECTIVE TRACK DENSITY FOR FLUENCE MONITOR (tracks/cm^2): 6.440E+05
RELATIVE ERROR (%): 1.57
EFFECTIVE URANIUM CONTENT OF MONITOR (ppm): 50.00
ZETA FACTOR AND STANDARD ERROR (yr cm^2): 119.60 5.40
SIZE OF COUNTER SQUARE (cm^2): 1.000E-06

------ GRAIN AGES IN ORIGINAL ORDER ------

Grain no.	**RhoS (cm^-2)**	**(Ns)**	**RhoI (cm^-2)**	**(Ni)**	**Squares**	**U+/-2s**		**Grain Age**	**Age (Ma) --95% CI--**	
1	7.50E+06	(45)	1.67E+06	(10)	6	129	80	168.9	85.5	374.8
2	9.86E+06	(355)	3.14E+06	(113)	36	244	46	119.5	95.0	150.2
3	4.86E+06	(34)	3.57E+06	(25)	7	277	110	52.1	30.2	91.0
4	7.31E+06	(117)	2.81E+06	(45)	16	218	65	99.1	69.9	143.2
5	9.00E+06	(54)	1.83E+06	(11)	6	142	84	184.2	96.9	389.3
6	7.12E+06	(121)	2.82E+06	(48)	17	219	63	96.2	68.5	137.4
7	7.30E+06	(73)	3.90E+06	(39)	10	303	97	71.6	48.0	108.5
8	3.52E+06	(197)	1.07E+06	(60)	56	83	22	125.0	93.4	169.8
9	1.18E+07	(71)	4.33E+06	(26)	6	336	131	103.9	65.8	169.7
10	4.92E+06	(59)	1.17E+06	(14)	12	91	48	158.9	88.8	307.6
11	1.17E+07	(316)	3.67E+06	(99)	27	285	58	121.4	95.3	154.5
12	4.50E+06	(27)	2.33E+06	(14)	6	181	95	73.4	37.5	151.6
13	9.25E+06	(37)	3.50E+06	(14)	4	272	143	100.3	53.5	200.8
14	1.23E+07	(49)	5.00E+06	(20)	4	388	172	93.2	54.8	165.6
15	1.02E+07	(92)	3.44E+06	(31)	9	267	96	112.9	74.8	175.5
16	6.06E+06	(103)	1.53E+06	(26)	17	119	46	150.1	97.6	240.2
17	9.67E+06	(58)	2.33E+06	(14)	6	181	95	156.2	87.2	302.8
18	1.04E+07	(167)	3.63E+06	(58)	16	281	74	109.7	81.1	150.7
19	3.50E+06	(21)	1.00E+06	(6)	6	78	61	130.9	52.4	396.0
20	6.63E+06	(53)	1.88E+06	(15)	8	146	74	133.6	75.1	255.1
21	7.25E+06	(87)	1.75E+06	(21)	12	136	59	156.7	97.3	265.4
22	9.63E+06	(77)	2.75E+06	(22)	8	214	90	132.7	82.4	223.7
23	5.06E+06	(86)	8.82E+05	(15)	17	69	35	215.2	125.3	399.3
24	4.44E+06	(71)	1.63E+06	(26)	16	126	49	103.9	65.8	169.7
25	2.50E+06	(15)	1.17E+06	(7)	6	91	66	81.0	31.6	235.1
26	4.20E+06	(21)	2.60E+06	(13)	5	202	110	61.6	29.6	133.9
27	1.30E+07	(65)	2.00E+06	(10)	5	155	96	242.3	126.4	524.9
28	4.25E+06	(17)	1.00E+06	(4)	4	78	73	156.9	53.1	636.4
29	7.40E+06	(74)	2.00E+06	(20)	10	155	69	140.1	85.3	242.3
30	5.00E+06	(40)	1.00E+06	(8)	8	78	53	186.8	88.2	459.8
31	1.03E+07	(93)	2.56E+06	(23)	9	198	82	153.1	97.0	252.9
32	5.79E+06	(81)	2.00E+06	(28)	14	155	58	110.0	71.2	175.7
33	6.60E+06	(66)	1.30E+06	(13)	10	101	55	190.7	105.9	375.6
34	1.26E+07	(201)	4.50E+06	(72)	16	349	83	106.2	80.0	140.7
35	1.31E+07	(131)	5.10E+06	(51)	10	396	111	98.0	70.6	138.3
36	1.09E+07	(261)	2.58E+06	(62)	24	201	51	159.2	119.3	212.1
37	4.81E+06	(77)	1.19E+06	(19)	16	92	42	153.2	92.7	267.8
38	2.03E+07	(122)	6.17E+06	(37)	6	479	157	125.4	86.6	186.3
39	6.24E+06	(287)	1.83E+06	(84)	46	142	31	129.7	100.2	167.7
40	7.52E+06	(218)	2.66E+06	(77)	29	206	47	107.7	81.9	141.5
41	1.00E+07	(90)	3.22E+06	(29)	9	250	92	118.0	77.3	186.0
42	1.07E+07	(300)	4.39E+06	(123)	28	341	62	93.0	74.1	116.8
43	3.29E+06	(46)	9.29E+05	(13)	14	72	39	133.7	71.9	269.5
44	5.00E+06	(40)	1.75E+06	(14)	8	136	71	108.3	58.3	215.5
45	7.00E+06	(56)	3.75E+06	(30)	8	291	106	71.3	45.1	115.1
46	1.13E+07	(203)	3.56E+06	(64)	18	276	69	120.8	91.0	162.7
47	9.58E+06	(115)	2.58E+06	(31)	12	201	72	140.8	94.6	216.5
48	1.55E+07	(93)	4.33E+06	(26)	6	336	131	135.7	87.7	218.3
49	9.00E+06	(54)	2.33E+06	(14)	6	181	95	145.6	80.8	283.5
50	8.42E+06	(101)	4.08E+06	(49)	12	317	91	78.8	55.6	113.2
51	4.00E+06	(32)	2.00E+06	(16)	8	155	77	76.2	40.9	148.7
52	6.20E+06	(124)	1.95E+06	(39)	20	151	48	121.0	84.2	178.1

53	2.00E+06	(12)	2.00E+06	(12)	6	155	88	38.4	15.8	93.1
54	8.29E+06	(199)	3.87E+06	(93)	24	301	63	81.7	62.9	106.0
55	6.57E+06	(230)	1.80E+06	(63)	35	140	35	138.3	103.4	184.7
56	6.25E+06	(150)	1.75E+06	(42)	24	136	42	135.7	96.2	195.9
57	1.24E+07	(87)	5.14E+06	(36)	7	399	133	92.2	62.1	140.0
58	2.12E+07	(254)	5.83E+06	(70)	12	453	109	137.5	104.2	181.4
59	9.56E+06	(86)	3.00E+06	(27)	9	233	89	121.0	78.2	194.0
60	1.25E+07	(75)	4.83E+06	(29)	6	375	139	98.5	63.7	156.9
61	4.75E+06	(19)	1.75E+06	(7)	4	136	99	102.2	41.9	287.9
62	4.30E+06	(43)	1.90E+06	(19)	10	148	67	86.2	49.5	156.6
63	5.17E+06	(62)	1.33E+06	(16)	12	104	51	146.4	84.4	271.5
64	8.88E+06	(71)	2.88E+06	(23)	8	223	92	117.2	72.9	196.6
65	4.80E+06	(192)	1.68E+06	(67)	40	130	32	108.9	81.4	145.5
66	4.00E+06	(60)	9.33E+05	(14)	15	72	38	161.5	90.4	312.4
67	1.44E+07	(345)	5.25E+06	(126)	24	408	74	104.3	83.5	130.3
68	1.30E+06	(13)	1.40E+06	(14)	10	109	57	35.7	15.4	81.6
69	1.02E+07	(61)	2.50E+06	(15)	6	194	99	153.5	87.3	290.3
70	6.10E+06	(61)	3.10E+06	(31)	10	241	86	75.2	48.2	119.9
71	9.67E+06	(87)	4.78E+06	(43)	9	371	113	77.3	53.2	114.2
72	4.80E+06	(48)	1.50E+06	(15)	10	116	59	121.2	67.4	232.9
73	4.83E+06	(29)	1.33E+06	(8)	6	104	71	136.1	61.9	344.3
74	1.37E+07	(137)	3.90E+06	(39)	10	303	97	133.5	93.4	195.7
75	1.01E+07	(101)	1.70E+06	(17)	10	132	63	223.1	134.5	396.1
76	5.58E+06	(67)	2.75E+06	(33)	12	214	74	77.5	50.5	121.5
77	7.68E+06	(215)	2.54E+06	(71)	28	197	47	115.0	86.8	152.3
78	6.31E+06	(101)	1.69E+06	(27)	16	131	50	141.9	92.7	225.5
79	6.24E+06	(131)	2.10E+06	(44)	21	163	49	113.4	80.3	163.4
80	7.83E+06	(47)	3.83E+06	(23)	6	298	123	77.9	46.6	134.5
81	8.83E+06	(265)	2.37E+06	(71)	30	184	44	141.4	107.5	186.0
82	7.08E+06	(92)	2.92E+06	(38)	13	227	73	92.3	62.9	138.6
83	6.06E+06	(97)	2.19E+06	(35)	16	170	57	105.6	71.3	160.1
84	9.00E+06	(216)	3.71E+06	(89)	24	288	62	92.5	71.2	120.1
85	5.42E+06	(271)	1.84E+06	(92)	50	143	30	112.1	87.1	144.1
86	6.29E+06	(283)	2.53E+06	(114)	45	197	37	94.7	74.8	119.7
87	6.17E+06	(148)	3.08E+06	(74)	24	239	56	76.3	57.0	102.1
88	1.06E+07	(95)	3.56E+06	(32)	9	276	97	113.0	75.3	174.3
89	6.36E+06	(178)	1.61E+06	(45)	28	125	37	150.2	108.2	213.0
90	7.25E+06	(58)	1.25E+06	(10)	8	97	60	216.7	112.1	472.8
91	5.07E+06	(71)	1.64E+06	(23)	14	128	53	117.2	72.9	196.6
92	5.88E+06	(94)	2.06E+06	(33)	16	160	56	108.4	72.6	166.5
93	6.08E+06	(73)	2.33E+06	(28)	12	181	68	99.3	63.7	159.5
94	9.10E+06	(182)	4.50E+06	(90)	20	349	74	77.2	59.1	100.8
95	2.50E+06	(30)	1.42E+06	(17)	12	110	53	67.3	36.2	130.2
96	1.23E+07	(98)	5.13E+06	(41)	8	398	124	91.2	62.9	134.8
97	1.33E+06	(8)	8.33E+05	(5)	6	65	55	60.6	17.7	235.2
98	1.09E+07	(87)	4.50E+06	(36)	8	349	116	92.2	62.1	140.0
99	6.13E+06	(98)	1.50E+06	(24)	16	116	47	154.6	98.9	252.3
100	4.21E+06	(59)	2.29E+06	(32)	14	177	63	70.5	45.2	112.0
101	5.56E+06	(50)	2.56E+06	(23)	9	198	82	82.9	49.9	142.3
102	4.50E+06	(45)	3.90E+06	(39)	10	303	97	44.3	28.2	69.8
103	4.70E+06	(47)	2.80E+06	(28)	10	217	82	64.2	39.5	106.4
104	5.14E+06	(108)	2.43E+06	(51)	21	189	53	80.9	57.6	115.3
105	7.67E+06	(46)	5.50E+06	(33)	6	427	148	53.4	33.5	86.2

KLD25 (Yukon), modern sand, TU11z (counted by Sarah Falkowski, April 2014)

EFFECTIVE TRACK DENSITY FOR FLUENCE MONITOR (tracks/cm^2): 6.430E+05
RELATIVE ERROR (%): 1.57
EFFECTIVE URANIUM CONTENT OF MONITOR (ppm): 50.00
ZETA FACTOR AND STANDARD ERROR (yr cm^2): 119.60 5.40
SIZE OF COUNTER SQUARE (cm^2): 1.000E-06

------ GRAIN AGES IN ORIGINAL ORDER ------

Grain no.	**RhoS (cm^-2)**	**(Ns)**	**RhoI (cm^-2)**	**(Ni)**	**Squares**	**U+/-2s**		**Grain Age**	**Age (Ma) --95% CI--**	
1	8.89E+05	(16)	4.44E+05	(8)	18	35	24	75.7	31.0	204.4
2	7.62E+05	(16)	2.86E+05	(6)	21	22	17	100.1	38.0	312.4
3	3.81E+06	(61)	1.38E+06	(22)	16	107	45	105.3	64.1	180.0
4	3.94E+06	(63)	8.13E+05	(13)	16	63	34	181.9	100.6	359.2
5	1.39E+06	(86)	1.06E+06	(66)	62	83	20	49.9	35.8	69.9
6	7.33E+06	(198)	3.00E+06	(81)	27	233	52	93.0	70.8	122.1
7	1.75E+06	(7)	5.00E+05	(2)	4	39	49	126.5	25.6	1207.7
8	1.33E+06	(16)	9.17E+05	(11)	12	71	42	55.4	24.3	132.0
9	6.43E+05	(18)	1.43E+05	(4)	28	11	10	165.7	56.7	667.5
10	4.63E+06	(37)	7.50E+05	(6)	8	58	46	227.8	98.4	653.5
11	1.11E+06	(50)	4.22E+05	(19)	45	33	15	99.9	58.3	179.4
12	1.25E+06	(20)	1.13E+06	(18)	16	87	41	42.5	21.4	85.2
13	1.08E+06	(43)	1.00E+06	(40)	40	78	25	41.2	26.2	65.0
14	1.33E+06	(16)	6.67E+05	(8)	12	52	36	75.7	31.0	204.4
15	4.54E+06	(109)	1.13E+06	(27)	24	87	33	152.7	100.2	241.9
16	4.81E+06	(77)	2.88E+06	(46)	16	224	66	64.0	43.9	94.3
17	5.00E+05	(6)	6.67E+05	(8)	12	52	36	29.0	8.2	94.1
18	1.25E+06	(15)	9.17E+05	(11)	12	71	42	52.0	22.5	125.1
19	6.67E+05	(4)	5.00E+05	(3)	6	39	42	50.4	8.7	341.0
20	1.08E+06	(13)	5.00E+05	(6)	12	39	31	81.6	29.5	262.1
21	3.52E+06	(74)	2.86E+06	(60)	21	222	58	47.2	33.2	67.6
22	1.63E+06	(13)	7.50E+05	(6)	8	58	46	81.6	29.5	262.1
23	6.21E+06	(211)	1.97E+06	(67)	34	153	38	119.4	89.6	159.0
24	1.30E+06	(13)	5.00E+05	(5)	10	39	33	97.3	33.3	348.8
25	7.50E+06	(75)	4.80E+06	(48)	10	373	108	59.7	41.1	87.7
26	1.75E+06	(35)	1.85E+06	(37)	20	144	47	36.3	22.2	59.2
27	3.29E+06	(69)	1.33E+06	(28)	21	104	39	93.7	59.9	151.1
28	4.13E+06	(66)	1.25E+06	(20)	16	97	43	125.0	75.4	217.5
29	2.00E+06	(64)	1.00E+06	(32)	32	78	27	76.3	49.3	120.5
30	6.50E+06	(156)	2.46E+06	(59)	24	191	50	100.7	74.3	138.4
31	1.63E+06	(39)	1.46E+06	(35)	24	113	38	42.7	26.4	69.4
32	4.04E+06	(113)	1.61E+06	(45)	28	125	37	95.6	67.3	138.3
33	4.50E+06	(27)	2.17E+06	(13)	6	168	92	78.9	39.7	166.6
34	1.42E+06	(17)	1.00E+06	(12)	12	78	44	54.0	24.5	123.9
35	1.25E+05	(2)	4.38E+05	(7)	16	34	25	11.6	1.1	57.5
36	3.92E+06	(47)	1.08E+06	(13)	12	84	46	136.3	73.5	274.4
37	9.00E+05	(36)	1.23E+06	(49)	40	95	27	28.2	17.8	44.2
38	1.97E+06	(59)	2.03E+06	(61)	30	158	41	37.1	25.5	53.9
39	1.50E+06	(18)	6.67E+05	(8)	12	52	36	85.0	35.7	226.1
40	2.00E+06	(12)	6.67E+05	(4)	6	52	49	111.4	34.9	473.2
41	2.13E+06	(17)	2.00E+06	(16)	8	156	77	40.7	19.4	85.9
42	1.86E+06	(39)	1.33E+06	(28)	21	104	39	53.3	32.0	89.8
43	7.14E+05	(20)	7.14E+05	(20)	28	56	25	38.3	19.6	74.9
44	3.28E+06	(59)	1.56E+06	(28)	18	121	45	80.3	50.6	130.8
45	3.50E+06	(35)	2.40E+06	(24)	10	187	76	55.7	32.3	97.9
46	2.52E+06	(53)	9.05E+05	(19)	21	70	32	105.8	62.1	189.2
47	3.12E+06	(187)	2.27E+06	(136)	60	176	31	52.6	41.4	66.8
48	2.42E+06	(121)	1.58E+06	(79)	50	123	28	58.6	43.8	78.9
49	2.88E+06	(23)	5.00E+05	(4)	8	39	37	210.6	75.1	824.9
50	4.58E+06	(110)	1.96E+06	(47)	24	152	44	89.2	63.0	128.4
51	1.40E+06	(28)	1.10E+06	(22)	20	86	36	48.7	26.9	89.2
52	1.77E+06	(85)	1.58E+06	(76)	48	123	28	42.9	31.1	59.2

53	1.00E+06	(20)	1.25E+06	(25)	20	97	39	30.7	16.2	57.5
54	8.33E+05	(10)	5.00E+05	(6)	12	39	31	63.1	21.1	211.2
55	4.63E+06	(37)	1.63E+06	(13)	8	126	69	107.7	56.6	220.7
56	3.38E+06	(27)	1.13E+06	(9)	8	87	57	113.0	52.4	273.1
57	4.11E+06	(37)	2.11E+06	(19)	9	164	75	74.1	41.8	136.5
58	1.14E+07	(91)	4.13E+06	(33)	8	321	111	104.8	70.0	161.3
59	1.50E+06	(12)	3.75E+05	(3)	8	29	31	146.4	41.4	798.2
60	1.33E+06	(16)	5.83E+05	(7)	12	45	33	86.2	34.1	248.0
61	4.50E+06	(81)	2.22E+06	(40)	18	173	55	77.2	52.4	115.9
62	1.33E+06	(16)	1.33E+06	(16)	12	104	51	38.3	18.0	81.7
63	1.71E+06	(24)	1.50E+06	(21)	14	117	50	43.8	23.4	82.6
64	2.75E+06	(33)	8.33E+05	(10)	12	65	40	124.3	60.8	282.6
65	7.08E+05	(17)	4.58E+05	(11)	24	36	21	58.9	26.2	139.0
66	1.38E+06	(33)	9.58E+05	(23)	24	75	31	54.8	31.3	97.8
67	6.44E+06	(58)	7.56E+06	(68)	9	588	143	32.7	22.6	47.2
68	2.38E+06	(57)	5.42E+05	(13)	24	42	23	164.9	90.5	327.6
69	3.83E+06	(23)	4.00E+06	(24)	6	311	126	36.8	19.8	67.9
70	1.47E+06	(22)	8.67E+05	(13)	15	67	37	64.4	31.3	139.2
71	2.25E+06	(27)	1.00E+06	(12)	12	78	44	85.3	42.2	184.9
72	1.04E+07	(94)	3.00E+06	(27)	9	233	89	131.9	85.8	210.5
73	2.00E+06	(48)	1.04E+06	(25)	24	81	32	73.2	44.4	123.9
74	3.88E+06	(155)	1.45E+06	(58)	40	113	30	101.8	75.0	140.2
75	3.40E+06	(34)	2.70E+06	(27)	10	210	80	48.2	28.3	83.0
76	7.80E+05	(39)	6.00E+05	(30)	50	47	17	49.7	30.2	82.9
77	3.87E+06	(116)	3.60E+06	(108)	30	280	54	41.2	31.2	54.3
78	2.25E+06	(27)	2.42E+06	(29)	12	188	69	35.7	20.3	62.4
79	7.92E+05	(19)	7.08E+05	(17)	24	55	26	42.8	21.1	87.5
80	9.17E+05	(22)	4.17E+05	(10)	24	32	20	83.3	38.3	197.2
81	7.78E+05	(7)	2.22E+05	(2)	9	17	22	126.5	25.6	1207.7
82	8.75E+05	(14)	5.00E+05	(8)	16	39	27	66.4	26.3	182.6
83	4.17E+05	(5)	1.08E+06	(13)	12	84	46	15.1	4.1	44.1
84	1.04E+06	(25)	6.67E+05	(16)	24	52	26	59.6	30.7	119.4
85	1.83E+06	(73)	2.10E+06	(84)	40	163	36	33.3	24.0	46.2
86	1.73E+06	(26)	1.00E+06	(15)	15	78	40	66.0	33.9	134.1
87	2.11E+06	(19)	6.67E+05	(6)	9	52	41	118.5	46.6	362.4
88	2.03E+06	(61)	7.33E+05	(22)	30	57	24	105.3	64.1	180.0
89	2.64E+06	(132)	4.74E+06	(237)	50	369	49	21.4	17.0	27.0
90	8.57E+05	(18)	8.10E+05	(17)	21	63	30	40.6	19.8	83.6
91	2.00E+06	(18)	1.11E+06	(10)	9	86	53	68.4	30.2	165.8
92	2.13E+06	(32)	4.07E+06	(61)	15	316	81	20.2	12.7	31.4
93	1.00E+06	(9)	1.78E+06	(16)	9	138	68	21.8	8.4	51.8
94	1.45E+06	(29)	1.00E+06	(20)	20	78	34	55.4	30.4	103.3
95	4.17E+05	(5)	8.33E+04	(1)	12	6	11	170.8	21.5	5673.0
96	7.50E+05	(6)	7.50E+05	(6)	8	58	46	38.3	10.3	142.3
97	3.67E+06	(55)	8.67E+05	(13)	15	67	37	159.2	87.1	317.0
98	1.50E+06	(18)	7.50E+05	(9)	12	58	38	75.8	32.7	191.6
99	6.25E+06	(25)	6.00E+06	(24)	4	467	189	39.9	21.9	72.9
100	1.50E+06	(24)	1.31E+06	(21)	16	102	44	43.8	23.4	82.6
101	1.39E+06	(25)	7.22E+05	(13)	18	56	31	73.1	36.3	155.6
102	2.40E+06	(36)	2.47E+06	(37)	15	192	63	37.3	22.9	60.7
103	5.92E+06	(148)	5.36E+06	(134)	25	417	73	42.3	32.9	54.4
104	5.00E+05	(5)	1.20E+06	(12)	10	93	53	16.3	4.4	48.7
105	1.53E+06	(46)	1.73E+06	(52)	30	135	37	33.9	22.3	51.4

KLD26 (Yukon), modern sand, TU11z (counted by Sarah Falkowski, April 2014)

EFFECTIVE TRACK DENSITY FOR FLUENCE MONITOR (tracks/cm^2): 6.410E+05
RELATIVE ERROR (%): 1.57
EFFECTIVE URANIUM CONTENT OF MONITOR (ppm): 50.00
ZETA FACTOR AND STANDARD ERROR (yr cm^2): 119.60 5.40
SIZE OF COUNTER SQUARE (cm^2): 1.000E-06

------ GRAIN AGES IN ORIGINAL ORDER ------

Grain no.	RhoS (cm^-2)	(Ns)	RhoI (cm^-2)	(Ni)	Squares	U+/-2s		Grain Age	Age (Ma) --95% CI--	
1	3.25E+06	(13)	2.50E+06	(10)	4	195	121	49.5	20.1	125.8
2	1.53E+07	(61)	5.50E+06	(22)	4	429	181	104.9	63.9	179.4
3	8.17E+06	(49)	2.17E+06	(13)	6	169	92	141.6	76.7	284.2
4	7.67E+06	(46)	4.00E+06	(24)	6	312	126	72.8	43.7	124.8
5	2.00E+06	(12)	3.33E+05	(2)	6	26	33	212.7	51.0	1830.3
6	1.32E+07	(79)	6.67E+06	(40)	6	520	164	75.1	50.9	112.9
7	9.00E+06	(243)	2.26E+06	(61)	27	176	45	150.6	113.7	202.8
8	5.35E+06	(107)	3.05E+06	(61)	20	238	61	66.8	48.4	93.1
9	6.00E+06	(24)	2.25E+06	(9)	4	176	114	100.3	45.7	245.3
10	5.25E+06	(21)	3.00E+06	(12)	4	234	133	66.4	31.4	148.0
11	7.35E+06	(147)	2.55E+06	(51)	20	199	56	109.3	79.2	153.5
12	1.67E+06	(10)	3.33E+06	(20)	6	260	115	19.3	8.0	42.8
13	8.40E+06	(84)	3.70E+06	(37)	10	289	95	86.2	58.1	130.7
14	7.38E+06	(59)	2.50E+06	(20)	8	195	86	111.5	66.7	195.5
15	4.25E+06	(17)	7.50E+05	(3)	4	59	63	205.0	62.5	1064.5
16	7.25E+06	(29)	1.75E+06	(7)	4	137	100	154.2	67.7	416.0
17	1.65E+07	(66)	4.75E+06	(19)	4	371	168	131.0	78.4	231.0
18	6.67E+05	(4)	1.50E+06	(9)	6	117	76	17.4	3.8	60.8
19	5.50E+06	(33)	1.27E+07	(76)	6	988	228	16.7	10.7	25.3
20	6.77E+06	(88)	2.69E+06	(35)	13	210	71	95.4	64.1	145.5
21	4.75E+06	(38)	2.13E+06	(17)	8	166	79	84.7	47.0	160.0
22	9.89E+06	(89)	3.67E+06	(33)	9	286	99	102.2	68.2	157.5
23	7.25E+06	(29)	1.00E+06	(4)	4	78	74	263.2	96.8	1005.8
24	7.58E+06	(91)	2.17E+06	(26)	12	169	66	132.2	85.3	212.9
25	9.38E+06	(75)	3.13E+06	(25)	8	244	97	113.5	71.8	186.3
26	7.50E+06	(45)	1.50E+06	(9)	6	117	76	186.2	91.8	431.5
27	1.33E+06	(8)	6.67E+05	(4)	6	52	49	74.8	20.5	339.0
28	2.14E+07	(107)	7.00E+06	(35)	5	546	184	115.8	78.7	174.8
29	1.28E+06	(23)	1.17E+06	(21)	18	91	39	41.8	22.2	79.3
30	8.83E+06	(106)	3.08E+06	(37)	12	241	79	108.6	74.4	162.5
31	1.03E+07	(205)	4.60E+06	(92)	20	359	75	84.6	65.2	109.8
32	9.00E+06	(99)	5.09E+06	(56)	11	397	106	67.3	48.1	95.3
33	7.38E+06	(59)	3.38E+06	(27)	8	263	101	83.0	52.0	136.1
34	4.00E+06	(32)	3.75E+06	(30)	8	293	106	40.7	24.0	69.4
35	8.08E+06	(194)	8.12E+06	(195)	24	634	93	38.0	30.5	47.3
36	6.60E+06	(132)	2.90E+06	(58)	20	226	60	86.5	63.2	120.0
37	1.33E+06	(8)	8.33E+05	(5)	6	65	55	60.3	17.7	234.1
38	1.13E+06	(9)	1.25E+05	(1)	8	10	16	299.3	47.6	7786.2
39	6.00E+06	(36)	3.17E+06	(19)	6	247	112	71.9	40.4	132.8
40	7.17E+06	(43)	1.17E+06	(7)	6	91	67	227.0	104.1	592.7
41	5.38E+06	(43)	1.88E+06	(15)	8	146	74	108.2	59.5	209.7
42	7.22E+06	(65)	2.67E+06	(24)	9	208	84	102.6	63.7	171.3
43	8.81E+06	(238)	3.67E+06	(99)	27	286	58	91.2	71.0	117.1
44	1.19E+07	(83)	2.86E+06	(20)	7	223	99	156.2	95.9	268.4
45	1.15E+07	(69)	5.17E+06	(31)	6	403	144	84.5	54.8	133.7
46	3.83E+06	(23)	1.17E+06	(7)	6	91	67	122.8	52.1	338.7
47	1.16E+07	(116)	5.40E+06	(54)	10	421	115	81.7	58.8	115.1
48	4.28E+06	(77)	1.56E+06	(28)	18	121	46	104.2	67.2	166.8
49	9.00E+06	(36)	2.00E+06	(8)	4	156	107	167.6	78.3	416.2
50	6.00E+06	(72)	2.00E+06	(24)	12	156	63	113.5	71.1	188.3
51	4.33E+06	(52)	1.67E+06	(20)	12	130	58	98.4	58.2	174.1
52	6.67E+05	(4)	1.33E+06	(8)	6	104	71	19.5	4.2	71.2

53	6.33E+06	(38)	3.00E+06	(18)	6	234	109	80.0	44.9	149.0
54	9.00E+06	(36)	7.00E+06	(28)	4	546	205	49.0	29.2	83.4
55	9.00E+06	(45)	6.00E+06	(30)	5	468	170	57.1	35.3	94.0
56	7.89E+06	(71)	3.22E+06	(29)	9	251	93	92.9	59.8	148.4
57	1.50E+06	(9)	1.00E+06	(6)	6	78	61	56.8	18.2	193.5
58	1.18E+07	(282)	4.33E+06	(104)	24	338	67	102.8	80.7	130.8
59	9.42E+06	(113)	4.42E+06	(53)	12	345	95	81.1	58.1	114.7
60	9.08E+06	(109)	3.75E+06	(45)	12	293	87	92.0	64.6	133.3
61	1.25E+06	(10)	2.00E+06	(16)	8	156	77	24.1	9.7	56.0
62	1.45E+07	(58)	5.25E+06	(21)	4	410	177	104.5	62.9	181.3
63	1.22E+06	(11)	1.44E+06	(13)	9	113	61	32.4	13.1	78.0
64	4.80E+06	(24)	6.00E+05	(3)	5	47	50	286.7	92.4	1422.4
65	5.03E+06	(201)	1.98E+06	(79)	40	154	35	96.4	73.3	126.8
66	7.17E+06	(43)	3.17E+06	(19)	6	247	112	85.8	49.2	155.9
67	8.10E+06	(170)	3.95E+06	(83)	21	308	68	77.8	59.0	102.5
68	9.40E+06	(94)	5.70E+06	(57)	10	445	118	62.8	44.8	89.0
69	4.75E+06	(57)	4.00E+06	(48)	12	312	90	45.3	30.4	68.0
70	7.22E+06	(65)	2.00E+06	(18)	9	156	73	136.1	80.5	243.6
71	8.21E+06	(115)	5.07E+06	(71)	14	396	94	61.7	45.6	84.3
72	1.18E+07	(94)	5.63E+06	(45)	8	439	131	79.4	55.2	116.0
73	1.21E+07	(182)	4.47E+06	(67)	15	348	86	103.1	77.7	138.7
74	2.00E+06	(18)	2.00E+06	(18)	9	156	73	38.2	18.8	77.7
75	5.20E+06	(52)	2.30E+06	(23)	10	179	74	85.8	51.8	146.8
76	6.70E+06	(201)	2.30E+06	(69)	30	179	43	110.2	82.8	146.6
77	8.00E+06	(128)	2.38E+06	(38)	16	185	60	127.5	88.5	188.2
78	5.83E+06	(35)	2.50E+06	(15)	6	195	99	88.3	47.4	174.1
79	8.00E+06	(48)	1.67E+06	(10)	6	130	80	179.1	91.2	395.8
80	5.33E+06	(96)	3.44E+06	(62)	18	269	68	59.0	42.5	82.7
81	5.50E+06	(44)	2.63E+06	(21)	8	205	89	79.5	46.5	140.8
82	5.89E+06	(106)	2.61E+06	(47)	18	204	59	85.7	60.4	123.6
83	5.81E+06	(93)	2.63E+06	(42)	16	205	63	84.2	58.0	124.3
84	2.17E+06	(13)	2.00E+06	(12)	6	156	88	41.4	17.4	98.9
85	1.00E+07	(60)	3.17E+06	(19)	6	247	112	119.2	70.8	211.5
86	3.43E+06	(48)	1.00E+06	(14)	14	78	41	129.1	70.8	253.3
87	8.75E+06	(105)	3.75E+06	(45)	12	293	87	88.6	62.1	128.7
88	9.53E+06	(381)	3.00E+06	(120)	40	234	43	120.2	96.2	150.2
89	5.75E+06	(46)	3.00E+06	(24)	8	234	95	72.8	43.7	124.8
90	1.00E+05	(2)	8.00E+05	(16)	20	62	31	5.1	0.5	20.4
91	1.10E+06	(11)	1.20E+06	(12)	10	94	53	35.1	14.0	86.5
92	5.31E+06	(191)	1.53E+06	(55)	36	119	32	131.5	97.2	180.9
93	1.04E+07	(104)	4.60E+06	(46)	10	359	106	85.9	60.3	124.4
94	2.00E+06	(16)	3.75E+05	(3)	8	29	31	193.2	58.2	1011.6
95	1.10E+07	(132)	5.33E+06	(64)	12	416	104	78.5	57.9	107.6
96	1.00E+07	(90)	3.00E+06	(27)	9	234	90	126.0	81.7	201.5
97	7.33E+06	(66)	4.44E+06	(40)	9	347	109	62.8	41.9	95.6
98	1.03E+07	(82)	4.50E+06	(36)	8	351	117	86.5	58.0	131.9
99	6.00E+06	(54)	2.56E+06	(23)	9	199	82	89.0	54.0	152.0
100	7.00E+06	(56)	2.38E+06	(19)	8	185	84	111.4	65.7	198.5
101	1.33E+06	(8)	3.83E+06	(23)	6	299	124	13.5	5.2	30.8
102	3.25E+06	(26)	3.00E+06	(24)	8	234	95	41.4	22.9	75.2
103	6.63E+06	(53)	1.75E+06	(14)	8	137	72	142.3	78.8	277.4
104	8.83E+06	(53)	2.67E+06	(16)	6	208	103	124.9	71.0	233.9
105	7.53E+06	(113)	1.40E+06	(21)	15	109	47	201.8	127.3	337.5

KLD29 (Yukon), modern sand, TU11z (counted by Sarah Falkowski, April 2014)

EFFECTIVE TRACK DENSITY FOR FLUENCE MONITOR (tracks/cm^2): 6.410E+05

RELATIVE ERROR (%): 1.57

EFFECTIVE URANIUM CONTENT OF MONITOR (ppm): 50.00

ZETA FACTOR AND STANDARD ERROR (yr cm^2): 119.60 5.40

SIZE OF COUNTER SQUARE (cm^2): 1.000E-06

------ GRAIN AGES IN ORIGINAL ORDER ------

Grain no.	RhoS (cm^-2)	(Ns)	RhoI (cm^-2)	(Ni)	Squares	U	+/-2s	Grain Age	Age (Ma) --95% CI--	
1	3.33E+06	(20)	7.67E+06	(46)	6	598	176	16.7	9.3	28.7
2	6.83E+06	(41)	8.00E+06	(48)	6	624	180	32.7	21.0	50.6
3	5.60E+06	(28)	7.40E+06	(37)	5	577	189	29.0	17.1	48.6
4	2.90E+06	(29)	4.90E+06	(49)	10	382	109	22.7	13.8	36.6
5	1.00E+07	(60)	2.10E+07	(126)	6	1638	296	18.3	13.2	25.0
6	5.61E+06	(101)	1.13E+07	(204)	18	884	127	19.0	14.7	24.5
7	8.00E+06	(40)	1.80E+06	(9)	5	140	91	165.9	80.8	387.7
8	1.66E+07	(83)	1.80E+07	(90)	5	1404	298	35.3	25.8	48.1
9	6.17E+06	(37)	1.83E+06	(11)	6	143	84	126.4	64.0	274.5
10	7.36E+06	(103)	8.71E+06	(122)	14	680	125	32.3	24.5	42.6
11	9.80E+06	(49)	3.20E+06	(16)	5	250	123	115.6	65.2	217.6
12	8.33E+06	(125)	7.20E+06	(108)	15	562	109	44.2	33.6	58.0
13	1.08E+07	(97)	1.96E+07	(176)	9	1525	235	21.1	16.2	27.5
14	2.83E+06	(17)	6.17E+06	(37)	6	481	158	17.7	9.3	32.0
15	4.13E+06	(33)	4.88E+06	(39)	8	380	122	32.4	19.7	52.8
16	8.70E+06	(235)	1.22E+07	(329)	27	950	109	27.3	22.6	33.1
17	1.64E+07	(148)	1.30E+07	(117)	9	1014	190	48.3	37.3	62.5
18	1.22E+07	(122)	1.29E+07	(129)	10	1006	180	36.2	27.8	47.1
19	5.43E+06	(38)	5.00E+06	(35)	7	390	131	41.5	25.5	67.6
20	5.14E+06	(36)	9.86E+06	(69)	7	769	186	20.0	13.0	30.3
21	9.00E+06	(72)	6.88E+06	(55)	8	536	145	50.0	34.7	72.3
22	4.27E+06	(64)	2.00E+06	(30)	15	156	57	81.0	52.0	129.6
23	4.83E+06	(87)	4.17E+06	(75)	18	325	76	44.3	32.1	61.2
24	5.71E+06	(80)	8.93E+06	(125)	14	696	126	24.5	18.2	32.7
25	9.00E+06	(81)	1.30E+07	(117)	9	1014	190	26.5	19.7	35.5
26	6.33E+06	(57)	1.07E+07	(96)	9	832	171	22.7	16.1	31.9
27	1.93E+07	(154)	1.29E+07	(103)	8	1004	200	57.0	43.7	74.2
28	2.93E+06	(44)	7.73E+06	(116)	15	603	113	14.6	10.0	20.7
29	7.69E+06	(123)	1.27E+07	(203)	16	990	142	23.2	18.2	29.6
30	4.50E+06	(27)	2.17E+06	(13)	6	169	92	78.6	39.5	166.0
31	9.38E+06	(75)	4.25E+06	(34)	8	332	113	83.8	55.4	129.7
32	2.00E+06	(24)	3.08E+06	(37)	12	241	79	24.9	14.2	42.6
33	1.03E+07	(62)	4.00E+06	(24)	6	312	126	97.9	60.6	164.0
34	3.80E+06	(76)	2.15E+06	(43)	20	168	51	67.3	45.8	100.3
35	4.21E+06	(101)	8.50E+06	(204)	24	663	95	19.0	14.7	24.5
36	6.05E+06	(127)	4.29E+06	(90)	21	334	71	53.8	40.5	71.4
37	1.11E+07	(100)	3.67E+06	(33)	9	286	99	114.8	77.1	175.6
38	6.33E+06	(57)	7.89E+06	(71)	9	615	147	30.7	21.3	44.2
39	2.94E+06	(53)	5.56E+06	(100)	18	433	88	20.3	14.2	28.6
40	1.60E+07	(64)	1.20E+07	(48)	4	936	270	50.9	34.5	75.6
41	5.25E+06	(42)	6.75E+06	(54)	8	527	144	29.8	19.4	45.4
42	7.80E+06	(78)	3.60E+06	(36)	10	281	93	82.3	55.0	125.9
43	5.36E+06	(75)	6.00E+06	(84)	14	468	103	34.1	24.6	47.2
44	8.33E+06	(50)	1.28E+07	(77)	6	1001	230	24.9	17.0	36.0
45	7.50E+06	(90)	1.37E+07	(164)	12	1066	170	21.1	16.0	27.7
46	5.00E+06	(35)	1.00E+07	(70)	7	780	187	19.2	12.4	29.1
47	1.00E+06	(6)	1.50E+06	(9)	6	117	76	25.7	7.5	79.9
48	2.00E+06	(48)	3.38E+06	(81)	24	263	59	22.7	15.5	32.8
49	3.58E+06	(215)	4.88E+06	(293)	60	381	46	28.1	23.0	34.3
50	6.47E+06	(97)	1.19E+07	(179)	15	931	142	20.8	16.0	27.0
51	2.78E+06	(25)	2.11E+06	(19)	9	165	75	50.1	26.6	96.3
52	5.60E+06	(28)	1.94E+07	(97)	5	1513	310	11.1	7.0	17.0

53	4.08E+06	(49)	3.67E+06	(44)	12	286	86	42.5	27.7	65.4
54	5.40E+06	(54)	8.60E+06	(86)	10	671	146	24.1	16.8	34.2
55	2.67E+06	(32)	1.33E+06	(16)	12	104	51	75.8	40.7	148.0
56	4.33E+06	(26)	8.17E+06	(49)	6	637	182	20.4	12.1	33.3
57	1.04E+07	(94)	1.31E+07	(118)	9	1023	191	30.5	22.9	40.6
58	1.08E+07	(43)	2.85E+07	(114)	4	2223	421	14.5	9.9	20.7
59	2.63E+06	(21)	3.63E+06	(29)	8	283	104	27.8	15.0	50.2
60	3.94E+06	(63)	6.75E+06	(108)	16	527	102	22.3	16.1	30.8
61	3.17E+06	(38)	5.17E+06	(62)	12	403	103	23.5	15.2	35.7
62	8.08E+06	(97)	1.49E+07	(179)	12	1164	177	20.8	16.0	27.0
63	2.90E+06	(87)	4.43E+06	(133)	30	346	61	25.1	18.9	33.3
64	8.00E+06	(32)	2.65E+07	(106)	4	2067	406	11.6	7.5	17.3
65	1.24E+07	(62)	3.20E+06	(16)	5	250	123	145.8	84.0	270.3
66	6.80E+06	(34)	6.20E+06	(31)	5	484	173	41.9	25.0	70.4
67	5.92E+06	(71)	9.00E+06	(108)	12	702	137	25.2	18.4	34.3
68	3.44E+06	(55)	4.81E+06	(77)	16	375	86	27.3	19.0	39.2
69	3.83E+06	(23)	8.83E+06	(53)	6	689	190	16.7	9.7	27.6
70	4.75E+06	(38)	2.38E+06	(19)	8	185	84	75.9	42.9	139.4
71	4.50E+06	(54)	2.33E+06	(28)	12	182	68	73.3	45.8	120.2
72	5.20E+06	(52)	1.48E+07	(148)	10	1154	193	13.5	9.6	18.6
73	9.70E+06	(291)	4.00E+06	(120)	30	312	58	92.1	73.1	115.9
74	5.83E+06	(35)	6.00E+06	(36)	6	468	156	37.2	22.7	60.9
75	4.17E+06	(50)	8.75E+06	(105)	12	683	135	18.3	12.7	25.8
76	2.92E+06	(35)	2.25E+06	(27)	12	176	67	49.4	29.1	84.9
77	5.08E+06	(61)	3.83E+06	(46)	12	299	88	50.6	34.0	75.9
78	3.00E+06	(63)	5.05E+06	(106)	21	394	77	22.8	16.4	31.4
79	1.53E+07	(92)	3.75E+07	(225)	6	2925	400	15.7	12.1	20.4
80	6.33E+06	(76)	3.50E+06	(42)	12	273	84	68.9	46.7	103.0
81	5.33E+06	(32)	9.17E+06	(55)	6	715	193	22.3	13.9	35.1
82	3.78E+06	(68)	6.94E+06	(125)	18	542	98	20.8	15.2	28.2
83	3.81E+06	(61)	5.81E+06	(93)	16	453	95	25.1	17.8	35.1
84	9.10E+06	(91)	3.00E+06	(30)	10	234	85	114.8	75.7	179.7
85	6.04E+06	(145)	9.38E+06	(225)	24	731	100	24.7	19.7	31.0
86	2.11E+06	(19)	6.67E+05	(6)	9	52	41	118.1	46.4	361.3
87	6.67E+06	(120)	8.50E+06	(153)	18	663	109	30.0	23.2	38.8
88	1.20E+06	(12)	7.00E+05	(7)	10	55	40	64.8	23.8	194.2
89	3.67E+06	(33)	6.33E+06	(57)	9	494	131	22.2	14.0	34.6
90	7.34E+06	(235)	1.15E+07	(369)	32	899	98	24.4	20.2	29.4
91	1.09E+07	(152)	9.50E+06	(133)	14	741	130	43.6	34.0	56.0
92	7.47E+06	(112)	1.23E+07	(184)	15	957	144	23.3	18.1	30.0
93	1.17E+06	(14)	1.83E+06	(22)	12	143	60	24.5	11.5	49.7
94	6.00E+06	(24)	1.15E+07	(46)	4	897	265	20.0	11.7	33.4
95	1.16E+07	(58)	1.80E+07	(90)	5	1404	298	24.7	17.4	34.7
96	6.38E+06	(51)	1.05E+07	(84)	8	819	180	23.3	16.1	33.3
97	1.60E+06	(24)	5.73E+06	(86)	15	447	97	10.7	6.5	17.0
98	2.93E+06	(79)	5.22E+06	(141)	27	407	70	21.5	16.1	28.7
99	7.87E+06	(189)	3.87E+06	(93)	24	302	63	77.2	59.3	100.5
100	6.86E+06	(48)	7.00E+06	(49)	7	546	156	37.4	24.6	56.9
101	5.83E+05	(7)	2.08E+06	(25)	12	163	65	10.9	3.9	25.5
102	4.40E+06	(22)	9.00E+06	(45)	5	702	209	18.8	10.7	31.8
103	7.00E+06	(70)	7.10E+06	(71)	10	554	132	37.7	26.7	53.2
104	6.00E+06	(72)	2.00E+06	(24)	12	156	63	113.5	71.1	188.3
105	4.13E+06	(33)	7.13E+06	(57)	8	556	148	22.2	14.0	34.6

KLD33 (Yukon), modern sand, UC2z (counted by Sarah Falkowski May 2014)

EFFECTIVE TRACK DENSITY FOR FLUENCE MONITOR (tracks/cm^2): 4.190E+05

RELATIVE ERROR (%): 1.57

EFFECTIVE URANIUM CONTENT OF MONITOR (ppm): 50.00

ZETA FACTOR AND STANDARD ERROR (yr cm^2): 119.60 5.40

SIZE OF COUNTER SQUARE (cm^2): 1.000E-06

------ GRAIN AGES IN ORIGINAL ORDER ------

Grain no.	**RhoS (cm^-2)**	**(Ns)**	**RhoI (cm^-2)**	**(Ni)**	**Squares**	**U+/-2s**		**Grain Age**	**Age (Ma) --95% CI--**	
1	8.47E+06	(254)	1.77E+06	(53)	30	211	58	118.7	88.3	162.9
2	1.18E+07	(378)	2.28E+06	(73)	32	272	64	127.8	98.1	166.3
3	1.09E+07	(328)	2.17E+06	(65)	30	259	64	124.5	94.2	164.4
4	9.58E+06	(115)	1.75E+06	(21)	12	209	90	134.9	85.0	226.3
5	1.02E+07	(102)	2.10E+06	(21)	10	251	108	119.8	75.0	202.0
6	1.55E+07	(186)	2.50E+06	(30)	12	298	108	152.8	104.2	232.8
7	1.28E+07	(204)	2.38E+06	(38)	16	283	92	132.7	93.9	192.9
8	1.26E+07	(377)	2.40E+06	(72)	30	286	68	129.2	99.0	168.4
9	9.24E+06	(388)	1.24E+06	(52)	42	148	41	183.8	138.0	250.3
10	1.11E+07	(311)	2.64E+06	(74)	28	315	74	103.9	79.5	135.7
11	1.13E+07	(135)	2.33E+06	(28)	12	278	105	119.1	79.4	186.1
12	9.63E+06	(385)	1.80E+06	(72)	40	215	51	131.9	101.1	171.8
13	9.00E+06	(189)	1.90E+06	(40)	21	227	72	116.9	83.1	169.0
14	6.56E+06	(295)	1.56E+06	(70)	45	186	45	104.2	79.2	137.0
15	9.63E+06	(154)	2.81E+06	(45)	16	336	100	85.0	60.8	121.4
16	1.19E+07	(215)	2.28E+06	(41)	18	272	85	129.7	92.9	185.9
17	1.00E+07	(300)	1.73E+06	(52)	30	207	57	142.6	106.3	195.3
18	9.10E+06	(364)	1.40E+06	(56)	40	167	45	160.5	121.3	216.5
19	1.33E+07	(200)	2.53E+06	(38)	15	302	98	130.1	92.1	189.3
20	1.27E+07	(266)	2.86E+06	(60)	21	341	88	109.9	83.0	148.1
21	6.03E+06	(181)	1.47E+06	(44)	30	175	53	102.0	73.3	145.3
22	9.50E+06	(380)	1.90E+06	(76)	40	227	52	123.4	95.1	160.1
23	1.29E+07	(258)	2.15E+06	(43)	20	257	78	148.2	107.5	209.7
24	1.10E+07	(331)	1.70E+06	(51)	30	203	57	160.2	119.5	219.5
25	1.38E+07	(248)	2.22E+06	(40)	18	265	84	153.0	109.8	219.3
26	1.07E+07	(320)	2.27E+06	(68)	30	270	66	116.2	88.2	152.9
27	1.89E+07	(189)	2.90E+06	(29)	10	346	128	160.5	109.0	246.1
28	1.28E+07	(255)	2.10E+06	(42)	20	251	77	149.9	108.3	213.0
29	1.82E+07	(291)	2.31E+06	(37)	16	276	91	193.4	137.9	279.8
30	8.63E+06	(259)	2.07E+06	(62)	30	247	63	103.2	77.3	137.8
31	2.00E+07	(240)	2.92E+06	(35)	12	348	117	168.9	118.9	248.0
32	9.05E+06	(181)	2.00E+06	(40)	20	239	75	112.0	79.5	162.1
33	1.47E+07	(293)	2.25E+06	(45)	20	268	80	160.6	117.6	225.0
34	1.55E+07	(309)	3.10E+06	(62)	20	370	94	122.9	92.4	163.3
35	1.40E+07	(279)	1.80E+06	(36)	20	215	71	190.6	135.3	277.3
36	1.43E+07	(428)	2.37E+06	(71)	30	282	67	148.4	113.9	193.3
37	1.05E+07	(189)	1.67E+06	(30)	18	199	72	155.3	106.0	236.4
38	1.19E+07	(143)	1.67E+06	(20)	12	199	88	175.5	110.7	295.6
39	1.13E+07	(169)	2.40E+06	(36)	15	286	95	116.2	81.1	171.5
40	9.53E+06	(286)	1.57E+06	(47)	30	187	55	150.3	110.5	209.2
41	2.26E+07	(113)	6.00E+06	(30)	5	716	260	93.3	62.2	144.8
42	1.19E+07	(380)	2.59E+06	(83)	32	310	68	113.2	87.9	145.6
43	1.51E+07	(136)	2.11E+06	(19)	9	252	114	175.6	109.5	300.3
44	6.75E+06	(270)	1.23E+06	(49)	40	146	42	136.2	100.6	188.7
45	7.30E+06	(146)	1.70E+06	(34)	20	203	69	106.3	73.1	159.5
46	1.07E+07	(214)	1.95E+06	(39)	20	233	74	135.6	96.5	196.0
47	1.32E+07	(317)	2.88E+06	(69)	24	343	83	113.5	86.3	149.1
48	7.06E+06	(353)	1.80E+06	(90)	50	215	46	97.1	75.8	124.4
49	5.80E+06	(116)	1.15E+06	(23)	20	137	57	124.4	79.7	204.2
50	1.10E+07	(331)	1.93E+06	(58)	30	231	61	140.4	105.0	187.6
51	9.26E+06	(250)	1.33E+06	(36)	27	159	53	171.0	121.0	249.6
52	8.41E+06	(227)	1.59E+06	(43)	27	190	58	130.5	94.3	185.4

53	8.75E+06 (140)	1.88E+06 (30)	16	224	81	115.4	77.8	177.5
54	1.11E+07 (133)	2.00E+06 (24)	12	239	97	136.6	88.7	220.8
55	7.93E+06 (214)	1.70E+06 (46)	27	203	60	115.2	83.8	162.2
56	9.70E+06 (262)	2.04E+06 (55)	27	243	66	118.0	88.2	160.9
57	6.64E+06 (93)	1.64E+06 (23)	14	196	81	100.0	63.3	165.7
58	1.13E+07 (304)	2.26E+06 (61)	27	270	69	122.9	92.2	163.6
59	8.76E+06 (184)	1.67E+06 (35)	21	199	67	129.9	90.6	192.3
60	9.58E+06 (230)	2.00E+06 (48)	24	239	69	118.6	86.9	165.6
61	1.14E+07 (91)	2.38E+06 (19)	8	283	129	118.1	72.1	205.3
62	6.50E+06 (78)	1.92E+06 (23)	12	229	95	84.0	52.5	140.4
63	1.60E+07 (128)	2.50E+06 (20)	8	298	132	157.3	98.7	266.1
64	9.70E+06 (97)	2.10E+06 (21)	10	251	108	114.0	71.2	192.7
65	1.51E+07 (301)	3.15E+06 (63)	20	376	95	117.9	88.7	156.5
66	6.44E+06 (116)	1.39E+06 (25)	18	166	66	114.6	74.4	184.6
67	1.11E+07 (299)	2.59E+06 (70)	27	309	74	105.6	80.3	138.8
68	9.10E+06 (273)	1.63E+06 (49)	30	195	56	137.7	101.7	190.8
69	8.93E+06 (268)	1.87E+06 (56)	30	223	60	118.5	88.8	161.2
70	1.30E+07 (259)	2.45E+06 (49)	20	292	84	130.8	96.4	181.3
71	7.50E+06 (90)	9.17E+05 (11)	12	109	65	199.3	108.3	412.2
72	9.63E+06 (289)	1.67E+06 (50)	30	199	56	142.8	105.9	197.0
73	1.52E+07 (137)	2.89E+06 (26)	9	345	134	130.0	85.7	206.2
74	1.32E+07 (263)	2.40E+06 (48)	20	286	83	135.5	99.7	188.4
75	1.03E+07 (206)	1.85E+06 (37)	20	221	72	137.5	97.1	200.8
76	1.20E+07 (216)	2.28E+06 (41)	18	272	85	130.3	93.4	186.7
77	1.04E+07 (156)	1.80E+06 (27)	15	215	82	142.5	95.0	223.0
78	1.30E+07 (195)	2.87E+06 (43)	15	342	104	112.3	80.7	160.2
79	1.58E+07 (190)	2.67E+06 (32)	12	318	112	146.5	101.0	220.2
80	5.98E+06 (239)	1.45E+06 (58)	40	173	46	102.2	76.6	138.8
81	1.39E+07 (416)	2.60E+06 (78)	30	310	71	131.6	101.8	169.9
82	1.74E+07 (157)	3.89E+06 (35)	9	464	156	111.0	76.9	165.2
83	2.14E+07 (171)	3.50E+06 (28)	8	418	157	150.5	101.3	233.1
84	8.86E+06 (62)	7.14E+05 (5)	7	85	73	294.9	124.9	921.8
85	1.46E+07 (262)	3.72E+06 (67)	18	444	109	96.7	73.0	128.1
86	1.03E+07 (124)	1.25E+06 (15)	12	149	76	202.0	119.6	370.7
87	5.94E+06 (107)	1.00E+06 (18)	18	119	56	146.2	89.2	256.0
88	1.33E+07 (120)	4.33E+06 (39)	9	517	165	76.4	53.0	112.8
89	1.34E+07 (402)	2.50E+06 (75)	30	298	69	132.2	101.9	171.5
90	1.74E+07 (279)	2.63E+06 (42)	16	313	97	163.8	118.7	232.2
91	1.24E+07 (373)	3.23E+06 (97)	30	386	79	95.3	74.9	121.1
92	9.70E+06 (194)	2.20E+06 (44)	20	263	79	109.2	78.7	155.3
93	1.90E+07 (190)	3.10E+06 (31)	10	370	132	151.1	103.7	228.6
94	8.93E+06 (268)	2.03E+06 (61)	30	243	62	108.5	81.1	144.9
95	1.87E+07 (336)	3.00E+06 (54)	18	358	98	153.7	115.4	208.8
96	1.29E+07 (309)	2.38E+06 (57)	24	283	75	134.1	101.1	181.3
97	1.14E+07 (182)	2.25E+06 (36)	16	268	89	125.0	87.5	184.1
98	1.26E+07 (251)	1.60E+06 (32)	20	191	67	192.8	134.1	287.4
99	1.13E+07 (226)	1.90E+06 (38)	20	227	73	146.8	104.3	212.8
100	1.29E+07 (388)	2.70E+06 (81)	30	322	72	118.3	91.8	152.5
101	9.65E+06 (193)	1.75E+06 (35)	20	209	70	136.2	95.2	201.3
102	6.00E+06 (120)	1.35E+06 (27)	20	161	62	109.9	72.4	173.8
103	7.89E+06 (213)	1.19E+06 (32)	27	141	50	164.0	113.5	245.6
104	1.16E+07 (232)	1.95E+06 (39)	20	233	74	146.9	104.8	211.8

KLD39 (Yukon), modern sand, TU11z (counted by Sarah Falkowski, April 2014)

EFFECTIVE TRACK DENSITY FOR FLUENCE MONITOR (tracks/cm^2): 6.400E+05
RELATIVE ERROR (%): 1.57
EFFECTIVE URANIUM CONTENT OF MONITOR (ppm): 50.00
ZETA FACTOR AND STANDARD ERROR (yr cm^2): 119.60 5.40
SIZE OF COUNTER SQUARE (cm^2): 1.000E-06

------ GRAIN AGES IN ORIGINAL ORDER ------

Grain no.	RhoS (cm^-2)	(Ns)	RhoI (cm^-2)	(Ni)	Squares	U	+/-2s	Grain Age	Age (Ma) --95% CI--	
1	1.01E+07	(202)	3.75E+06	(75)	20	293	68	101.8	77.1	134.5
2	3.25E+06	(13)	1.00E+06	(4)	4	78	74	120.0	38.3	503.7
3	6.33E+06	(253)	2.70E+06	(108)	40	211	41	88.8	69.7	113.1
4	1.20E+07	(48)	5.00E+06	(20)	4	391	173	90.8	53.2	161.5
5	1.02E+07	(245)	4.17E+06	(100)	24	326	66	92.8	72.4	119.0
6	3.00E+06	(150)	1.16E+06	(58)	50	91	24	98.1	72.1	135.2
7	8.94E+06	(143)	5.63E+06	(90)	16	439	93	60.4	45.7	79.7
8	2.18E+07	(87)	8.75E+06	(35)	4	684	230	94.2	63.2	143.7
9	1.16E+07	(243)	4.33E+06	(91)	21	339	72	101.1	78.2	130.5
10	8.50E+06	(68)	3.00E+06	(24)	8	234	95	107.1	66.8	178.3
11	1.34E+07	(107)	4.63E+06	(37)	8	361	119	109.4	75.0	163.6
12	8.81E+06	(185)	3.38E+06	(71)	21	264	63	98.5	74.0	131.2
13	6.70E+06	(134)	2.30E+06	(46)	20	180	53	110.3	78.6	157.7
14	2.38E+07	(143)	6.67E+06	(40)	6	521	164	135.0	94.9	196.7
15	1.12E+07	(112)	2.10E+06	(21)	10	164	71	199.7	125.9	334.2
16	7.05E+06	(148)	2.48E+06	(52)	21	193	54	107.8	78.3	150.9
17	1.17E+07	(117)	3.20E+06	(32)	10	250	88	137.9	93.2	210.7
18	7.25E+06	(58)	4.63E+06	(37)	8	361	119	59.6	38.9	92.7
19	1.12E+07	(224)	3.35E+06	(67)	20	262	64	126.0	94.8	167.5
20	1.07E+07	(107)	4.70E+06	(47)	10	367	107	86.4	60.9	124.5
21	8.15E+06	(212)	4.04E+06	(105)	26	316	62	76.6	59.7	98.4
22	7.75E+06	(93)	2.67E+06	(32)	12	208	73	109.9	73.2	169.8
23	1.12E+07	(303)	5.26E+06	(142)	27	411	70	81.0	65.1	100.8
24	1.37E+07	(137)	6.30E+06	(63)	10	492	124	82.6	60.9	113.2
25	9.15E+06	(183)	3.95E+06	(79)	20	309	70	87.7	66.5	115.8
26	1.44E+07	(287)	5.55E+06	(111)	20	434	83	97.9	77.3	124.0
27	1.41E+07	(113)	4.13E+06	(33)	8	322	112	129.3	87.5	196.7
28	1.17E+07	(164)	3.93E+06	(55)	14	307	83	112.9	82.9	156.2
29	9.92E+06	(119)	4.83E+06	(58)	12	378	99	77.9	56.6	108.7
30	1.76E+07	(281)	6.25E+06	(100)	16	488	99	106.3	83.3	135.7
31	1.33E+07	(53)	4.25E+06	(17)	4	332	159	117.5	67.6	216.4
32	7.88E+06	(63)	2.25E+06	(18)	8	176	82	131.7	77.8	236.2
33	9.00E+06	(63)	3.43E+06	(24)	7	268	109	99.3	61.5	166.2
34	7.60E+06	(114)	3.93E+06	(59)	15	307	80	73.4	53.2	102.4
35	1.74E+07	(139)	3.50E+06	(28)	8	273	103	186.4	124.5	290.0
36	7.22E+06	(65)	3.78E+06	(34)	9	295	101	72.6	47.4	113.4
37	1.50E+07	(90)	6.00E+06	(36)	6	469	156	94.7	63.9	143.6
38	1.11E+07	(100)	4.00E+06	(36)	9	312	104	105.1	71.5	158.5
39	1.04E+07	(415)	3.50E+06	(140)	40	273	47	112.2	90.8	138.5
40	1.36E+07	(122)	4.00E+06	(36)	9	312	104	128.0	88.1	191.1
41	1.70E+07	(153)	8.22E+06	(74)	9	642	150	78.4	58.6	104.8
42	9.28E+06	(167)	2.11E+06	(38)	18	165	53	165.5	116.4	241.7
43	1.30E+07	(104)	8.63E+06	(69)	8	674	163	57.4	41.9	79.0
44	7.75E+06	(93)	2.75E+06	(33)	12	215	75	106.6	71.3	163.8
45	1.21E+07	(242)	4.15E+06	(83)	20	324	72	110.2	84.7	143.4
46	7.83E+06	(141)	3.33E+06	(60)	18	260	67	89.2	65.6	122.8
47	1.60E+07	(192)	6.67E+06	(80)	12	521	117	90.9	69.0	119.6
48	8.38E+06	(67)	3.00E+06	(24)	8	234	95	105.5	65.7	175.9
49	7.85E+06	(157)	3.60E+06	(72)	20	281	67	82.6	61.7	110.6
50	6.17E+06	(185)	1.60E+06	(48)	30	125	36	145.5	105.8	204.2
51	1.28E+07	(154)	7.50E+06	(90)	12	586	125	65.0	49.4	85.5
52	1.74E+07	(244)	4.36E+06	(61)	14	340	87	151.0	114.0	203.3

53	1.38E+07	(55)	7.50E+06	(30)	4	586	213	69.6	44.0	112.6
54	9.63E+06	(154)	5.19E+06	(83)	16	405	90	70.4	53.2	93.2
55	8.31E+06	(349)	4.10E+06	(172)	42	320	50	77.1	62.9	94.5
56	4.25E+06	(34)	1.75E+06	(14)	8	137	72	91.7	48.4	185.0
57	1.34E+07	(161)	5.08E+06	(61)	12	397	102	100.1	74.2	136.7
58	1.05E+07	(84)	4.38E+06	(35)	8	342	115	91.0	60.9	139.1
59	8.37E+06	(201)	2.83E+06	(68)	24	221	54	111.6	83.7	148.7
60	1.16E+07	(104)	2.44E+06	(22)	9	191	81	177.4	112.3	294.6
61	5.67E+06	(68)	3.00E+06	(36)	12	234	78	71.7	47.4	110.7
62	9.00E+06	(81)	5.11E+06	(46)	9	399	118	66.9	46.1	98.4
63	8.00E+06	(48)	4.17E+06	(25)	6	326	129	72.8	44.2	123.3
64	9.83E+06	(59)	5.17E+06	(31)	6	404	144	72.3	46.2	115.5
65	1.25E+07	(337)	5.52E+06	(149)	27	431	72	85.8	69.4	106.2
66	9.67E+06	(87)	5.22E+06	(47)	9	408	119	70.4	48.9	102.6
67	8.08E+06	(97)	4.00E+06	(48)	12	312	90	76.8	53.9	110.9
68	1.50E+07	(60)	4.75E+06	(19)	4	371	168	119.1	70.7	211.2
69	9.25E+06	(74)	4.00E+06	(32)	8	313	110	87.7	57.4	137.2
70	1.51E+07	(121)	3.50E+06	(28)	8	273	103	162.6	107.9	254.4
71	1.06E+07	(190)	3.89E+06	(70)	18	304	73	102.6	77.0	136.6
72	4.94E+06	(79)	3.56E+06	(57)	16	278	74	52.8	37.1	75.6
73	1.03E+07	(82)	4.00E+06	(32)	8	313	110	97.0	64.1	151.0
74	1.54E+07	(123)	3.88E+06	(31)	8	303	108	149.5	100.8	229.2
75	1.25E+07	(200)	6.81E+06	(109)	16	532	103	69.7	54.3	89.5
76	7.55E+06	(151)	1.60E+06	(32)	20	125	44	177.4	121.4	268.1
77	1.57E+07	(141)	5.44E+06	(49)	9	425	122	109.0	78.4	154.1
78	1.32E+07	(316)	4.12E+06	(99)	24	322	65	120.6	94.7	153.5
79	1.28E+07	(77)	7.17E+06	(43)	6	560	171	68.1	46.4	101.3
80	9.58E+06	(115)	2.67E+06	(32)	12	208	73	135.6	91.5	207.3
81	1.25E+07	(188)	4.27E+06	(64)	15	333	84	111.3	83.5	150.2
82	1.01E+07	(101)	3.30E+06	(33)	10	258	89	115.7	77.8	177.0
83	7.83E+06	(47)	6.33E+06	(38)	6	495	160	47.1	30.1	74.3
84	8.60E+06	(258)	3.47E+06	(104)	30	271	54	94.0	73.6	119.9
85	1.06E+07	(85)	3.63E+06	(29)	8	283	105	110.8	72.3	175.2
86	1.08E+07	(216)	4.10E+06	(82)	20	320	71	99.7	76.2	130.3
87	1.45E+07	(58)	4.25E+06	(17)	4	332	159	128.4	74.5	235.1
88	8.00E+06	(144)	3.61E+06	(65)	18	282	70	84.1	62.4	114.6
89	1.18E+07	(189)	6.06E+06	(97)	16	474	97	74.0	57.0	95.9
90	1.01E+07	(202)	4.05E+06	(81)	20	316	71	94.4	71.9	123.8
91	1.10E+07	(88)	5.50E+06	(44)	8	430	130	76.0	52.4	111.8
92	1.00E+07	(70)	7.29E+06	(51)	7	569	160	52.3	36.0	76.6
93	1.75E+07	(105)	5.83E+06	(35)	6	456	154	113.5	77.1	171.4
94	1.61E+07	(129)	8.38E+06	(67)	8	654	161	73.2	54.1	99.9
95	1.74E+07	(139)	8.50E+06	(68)	8	664	162	77.7	57.8	105.5
96	9.58E+06	(115)	6.42E+06	(77)	12	501	115	56.9	42.3	77.0
97	1.80E+07	(108)	4.83E+06	(29)	6	378	140	140.4	93.1	219.3
98	2.00E+07	(140)	6.86E+06	(48)	7	536	155	110.4	79.3	156.7
99	9.17E+06	(55)	3.00E+06	(18)	6	234	109	115.2	67.2	208.4
100	1.28E+07	(77)	9.67E+06	(58)	6	755	199	50.6	35.5	72.4
101	8.00E+06	(64)	4.13E+06	(33)	8	322	112	73.6	47.8	115.8
102	1.46E+07	(73)	3.20E+06	(16)	5	250	123	171.0	99.8	314.0

KLD40 (Yukon), modern sand, TU11z (counted by Sarah Falkowski, May 2014)

EFFECTIVE TRACK DENSITY FOR FLUENCE MONITOR (tracks/cm^2): 6.390E+05

RELATIVE ERROR (%): 1.57

EFFECTIVE URANIUM CONTENT OF MONITOR (ppm): 50.00

ZETA FACTOR AND STANDARD ERROR (yr cm^2): 119.60 5.40

SIZE OF COUNTER SQUARE (cm^2): 1.000E-06

------ GRAIN AGES IN ORIGINAL ORDER ------

Grain no.	**RhoS (cm^-2)**	**(Ns)**	**RhoI (cm^-2)**	**(Ni)**	**Squares**	**U+/-2s**		**Grain Age**	**Age (Ma) --95% CI--**	
1	2.00E+06	(12)	2.00E+06	(12)	6	156	89	38.1	15.7	92.4
2	2.20E+06	(11)	7.80E+06	(39)	5	610	195	10.9	5.0	21.4
3	9.67E+06	(58)	3.50E+06	(21)	6	274	118	104.2	62.7	180.7
4	1.31E+07	(118)	6.89E+06	(62)	9	539	137	72.2	52.7	100.0
5	9.70E+06	(97)	2.00E+06	(20)	10	156	69	181.6	112.6	309.5
6	6.67E+05	(12)	4.22E+06	(76)	18	330	76	6.1	3.0	11.2
7	2.00E+07	(120)	5.33E+06	(32)	6	417	147	141.2	95.5	215.4
8	1.43E+07	(129)	7.78E+06	(70)	9	609	146	70.0	51.9	95.1
9	1.50E+07	(180)	5.33E+06	(64)	12	417	105	106.4	79.7	143.9
10	1.18E+07	(94)	2.25E+06	(18)	8	176	82	195.1	118.4	342.3
11	1.06E+07	(159)	4.07E+06	(61)	15	318	82	98.7	73.2	134.9
12	1.11E+07	(133)	4.75E+06	(57)	12	372	99	88.4	64.5	122.9
13	1.71E+06	(12)	1.09E+07	(76)	7	850	196	6.1	3.0	11.2
14	1.60E+06	(16)	8.90E+06	(89)	10	696	149	6.9	3.8	11.8
15	1.22E+06	(11)	1.78E+06	(16)	9	139	69	26.3	11.0	60.0
16	4.00E+06	(32)	2.39E+07	(191)	8	1868	276	6.4	4.3	9.4
17	8.57E+05	(6)	7.00E+06	(49)	7	548	157	4.8	1.6	10.9
18	8.89E+05	(8)	3.22E+06	(29)	9	252	93	10.7	4.2	23.6
19	2.06E+06	(33)	8.19E+06	(131)	16	641	114	9.7	6.4	14.2
20	7.50E+05	(6)	6.25E+06	(50)	8	489	138	4.7	1.6	10.7
21	9.17E+06	(55)	5.83E+06	(35)	6	456	154	59.7	38.4	94.0
22	1.07E+07	(64)	5.33E+06	(32)	6	417	147	75.8	49.0	119.8
23	2.71E+06	(19)	1.14E+07	(80)	7	894	201	9.1	5.2	15.1
24	5.88E+06	(94)	1.81E+06	(29)	16	142	52	122.2	80.3	192.2
25	5.00E+05	(5)	2.90E+06	(29)	10	227	84	6.8	2.0	17.2
26	9.33E+05	(14)	2.40E+06	(36)	15	188	62	15.0	7.4	28.2
27	4.67E+06	(56)	2.73E+07	(327)	12	2132	245	6.6	4.8	8.7
28	1.13E+06	(45)	4.15E+06	(166)	40	325	51	10.4	7.3	14.5
29	1.50E+06	(18)	1.05E+07	(126)	12	822	148	5.5	3.1	9.0
30	1.04E+06	(29)	6.32E+06	(177)	28	495	76	6.3	4.1	9.3
31	9.75E+05	(39)	5.00E+06	(200)	40	391	57	7.5	5.1	10.6
32	1.33E+06	(12)	7.00E+06	(63)	9	548	139	7.4	3.6	13.6
33	1.72E+06	(31)	7.61E+06	(137)	18	596	103	8.7	5.6	12.9
34	2.38E+07	(95)	5.50E+06	(22)	4	430	182	162.0	102.0	270.2
35	1.17E+06	(21)	5.94E+06	(107)	18	465	91	7.5	4.5	12.1
36	1.58E+07	(95)	7.33E+06	(44)	6	574	173	81.8	56.8	119.8
37	3.56E+06	(32)	3.78E+06	(34)	9	296	101	35.9	21.4	59.9
38	5.71E+06	(40)	3.71E+06	(26)	7	291	113	58.4	34.9	99.7
39	6.69E+06	(87)	3.77E+06	(49)	13	295	84	67.4	47.0	97.8
40	1.10E+07	(165)	4.27E+06	(64)	15	334	84	97.6	72.9	132.5
41	4.56E+06	(73)	2.38E+07	(380)	16	1858	199	7.4	5.7	9.6
42	1.33E+06	(20)	1.03E+07	(155)	15	809	132	5.0	2.9	7.9
43	1.23E+07	(98)	6.63E+06	(53)	8	518	143	70.2	49.8	100.0
44	1.02E+07	(306)	3.80E+06	(114)	30	297	56	101.5	80.4	128.0
45	1.43E+07	(200)	6.36E+06	(89)	14	497	106	85.0	65.3	110.8
46	1.10E+07	(88)	2.50E+06	(20)	8	196	87	165.0	101.7	282.6
47	7.50E+05	(6)	3.25E+06	(26)	8	254	99	9.0	3.0	21.9
48	8.78E+06	(79)	2.33E+06	(21)	9	183	79	141.4	87.2	240.7
49	6.88E+06	(55)	4.50E+06	(36)	8	352	117	58.0	37.5	91.0
50	1.36E+06	(57)	5.05E+06	(212)	42	395	56	10.3	7.5	13.8
51	1.75E+06	(14)	1.00E+07	(80)	8	782	176	6.7	3.5	11.9
52	1.83E+06	(44)	9.04E+06	(217)	24	707	98	7.8	5.5	10.8

53	1.28E+07	(269)	4.52E+06	(95)	21	354	73	106.9	83.3	137.2
54	2.00E+06	(18)	9.56E+06	(86)	9	748	162	8.1	4.5	13.4
55	2.10E+06	(21)	1.09E+07	(109)	10	853	165	7.4	4.4	11.8
56	1.10E+06	(11)	4.20E+06	(42)	10	329	101	10.1	4.6	19.8
57	7.14E+05	(10)	4.21E+06	(59)	14	330	86	6.6	3.0	12.8
58	2.20E+06	(44)	7.85E+06	(157)	20	614	100	10.7	7.5	15.1
59	1.13E+06	(18)	3.69E+06	(59)	16	289	75	11.7	6.5	20.0
60	1.44E+06	(13)	9.67E+06	(87)	9	756	163	5.8	2.9	10.3
61	4.67E+05	(7)	3.13E+06	(47)	15	245	72	5.8	2.2	12.7
62	1.12E+07	(67)	5.67E+06	(34)	6	443	152	74.7	48.9	116.5
63	5.00E+05	(5)	1.20E+06	(12)	10	94	53	16.2	4.4	48.4
64	7.38E+06	(332)	4.73E+06	(213)	45	370	52	59.2	48.7	72.0
65	1.38E+06	(11)	1.43E+07	(114)	8	1115	211	3.7	1.8	6.9
66	3.46E+05	(9)	1.88E+06	(49)	26	147	42	7.1	3.0	14.4
67	1.81E+07	(145)	5.00E+06	(40)	8	391	124	136.7	96.2	199.0
68	7.78E+05	(14)	3.83E+06	(69)	18	300	73	7.8	4.0	13.9
69	1.25E+06	(10)	6.13E+06	(49)	8	479	137	7.9	3.5	15.6
70	1.52E+07	(91)	3.00E+06	(18)	6	235	109	189.0	114.5	332.1
71	1.08E+07	(301)	2.82E+06	(79)	28	221	50	143.3	110.3	186.0
72	9.47E+05	(18)	5.84E+06	(111)	19	457	88	6.2	3.5	10.3
73	1.11E+07	(89)	6.13E+06	(49)	8	479	137	68.9	48.2	99.8
74	1.38E+07	(165)	5.75E+06	(69)	12	450	109	90.6	68.1	121.9
75	2.88E+06	(46)	1.81E+06	(29)	16	142	52	60.2	37.1	99.4
76	1.11E+07	(311)	3.07E+06	(86)	28	240	52	136.2	105.7	175.3
77	5.83E+05	(7)	2.67E+06	(32)	12	209	73	8.5	3.1	19.3
78	4.70E+06	(127)	2.29E+07	(619)	27	1794	155	7.9	6.4	9.7
79	1.55E+06	(31)	5.65E+06	(113)	20	442	84	10.5	6.8	15.7
80	5.33E+05	(8)	2.40E+06	(36)	15	188	62	8.6	3.4	18.6
81	3.06E+06	(55)	2.78E+07	(500)	18	2174	206	4.2	3.2	5.7
82	1.17E+07	(350)	5.17E+06	(155)	30	404	66	85.6	69.4	105.5
83	6.67E+05	(8)	6.08E+06	(73)	12	476	112	4.3	1.7	8.7
84	8.67E+05	(13)	5.20E+06	(78)	15	407	93	6.4	3.2	11.5
85	9.00E+06	(63)	4.57E+06	(32)	7	358	126	74.6	48.2	118.1
86	1.45E+07	(87)	8.00E+06	(48)	6	626	181	68.8	47.9	100.1
87	1.33E+06	(36)	4.04E+06	(109)	27	316	61	12.6	8.4	18.6
88	1.85E+06	(37)	5.75E+06	(115)	20	450	85	12.3	8.2	18.0
89	1.50E+06	(9)	9.83E+06	(59)	6	769	201	5.9	2.5	11.8
90	1.00E+06	(8)	3.38E+06	(27)	8	264	101	11.5	4.4	25.6
91	1.70E+06	(68)	5.75E+06	(230)	40	450	61	11.3	8.5	15.1
92	2.00E+06	(12)	5.33E+06	(32)	6	417	147	14.4	6.7	28.5
93	1.10E+06	(11)	7.60E+06	(76)	10	595	137	5.6	2.6	10.5
94	5.56E+05	(5)	2.44E+06	(22)	9	191	81	8.9	2.6	23.5
95	6.67E+05	(8)	1.50E+06	(18)	12	117	55	17.2	6.4	41.0
96	1.21E+06	(29)	9.13E+06	(219)	24	714	99	5.1	3.3	7.5
97	1.30E+06	(13)	3.10E+06	(31)	10	243	87	16.1	7.7	31.5
98	2.00E+06	(18)	7.89E+06	(71)	9	617	147	9.7	5.4	16.4
99	8.89E+05	(8)	5.33E+06	(48)	9	417	121	6.5	2.6	13.6
100	1.09E+06	(12)	3.27E+06	(36)	11	256	85	12.8	6.0	25.0
101	3.68E+05	(7)	2.32E+06	(44)	19	181	55	6.2	2.3	13.6
102	2.79E+06	(78)	1.83E+07	(513)	28	1434	134	5.8	4.5	7.5
103	1.75E+06	(35)	7.60E+06	(152)	20	595	98	8.8	5.9	12.8
104	1.67E+06	(15)	8.00E+06	(72)	9	626	148	8.0	4.2	14.0
105	6.00E+05	(12)	3.80E+06	(76)	20	297	69	6.1	3.0	11.2

KLD65 (Yukon), modern sand, TU11z (counted by Sarah Falkowski, May 2014)

EFFECTIVE TRACK DENSITY FOR FLUENCE MONITOR (tracks/cm^2): 6.380E+05

RELATIVE ERROR (%): 1.57

EFFECTIVE URANIUM CONTENT OF MONITOR (ppm): 50.00

ZETA FACTOR AND STANDARD ERROR (yr cm^2): 119.60 5.40

SIZE OF COUNTER SQUARE (cm^2): 1.000E-06

------ GRAIN AGES IN ORIGINAL ORDER ------

Grain no.	**RhoS (cm^-2)**	**(Ns)**	**RhoI (cm^-2)**	**(Ni)**	**Squares**	**U**	**+/-2s**	**Grain Age**	**Age (Ma) --95%**	**CI--**
1	2.00E+07	(120)	6.00E+06	(36)	6	470	156	125.5	86.3	187.6
2	1.13E+07	(45)	1.10E+07	(44)	4	862	260	38.9	25.1	60.3
3	8.10E+06	(81)	3.40E+06	(34)	10	266	91	90.0	59.8	138.6
4	2.25E+07	(90)	6.25E+06	(25)	4	490	195	135.3	86.7	219.8
5	1.14E+07	(57)	6.00E+06	(30)	5	470	171	71.9	45.6	115.9
6	9.29E+06	(65)	6.57E+06	(46)	7	515	152	53.6	36.2	80.1
7	1.78E+07	(71)	1.23E+07	(49)	4	960	275	55.0	37.7	80.9
8	1.87E+07	(112)	1.15E+07	(69)	6	901	218	61.6	45.2	84.4
9	2.30E+07	(138)	1.17E+07	(70)	6	914	220	74.7	55.7	101.2
10	1.35E+07	(108)	5.38E+06	(43)	8	421	128	94.9	66.3	138.5
11	7.00E+06	(28)	2.50E+06	(10)	4	196	121	104.9	50.1	242.1
12	1.31E+07	(157)	4.58E+06	(55)	12	359	97	107.8	79.0	149.4
13	1.98E+07	(79)	1.13E+07	(45)	4	882	263	66.5	45.7	98.2
14	1.25E+07	(276)	3.64E+06	(80)	22	285	64	129.7	99.7	168.6
15	2.05E+07	(123)	6.50E+06	(39)	6	509	163	118.9	82.7	175.1
16	2.40E+07	(96)	5.75E+06	(23)	4	451	186	156.5	99.3	258.2
17	1.07E+07	(193)	3.17E+06	(57)	18	248	66	127.7	94.8	174.7
18	1.08E+07	(129)	5.00E+06	(60)	12	392	102	81.4	59.6	112.6
19	1.55E+07	(62)	9.75E+06	(39)	4	764	244	60.3	39.8	92.5
20	2.24E+07	(269)	7.67E+06	(92)	12	601	126	110.2	85.6	141.7
21	1.17E+07	(245)	2.52E+06	(53)	21	198	54	173.6	129.1	238.0
22	9.56E+06	(172)	3.56E+06	(64)	18	279	70	101.6	75.9	137.6
23	1.23E+07	(246)	5.95E+06	(119)	20	466	87	78.2	61.8	99.1
24	9.67E+06	(116)	3.25E+06	(39)	12	255	81	112.2	77.8	165.7
25	1.02E+07	(61)	3.67E+06	(22)	6	287	121	104.4	63.7	178.6
26	1.13E+07	(124)	3.82E+06	(42)	11	299	92	111.4	78.2	162.1
27	1.58E+07	(190)	5.42E+06	(65)	12	425	106	110.4	83.0	148.7
28	7.50E+06	(30)	4.00E+06	(16)	4	313	155	70.8	37.6	139.1
29	1.91E+07	(191)	4.00E+06	(40)	10	313	99	179.1	127.5	258.2
30	1.73E+07	(104)	7.50E+06	(45)	6	588	175	87.4	61.2	127.0
31	2.22E+07	(133)	7.50E+06	(45)	6	588	175	111.5	79.3	160.1
32	3.20E+07	(128)	9.75E+06	(39)	4	764	244	123.7	86.2	181.8
33	1.25E+07	(125)	2.50E+06	(25)	10	196	78	187.0	122.1	299.3
34	1.27E+07	(344)	5.37E+06	(145)	27	421	71	89.7	72.4	111.1
35	1.08E+07	(108)	3.90E+06	(39)	10	306	98	104.5	72.1	154.9
36	4.83E+06	(29)	3.33E+06	(20)	6	261	116	55.0	30.1	102.5
37	9.13E+06	(73)	4.25E+06	(34)	8	333	114	81.2	53.5	125.9
38	1.56E+07	(281)	4.44E+06	(80)	18	348	78	132.1	101.6	171.6
39	6.22E+06	(56)	1.22E+06	(11)	9	96	57	189.1	99.8	398.9
40	1.93E+07	(116)	7.50E+06	(45)	6	588	175	97.4	68.7	140.7
41	1.40E+07	(56)	1.05E+07	(42)	4	823	254	50.6	33.4	77.4
42	1.18E+07	(94)	3.13E+06	(25)	8	245	97	141.2	90.7	229.0
43	1.75E+07	(350)	6.55E+06	(131)	20	513	91	100.9	81.0	125.6
44	1.97E+07	(197)	1.02E+07	(102)	10	799	160	73.1	56.6	94.3
45	1.60E+07	(64)	8.50E+06	(34)	4	666	228	71.3	46.4	111.5
46	1.75E+07	(105)	1.20E+07	(72)	6	940	223	55.4	40.6	75.9
47	8.30E+06	(83)	2.00E+06	(20)	10	157	69	155.5	95.5	267.1
48	1.68E+07	(101)	3.00E+06	(18)	6	235	110	209.1	127.4	365.6
49	1.55E+07	(93)	6.33E+06	(38)	6	496	161	92.5	63.0	138.7
50	1.08E+07	(151)	3.64E+06	(51)	14	285	80	111.8	81.1	156.7
51	1.10E+07	(99)	8.67E+06	(78)	9	679	155	48.2	35.5	65.8
52	1.23E+07	(74)	5.17E+06	(31)	6	405	145	90.2	58.8	142.0

53	1.05E+07	(84)	3.50E+06	(28)	8	274	103	113.0	73.3	180.1
54	1.63E+07	(147)	3.44E+06	(31)	9	270	97	177.7	120.8	270.5
55	1.88E+07	(282)	6.27E+06	(94)	15	491	102	113.1	88.1	145.0
56	1.80E+07	(72)	7.75E+06	(31)	4	607	217	87.8	57.1	138.4
57	1.87E+07	(112)	7.50E+06	(45)	6	588	175	94.1	66.2	136.1
58	1.68E+07	(101)	6.17E+06	(37)	6	483	159	103.0	70.3	154.5
59	1.44E+07	(130)	6.44E+06	(58)	9	505	133	84.8	61.9	117.8
60	1.22E+07	(110)	6.56E+06	(59)	9	514	134	70.7	51.1	98.7
61	2.08E+07	(208)	7.80E+06	(78)	10	611	139	100.5	76.4	132.2
62	9.08E+06	(109)	1.83E+06	(22)	12	144	61	185.2	117.5	306.9
63	9.25E+06	(37)	5.00E+06	(20)	4	392	174	69.9	39.8	127.2
64	1.81E+07	(145)	9.00E+06	(72)	8	705	167	76.3	57.2	102.8
65	1.47E+07	(88)	1.00E+07	(60)	6	784	203	55.7	39.7	78.7
66	1.23E+07	(147)	5.08E+06	(61)	12	398	102	91.2	67.3	125.0
67	5.58E+06	(67)	2.17E+06	(26)	12	170	66	97.2	61.3	159.3
68	1.45E+07	(87)	1.02E+07	(61)	6	797	205	54.1	38.6	76.4
69	1.73E+07	(173)	4.40E+06	(44)	10	345	104	147.9	106.2	210.7
70	9.14E+06	(64)	2.14E+06	(15)	7	168	85	159.5	91.0	300.8
71	8.00E+06	(48)	2.50E+06	(15)	6	196	100	120.1	66.8	230.8
72	8.60E+06	(86)	2.10E+06	(21)	10	165	71	153.5	95.3	260.1
73	1.27E+07	(76)	4.67E+06	(28)	6	366	137	102.4	65.9	164.0
74	5.88E+06	(47)	1.50E+06	(12)	8	118	67	146.3	77.5	302.5
75	3.50E+06	(14)	3.25E+06	(13)	4	255	139	40.9	17.9	94.3
76	1.58E+07	(95)	3.83E+06	(23)	6	300	124	154.9	98.2	255.6
77	1.30E+07	(78)	5.17E+06	(31)	6	405	145	95.0	62.2	149.1
78	1.50E+07	(90)	2.83E+06	(17)	6	222	106	197.4	118.2	352.5
79	1.47E+07	(176)	6.50E+06	(78)	12	509	116	85.2	64.4	112.7
80	1.42E+07	(170)	4.42E+06	(53)	12	346	95	121.0	88.7	168.0
81	1.08E+07	(65)	5.00E+06	(30)	6	392	142	81.9	52.6	130.8
82	6.00E+06	(36)	4.33E+06	(26)	6	340	132	52.5	30.9	90.6
83	8.75E+06	(35)	3.00E+06	(12)	4	235	133	109.4	56.1	231.4
84	1.53E+07	(214)	5.14E+06	(72)	14	403	96	111.9	84.6	148.0
85	1.23E+07	(123)	2.80E+06	(28)	10	219	82	164.7	109.4	257.6
86	3.00E+07	(120)	9.00E+06	(36)	4	705	235	125.5	86.3	187.6
87	1.80E+07	(180)	9.20E+06	(92)	10	721	152	74.0	56.7	96.6
88	1.87E+07	(168)	6.22E+06	(56)	9	488	131	113.2	83.4	156.1
89	1.85E+07	(111)	1.17E+07	(70)	6	914	220	60.2	44.2	82.4
90	1.24E+07	(62)	5.40E+06	(27)	5	423	162	86.7	54.6	141.8
91	1.72E+07	(309)	7.50E+06	(135)	18	588	103	86.6	69.4	108.0
92	1.04E+07	(125)	4.58E+06	(55)	12	359	97	86.0	62.3	120.4
93	1.43E+07	(228)	6.56E+06	(105)	16	514	101	82.1	64.1	105.1
94	1.05E+07	(84)	2.88E+06	(23)	8	225	93	137.2	86.3	227.8
95	1.43E+07	(228)	4.63E+06	(74)	16	362	85	116.0	88.0	152.7
96	9.50E+06	(38)	4.75E+06	(19)	4	372	169	75.5	42.7	138.8
97	1.50E+07	(150)	7.20E+06	(72)	10	564	134	78.9	59.2	106.1
98	1.59E+07	(318)	7.25E+06	(145)	20	568	96	83.0	66.9	103.0
99	1.35E+07	(108)	6.38E+06	(51)	8	500	140	80.2	57.1	114.2
100	2.23E+07	(134)	8.17E+06	(49)	6	640	183	103.3	74.2	146.4
101	1.60E+07	(64)	7.75E+06	(31)	4	607	217	78.1	50.3	124.1
102	1.14E+07	(114)	5.30E+06	(53)	10	415	114	81.4	58.4	115.1
103	1.20E+07	(192)	3.19E+06	(51)	16	250	70	141.7	104.0	196.9
104	1.53E+07	(153)	6.30E+06	(63)	10	494	125	91.9	68.2	125.3

KLD66 (Yukon), modern sand, TU11z (counted by Sarah Falkowski, May 2014)

EFFECTIVE TRACK DENSITY FOR FLUENCE MONITOR (tracks/cm^2): 6.380E+05
RELATIVE ERROR (%): 1.57
EFFECTIVE URANIUM CONTENT OF MONITOR (ppm): 50.00
ZETA FACTOR AND STANDARD ERROR (yr cm^2): 119.60 5.40
SIZE OF COUNTER SQUARE (cm^2): 1.000E-06

------ GRAIN AGES IN ORIGINAL ORDER ------

Grain no.	**RhoS (cm^-2)**	**(Ns)**	**RhoI (cm^-2)**	**(Ni)**	**Squares**	**U+/-2s**		**Grain Age**	**Age (Ma) --95% CI--**	
1	8.13E+06	(65)	1.50E+06	(12)	8	118	67	201.2	109.6	407.6
2	1.27E+07	(76)	6.33E+06	(38)	6	496	161	75.7	50.8	114.9
3	1.44E+07	(130)	7.11E+06	(64)	9	557	140	76.9	56.7	105.6
4	1.50E+06	(9)	1.00E+06	(6)	6	78	62	56.5	18.2	192.6
5	9.90E+06	(99)	6.50E+06	(65)	10	509	127	57.8	41.9	80.4
6	1.73E+07	(69)	8.50E+06	(34)	4	666	228	76.8	50.4	119.5
7	5.17E+06	(93)	2.72E+06	(49)	18	213	61	71.9	50.4	103.9
8	1.40E+07	(84)	6.67E+06	(40)	6	522	165	79.5	54.1	118.9
9	1.15E+07	(92)	4.75E+06	(38)	8	372	121	91.5	62.3	137.3
10	4.20E+06	(63)	9.33E+05	(14)	15	73	38	167.9	94.4	323.8
11	7.31E+06	(95)	3.08E+06	(40)	13	241	76	89.8	61.6	133.4
12	4.50E+06	(72)	1.69E+06	(27)	16	132	51	100.6	64.2	162.9
13	5.63E+06	(180)	1.84E+06	(59)	32	144	38	115.2	85.6	157.3
14	7.33E+06	(88)	1.42E+06	(17)	12	111	53	193.1	115.4	345.1
15	1.19E+07	(95)	2.75E+06	(22)	8	216	91	161.8	101.8	269.8
16	3.33E+06	(20)	1.67E+06	(10)	6	131	81	75.3	34.0	180.1
17	1.10E+07	(264)	3.21E+06	(77)	24	251	58	128.9	98.6	168.3
18	1.19E+07	(95)	3.50E+06	(28)	8	274	103	127.6	83.5	202.0
19	7.59E+06	(205)	2.56E+06	(69)	27	200	48	111.8	84.1	148.7
20	1.82E+07	(91)	1.20E+07	(60)	5	940	244	57.6	41.1	81.2
21	6.50E+06	(156)	2.29E+06	(55)	24	180	49	107.1	78.5	148.5
22	5.14E+06	(36)	2.57E+06	(18)	7	202	94	75.5	42.0	141.3
23	5.40E+06	(54)	2.70E+06	(27)	10	212	81	75.6	47.0	124.9
24	1.35E+07	(81)	4.50E+06	(27)	6	353	135	113.0	72.7	181.7
25	3.86E+06	(27)	1.57E+06	(11)	7	123	73	92.2	44.8	206.0
26	1.22E+07	(73)	6.33E+06	(38)	6	496	161	72.7	48.6	110.7
27	3.62E+06	(76)	1.90E+06	(40)	21	149	47	72.0	48.6	108.4
28	1.33E+07	(80)	5.67E+06	(34)	6	444	152	88.9	59.1	137.0
29	2.58E+06	(31)	5.00E+05	(6)	12	39	31	190.1	80.5	553.8
30	5.19E+06	(83)	3.56E+06	(57)	16	279	74	55.3	39.0	78.9
31	8.50E+06	(51)	3.67E+06	(22)	6	287	121	87.5	52.4	151.5
32	1.26E+07	(101)	6.13E+06	(49)	8	480	137	78.0	55.1	112.2
33	1.07E+07	(107)	4.20E+06	(42)	10	329	102	96.3	67.0	141.1
34	1.24E+07	(336)	3.52E+06	(95)	27	276	57	133.0	104.3	169.6
35	5.00E+06	(30)	3.83E+06	(23)	6	300	124	49.5	27.9	89.2
36	5.00E+06	(40)	1.63E+06	(13)	8	127	69	115.4	61.2	235.1
37	7.43E+06	(104)	2.57E+06	(36)	14	202	67	109.0	74.3	163.9
38	1.13E+07	(45)	5.50E+06	(22)	4	431	182	77.3	45.7	135.2
39	7.88E+06	(315)	2.55E+06	(102)	40	200	40	116.4	91.6	147.8
40	1.09E+07	(76)	3.57E+06	(25)	7	280	111	114.5	72.5	187.7
41	8.44E+06	(76)	2.11E+06	(19)	9	165	75	149.9	90.6	262.1
42	8.90E+06	(89)	5.20E+06	(52)	10	408	113	64.9	45.6	93.3
43	2.13E+06	(17)	8.75E+05	(7)	8	69	50	90.8	36.4	259.2
44	5.31E+06	(85)	1.50E+06	(24)	16	118	48	133.1	84.4	218.8
45	6.50E+06	(52)	2.38E+06	(19)	8	186	85	103.0	60.4	184.5
46	7.50E+06	(60)	5.25E+06	(42)	8	411	127	54.2	36.0	82.5
47	7.17E+06	(43)	2.00E+06	(12)	6	157	89	134.0	70.4	278.9
48	1.25E+07	(150)	5.58E+06	(67)	12	438	107	84.7	63.2	114.9
49	1.78E+07	(71)	6.00E+06	(24)	4	470	191	111.4	69.7	185.1
50	6.75E+06	(81)	2.50E+06	(30)	12	196	71	101.9	66.6	160.5
51	8.67E+06	(78)	2.11E+06	(19)	9	165	75	153.8	93.1	268.6
52	1.05E+07	(209)	3.85E+06	(77)	20	302	69	102.3	77.7	134.6

53	1.48E+07 (89)	7.33E+06 (44)	6	575	173	76.6	52.9	112.6
54	3.89E+06 (35)	1.67E+06 (15)	9	131	66	87.9	47.2	173.3
55	1.18E+07 (296)	4.36E+06 (109)	25	342	66	102.5	80.9	129.8
56	5.00E+06 (20)	7.50E+05 (3)	4	59	63	239.0	75.0	1215.1
57	9.19E+06 (239)	2.81E+06 (73)	26	220	52	123.1	93.5	162.0
58	7.00E+06 (28)	3.50E+06 (14)	4	274	144	75.4	38.7	155.1
59	1.28E+07 (102)	3.75E+06 (30)	8	294	107	127.9	84.9	199.1
60	9.17E+06 (55)	4.17E+06 (25)	6	327	130	83.1	51.2	139.2
61	4.00E+06 (16)	1.50E+06 (6)	4	118	92	99.3	37.7	310.1
62	1.04E+07 (83)	5.13E+06 (41)	8	402	125	76.6	52.2	114.3
63	7.00E+06 (70)	3.90E+06 (39)	10	306	98	68.0	45.4	103.4
64	1.43E+07 (286)	6.45E+06 (129)	20	505	90	83.9	66.9	105.1
65	5.15E+06 (103)	1.90E+06 (38)	20	149	48	102.3	70.2	152.6
66	7.50E+06 (45)	4.33E+06 (26)	6	340	132	65.5	39.7	110.7
67	1.26E+07 (113)	3.44E+06 (31)	9	270	97	137.1	92.0	211.0
68	8.75E+06 (35)	1.00E+06 (4)	4	78	74	314.6	118.2	1179.0
69	2.10E+07 (126)	7.33E+06 (44)	6	575	173	108.1	76.4	156.0
70	1.29E+07 (129)	4.50E+06 (45)	10	353	105	108.2	76.8	155.5
71	6.28E+06 (113)	2.89E+06 (52)	18	226	63	82.2	58.8	116.6
72	9.63E+06 (77)	4.50E+06 (36)	8	353	117	80.9	54.0	123.8
73	1.58E+07 (285)	6.00E+06 (108)	18	470	91	99.6	78.5	126.4
74	7.87E+06 (118)	2.33E+06 (35)	15	183	62	127.0	86.8	190.8
75	7.50E+06 (45)	1.33E+06 (8)	6	104	72	207.7	99.3	507.0
76	8.56E+06 (77)	2.89E+06 (26)	9	226	88	111.6	71.1	181.3
77	1.03E+07 (41)	2.75E+06 (11)	4	216	127	139.2	71.3	299.9
78	3.50E+06 (21)	2.33E+06 (14)	6	183	96	56.8	27.7	120.6
79	6.86E+06 (192)	1.68E+06 (47)	28	132	38	153.6	111.6	215.9
80	5.20E+06 (52)	7.00E+05 (7)	10	55	40	272.0	126.9	700.6
81	5.25E+06 (63)	1.58E+06 (19)	12	124	56	124.5	74.2	220.2
82	1.88E+07 (75)	4.75E+06 (19)	4	372	169	147.9	89.4	258.9
83	8.22E+06 (148)	3.17E+06 (57)	18	248	66	98.1	72.0	135.7
84	1.29E+07 (90)	6.14E+06 (43)	7	481	147	79.2	54.6	116.8
85	7.39E+06 (133)	2.06E+06 (37)	18	161	53	135.3	93.8	200.3
86	1.38E+07 (124)	3.33E+06 (30)	9	261	95	155.2	104.1	239.3
87	5.33E+06 (32)	2.17E+06 (13)	6	170	93	92.6	47.7	192.2
88	1.35E+07 (54)	3.75E+06 (15)	4	294	150	134.9	75.9	257.1
89	7.94E+06 (127)	2.00E+06 (32)	16	157	55	149.1	101.1	226.9
90	5.05E+06 (101)	1.95E+06 (39)	20	153	49	97.8	67.2	145.4
91	7.05E+06 (141)	3.05E+06 (61)	20	239	61	87.5	64.4	120.2
92	2.32E+07 (139)	7.17E+06 (43)	6	562	171	121.9	86.3	175.8
93	8.67E+06 (78)	3.00E+06 (27)	9	235	90	108.9	69.9	175.5
94	8.05E+06 (161)	2.45E+06 (49)	20	192	55	123.9	89.8	174.2
95	6.25E+06 (25)	3.75E+06 (15)	4	294	150	63.0	32.1	128.6
96	8.00E+06 (32)	2.00E+06 (8)	4	157	108	148.6	68.5	372.6
97	1.29E+07 (103)	2.13E+06 (17)	8	167	80	225.3	136.0	399.8
98	1.11E+07 (89)	4.25E+06 (34)	8	333	114	98.8	66.1	151.4
99	9.00E+06 (63)	3.71E+06 (26)	7	291	113	91.5	57.4	150.5
100	1.80E+07 (72)	4.00E+06 (16)	4	313	155	168.1	98.0	309.0
101	4.38E+06 (35)	1.63E+06 (13)	8	127	69	101.1	52.8	208.3
102	1.03E+07 (41)	1.25E+06 (5)	4	98	84	297.3	122.5	942.5
103	1.20E+07 (108)	2.89E+06 (26)	9	226	88	155.8	101.6	248.9

KLD67 (Yukon), modern sand, TU11z (counted by Sarah Falkowski, May 2014)

EFFECTIVE TRACK DENSITY FOR FLUENCE MONITOR (tracks/cm^2): 6.360E+05

RELATIVE ERROR (%): 1.57

EFFECTIVE URANIUM CONTENT OF MONITOR (ppm): 50.00

ZETA FACTOR AND STANDARD ERROR (yr cm^2): 119.60 5.40

SIZE OF COUNTER SQUARE (cm^2): 1.000E-06

------ GRAIN AGES IN ORIGINAL ORDER ------

Grain no.	RhoS (cm^-2)	(Ns)	RhoI (cm^-2)	(Ni)	Squares	U	+/-2s	Grain Age	Age (Ma) --95% CI--	
1	1.30E+07	(78)	3.33E+06	(20)	6	262	116	145.8	89.1	251.3
2	1.44E+07	(130)	4.89E+06	(44)	9	384	116	111.1	78.7	160.2
3	2.02E+07	(101)	7.20E+06	(36)	5	566	188	105.5	71.8	159.0
4	1.61E+07	(129)	6.50E+06	(52)	8	511	142	93.5	67.4	131.7
5	1.12E+07	(279)	2.96E+06	(74)	25	233	54	141.1	107.8	184.7
6	1.87E+07	(262)	6.07E+06	(85)	14	477	104	115.7	89.3	149.9
7	6.42E+06	(77)	3.17E+06	(38)	12	249	81	76.4	51.3	116.0
8	1.96E+07	(176)	5.78E+06	(52)	9	454	126	127.2	93.2	176.8
9	9.38E+06	(75)	1.75E+06	(14)	8	138	72	198.7	113.1	379.4
10	1.55E+07	(124)	6.63E+06	(53)	8	521	143	88.2	63.6	124.2
11	2.53E+07	(101)	1.05E+07	(42)	4	825	255	90.6	62.8	133.2
12	1.48E+07	(89)	7.50E+06	(45)	6	590	176	74.7	51.7	109.4
13	1.16E+07	(418)	4.89E+06	(176)	36	384	59	89.6	73.5	109.1
14	1.35E+07	(81)	5.33E+06	(32)	6	419	148	95.3	62.8	148.3
15	2.10E+07	(84)	7.50E+06	(30)	4	590	214	105.3	69.0	165.5
16	1.24E+07	(348)	4.14E+06	(116)	28	326	61	112.8	89.8	141.6
17	1.99E+07	(159)	6.75E+06	(54)	8	531	145	110.8	81.1	153.9
18	1.05E+07	(84)	2.00E+06	(16)	8	157	78	195.1	114.9	355.6
19	1.39E+07	(292)	4.86E+06	(102)	21	382	76	107.6	84.5	137.0
20	8.30E+06	(83)	4.30E+06	(43)	10	338	103	72.9	49.9	108.0
21	1.93E+07	(135)	1.27E+07	(89)	7	1000	214	57.3	43.2	76.0
22	1.97E+07	(118)	1.03E+07	(62)	6	812	207	71.9	52.5	99.5
23	1.18E+07	(142)	4.33E+06	(52)	12	341	95	102.8	74.5	144.2
24	1.33E+07	(106)	3.88E+06	(31)	8	305	109	128.3	85.8	198.0
25	2.15E+07	(129)	7.83E+06	(47)	6	616	180	103.3	73.7	147.6
26	1.98E+07	(119)	1.07E+07	(64)	6	839	210	70.3	51.5	96.8
27	2.63E+07	(105)	1.10E+07	(44)	4	865	261	89.9	62.9	131.0
28	1.72E+07	(103)	9.00E+06	(54)	6	708	193	72.0	51.4	102.1
29	1.24E+07	(174)	3.36E+06	(47)	14	264	77	138.9	100.5	196.0
30	1.78E+07	(89)	6.80E+06	(34)	5	535	183	98.5	65.9	150.9
31	1.32E+07	(79)	6.33E+06	(38)	6	498	161	78.4	52.8	118.8
32	2.08E+07	(166)	5.00E+06	(40)	8	393	124	155.5	110.1	225.2
33	1.20E+07	(72)	9.33E+06	(56)	6	734	197	48.7	33.9	70.4
34	9.38E+06	(75)	4.50E+06	(36)	8	354	118	78.6	52.3	120.4
35	1.43E+07	(57)	2.75E+06	(11)	4	216	128	191.9	101.4	404.2
36	1.78E+07	(71)	8.50E+06	(34)	4	668	229	78.7	51.8	122.3
37	1.10E+07	(44)	5.75E+06	(23)	4	452	187	72.1	42.8	125.1
38	1.51E+07	(121)	4.38E+06	(35)	8	344	116	129.7	88.9	194.7
39	2.13E+07	(170)	8.38E+06	(67)	8	658	162	95.7	71.8	129.0
40	1.04E+07	(104)	5.40E+06	(54)	10	425	116	72.7	51.9	103.1
41	1.27E+07	(76)	3.33E+06	(20)	6	262	116	142.1	86.7	245.3
42	1.35E+07	(54)	1.20E+07	(48)	4	943	273	42.6	28.4	64.3
43	7.13E+06	(57)	1.50E+06	(12)	8	118	67	176.3	95.1	360.0
44	2.75E+07	(165)	7.67E+06	(46)	6	603	178	134.7	97.0	191.0
45	1.24E+07	(112)	8.67E+06	(78)	9	681	155	54.4	40.3	73.6
46	1.37E+07	(82)	5.50E+06	(33)	6	432	150	93.6	62.0	144.7
47	1.33E+07	(80)	5.33E+06	(32)	6	419	148	94.1	62.0	146.6
48	1.27E+07	(76)	3.83E+06	(23)	6	301	125	123.9	77.4	206.9
49	1.12E+07	(67)	4.33E+06	(26)	6	341	133	96.9	61.1	158.9
50	1.49E+07	(134)	7.78E+06	(70)	9	611	147	72.3	53.8	98.1
51	1.02E+07	(215)	4.48E+06	(94)	21	352	73	86.2	66.6	111.4
52	7.83E+06	(94)	3.17E+06	(38)	12	249	81	93.2	63.5	139.7

53	8.80E+06 (176)	3.25E+06 (65)	20	256	64	102.0	76.5	137.8
54	7.50E+06 (60)	4.25E+06 (34)	8	334	114	66.6	43.2	104.7
55	1.56E+07 (78)	1.32E+07 (66)	5	1038	257	44.8	31.8	63.2
56	1.63E+07 (343)	7.19E+06 (151)	21	565	94	85.7	69.3	105.8
57	1.55E+07 (62)	6.25E+06 (25)	4	491	195	93.3	58.1	155.0
58	2.33E+07 (93)	1.00E+07 (40)	4	786	248	87.6	60.1	130.4
59	8.56E+06 (231)	3.63E+06 (98)	27	285	58	88.8	69.0	114.2
60	6.00E+06 (120)	2.05E+06 (41)	20	161	50	110.1	76.9	161.0
61	7.17E+06 (86)	1.75E+06 (21)	12	138	59	153.0	95.0	259.3
62	1.93E+07 (116)	8.67E+06 (52)	6	681	189	84.2	60.3	119.1
63	1.09E+07 (87)	4.75E+06 (38)	8	373	121	86.3	58.5	129.9
64	4.72E+06 (85)	1.06E+06 (19)	18	83	38	166.8	101.7	290.1
65	2.17E+07 (130)	8.67E+06 (52)	6	681	189	94.2	68.0	132.6
66	1.03E+07 (93)	5.11E+06 (46)	9	402	119	76.3	53.2	111.2
67	1.69E+07 (152)	6.89E+06 (62)	9	542	138	92.4	68.5	126.4
68	8.30E+06 (166)	2.20E+06 (44)	20	173	52	141.5	101.4	202.0
69	7.17E+06 (86)	2.17E+06 (26)	12	170	66	124.1	79.7	200.4
70	1.24E+07 (224)	4.17E+06 (75)	18	328	76	112.1	85.2	147.5
71	1.87E+07 (168)	5.00E+06 (45)	9	393	117	140.1	100.7	199.2
72	2.01E+07 (241)	1.00E+07 (120)	12	786	145	75.8	59.8	96.0
73	1.75E+07 (210)	5.33E+06 (64)	12	419	105	123.4	93.1	165.9
74	1.52E+07 (213)	8.57E+06 (120)	14	674	125	67.0	52.7	85.3
75	2.25E+07 (90)	9.50E+06 (38)	4	747	242	89.2	60.6	134.1
76	2.46E+07 (221)	8.67E+06 (78)	9	681	155	106.4	81.1	139.6
77	1.03E+07 (82)	3.63E+06 (29)	8	285	105	106.3	69.2	168.4
78	1.80E+07 (144)	5.50E+06 (44)	8	432	130	123.0	87.5	176.5
79	8.50E+06 (51)	5.50E+06 (33)	6	432	150	58.4	37.1	93.5
80	6.25E+06 (125)	2.00E+06 (40)	20	157	50	117.5	82.0	172.1
81	1.36E+07 (109)	8.38E+06 (67)	8	658	162	61.5	45.0	84.8
82	9.20E+06 (92)	4.10E+06 (41)	10	322	101	84.6	58.1	125.5
83	1.04E+07 (146)	5.29E+06 (74)	14	416	97	74.5	56.0	100.1
84	7.71E+06 (108)	3.14E+06 (44)	14	247	74	92.5	64.8	134.5
85	1.69E+07 (236)	8.00E+06 (112)	14	629	120	79.5	62.4	101.2
86	1.19E+07 (215)	3.00E+06 (54)	18	236	64	149.3	110.8	205.1
87	1.63E+07 (326)	6.55E+06 (131)	20	515	91	93.7	75.1	117.0
88	1.48E+07 (178)	1.00E+07 (120)	12	786	145	56.1	43.8	71.9
89	1.72E+07 (155)	7.56E+06 (68)	9	594	145	86.0	64.3	116.2
90	1.77E+07 (106)	6.33E+06 (38)	6	498	161	104.9	72.1	156.3
91	1.20E+07 (120)	4.40E+06 (44)	10	346	104	102.7	72.3	148.6
92	1.29E+07 (103)	8.75E+06 (70)	8	688	165	55.7	40.7	76.6
93	1.15E+07 (69)	8.00E+06 (48)	6	629	182	54.4	37.1	80.4
94	1.66E+07 (199)	5.50E+06 (66)	12	432	107	113.1	84.6	151.1
95	1.58E+07 (142)	7.56E+06 (68)	9	594	145	78.8	58.7	107.0
96	1.28E+07 (153)	3.92E+06 (47)	12	308	90	122.3	88.0	173.5
97	1.40E+07 (140)	8.80E+06 (88)	10	692	149	60.1	45.4	79.6
98	1.52E+07 (137)	8.67E+06 (78)	9	681	155	66.3	49.5	88.7
99	1.88E+07 (150)	6.88E+06 (55)	8	540	146	102.7	75.1	142.6
100	8.56E+06 (154)	3.39E+06 (61)	18	266	68	95.2	70.4	130.3
101	1.02E+07 (163)	4.25E+06 (68)	16	334	81	90.4	67.8	121.9
102	6.67E+06 (80)	2.50E+06 (30)	12	197	71	100.3	65.5	158.1
103	5.30E+06 (53)	2.10E+06 (21)	10	165	71	94.8	56.6	165.6

KLD78 (Yukon), modern sand, UC2z (counted by Sarah Falkowski, May 2014)

EFFECTIVE TRACK DENSITY FOR FLUENCE MONITOR (tracks/cm^2): 4.090E+05
RELATIVE ERROR (%): 1.57
EFFECTIVE URANIUM CONTENT OF MONITOR (ppm): 50.00
ZETA FACTOR AND STANDARD ERROR (yr cm^2): 119.60 5.40
SIZE OF COUNTER SQUARE (cm^2): 1.000E-06

------ GRAIN AGES IN ORIGINAL ORDER ------

Grain no.	**RhoS (cm^-2)**	**(Ns)**	**RhoI (cm^-2)**	**(Ni)**	**Squares**	**U+/-2s**		**Grain Age**	**Age (Ma) --95% CI--**	
1	2.60E+06	(13)	9.20E+06	(46)	5	1125	332	7.0	3.4	13.0
2	3.80E+06	(38)	8.10E+06	(81)	10	990	222	11.5	7.6	17.1
3	2.05E+06	(39)	4.79E+06	(91)	19	586	124	10.5	7.0	15.4
4	1.33E+07	(159)	9.08E+06	(109)	12	1110	215	35.5	27.4	46.1
5	3.13E+05	(5)	1.88E+06	(30)	16	229	83	4.2	1.2	10.6
6	2.03E+06	(61)	6.60E+06	(198)	30	807	117	7.5	5.5	10.1
7	5.71E+05	(12)	1.14E+06	(24)	21	140	57	12.3	5.6	25.4
8	1.17E+06	(7)	2.50E+06	(15)	6	306	156	11.5	3.9	29.7
9	2.79E+06	(67)	6.54E+06	(157)	24	800	130	10.4	7.7	14.0
10	7.50E+05	(9)	1.58E+06	(19)	12	194	88	11.7	4.6	26.8
11	8.75E+05	(21)	1.96E+06	(47)	24	239	70	11.0	6.2	18.6
12	1.11E+06	(10)	1.89E+06	(17)	9	231	111	14.5	5.9	33.2
13	6.13E+06	(49)	8.38E+06	(67)	8	1024	251	17.9	12.1	26.2
14	5.00E+05	(4)	1.25E+06	(10)	8	153	94	10.0	2.2	33.9
15	1.50E+06	(12)	4.38E+06	(35)	8	535	180	8.5	4.0	16.5
16	7.10E+06	(71)	1.68E+07	(168)	10	2054	323	10.4	7.7	13.9
17	8.67E+05	(13)	2.40E+06	(36)	15	293	98	8.9	4.3	17.0
18	1.67E+05	(1)	8.33E+05	(5)	6	102	87	5.4	0.1	43.6
19	3.08E+06	(37)	4.58E+06	(55)	12	560	151	16.5	10.5	25.4
20	1.63E+06	(13)	2.38E+06	(19)	8	290	132	16.8	7.6	35.7
21	2.29E+06	(16)	5.14E+06	(36)	7	629	209	10.9	5.6	20.1
22	1.94E+06	(35)	4.67E+06	(84)	18	570	125	10.2	6.7	15.3
23	2.33E+06	(70)	4.50E+06	(135)	30	550	96	12.7	9.3	17.1
24	3.00E+06	(24)	9.88E+06	(79)	8	1207	273	7.5	4.5	11.9
25	2.33E+06	(14)	1.83E+06	(11)	6	224	132	31.0	13.1	75.4
26	8.50E+05	(17)	1.65E+06	(33)	20	202	70	12.6	6.6	23.3
27	2.71E+06	(65)	5.13E+06	(123)	24	627	114	12.9	9.4	17.6
28	7.50E+05	(15)	2.45E+06	(49)	20	300	86	7.5	3.9	13.6
29	3.65E+06	(73)	1.06E+07	(212)	20	1296	182	8.5	6.4	11.2
30	4.29E+05	(6)	1.00E+06	(14)	14	122	64	10.6	3.3	29.0
31	7.50E+05	(12)	1.38E+06	(22)	16	168	71	13.4	6.0	28.1
32	7.50E+05	(9)	1.25E+06	(15)	12	153	78	14.8	5.7	35.7
33	2.75E+06	(55)	7.50E+06	(150)	20	917	152	9.0	6.4	12.3
34	4.00E+05	(4)	1.20E+06	(12)	10	147	83	8.4	1.9	26.9
35	3.17E+06	(95)	6.20E+06	(186)	30	758	114	12.5	9.6	16.3
36	6.67E+05	(8)	2.50E+06	(30)	12	306	111	6.6	2.6	14.6
37	1.11E+05	(1)	2.00E+06	(18)	9	244	114	1.5	0.0	8.6
38	5.42E+06	(65)	1.27E+07	(152)	12	1548	255	10.5	7.7	14.1
39	4.00E+06	(24)	4.50E+06	(27)	6	550	211	21.7	12.0	39.1
40	2.22E+05	(2)	1.67E+06	(15)	9	204	104	3.5	0.4	14.0
41	3.54E+06	(46)	7.38E+06	(96)	13	903	186	11.7	8.0	16.8
42	6.25E+04	(1)	1.25E+06	(20)	16	153	68	1.4	0.0	7.6
43	2.89E+06	(26)	9.78E+06	(88)	9	1195	257	7.3	4.5	11.3
44	3.60E+06	(72)	1.06E+07	(212)	20	1296	182	8.3	6.3	11.1
45	5.00E+05	(7)	1.71E+06	(24)	14	210	85	7.2	2.6	17.1
46	4.50E+06	(36)	8.50E+06	(68)	8	1039	253	13.0	8.4	19.7
47	2.40E+06	(24)	4.90E+06	(49)	10	599	171	12.0	7.0	19.9
48	8.00E+05	(12)	3.07E+06	(46)	15	375	111	6.4	3.1	12.2
49	5.38E+06	(43)	1.14E+07	(91)	8	1391	294	11.6	7.8	16.8
50	4.88E+06	(78)	1.14E+07	(182)	16	1391	210	10.5	7.9	13.9
51	4.93E+06	(69)	1.03E+07	(144)	14	1257	213	11.7	8.6	15.7
52	9.33E+05	(14)	1.33E+06	(20)	15	163	72	17.2	8.0	35.6

53	7.33E+06	(44)	8.33E+06	(50)	6	1019	288	21.5	14.0	32.9
54	4.21E+06	(80)	1.12E+07	(212)	19	1364	192	9.3	7.0	12.2
55	2.75E+05	(11)	6.00E+05	(24)	40	73	30	11.3	5.0	23.8
56	4.00E+06	(40)	7.40E+06	(74)	10	905	212	13.2	8.8	19.7
57	5.83E+05	(7)	1.17E+06	(14)	12	143	75	12.4	4.2	32.3
58	2.47E+06	(37)	3.67E+06	(55)	15	448	121	16.5	10.5	25.4
59	7.00E+06	(42)	1.50E+07	(90)	6	1834	390	11.4	7.7	16.6
60	1.30E+06	(13)	1.30E+06	(13)	10	159	87	24.4	10.4	57.1
61	4.70E+06	(47)	1.01E+07	(101)	10	1235	248	11.4	7.9	16.2
62	9.17E+05	(11)	4.33E+06	(52)	12	530	147	5.2	2.4	10.0
63	6.25E+04	(1)	1.56E+06	(25)	16	191	76	1.1	0.0	6.0
64	3.13E+06	(94)	5.23E+06	(157)	30	640	104	14.7	11.2	19.2
65	4.17E+06	(25)	3.17E+06	(19)	6	387	176	32.0	17.0	61.6
66	2.92E+06	(35)	8.33E+06	(100)	12	1019	206	8.6	5.6	12.7
67	2.59E+05	(7)	1.78E+06	(48)	27	217	63	3.6	1.4	7.9
68	8.75E+05	(35)	2.65E+06	(106)	40	324	64	8.1	5.3	11.9
69	2.67E+05	(4)	1.00E+06	(15)	15	122	62	6.7	1.6	20.5
70	6.80E+06	(68)	1.22E+07	(122)	10	1491	274	13.6	10.0	18.5
71	2.00E+05	(4)	1.10E+06	(22)	20	134	57	4.6	1.1	13.1
72	1.04E+06	(25)	3.08E+06	(74)	24	377	88	8.3	5.0	13.2
73	1.15E+06	(46)	2.33E+06	(93)	40	284	59	12.1	8.3	17.4
74	2.30E+06	(46)	4.25E+06	(85)	20	520	114	13.2	9.0	19.2
75	5.00E+05	(12)	1.33E+06	(32)	24	163	57	9.2	4.3	18.3
76	2.33E+06	(56)	4.04E+06	(97)	24	494	101	14.1	10.0	19.8
77	3.50E+05	(14)	6.50E+05	(26)	40	79	31	13.2	6.3	26.1
78	1.43E+05	(4)	3.93E+05	(11)	28	48	28	9.1	2.1	30.0
79	6.07E+05	(17)	1.57E+06	(44)	28	192	58	9.5	5.1	16.9
80	8.75E+05	(14)	9.38E+05	(15)	16	115	58	22.8	10.2	50.6
81	1.27E+07	(152)	3.00E+07	(360)	12	3667	403	10.3	8.4	12.8
82	1.21E+06	(17)	3.00E+06	(42)	14	367	113	10.0	5.3	17.8
83	3.33E+05	(8)	9.58E+05	(23)	24	117	48	8.6	3.3	19.7
84	5.83E+05	(14)	1.79E+06	(43)	24	219	67	8.0	4.0	14.8
85	3.57E+06	(50)	1.04E+07	(145)	14	1266	214	8.4	6.0	11.7
86	1.07E+06	(16)	2.47E+06	(37)	15	302	99	10.6	5.5	19.5
87	7.50E+05	(9)	1.17E+06	(14)	12	143	75	15.8	6.0	38.9
88	8.31E+06	(133)	3.63E+06	(58)	16	443	117	55.8	40.7	77.4
89	9.29E+06	(130)	3.93E+06	(55)	14	480	130	57.5	41.7	80.4
90	2.10E+06	(21)	3.60E+06	(36)	10	440	146	14.3	7.9	25.1
91	6.00E+05	(9)	6.67E+05	(10)	15	81	50	22.0	7.9	60.0
92	8.00E+05	(8)	4.00E+05	(4)	10	49	46	47.8	13.1	218.4
93	3.75E+06	(75)	2.25E+06	(45)	20	275	82	40.6	27.7	60.2
94	3.50E+06	(42)	6.25E+06	(75)	12	764	177	13.7	9.1	20.2
95	4.47E+06	(85)	9.58E+06	(182)	19	1171	177	11.4	8.7	15.0
96	1.40E+06	(21)	4.53E+06	(68)	15	554	135	7.6	4.4	12.5
97	3.10E+06	(62)	6.00E+06	(120)	20	733	136	12.6	9.1	17.3
98	7.50E+05	(9)	1.67E+06	(20)	12	204	90	11.1	4.4	25.3
99	4.12E+06	(70)	7.18E+06	(122)	17	877	161	14.0	10.3	19.0
100	4.50E+05	(9)	1.85E+06	(37)	20	226	74	6.0	2.5	12.6
101	2.56E+06	(46)	8.50E+06	(153)	18	1039	171	7.4	5.2	10.3
102	2.92E+06	(35)	6.67E+06	(80)	12	815	183	10.7	7.0	16.1
103	2.50E+06	(75)	8.67E+05	(26)	30	106	41	69.9	44.4	114.0
104	4.20E+05	(21)	9.80E+05	(49)	50	120	34	10.5	6.0	17.8

KLD85 (Yukon), modern sand, TU11z (counted by Sarah Falkowski, May 2014)

EFFECTIVE TRACK DENSITY FOR FLUENCE MONITOR (tracks/cm^2): 6.340E+05
RELATIVE ERROR (%): 1.57
EFFECTIVE URANIUM CONTENT OF MONITOR (ppm): 50.00
ZETA FACTOR AND STANDARD ERROR (yr cm^2): 119.60 5.40
SIZE OF COUNTER SQUARE (cm^2): 1.000E-06

------ GRAIN AGES IN ORIGINAL ORDER ------

Grain no.	**RhoS (cm^-2)**	**(Ns)**	**RhoI (cm^-2)**	**(Ni)**	**Squares**	**U+/-2s**		**Grain Age (Ma)**	--95% CI--	
1	1.98E+07	(119)	7.83E+06	(47)	6	618	180	95.1	67.5	136.3
2	1.23E+07	(86)	7.43E+06	(52)	7	586	163	62.3	43.7	89.8
3	6.70E+06	(67)	7.00E+06	(70)	10	552	133	36.2	25.5	51.4
4	9.75E+06	(39)	1.10E+07	(44)	4	868	262	33.5	21.2	52.8
5	8.17E+06	(49)	7.33E+06	(44)	6	578	174	42.1	27.4	64.7
6	1.44E+07	(144)	4.90E+06	(49)	10	386	111	110.2	79.4	155.8
7	9.50E+06	(38)	6.00E+06	(24)	4	473	192	59.6	35.0	103.9
8	6.40E+06	(32)	6.60E+06	(33)	5	521	181	36.7	21.8	61.5
9	1.02E+07	(61)	5.17E+06	(31)	6	407	146	74.0	47.4	118.0
10	7.63E+06	(61)	3.38E+06	(27)	8	266	102	84.8	53.3	138.8
11	7.25E+06	(29)	2.00E+06	(8)	4	158	108	134.1	61.0	339.1
12	1.32E+07	(132)	3.90E+06	(39)	10	308	98	126.7	88.4	186.0
13	9.89E+06	(89)	5.11E+06	(46)	9	403	119	72.8	50.6	106.4
14	1.01E+07	(101)	3.90E+06	(39)	10	308	98	97.2	66.8	144.5
15	7.17E+06	(43)	3.33E+06	(20)	6	263	116	80.7	46.7	144.8
16	2.07E+07	(124)	5.17E+06	(31)	6	407	146	149.3	100.7	228.9
17	2.10E+07	(126)	8.33E+06	(50)	6	657	186	94.7	67.9	134.2
18	1.21E+07	(121)	5.10E+06	(51)	10	402	113	89.2	63.9	126.3
19	9.00E+06	(36)	9.00E+06	(36)	4	710	236	37.8	23.1	61.7
20	9.39E+06	(169)	4.11E+06	(74)	18	324	76	85.7	64.3	114.0
21	8.25E+06	(66)	4.13E+06	(33)	8	325	113	75.2	49.0	118.0
22	9.78E+06	(176)	3.61E+06	(65)	18	285	71	101.7	76.2	137.4
23	1.00E+07	(80)	6.13E+06	(49)	8	483	138	61.5	42.6	89.7
24	1.49E+07	(119)	6.50E+06	(52)	8	513	142	86.0	61.7	121.7
25	1.33E+07	(53)	3.50E+06	(14)	4	276	145	140.8	78.0	274.4
26	5.78E+06	(52)	1.00E+06	(9)	9	79	51	212.3	106.0	487.1
27	1.69E+07	(118)	6.86E+06	(48)	7	541	156	92.4	65.7	132.1
28	1.57E+07	(94)	8.67E+06	(52)	6	683	190	68.1	48.1	97.5
29	1.90E+07	(152)	8.38E+06	(67)	8	660	162	85.3	63.7	115.6
30	7.67E+06	(69)	5.56E+06	(50)	9	438	124	52.1	35.7	76.5
31	1.40E+07	(56)	7.25E+06	(29)	4	572	211	72.6	45.7	118.0
32	1.50E+07	(60)	8.50E+06	(34)	4	670	229	66.4	43.0	104.4
33	1.35E+07	(81)	2.67E+06	(16)	6	210	104	187.6	110.3	342.7
34	1.23E+07	(74)	1.02E+07	(61)	6	802	206	45.8	32.2	65.4
35	1.12E+07	(67)	6.83E+06	(41)	6	539	168	61.6	41.2	93.2
36	9.33E+06	(112)	4.33E+06	(52)	12	342	95	81.0	57.9	114.9
37	9.06E+06	(145)	5.69E+06	(91)	16	449	95	60.0	45.5	79.1
38	6.63E+06	(53)	5.25E+06	(42)	8	414	128	47.6	31.2	73.2
39	1.20E+07	(239)	4.40E+06	(88)	20	347	75	101.8	78.5	131.9
40	1.59E+07	(222)	6.86E+06	(96)	14	541	111	86.8	67.3	112.0
41	1.22E+07	(122)	6.90E+06	(69)	10	544	132	66.6	49.2	90.9
42	1.26E+07	(151)	4.58E+06	(55)	12	361	98	103.1	75.4	143.1
43	1.07E+07	(150)	5.64E+06	(79)	14	445	101	71.4	53.6	95.0
44	1.54E+07	(123)	7.50E+06	(60)	8	591	153	77.2	56.3	107.0
45	8.89E+06	(80)	5.11E+06	(46)	9	403	119	65.5	45.1	96.4
46	8.80E+06	(132)	2.20E+06	(33)	15	174	60	149.4	101.9	225.7
47	8.14E+06	(114)	4.14E+06	(58)	14	327	86	74.0	53.6	103.4
48	1.30E+07	(52)	6.75E+06	(27)	4	532	204	72.4	44.8	119.9
49	1.26E+07	(126)	7.10E+06	(71)	10	560	134	66.9	49.6	90.8
50	9.70E+06	(97)	5.30E+06	(53)	10	418	115	68.9	48.9	98.3
51	1.61E+07	(145)	6.56E+06	(59)	9	517	135	92.4	67.9	127.3
52	7.83E+06	(47)	2.33E+06	(14)	6	184	97	125.0	68.5	245.8

53	5.10E+06 (107)	4.19E+06 (88)	21	330	71	45.9	34.3	61.7
54	1.38E+07 (83)	5.67E+06 (34)	6	447	153	91.6	61.0	140.9
55	1.43E+07 (114)	9.25E+06 (74)	8	729	171	58.1	43.0	79.0
56	1.43E+07 (114)	6.88E+06 (55)	8	542	147	78.0	56.1	109.7
57	1.56E+07 (140)	7.11E+06 (64)	9	561	141	82.3	60.9	112.5
58	9.10E+06 (191)	4.14E+06 (87)	21	327	71	82.4	63.1	107.8
59	1.69E+07 (135)	7.88E+06 (63)	8	621	157	80.6	59.4	110.6
60	9.64E+06 (106)	4.45E+06 (49)	11	351	100	81.4	57.6	116.7
61	1.30E+07 (78)	4.83E+06 (29)	6	381	141	100.8	65.4	160.2
62	7.78E+06 (70)	4.56E+06 (41)	9	359	112	64.3	43.2	97.0
63	1.99E+07 (279)	6.36E+06 (89)	14	501	107	117.3	91.0	151.1
64	1.86E+07 (279)	7.13E+06 (107)	15	563	110	97.8	77.0	124.3
65	1.70E+07 (136)	7.25E+06 (58)	8	572	151	88.2	64.5	122.1
66	1.25E+07 (100)	6.63E+06 (53)	8	522	144	71.0	50.5	101.1
67	1.00E+07 (60)	2.50E+06 (15)	6	197	100	148.7	84.4	281.6
68	1.00E+07 (40)	2.50E+06 (10)	4	197	122	148.1	74.0	331.7
69	2.08E+07 (104)	9.00E+06 (45)	5	710	212	86.9	60.8	126.2
70	9.75E+06 (195)	4.25E+06 (85)	20	335	73	86.1	65.8	112.7
71	1.70E+07 (153)	6.11E+06 (55)	9	482	130	104.4	76.4	144.9
72	1.74E+07 (87)	8.20E+06 (41)	5	647	202	79.8	54.6	118.7
73	1.40E+07 (56)	7.25E+06 (29)	4	572	211	72.6	45.7	118.0
74	2.10E+07 (126)	9.33E+06 (56)	6	736	197	84.6	61.4	118.2
75	1.47E+07 (88)	7.83E+06 (47)	6	618	180	70.5	49.0	102.8
76	1.25E+07 (100)	4.50E+06 (36)	8	355	118	104.2	70.8	157.0
77	1.47E+07 (147)	6.00E+06 (60)	10	473	123	92.1	67.9	126.6
78	1.12E+07 (179)	5.19E+06 (83)	16	409	90	81.0	61.5	106.5
79	9.11E+06 (82)	2.56E+06 (23)	9	202	83	133.1	83.6	221.4
80	7.56E+06 (68)	2.67E+06 (24)	9	210	85	106.1	66.2	176.7
81	1.93E+07 (77)	1.25E+07 (50)	4	986	279	58.1	40.2	84.7
82	1.27E+07 (191)	5.27E+06 (79)	15	415	94	90.7	68.8	119.5
83	5.11E+06 (92)	3.28E+06 (59)	18	258	68	58.8	42.0	83.0
84	1.18E+07 (94)	9.13E+06 (73)	8	720	169	48.6	35.4	67.0
85	1.25E+07 (150)	5.33E+06 (64)	12	421	106	88.1	65.4	120.1
86	1.46E+07 (131)	4.22E+06 (38)	9	333	108	129.0	89.7	190.3
87	1.34E+07 (121)	5.56E+06 (50)	9	438	124	90.9	65.0	129.2
88	1.09E+07 (217)	5.50E+06 (110)	20	434	84	74.2	58.0	94.9
89	1.26E+07 (101)	4.88E+06 (39)	8	384	123	97.2	66.8	144.5
90	1.98E+07 (79)	1.25E+07 (50)	4	986	279	59.6	41.3	86.7
91	5.80E+06 (58)	3.20E+06 (32)	10	252	89	68.2	43.7	108.6
92	9.81E+06 (157)	5.38E+06 (86)	16	424	92	68.7	52.0	90.6
93	1.01E+07 (81)	5.00E+06 (40)	8	394	125	76.2	51.7	114.3
94	1.24E+07 (198)	3.50E+06 (56)	16	276	74	132.4	98.3	181.5
95	7.75E+06 (62)	4.13E+06 (33)	8	325	113	70.7	45.8	111.4
96	1.03E+07 (82)	6.75E+06 (54)	8	532	145	57.3	40.2	82.3
97	1.40E+07 (56)	8.00E+06 (32)	4	631	222	65.9	42.0	105.1
98	9.25E+06 (37)	2.50E+06 (10)	4	197	122	137.2	68.0	309.0
99	9.40E+06 (94)	4.00E+06 (40)	10	315	100	88.3	60.6	131.3
100	9.00E+06 (108)	4.08E+06 (49)	12	322	92	82.9	58.7	118.7
101	1.61E+07 (129)	4.50E+06 (36)	8	355	118	134.0	92.5	199.6
102	1.30E+07 (104)	3.75E+06 (30)	8	296	108	129.6	86.1	201.5
103	1.61E+07 (129)	4.00E+06 (32)	8	315	111	150.5	102.2	228.9
104	1.20E+07 (120)	3.10E+06 (31)	10	244	87	144.6	97.3	221.9
105	9.00E+06 (162)	3.50E+06 (63)	18	276	70	96.6	71.9	131.5

KLD105 (Yukon), modern sand, TU11z (counted by Sarah Falkowski, April 2014)

EFFECTIVE TRACK DENSITY FOR FLUENCE MONITOR (tracks/cm^2): 6.330E+05
RELATIVE ERROR (%): 1.57
EFFECTIVE URANIUM CONTENT OF MONITOR (ppm): 50.00
ZETA FACTOR AND STANDARD ERROR (yr cm^2): 119.60 5.40
SIZE OF COUNTER SQUARE (cm^2): 1.000E-06

------ GRAIN AGES IN ORIGINAL ORDER ------

Grain no.	RhoS (cm^-2)	(Ns)	RhoI (cm^-2)	(Ni)	Squares	U+/-2s		Grain Age	Age (Ma) --95% CI--	
1	8.75E+06	(175)	4.10E+06	(82)	20	324	72	80.0	60.7	105.5
2	1.23E+07	(49)	4.25E+06	(17)	4	336	161	107.5	61.4	199.2
3	6.75E+06	(27)	2.50E+06	(10)	4	197	122	100.4	47.7	232.6
4	7.17E+06	(43)	1.83E+06	(11)	6	145	86	144.7	74.5	310.8
5	1.87E+07	(112)	7.17E+06	(43)	6	566	173	97.6	68.3	142.2
6	1.18E+07	(71)	5.67E+06	(34)	6	448	153	78.4	51.6	121.7
7	8.67E+06	(104)	2.75E+06	(33)	12	217	75	117.8	79.4	180.0
8	8.75E+06	(105)	3.17E+06	(38)	12	250	81	103.5	71.1	154.2
9	1.01E+07	(242)	3.04E+06	(73)	24	240	57	123.7	94.0	162.7
10	1.24E+07	(223)	4.44E+06	(80)	18	351	79	104.2	79.6	136.4
11	6.00E+06	(48)	2.50E+06	(20)	8	197	87	89.8	52.6	159.8
12	1.45E+07	(116)	6.50E+06	(52)	8	513	143	83.8	60.0	118.6
13	1.02E+07	(61)	2.83E+06	(17)	6	224	107	133.5	77.8	243.6
14	1.04E+07	(52)	3.40E+06	(17)	5	269	129	114.0	65.5	210.3
15	5.42E+06	(130)	1.58E+06	(38)	24	125	41	127.8	88.9	188.6
16	1.05E+07	(42)	7.00E+06	(28)	4	553	208	56.4	34.3	94.5
17	6.67E+06	(40)	2.00E+06	(12)	6	158	90	123.8	64.5	259.1
18	2.00E+07	(80)	8.25E+06	(33)	4	652	226	90.9	60.1	140.8
19	1.08E+07	(43)	3.00E+06	(12)	4	237	134	133.0	69.8	276.8
20	8.00E+06	(32)	2.75E+06	(11)	4	217	128	108.2	53.8	237.9
21	7.63E+06	(61)	3.00E+06	(24)	8	237	96	95.1	58.8	159.6
22	1.53E+07	(92)	5.33E+06	(32)	6	421	148	107.6	71.6	166.3
23	7.50E+06	(45)	4.17E+06	(25)	6	329	131	67.6	40.7	115.0
24	9.88E+06	(79)	4.25E+06	(34)	8	336	115	87.1	57.8	134.4
25	1.60E+07	(240)	6.27E+06	(94)	15	495	103	95.6	74.2	123.2
26	1.03E+07	(82)	4.38E+06	(35)	8	346	117	87.9	58.7	134.5
27	9.83E+06	(118)	4.83E+06	(58)	12	382	101	76.5	55.5	106.6
28	9.75E+06	(39)	6.50E+06	(26)	4	513	200	56.4	33.6	96.5
29	3.88E+06	(31)	1.75E+06	(14)	8	138	73	82.8	43.1	168.5
30	6.00E+06	(24)	4.50E+06	(18)	4	355	166	50.2	26.2	98.0
31	1.08E+07	(43)	4.00E+06	(16)	4	316	156	100.3	55.9	190.8
32	1.18E+07	(47)	3.00E+06	(12)	4	237	134	145.1	76.9	300.2
33	1.03E+07	(103)	4.20E+06	(42)	10	332	102	92.0	63.8	135.0
34	1.15E+07	(46)	4.75E+06	(19)	4	375	170	90.6	52.4	163.7
35	1.55E+07	(62)	3.75E+06	(15)	4	296	151	153.3	87.3	289.8
36	8.63E+06	(69)	2.75E+06	(22)	8	217	92	117.1	72.1	198.7
37	1.25E+07	(75)	6.67E+06	(40)	6	527	166	70.5	47.5	106.2
38	9.22E+06	(83)	3.44E+06	(31)	9	272	97	100.2	65.9	156.7
39	1.16E+07	(104)	4.56E+06	(41)	9	360	112	95.1	65.9	140.1
40	7.60E+06	(76)	3.20E+06	(32)	10	253	89	89.0	58.4	139.1
41	1.03E+07	(62)	8.17E+06	(49)	6	645	184	47.7	32.3	70.9
42	5.38E+06	(129)	2.67E+06	(64)	24	211	53	75.8	55.8	104.0
43	1.38E+07	(55)	4.00E+06	(16)	4	316	156	127.9	73.0	239.0
44	5.70E+06	(171)	2.17E+06	(65)	30	171	43	98.7	73.9	133.5
45	7.33E+06	(88)	3.58E+06	(43)	12	283	86	76.9	52.9	113.5
46	4.70E+06	(47)	1.50E+06	(15)	10	118	60	116.7	64.8	224.6
47	4.13E+06	(33)	2.13E+06	(17)	8	168	80	72.7	39.6	139.3
48	8.63E+06	(69)	2.75E+06	(22)	8	217	92	117.1	72.1	198.7
49	9.50E+06	(190)	3.25E+06	(65)	20	257	64	109.5	82.4	147.6
50	7.00E+06	(42)	1.67E+06	(10)	6	132	81	155.2	78.0	346.2
51	1.07E+07	(171)	4.00E+06	(64)	16	316	79	100.2	74.9	135.8
52	8.60E+06	(43)	7.00E+06	(35)	5	553	186	46.3	29.0	74.5

53	8.50E+06	(34)	3.25E+06	(13)	4	257	140	97.5	50.7	201.4
54	5.80E+06	(29)	1.40E+06	(7)	5	111	81	152.3	66.8	411.0
55	7.25E+06	(29)	6.50E+06	(26)	4	513	200	42.1	23.9	74.3
56	1.20E+07	(216)	4.44E+06	(80)	18	351	79	101.0	77.1	132.3
57	7.20E+06	(72)	3.40E+06	(34)	10	269	92	79.5	52.3	123.3
58	8.25E+06	(66)	3.75E+06	(30)	8	296	108	82.5	53.0	131.7
59	6.00E+06	(36)	6.50E+06	(39)	6	513	164	34.9	21.5	56.3
60	8.25E+06	(33)	3.50E+06	(14)	4	276	145	88.0	46.3	178.1
61	1.10E+07	(165)	3.93E+06	(59)	15	311	81	104.8	77.6	143.7
62	9.50E+06	(57)	8.17E+06	(49)	6	645	184	43.9	29.4	65.6
63	1.10E+07	(88)	5.50E+06	(44)	8	434	131	75.1	51.9	110.5
64	1.15E+07	(46)	4.25E+06	(17)	4	336	161	101.0	57.3	188.0
65	1.08E+07	(162)	3.93E+06	(59)	15	311	81	102.9	76.1	141.2
66	7.75E+06	(31)	1.50E+06	(6)	4	118	93	188.6	79.8	549.6
67	5.60E+06	(28)	2.00E+06	(10)	5	158	98	104.1	49.7	240.2
68	6.00E+06	(36)	5.17E+06	(31)	6	408	146	43.8	26.4	73.2
69	6.83E+06	(41)	2.17E+06	(13)	6	171	93	117.3	62.4	238.6
70	9.83E+06	(59)	7.83E+06	(47)	6	619	181	47.3	31.7	71.0
71	8.67E+06	(104)	3.75E+06	(45)	12	296	88	86.7	60.7	126.0
72	6.25E+06	(25)	5.25E+06	(21)	4	415	179	44.9	24.2	84.2
73	1.33E+07	(80)	3.33E+06	(20)	6	263	117	148.8	91.1	256.1
74	5.75E+06	(23)	2.25E+06	(9)	4	178	115	95.0	42.9	233.4
75	1.29E+07	(116)	4.44E+06	(40)	9	351	111	108.6	75.5	159.7
76	7.00E+06	(28)	7.00E+06	(28)	4	553	208	37.7	21.5	66.1
77	1.00E+07	(80)	2.38E+06	(19)	8	188	85	156.4	94.9	272.9
78	1.33E+07	(106)	6.25E+06	(50)	8	494	140	79.6	56.5	113.9
79	1.34E+07	(267)	5.30E+06	(106)	20	419	82	94.4	74.1	120.1
80	9.13E+06	(73)	3.25E+06	(26)	8	257	100	105.0	66.7	171.2
81	8.50E+06	(34)	2.75E+06	(11)	4	217	128	114.8	57.6	251.2
82	1.42E+07	(85)	4.83E+06	(29)	6	382	141	109.6	71.5	173.3
83	5.75E+06	(23)	1.25E+06	(5)	4	99	84	167.7	64.4	561.5
84	9.50E+06	(57)	6.50E+06	(39)	6	513	164	55.0	36.0	84.9
85	1.04E+07	(83)	3.13E+06	(25)	8	247	98	123.9	79.0	202.2
86	6.75E+06	(54)	2.00E+06	(16)	8	158	78	125.6	71.6	235.0
87	5.50E+06	(22)	1.00E+06	(4)	4	79	75	198.5	70.3	782.1
88	1.06E+07	(53)	5.80E+06	(29)	5	458	169	68.6	43.0	112.0
89	1.27E+07	(76)	5.00E+06	(30)	6	395	144	94.9	61.7	150.0
90	9.83E+06	(59)	4.67E+06	(28)	6	369	139	79.0	49.8	128.8
91	6.75E+06	(27)	3.00E+06	(12)	4	237	134	84.0	41.6	182.1
92	9.25E+06	(37)	6.00E+06	(24)	4	474	192	58.0	33.9	101.3
93	1.30E+07	(78)	7.83E+06	(47)	6	619	181	62.4	43.0	91.7
94	7.25E+06	(58)	1.75E+06	(14)	8	138	73	153.6	85.7	297.7
95	1.13E+07	(45)	2.50E+06	(10)	4	197	122	166.1	84.0	368.6
96	1.00E+07	(40)	3.50E+06	(14)	4	276	145	106.5	57.3	211.9
97	7.67E+06	(46)	2.17E+06	(13)	6	171	93	131.4	70.7	265.0
98	9.40E+06	(94)	3.40E+06	(34)	10	269	92	103.5	69.5	158.1
99	8.75E+06	(70)	2.50E+06	(20)	8	197	87	130.4	79.1	226.2
100	1.03E+07	(82)	2.50E+06	(20)	8	197	87	152.4	93.5	262.1
101	7.25E+06	(29)	2.25E+06	(9)	4	178	115	119.4	55.9	286.7
102	1.15E+07	(46)	8.75E+06	(35)	4	691	233	49.5	31.3	79.2
103	6.25E+06	(50)	2.00E+06	(16)	8	158	78	116.4	65.9	219.0
104	1.17E+07	(70)	3.83E+06	(23)	6	303	125	113.7	70.6	190.8

KLD106 (Yukon), modern sand, TU11z (counted by Sarah Falkowski 5 April 2014)

EFFECTIVE TRACK DENSITY FOR FLUENCE MONITOR (tracks/cm^2): 6.320E+05
RELATIVE ERROR (%): 1.57
EFFECTIVE URANIUM CONTENT OF MONITOR (ppm): 50.00
ZETA FACTOR AND STANDARD ERROR (yr cm^2): 119.60 5.40
SIZE OF COUNTER SQUARE (cm^2): 1.000E-06

------ GRAIN AGES IN ORIGINAL ORDER ------

Grain no.	**RhoS (cm^-2)**	**(Ns)**	**RhoI (cm^-2)**	**(Ni)**	**Squares**	**U+/-2s**		**Grain Age**	**Age (Ma) --95% CI--**	
1	9.67E+06	(58)	3.00E+06	(18)	6	237	111	119.9	70.3	216.2
2	1.10E+07	(66)	3.67E+06	(22)	6	290	123	111.9	68.6	190.3
3	8.17E+06	(98)	3.33E+06	(40)	12	264	83	91.7	63.1	136.1
4	7.71E+06	(54)	4.43E+06	(31)	7	350	125	65.4	41.4	105.2
5	1.15E+07	(46)	4.50E+06	(18)	4	356	166	95.3	54.6	174.8
6	9.89E+06	(89)	4.78E+06	(43)	9	378	115	77.6	53.5	114.5
7	1.46E+07	(117)	5.38E+06	(43)	8	425	130	101.8	71.4	148.0
8	7.50E+06	(60)	2.63E+06	(21)	8	208	90	106.6	64.3	184.4
9	1.40E+07	(84)	8.00E+06	(48)	6	633	183	65.7	45.6	95.8
10	9.19E+06	(147)	4.38E+06	(70)	16	346	83	78.8	58.9	106.4
11	1.24E+07	(224)	5.17E+06	(93)	18	409	86	90.1	69.7	116.5
12	1.14E+07	(57)	7.40E+06	(37)	5	585	192	57.9	37.7	90.1
13	4.00E+06	(24)	2.83E+06	(17)	6	224	107	53.0	27.4	105.1
14	1.23E+07	(49)	7.00E+06	(28)	4	554	208	65.6	40.6	108.5
15	1.21E+07	(97)	2.63E+06	(21)	8	208	90	171.2	107.1	288.5
16	9.00E+06	(54)	3.67E+06	(22)	6	290	123	91.7	55.3	158.2
17	9.88E+06	(79)	5.13E+06	(41)	8	405	127	72.3	49.1	108.2
18	8.40E+06	(42)	4.00E+06	(20)	5	316	140	78.6	45.4	141.3
19	1.75E+07	(105)	7.50E+06	(45)	6	593	177	87.4	61.3	126.9
20	7.50E+06	(105)	2.50E+06	(35)	14	198	67	112.1	76.1	169.3
21	1.42E+07	(213)	5.13E+06	(77)	15	406	93	103.3	78.5	135.8
22	1.33E+07	(106)	4.88E+06	(39)	8	386	123	101.7	70.1	150.8
23	1.27E+07	(76)	5.83E+06	(35)	6	461	156	81.4	54.0	125.2
24	9.25E+06	(74)	5.50E+06	(44)	8	435	131	63.2	43.0	94.0
25	5.00E+06	(30)	3.00E+06	(18)	6	237	111	62.5	33.9	119.0
26	1.28E+07	(154)	6.17E+06	(74)	12	488	114	77.9	58.3	104.1
27	1.04E+07	(166)	4.31E+06	(69)	16	341	83	90.2	67.8	121.3
28	8.50E+06	(68)	3.00E+06	(24)	8	237	96	105.7	66.0	176.1
29	1.55E+07	(62)	2.50E+06	(10)	4	198	122	227.1	118.1	493.6
30	1.39E+07	(97)	5.43E+06	(38)	7	429	139	95.5	65.2	142.9
31	1.35E+07	(108)	9.13E+06	(73)	8	722	170	55.6	41.0	76.0
32	1.72E+07	(86)	6.40E+06	(32)	5	506	178	100.5	66.5	155.9
33	8.83E+06	(106)	3.50E+06	(42)	12	277	85	94.5	65.7	138.5
34	1.00E+07	(40)	6.25E+06	(25)	4	494	196	60.0	35.7	103.3
35	1.37E+07	(82)	4.50E+06	(27)	6	356	136	113.3	73.0	182.1
36	9.15E+06	(119)	3.69E+06	(48)	13	292	84	92.8	66.0	132.7
37	1.24E+07	(99)	5.25E+06	(42)	8	415	128	88.3	61.1	129.9
38	9.78E+06	(176)	3.72E+06	(67)	18	294	72	98.4	74.0	132.5
39	1.40E+07	(112)	4.00E+06	(32)	8	316	111	130.5	87.9	199.7
40	8.67E+06	(52)	2.67E+06	(16)	6	211	104	120.8	68.6	226.7
41	1.40E+07	(56)	5.25E+06	(21)	4	415	180	99.5	59.7	173.1
42	1.65E+07	(99)	5.67E+06	(34)	6	448	153	108.8	73.3	165.7
43	1.02E+07	(102)	4.40E+06	(44)	10	348	105	86.8	60.6	126.7
44	5.90E+06	(413)	1.97E+06	(138)	70	156	27	111.9	90.5	138.3
45	5.00E+06	(30)	3.33E+06	(20)	6	264	117	56.3	31.0	104.6
46	7.39E+06	(133)	1.83E+06	(33)	18	145	50	150.0	102.4	226.6
47	1.20E+07	(48)	6.00E+06	(24)	4	475	192	74.9	45.2	127.9
48	5.94E+06	(95)	3.31E+06	(53)	16	262	72	67.3	47.7	96.1
49	1.05E+07	(42)	6.25E+06	(25)	4	494	196	63.0	37.7	107.9
50	6.25E+06	(25)	2.00E+06	(8)	4	158	109	115.5	51.4	296.2
51	8.32E+06	(208)	4.84E+06	(121)	25	383	71	64.5	50.7	82.1
52	7.81E+06	(164)	3.52E+06	(74)	21	279	65	82.9	62.2	110.5

53	8.17E+06	(49)	3.50E+06	(21)	6	277	120	87.2	51.6	153.1
54	9.29E+06	(65)	2.57E+06	(18)	7	203	95	134.2	79.4	240.2
55	8.80E+06	(44)	5.00E+06	(25)	5	396	157	66.0	39.7	112.6
56	7.07E+06	(106)	2.07E+06	(31)	15	164	58	127.5	85.2	196.8
57	1.16E+07	(58)	2.60E+06	(13)	5	206	112	164.9	90.6	327.3
58	8.75E+06	(105)	4.33E+06	(52)	12	343	95	75.8	53.9	107.8
59	1.01E+07	(91)	2.89E+06	(26)	9	229	89	130.4	84.1	210.0
60	1.94E+07	(97)	3.20E+06	(16)	5	253	125	223.3	132.7	404.2
61	9.20E+06	(92)	5.70E+06	(57)	10	451	120	60.7	43.2	86.0
62	1.31E+07	(196)	4.20E+06	(63)	15	332	84	116.3	87.4	157.1
63	9.50E+06	(57)	3.00E+06	(18)	6	237	111	117.9	69.0	212.7
64	9.00E+06	(72)	5.25E+06	(42)	8	415	128	64.4	43.5	96.6
65	1.07E+07	(64)	5.83E+06	(35)	6	461	156	68.6	44.9	106.8
66	1.40E+07	(56)	2.50E+06	(10)	4	198	122	205.5	106.0	449.6
67	1.63E+07	(65)	5.25E+06	(21)	4	415	180	115.3	70.1	198.6
68	1.07E+07	(64)	1.67E+06	(10)	6	132	81	234.3	122.1	508.2
69	1.02E+07	(61)	3.00E+06	(18)	6	237	111	126.0	74.2	226.5
70	1.48E+07	(178)	5.33E+06	(64)	12	422	106	104.1	78.0	140.9
71	1.67E+07	(100)	5.17E+06	(31)	6	409	146	120.3	80.2	186.3
72	7.38E+06	(59)	3.63E+06	(29)	8	287	106	76.2	48.3	123.4
73	5.25E+06	(21)	3.00E+06	(12)	4	237	134	65.4	31.0	145.9
74	5.33E+06	(32)	3.83E+06	(23)	6	303	125	52.3	29.7	93.5
75	8.88E+06	(71)	4.25E+06	(34)	8	336	115	78.3	51.5	121.5
76	7.50E+06	(30)	1.00E+06	(4)	4	79	75	268.3	99.1	1022.4
77	1.53E+07	(244)	4.00E+06	(64)	16	316	79	141.7	106.3	188.7
78	1.17E+07	(164)	5.50E+06	(77)	14	435	100	79.7	60.0	105.9
79	8.33E+06	(50)	2.33E+06	(14)	6	185	97	132.5	73.0	259.3
80	9.00E+06	(54)	5.50E+06	(33)	6	435	151	61.4	39.2	97.8
81	1.65E+07	(66)	9.50E+06	(38)	4	752	243	65.2	43.2	99.9
82	1.28E+07	(179)	4.36E+06	(61)	14	345	89	109.8	81.8	149.4
83	1.22E+07	(61)	8.00E+06	(40)	5	633	200	57.3	37.9	87.7
84	1.83E+07	(73)	6.75E+06	(27)	4	534	204	101.0	64.5	163.4
85	9.17E+06	(55)	2.33E+06	(14)	6	185	97	145.5	80.9	283.1
86	1.18E+07	(47)	4.50E+06	(18)	4	356	166	97.4	55.9	178.2
87	2.34E+07	(117)	5.80E+06	(29)	5	459	170	150.1	99.9	233.6
88	1.62E+07	(97)	5.83E+06	(35)	6	461	156	103.6	70.0	157.2
89	1.22E+07	(73)	2.00E+06	(12)	6	158	90	223.4	122.7	449.6
90	1.45E+07	(58)	4.50E+06	(18)	4	356	166	119.9	70.3	216.2
91	2.58E+07	(103)	1.00E+07	(40)	4	791	250	96.4	66.5	142.6
92	1.88E+07	(75)	4.50E+06	(18)	4	356	166	154.5	92.4	274.3
93	2.44E+07	(195)	6.13E+06	(49)	8	485	139	148.3	108.4	207.1
94	1.91E+07	(286)	4.60E+06	(69)	15	364	88	153.9	116.9	202.6
95	2.05E+07	(82)	6.00E+06	(24)	4	475	192	127.2	80.5	209.7
96	1.42E+07	(85)	4.00E+06	(24)	6	316	128	131.8	83.6	216.8
97	1.98E+07	(79)	6.00E+06	(24)	4	475	192	122.6	77.4	202.5
98	2.43E+07	(97)	6.25E+06	(25)	4	494	196	144.3	92.9	233.6
99	1.47E+07	(88)	4.67E+06	(28)	6	369	139	117.2	76.3	186.3
100	1.38E+07	(83)	6.83E+06	(41)	6	541	169	75.9	51.7	113.3
101	1.73E+07	(156)	7.78E+06	(70)	9	615	148	83.6	62.7	112.5
102	1.78E+07	(107)	5.33E+06	(32)	6	422	149	124.7	83.8	191.3
103	1.88E+07	(75)	5.00E+06	(20)	4	396	175	139.4	85.0	240.8

KLD110 (Yukon), modern sand, UC2z (counted by Sarah Falkowski 4 July 2014)

EFFECTIVE TRACK DENSITY FOR FLUENCE MONITOR (tracks/cm^2): 3.820E+05
RELATIVE ERROR (%): 1.57
EFFECTIVE URANIUM CONTENT OF MONITOR (ppm): 50.00
ZETA FACTOR AND STANDARD ERROR (yr cm^2): 119.60 5.40
SIZE OF COUNTER SQUARE (cm^2): 1.000E-06

------ GRAIN AGES IN ORIGINAL ORDER ------

Grain no.	RhoS (cm^-2)	(Ns)	RhoI (cm^-2)	(Ni)	Squares	U+/-2s		Grain Age	Age (Ma) --95% CI--	
1	5.80E+06	(58)	3.00E+05	(3)	10	39	42	407.4	142.1	1896.3
2	6.71E+06	(47)	5.71E+06	(40)	7	748	236	26.8	17.2	41.9
3	2.56E+06	(23)	4.56E+06	(41)	9	596	186	12.8	7.3	21.9
4	2.07E+06	(31)	3.87E+06	(58)	15	506	133	12.2	7.6	19.2
5	1.90E+06	(19)	6.40E+06	(64)	10	838	210	6.8	3.8	11.5
6	1.50E+06	(12)	4.50E+06	(36)	8	589	196	7.7	3.6	15.0
7	3.33E+06	(20)	2.12E+07	(127)	6	2771	498	3.6	2.1	5.8
8	2.80E+06	(14)	5.20E+06	(26)	5	681	265	12.4	5.9	24.4
9	4.80E+06	(72)	7.07E+06	(106)	15	925	182	15.5	11.3	21.1
10	5.63E+05	(9)	1.00E+06	(16)	16	131	65	12.9	5.0	30.8
11	3.50E+06	(21)	6.33E+06	(38)	6	829	268	12.7	7.0	22.1
12	8.75E+05	(7)	2.88E+06	(23)	8	376	156	7.1	2.5	16.7
13	9.52E+05	(20)	1.81E+06	(38)	21	237	77	12.1	6.6	21.2
14	3.55E+06	(71)	6.40E+06	(128)	20	838	150	12.7	9.3	17.1
15	3.00E+06	(18)	7.50E+06	(45)	6	982	293	9.2	5.0	16.1
16	2.13E+06	(17)	2.38E+06	(19)	8	311	141	20.4	10.0	41.4
17	2.35E+07	(94)	3.75E+06	(15)	4	491	250	140.3	81.9	260.8
18	3.59E+06	(115)	7.66E+06	(245)	32	1002	132	10.7	8.4	13.7
19	6.35E+06	(127)	1.80E+06	(36)	20	236	78	79.8	55.0	119.2
20	2.30E+06	(46)	6.15E+06	(123)	20	805	147	8.6	5.9	12.1
21	1.67E+06	(35)	3.19E+06	(67)	21	418	102	12.0	7.7	18.2
22	1.60E+06	(16)	6.80E+06	(68)	10	890	217	5.4	2.9	9.4
23	1.11E+06	(10)	8.89E+05	(8)	9	116	80	28.4	10.1	82.8
24	3.86E+06	(54)	9.86E+06	(138)	14	1290	223	9.0	6.4	12.3
25	1.00E+06	(9)	2.11E+06	(19)	9	276	125	10.9	4.3	25.1
26	7.70E+06	(154)	1.90E+07	(379)	20	2480	266	9.3	7.5	11.5
27	1.25E+06	(5)	2.00E+06	(8)	4	262	180	14.4	3.7	49.3
28	3.15E+06	(63)	6.70E+06	(134)	20	877	154	10.7	7.8	14.6
29	2.46E+06	(59)	6.46E+06	(155)	24	845	138	8.7	6.3	11.8
30	2.21E+06	(53)	5.33E+06	(128)	24	698	125	9.5	6.7	13.1
31	1.88E+07	(113)	8.33E+05	(5)	6	109	93	482.3	211.2	1446.4
32	1.65E+07	(99)	2.33E+06	(14)	6	305	161	158.0	91.1	299.4
33	5.19E+06	(83)	9.56E+06	(153)	16	1252	206	12.4	9.4	16.5
34	2.93E+06	(79)	6.26E+06	(169)	27	819	128	10.7	8.1	14.2
35	2.25E+06	(18)	3.25E+06	(26)	8	425	166	15.8	8.2	29.9
36	7.50E+05	(6)	1.63E+06	(13)	8	213	116	10.7	3.3	29.7
37	7.20E+06	(36)	1.74E+07	(87)	5	2277	492	9.5	6.2	14.1
38	6.88E+05	(11)	1.31E+06	(21)	16	172	74	12.0	5.2	25.9
39	1.25E+06	(30)	4.96E+06	(119)	24	649	120	5.8	3.7	8.7
40	1.33E+07	(93)	9.14E+06	(64)	7	1197	300	33.1	23.8	46.3
41	2.27E+06	(34)	7.87E+06	(118)	15	1030	192	6.6	4.4	9.7
42	3.17E+06	(38)	5.00E+06	(60)	12	654	170	14.5	9.4	22.1
43	1.15E+07	(46)	7.50E+05	(3)	4	98	105	325.4	111.6	1557.2
44	4.63E+06	(37)	1.45E+07	(116)	8	1898	357	7.3	4.9	10.6
45	8.94E+06	(143)	1.67E+07	(267)	16	2184	276	12.2	9.8	15.3
46	1.50E+06	(6)	1.20E+07	(48)	4	1571	454	2.9	1.0	6.7
47	6.33E+06	(76)	1.92E+06	(23)	12	251	104	74.7	46.6	125.1
48	6.43E+05	(9)	2.36E+06	(33)	14	309	107	6.3	2.6	13.3
49	1.67E+05	(1)	1.17E+06	(7)	6	153	112	3.7	0.1	25.4
50	1.32E+07	(79)	1.13E+07	(68)	6	1483	361	26.5	18.9	37.2
51	1.83E+06	(66)	4.92E+06	(177)	36	644	99	8.5	6.3	11.4
52	1.67E+06	(10)	1.17E+06	(7)	6	153	112	32.3	11.2	100.3

53	2.00E+06	(12)	3.50E+06	(21)	6	458	198	13.1	5.8	27.7
54	3.21E+06	(154)	7.06E+06	(339)	48	924	104	10.4	8.4	12.8
55	4.50E+06	(81)	1.38E+07	(249)	18	1811	236	7.5	5.7	9.7
56	1.00E+06	(4)	5.00E+05	(2)	4	65	83	43.9	6.5	486.4
57	6.44E+06	(58)	2.44E+07	(220)	9	3200	442	6.0	4.4	8.1
58	1.00E+07	(40)	1.30E+07	(52)	4	1702	473	17.6	11.3	27.0
59	1.08E+07	(65)	1.50E+06	(9)	6	196	128	160.4	81.2	366.5
60	1.30E+07	(130)	3.50E+06	(35)	10	458	154	84.0	57.7	126.0
61	6.78E+06	(122)	1.18E+07	(212)	18	1542	217	13.2	10.3	16.7
62	4.25E+06	(68)	1.03E+07	(164)	16	1342	213	9.5	7.0	12.7
63	1.62E+07	(97)	1.50E+06	(9)	6	196	128	237.8	123.2	532.4
64	4.67E+06	(28)	9.50E+06	(57)	6	1243	330	11.2	6.9	17.9
65	2.00E+06	(12)	3.33E+06	(20)	6	436	193	13.8	6.1	29.4
66	3.53E+06	(141)	7.10E+06	(284)	40	929	114	11.4	9.1	14.2
67	1.10E+07	(88)	8.75E+05	(7)	8	115	84	275.2	132.2	696.6
68	1.29E+06	(31)	3.46E+06	(83)	24	453	100	8.6	5.4	13.0
69	1.89E+06	(68)	3.94E+06	(142)	36	516	88	10.9	8.1	14.7
70	1.33E+06	(8)	5.83E+06	(35)	6	764	257	5.3	2.1	11.5
71	2.00E+06	(18)	1.78E+06	(16)	9	233	115	25.6	12.4	53.7
72	8.75E+06	(140)	4.06E+06	(65)	16	532	132	49.0	36.2	66.9
73	4.29E+05	(9)	1.95E+06	(41)	21	256	80	5.1	2.1	10.5
74	2.00E+06	(16)	8.38E+06	(67)	8	1096	269	5.5	2.9	9.5
75	5.40E+06	(81)	1.13E+07	(169)	15	1475	231	11.0	8.3	14.5
76	1.15E+07	(69)	6.67E+05	(4)	6	87	82	368.9	145.4	1338.6
77	4.75E+06	(38)	2.25E+06	(18)	8	295	137	47.8	26.8	89.2
78	1.33E+06	(20)	4.20E+06	(63)	15	550	139	7.3	4.1	12.2
79	1.47E+07	(176)	8.33E+05	(10)	12	109	67	384.3	209.9	801.7
80	1.00E+06	(12)	4.75E+06	(57)	12	622	165	4.9	2.3	9.1
81	2.63E+06	(63)	6.04E+06	(145)	24	791	133	9.9	7.2	13.4
82	1.62E+06	(73)	3.98E+06	(179)	45	521	79	9.3	7.0	12.5
83	4.80E+06	(24)	1.76E+07	(88)	5	2304	495	6.3	3.8	9.9
84	1.66E+07	(133)	6.63E+06	(53)	8	867	239	57.0	41.2	80.0
85	1.13E+06	(9)	1.38E+06	(11)	8	180	106	18.7	6.8	49.5
86	7.47E+06	(112)	2.67E+05	(4)	15	35	33	588.1	238.3	2032.6
87	5.04E+06	(121)	1.21E+06	(29)	24	158	58	94.2	62.7	146.8
88	1.30E+06	(26)	2.05E+06	(41)	20	268	84	14.5	8.5	24.2
89	1.25E+06	(15)	2.92E+06	(35)	12	382	129	9.8	5.0	18.4
90	7.75E+06	(31)	5.00E+05	(2)	4	65	83	322.0	89.4	2500.3
91	1.80E+07	(108)	1.33E+06	(8)	6	175	120	295.8	149.2	694.2
92	2.00E+06	(8)	3.25E+06	(13)	4	425	232	14.2	5.0	36.5
93	7.42E+06	(89)	2.04E+07	(245)	12	2672	351	8.3	6.4	10.8
94	1.00E+07	(160)	8.13E+05	(13)	16	106	58	272.1	157.7	518.6
95	2.90E+06	(29)	4.10E+06	(41)	10	537	167	16.2	9.7	26.6
96	1.00E+06	(5)	6.20E+06	(31)	5	812	290	3.8	1.1	9.6
97	1.93E+06	(27)	1.93E+06	(27)	14	252	97	22.8	12.9	40.4
98	3.21E+06	(77)	6.96E+06	(167)	24	911	144	10.6	7.9	14.0
99	8.50E+06	(34)	1.25E+07	(50)	4	1636	463	15.5	9.7	24.5

EFFECTIVE TRACK DENSITY FOR FLUENCE MONITOR (tracks/cm^2): 3.800E+05
RELATIVE ERROR (%): 1.57
EFFECTIVE URANIUM CONTENT OF MONITOR (ppm): 50.00
ZETA FACTOR AND STANDARD ERROR (yr cm^2): 119.60 5.40
SIZE OF COUNTER SQUARE (cm^2): 1.000E-06

------ GRAIN AGES IN ORIGINAL ORDER ------

Grain no.	**RhoS (cm^-2)**	**(Ns)**	**RhoI (cm^-2)**	**(Ni)**	**Squares**	**U**	**+/-2s**	**Grain Age**	**Age (Ma) --95% CI--**	
100	1.52E+07	(91)	2.72E+07	(163)	6	3575	570	12.7	9.7	16.7
101	8.17E+06	(49)	2.22E+07	(133)	6	2917	513	8.4	5.9	11.7
102	1.53E+07	(61)	2.60E+07	(104)	4	3421	678	13.3	9.5	18.5
103	1.11E+07	(111)	2.10E+06	(21)	10	276	119	118.3	74.3	198.8

EFFECTIVE TRACK DENSITY FOR FLUENCE MONITOR (tracks/cm^2): 3.810E+05
RELATIVE ERROR (%): 1.57
EFFECTIVE URANIUM CONTENT OF MONITOR (ppm): 50.00

ZETA FACTOR AND STANDARD ERROR (yr cm^2): 119.60 5.40
SIZE OF COUNTER SQUARE (cm^2): 1.000E-06

------ GRAIN AGES IN ORIGINAL ORDER ------

Grain no.	RhoS (cm^-2)	(Ns)	RhoI (cm^-2)	(Ni)	Squares	U+/-2s		Grain Age	Age (Ma) --95% CI--	
104	1.47E+07	(88)	3.12E+07	(187)	6	4090	611	10.7	8.2	14.1

Dataset B-5. Single-grain apatite fission-track ages of KLD samples

==================ZetaAge Program v. 4.8 (Brandon 8/13/02)===================

KLD_9 Kluane detrital UC03A- (Counted by Eva Enkelmann 28 Nov 2014)

EFFECTIVE TRACK DENSITY FOR FLUENCE MONITOR (tracks/cm^2): 7.856E+05
RELATIVE ERROR (%): 1.80
EFFECTIVE URANIUM CONTENT OF MONITOR (ppm): 15.00
ZETA FACTOR AND STANDARD ERROR (yr cm^2): 237.00 5.00
SIZE OF COUNTER SQUARE (cm^2): 1.000E-06

------ GRAIN AGES IN ORIGINAL ORDER ------

Grain no.	RhoS (cm^-2)	(Ns)	RhoI (cm^-2)	(Ni)	Squares	U+/-2s		Grain Age	Age (Ma) --95% CI--	
1	1.58E+06	(19)	1.42E+06	(17)	12	27	13	103.1	51.0	209.9
2	8.50E+05	(34)	4.75E+05	(19)	40	9	4	163.9	91.6	302.3
3	8.89E+05	(8)	2.22E+05	(2)	9	4	5	343.1	73.8	2860.6
4	2.00E+06	(24)	1.33E+06	(16)	12	25	13	137.7	70.7	275.6
5	1.00E+06	(30)	6.00E+05	(18)	30	11	5	152.8	83.1	289.3
6	1.24E+06	(26)	9.52E+05	(20)	21	18	8	119.7	64.6	224.9
7	1.04E+06	(26)	6.40E+05	(16)	25	12	6	149.0	77.6	295.3
8	1.08E+06	(43)	6.75E+05	(27)	40	13	5	146.3	88.8	245.1
9	1.07E+06	(15)	9.29E+05	(13)	14	18	10	106.4	47.5	241.0
10	7.00E+05	(14)	9.00E+05	(18)	20	17	8	72.2	33.2	152.4
11	9.05E+05	(19)	1.05E+06	(22)	21	20	8	80.0	41.0	154.0
12	7.60E+05	(38)	6.60E+05	(33)	50	13	4	106.2	65.0	174.2
13	2.56E+06	(64)	1.88E+06	(47)	25	36	10	125.4	84.9	186.5
14	7.08E+05	(17)	1.00E+06	(24)	24	19	8	65.8	33.1	126.9
15	5.00E+05	(15)	5.67E+05	(17)	30	11	5	81.7	38.0	172.7
16	1.37E+06	(41)	1.37E+06	(41)	30	26	8	92.4	58.5	145.7
17	9.58E+05	(23)	3.33E+05	(8)	24	6	4	258.9	114.4	657.9
18	4.50E+05	(18)	6.25E+05	(25)	40	12	5	66.9	34.3	126.8
19	6.60E+05	(33)	7.60E+05	(38)	50	15	5	80.4	48.9	131.2
20	1.22E+06	(11)	7.78E+05	(7)	9	15	11	143.5	51.5	430.7
21	9.50E+05	(19)	8.50E+05	(17)	20	16	8	103.1	51.0	209.9
22	1.05E+06	(22)	1.14E+06	(24)	21	22	9	84.8	45.4	157.1
23	2.35E+06	(47)	1.45E+06	(29)	20	28	10	148.8	92.2	244.2
24	6.33E+05	(19)	5.00E+05	(15)	30	10	5	116.6	56.5	244.9
25	1.50E+06	(45)	7.67E+05	(23)	30	15	6	179.0	106.9	308.3
26	3.67E+05	(11)	3.67E+05	(11)	30	7	4	92.4	36.5	232.7
27	8.67E+05	(13)	6.67E+05	(10)	15	13	8	119.5	48.8	301.4
28	3.67E+05	(11)	3.00E+05	(9)	30	6	4	112.4	42.7	303.6
29	1.21E+06	(29)	4.58E+05	(11)	24	9	5	238.7	117.8	523.2
30	6.33E+05	(19)	9.00E+05	(27)	30	17	7	65.3	34.3	121.3
31	2.50E+05	(5)	2.00E+05	(4)	20	4	4	114.5	25.0	561.5
32	7.75E+05	(31)	9.50E+05	(38)	40	18	6	75.6	45.5	124.3
33	1.65E+06	(33)	1.40E+06	(28)	20	27	10	108.7	63.9	186.0
34	2.33E+06	(35)	1.47E+06	(22)	15	28	12	146.0	83.8	260.0
35	1.08E+06	(43)	2.50E+05	(10)	40	5	3	383.7	194.9	837.3
36	1.08E+06	(26)	9.58E+05	(23)	24	18	8	104.3	57.4	190.4
37	7.25E+05	(29)	9.25E+05	(37)	40	18	6	72.6	43.1	121.0
38	1.67E+06	(25)	8.00E+05	(12)	15	15	9	189.8	93.1	410.7
39	1.04E+06	(26)	1.24E+06	(31)	25	24	8	77.7	44.3	134.7
40	8.52E+05	(23)	9.63E+05	(26)	27	18	7	81.9	44.7	148.6
41	1.08E+06	(43)	1.23E+06	(49)	40	23	7	81.2	52.7	124.6
42	9.00E+05	(45)	9.00E+05	(45)	50	17	5	92.4	59.8	142.6
43	3.75E+05	(6)	1.00E+06	(16)	16	19	9	35.4	11.2	93.3
44	1.50E+06	(30)	1.95E+06	(39)	20	37	12	71.3	42.8	117.4
45	4.00E+05	(16)	4.50E+05	(18)	40	9	4	82.3	39.3	169.8
46	1.57E+06	(33)	1.48E+06	(31)	21	28	10	98.3	58.5	165.4
47	1.65E+06	(33)	1.85E+06	(37)	20	35	12	82.5	50.1	135.2

48	7.33E+05	(22)	1.10E+06	(33)	30	21	7	61.9	34.3	108.9
49	1.00E+06	(9)	7.78E+05	(7)	9	15	11	118.0	39.5	367.8
50	9.64E+05	(27)	5.36E+05	(15)	28	10	5	164.6	85.4	330.6
51	1.19E+06	(19)	5.00E+05	(8)	16	10	7	214.9	91.7	559.3
52	1.75E+05	(7)	3.25E+05	(13)	40	6	3	50.5	16.9	133.9
53	1.50E+06	(45)	1.03E+06	(31)	30	20	7	133.5	83.0	217.5
54	4.64E+05	(13)	4.29E+05	(12)	28	8	5	100.0	42.2	237.6
55	9.25E+05	(37)	9.00E+05	(36)	40	17	6	95.0	58.5	154.2
56	6.00E+05	(30)	6.40E+05	(32)	50	12	4	86.7	51.0	146.8
57	2.27E+06	(34)	2.33E+06	(35)	15	45	15	89.8	54.4	147.8
58	6.67E+05	(10)	7.33E+05	(11)	15	14	8	84.2	32.1	216.0
59	1.05E+06	(21)	9.50E+05	(19)	20	18	8	102.0	52.4	199.4
60	5.33E+05	(16)	7.67E+05	(23)	30	15	6	64.6	31.9	126.9
61	5.00E+05	(20)	5.50E+05	(22)	40	11	4	84.1	43.6	160.7
62	1.00E+06	(15)	2.60E+06	(39)	15	50	16	35.9	18.3	66.2
63	7.62E+05	(16)	7.62E+05	(16)	21	15	7	92.4	43.4	196.0
64	2.56E+06	(23)	1.33E+06	(12)	9	25	14	174.9	84.6	382.3
65	1.14E+06	(24)	1.57E+06	(33)	21	30	10	67.5	38.1	117.2
66	1.89E+06	(17)	2.78E+06	(25)	9	53	21	63.2	32.0	121.0
67	2.25E+06	(9)	1.75E+06	(7)	4	33	24	118.0	39.5	367.8
68	6.00E+05	(30)	5.00E+05	(25)	50	10	4	110.6	63.1	195.4
69	3.20E+05	(8)	4.40E+05	(11)	25	8	5	67.7	23.6	182.3
70	6.50E+05	(13)	4.00E+05	(8)	20	8	5	148.4	57.8	408.1
71	3.00E+05	(12)	5.25E+05	(21)	40	10	4	53.3	23.8	112.3
72	1.44E+06	(13)	8.89E+05	(8)	9	17	12	148.4	57.8	408.1

KLD_13 Kluane detrital UC03A- (Counted by Eva Enkelmann 30 Nov 2014)

EFFECTIVE TRACK DENSITY FOR FLUENCE MONITOR (tracks/cm^2): 7.556E+05
RELATIVE ERROR (%): 1.80
EFFECTIVE URANIUM CONTENT OF MONITOR (ppm): 15.00
ZETA FACTOR AND STANDARD ERROR (yr cm^2): 237.00 5.00
SIZE OF COUNTER SQUARE (cm^2): 1.000E-06

------ GRAIN AGES IN ORIGINAL ORDER ------

Grain no.	**RhoS (cm^-2)**	**(Ns)**	**RhoI (cm^-2)**	**(Ni)**	**Squares**	**U+/-2s**		**Grain Age**	**Age (Ma) --95% CI--**	
1	4.50E+05	(45)	4.90E+05	(49)	100	10	3	81.7	53.3	124.8
2	1.29E+05	(9)	2.86E+05	(20)	70	6	3	40.6	16.1	92.0
3	6.00E+05	(15)	9.60E+05	(24)	25	19	8	55.9	27.2	110.3
4	7.14E+05	(10)	8.57E+05	(12)	14	17	10	74.4	28.8	185.9
5	2.20E+06	(44)	1.90E+06	(38)	20	38	12	102.8	65.2	162.6
6	1.79E+05	(5)	2.86E+05	(8)	28	6	4	56.4	14.4	191.3
7	1.47E+06	(44)	1.57E+06	(47)	30	31	9	83.3	54.0	128.2
8	1.60E+05	(8)	6.20E+05	(31)	50	12	4	23.4	9.2	51.2
9	1.28E+06	(23)	7.22E+05	(13)	18	14	8	155.7	76.4	332.1
10	3.50E+05	(14)	5.75E+05	(23)	40	11	5	54.5	25.9	109.7
11	1.33E+05	(4)	4.33E+05	(13)	30	9	5	28.2	6.5	88.6
12	2.86E+05	(20)	3.29E+05	(23)	70	7	3	77.5	40.4	146.7
13	3.44E+05	(11)	4.69E+05	(15)	32	9	5	65.6	27.2	151.4
14	5.80E+05	(29)	4.20E+05	(21)	50	8	4	122.2	67.7	224.4
15	9.60E+05	(48)	8.40E+05	(42)	50	17	5	101.5	65.8	157.0
16	4.50E+05	(18)	6.50E+05	(26)	40	13	5	61.9	31.9	116.6
17	3.60E+05	(18)	5.60E+05	(28)	50	11	4	57.5	29.9	107.0
18	2.20E+05	(11)	3.00E+05	(15)	50	6	3	65.6	27.2	151.4
19	7.00E+05	(35)	8.60E+05	(43)	50	17	5	72.5	45.1	115.7
20	4.40E+05	(22)	4.40E+05	(22)	50	9	4	88.9	47.1	167.5
21	8.33E+05	(25)	7.67E+05	(23)	30	15	6	96.5	52.7	177.2
22	2.33E+05	(7)	5.33E+05	(16)	30	11	5	39.6	13.6	100.0
23	2.57E+05	(9)	5.71E+05	(20)	35	11	5	40.6	16.1	92.0
24	1.42E+06	(17)	9.17E+05	(11)	12	18	11	136.2	60.8	319.1
25	2.03E+06	(61)	1.87E+06	(56)	30	37	10	96.8	66.3	141.5
26	2.22E+05	(4)	5.56E+05	(10)	18	11	7	36.6	8.2	123.1
27	2.86E+05	(6)	4.76E+05	(10)	21	9	6	54.1	16.0	161.2
28	2.25E+05	(9)	2.00E+05	(8)	40	4	3	99.7	34.4	293.5
29	1.06E+06	(53)	1.18E+06	(59)	50	23	6	80.0	54.1	117.7
30	5.50E+05	(11)	7.50E+05	(15)	20	15	8	65.6	27.2	151.4
31	2.86E+05	(6)	2.86E+05	(6)	21	6	4	88.9	23.9	326.7
32	1.94E+06	(68)	1.86E+06	(65)	35	37	9	93.0	65.2	132.6
33	3.40E+05	(17)	6.00E+05	(30)	50	12	4	50.8	26.2	94.4
34	1.13E+06	(34)	1.10E+06	(33)	30	22	8	91.6	55.1	152.1
35	1.28E+06	(51)	1.45E+06	(58)	40	29	8	78.3	52.7	115.9
36	3.75E+05	(15)	5.25E+05	(21)	40	10	5	63.8	30.6	129.0
37	2.33E+05	(14)	4.50E+05	(27)	60	9	3	46.5	22.4	91.2
38	2.00E+05	(4)	4.00E+05	(8)	20	8	5	45.5	9.9	165.1
39	3.50E+05	(14)	7.00E+05	(28)	40	14	5	44.9	21.7	87.4
40	1.75E+06	(14)	1.25E+06	(10)	8	25	15	123.6	51.5	308.2
41	4.00E+05	(24)	6.00E+05	(36)	60	12	4	59.6	33.9	102.2
42	1.50E+05	(6)	5.75E+05	(23)	40	11	5	23.8	7.8	58.8
43	1.81E+06	(38)	1.43E+06	(30)	21	28	10	112.3	68.0	187.1
44	2.80E+05	(14)	4.00E+05	(20)	50	8	4	62.6	29.2	129.3
45	3.60E+05	(18)	4.40E+05	(22)	50	9	4	73.0	36.9	141.7
46	5.25E+05	(21)	5.25E+05	(21)	40	10	5	88.9	46.3	170.2
47	3.13E+05	(5)	5.63E+05	(9)	16	11	7	50.2	13.1	163.3
48	1.00E+05	(4)	2.75E+05	(11)	40	5	3	33.3	7.6	109.0
49	5.83E+05	(7)	4.17E+05	(5)	12	8	7	123.1	34.1	482.6
50	8.33E+05	(10)	5.00E+05	(6)	12	10	8	146.0	48.9	481.5
51	1.33E+05	(4)	3.00E+05	(9)	30	6	4	40.5	8.9	141.1

52	7.78E+05	(	7)	1.00E+06	(	9)	9	20	13	69.6	22.0	206.9
53	1.75E+05	(	7)	3.25E+05	(	13)	40	6	4	48.5	16.3	128.8
54	2.34E+06	(	117)	5.80E+05	(	29)	50	12	4	350.0	234.1	540.4
55	4.29E+05	(	15)	2.86E+05	(	10)	35	6	4	132.2	56.1	326.2
56	1.10E+06	(	33)	7.67E+05	(	23)	30	15	6	126.9	72.7	225.4
57	1.17E+06	(	21)	1.39E+06	(	25)	18	28	11	74.9	39.9	138.6
58	4.00E+05	(	16)	9.25E+05	(	37)	40	18	6	38.8	20.1	71.0
59	1.19E+06	(	25)	4.29E+05	(	9)	21	9	6	241.3	111.2	579.2
60	1.00E+06	(	40)	1.13E+06	(	45)	40	22	7	79.1	50.4	123.6
61	2.67E+05	(	8)	3.67E+05	(	11)	30	7	4	65.1	22.7	175.5
62	6.33E+05	(	19)	4.67E+05	(	14)	30	9	5	120.0	57.5	257.0
63	1.30E+06	(	39)	1.03E+06	(	31)	30	21	7	111.6	68.0	184.3
64	1.56E+05	(	5)	6.88E+05	(	22)	32	14	6	20.8	6.0	54.9
65	2.67E+05	(	4)	4.00E+05	(	6)	15	8	6	60.2	12.4	247.1
66	2.00E+05	(	5)	8.00E+05	(	20)	25	16	7	22.9	6.6	61.2
67	5.75E+05	(	23)	7.00E+05	(	28)	40	14	5	73.2	40.3	131.2
68	9.50E+05	(	38)	8.50E+05	(	34)	40	17	6	99.3	61.0	162.1
69	1.50E+05	(	6)	3.75E+05	(	15)	40	7	4	36.3	11.4	97.0
70	1.27E+06	(	38)	1.83E+06	(	55)	30	36	10	61.7	39.6	94.7
71	2.47E+06	(	74)	2.03E+06	(	61)	30	40	10	107.7	75.7	153.5
72	9.67E+05	(	29)	1.03E+06	(	31)	30	21	7	83.3	48.5	142.3
73	1.50E+06	(	18)	6.67E+05	(	8)	12	13	9	196.2	82.7	514.8
74	5.83E+05	(	7)	7.50E+05	(	9)	12	15	10	69.6	22.0	206.9
75	4.80E+05	(	24)	6.20E+05	(	31)	50	12	4	69.1	38.8	121.0
76	3.40E+05	(	17)	5.00E+05	(	25)	50	10	4	60.8	30.8	116.4
77	3.25E+05	(	13)	4.75E+05	(	19)	40	9	4	61.2	27.7	129.6
78	4.58E+05	(	11)	7.50E+05	(	18)	24	15	7	54.8	23.3	121.3
79	7.50E+05	(	12)	1.25E+05	(	2)	16	2	3	486.3	118.4	3669.5
80	2.03E+06	(	61)	1.53E+06	(	46)	30	30	9	117.6	79.0	176.0
81	7.25E+05	(	29)	9.75E+05	(	39)	40	19	6	66.3	39.5	109.7
82	5.00E+05	(	20)	6.50E+05	(	26)	40	13	5	68.6	36.3	127.2
83	1.25E+06	(	20)	7.50E+05	(	12)	16	15	8	146.7	69.0	326.7
84	3.50E+05	(	14)	5.00E+05	(	20)	40	10	4	62.6	29.2	129.3
85	1.73E+06	(	52)	2.17E+06	(	65)	30	43	11	71.3	48.5	104.1
86	1.07E+06	(	32)	1.37E+06	(	41)	30	27	8	69.6	42.4	112.9
87	1.20E+06	(	36)	1.10E+06	(	33)	30	22	8	96.9	58.8	159.9
88	3.33E+06	(	40)	2.92E+06	(	35)	12	58	20	101.5	63.0	164.1
89	8.80E+05	(	22)	1.12E+06	(	28)	25	22	8	70.1	38.2	126.4
90	4.40E+05	(	22)	4.20E+05	(	21)	50	8	4	93.1	49.0	177.1
91	2.00E+05	(	7)	3.71E+05	(	13)	35	7	4	48.5	16.3	128.8
92	1.08E+06	(	13)	9.17E+05	(	11)	12	18	11	104.7	43.6	255.9
93	5.50E+05	(	22)	7.25E+05	(	29)	40	14	5	67.7	37.0	121.4
94	3.75E+05	(	15)	4.50E+05	(	18)	40	9	4	74.3	34.9	155.1
95	5.50E+05	(	22)	7.25E+05	(	29)	40	14	5	67.7	37.0	121.4
96	3.75E+05	(	6)	1.00E+06	(	16)	16	20	10	34.1	10.7	89.8
97	2.60E+05	(	26)	4.50E+05	(	45)	100	9	3	51.7	30.5	85.2
98	6.25E+05	(	25)	4.25E+05	(	17)	40	8	4	130.0	67.9	255.0
99	8.00E+05	(	24)	1.57E+06	(	47)	30	31	9	45.7	26.7	76.0
100	1.33E+05	(	4)	1.67E+05	(	5)	30	3	3	71.8	14.2	324.7
101	4.50E+05	(	18)	6.25E+05	(	25)	40	12	5	64.3	33.0	122.0
102	2.20E+05	(	11)	3.80E+05	(	19)	50	8	3	52.0	22.2	113.7
103	5.75E+05	(	23)	7.00E+05	(	28)	40	14	5	73.2	40.3	131.2
104	9.00E+05	(	9)	1.20E+06	(	12)	10	24	14	67.1	24.9	171.5

KLD_18 Kluane detrital UC03A- (Counted by Eva Enkelmann 24 Nov 2014)

EFFECTIVE TRACK DENSITY FOR FLUENCE MONITOR (tracks/cm^2): 7.456E+05
RELATIVE ERROR (%): 1.80
EFFECTIVE URANIUM CONTENT OF MONITOR (ppm): 15.00
ZETA FACTOR AND STANDARD ERROR (yr cm^2): 237.00 5.00
SIZE OF COUNTER SQUARE (cm^2): 1.000E-06

------ GRAIN AGES IN ORIGINAL ORDER ------

Grain no.	RhoS (cm^-2)	(Ns)	RhoI (cm^-2)	(Ni)	Squares	U	+/-2s	Grain Age	--95% CI--	
1	1.79E+06	(43)	8.33E+05	(20)	24	17	7	186.4	108.3	332.5
2	1.75E+05	(7)	4.25E+05	(17)	40	9	4	36.8	12.7	91.7
3	2.00E+05	(10)	8.00E+05	(40)	50	16	5	22.3	9.8	44.8
4	3.00E+04	(3)	1.90E+05	(19)	100	4	2	14.6	2.6	47.3
5	4.00E+05	(12)	9.33E+05	(28)	30	19	7	38.1	17.5	76.5
6	2.23E+06	(67)	1.33E+06	(40)	30	27	8	146.1	97.7	221.3
7	5.00E+05	(25)	5.80E+05	(29)	50	12	4	75.8	42.6	133.5
8	3.75E+05	(15)	7.50E+05	(30)	40	15	5	44.3	22.0	84.3
9	3.89E+05	(7)	2.78E+05	(5)	18	6	5	121.5	33.7	476.5
10	5.00E+06	(30)	4.33E+06	(26)	6	87	34	101.1	57.9	177.2
11	4.67E+05	(14)	4.67E+05	(14)	30	9	5	87.8	38.9	197.1
12	9.38E+05	(15)	9.38E+05	(15)	16	19	10	87.8	40.1	191.3
13	1.50E+05	(15)	5.60E+05	(56)	100	11	3	23.8	12.4	42.3
14	4.20E+05	(21)	1.04E+06	(52)	50	21	6	35.8	20.4	60.1
15	1.75E+05	(7)	1.00E+06	(40)	40	20	6	15.7	5.8	34.8
16	5.00E+05	(15)	9.00E+05	(27)	30	18	7	49.1	24.2	95.0
17	5.00E+05	(10)	6.00E+05	(12)	20	12	7	73.4	28.4	183.5
18	2.25E+05	(9)	5.50E+05	(22)	40	11	5	36.4	14.6	81.2
19	6.60E+05	(33)	1.66E+06	(83)	50	33	7	35.1	22.7	53.1
20	6.00E+04	(6)	1.90E+05	(19)	100	4	2	28.4	9.1	72.3
21	6.00E+04	(6)	1.40E+05	(14)	100	3	1	38.3	11.9	104.1
22	1.50E+06	(27)	4.44E+05	(8)	18	9	6	287.5	130.3	718.5
23	6.60E+05	(33)	7.40E+05	(37)	50	15	5	78.4	47.5	128.4
24	4.70E+05	(47)	2.10E+05	(21)	100	4	2	193.9	114.7	339.6
25	4.20E+05	(21)	7.80E+05	(39)	50	16	5	47.6	26.5	82.5
26	4.44E+05	(4)	7.78E+05	(7)	9	16	11	51.1	10.8	195.7
27	2.40E+05	(12)	4.00E+05	(20)	50	8	4	53.1	23.6	113.0
28	2.67E+05	(8)	5.67E+05	(17)	30	11	5	41.9	15.5	101.0
29	4.00E+04	(1)	5.60E+05	(14)	25	11	6	7.1	0.1	41.4
30	2.00E+05	(5)	4.40E+05	(11)	25	9	5	40.7	10.9	124.3
31	1.78E+06	(16)	4.44E+05	(4)	9	9	8	334.4	112.9	1310.7
32	2.20E+05	(11)	6.00E+05	(30)	50	12	4	32.6	14.6	66.2
33	2.80E+05	(7)	1.60E+05	(4)	25	3	3	150.3	39.2	683.1

KLD_20 Kluane detrital UC03A- (Counted by Eva Enkelmann 28 Nov 2014)

EFFECTIVE TRACK DENSITY FOR FLUENCE MONITOR (tracks/cm^2): 7.356E+05
RELATIVE ERROR (%): 1.80
EFFECTIVE URANIUM CONTENT OF MONITOR (ppm): 15.00
ZETA FACTOR AND STANDARD ERROR (yr cm^2): 237.00 5.00
SIZE OF COUNTER SQUARE (cm^2): 1.000E-06

------ GRAIN AGES IN ORIGINAL ORDER ------

Grain no.	**RhoS (cm^-2)**	**(Ns)**	**RhoI (cm^-2)**	**(Ni)**	**Squares**	**U+/-2s**		**Grain Age**	**Age (Ma) --95% CI--**	
1	6.00E+05	(18)	1.00E+06	(30)	30	20	7	52.3	27.4	96.3
2	1.13E+06	(34)	9.33E+05	(28)	30	19	7	104.9	61.9	178.9
3	9.17E+05	(11)	1.08E+06	(13)	12	22	12	73.5	29.8	176.2
4	2.80E+05	(7)	3.60E+05	(9)	25	7	5	67.8	21.4	201.6
5	1.73E+06	(52)	1.43E+06	(43)	30	29	9	104.5	68.5	160.0
6	3.50E+05	(14)	3.75E+05	(15)	40	8	4	80.9	36.2	178.5
7	4.75E+05	(19)	5.75E+05	(23)	40	12	5	71.7	36.9	136.9
8	3.00E+04	(3)	3.70E+05	(37)	100	8	2	7.4	1.4	22.3
9	7.50E+05	(30)	6.75E+05	(27)	40	14	5	96.1	55.3	167.4
10	1.00E+05	(2)	9.50E+05	(19)	20	19	9	9.8	1.0	38.0
11	8.89E+05	(8)	6.67E+05	(6)	9	14	11	114.4	35.2	394.3
12	2.33E+06	(21)	7.78E+05	(7)	9	16	12	252.5	106.1	690.4
13	2.07E+06	(62)	3.00E+06	(90)	30	61	13	59.8	42.5	83.5
14	2.75E+06	(44)	1.13E+06	(18)	16	23	11	208.5	119.4	380.8
15	2.00E+06	(12)	1.67E+06	(10)	6	34	21	103.5	41.3	265.0
16	1.20E+05	(3)	1.20E+05	(3)	25	2	3	86.6	11.7	620.3
17	4.00E+05	(12)	6.67E+05	(20)	30	14	6	52.4	23.2	111.5
18	1.33E+06	(16)	1.25E+06	(15)	12	25	13	92.3	42.9	199.0
19	5.80E+05	(29)	8.80E+05	(44)	50	18	5	57.3	34.5	93.4
20	1.57E+06	(47)	1.23E+06	(37)	30	25	8	109.7	70.0	173.1
21	3.67E+05	(11)	1.53E+06	(46)	30	31	9	21.0	9.7	40.8
22	5.67E+05	(17)	2.00E+05	(6)	30	4	3	238.3	92.2	723.4
23	7.00E+05	(14)	4.50E+05	(9)	20	9	6	133.3	54.4	346.0
24	1.55E+06	(62)	1.65E+06	(66)	40	34	8	81.4	56.6	116.8
25	1.75E+06	(70)	1.88E+06	(75)	40	38	9	80.9	57.5	113.5
26	5.60E+05	(28)	9.20E+05	(46)	50	19	6	53.0	31.8	86.3
27	1.03E+06	(31)	1.47E+06	(44)	30	30	9	61.2	37.3	98.9
28	3.20E+05	(16)	5.00E+05	(25)	50	10	4	55.8	27.7	107.9
29	2.50E+06	(15)	1.67E+06	(10)	6	34	21	128.8	54.7	317.8
30	2.67E+06	(16)	1.50E+06	(9)	6	31	20	152.0	64.1	386.4
31	3.25E+05	(13)	6.75E+05	(27)	40	14	5	42.1	19.8	83.7
32	1.97E+06	(59)	2.57E+06	(77)	30	52	12	66.5	46.5	94.5
33	3.25E+05	(13)	1.25E+06	(50)	40	25	7	22.8	11.3	42.3
34	4.44E+05	(8)	6.11E+05	(11)	18	12	7	63.4	22.1	170.9
35	3.25E+05	(13)	1.43E+06	(57)	40	29	8	20.0	10.0	36.7
36	1.00E+06	(20)	9.50E+05	(19)	20	19	9	91.1	46.3	179.4
37	1.50E+05	(6)	7.25E+05	(29)	40	15	5	18.4	6.1	44.1
38	8.00E+04	(4)	1.06E+06	(53)	50	22	6	6.8	1.7	17.9
39	3.00E+05	(12)	2.50E+05	(10)	40	5	3	103.5	41.3	265.0
40	2.25E+05	(9)	1.75E+05	(7)	40	4	3	110.6	37.0	345.0
41	2.00E+05	(8)	3.50E+05	(14)	40	7	4	50.0	18.1	126.1
42	6.25E+05	(25)	1.03E+06	(41)	40	21	7	53.1	30.9	89.0
43	1.96E+06	(49)	1.92E+06	(48)	25	39	11	88.4	58.2	134.2
44	6.25E+05	(10)	6.88E+05	(11)	16	14	8	78.9	30.1	202.5
45	3.75E+05	(15)	3.75E+05	(15)	40	8	4	86.6	39.6	188.7
46	1.11E+06	(31)	1.04E+06	(29)	28	21	8	92.5	54.0	158.5
47	4.64E+05	(13)	8.57E+05	(24)	28	17	7	47.3	22.0	95.9
48	2.25E+05	(9)	4.25E+05	(17)	40	9	4	46.4	18.1	108.6
49	1.08E+06	(13)	6.67E+05	(8)	12	14	9	139.1	54.1	382.9
50	3.33E+05	(10)	4.00E+05	(12)	30	8	5	72.4	28.0	181.0
51	1.04E+06	(26)	1.64E+06	(41)	25	33	10	55.2	32.3	92.0

52	1.33E+06	(	20)	1.20E+06	(	18)	15	24	11	96.0	48.4	191.5
53	3.00E+05	(	6)	6.00E+05	(	12)	20	12	7	44.0	13.4	124.4
54	8.25E+05	(	33)	4.50E+05	(	18)	40	9	4	157.2	86.7	294.9
55	2.25E+05	(	9)	3.25E+05	(	13)	40	7	4	60.4	22.7	151.0
56	4.50E+05	(	9)	6.50E+05	(	13)	20	13	7	60.4	22.7	151.0
57	6.00E+05	(	12)	1.30E+06	(	26)	20	27	10	40.4	18.5	82.2
58	2.93E+06	(	44)	2.07E+06	(	31)	15	42	15	122.4	75.8	199.8
59	1.95E+06	(	39)	1.55E+06	(	31)	20	32	11	108.6	66.2	179.5
60	6.00E+05	(	18)	9.00E+05	(	27)	30	18	7	58.0	30.0	108.7
61	8.50E+05	(	34)	1.13E+06	(	45)	40	23	7	65.6	40.7	104.5
62	3.33E+05	(	6)	6.67E+05	(	12)	18	14	8	44.0	13.4	124.4
63	4.38E+05	(	7)	1.88E+05	(	3)	16	4	4	194.6	46.2	1116.9
64	2.75E+05	(	11)	9.00E+05	(	36)	40	18	6	26.9	12.2	53.3
65	1.60E+05	(	8)	5.20E+05	(	26)	50	11	4	27.1	10.5	60.8
66	3.50E+05	(	14)	4.75E+05	(	19)	40	10	4	64.1	29.7	133.9
67	6.00E+05	(	18)	9.33E+05	(	28)	30	19	7	56.0	29.1	104.2
68	8.40E+05	(	21)	7.20E+05	(	18)	25	15	7	100.8	51.3	199.6
69	5.60E+05	(	14)	3.20E+05	(	8)	25	7	4	149.5	59.4	406.9
70	1.00E+06	(	30)	7.33E+05	(	22)	30	15	6	117.6	65.9	213.0
71	7.67E+05	(	23)	9.33E+05	(	28)	30	19	7	71.3	39.2	127.8
72	1.33E+06	(	32)	1.58E+06	(	38)	24	32	10	73.1	44.2	119.7
73	6.67E+04	(	2)	5.00E+05	(	15)	30	10	5	12.4	1.3	49.8
74	1.60E+06	(	64)	1.35E+06	(	54)	40	28	8	102.4	70.3	149.8
75	1.20E+06	(	12)	1.30E+06	(	13)	10	27	14	80.0	33.4	188.7
76	1.25E+05	(	5)	5.50E+05	(	22)	40	11	5	20.3	5.9	53.4
77	2.43E+06	(	97)	1.93E+06	(	77)	40	39	9	108.8	79.9	148.7
78	3.60E+05	(	18)	4.40E+05	(	22)	50	9	4	71.0	35.9	138.0
79	3.07E+06	(	46)	2.07E+06	(	31)	15	42	15	127.8	79.7	207.9
80	6.67E+05	(	14)	5.71E+05	(	12)	21	12	7	100.7	43.5	236.5
81	1.07E+06	(	16)	1.13E+06	(	17)	15	23	11	81.6	38.6	170.6
82	3.50E+05	(	7)	1.50E+05	(	3)	20	3	3	194.6	46.2	1116.9
83	1.67E+05	(	5)	5.67E+05	(	17)	30	12	6	26.2	7.4	72.1
84	9.00E+05	(	27)	8.00E+05	(	24)	30	16	7	97.3	54.2	175.4
85	2.14E+05	(	3)	1.14E+06	(	16)	14	23	12	17.0	3.0	56.9
86	1.31E+06	(	21)	1.56E+06	(	25)	16	32	13	72.9	38.8	135.0
87	2.78E+05	(	10)	1.94E+05	(	7)	36	4	3	122.5	42.6	374.6
88	3.00E+05	(	15)	2.80E+05	(	14)	50	6	3	92.7	41.9	205.7
89	1.50E+05	(	6)	5.25E+05	(	21)	40	11	5	25.3	8.2	63.5
90	1.13E+06	(	17)	1.73E+06	(	26)	15	35	14	56.9	28.9	108.3
91	2.20E+05	(	11)	4.00E+05	(	20)	50	8	4	48.1	20.7	104.2
92	1.50E+05	(	3)	1.10E+06	(	22)	20	22	9	12.4	2.3	39.5
93	2.75E+06	(	44)	3.25E+06	(	52)	16	66	18	73.4	48.0	111.6
94	4.00E+05	(	8)	6.50E+05	(	13)	20	13	7	53.8	19.2	138.3
95	7.14E+05	(	15)	7.62E+05	(	16)	21	16	8	81.3	37.5	174.3

KLD_23 Kluane detrital UC03A- (Counted by Eva Enkelmann 25 Nov 2014)

EFFECTIVE TRACK DENSITY FOR FLUENCE MONITOR (tracks/cm^2): 7.256E+05

RELATIVE ERROR (%): 1.80

EFFECTIVE URANIUM CONTENT OF MONITOR (ppm): 15.00

ZETA FACTOR AND STANDARD ERROR (yr cm^2): 237.00 5.00

SIZE OF COUNTER SQUARE (cm^2): 1.000E-06

------ GRAIN AGES IN ORIGINAL ORDER ------

Grain no.	**RhoS (cm^-2)**	**(Ns)**	**RhoI (cm^-2)**	**(Ni)**	**Squares**	**U+/-2s**		**Grain Age**	**Age (Ma) --95% CI--**	
1	8.00E+04	(4)	3.40E+05	(17)	50	7	3	20.8	4.9	61.8
2	3.25E+05	(13)	1.20E+06	(48)	40	25	7	23.5	11.6	43.6
3	2.00E+05	(4)	1.45E+06	(29)	20	30	11	12.3	3.0	33.7
4	9.50E+05	(19)	1.80E+06	(36)	20	37	12	45.4	24.5	80.8
5	0.00E+00	(0)	4.33E+05	(13)	30	9	5	4.7	0.2	28.2
6	3.33E+05	(5)	2.13E+06	(32)	15	44	16	13.8	4.1	34.7
7	8.33E+04	(2)	4.58E+05	(11)	24	9	6	16.6	1.7	71.3
8	2.25E+05	(9)	8.25E+05	(33)	40	17	6	23.7	9.9	50.0
9	2.92E+05	(7)	2.83E+06	(68)	24	59	14	9.0	3.4	19.2
10	4.64E+05	(13)	1.50E+06	(42)	28	31	10	26.8	13.1	50.4
11	7.78E+05	(7)	2.78E+06	(25)	9	57	23	24.4	8.8	57.1
12	6.00E+04	(3)	8.20E+05	(41)	50	17	5	6.6	1.2	19.7
13	6.00E+04	(3)	6.40E+05	(32)	50	13	5	8.4	1.6	25.7
14	4.00E+05	(10)	2.84E+06	(71)	25	59	14	12.3	5.6	23.6
15	2.50E+05	(7)	6.79E+05	(19)	28	14	6	32.1	11.2	78.3
16	5.00E+04	(1)	1.35E+06	(27)	20	28	11	3.6	0.1	19.3
17	3.67E+05	(11)	1.03E+06	(31)	30	21	8	30.7	13.8	62.1
18	2.00E+05	(8)	1.30E+06	(52)	40	27	7	13.4	5.4	28.0
19	4.17E+05	(25)	3.73E+06	(224)	60	77	11	9.6	6.1	14.6
20	1.00E+05	(3)	8.00E+05	(24)	30	17	7	11.2	2.1	35.3
21	2.75E+06	(22)	1.75E+06	(14)	8	36	19	133.2	65.7	279.7
22	1.25E+05	(5)	2.08E+06	(83)	40	43	10	5.3	1.6	12.6
23	4.06E+05	(13)	1.22E+06	(39)	32	25	8	28.8	14.0	54.7
24	3.33E+05	(5)	2.13E+06	(32)	15	44	16	13.8	4.1	34.7
25	6.50E+05	(13)	1.15E+06	(23)	20	24	10	48.7	22.6	99.4
26	1.33E+06	(20)	3.67E+06	(55)	15	76	21	31.4	17.7	52.9
27	5.00E+04	(2)	4.50E+05	(18)	40	9	4	10.2	1.1	39.8
28	3.33E+04	(2)	6.17E+05	(37)	60	13	4	5.0	0.5	18.0
29	2.00E+05	(8)	2.15E+06	(86)	40	44	10	8.1	3.3	16.5
30	3.00E+05	(12)	7.50E+05	(30)	40	16	6	34.6	16.0	68.9
31	6.75E+05	(27)	8.00E+05	(32)	40	17	6	72.2	41.6	124.0
32	4.38E+05	(7)	1.13E+06	(18)	16	23	11	33.8	11.8	83.4
33	1.20E+05	(3)	2.56E+06	(64)	25	53	13	4.2	0.8	12.3
34	1.40E+05	(7)	9.80E+05	(49)	50	20	6	12.5	4.7	27.2
35	5.75E+05	(23)	2.50E+06	(100)	40	52	10	19.9	12.0	31.3
36	6.67E+04	(2)	3.00E+05	(9)	30	6	4	20.2	2.0	91.7
37	1.57E+05	(11)	1.26E+06	(88)	70	26	6	10.9	5.2	20.2
38	4.64E+05	(13)	1.29E+06	(36)	28	27	9	31.2	15.1	59.8
39	3.93E+05	(11)	1.82E+06	(51)	28	38	11	18.7	8.7	36.0
40	2.00E+05	(6)	2.30E+06	(69)	30	48	12	7.7	2.7	17.1
41	4.64E+05	(13)	1.82E+06	(51)	28	38	11	22.1	10.9	40.8
42	8.00E+04	(2)	1.20E+06	(30)	25	25	9	6.1	0.7	22.6
43	3.75E+05	(15)	9.25E+05	(37)	40	19	6	35.0	17.7	64.8
44	1.60E+05	(8)	6.60E+05	(33)	50	14	5	21.1	8.3	45.9
45	4.40E+05	(22)	9.60E+05	(48)	50	20	6	39.5	22.6	66.3
46	8.75E+05	(14)	6.88E+05	(11)	16	14	8	108.2	45.9	261.2
47	5.00E+05	(12)	2.54E+06	(61)	24	53	14	17.1	8.3	31.7
48	1.83E+05	(11)	7.50E+05	(45)	60	16	5	21.2	9.8	41.2
49	3.75E+05	(15)	2.80E+06	(112)	40	58	11	11.6	6.2	19.8
50	2.67E+05	(8)	1.80E+06	(54)	30	37	10	12.9	5.2	26.9
51	1.00E+05	(2)	1.40E+06	(28)	20	29	11	6.6	0.7	24.3

52	1.90E+05	(8)	2.45E+06	(103)	42	51	10	6.8	2.8	13.7
53	1.04E+06	(26)	4.96E+06	(124)	25	103	19	18.1	11.3	27.7
54	1.00E+05	(4)	1.73E+06	(69)	40	36	9	5.2	1.3	13.4
55	6.00E+05	(18)	3.37E+06	(101)	30	70	14	15.4	8.7	25.5
56	6.75E+05	(27)	9.25E+05	(37)	40	19	6	62.5	36.6	105.2
57	5.00E+04	(2)	3.50E+05	(14)	40	7	4	13.1	1.4	53.3
58	6.33E+05	(19)	1.53E+06	(46)	30	32	9	35.6	19.6	61.6
59	1.00E+05	(3)	9.00E+05	(27)	30	19	7	10.0	1.9	31.0
60	4.40E+05	(22)	3.84E+06	(192)	50	79	12	9.9	6.0	15.4
61	2.75E+05	(11)	1.00E+06	(40)	40	21	7	23.9	10.9	46.8
62	3.75E+05	(15)	1.28E+06	(51)	40	26	7	25.4	13.2	45.6
63	3.33E+05	(8)	1.92E+06	(46)	24	40	12	15.2	6.1	32.0
64	1.33E+05	(2)	3.33E+05	(5)	15	7	6	35.8	3.3	206.8
65	3.33E+04	(2)	6.83E+05	(41)	60	14	4	4.5	0.5	16.1
66	4.33E+05	(13)	8.33E+05	(25)	30	17	7	44.8	21.0	90.2
67	5.50E+05	(22)	1.23E+06	(49)	40	25	7	38.7	22.2	64.8
68	8.33E+04	(2)	1.04E+06	(25)	24	22	9	7.4	0.8	27.6
69	4.00E+05	(12)	3.73E+06	(112)	30	77	15	9.3	4.6	16.7
70	3.00E+05	(12)	2.78E+06	(111)	40	57	11	9.4	4.7	16.9
71	6.25E+04	(1)	2.50E+05	(4)	16	5	5	23.7	0.4	213.7
72	0.00E+00	(0)	3.50E+05	(7)	20	7	5	8.9	0.3	59.4
73	2.50E+05	(6)	1.58E+06	(38)	24	33	11	13.9	4.7	32.3
74	1.43E+06	(57)	2.93E+06	(117)	40	60	11	41.8	29.8	57.8
75	3.33E+04	(1)	1.13E+06	(34)	30	23	8	2.9	0.1	15.1
76	4.00E+04	(2)	2.40E+05	(12)	50	5	3	15.2	1.6	64.1
77	6.67E+04	(2)	7.67E+05	(23)	30	16	7	8.0	0.9	30.2
78	4.00E+04	(2)	7.40E+05	(37)	50	15	5	5.0	0.5	18.0
79	2.38E+05	(10)	1.55E+06	(65)	42	32	8	13.4	6.1	25.9
80	4.25E+05	(17)	2.93E+06	(117)	40	60	11	12.6	7.0	20.9
81	5.00E+04	(4)	3.00E+05	(24)	80	6	3	14.8	3.6	41.6
82	3.21E+05	(9)	1.07E+06	(30)	28	22	8	26.1	10.8	55.6
83	1.80E+05	(9)	4.20E+05	(21)	50	9	4	37.1	14.8	83.5
84	4.00E+05	(8)	1.60E+06	(32)	20	33	12	21.8	8.5	47.5
85	1.02E+05	(5)	1.37E+06	(67)	49	28	7	6.6	2.0	15.7
86	5.00E+05	(18)	1.61E+06	(58)	36	33	9	26.8	14.8	45.8
87	5.50E+05	(22)	4.50E+05	(18)	40	9	4	104.1	53.5	204.8
88	4.64E+05	(13)	2.46E+06	(69)	28	51	12	16.3	8.2	29.5
89	1.33E+05	(4)	5.33E+05	(16)	30	11	5	22.1	5.2	66.4
90	3.33E+04	(2)	9.00E+05	(54)	60	19	5	3.4	0.4	12.1
91	6.67E+04	(2)	2.33E+05	(7)	30	5	4	25.8	2.5	127.8
92	8.33E+04	(5)	9.33E+05	(56)	60	19	5	7.9	2.4	19.0
93	1.23E+06	(49)	1.38E+06	(55)	40	28	8	76.2	50.8	113.9
94	4.33E+05	(13)	2.43E+06	(73)	30	50	12	15.5	7.8	27.8
95	8.25E+05	(33)	1.63E+06	(65)	40	34	8	43.6	27.7	67.1
96	4.40E+05	(22)	7.40E+05	(37)	50	15	5	51.1	28.6	88.5
97	8.00E+04	(2)	4.80E+05	(12)	25	10	6	15.2	1.6	64.1
98	4.83E+05	(29)	1.07E+06	(64)	60	22	6	39.0	24.1	61.1
99	1.88E+05	(15)	3.31E+06	(265)	80	68	9	4.9	2.7	8.2
100	3.75E+05	(15)	2.25E+06	(90)	40	47	10	14.4	7.7	24.9
101	4.00E+05	(8)	7.50E+05	(15)	20	16	8	46.1	16.8	114.3
102	1.00E+05	(4)	2.75E+05	(11)	40	6	3	32.0	7.3	104.7
103	3.50E+05	(14)	1.88E+06	(75)	40	39	9	16.2	8.4	28.6
104	2.60E+05	(13)	2.32E+06	(116)	50	48	9	9.7	5.0	17.1
105	1.96E+06	(49)	3.72E+06	(93)	25	77	16	45.2	31.2	64.5

KLD_26 Kluane detrital UC03A- (Counted by Eva Enkelmann 24 Nov 2014)

EFFECTIVE TRACK DENSITY FOR FLUENCE MONITOR (tracks/cm^2): 7.056E+05

RELATIVE ERROR (%): 1.80

EFFECTIVE URANIUM CONTENT OF MONITOR (ppm): 15.00

ZETA FACTOR AND STANDARD ERROR (yr cm^2): 237.00 5.00

SIZE OF COUNTER SQUARE (cm^2): 1.000E-06

------ GRAIN AGES IN ORIGINAL ORDER ------

Grain no.	RhoS (cm^-2)	(Ns)	RhoI (cm^-2)	(Ni)	Squares	U+/-2s		Grain Age	Age (Ma) --95% CI--	
1	7.50E+04	(3)	4.25E+05	(17)	40	9	4	15.4	2.8	50.9
2	1.00E+05	(5)	2.60E+05	(13)	50	6	3	32.7	9.0	95.5
3	8.33E+04	(2)	6.67E+05	(16)	24	14	7	11.1	1.2	44.3
4	3.00E+04	(3)	2.30E+05	(23)	100	5	2	11.4	2.1	36.0
5	2.00E+04	(2)	8.00E+04	(8)	100	2	1	22.1	2.2	104.0
6	4.00E+04	(2)	6.00E+04	(3)	50	1	1	56.8	4.7	469.3
7	1.00E+05	(5)	2.40E+05	(12)	50	5	3	35.4	9.6	105.5
8	4.00E+04	(2)	4.00E+04	(2)	50	1	1	83.1	6.1	1061.5
9	0.00E+00	(0)	1.60E+05	(8)	50	3	2	7.6	0.3	48.8
10	1.29E+05	(9)	1.86E+05	(13)	70	4	2	57.9	21.8	144.9
11	4.00E+04	(2)	8.00E+04	(4)	50	2	2	43.2	3.8	285.4
12	0.00E+00	(0)	3.33E+04	(2)	60	1	1	34.5	1.1	430.6
13	3.33E+05	(5)	1.80E+06	(27)	15	38	15	15.9	4.7	40.7
14	3.33E+04	(1)	3.67E+05	(11)	30	8	5	8.6	0.2	52.1
15	5.00E+04	(2)	8.25E+05	(33)	40	18	6	5.4	0.6	19.8
16	6.67E+04	(2)	1.33E+05	(4)	30	3	3	43.2	3.8	285.4
17	5.00E+04	(5)	7.00E+04	(7)	100	1	1	60.0	14.9	215.1
18	1.00E+05	(6)	6.33E+05	(38)	60	13	4	13.5	4.6	31.4
19	2.00E+04	(1)	1.20E+05	(6)	50	3	2	15.5	0.3	113.9
20	8.00E+04	(4)	1.58E+06	(79)	50	34	8	4.4	1.1	11.3
21	5.00E+04	(3)	1.52E+06	(91)	60	32	7	2.9	0.6	8.3
22	2.86E+04	(2)	1.00E+05	(7)	70	2	2	25.1	2.4	124.3
23	1.00E+04	(1)	8.00E+04	(8)	100	2	1	11.7	0.2	77.5
24	1.80E+05	(9)	1.40E+05	(7)	50	3	2	106.1	35.5	331.2
25	1.15E+06	(46)	2.33E+06	(93)	40	49	10	41.3	28.3	59.3
26	5.00E+04	(1)	6.00E+05	(12)	20	13	7	7.9	0.2	47.0
27	2.50E+05	(10)	2.00E+06	(80)	40	43	10	10.6	4.8	20.2
28	8.57E+04	(6)	7.57E+05	(53)	70	16	4	9.7	3.3	22.0
29	3.00E+05	(6)	1.35E+06	(27)	20	29	11	18.9	6.3	45.8
30	2.50E+04	(1)	1.75E+05	(7)	40	4	3	13.4	0.3	92.4
31	4.00E+04	(2)	6.00E+05	(30)	50	13	5	6.0	0.6	22.0
32	2.00E+04	(1)	1.00E+05	(5)	50	2	2	18.6	0.4	147.8
33	2.50E+04	(1)	2.50E+05	(10)	40	5	3	9.4	0.2	58.5
34	4.00E+04	(4)	3.00E+04	(3)	100	1	1	109.2	18.8	719.7
35	2.00E+04	(1)	4.40E+05	(22)	50	9	4	4.3	0.1	23.5
36	1.20E+06	(48)	1.70E+06	(68)	40	36	9	58.8	39.7	86.3
37	1.20E+05	(12)	7.70E+05	(77)	100	16	4	13.2	6.4	24.1
38	6.67E+04	(2)	6.33E+05	(19)	30	13	6	9.4	1.0	36.4
39	3.33E+04	(2)	2.00E+05	(12)	60	4	2	14.8	1.5	62.3
40	1.00E+04	(1)	1.50E+05	(15)	100	3	2	6.3	0.1	36.2
41	3.33E+04	(2)	1.83E+05	(11)	60	4	2	16.1	1.6	69.3
42	1.40E+05	(14)	1.44E+06	(144)	100	31	5	8.2	4.3	14.1
43	2.00E+04	(1)	1.80E+05	(9)	50	4	2	10.5	0.2	66.7
44	1.00E+04	(1)	1.00E+05	(10)	100	2	1	9.4	0.2	58.5
45	3.00E+04	(3)	9.60E+05	(96)	100	20	4	2.7	0.5	7.9
46	8.33E+04	(5)	1.50E+05	(9)	60	3	2	46.9	12.2	152.6
47	2.00E+04	(1)	2.60E+05	(13)	50	6	3	7.3	0.2	42.7
48	5.00E+04	(1)	4.50E+05	(9)	20	10	6	10.5	0.2	66.7
49	1.67E+05	(3)	1.50E+06	(27)	18	32	12	9.7	1.8	30.1
50	8.00E+04	(4)	1.40E+05	(7)	50	3	2	48.4	10.2	185.4
51	4.00E+04	(2)	2.00E+05	(10)	50	4	3	17.7	1.8	78.1

52	1.10E+05	(11)	3.70E+05	(37)	100	8	3	25.1	11.4	49.6
53	1.20E+05	(12)	5.30E+05	(53)	100	11	3	19.1	9.2	35.8
54	3.00E+05	(15)	2.26E+06	(113)	50	48	9	11.2	6.0	19.1
55	1.00E+04	(1)	5.00E+04	(5)	100	1	1	18.6	0.4	147.8
56	6.67E+05	(8)	5.00E+05	(6)	12	11	8	109.8	33.8	378.7
57	1.00E+05	(3)	9.00E+05	(27)	30	19	7	9.7	1.8	30.1
58	4.00E+04	(2)	6.00E+04	(3)	50	1	1	56.8	4.7	469.3
59	0.00E+00	(0)	3.00E+05	(12)	40	6	4	5.0	0.2	30.0
60	4.00E+05	(12)	5.00E+05	(15)	30	11	5	66.7	28.5	151.4
61	0.00E+00	(0)	5.00E+04	(5)	100	1	1	12.4	0.4	90.7
62	1.67E+04	(1)	5.17E+05	(31)	60	11	4	3.1	0.1	16.2
63	0.00E+00	(0)	1.33E+05	(4)	30	3	3	15.8	0.5	125.5
64	2.00E+04	(1)	2.00E+05	(10)	50	4	3	9.4	0.2	58.5
65	7.50E+04	(3)	7.75E+05	(31)	40	16	6	8.5	1.6	25.9
66	2.67E+05	(4)	3.13E+06	(47)	15	67	19	7.4	1.9	19.5
67	1.00E+05	(5)	8.00E+04	(4)	50	2	2	102.9	22.4	506.6
68	7.50E+04	(3)	1.25E+05	(5)	40	3	2	51.0	7.8	253.0
69	2.00E+05	(6)	5.67E+05	(17)	30	12	6	30.0	9.5	78.0
70	6.67E+04	(2)	3.00E+05	(9)	30	6	4	19.6	2.0	89.2
71	3.00E+04	(3)	2.50E+05	(25)	100	5	2	10.5	1.9	32.8
72	2.25E+05	(9)	4.75E+05	(19)	40	10	5	39.9	15.8	91.3
73	8.00E+04	(2)	2.40E+05	(6)	25	5	4	29.2	2.7	154.1

KLD_27 Kluane detrital UC03A- (Counted by Eva Enkelmann 23 Nov 2014)

EFFECTIVE TRACK DENSITY FOR FLUENCE MONITOR (tracks/cm^2): 6.956E+05
RELATIVE ERROR (%): 1.80
EFFECTIVE URANIUM CONTENT OF MONITOR (ppm): 15.00
ZETA FACTOR AND STANDARD ERROR (yr cm^2): 237.00 5.00
SIZE OF COUNTER SQUARE (cm^2): 1.000E-06

------ GRAIN AGES IN ORIGINAL ORDER ------

Grain no.	RhoS (cm^-2)	(Ns)	RhoI (cm^-2)	(Ni)	Squares	U+/-2s		Grain Age	Age (Ma) --95% CI--	
1	1.00E+06	(30)	8.33E+05	(25)	30	18	7	98.1	55.9	173.3
2	9.33E+05	(14)	2.07E+06	(31)	15	45	16	37.4	18.3	71.8
3	5.00E+04	(5)	2.50E+05	(25)	100	5	2	16.9	4.9	43.7
4	1.40E+05	(7)	2.78E+06	(139)	50	60	10	4.2	1.6	8.8
5	7.22E+05	(26)	4.11E+06	(148)	36	89	15	14.5	9.1	22.1
6	1.20E+05	(12)	9.20E+05	(92)	100	20	4	10.9	5.4	19.7
7	6.50E+05	(13)	1.00E+06	(20)	20	22	10	53.6	24.4	112.3
8	6.00E+04	(6)	8.00E+05	(80)	100	17	4	6.3	2.2	14.1
9	1.10E+05	(11)	5.20E+05	(52)	100	11	3	17.6	8.2	33.8
10	7.00E+04	(7)	2.30E+05	(23)	100	5	2	25.4	9.1	60.2
11	3.33E+04	(1)	1.00E+05	(3)	30	2	2	29.9	0.5	333.6
12	1.00E+05	(3)	5.33E+05	(16)	30	12	6	16.1	2.9	53.8
13	2.50E+05	(25)	8.30E+05	(83)	100	18	4	24.9	15.2	39.2
14	8.33E+04	(5)	4.17E+05	(25)	60	9	4	16.9	4.9	43.7
15	1.13E+05	(9)	2.63E+05	(21)	80	6	2	35.6	14.2	80.0
16	1.33E+05	(2)	1.93E+06	(29)	15	42	15	6.1	0.7	22.5
17	1.20E+05	(6)	1.72E+06	(86)	50	37	8	5.9	2.1	13.0
18	2.60E+05	(26)	8.30E+05	(83)	100	18	4	25.9	15.9	40.5
19	2.78E+05	(5)	1.00E+06	(18)	18	22	10	23.4	6.6	63.7
20	5.00E+04	(5)	1.90E+05	(19)	100	4	2	22.2	6.3	59.8
21	6.67E+04	(4)	1.50E+05	(9)	60	3	2	37.3	8.2	130.0
22	3.33E+05	(2)	3.33E+05	(2)	6	7	9	81.9	6.0	1047.6
23	7.00E+05	(14)	2.90E+06	(58)	20	63	17	20.0	10.2	36.1
24	4.50E+05	(9)	2.00E+06	(40)	20	43	14	18.8	7.9	38.8
25	2.50E+05	(3)	3.33E+05	(4)	12	7	7	62.3	9.0	355.6
26	6.67E+05	(6)	1.22E+06	(11)	9	26	16	45.3	13.6	131.4
27	2.14E+05	(3)	9.29E+05	(13)	14	20	11	19.8	3.5	68.9
28	6.00E+04	(6)	3.80E+05	(38)	100	8	3	13.3	4.5	31.0
29	4.33E+05	(13)	2.53E+06	(76)	30	55	13	14.2	7.2	25.6
30	0.00E+00	(0)	2.33E+05	(14)	60	5	3	4.2	0.1	24.8
31	6.00E+04	(3)	4.60E+05	(23)	50	10	4	11.2	2.1	35.5
32	1.67E+06	(25)	3.33E+06	(50)	15	72	20	41.2	24.4	67.6
33	1.33E+05	(4)	1.90E+06	(57)	30	41	11	6.0	1.5	15.6
34	1.00E+05	(5)	1.80E+05	(9)	50	4	3	46.3	12.0	150.5
35	2.50E+05	(3)	1.00E+06	(12)	12	22	12	21.4	3.7	76.0
36	3.00E+06	(12)	4.50E+06	(18)	4	97	45	55.0	24.1	119.6
37	3.13E+04	(1)	3.44E+05	(11)	32	7	4	8.5	0.2	51.4
38	8.52E+05	(23)	1.22E+06	(33)	27	26	9	57.3	32.1	100.2
39	7.14E+05	(10)	4.29E+05	(6)	14	9	7	134.5	45.0	444.5
40	4.00E+05	(8)	4.50E+05	(9)	20	10	6	73.0	24.5	210.6
41	4.67E+05	(14)	2.63E+06	(79)	30	57	13	14.7	7.6	26.0
42	4.00E+04	(4)	2.10E+05	(21)	100	5	2	16.2	3.9	46.4
43	5.67E+05	(17)	4.00E+06	(120)	30	86	16	11.8	6.6	19.5
44	1.00E+04	(1)	3.70E+05	(37)	100	8	3	2.5	0.1	13.2
45	7.00E+05	(21)	4.43E+06	(133)	30	96	17	13.1	7.8	20.7
46	4.00E+04	(4)	3.50E+05	(35)	100	8	3	9.7	2.4	26.3
47	4.44E+05	(4)	4.44E+05	(4)	9	10	9	81.9	15.3	428.2
48	1.88E+05	(3)	2.81E+06	(45)	16	61	18	5.8	1.1	17.1
49	1.20E+05	(6)	4.80E+05	(24)	50	10	4	21.0	6.9	51.6
50	8.00E+04	(4)	4.00E+05	(20)	50	9	4	17.0	4.1	49.1
51	7.67E+05	(23)	1.80E+06	(54)	30	39	11	35.2	20.5	58.0

52	6.11E+05	(	11)	1.22E+06	(	22)	18	26	11	41.4	18.0	88.2
53	2.75E+05	(	11)	7.00E+05	(	28)	40	15	6	32.6	14.5	66.8
54	8.00E+04	(	4)	6.40E+05	(	32)	50	14	5	10.7	2.6	29.0
55	1.00E+05	(	3)	5.00E+05	(	15)	30	11	5	17.2	3.1	58.1
56	2.29E+05	(	16)	2.83E+06	(	198)	70	61	9	6.7	3.7	11.1
57	4.50E+05	(	9)	3.50E+05	(	7)	20	8	6	104.6	35.0	326.7
58	2.00E+05	(	8)	1.15E+06	(	46)	40	25	7	14.6	5.8	30.6
59	9.00E+05	(	36)	9.50E+05	(	38)	40	20	7	77.6	47.9	125.5
60	3.33E+05	(	3)	2.22E+05	(	2)	9	5	6	119.7	14.1	1333.0
61	3.10E+05	(	31)	8.90E+05	(	89)	100	19	4	28.7	18.4	43.6
62	1.45E+06	(	29)	1.70E+06	(	34)	20	37	13	70.0	41.1	118.0
63	3.50E+05	(	7)	1.10E+06	(	22)	20	24	10	26.6	9.5	63.3
64	6.40E+05	(	32)	2.06E+06	(	103)	50	44	9	25.7	16.6	38.4
65	1.60E+05	(	8)	5.40E+05	(	27)	50	12	4	24.7	9.6	55.1
66	6.25E+05	(	25)	2.70E+06	(	108)	40	58	11	19.2	11.8	29.7
67	1.00E+05	(	5)	4.20E+05	(	21)	50	9	4	20.1	5.8	53.3
68	5.00E+05	(	10)	1.60E+06	(	32)	20	35	12	26.0	11.3	53.5
69	1.40E+06	(	28)	3.70E+06	(	74)	20	80	19	31.2	19.4	48.7
70	8.00E+05	(	24)	7.33E+05	(	22)	30	16	7	89.2	48.1	166.2
71	8.13E+05	(	13)	3.69E+06	(	59)	16	80	21	18.3	9.1	33.5
72	1.25E+05	(	5)	5.50E+05	(	22)	40	12	5	19.2	5.5	50.6
73	1.00E+05	(	5)	1.60E+05	(	8)	50	3	2	51.9	13.2	176.3
74	2.86E+04	(	2)	4.00E+05	(	28)	70	9	3	6.3	0.7	23.3
75	5.00E+05	(	10)	1.85E+06	(	37)	20	40	13	22.5	9.9	45.6
76	1.60E+05	(	4)	3.60E+05	(	9)	25	8	5	37.3	8.2	130.0
77	2.00E+05	(	4)	3.00E+05	(	6)	20	6	5	55.4	11.4	227.8
78	1.33E+05	(	4)	5.33E+05	(	16)	30	12	6	21.2	5.0	63.6
79	2.00E+04	(	2)	2.80E+05	(	28)	100	6	2	6.3	0.7	23.3
80	1.25E+06	(	20)	2.81E+06	(	45)	16	61	18	36.7	20.4	63.1
81	2.50E+05	(	10)	1.13E+06	(	45)	40	24	7	18.5	8.2	36.8
82	4.50E+05	(	18)	2.43E+06	(	97)	40	52	11	15.4	8.7	25.5
83	5.00E+04	(	2)	3.25E+05	(	13)	40	7	4	13.5	1.4	55.8
84	1.00E+05	(	10)	2.40E+05	(	24)	100	5	2	34.6	14.6	74.2
85	9.00E+05	(	45)	1.82E+06	(	91)	50	39	8	40.7	27.8	58.7
86	1.87E+06	(	28)	4.80E+06	(	72)	15	104	25	32.1	19.9	50.1
87	7.33E+05	(	11)	1.67E+06	(	25)	15	36	14	36.5	16.1	76.1
88	2.17E+05	(	13)	3.50E+05	(	21)	60	8	3	51.1	23.4	106.0
89	2.17E+05	(	13)	3.50E+05	(	21)	60	8	3	51.1	23.4	106.0
90	7.22E+05	(	13)	8.33E+05	(	15)	18	18	9	71.2	31.2	159.1
91	5.60E+05	(	14)	6.40E+05	(	16)	25	14	7	71.8	32.5	156.0
92	7.50E+04	(	3)	6.75E+05	(	27)	40	15	6	9.6	1.8	29.7
93	3.00E+04	(	3)	1.60E+05	(	16)	100	3	2	16.1	2.9	53.8
94	6.33E+06	(	57)	6.44E+06	(	58)	9	139	37	80.5	54.9	118.0
95	6.00E+05	(	24)	1.45E+06	(	58)	40	31	8	34.2	20.2	55.6
96	5.00E+04	(	5)	7.00E+04	(	7)	100	2	1	59.1	14.7	212.1
97	2.38E+05	(	19)	3.88E+05	(	31)	80	8	3	50.5	26.9	91.8
98	4.00E+04	(	4)	2.70E+05	(	27)	100	6	2	12.6	3.1	35.0
99	8.33E+05	(	15)	8.89E+05	(	16)	18	19	9	76.9	35.5	164.9
100	8.57E+04	(	3)	4.00E+05	(	14)	35	9	5	18.4	3.3	63.0
101	2.75E+05	(	11)	3.25E+05	(	13)	40	7	4	69.5	28.2	166.7
102	1.20E+05	(	6)	7.20E+05	(	36)	50	16	5	14.0	4.7	32.9
103	4.50E+05	(	18)	5.25E+05	(	21)	40	11	5	70.4	35.4	137.9
104	2.40E+06	(	48)	2.40E+06	(	48)	20	52	15	81.9	53.8	124.6
105	0.00E+00	(	0)	2.00E+05	(	8)	40	4	3	7.5	0.3	48.1
106	8.13E+05	(	13)	6.25E+05	(	10)	16	13	8	105.9	43.2	267.6
107	1.15E+06	(	23)	7.00E+05	(	14)	20	15	8	133.4	66.4	278.8

KLD_29 Kluane detrital UC03A- (Counted by Eva Enkelmann 20 Nov 2014)

EFFECTIVE TRACK DENSITY FOR FLUENCE MONITOR (tracks/cm^2): 6.756E+05
RELATIVE ERROR (%): 1.80
EFFECTIVE URANIUM CONTENT OF MONITOR (ppm): 15.00
ZETA FACTOR AND STANDARD ERROR (yr cm^2): 237.00 5.00
SIZE OF COUNTER SQUARE (cm^2): 1.000E-06

------ GRAIN AGES IN ORIGINAL ORDER ------

Grain no.	**RhoS (cm^-2)**	**(Ns)**	**RhoI (cm^-2)**	**(Ni)**	**Squares**	**U+/-2s**		**Grain Age**	**Age (Ma) --95% CI--**	
1	1.70E+05	(17)	5.70E+05	(57)	100	13	3	24.0	13.0	41.6
2	5.00E+05	(7)	1.64E+06	(23)	14	36	15	24.7	8.8	58.4
3	2.00E+05	(6)	1.07E+06	(32)	30	24	8	15.3	5.1	36.3
4	1.75E+05	(7)	1.30E+06	(52)	40	29	8	11.0	4.1	23.8
5	1.60E+05	(8)	1.08E+06	(54)	50	24	7	12.1	4.9	25.1
6	4.00E+05	(16)	2.18E+06	(87)	40	48	10	14.8	8.0	25.3
7	2.50E+05	(10)	1.35E+06	(54)	40	30	8	15.0	6.7	29.4
8	5.60E+05	(28)	1.82E+06	(91)	50	40	9	24.7	15.5	37.9
9	1.67E+05	(10)	1.20E+06	(72)	60	27	6	11.3	5.1	21.6
10	4.00E+05	(12)	2.27E+06	(68)	30	50	12	14.3	6.9	26.3
11	3.17E+05	(19)	8.50E+05	(51)	60	19	5	29.9	16.6	51.3
12	2.40E+05	(6)	2.44E+06	(61)	25	54	14	8.1	2.8	18.1
13	6.67E+04	(2)	3.33E+05	(10)	30	7	5	17.0	1.7	74.8
14	1.70E+05	(17)	6.90E+05	(69)	100	15	4	19.8	10.9	33.9
15	1.20E+05	(6)	7.00E+05	(35)	50	16	5	14.0	4.7	32.9
16	3.50E+05	(35)	1.75E+06	(175)	100	39	6	16.1	10.8	23.1
17	1.00E+05	(5)	3.80E+05	(19)	50	8	4	21.5	6.1	58.1
18	2.00E+05	(4)	1.00E+06	(20)	20	22	10	16.5	4.0	47.7
19	7.50E+04	(3)	1.43E+06	(57)	40	32	8	4.4	0.8	13.0
20	5.25E+05	(42)	1.80E+06	(144)	80	40	7	23.4	16.1	33.1
21	2.20E+05	(11)	4.20E+05	(21)	50	9	4	42.1	18.2	90.4
22	3.00E+05	(15)	1.98E+06	(99)	50	44	9	12.2	6.5	21.0
23	4.00E+04	(2)	5.60E+05	(28)	50	12	5	6.1	0.7	22.7
24	7.67E+05	(23)	3.23E+06	(97)	30	72	15	19.1	11.5	30.1
25	5.00E+04	(2)	1.33E+06	(53)	40	29	8	3.2	0.4	11.5
26	2.50E+05	(4)	5.00E+05	(8)	16	11	8	40.7	8.8	147.8
27	1.67E+04	(1)	1.00E+05	(6)	60	2	2	14.9	0.3	109.1
28	6.00E+04	(3)	2.40E+05	(12)	50	5	3	20.8	3.6	73.8
29	1.25E+05	(5)	6.50E+05	(26)	40	14	6	15.8	4.6	40.7
30	1.25E+05	(2)	3.13E+05	(5)	16	7	6	33.4	3.0	192.8
31	1.00E+05	(4)	3.75E+05	(15)	40	8	4	21.9	5.2	66.7
32	8.13E+05	(13)	2.88E+06	(46)	16	64	19	22.8	11.2	42.5
33	8.33E+04	(5)	2.83E+05	(17)	60	6	3	24.0	6.8	66.2
34	3.33E+04	(1)	6.67E+04	(2)	30	1	2	42.5	0.7	726.6
35	6.67E+04	(4)	8.17E+05	(49)	60	18	5	6.8	1.7	17.8
36	1.20E+05	(6)	6.80E+05	(34)	50	15	5	14.4	4.8	34.0
37	4.20E+05	(21)	2.66E+06	(133)	50	59	10	12.7	7.6	20.1
38	3.54E+05	(17)	6.46E+05	(31)	48	14	5	43.9	22.7	81.4
39	1.00E+05	(9)	9.11E+05	(82)	90	20	5	8.9	3.9	17.5
40	2.50E+04	(1)	2.50E+05	(10)	40	6	3	9.0	0.2	56.1
41	1.11E+05	(9)	3.09E+05	(25)	81	7	3	29.1	11.8	63.6
42	1.00E+05	(3)	1.03E+06	(31)	30	23	8	8.1	1.5	24.8
43	3.33E+04	(1)	5.00E+05	(15)	30	11	6	6.1	0.1	34.6
44	1.00E+06	(6)	5.83E+06	(35)	6	130	44	14.0	4.7	32.9
45	4.00E+05	(16)	9.00E+05	(36)	40	20	7	35.7	18.4	65.5
46	5.00E+05	(6)	2.75E+06	(33)	12	61	21	14.9	5.0	35.1
47	9.33E+05	(14)	2.40E+06	(36)	15	53	18	31.3	15.5	59.0
48	7.50E+04	(3)	6.50E+05	(26)	40	14	6	9.7	1.8	30.1
49	9.50E+05	(19)	3.50E+06	(70)	20	78	19	21.8	12.3	36.5
50	9.38E+05	(15)	2.69E+06	(43)	16	60	18	28.1	14.4	51.1
51	8.89E+05	(16)	1.94E+06	(35)	18	43	15	36.7	18.9	67.6

52	4.60E+05 (23)	2.78E+06 (139)	50	62	11	13.3	8.1	20.7
53	3.33E+04 (2)	3.33E+04 (2)	60	1	1	79.6	5.8	1019.8
54	1.60E+05 (8)	1.50E+06 (75)	50	33	8	8.7	3.6	17.7
55	6.00E+05 (9)	8.00E+05 (12)	15	18	10	60.0	22.3	153.6
56	9.33E+05 (14)	5.33E+06 (80)	15	118	27	14.1	7.3	24.9
57	6.00E+05 (30)	1.10E+06 (55)	50	24	7	43.6	26.9	69.1
58	8.00E+04 (4)	4.60E+05 (23)	50	10	4	14.4	3.5	40.7
59	2.67E+05 (8)	1.80E+06 (54)	30	40	11	12.1	4.9	25.1
60	8.25E+05 (33)	4.80E+06 (192)	40	107	16	13.8	9.2	20.0
61	6.50E+05 (26)	1.68E+06 (67)	40	37	9	31.1	18.9	49.4
62	5.63E+05 (9)	2.75E+06 (44)	16	61	18	16.6	7.0	33.9
63	1.79E+05 (5)	9.29E+05 (26)	28	21	8	15.8	4.6	40.7
64	1.33E+05 (4)	8.67E+05 (26)	30	19	8	12.7	3.1	35.4
65	2.17E+05 (13)	1.17E+06 (70)	60	26	6	15.0	7.5	27.1
66	8.33E+05 (25)	2.03E+06 (61)	30	45	12	32.9	19.7	52.9
67	4.00E+05 (12)	1.87E+06 (56)	30	41	11	17.3	8.4	32.3
68	6.00E+05 (9)	3.27E+06 (49)	15	73	21	14.9	6.3	30.2
69	1.80E+05 (9)	1.14E+06 (57)	50	25	7	12.8	5.5	25.7
70	1.20E+05 (12)	2.50E+05 (25)	100	6	2	38.6	17.6	79.0
71	2.75E+05 (11)	1.03E+06 (41)	40	23	7	21.7	9.9	42.5
72	8.21E+05 (23)	3.04E+06 (85)	28	67	15	21.7	13.0	34.6
73	3.50E+05 (14)	2.45E+06 (98)	40	54	11	11.5	6.0	20.1
74	6.00E+05 (30)	2.64E+06 (132)	50	59	10	18.2	11.8	27.2
75	2.00E+05 (6)	9.67E+05 (29)	30	21	8	16.9	5.6	40.5
76	1.33E+05 (4)	4.00E+05 (12)	30	9	5	27.3	6.3	87.5
77	2.25E+05 (9)	2.08E+06 (83)	40	46	10	8.8	3.8	17.3
78	1.40E+05 (7)	9.20E+05 (46)	50	20	6	12.4	4.6	27.1
79	2.00E+05 (12)	8.33E+05 (50)	60	19	5	19.4	9.3	36.5
80	3.00E+05 (30)	7.60E+05 (76)	100	17	4	31.6	19.9	48.7
81	2.50E+05 (25)	1.43E+06 (143)	100	32	5	14.1	8.7	21.5
82	3.20E+05 (16)	1.26E+06 (63)	50	28	7	20.5	10.9	35.6
83	2.00E+04 (1)	1.40E+05 (7)	50	3	2	12.8	0.3	88.5
84	1.67E+05 (5)	3.33E+05 (10)	30	7	5	40.5	10.7	127.4
85	9.33E+05 (28)	3.37E+06 (101)	30	75	15	22.3	14.0	34.0
86	7.25E+05 (29)	3.85E+06 (154)	40	85	14	15.1	9.7	22.5
87	4.00E+05 (16)	1.25E+06 (50)	40	28	8	25.7	13.6	45.6
88	5.50E+05 (22)	1.95E+06 (78)	40	43	10	22.7	13.4	36.6
89	1.50E+05 (6)	1.35E+06 (54)	40	30	8	9.1	3.1	20.6
90	4.00E+05 (20)	2.08E+06 (104)	50	46	9	15.5	9.0	25.0
91	4.20E+05 (21)	1.92E+06 (96)	50	43	9	17.6	10.3	28.3
92	1.53E+06 (46)	6.30E+06 (189)	30	140	21	19.5	13.8	27.0
93	5.25E+05 (21)	2.45E+06 (98)	40	54	11	17.2	10.1	27.7
94	3.00E+04 (3)	2.90E+05 (29)	100	6	2	8.7	1.6	26.7
95	5.00E+04 (2)	2.65E+06 (106)	40	59	12	1.6	0.2	5.6
96	6.50E+05 (26)	2.25E+06 (90)	40	50	11	23.2	14.3	36.1
97	1.94E+05 (7)	7.50E+05 (27)	36	17	6	21.1	7.6	48.7
98	9.00E+04 (9)	3.80E+05 (38)	100	8	3	19.2	8.1	39.8
99	2.75E+05 (11)	1.53E+06 (61)	40	34	9	14.6	6.8	27.7
100	2.20E+05 (11)	1.72E+06 (86)	50	38	8	10.4	4.9	19.3
101	1.00E+05 (3)	1.07E+06 (32)	30	24	8	7.9	1.5	24.0
102	2.00E+05 (8)	9.00E+05 (36)	40	20	7	18.0	7.1	38.9
103	4.00E+05 (12)	1.30E+06 (39)	30	29	9	24.8	11.7	47.9

KLD_33 Kluane detrital UC03A- (Counted by Eva Enkelmann 1 Dec 2014)

EFFECTIVE TRACK DENSITY FOR FLUENCE MONITOR (tracks/cm^2): 6.355E+05
RELATIVE ERROR (%): 1.80
EFFECTIVE URANIUM CONTENT OF MONITOR (ppm): 15.00
ZETA FACTOR AND STANDARD ERROR (yr cm^2): 237.00 5.00
SIZE OF COUNTER SQUARE (cm^2): 1.000E-06

------ GRAIN AGES IN ORIGINAL ORDER ------

Grain no.	**RhoS (cm^-2)**	**(Ns)**	**RhoI (cm^-2)**	**(Ni)**	**Squares**	**U+/-2s**		**Grain Age**	**Age (Ma) --95% CI--**	
1	3.00E+04	(3)	1.90E+05	(19)	100	4	2	12.4	2.3	40.3
2	2.50E+05	(3)	8.33E+04	(1)	12	2	3	204.1	18.1	6729.2
3	1.20E+05	(6)	2.80E+05	(14)	50	7	3	32.7	10.2	88.9
4	2.86E+04	(2)	2.00E+05	(14)	70	5	2	11.5	1.2	46.7
5	1.43E+04	(1)	1.14E+05	(8)	70	3	2	10.6	0.2	69.9
6	5.00E+04	(5)	1.80E+05	(18)	100	4	2	21.4	6.1	58.3
7	4.00E+04	(4)	3.40E+05	(34)	100	8	3	9.2	2.3	24.8
8	0.00E+00	(0)	1.40E+05	(7)	50	3	2	7.8	0.3	52.1
9	4.29E+04	(3)	2.00E+05	(14)	70	5	2	16.8	3.0	57.6
10	3.00E+04	(3)	2.00E+05	(20)	100	5	2	11.8	2.1	38.0
11	3.00E+04	(3)	2.70E+05	(27)	100	6	2	8.8	1.6	27.2
12	2.80E+05	(7)	5.20E+05	(13)	25	12	7	40.9	13.7	108.5
13	1.40E+05	(14)	6.30E+05	(63)	100	15	4	16.9	8.6	30.2
14	6.00E+04	(6)	9.70E+05	(97)	100	23	5	4.8	1.7	10.5
15	4.00E+04	(2)	1.60E+05	(8)	50	4	3	19.9	1.9	93.7
16	1.30E+05	(13)	3.90E+05	(39)	100	9	3	25.3	12.3	47.9
17	1.00E+05	(4)	5.25E+05	(21)	40	12	5	14.8	3.6	42.4
18	0.00E+00	(0)	7.50E+04	(3)	40	2	2	19.5	0.6	179.8
19	1.33E+05	(4)	4.67E+05	(14)	30	11	6	22.1	5.2	68.2
20	8.00E+04	(8)	2.90E+05	(29)	100	7	3	21.0	8.2	46.5
21	6.00E+04	(6)	4.60E+05	(46)	100	11	3	10.0	3.4	23.0
22	2.50E+05	(25)	6.30E+05	(63)	100	15	4	29.9	18.0	48.1
23	2.38E+05	(5)	8.10E+05	(17)	21	19	9	22.6	6.4	62.3
24	1.00E+04	(1)	2.10E+05	(21)	100	5	2	4.1	0.1	22.3
25	1.43E+04	(1)	8.57E+04	(6)	70	2	2	14.0	0.3	102.7
26	0.00E+00	(0)	6.00E+05	(12)	20	14	8	4.5	0.2	27.1
27	2.80E+05	(14)	2.22E+06	(111)	50	52	10	9.6	5.0	16.6
28	4.10E+05	(41)	1.45E+06	(145)	100	34	6	21.3	14.6	30.3
29	2.00E+04	(2)	2.20E+05	(22)	100	5	2	7.3	0.8	27.8
30	1.11E+05	(2)	3.89E+05	(7)	18	9	7	22.6	2.2	112.1
31	5.00E+04	(2)	1.50E+05	(6)	40	4	3	26.3	2.5	139.0
32	1.00E+05	(4)	3.25E+05	(13)	40	8	4	23.8	5.5	74.6
33	3.33E+04	(1)	5.00E+05	(15)	30	12	6	5.7	0.1	32.6
34	2.40E+05	(6)	1.04E+06	(26)	25	25	10	17.7	5.8	43.1
35	5.71E+04	(4)	3.86E+05	(27)	70	9	3	11.5	2.8	32.0
36	3.40E+05	(34)	7.20E+05	(72)	100	17	4	35.6	22.9	54.1
37	6.00E+04	(3)	4.20E+05	(21)	50	10	4	11.2	2.1	36.0
38	1.00E+05	(4)	3.50E+05	(14)	40	8	4	22.1	5.2	68.2
39	1.90E+05	(19)	6.40E+05	(64)	100	15	4	22.5	12.6	37.7
40	7.50E+04	(3)	4.50E+05	(18)	40	11	5	13.1	2.4	42.9
41	3.00E+04	(3)	3.10E+05	(31)	100	7	3	7.6	1.4	23.3
42	1.20E+05	(3)	3.04E+06	(76)	25	72	17	3.1	0.6	9.0
43	2.00E+05	(8)	1.03E+06	(41)	40	24	8	14.9	5.9	31.7
44	1.10E+05	(11)	6.90E+05	(69)	100	16	4	12.1	5.7	22.8
45	4.00E+05	(12)	9.67E+05	(29)	30	23	8	31.3	14.5	62.7
46	1.50E+05	(3)	5.50E+05	(11)	20	13	8	21.3	3.7	77.3
47	6.00E+04	(3)	4.60E+05	(23)	50	11	4	10.3	1.9	32.5
48	2.50E+04	(1)	2.25E+05	(9)	40	5	3	9.4	0.2	60.1
49	1.43E+04	(1)	1.29E+05	(9)	70	3	2	9.4	0.2	60.1
50	1.00E+05	(4)	3.50E+05	(14)	40	8	4	22.1	5.2	68.2
51	4.00E+04	(4)	6.50E+05	(65)	100	15	4	4.8	1.2	12.4

52	1.20E+05 (6)	3.20E+05 (16)	50	8	4	28.7	9.0	75.6
53	1.67E+05 (5)	3.33E+05 (10)	30	8	5	38.1	10.1	119.9
54	1.25E+05 (5)	9.00E+05 (36)	40	21	7	10.7	3.2	26.7
55	0.00E+00 (0)	2.00E+05 (6)	30	5	4	9.2	0.3	63.7
56	7.50E+04 (3)	2.75E+05 (11)	40	6	4	21.3	3.7	77.3
57	3.70E+05 (37)	1.19E+06 (119)	100	28	5	23.4	15.7	34.1
58	6.00E+04 (3)	4.40E+05 (22)	50	10	4	10.7	2.0	34.1
59	3.00E+05 (12)	3.25E+05 (13)	40	8	4	69.2	28.9	163.3
60	1.80E+05 (9)	7.60E+05 (38)	50	18	6	18.1	7.6	37.5
61	1.60E+05 (8)	1.10E+06 (55)	50	26	7	11.1	4.5	23.1
62	1.00E+05 (5)	4.80E+05 (24)	50	11	5	16.1	4.7	41.9
63	3.00E+05 (3)	1.40E+06 (14)	10	33	17	16.8	3.0	57.6
64	0.00E+00 (0)	2.40E+05 (12)	50	6	3	4.5	0.2	27.1
65	3.17E+05 (19)	1.50E+06 (90)	60	35	8	16.0	9.1	26.3
66	1.00E+06 (9)	3.44E+06 (31)	9	81	29	22.1	9.1	46.9
67	1.00E+05 (5)	1.60E+05 (8)	50	4	3	47.4	12.1	161.3
68	5.00E+04 (2)	9.75E+05 (39)	40	23	7	4.1	0.5	14.9
69	3.75E+05 (15)	4.75E+05 (19)	40	11	5	59.3	28.0	122.4
70	1.20E+05 (12)	5.30E+05 (53)	100	13	3	17.2	8.3	32.3
71	1.40E+05 (7)	4.40E+05 (22)	50	10	4	24.3	8.6	57.9
72	6.80E+05 (68)	1.42E+06 (142)	100	34	6	36.1	26.9	48.4
73	2.40E+05 (12)	1.34E+06 (67)	50	32	8	13.6	6.6	25.1
74	1.00E+05 (3)	1.67E+05 (5)	30	4	3	45.9	7.0	228.3
75	1.20E+05 (6)	7.40E+05 (37)	50	17	6	12.5	4.2	29.2
76	5.00E+04 (2)	9.25E+05 (37)	40	22	7	4.4	0.5	15.8
77	7.00E+04 (7)	5.40E+05 (54)	100	13	3	10.0	3.7	21.5
78	1.29E+05 (9)	7.71E+05 (54)	70	18	5	12.7	5.4	25.6
79	7.50E+04 (3)	5.75E+05 (23)	40	14	6	10.3	1.9	32.5
80	1.00E+04 (1)	1.70E+05 (17)	100	4	2	5.0	0.1	28.2
81	2.00E+05 (6)	6.00E+05 (18)	30	14	7	25.5	8.1	65.7
82	2.50E+04 (1)	1.75E+05 (7)	40	4	3	12.0	0.2	83.3
83	1.00E+05 (5)	3.40E+05 (17)	50	8	4	22.6	6.4	62.3
84	2.00E+04 (2)	2.50E+05 (25)	100	6	2	6.4	0.7	24.1
85	3.67E+05 (11)	6.67E+05 (20)	30	16	7	41.6	17.9	90.1
86	5.63E+05 (9)	1.81E+06 (29)	16	43	16	23.6	9.7	50.6
87	0.00E+00 (0)	2.33E+05 (7)	30	6	4	7.8	0.3	52.1
88	1.75E+05 (7)	2.75E+05 (11)	40	6	4	48.1	15.7	134.1
89	3.33E+04 (1)	1.33E+05 (4)	30	3	3	20.7	0.4	187.6
90	1.00E+06 (12)	2.00E+06 (24)	12	47	19	37.8	17.1	77.9
91	1.60E+05 (4)	4.00E+05 (10)	25	9	6	30.8	6.9	103.7
92	1.67E+05 (5)	5.33E+05 (16)	30	13	6	24.0	6.7	66.9
93	6.60E+05 (33)	1.74E+06 (87)	50	41	9	28.6	18.5	43.0
94	8.00E+04 (4)	3.00E+05 (15)	50	7	4	20.6	4.8	62.8
95	4.00E+04 (2)	2.00E+05 (10)	50	5	3	16.0	1.6	70.3

KLD_39 Kluane detrital UC03A- (Counted by Eva Enkelmann 18 July 2015)

EFFECTIVE TRACK DENSITY FOR FLUENCE MONITOR (tracks/cm^2): 5.899E+05
RELATIVE ERROR (%): 1.80
EFFECTIVE URANIUM CONTENT OF MONITOR (ppm): 15.00
ZETA FACTOR AND STANDARD ERROR (yr cm^2): 237.00 5.00
SIZE OF COUNTER SQUARE (cm^2): 1.000E-06

------ GRAIN AGES IN ORIGINAL ORDER ------

Grain no.	**RhoS (cm^-2)**	**(Ns)**	**RhoI (cm^-2)**	**(Ni)**	**Squares**	**U+/-2s**		**Grain Age**	**Age (Ma) --95% CI--**	
1	1.28E+06	(51)	1.08E+06	(43)	40	27	8	82.3	53.9	126.4
2	1.90E+06	(38)	1.85E+06	(37)	20	47	15	71.4	44.2	115.2
3	2.40E+06	(48)	1.15E+06	(23)	20	29	12	143.7	86.3	246.8
4	8.00E+05	(40)	6.20E+05	(31)	50	16	6	89.5	54.7	147.6
5	1.00E+06	(20)	8.00E+05	(16)	20	20	10	86.6	42.8	178.0
6	1.07E+06	(32)	8.00E+05	(24)	30	20	8	92.4	52.9	163.5
7	2.31E+06	(37)	1.31E+06	(21)	16	33	14	121.6	69.8	218.0
8	4.75E+05	(19)	1.43E+06	(57)	40	36	10	23.4	13.1	39.7
9	2.20E+05	(11)	9.40E+05	(47)	50	24	7	16.5	7.6	32.0
10	6.67E+05	(20)	4.33E+05	(13)	30	11	6	106.2	50.7	231.3
11	7.00E+05	(21)	6.67E+05	(20)	30	17	8	73.0	37.7	141.3
12	6.75E+05	(27)	1.68E+06	(67)	40	43	10	28.2	17.3	44.6
13	3.11E+06	(28)	2.56E+06	(23)	9	65	27	84.4	47.0	153.0
14	3.25E+06	(13)	5.00E+06	(20)	4	127	56	45.5	20.7	95.4
15	8.33E+05	(10)	6.67E+05	(8)	12	17	12	86.5	31.0	250.0
16	9.33E+05	(14)	4.00E+05	(6)	15	10	8	158.7	58.6	498.4
17	4.50E+05	(9)	9.00E+05	(18)	20	23	11	35.2	13.8	81.5
18	7.50E+05	(30)	5.75E+05	(23)	40	15	6	90.4	50.9	162.5
19	1.89E+06	(17)	4.44E+05	(4)	9	11	11	282.1	96.1	1112.4
20	4.67E+05	(14)	2.67E+05	(8)	30	7	5	120.2	47.7	328.3
21	2.33E+05	(7)	3.00E+05	(9)	30	8	5	54.4	17.2	162.1
22	5.00E+05	(10)	2.00E+05	(4)	20	5	5	168.5	50.2	721.8
23	3.00E+05	(24)	1.55E+06	(124)	80	39	7	13.6	8.3	21.1
24	2.38E+06	(38)	2.13E+06	(34)	16	54	19	77.6	47.6	126.9
25	5.00E+05	(15)	3.00E+05	(9)	30	8	5	114.6	47.5	295.3
26	3.50E+05	(7)	3.00E+05	(6)	20	8	6	80.7	23.4	287.4
27	3.00E+05	(15)	8.60E+05	(43)	50	22	7	24.5	12.6	44.7
28	4.75E+05	(19)	3.00E+05	(12)	40	8	4	109.2	50.8	245.5
29	2.85E+06	(57)	2.55E+06	(51)	20	65	18	77.6	52.3	115.5
30	7.33E+05	(22)	6.33E+05	(19)	30	16	7	80.3	41.6	156.4
31	8.75E+05	(14)	6.25E+05	(10)	16	16	10	96.7	40.3	241.9
32	4.20E+05	(21)	4.00E+05	(20)	50	10	5	73.0	37.7	141.3
33	5.75E+05	(23)	3.25E+05	(13)	40	8	5	121.8	59.7	260.7
34	5.50E+05	(22)	7.00E+05	(28)	40	18	7	54.8	29.8	98.9
35	7.50E+05	(12)	5.00E+05	(8)	16	13	9	103.3	39.3	289.3
36	2.20E+05	(11)	8.80E+05	(44)	50	22	7	17.6	8.1	34.3
37	4.76E+05	(10)	4.76E+05	(10)	21	12	7	69.5	26.0	184.6
38	1.25E+05	(5)	1.18E+06	(47)	40	30	9	7.6	2.3	18.6
39	6.67E+05	(4)	1.83E+06	(11)	6	47	28	26.0	5.9	85.3
40	1.03E+06	(41)	8.00E+05	(32)	40	20	7	88.8	54.7	145.5
41	5.67E+05	(17)	8.00E+05	(24)	30	20	8	49.5	24.9	95.5
42	5.00E+04	(5)	1.30E+05	(13)	100	3	2	27.4	7.5	79.9
43	3.00E+05	(9)	3.00E+05	(9)	30	8	5	69.5	24.5	195.9
44	3.65E+06	(73)	2.55E+06	(51)	20	65	18	99.2	68.5	144.7
45	1.00E+06	(30)	7.33E+05	(22)	30	19	8	94.4	52.9	171.3
46	1.60E+05	(8)	1.00E+06	(50)	50	25	7	11.4	4.6	23.8
47	1.40E+05	(7)	2.20E+05	(11)	50	6	3	44.7	14.6	124.5
48	5.00E+04	(2)	5.50E+05	(22)	40	14	6	6.8	0.7	25.8
49	5.00E+05	(10)	6.00E+05	(12)	20	15	9	58.1	22.5	145.6
50	6.67E+05	(20)	8.33E+05	(25)	30	21	8	55.8	29.4	104.1
51	4.67E+06	(42)	2.33E+06	(21)	9	59	26	137.8	80.3	244.1

52	2.44E+06	(	22)	1.67E+06	(	15)	9	42	22	101.4	50.6	209.3
53	5.25E+05	(	21)	4.75E+05	(	19)	40	12	5	76.7	39.4	150.3
54	1.33E+05	(	4)	2.00E+05	(	6)	30	5	4	47.0	9.7	193.7
55	2.22E+06	(	20)	1.67E+06	(	15)	9	42	22	92.3	45.2	192.9
56	1.00E+06	(	16)	6.25E+05	(	10)	16	16	10	110.2	47.5	270.2
57	1.25E+05	(	5)	4.50E+05	(	18)	40	11	5	19.8	5.6	54.1
58	4.25E+05	(	17)	3.75E+05	(	15)	40	10	5	78.6	37.1	168.3
59	4.25E+05	(	17)	3.75E+05	(	15)	40	10	5	78.6	37.1	168.3
60	7.67E+05	(	23)	5.33E+05	(	16)	30	14	7	99.4	50.6	200.6
61	5.50E+05	(	11)	2.90E+06	(	58)	20	74	19	13.4	6.3	25.5
62	6.00E+05	(	12)	5.50E+05	(	11)	20	14	8	75.7	30.7	188.1
63	3.35E+06	(	67)	3.70E+06	(	74)	20	94	22	63.0	44.5	88.9
64	4.56E+06	(	41)	4.44E+06	(	40)	9	113	36	71.3	45.0	112.8
65	1.37E+06	(	41)	8.67E+05	(	26)	30	22	9	109.0	65.4	185.3
66	1.13E+06	(	45)	6.25E+05	(	25)	40	16	6	124.3	75.0	210.9
67	6.00E+05	(	12)	1.00E+06	(	20)	20	25	11	42.0	18.7	89.6
68	2.25E+05	(	9)	4.25E+05	(	17)	40	11	5	37.2	14.5	87.3
69	1.65E+06	(	33)	1.50E+06	(	30)	20	38	14	76.4	45.2	129.4
70	1.50E+05	(	3)	7.50E+05	(	15)	20	19	10	14.5	2.6	49.3
71	3.67E+05	(	11)	4.67E+05	(	14)	30	12	6	54.9	22.5	129.1
72	2.40E+06	(	48)	1.50E+06	(	30)	20	38	14	110.7	69.0	180.5
73	8.80E+05	(	22)	1.00E+06	(	25)	25	25	10	61.3	32.9	112.8
74	1.57E+06	(	47)	1.20E+06	(	36)	30	31	10	90.5	57.5	143.6
75	1.12E+06	(	28)	1.00E+06	(	25)	25	25	10	77.8	43.8	138.7
76	7.00E+05	(	21)	3.67E+05	(	11)	30	9	6	131.2	61.2	299.7
77	1.02E+06	(	51)	6.40E+05	(	32)	50	16	6	110.2	69.7	176.9
78	6.25E+05	(	25)	1.13E+06	(	45)	40	29	9	38.8	22.8	64.5
79	1.00E+06	(	9)	1.22E+06	(	11)	9	31	18	57.1	20.9	150.2
80	1.00E+06	(	16)	4.38E+05	(	7)	16	11	8	155.8	61.8	443.9
81	1.75E+05	(	7)	5.75E+05	(	23)	40	15	6	21.6	7.7	51.1
82	2.56E+06	(	23)	2.22E+06	(	20)	9	57	25	79.8	42.0	152.7
83	6.00E+05	(	18)	4.33E+05	(	13)	30	11	6	95.7	44.6	211.6
84	4.00E+05	(	12)	2.67E+05	(	8)	30	7	5	103.3	39.3	289.3
85	5.50E+05	(	22)	7.75E+05	(	31)	40	20	7	49.5	27.3	88.0
86	1.20E+06	(	18)	9.33E+05	(	14)	15	24	12	89.0	42.1	192.5
87	1.00E+06	(	25)	5.60E+05	(	14)	25	14	7	123.0	62.1	254.9
88	1.25E+06	(	25)	9.00E+05	(	18)	20	23	11	96.1	50.6	186.4
89	3.22E+06	(	29)	2.11E+06	(	19)	9	54	24	105.5	57.5	198.5
90	2.50E+06	(	50)	1.75E+06	(	35)	20	44	15	99.0	63.1	156.8
91	2.00E+06	(	40)	1.35E+06	(	27)	20	34	13	102.5	61.6	173.4
92	1.45E+06	(	29)	3.85E+06	(	77)	20	98	23	26.4	16.5	40.8
93	1.28E+06	(	51)	1.43E+06	(	57)	40	36	10	62.3	41.8	92.4
94	1.38E+06	(	11)	1.00E+06	(	8)	8	25	17	94.9	35.1	269.7
95	7.67E+05	(	23)	1.03E+06	(	31)	30	26	9	51.8	28.8	91.4
96	7.00E+05	(	14)	7.50E+05	(	15)	20	19	10	65.0	29.1	143.5
97	6.33E+05	(	19)	1.03E+06	(	31)	30	26	9	42.8	22.8	77.9
98	2.47E+06	(	74)	1.77E+06	(	53)	30	45	12	96.8	67.2	140.3
99	2.44E+06	(	39)	1.69E+06	(	27)	16	43	16	100.0	59.9	169.5
100	2.33E+05	(	7)	3.67E+05	(	11)	30	9	6	44.7	14.6	124.5
101	5.50E+06	(	22)	1.75E+06	(	7)	4	44	33	212.7	89.9	582.2
102	1.73E+06	(	52)	1.20E+06	(	36)	30	31	10	100.0	64.3	157.3
103	7.50E+05	(	15)	8.50E+05	(	17)	20	22	10	61.5	28.6	130.1
104	1.17E+06	(	35)	1.10E+06	(	33)	30	28	10	73.7	44.5	122.1
105	5.33E+05	(	16)	5.00E+05	(	15)	30	13	6	74.1	34.4	160.1
106	2.56E+06	(	41)	2.13E+06	(	34)	16	54	19	83.7	51.9	135.7

KLD_40 Kluane detrital UC03A- (Counted by Eva Enkelmann 26 Nov 2014)

EFFECTIVE TRACK DENSITY FOR FLUENCE MONITOR (tracks/cm^2): 5.847E+05
RELATIVE ERROR (%): 1.80
EFFECTIVE URANIUM CONTENT OF MONITOR (ppm): 15.00
ZETA FACTOR AND STANDARD ERROR (yr cm^2): 237.00 5.00
SIZE OF COUNTER SQUARE (cm^2): 1.000E-06

------ GRAIN AGES IN ORIGINAL ORDER ------

Grain no.	RhoS (cm^-2)	(Ns)	RhoI (cm^-2)	(Ni)	Squares	U+/-2s		Grain Age	Age (Ma) --95% CI--	
1	7.50E+04	(3)	3.00E+05	(12)	40	8	4	18.0	3.1	63.9
2	9.00E+05	(36)	3.25E+05	(13)	40	8	5	187.6	98.5	383.0
3	8.50E+05	(17)	5.00E+05	(10)	20	13	8	116.0	50.7	281.8
4	2.00E+04	(2)	4.50E+05	(45)	100	12	3	3.3	0.4	11.8
5	2.00E+06	(18)	1.44E+06	(13)	9	37	20	94.9	44.2	209.7
6	1.22E+06	(11)	3.33E+05	(3)	9	9	9	240.3	66.7	1282.4
7	5.00E+04	(2)	3.00E+05	(12)	40	8	4	12.3	1.3	51.7
8	1.10E+06	(22)	1.15E+06	(23)	20	30	12	66.0	35.1	123.4
9	1.92E+06	(23)	1.42E+06	(17)	12	36	17	92.8	47.7	184.5
10	6.00E+04	(3)	2.40E+05	(12)	50	6	3	18.0	3.1	63.9
11	1.94E+06	(31)	1.94E+06	(31)	16	50	18	68.9	40.6	116.9
12	0.00E+00	(0)	3.13E+05	(25)	80	8	3	1.9	0.1	11.0
13	6.50E+05	(13)	3.50E+05	(7)	20	9	7	126.1	47.5	370.3
14	1.70E+06	(51)	8.67E+05	(26)	30	22	9	134.1	82.5	223.5
15	3.33E+05	(10)	2.33E+05	(7)	30	6	4	97.6	33.9	299.5
16	1.38E+06	(11)	1.50E+06	(12)	8	38	22	63.3	25.3	155.5
17	5.00E+04	(2)	9.25E+05	(37)	40	24	8	4.0	0.4	14.5
18	6.67E+04	(2)	2.33E+05	(7)	30	6	4	20.8	2.0	103.2
19	5.50E+05	(11)	4.50E+05	(9)	20	12	8	83.9	31.8	227.3
20	1.00E+05	(4)	1.50E+05	(6)	40	4	3	46.6	9.6	192.0
21	3.33E+04	(1)	4.33E+05	(13)	30	11	6	6.0	0.1	35.4
22	5.83E+05	(7)	1.17E+06	(14)	12	30	16	34.9	11.8	91.2
23	1.67E+04	(1)	5.17E+05	(31)	60	13	5	2.5	0.1	13.4
24	1.15E+06	(46)	5.00E+05	(20)	40	13	6	156.7	91.6	278.6
25	8.75E+05	(14)	3.13E+05	(5)	16	8	7	187.4	65.6	654.3
26	1.25E+05	(5)	5.75E+05	(23)	40	15	6	15.4	4.5	40.4
27	0.00E+00	(0)	2.75E+05	(11)	40	7	4	4.5	0.2	27.6
28	5.00E+04	(2)	3.00E+05	(12)	40	8	4	12.3	1.3	51.7
29	9.25E+05	(37)	7.25E+05	(29)	40	19	7	87.7	52.6	147.5
30	0.00E+00	(0)	5.00E+05	(15)	30	13	7	3.3	0.1	19.3
31	2.00E+05	(4)	2.50E+05	(5)	20	6	5	55.6	11.0	252.7
32	1.33E+05	(4)	1.60E+06	(48)	30	41	12	6.0	1.5	15.8
33	0.00E+00	(0)	8.00E+05	(24)	30	21	8	2.0	0.1	11.5
34	3.33E+04	(1)	3.00E+05	(9)	30	8	5	8.7	0.2	55.4
35	7.50E+05	(6)	6.25E+05	(5)	8	16	14	82.2	21.1	335.7
36	2.86E+04	(2)	7.14E+04	(5)	70	2	2	28.9	2.6	167.2
37	6.00E+04	(3)	5.00E+05	(25)	50	13	5	8.7	1.6	27.2
38	5.50E+05	(22)	4.50E+05	(18)	40	12	5	84.0	43.2	165.6
39	8.00E+05	(24)	6.33E+05	(19)	30	16	7	86.8	45.7	167.0
40	5.00E+04	(1)	5.00E+05	(10)	20	13	8	7.8	0.2	48.6
41	8.00E+04	(4)	3.80E+05	(19)	50	10	4	15.0	3.6	43.8
42	6.67E+04	(1)	6.00E+05	(9)	15	15	10	8.7	0.2	55.4
43	2.00E+04	(1)	3.40E+05	(17)	50	9	4	4.6	0.1	26.0
44	3.25E+05	(13)	1.75E+05	(7)	40	4	3	126.1	47.5	370.3
45	7.50E+04	(3)	6.75E+05	(27)	40	17	7	8.1	1.5	25.0
46	1.00E+05	(4)	3.00E+05	(12)	40	8	4	23.7	5.4	75.8
47	1.25E+04	(1)	7.00E+05	(56)	80	18	5	1.4	0.0	7.2
48	2.00E+04	(2)	3.10E+05	(31)	100	8	3	4.8	0.5	17.6
49	1.60E+06	(32)	1.25E+06	(25)	20	32	13	88.0	50.7	154.4
50	6.00E+04	(6)	4.20E+05	(42)	100	11	3	10.1	3.4	23.4
51	6.00E+04	(3)	5.60E+05	(28)	50	14	5	7.8	1.4	24.0

52	1.00E+05	(2)	6.00E+05	(12)	20	15	9	12.3	1.3	51.7
53	1.00E+05	(3)	6.00E+05	(18)	30	15	7	12.0	2.2	39.5
54	1.00E+05	(3)	8.33E+05	(25)	30	21	9	8.7	1.6	27.2
55	2.78E+06	(25)	1.44E+06	(13)	9	37	20	131.1	65.2	277.8
56	1.80E+06	(45)	1.72E+06	(43)	25	44	13	72.1	46.4	112.0
57	3.00E+05	(9)	8.00E+05	(24)	30	21	8	26.2	10.6	57.7
58	2.50E+05	(10)	3.00E+05	(12)	40	8	4	57.6	22.3	144.3
59	9.50E+05	(19)	1.25E+06	(25)	20	32	13	52.6	27.3	98.9
60	4.20E+05	(21)	4.20E+05	(21)	50	11	5	68.9	35.9	132.1
61	6.67E+04	(2)	2.00E+05	(6)	30	5	4	24.2	2.3	128.0
62	1.00E+05	(5)	2.80E+05	(14)	50	7	4	25.2	7.0	72.4
63	7.00E+05	(14)	9.50E+05	(19)	20	24	11	51.0	23.6	106.6
64	6.00E+04	(3)	3.20E+05	(16)	50	8	4	13.5	2.4	45.3
65	4.80E+05	(12)	4.00E+05	(10)	25	10	6	82.4	32.8	211.5
66	4.80E+05	(12)	4.00E+05	(10)	25	10	6	82.4	32.8	211.5
67	4.00E+05	(12)	3.00E+05	(9)	30	8	5	91.3	35.6	243.8
68	2.13E+06	(34)	9.38E+05	(15)	16	24	12	154.2	82.6	303.4
69	1.33E+05	(8)	3.17E+05	(19)	60	8	4	29.4	11.0	69.5
70	5.00E+05	(15)	2.33E+05	(7)	30	6	4	145.0	56.7	417.0
71	5.00E+05	(10)	8.00E+05	(16)	20	21	10	43.4	17.5	100.8
72	6.50E+05	(13)	5.00E+05	(10)	20	13	8	89.1	36.4	225.7
73	1.25E+05	(5)	9.00E+05	(36)	40	23	8	9.9	2.9	24.6
74	8.33E+04	(5)	3.17E+05	(19)	60	8	4	18.6	5.3	50.3
75	4.00E+04	(1)	3.60E+05	(9)	25	9	6	8.7	0.2	55.4
76	2.78E+06	(25)	2.44E+06	(22)	9	63	27	78.2	42.4	145.0
77	2.10E+06	(42)	2.20E+06	(44)	20	56	17	65.8	42.1	102.7
78	3.00E+05	(15)	3.40E+05	(17)	50	9	4	60.9	28.3	129.0
79	4.56E+06	(41)	3.44E+06	(31)	9	88	32	90.9	55.8	149.6
80	1.00E+05	(3)	4.67E+05	(14)	30	12	6	15.4	2.7	53.0
81	4.29E+05	(15)	4.00E+05	(14)	35	10	5	73.8	33.3	164.0
82	5.00E+05	(20)	5.00E+05	(20)	40	13	6	68.9	35.2	134.4
83	0.00E+00	(0)	5.20E+05	(13)	25	13	7	3.8	0.1	22.7
84	4.29E+04	(3)	5.14E+05	(36)	70	13	4	6.1	1.1	18.3
85	8.33E+04	(2)	4.17E+05	(10)	24	11	7	14.7	1.5	64.7
86	2.86E+04	(2)	3.86E+05	(27)	70	10	4	5.5	0.6	20.4
87	2.50E+04	(1)	4.00E+05	(16)	40	10	5	4.9	0.1	27.8
88	1.00E+05	(2)	4.00E+05	(8)	20	10	7	18.3	1.8	86.3
89	4.00E+04	(2)	3.80E+05	(19)	50	10	4	7.8	0.8	30.2
90	7.50E+04	(3)	2.00E+05	(8)	40	5	4	26.8	4.4	107.4
91	5.00E+04	(5)	4.20E+05	(42)	100	11	3	8.5	2.5	20.8
92	5.00E+04	(2)	2.25E+05	(9)	40	6	4	16.3	1.6	74.0
93	4.00E+04	(2)	2.40E+05	(12)	50	6	3	12.3	1.3	51.7
94	6.00E+04	(3)	3.00E+05	(15)	50	8	4	14.4	2.6	48.8
95	4.75E+05	(19)	4.75E+05	(19)	40	12	6	68.9	34.6	137.0
96	2.00E+04	(1)	7.00E+05	(35)	50	18	6	2.3	0.0	11.8
97	4.00E+04	(1)	4.00E+05	(10)	25	10	6	7.8	0.2	48.6
98	7.14E+04	(5)	3.14E+05	(22)	70	8	3	16.1	4.7	42.5
99	3.20E+05	(16)	3.80E+05	(19)	50	10	4	58.2	28.0	118.8
100	1.25E+05	(5)	4.75E+05	(19)	40	12	6	18.6	5.3	50.3
101	4.00E+04	(4)	3.00E+05	(30)	100	8	3	9.6	2.4	26.2
102	5.00E+04	(1)	3.00E+05	(6)	20	8	6	12.9	0.3	94.5
103	5.50E+05	(11)	4.50E+05	(9)	20	12	8	83.9	31.8	227.3
104	7.75E+05	(31)	4.50E+05	(18)	40	12	5	117.8	64.3	222.9
105	2.00E+04	(1)	2.80E+05	(14)	50	7	4	5.6	0.1	32.5

KLD_65 Kluane detrital UC03A- (Counted by Eva Enkelmann 15 July 2015)

EFFECTIVE TRACK DENSITY FOR FLUENCE MONITOR (tracks/cm^2): 5.795E+05
RELATIVE ERROR (%): 1.80
EFFECTIVE URANIUM CONTENT OF MONITOR (ppm): 15.00
ZETA FACTOR AND STANDARD ERROR (yr cm^2): 237.00 5.00
SIZE OF COUNTER SQUARE (cm^2): 1.000E-06

------ GRAIN AGES IN ORIGINAL ORDER ------

Grain no.	**RhoS (cm^-2)**	**(Ns)**	**RhoI (cm^-2)**	**(Ni)**	**Squares**	**U**	**+/-2s**	**Grain Age**	**Age (Ma) --95% CI--**	
1	2.40E+05	(24)	2.90E+05	(29)	100	8	3	56.7	31.6	100.4
2	3.29E+05	(23)	2.57E+05	(18)	70	7	3	87.0	45.1	170.5
3	1.35E+06	(54)	7.75E+05	(31)	40	20	7	118.3	75.0	190.0
4	2.00E+05	(10)	6.00E+04	(3)	50	2	2	217.2	58.6	1180.0
5	3.75E+05	(9)	5.42E+05	(13)	24	14	8	47.6	17.9	119.2
6	3.33E+05	(10)	5.67E+05	(17)	30	15	7	40.5	16.5	92.8
7	5.80E+05	(29)	4.40E+05	(22)	50	11	5	89.7	50.0	163.4
8	3.81E+05	(8)	2.86E+05	(6)	21	7	6	90.3	27.8	312.6
9	2.33E+05	(14)	4.17E+05	(25)	60	11	4	38.5	18.4	76.5
10	4.64E+05	(13)	1.43E+05	(4)	28	4	3	213.7	68.5	877.5
11	4.90E+05	(49)	4.60E+05	(46)	100	12	4	72.7	47.7	111.1
12	3.20E+05	(8)	1.60E+05	(4)	25	4	4	133.3	36.7	595.2
13	3.60E+05	(36)	3.00E+05	(30)	100	8	3	81.8	49.1	137.2
14	1.00E+05	(10)	7.00E+04	(7)	100	2	1	96.7	33.6	296.9
15	1.03E+06	(31)	7.33E+05	(22)	30	19	8	95.8	54.0	173.3
16	5.10E+05	(51)	3.10E+05	(31)	100	8	3	111.8	70.4	180.4
17	3.30E+05	(33)	2.40E+05	(24)	100	6	3	93.6	53.8	165.0
18	4.33E+05	(13)	3.33E+05	(10)	30	9	5	88.3	36.0	223.7
19	3.20E+05	(16)	5.20E+05	(26)	50	13	5	42.3	21.1	81.4
20	1.00E+05	(6)	8.33E+04	(5)	60	2	2	81.5	20.9	332.8
21	4.25E+05	(17)	4.25E+05	(17)	40	11	5	68.3	32.8	141.7
22	6.00E+05	(18)	2.33E+05	(7)	30	6	4	171.8	69.9	482.1
23	5.90E+05	(59)	3.50E+05	(35)	100	9	3	114.5	74.4	179.0
24	2.00E+05	(20)	3.20E+05	(32)	100	8	3	42.9	23.2	77.0
25	5.00E+05	(25)	5.20E+05	(26)	50	13	5	65.7	36.4	118.0
26	1.81E+06	(29)	9.38E+05	(15)	16	24	12	130.7	68.4	261.3
27	1.36E+06	(68)	1.48E+06	(74)	50	38	9	62.8	44.5	88.5
28	3.67E+05	(33)	3.44E+05	(31)	90	9	3	72.7	43.2	122.4
29	4.20E+05	(21)	3.20E+05	(16)	50	8	4	89.3	44.6	182.3
30	2.67E+05	(16)	1.00E+05	(6)	60	3	2	177.6	67.6	547.8
31	1.50E+05	(6)	2.50E+05	(10)	40	6	4	41.5	12.3	124.0
32	8.15E+05	(22)	5.56E+05	(15)	27	14	7	99.6	49.7	205.6
33	4.30E+05	(43)	3.00E+05	(30)	100	8	3	97.5	60.0	160.7
34	3.80E+05	(19)	1.80E+05	(9)	50	5	3	142.0	62.1	354.2
35	1.87E+06	(56)	1.93E+06	(58)	30	50	13	66.0	44.9	96.9
36	1.37E+06	(41)	2.00E+06	(60)	30	52	13	46.8	30.6	70.7
37	2.40E+05	(12)	4.00E+04	(2)	50	1	1	376.2	91.0	2982.0
38	5.00E+05	(25)	8.20E+05	(41)	50	21	7	41.8	24.3	70.2
39	1.65E+06	(33)	1.25E+06	(25)	20	32	13	89.9	52.0	157.3
40	4.17E+05	(25)	4.83E+05	(29)	60	13	5	59.0	33.1	104.0
41	4.40E+05	(22)	2.80E+05	(14)	50	7	4	106.6	52.5	224.3
42	6.00E+05	(18)	1.10E+06	(33)	30	28	10	37.5	19.8	68.2
43	3.90E+05	(39)	4.50E+05	(45)	100	12	3	59.3	37.6	92.9
44	7.50E+05	(15)	3.50E+05	(7)	20	9	7	143.8	56.2	413.4
45	6.20E+05	(31)	3.60E+05	(18)	50	9	4	116.8	63.7	220.9
46	2.75E+05	(11)	2.00E+05	(8)	40	5	4	93.2	34.5	265.1
47	6.00E+05	(18)	3.67E+05	(11)	30	9	6	110.8	50.0	258.3
48	1.40E+05	(7)	1.80E+05	(9)	50	5	3	53.5	16.9	159.3
49	2.56E+06	(41)	1.50E+06	(24)	16	39	16	115.9	68.8	200.1
50	4.00E+05	(16)	3.00E+05	(12)	40	8	4	90.6	40.5	208.8
51	2.67E+05	(8)	1.67E+05	(5)	30	4	4	107.7	31.6	413.6

52	3.67E+05	(	11)	3.33E+05	(	10)	30	9	5	75.0	29.0	195.6

KLD_67 Kluane detrital UC03A- (Counted by Eva Enkelmann 15 July 2015)

EFFECTIVE TRACK DENSITY FOR FLUENCE MONITOR (tracks/cm^2): 5.743E+05
RELATIVE ERROR (%): 1.80
EFFECTIVE URANIUM CONTENT OF MONITOR (ppm): 15.00
ZETA FACTOR AND STANDARD ERROR (yr cm^2): 237.00 5.00
SIZE OF COUNTER SQUARE (cm^2): 1.000E-06

------ GRAIN AGES IN ORIGINAL ORDER ------

Grain no.	**RhoS (cm^-2)**	**(Ns)**	**RhoI (cm^-2)**	**(Ni)**	**Squares**	**U+/-2s**		**Grain Age**	**Age (Ma) --95% CI--**	
1	2.00E+05	(10)	2.00E+05	(10)	50	5	3	67.7	25.4	179.8
2	5.40E+05	(27)	5.40E+05	(27)	50	14	5	67.7	38.3	119.6
3	2.00E+05	(6)	2.00E+05	(6)	30	5	4	67.7	18.2	249.8
4	2.50E+05	(4)	1.88E+05	(3)	16	5	5	89.0	15.3	591.7
5	1.37E+06	(41)	5.67E+05	(17)	30	15	7	161.2	90.5	301.3
6	3.25E+05	(13)	5.25E+05	(21)	40	14	6	42.2	19.3	87.7
7	3.00E+06	(18)	2.17E+06	(13)	6	57	31	93.2	43.5	206.0
8	7.57E+05	(53)	5.43E+05	(38)	70	14	5	94.1	61.0	146.5
9	6.40E+05	(32)	7.40E+05	(37)	50	19	6	58.6	35.4	96.5
10	2.67E+05	(8)	1.00E+05	(3)	30	3	3	173.5	43.4	983.5
11	8.25E+05	(33)	6.00E+05	(24)	40	16	6	92.7	53.4	163.6
12	1.40E+05	(7)	1.60E+05	(8)	50	4	3	59.4	18.3	185.4
13	3.40E+05	(17)	6.00E+04	(3)	50	2	2	359.5	110.5	1783.6
14	3.80E+05	(38)	3.70E+05	(37)	100	10	3	69.5	43.1	112.2
15	2.20E+05	(11)	2.00E+05	(10)	50	5	3	74.3	28.8	193.8
16	1.72E+06	(31)	7.22E+05	(13)	18	19	10	159.1	81.9	329.6
17	3.00E+05	(9)	6.33E+05	(19)	30	17	8	32.5	12.8	74.4
18	2.29E+05	(16)	3.71E+05	(26)	70	10	4	41.9	20.9	80.7
19	3.00E+05	(12)	2.00E+05	(8)	40	5	4	100.6	38.2	281.9
20	4.60E+05	(23)	3.00E+05	(15)	50	8	4	103.1	51.9	211.8
21	3.80E+05	(19)	4.00E+05	(20)	50	10	5	64.4	32.5	126.5
22	2.60E+05	(13)	8.00E+04	(4)	50	2	2	211.8	67.9	870.2
23	2.50E+05	(25)	3.10E+05	(31)	100	8	3	54.7	31.0	95.5
24	3.25E+05	(13)	1.75E+05	(7)	40	5	3	123.9	46.7	363.9
25	3.00E+05	(18)	2.17E+05	(13)	60	6	3	93.2	43.5	206.0
26	6.00E+05	(9)	3.33E+05	(5)	15	9	7	119.7	36.7	449.5
27	2.25E+05	(9)	2.75E+05	(11)	40	7	4	55.6	20.3	146.3
28	1.20E+05	(6)	1.40E+05	(7)	50	4	3	58.3	16.2	199.7
29	2.00E+05	(3)	4.00E+05	(6)	15	10	8	34.8	5.5	157.5
30	2.67E+05	(8)	1.67E+05	(5)	30	4	4	106.7	31.3	410.0
31	1.00E+05	(7)	7.14E+04	(5)	70	2	2	93.7	26.0	370.1
32	3.00E+05	(12)	4.25E+05	(17)	40	11	5	48.1	20.9	106.0
33	2.40E+05	(12)	2.80E+05	(14)	50	7	4	58.2	24.6	134.6
34	4.30E+05	(43)	4.40E+05	(44)	100	11	3	66.2	42.4	103.0
35	3.40E+05	(17)	3.20E+05	(16)	50	8	4	71.9	34.2	151.3
36	4.50E+05	(18)	5.25E+05	(21)	40	14	6	58.1	29.2	114.1
37	9.00E+04	(9)	6.00E+04	(6)	100	2	1	100.4	32.3	339.6
38	6.25E+05	(25)	4.00E+05	(16)	40	10	5	105.1	54.3	209.9
39	1.80E+05	(18)	1.60E+05	(16)	100	4	2	76.0	36.7	158.7
40	4.60E+05	(23)	1.20E+05	(6)	50	3	2	250.8	102.3	739.6
41	1.12E+06	(28)	3.60E+05	(9)	25	9	6	205.8	96.3	491.2
42	4.60E+05	(23)	3.80E+05	(19)	50	10	5	81.7	42.7	158.2
43	4.20E+05	(42)	3.20E+05	(32)	100	8	3	88.6	54.7	144.8
44	8.00E+05	(24)	5.00E+05	(15)	30	13	7	107.5	54.5	219.7
45	6.00E+05	(6)	8.00E+05	(8)	10	21	14	51.2	14.6	165.7
46	1.23E+06	(37)	1.03E+06	(31)	30	27	10	80.7	48.8	134.2
47	1.50E+05	(6)	2.50E+05	(10)	40	7	4	41.1	12.2	122.9
48	4.00E+06	(36)	6.22E+06	(56)	9	163	44	43.7	27.9	67.4
49	6.00E+05	(18)	5.33E+05	(16)	30	14	7	76.0	36.7	158.7
50	2.80E+05	(14)	3.80E+05	(19)	50	10	5	50.1	23.2	104.7
51	2.80E+05	(14)	2.00E+05	(10)	50	5	3	94.1	39.2	235.6

52	2.50E+05	(10)	2.50E+05	(10)	40	7	4	67.7	25.4	179.8
53	3.00E+05	(15)	3.20E+05	(16)	50	8	4	63.5	29.3	136.5
54	3.00E+05	(30)	3.10E+05	(31)	100	8	3	65.5	38.3	111.7
55	2.63E+05	(21)	3.38E+05	(27)	80	9	3	52.8	28.4	96.6
56	6.00E+05	(18)	4.00E+05	(12)	30	10	6	100.8	46.3	228.4
57	6.00E+05	(30)	2.20E+05	(11)	50	6	3	181.3	89.7	398.3
58	6.00E+05	(18)	2.33E+05	(7)	30	6	4	170.3	69.3	477.9
59	3.00E+05	(12)	1.75E+05	(7)	40	5	3	114.5	42.2	340.8
60	2.80E+05	(28)	4.30E+05	(43)	100	11	3	44.3	26.4	72.7
61	5.00E+05	(15)	5.33E+05	(16)	30	14	7	63.5	29.3	136.5
62	1.33E+05	(8)	6.67E+04	(4)	60	2	2	132.1	36.3	590.1
63	2.70E+05	(27)	4.70E+05	(47)	100	12	4	39.1	23.3	63.9
64	2.33E+05	(7)	2.67E+05	(8)	30	7	5	59.4	18.3	185.4
65	3.40E+05	(17)	3.60E+05	(18)	50	9	4	64.0	31.0	131.0
66	1.23E+06	(49)	1.75E+06	(70)	40	46	11	47.5	32.2	69.4
67	4.00E+05	(16)	6.50E+05	(26)	40	17	7	41.9	20.9	80.7
68	7.00E+05	(14)	1.00E+06	(20)	20	26	12	47.6	22.2	98.5
69	1.00E+06	(15)	1.47E+06	(22)	15	38	16	46.4	22.3	93.0
70	2.50E+05	(10)	2.00E+05	(8)	40	5	4	84.2	30.1	243.6
71	5.40E+05	(27)	4.20E+05	(21)	50	11	5	86.8	47.4	161.0
72	3.00E+05	(15)	1.80E+05	(9)	50	5	3	111.6	46.3	287.7
73	3.20E+05	(16)	2.60E+05	(13)	50	7	4	83.0	37.6	186.7
74	3.67E+05	(11)	3.00E+05	(9)	30	8	5	82.4	31.2	223.4
75	6.25E+05	(10)	3.75E+05	(6)	16	10	8	111.3	37.2	369.2
76	6.00E+05	(18)	1.00E+06	(30)	30	26	10	40.9	21.4	75.3
77	1.80E+05	(9)	5.60E+05	(28)	50	15	6	22.1	9.1	47.6
78	2.60E+05	(13)	3.20E+05	(16)	50	8	4	55.2	24.4	121.6
79	5.00E+04	(2)	1.50E+05	(6)	40	4	3	23.8	2.2	125.7
80	1.67E+05	(5)	3.33E+05	(10)	30	9	5	34.5	9.1	108.4
81	2.75E+05	(11)	4.00E+05	(16)	40	10	5	46.8	19.6	106.6
82	3.40E+05	(17)	3.80E+05	(19)	50	10	5	60.7	29.6	122.7
83	3.80E+05	(19)	2.40E+05	(12)	50	6	4	106.3	49.4	239.1
84	1.43E+05	(10)	2.29E+05	(16)	70	6	3	42.7	17.2	99.0
85	2.50E+05	(25)	2.80E+05	(28)	100	7	3	60.5	33.8	107.3
86	2.75E+05	(11)	3.50E+05	(14)	40	9	5	53.4	21.9	125.7
87	1.70E+05	(17)	1.30E+05	(13)	100	3	2	88.1	40.5	196.4
88	1.67E+06	(10)	2.00E+06	(12)	6	52	30	56.6	21.9	141.8
89	7.20E+05	(18)	2.80E+05	(7)	25	7	5	170.3	69.3	477.9
90	2.57E+05	(18)	2.14E+05	(15)	70	6	3	81.0	38.7	171.9
91	1.60E+05	(8)	4.00E+05	(20)	50	10	5	27.5	10.4	64.3
92	6.00E+04	(3)	2.20E+05	(11)	50	6	3	19.2	3.3	69.9
93	1.38E+06	(22)	1.31E+06	(21)	16	34	15	70.9	37.2	135.0
94	2.40E+05	(12)	3.20E+05	(16)	50	8	4	51.0	22.0	114.1
95	5.25E+05	(21)	7.75E+05	(31)	40	20	7	46.1	25.1	82.4
96	2.00E+05	(4)	4.00E+05	(8)	20	10	7	34.6	7.5	125.9
97	8.67E+05	(26)	7.33E+05	(22)	30	19	8	79.8	43.6	147.4

KLD_85 Kluane detrital UC03A- (Counted by Eva Enkelmann 18 July 2015)

EFFECTIVE TRACK DENSITY FOR FLUENCE MONITOR (tracks/cm^2): 5.640E+05
RELATIVE ERROR (%): 1.80
EFFECTIVE URANIUM CONTENT OF MONITOR (ppm): 15.00
ZETA FACTOR AND STANDARD ERROR (yr cm^2): 237.00 5.00
SIZE OF COUNTER SQUARE (cm^2): 1.000E-06

------ GRAIN AGES IN ORIGINAL ORDER ------

Grain no.	RhoS (cm^-2)	(Ns)	RhoI (cm^-2)	(Ni)	Squares	U	+/-2s	Grain Age	Age (Ma) --95% CI--	
1	1.10E+06	(22)	8.00E+05	(16)	20	21	11	91.0	45.9	184.7
2	7.67E+05	(23)	4.00E+05	(12)	30	11	6	126.0	60.8	276.7
3	4.40E+05	(22)	3.20E+05	(16)	50	9	4	91.0	45.9	184.7
4	1.53E+06	(46)	1.03E+06	(31)	30	27	10	98.2	61.2	160.0
5	2.22E+05	(4)	7.78E+05	(14)	18	21	11	19.6	4.6	60.6
6	3.33E+04	(2)	3.83E+05	(23)	60	10	4	6.2	0.7	23.5
7	1.25E+05	(5)	2.00E+05	(8)	40	5	4	42.1	10.7	143.3
8	3.33E+04	(2)	1.83E+05	(11)	60	5	3	12.9	1.3	55.5
9	6.17E+06	(37)	4.00E+06	(24)	6	106	43	102.0	59.7	177.8
10	8.00E+04	(2)	4.80E+05	(12)	25	13	7	11.8	1.2	49.9
11	6.67E+04	(4)	3.33E+05	(20)	60	9	4	13.8	3.3	39.8
12	0.00E+00	(0)	3.75E+05	(15)	40	10	5	3.2	0.1	18.6
13	3.25E+06	(65)	1.70E+06	(34)	20	45	15	126.2	82.5	196.8
14	9.00E+04	(9)	3.40E+05	(34)	100	9	3	17.9	7.5	37.6
15	1.20E+05	(6)	5.40E+05	(27)	50	14	6	15.1	5.0	36.7
16	1.33E+05	(4)	1.33E+05	(4)	30	4	3	66.5	12.4	349.4
17	5.00E+04	(1)	3.50E+05	(7)	20	9	7	10.7	0.2	73.9
18	1.20E+05	(6)	4.00E+05	(20)	50	11	5	20.4	6.6	51.6
19	8.00E+04	(4)	2.60E+05	(13)	50	7	4	21.1	4.9	66.3
20	0.00E+00	(0)	3.60E+05	(18)	50	10	4	2.6	0.1	15.2
21	8.60E+05	(43)	3.60E+05	(18)	50	10	4	156.9	89.4	287.9
22	2.15E+06	(43)	9.00E+05	(18)	20	24	11	156.9	89.4	287.9
23	7.00E+06	(28)	6.75E+06	(27)	4	180	69	68.9	39.2	121.2
24	5.67E+05	(17)	2.00E+05	(6)	30	5	4	183.5	70.8	561.7
25	2.33E+05	(7)	3.00E+05	(9)	30	8	5	52.0	16.4	155.1
26	6.67E+04	(2)	3.67E+05	(11)	30	10	6	12.9	1.3	55.5
27	2.50E+04	(1)	2.50E+05	(10)	40	7	4	7.5	0.2	46.8
28	1.25E+05	(5)	1.50E+05	(6)	40	4	3	55.7	13.4	215.5
29	2.50E+04	(1)	2.25E+05	(9)	40	6	4	8.4	0.2	53.4
30	4.00E+04	(2)	5.40E+05	(27)	50	14	6	5.3	0.6	19.7
31	1.56E+06	(25)	1.38E+06	(22)	16	37	15	75.4	40.9	139.9
32	2.75E+05	(11)	1.40E+06	(56)	40	37	10	13.3	6.2	25.3
33	3.00E+05	(12)	3.00E+05	(12)	40	8	5	66.5	27.4	160.8
34	1.00E+05	(5)	3.40E+05	(17)	50	9	4	20.1	5.7	55.3
35	5.00E+04	(2)	1.25E+05	(5)	40	3	3	27.9	2.5	161.3
36	5.50E+05	(11)	3.00E+05	(6)	20	8	6	119.9	41.4	391.6
37	2.40E+05	(6)	4.80E+05	(12)	25	13	7	33.8	10.3	95.6
38	5.11E+06	(46)	2.67E+06	(24)	9	71	29	126.4	76.0	216.0
39	8.00E+04	(4)	1.80E+05	(9)	50	5	3	30.3	6.7	105.6
40	6.22E+06	(56)	1.89E+06	(17)	9	50	24	215.1	124.7	392.4
41	6.00E+04	(3)	6.60E+05	(33)	50	18	6	6.4	1.2	19.4
42	6.00E+06	(24)	3.25E+06	(13)	4	86	47	121.5	60.0	258.8
43	3.33E+04	(2)	5.67E+05	(34)	60	15	5	4.2	0.5	15.3
44	1.20E+05	(6)	6.40E+05	(32)	50	17	6	12.8	4.3	30.3
45	6.00E+04	(6)	2.20E+05	(22)	100	6	2	18.6	6.0	46.2
46	1.00E+05	(5)	2.60E+05	(13)	50	7	4	26.2	7.2	76.4
47	4.29E+04	(3)	2.00E+05	(14)	70	5	3	14.9	2.6	51.2
48	3.75E+06	(15)	4.50E+06	(18)	4	120	56	55.6	26.1	116.1
49	4.00E+06	(36)	3.00E+06	(27)	9	80	31	88.4	52.3	151.0
50	1.05E+06	(21)	6.00E+05	(12)	20	16	9	115.2	54.7	255.9
51	7.50E+04	(3)	4.00E+05	(16)	40	11	5	13.1	2.3	43.7

52	3.33E+04 (1)	2.33E+05 (7)	30	6	5	10.7	0.2	73.9
53	5.00E+05 (6)	8.33E+05 (10)	12	22	14	40.4	12.0	120.7
54	0.00E+00 (0)	3.25E+05 (13)	40	9	5	3.7	0.1	21.9
55	2.33E+06 (21)	1.89E+06 (17)	9	50	24	81.9	41.3	164.7
56	2.00E+05 (5)	5.20E+05 (13)	25	14	8	26.2	7.2	76.4
57	1.25E+06 (20)	1.75E+06 (28)	16	47	18	47.7	25.4	87.3
58	3.60E+06 (108)	2.50E+06 (75)	30	66	15	95.5	70.5	130.0
59	5.00E+04 (2)	3.00E+05 (12)	40	8	5	11.8	1.2	49.9
60	5.00E+04 (2)	3.50E+05 (14)	40	9	5	10.2	1.1	41.5
61	9.33E+05 (14)	1.00E+06 (15)	15	27	14	62.1	27.8	137.3
62	3.00E+04 (3)	2.90E+05 (29)	100	8	3	7.2	1.3	22.3
63	6.67E+05 (12)	1.67E+05 (3)	18	4	5	252.3	71.7	1329.8
64	4.00E+04 (4)	2.80E+05 (28)	100	7	3	9.9	2.4	27.3
65	0.00E+00 (0)	3.00E+05 (30)	100	8	3	1.6	0.1	8.7
66	8.33E+04 (5)	2.67E+05 (16)	60	7	4	21.3	6.0	59.4
67	1.20E+05 (3)	3.20E+05 (8)	25	9	6	25.8	4.3	103.7
68	1.00E+04 (1)	3.00E+05 (30)	100	8	3	2.5	0.1	13.4
69	1.00E+05 (10)	3.70E+05 (37)	100	10	3	18.3	8.0	37.0
70	2.00E+05 (4)	4.50E+05 (9)	20	12	8	30.3	6.7	105.6
71	6.67E+04 (2)	4.00E+05 (12)	30	11	6	11.8	1.2	49.9
72	0.00E+00 (0)	5.00E+05 (5)	10	13	11	9.9	0.3	72.6
73	1.33E+05 (4)	4.33E+05 (13)	30	12	6	21.1	4.9	66.3
74	8.57E+04 (6)	3.00E+05 (21)	70	8	3	19.4	6.3	48.8
75	6.67E+04 (2)	2.00E+05 (6)	30	5	4	23.3	2.2	123.5
76	7.50E+04 (3)	3.50E+05 (14)	40	9	5	14.9	2.6	51.2
77	1.33E+06 (12)	1.33E+06 (12)	9	35	20	66.5	27.4	160.8
78	5.24E+05 (11)	9.52E+04 (2)	21	3	3	337.0	79.7	2739.7
79	6.00E+04 (3)	3.40E+05 (17)	50	9	4	12.3	2.2	40.7
80	1.00E+05 (3)	3.00E+05 (9)	30	8	5	23.0	3.9	88.7
81	6.33E+05 (19)	1.90E+06 (57)	30	51	13	22.4	12.5	38.0
82	7.50E+04 (3)	5.00E+05 (20)	40	13	6	10.5	1.9	33.7
83	2.50E+06 (50)	1.35E+06 (27)	20	36	14	122.3	75.5	202.7
84	1.30E+06 (26)	6.80E+06 (136)	20	181	32	12.8	8.0	19.5
85	2.22E+05 (2)	3.33E+05 (3)	9	9	9	45.5	3.7	377.8
86	0.00E+00 (0)	3.00E+05 (12)	40	8	5	4.0	0.1	24.0
87	5.00E+06 (20)	2.25E+06 (9)	4	60	39	145.4	64.3	360.5
88	3.22E+06 (29)	3.44E+06 (31)	9	92	33	62.2	36.2	106.5
89	4.00E+04 (2)	4.40E+05 (22)	50	12	5	6.5	0.7	24.7
90	0.00E+00 (0)	2.00E+05 (6)	30	5	4	8.2	0.3	56.5
91	5.00E+04 (2)	1.75E+05 (7)	40	5	3	20.1	1.9	99.6
92	1.40E+05 (7)	7.00E+05 (35)	50	19	6	13.6	5.0	30.5
93	8.00E+04 (8)	3.60E+05 (36)	100	10	3	15.1	6.0	32.4
94	4.00E+04 (4)	4.40E+05 (44)	100	12	4	6.3	1.6	16.7
95	4.00E+04 (1)	5.20E+05 (13)	25	14	8	5.8	0.1	34.2
96	9.00E+04 (9)	4.20E+05 (42)	100	11	3	14.5	6.1	29.8
97	8.00E+04 (4)	2.20E+05 (11)	50	6	3	24.9	5.6	81.6
98	7.00E+04 (7)	9.40E+05 (94)	100	25	5	5.1	1.9	10.7
99	7.78E+05 (7)	5.56E+05 (5)	9	15	13	92.1	25.5	363.6
100	0.00E+00 (0)	3.40E+05 (17)	50	9	4	2.8	0.1	16.2
101	7.50E+04 (3)	3.75E+05 (15)	40	10	5	13.9	2.5	47.1
102	5.33E+05 (16)	3.00E+05 (9)	30	8	5	116.8	49.2	298.3
103	3.67E+06 (33)	2.00E+06 (18)	9	53	25	120.9	66.6	227.3
104	4.00E+06 (16)	2.75E+06 (11)	4	73	43	96.0	42.2	227.8
105	2.50E+04 (1)	3.00E+05 (12)	40	8	5	6.3	0.1	37.6

KLD_105 Kluane detrital UC03A- (Counted by Eva Enkelmann 16 July 2015)

EFFECTIVE TRACK DENSITY FOR FLUENCE MONITOR (tracks/cm^2): 5.276E+05

RELATIVE ERROR (%): 1.80

EFFECTIVE URANIUM CONTENT OF MONITOR (ppm): 15.00

ZETA FACTOR AND STANDARD ERROR (yr cm^2): 237.00 5.00

SIZE OF COUNTER SQUARE (cm^2): 1.000E-06

------ GRAIN AGES IN ORIGINAL ORDER ------

Grain no.	**RhoS (cm^-2)**	**(Ns)**	**RhoI (cm^-2)**	**(Ni)**	**Squares**	**U+/-2s**		**Grain Age**	**Age (Ma) --95% CI--**	
1	6.00E+05	(18)	3.00E+05	(9)	30	9	6	122.7	53.1	308.7
2	4.67E+05	(14)	2.00E+05	(6)	30	6	4	142.1	52.4	447.6
3	1.00E+06	(9)	2.22E+05	(2)	9	6	8	260.3	57.9	2238.8
4	4.44E+05	(8)	2.78E+05	(5)	18	8	7	98.1	28.8	377.6
5	8.33E+05	(25)	6.00E+05	(18)	30	17	8	86.0	45.3	166.9
6	6.00E+05	(9)	6.00E+05	(9)	15	17	11	62.2	21.9	175.5
7	3.50E+05	(14)	4.50E+05	(18)	40	13	6	48.6	22.3	102.8
8	1.00E+06	(9)	8.89E+05	(8)	9	25	17	69.8	24.0	206.3
9	2.75E+05	(11)	5.00E+04	(2)	40	1	2	315.8	74.6	2594.0
10	2.00E+05	(3)	3.33E+05	(5)	15	9	8	38.2	5.8	190.1
11	4.00E+05	(12)	4.33E+05	(13)	30	12	7	57.5	24.0	135.9
12	3.21E+05	(9)	4.29E+05	(12)	28	12	7	46.9	17.4	120.2
13	4.80E+05	(24)	4.00E+05	(20)	50	11	5	74.5	39.5	141.8
14	4.67E+05	(14)	2.00E+05	(6)	30	6	4	142.1	52.4	447.6
15	9.17E+05	(11)	2.50E+05	(3)	12	7	8	217.2	60.2	1167.8
16	1.00E+05	(1)	3.00E+05	(3)	10	9	9	22.7	0.4	254.6
17	1.67E+05	(5)	3.00E+05	(9)	30	9	6	35.1	9.1	114.5
18	5.00E+05	(15)	5.00E+05	(15)	30	14	7	62.2	28.4	135.9
19	7.78E+05	(7)	5.56E+05	(5)	9	16	13	86.2	23.9	340.8
20	5.00E+05	(15)	1.67E+05	(5)	30	5	4	181.1	64.4	628.4
21	4.67E+05	(14)	1.67E+05	(5)	30	5	4	169.3	59.3	593.2
22	4.38E+05	(7)	5.00E+05	(8)	16	14	10	54.6	16.9	170.5
23	4.00E+05	(6)	2.00E+05	(3)	15	6	6	120.8	26.6	730.1
24	2.00E+05	(6)	5.33E+05	(16)	30	15	7	23.8	7.5	62.8
25	7.00E+05	(28)	5.00E+05	(20)	40	14	6	86.7	47.3	162.0
26	5.50E+05	(11)	4.50E+05	(9)	20	13	8	75.7	28.7	205.5
27	2.75E+05	(11)	7.50E+04	(3)	40	2	2	217.2	60.2	1167.8
28	4.00E+05	(12)	2.33E+05	(7)	30	7	5	105.3	38.8	313.8
29	4.00E+05	(4)	2.00E+05	(2)	10	6	7	119.5	17.9	1252.7
30	4.33E+05	(13)	2.67E+05	(8)	30	8	5	100.0	38.9	276.9
31	8.89E+05	(16)	2.78E+05	(5)	18	8	7	192.8	69.6	663.4
32	1.00E+05	(4)	2.00E+05	(8)	40	6	4	31.8	6.9	115.7
33	4.00E+05	(8)	3.50E+05	(7)	20	10	7	70.9	22.6	227.6
34	1.00E+06	(20)	4.50E+05	(9)	20	13	8	136.1	60.1	337.8
35	5.50E+05	(11)	4.00E+05	(8)	20	11	8	84.9	31.4	241.8
36	1.70E+05	(17)	4.00E+04	(4)	100	1	1	252.8	86.0	1003.6
37	1.05E+06	(21)	8.00E+05	(16)	20	23	11	81.3	40.6	166.2
38	5.00E+05	(8)	4.38E+05	(7)	16	12	9	70.9	22.6	227.6
39	6.00E+05	(18)	3.00E+05	(9)	30	9	6	122.7	53.1	308.7
40	3.00E+05	(9)	4.67E+05	(14)	30	13	7	40.3	15.3	99.0
41	5.83E+05	(7)	5.83E+05	(7)	12	17	12	62.2	18.7	205.7
42	9.00E+05	(27)	4.67E+05	(14)	30	13	7	118.8	60.7	244.3
43	7.33E+05	(11)	6.00E+05	(9)	15	17	11	75.7	28.7	205.5
44	4.75E+05	(19)	4.50E+05	(18)	40	13	6	65.6	32.7	132.1
45	8.00E+05	(12)	8.00E+05	(12)	15	23	13	62.2	25.6	150.5
46	8.00E+05	(16)	4.50E+05	(9)	20	13	8	109.3	46.0	279.4
47	1.14E+05	(8)	7.14E+04	(5)	70	2	2	98.1	28.8	377.6
48	3.17E+05	(19)	2.67E+05	(16)	60	8	4	73.7	36.0	152.7
49	6.00E+04	(3)	4.00E+04	(2)	50	1	1	91.0	10.7	1035.4
50	5.00E+05	(10)	5.50E+05	(11)	20	16	9	56.7	21.6	145.9
51	5.00E+05	(15)	3.67E+05	(11)	30	10	6	84.4	36.5	202.2

52	1.19E+06	(19)	8.75E+05	(14)	16	25	13	84.0	40.2	180.5
53	4.67E+05	(14)	3.67E+05	(11)	30	10	6	78.8	33.4	191.0
54	4.80E+05	(12)	1.08E+06	(27)	25	31	12	27.9	12.8	56.5
55	2.78E+05	(5)	2.22E+05	(4)	18	6	6	77.1	16.8	382.5
56	8.33E+05	(25)	6.00E+05	(18)	30	17	8	86.0	45.3	166.9
57	9.50E+05	(19)	4.00E+05	(8)	20	11	8	145.1	61.7	380.9
58	4.80E+05	(12)	4.80E+05	(12)	25	14	8	62.2	25.6	150.5
59	1.40E+05	(7)	6.00E+04	(3)	50	2	2	140.2	33.2	820.2
60	1.50E+05	(3)	5.00E+05	(10)	20	14	9	19.4	3.3	72.5
61	6.00E+05	(15)	3.20E+05	(8)	25	9	6	115.1	46.4	311.8
62	3.67E+05	(11)	3.33E+05	(10)	30	9	6	68.3	26.4	178.3
63	7.67E+05	(23)	4.33E+05	(13)	30	12	7	109.1	53.5	233.7
64	4.67E+05	(14)	3.33E+05	(10)	30	9	6	86.5	36.0	216.7
65	6.00E+05	(15)	4.80E+05	(12)	25	14	8	77.5	34.0	180.5
66	4.33E+05	(13)	2.67E+05	(8)	30	8	5	100.0	38.9	276.9
67	2.50E+05	(3)	5.00E+05	(6)	12	14	11	32.0	5.1	144.8
68	4.44E+05	(4)	1.00E+06	(9)	9	28	18	28.3	6.2	98.9
69	1.70E+06	(34)	1.15E+06	(23)	20	33	14	91.6	52.6	162.5
70	7.00E+05	(28)	3.25E+05	(13)	40	9	5	132.4	67.1	277.4
71	5.50E+05	(22)	4.25E+05	(17)	40	12	6	80.2	40.9	160.4
72	8.00E+05	(24)	2.67E+05	(8)	30	8	5	182.4	80.9	466.1
73	4.20E+05	(21)	2.40E+05	(12)	50	7	4	107.9	51.2	239.7
74	9.00E+05	(18)	5.50E+05	(11)	20	16	9	100.9	45.6	235.6
75	1.00E+05	(3)	6.67E+04	(2)	30	2	2	91.0	10.7	1035.4
76	6.80E+05	(17)	5.20E+05	(13)	25	15	8	81.0	37.3	180.7
77	1.93E+06	(58)	1.83E+06	(55)	30	52	14	65.6	44.6	96.6
78	5.50E+05	(11)	4.50E+05	(9)	20	13	8	75.7	28.7	205.5
79	1.00E+05	(5)	4.00E+04	(2)	50	1	1	147.9	25.5	1462.7
80	2.50E+05	(10)	7.50E+04	(3)	40	2	2	198.0	53.4	1082.7
81	4.75E+05	(19)	3.50E+05	(14)	40	10	5	84.0	40.2	180.5
82	5.00E+05	(25)	3.00E+05	(15)	50	9	4	102.9	52.6	209.4
83	4.00E+05	(20)	4.40E+05	(22)	50	13	5	56.6	29.3	108.4
84	5.00E+05	(15)	1.67E+05	(5)	30	5	4	181.1	64.4	628.4
85	2.00E+06	(18)	2.33E+06	(21)	9	66	29	53.4	26.8	104.9
86	4.25E+05	(17)	5.00E+05	(20)	40	14	6	53.0	26.1	106.1
87	4.00E+05	(12)	2.00E+05	(6)	30	6	4	122.2	43.3	394.0
88	4.40E+05	(11)	4.00E+05	(10)	25	11	7	68.3	26.4	178.3
89	3.00E+05	(15)	1.60E+05	(8)	50	5	3	115.1	46.4	311.8
90	5.75E+05	(23)	2.75E+05	(11)	40	8	5	128.4	60.9	290.6
91	8.00E+05	(8)	4.00E+05	(4)	10	11	11	121.5	33.4	544.1
92	8.89E+05	(8)	1.00E+06	(9)	9	28	18	55.5	18.6	160.4
93	8.00E+05	(16)	3.00E+05	(6)	20	9	7	161.9	61.6	500.6
94	6.67E+05	(14)	3.81E+05	(8)	21	11	7	107.6	42.7	294.4
95	2.40E+05	(12)	6.00E+04	(3)	50	2	2	236.3	67.1	1251.7
96	7.50E+05	(15)	3.50E+05	(7)	20	10	7	131.0	51.2	377.4
97	3.00E+05	(3)	7.00E+05	(7)	10	20	15	27.5	4.5	116.4
98	1.40E+06	(28)	1.00E+06	(20)	20	28	13	86.7	47.3	162.0